Measurement of the effective diffusivity of carbon monoxide in commercial catalytic monolith converters

Zhang, Fan

Award date:
2005

Awarding institution:
University of Bath

MEASUREMENT OF THE EFFECTIVE DIFFUSIVITY OF CARBON MONOXIDE IN COMMERCIAL CATALYTIC MONOLITH CONVERTERS

Submitted by

Fan Zhang

For the degree of PhD of the University of Bath, 2005

COPYRIGHT

Fan Zhang

Dec 2005

ProQuest LLC
789 East Eisenhower Parkway
P.O. Box 1346
Ann Arbor, MI 48106-1346

Abstract

Catalytic converters are widely used to control emissions from motor vehicles, and carbon monoxide is one of the main components that are controlled. In catalytic converters, noble metal catalysts (*e.g.* Pt, Pd and Rh) are dispersed in a washcoated monolith, and these promote favourable oxidation and reduction reactions to reduce undesirable emissions. At normal working temperatures in a catalytic converter, *e.g.* 400 to 800 °C, these catalytic reactions are extremely fast, and so both interphase and intraphase transport limitations may have significant influence on overall reaction rates. In order to model the performance of a catalytic converter, it is necessary to be able to quantify the extent of diffusion limitation in the washcoated layer.

In this thesis, a method is described for measuring the flux of a diffusing species through a single and multiple cell structures that have been cut from a commercial catalytic monolith. This method is suitable for porous monolith supports, *e.g.* cordierite. To illustrate the technique, the diffusion of CO in nitrogen is studied using a modified form of Wicke-Kallenbach type of diffusion cell. The inlet concentration of the diffusing component is 2.4% CO in nitrogen, and experiments are performed on a catalytic monolith with 62 cells/cm^2 at ambient temperature and pressures between 106 to 151 kPa. At experimental conditions (temperature 17.4 ± 2.3 °C; pressure in the diffusion cell 1.1100 ± 0.0001 bar (a); inlet gas flowrate 600 ± 2 ml/min), the measured effective diffusivity of CO in the different alumina based washcoats is found to lie in the range of (7.04 ± 3.48) × 10^{-7} m^2/s, whilst the value in the cordierite support is in the range of (10.81 ± 1.72) × 10^{-7} m^2/s.

To illustrate the importance of intraphase diffusion on reaction rates and conversion of pollutants, CO oxidation experiments are preformed using a commercial diesel-oxidation catalytic monolith. It is shown that even at high gas velocities in the channels (*e.g.* 140 to 166 m/s), intraphase mass transfer is significant. For the platinum based diesel oxidation catalyst, the rate expression was found to be of the following form:

$$(-R_{CO}) = 7.9433\times10^{15} \exp\left(-\frac{104000}{R_g T}\right) P^{-1.1}\, C_b\, Y_{CO} \quad (\text{mol.m}^{-2}.\text{s}^{-1})$$

Acknowledgements

It is my great pleasure to acknowledge those who have contributed to the thesis in the past years.

First of all, I would like to thank my supervisor, **Professor Stan Kolaczkowski**. He has very great learning and attainments, especially in chemical engineering, reaction engineering, chemistry and mathematics. He is always patient, and never feels tired of giving instructions to his students including me. He is so kindly that he always does his best to help me in many aspects. I feel very much indebted to him for all that he had done in these years for my family and myself.

My sincere thanks also go to the following people:

Professor R. E. Hayes in the chemical engineering department at University of Alberta (Canada), for many interesting discussions on mass transfer in monolithic reactors.

Dr Serpil Awdry and Dr Luong Nguyen for discussing the modelling and the Matlab programme used in the thesis.

Dr Jürgen Gieshoff and Dr Martin Votsmeier for giving me the opportunity to perform experiments in Automotive Catalyst Division, Degussa Metals Catalysts Cerdec (**dmc**^{2}), Frankfurt.

Professor John Howell & Dr Alexei Lapkin for their discussions and encouragement.

Dr Semali Perera for being as my examiner in the viva of my transfer report and giving many useful and helpful suggestions.

Mrs Sally Barker and Miss Charlotte Wilkes for their daily support.

Ms June Fish, Dr Gareth Williams and Dr Alex Shirley for helping me correct spelling and grammar mistakes in the thesis.

Dr George Manos and Mr Julian Perfect at University College London for their help in Mercury porosimetry and ASAP characterisation for my samples.

Dr Sungsoo Kim for always being willing to give competent help on the experimental skills.

Dr Gareth Williams for daily co-operation and good spirits.

Miss Katarina Persson from Sweden and Mrs Sonja Stark in **dmc^2** (Germany) for short but stimulating collaboration.

Dr Chris Flatley for assistance in building the rig of the catalytic combustion experiments and in preparing catalysts.

Mr Fernando Acosta and Mr Tony Comer for assistance in building the rig of CO diffusion experiments.

Mr Mac Forsyth, Mr Robert Brain, & Mr John Bishop for providing various experimental materials.

Mr Merv Newnes for his IT supports.

Ms Anne O'Reilly for helping me characterise many of the samples.

Mr Hugh Parrott in the Material Department for his help in electron microscopy.

Dr Mingguo Tang, Dr Tianxiang Xia, Dr Yutie Liu, Dr Rongsheng Zhang, Miss Dan Wu, Mr Gang Yuan and Miss Rong Chao for support and help on various issues.

All other friends and colleagues at Bath University for their help on numerous occasions.

My very special thanks go to my wife and my parents-in-law for their help in daily living in Bath.

Finally, **dmc^2** is acknowledged for the part-financial support of some of this work, and **Prof Stan Kolaczkowski** who part-funded the work from some of his consultancy income.

List of figures

List of tables

Nomenclature and abbreviations

A	Surface area available for diffusion in the diffusion cell	m^2
A_b	Surface area of the blank (uncoated) cordierite available for diffusion in the diffusion cell	m^2
A_w	Pre-exponential factor	$m.s^{-1}.pa^{-\alpha}$
$C_{1,CO}$	Inlet CO concentration in the upper chamber,	$mol.m^{-3}$
$C_{2,CO}$	Outlet CO concentration in the upper chamber	$mol.m^{-3}$
$C_{3,CO}$	Inlet CO concentration in the lower chamber	$mol.m^{-3}$
$C_{4,CO}$	Outlet CO concentration in the lower chamber	$mol.m^{-3}$
C_A	Molar concentration of Component A	$mol.m^{-3}$
C_p	Constant pressure heat capacity of air	$J.mol^{-1}.K^{-1}$
$C_{p,m}$	Mass heat capacity of air	$J.kg^{-1}.K^{-1}$
C_T	Total molar concentration of gas mixture in the porous media	$mol.m^{-3}$
D	Diameter of the circular hole available for diffusion in the washcoated sample	m
D_{AB}	Molecular diffusion coefficient of A in a mixture of A and B	$m^2.s\text{-}1$
$D_{AB,eff}$	Effective diffusivity of A in a mixture of A and B	$m^2.s\text{-}1$
D_b or D_{Bulk}	Bulk diffusion (molecular diffusion)	$m^2.s\text{-}1$
D_{bc}	Diameter of the circular hole available for diffusion in the blank (uncoated) cordierite sample	m
$D_{Bulk,0}$	Molecular diffusion coefficient of CO in a mixture of CO and N_2 evaluated at room temperature	$m^2.s^{-1}$
$D_{Bulk,T}$	Molecular diffusion coefficient of CO in a mixture of CO and N_2 evaluated at mean bulk temperature (T)	$m^2.s^{-1}$
D_c	Combined effective diffusivity in transition regime	$m^2.s^{-1}$
D_e or D_{eff}	Effective diffusivity of CO in air under reaction conditions in the catalyst	$m^2.s^{-1}$

$D_{eff,0}$	Effective diffusivity of CO in N_2 under room temperature (17.4 ± 2.3) °C in the catalyst	$m^2.s^{-1}$
$D_{eff,bc}$	Effective diffusivity of CO in blank (uncoated) cordierite	$m^2.s^{-1}$
$D_{eff,s}$	Effective diffusivity of CO in blank (uncoated) substrate (cordierite)	$m^2.s^{-1}$
$D_{eff,t}$	Effective diffusivity of CO in washcoated monolith	$m^2.s^{-1}$
$D_{eff,T}$	Effective diffusivity of CO in N_2 under temperature T in the catalyst	$m^2.s^{-1}$
$D_{eff,w}$	Effective diffusivity of CO in washcoat layer	$m^2.s^{-1}$
D_H	Hydraulic diameter of a single monolith channel	m
D_i	Diffusivity coefficient in micropore	$m^2.s^{-1}$
D_K	Knudsen diffusion coefficient	$m^2.s^{-1}$
$D_{K,0}$	Knudsen diffusion coefficient in the catalyst at room temperature	$m^2.s^{-1}$
$D_{K,a}$	Knudsen diffusion coefficient in macropore	$m^2.s^{-1}$
$D_{K,i}$	Knudsen diffusion coefficient in micropore	$m^2.s^{-1}$
$D_{K,T}$	Knudsen diffusion coefficient in the catalyst at temperature T	$m^2.s^{-1}$
$D_{K,A}$	Knudsen diffusivity of A in pores	$m^2.s^{-1}$
$D_{M,0}$	Diffusion coefficient of CO in N_2 under room temperature in the catalyst	$m^2.s^{-1}$
$D_{M,T}$	Diffusion coefficient of CO in N_2 under temperature T in the catalyst	$m^2.s^{-1}$
dp	Average pore diameter	m
E_w	Activation energy of CO oxidation reaction (based on the Pt catalyst in the washcoat)	$J.mol^{-1}$
F	Molar flowrate	$mol.s^{-1}$
$F_{1,CO}$	Inlet CO molar flowrate in the upper chamber	$mol.s^{-1}$
$F_{1,t}$	Inlet total molar flowrate in the upper chamber	$mol.s^{-1}$
$F_{2,CO}$	Outlet CO molar flowrate in the upper chamber	$mol.s^{-1}$

$F_{2,t}$	Outlet total molar flowrate in the upper chamber	$mol.s^{-1}$
$F_{3,CO}$	Inlet CO molar flowrate in the lower chamber	$mol.s^{-1}$
$F_{3,t}$	Inlet total molar flowrate in the lower chamber	$mol.s^{-1}$
$F_{4,CO}$	Outlet CO molar flowrate in the lower chamber	$mol.s^{-1}$
$F_{4,t}$	Outlet total molar flowrate in the lower chamber	$mol.s^{-1}$
Gz	Graetz number (heat transfer)	*dimensionless*
h	Heat transfer coefficient	$W.m^{-2}.K^{-1}$
$(\Delta H)_R$	Heat of reaction	$J.mol^{-1}$
k_f	Thermal conductivity of air	$W.m^{-1}.K^{-1}$
k_m	Mass transfer coefficient	$m.s^{-1}$
k_v	Reaction rate constant based on catalyst volume	$s^{-1}.Pa^{-\alpha}$
L	Length of capillary tubes	*m*
L_{bc}	Thickness of blank (uncoated) cordierite	*m*
Lc	The "effective" thickness of washcoat of the monolith reactor in Chapter 6	*m*
Len	The length of the monolith reactor in Chapter 6	*m*
L_t or L_{total}	Total thickness of the washcoated cordierite	*m*
L_w	Thickness of the washcoat	*m*
m	Mass	*kg*
M_A	Molar mass of species A	$g.mol^{-1}$
n	Avogadro's number, = 6.022045×10^{23}	*dimensionless*
N_1	Diffusion flux in a pore of mean radius (r_m)	$mol.m^{-2}.s^{-1}$
N_A	Diffusion flux of component A	$mol.m^{-2}.s^{-1}$
N_{co}	Molar flux of CO in the upper chamber	$mol.m^{-2}.s^{-1}$
Nu	Nusselt number	*dimensionless*

P	Pressure	Pa
$P_{2,s}$	Outlet pressure at standard condition (101325 Pa pressure and 273.15 K temperature) in the upper chamber	Pa
$P_{3,s}$	Inlet pressure at standard condition in the lower chamber	Pa
$P_{4,s}$	Outlet pressure at standard condition in the lower chamber	Pa
P_{cell}	Measured absolute pressure in the diffusion cell	Pa
Pr	Prandtl number	*dimensionless*
P_{room}	Room pressure	Pa
$Q_{1,c}$	Calibrated value of inlet flowrate in the upper chamber	$ml.min^{-1}$
$Q_{1,d}$	Displayed value of inlet flowrate in the upper chamber	$ml.min^{-1}$
$Q_{1,s}$	Inlet flowrate in the upper chamber at standard condition	$m^3.s^{-1}$
$Q_{2,c}$	Calibrated value of outlet flowrate in the upper chamber	$ml.min^{-1}$
$Q_{2,d}$	Displayed value of outlet flowrate in the upper chamber	$ml.min^{-1}$
$Q_{2,s}$	Outlet flowrate in the upper chamber at standard condition	$m^3.s^{-1}$
$Q_{3,c}$	Calibrated value of inlet flowrate in the lower chamber	$ml.min^{-1}$
$Q_{3,d}$	Displayed value of inlet flowrate in the lower chamber	$ml.min^{-1}$
$Q_{3,s}$	Inlet flowrate in the lower chamber at standard condition	$m^3.s^{-1}$
$Q_{4,c}$	Calibrated value of outlet flowrate in the lower chamber	$ml.min^{-1}$
$Q_{4,d}$	Displayed value of outlet flowrate in the lower chamber	$ml.min^{-1}$
$Q_{4,s}$	Outlet flowrate in the lower chamber at standard condition	$m^3.s^{-1}$
Q_c	Calibrated flowrate	$ml.min^{-1}$
Q_s	Flowrate at standard condition	$m^3.s^{-1}$
r	Average pore radius	m
R	Universal gas constant, 8.314 J/(mol.K)	$J.mol^{-1}.K^{-1}$
R_d	Diffusion resistance	$s.m^{-1}$

R_i	Electrical resistance (See Equation 3.6)	Ω
r_a	Macropore radius	m
$(-R_{CO})$	Rate of disappearance of species CO.	$mol.m^{-2}.s^{-1}$
Re	Reynolds number	*dimensionless*
r_i	Micropore radius	m
r_m	Mean radius in a pore	m
r_p	The capillary tube radius	m
Sc	Schmidt number	*dimensionless*
S_g	BET surface area (for unit mass of solid)	$m^2.g^{-1}$
Sh	Sherwood number	*dimensionless*
S_t	The total BET surfaces	m^2
S_w	Calculated washcoat BET surface	$m^2.g^{-1}$
t	Time	s
T	Absolute temperature	K
$T_{1,c}$	Inlet temperature at calibration condition in the upper chamber	K
T_b	The temperature in the bulk flow	K
T_{cal}	Temperature at calibration condition	K
Th_b	Thickness of blank (uncoated) cordierite	μm
Th_w	Thickness of washcoat layer	μm
T_{in}	Inlet temperature to the monolithic reactor	K
T_{out}	Outlet temperature from the monolithic reactor	K
T_{prime}	Definition of $\frac{dT}{dZ}$, outlet temperature distribution along the monolithic reactor length, see Equation 6.29	*dimensionless*
T_{room}	Room temperature	K

T_w	The temperature in the washcoat	*K*
u	Average velocity	$m.s^{-1}$
V_g	Pore volume (for unit mass of solid)	$m^3.g^{-1}$
y_0	The mole fraction of component A at z = 0	*dimensionless*
$Y_{1,CO}$	Inlet concentration of CO in the upper chamber	*ppm*
$Y_{2,CO}$	Outlet concentration of CO in the upper chamber	*ppm*
$Y_{2,CO,c}$	Calibrated outlet concentration of CO in the upper chamber	*ppm*
$Y_{2,CO,d}$	Displayed outlet concentration of CO in the upper chamber	*ppm*
$Y_{3,CO}$	Inlet CO concentration in the lower chamber	*ppm*
$Y_{4,CO}$	Outlet CO concentration in the lower chamber	*ppm*
y_A	Molar fraction of component A	*dimensionless*
Y_b	Mole fraction of CO in the bulk flow	*dimensionless*
Y_c	Calibrated CO concentration	*ppm*
Y_d	Displayed CO concentration	*ppm*
Y_{in}	Inlet CO fraction to the monolithic reactor	*dimensionless*
Y_{out}	Outlet CO fraction from the monolithic reactor	*dimensionless*
y_L	The mole fraction of A at z = L	*dimensionless*
yprime	Definition of $\frac{dy}{dZ}$, CO fraction distribution along the monolithic reactor length, see Equation 6.10	*dimensionless*
Y_w	Mole fraction of CO in the washcoat	*dimensionless*
z	Length of the capillary tube	*m*
z	Distance from the entrance in the direction of gas flow	*m*

Greek letters

μ	Dynamic viscosity of air	*Pa.s*
α	The order of pressure	*dimensionless*
β	$\beta = 1 + \frac{N_2}{N_1}$ (See Equation 2.17)	*dimensionless*
α_{AB}	Geometric correction factor for Weisz diffusion cell	*dimensionless*
γ_M	Activity coefficient in macropore	*dimensionless*
γ_μ	Activity coefficient in micropore	*dimensionless*
ε	Total porosity	*dimensionless*
ε_a	Macroporosity	*dimensionless*
ε_i	Microporosity	*dimensionless*
ε_M	Void fraction in macropore	*dimensionless*
ε_P	Porosity of solid	*dimensionless*
ε_μ	Void fraction in micropore	*dimensionless*
λ	Mean free path	*m*
ν	The average velocity of the mixture gases	$m.s^{-1}$
ν	Mean mass average velocity of the fluid	$m.s^{-1}$
ν_m	The mean molecular velocity	$m.s^{-1}$
ρ	Gas density	$kg.m^{-3}$
ρ_a	Apparent density of a solid	$kg.m^{-3}$
ρ_b	Density of the blank (uncoated) cordierite sample	$kg.m^{-3}$
ρ	Inlet mole density	$mol.m^{-3}$

ρ_m	Inlet mass density of air	$kg.m^{-3}$
ρ_w	Density of washcoats	$kg.m^{-3}$
σ	Minimum root-mean square errors of outlet temperatures and CO fractions between calculated and measured values in Chapter 6. The express formula is $$\sigma = \sum_{n=1}^{10}\left(\frac{T_{n,measured} - T_{n,\,calculated}}{T_{n,\,measured}}\right)^2 + \sum_{n=1}^{10}\left(\frac{Y_{n,measured} - Y_{n,\,calculated}}{Y_{n,\,measured}}\right)^2 + \sum_{n=1}^{10}\frac{\left[(-R_{CO,n,measured}) - (-R_{CO,n,calculated})\right]^2}{(-R_{CO,n,measured}) \times (-R_{CO,n,calculated})}$$	*dimensionless*
σ_{AB}	Parameter defined in Equation 2.3	*dimensionless*
τ	Tortuosity factor	*dimensionless*

Abbreviation

AFR	Air to Fuel Ratio
ASAP	Accelerated Surface Area and Porosimetry system
BET	Brunauer-Emmerit-Teller
cpsi	Cells per square inch
dmc^2	Degussa Metals Catalysts Cerdec, Germany
DPI	Difference Pressure Indicator
FID	Flame Ionisation Detector
GC	Gas Chromatography
OFA	Open Frontal Area
PGE	Platinum Group Element
PGM	Platinum Group Metals
PIXE	Proton Induced X ray Emission analysis
SCR	Selective Catalytic Reduction
SEM	Scanning Electron Microscopy
STP	Standard Temperature and Pressure (273.15 K and 101325 Pa)
TCD	Thermal Conductivity Detector
TEM	Transmission Electron Microscopy
TWC	Three-Way Catalysts
W-K	Wicke-Kallenbach
W-S	Wakao-Smith model
XRD	X-Ray Diffraction

Table of contents

Chapter 1 Introduction

1.1 General background

The use of automobiles as a comfortable and convenient transport system has become more and more popular since the first practical internal combustion engine-powered automobile was invented in 1886 by a German engineer Karl Benz.

The impact of automobiles on the global environment is considerable. They contribute to a wide range of different types of pollution. For example, motors and alarms may cause noise pollution; particulates in exhaust emissions may cause soil pollution; waste lubrication oil could contribute to water pollution, whilst polished car surfaces and windscreens possibly effect light pollution. Amongst them, some of more adverse impacts arise from exhaust emissions, which have already caused air and atmospheric pollution in many developed countries and in most developing countries.

The pollutants in vehicle exhaust emissions can be classed into the following six groups (Holmgren, 1999; Akama *et al.*, 2002):

CO (carbon monoxide). This is mainly formed as a result of incomplete combustion in the region of oxygen deficiency in an engine, especially in a cold region.

HC (hydrocarbons). These hydrocarbons arise from the incomplete combustion of fuel, or the volatilisation of dissolved fuel in the lubrication oil. Many of the aromatic and unsaturated hydrocarbons in the exhaust are carcinogens.

NOx (NO and NO_2). These are generally formed in the high temperature region where nitrogen is oxidised. In the atmosphere, NOx in the presence of hydrocarbons can react to form photochemical smog.

SOx (SO_2 and SO_3). These are formed by the oxidation of sulphur in fuel and lubrication oil, and in the atmosphere they react with water to form acids.

Greenhouse gases (CO_2, HC and N_2O). These gases are believed to raise the atmospheric temperature. Besides being a greenhouse gas, N_2O may reach the stratosphere, where it reacts with ozone and decreases the ozone layer.

PM (Particulate matter, including soluble organic fraction, sulphur and carbon particles). PM is produced mainly by lean-burn diesel-fuelled engines, which are operated on fuel-air mixtures having fuel-air ratios richer than the stoichiometric value.

The main components in the exhaust emissions from gasoline-fuelled engines are listed in Table 1.1.

Table 1.1 An indication of components in exhaust emissions from gasoline-fuelled engines.

(Based on data summarised from: Shishu, 1972; Voltz *et al.*, 1973; Bettman & Otto, 1983; Subramanlam & Varma, 1985; Koltsakis and Stamatelos, 1997A; Lox and Engler, 1997; Hu *et al.*, 2001).

Components	Concentration
CO	0.05 to 4.0 (mol %)
Hydrocarbons	100 to 5000 (ppm)
NOx	50 to 2500 (ppm)
SOx	20 to 45 (ppm)
CO_2	12.0 to 18.0 (mol %)
Water	9.0 to 10.0 (mol %)
O_2	0.1 to 5.0 (mol %)
N_2 and others	Balance (mol %)

The main components in the exhaust emissions from a diesel engine are listed in Table 1.2. They are more complex than those from gasoline-fuelled engines because they comprise not only gaseous components but also liquid and even solid components. The solid components are denoted as particulate matter.

Table 1.2 An indication of components in exhaust emissions from diesel engines. (Based on data from: Lox and Engler, 1997; Koltsakis & Stamatelos, 1997A; Jelles, 1999; Morlang *et al.*, 2005).

Components	Concentration
CO	100 to 2000 (ppm)
Hydrocarbons (C_1 - C_{15})	50 to 2000 (ppm)
NOx	30 to 1000 (ppm)
SOx	About 20 ppm
CO_2	2 to 12 (mol %)
Water	2 to 10 (mol %)
O_2	3 to 15 (mol %)
N_2 and others	Balance (mol %)
Particulate matter	20 to 200 (mg/m^3)

It is estimated that in the next decade most vehicles will still be fuelled mainly by gasoline or diesel rather than powered by electrical energy, solar energy or natural gas. To minimize emissions, many different factors need to be considered, *e.g.* road conditions, engines' performance, fuel components, after-treatment of exhaust emissions, *etc.* Catalytic automotive exhaust after-treatment is the last opportunity to minimize the emissions before they are emitted into the atmosphere.

Oxidation catalysts were first introduced to oxidize CO and HC in exhaust emissions in the USA before the 1970's (Koltsakis *et al.*, 1997). Several years later, they were replaced by three-way catalysts (TWC) and diesel-oxidation catalysts (DOC). The former were able to oxidize CO and hydrocarbons, and reduce NOx simultaneously. In

the end of 1990's, more than 55% of the world's 500 millions cars and over 85% of all new-produced cars worldwide were equipped with after-treatment systems (Searles, 2000).

Although auto-catalysts have been used for about 30 years, there are still improvements sought to their design. One of the main research challenges is how to increase the conversions of the pollutants to as high a level as possible; in other words, how to decrease the concentration of the harmful emissions to as low a level as possible, in order to match the increasingly strict emission standards throughout the world. Having reviewed the literature, it is clear that the following three factors still have an important effect on the performance of the converter.

Control of the air-fuel ratio (AFR). Since the oxidation of carbon monoxide and hydrocarbons, and the concomitant reduction of oxides of nitrogen occur simultaneously, the concentration of oxygen (or air-fuel ratio, so-called **AFR)** is a very significant factor. Figure 1.1 shows that only a very narrow range (14.48 to 14.62) is suitable for AFR values. Although sensitive oxygen-sensor control systems have been developed, it is difficult to control the AFR with sufficient accuracy throughout the process.

Control of reaction conditions. Catalytic converters are not always operating in their optimum temperature range (*e.g.* 400 to 800 °C) due to the transient nature of operation and variations in ambient conditions.

Avoidance of intraphase diffusion limitations. Although the thickness of the washcoat containing the dispersed catalyst on the monolith is normally thinner than 200 μm, the diffusion of reactants in this layer may be a significant rate-limiting step at high temperatures (*e.g.* Massing *et al.*, 2000; Mukadi & Hayes, 2002).

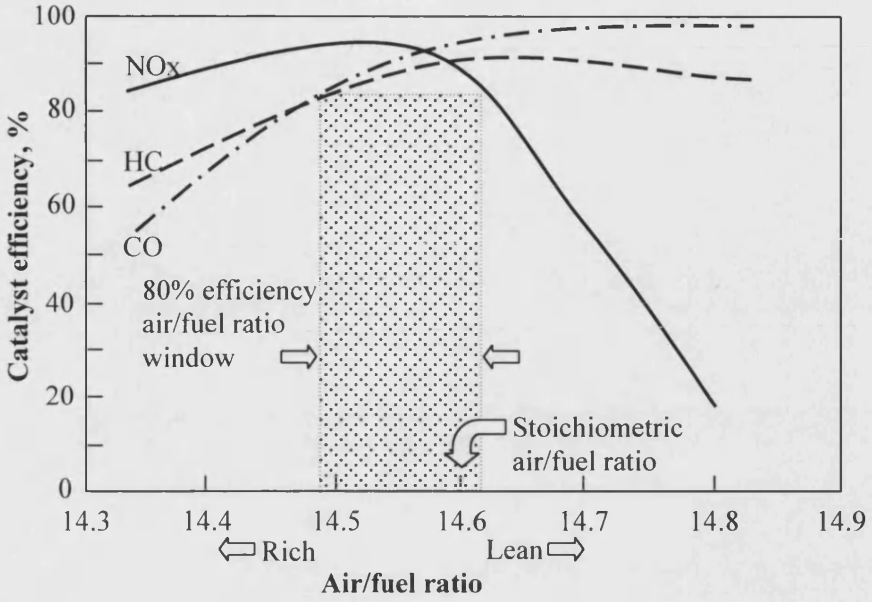

Figure 1.1 Conversion efficiency of NO, CO and HC as a function of the air-fuel ratio in a three way catalytic converter.

As the performance of catalytic converters is a complex function of operating conditions, converter geometries, and catalyst properties (OH *et al.*, 1980), and as there are still several challenges left for the development of catalytic converters, an empirical approach to these challenges could be very costly and time-consuming. Therefore, there is scope to make use of mathematical modelling to help with the development of catalytic converters and to support experimental studies.

In order to model the performance of a catalytic converter, it is necessary to consider diffusion limitations. Although there are many studies of effective diffusivity in catalyst pellets, there are very few studies on catalytic monoliths. From the literature, it appears that in the last three decades, most researchers have used calculated or estimated effective diffusivity values in their models rather than experimentally derived ones. This is not surprising as developers of mathematical models do not necessarily have access to experimental facilities, and it is also very difficult to measure the effective diffusivity of reactants in a sample of washcoated monolith.

1.2 Scope of work in this thesis

The main focus of the thesis is how to measure the effective diffusivity of a species in the washcoat of a realistic and representative structure, and then how to apply that knowledge in a model of a catalytic converter. As CO is one of the main reactants, it was selected for the purpose of this study. The intention was to develop a method to measure the effective diffusivity in a representative system, and then to back-calculate the values of tortuosity that were specific to the washcoat, that could be used in a more complex model of the converter.

1.3 Structure of the thesis

This thesis is organized as follows:

In Chapter 2, a brief review is provided to illustrate the history, development, current situation and the important role that catalytic converters have in controlling emissions. The classification, structure, and function of catalytic converters are also described. Mass transfer and diffusion, as well as various possible chemical reactions that may occur in a catalytic converter are introduced. This leads to the identification of challenges, including those arising from mass transfer limitation. A brief description is provided of the models used to describe mass transfer and diffusion in catalytic converters, and of methods to measure the effective diffusivity in commercial auto-catalysts.

In Chapter 3, the design of a modified Wicke-Kallenbach diffusion cell and the associated apparatus for the measurement of steady-state diffusion is described. Experimental conditions are carefully selected, and measurements are made on samples of a 400 cells per square inch (**cpsi**) of ceramic monolith. The values of effective diffusivity of CO in nitrogen are determined, through blank (uncoated) cordierite, either

with a smooth or with a rough surface, using either single-plate or multi-plate structures. Possible sources of errors are described.

In Chapter 4, a method is developed to washcoat plates of cordierite with two different types of commercial slurry. The coating of the samples was done during a one-week period of research work at **dmc**^{2} laboratories in Hanau (Germany). The samples were calcined at two different temperatures, so that different types of pore structure are obtained. The values of effective diffusivity of CO in nitrogen through these samples are measured, and possible sources of errors are discussed.

In Chapter 5, samples are prepared by cutting sections from commercial automotive catalysts, either in the form of a single-plate or a multi-plate structure. The values of effective diffusivity of CO through these samples are measured, and possible sources of errors are discussed. This led to the publication of a paper (see Appendix A), where the techniques developed in this thesis were combined with the modelling skills of Professor Hayes at the University of Alberta in Canada (Hayes *et al.*, 2000) to interpret the data.

In Chapter 6, the catalytic oxidation of CO on a commercially produced diesel-oxidation catalysts is investigated. Making use of the data acquired in Chapter 5, values of tortuosity are assigned in a model of the catalytic converter. This enables the rate constants in a kinetic rate expression to be back-calculated and the effect of pressure to be quantified. This example illustrates the value of the technique studied in this thesis, and how with the aid of the model the presence of diffusion limitations may be quantified. The errors in these experiments as well as the limitations of the rate expression used are discussed.

In Chapter 7, general conclusions are presented, and suggestions made for future work in this field.

In the appendices, example calculations are provided and experimental data are listed.

Chapter 2 Catalytic converters

2.1 Introduction

The initiative to introduce legislation to limit vehicles' exhaust emissions was taken in the USA. In 1966, California introduced limits for the exhaust emission of CO and hydrocarbons from passenger cars equipped with spark ignition engines. Soon after, similar measures were then taken in Japan, Australia and Switzerland. In 1985, the European Community passed respective strict legislation for passenger cars with spark ignition engines (Lox *et al.*, 1997).

In the last decade many countries paid more attention to vehicles' exhaust emission pollution than ever before. They set up their own emission standards for different vehicles. As a result, millions of catalytic converters are needed every year for the global automobile market.

During the process of improving the quality and function of catalytic converters, hundreds of patents have been filled in the world. Based on a review of numerous sources of literature (*e.g.*, Lox & Engler, 1997; Kruse *et al.*, 1998; Harrison, 2001), the requirements for the development of catalytic converters are summarized below:

To keep costs low. Many researchers are trying to make use of alkaline earth metals to partially replace noble Pt group metals (Pt, Pd, Rh, Ru, Os and Ir), and thereby lower the cost as well as save the limited noble metal resource.

To maintain a longer service life. The catalyst durability in catalytic converters should be the same order of magnitude as the vehicles lifetime. However, current catalytic converters fitted to vehicles have been designed to give service life that covers only 50,000 to 100,000 miles (see http://www.eurocats.co.uk/).

To improve operational performance. This means that a catalytic converter has the optimum design for mass transfer, heat transfer, flow distribution, pressure drop, *etc.*

To extend application range. This means the emission limits for other exhaust gas components, *e.g.* carbon dioxide, benzene and aldehydes; and for other transportation rather than passenger cars, *e.g.* motorbikes, trucks, buses, trains, ships; and for other fuel-powered equipment, *e.g.* small utility equipment, larger construction equipment, are being considered.

To achieve higher conversion of pollutants. New-generation catalytic converters tend to convert more than 98% of CO and HC, and 95% of NO_x into harmless products. A higher target is "zero emission" or to act as an "air cleaner". This means that the exhaust emissions after being treated by the catalytic converter results in an exhaust stream that could be cleaner than the surrounding air.

However, because of many limitations in catalytic converters, *e.g.* possible diffusion limitation and the effect of operating conditions, it is difficult for catalytic converters, especially those that have been in service for several years, to match the increasingly strict emission standards. Figure 2.1 shows the evolution of US federal emissions standards for light-duty vehicles over the last 27 years. After 2003, these emissions standards for NO, HC and CO will be limited to 0.2, 0.125 and 1.7 g/mile respectively (Koltsakis and Stamatelos, 1997A).

As illustrated in Figure 2.1, CO is the pollutant of highest concentration and is difficult to completely eliminate in vehicle exhaust emissions. This is the reason why CO emission limits are still as high as 1.7 g/mile for light-duty vehicles in the USA even after 2003. It is therefore not surprising that the oxidation of CO on noble metal catalysts is one of the most studied catalytic reactions (Drewsen *et al.*, 2000), although it was started with early work by Langmuir (1922). For this reaction, there is much experimental and kinetic data available in the literature. A large number of CO oxidation models have also been developed. The plentiful amount of data available

could be used to support the work contained in this thesis. Based on all of these considerations, CO was selected as the species to be used in this study.

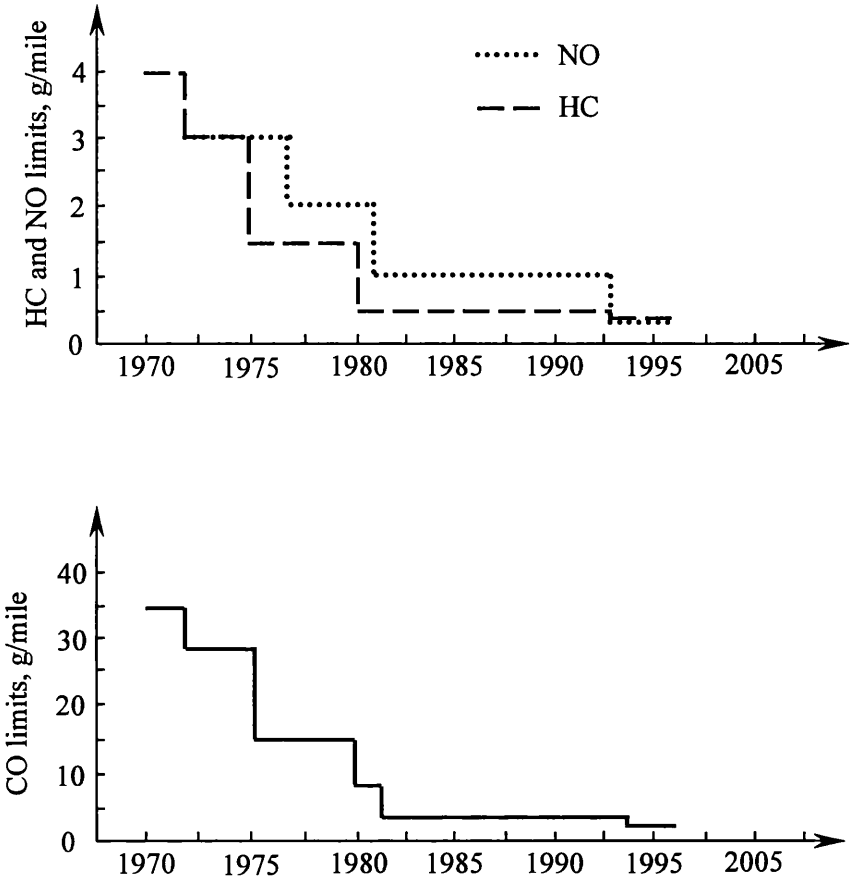

Figure 2.1 Historical evolutions of the federal emission standards in the USA for light-duty vehicles.

(Adapted from Koltsakis and Stamatelos, 1997).

2.2 The classification of catalytic converters

Catalytic converters have many different types and shapes. In simple terms they could be classified either by their functions, or by their support materials.

***By functions*:** A catalytic converter for a gasoline engine exhaust emissions is called a three-way catalyst (**TWC**) converter. Since the main harmful components from the exhaust emissions of a gasoline engine is CO, HC and NOx, a TWC converter focuses its function to oxidize CO and HC as well as to reduce NO_x simultaneously.

A catalytic converter that is used to purify the diesel engine exhaust emissions is called a diesel-oxidation catalyst (**DOC**) converter. Because diesel engines generally emit gaseous emissions as well as particulate matter, *e.g.* soot, inorganic oxides, sulphates, solid hydrocarbons (Koltsakis & Stamatelos, 1997A; Harrison, 2001; Tsolakis *et al.*, 2004), a DOC converter is normally combined with a filter to catch the particulate matter.

By support materials: Catalytic converters that have metal or alloy supports are called metallic monolith converters. Their honeycomb is formed by alternating flat and corrugated thin metal foils. These foils are made out of corrosion-and-high-temperature-resistant steel with a thickness of about 0.05 mm (Lox & Engler, 1997). Metallic monolith converters offer certain advantages (Silversand & Odenbrand, 1999) and are used in a number of specialist applications.

Catalytic converters that have porous ceramic supports with monolith or bead structure (*e.g.* spheres, or extruded short segments of a suitable refractory material), are called ceramic catalytic converters. Ceramic bead-structure converters have some obvious disadvantages, *e.g.* high pressure-drop, complex construction of the converter housing (compared to ceramic monolith converters). So the majority of passenger cars are now equipped with ceramic monolith converters (Lox & Engler, 1997). As ceramic monoliths are predominantly used as supports for catalytic converters, they are considered in more detail in this thesis.

2.3 The structure of catalytic converters

A catalytic converter is generally located close to the engine exhaust manifold (see Figure 2.2), so that it can be rapidly heated (within 1 or 2 minutes) to reaction temperature by the exhaust emissions.

Typically a catalytic converter is made up of 5 main parts: support, washcoat, catalyst, mat and housing. Figure 2.3 illustrates the structure of a ceramic-based monolith converter.

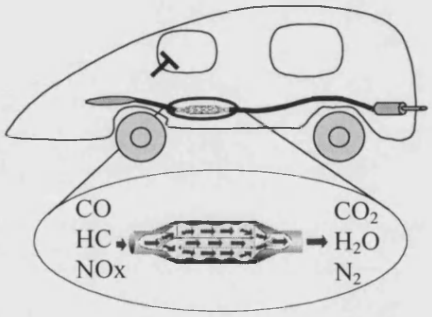

Figure 2.2 The location of a catalytic converter in a vehicle.

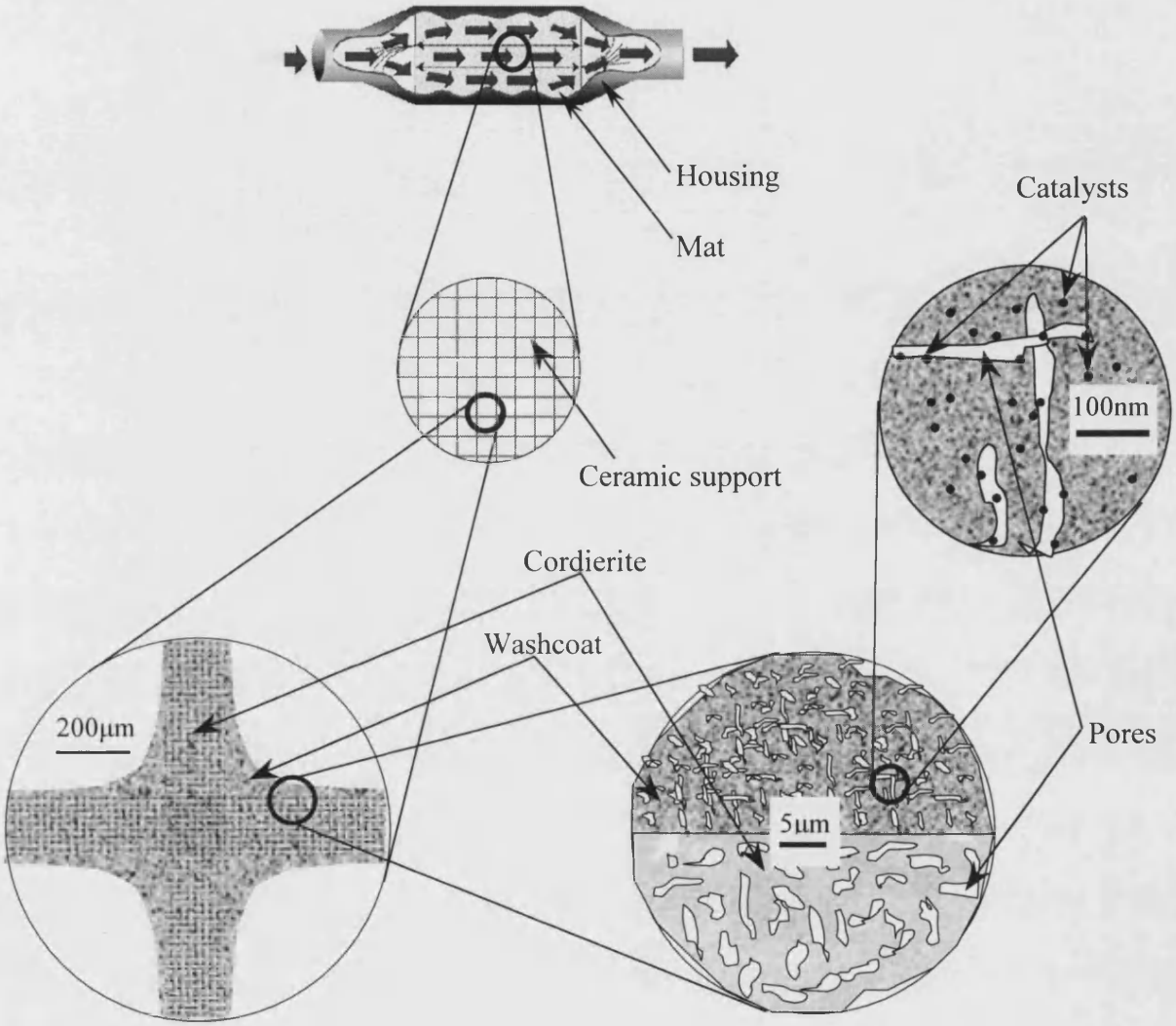

Figure 2.3 Schematic diagram illustrating the structure of the catalytic monolith converter.

2.3.1 Support

Support is like the skeleton of a catalytic converter. The basic requirements for a support are as follows:

- Reasonable mechanical strength and rigidity to endure a vehicle's acceleration, deceleration and vibration;
- A high temperature thermo-tolerance to face about 300 to 1000 °C of reaction temperature (Lox & Engler, 1997);
- Resistance to thermal shock to endure fast temperature-rise processes;
- Corrosion resistance to avoid being oxidized by oxygen, NO_2, or to be corroded by NH_3, SOx, *etc*;
- Low pressure-drop to allow exhaust emissions to be vented smoothly;
- Durability for a long life expectancy.

To match these requirements, channels with many different shapes were designed. Common shapes are square, triangle, hexagon, *etc* (see Figure 2.4). The cell/channel densities can also vary from 25 to 900 cells per square inch (**cpsi**) of monolith as illustrated in Table 2.1 (Williams, 2001).

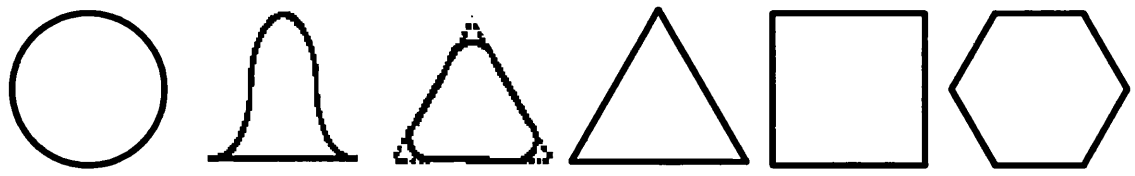

Figure 2.4 Different channel shapes commonly used in catalytic monoliths. (Adapted from Balakotaiah & West, 2002).

Table 2.1 Monolith substrate of interest for automotive converters.
(Adapted from Williams, 2001).

Cell density (cpsi)	**Wall thickness** (1 mil = 0.001 inch)	**Geometric surface area** (cm^2/cm^3)	**OFA** (Open Frontal Area) (%)
25	(35 mil) 0.889mm	6.51	0.681
50	(25 mil) 0.635mm	9.17	0.678
100	(15 mil) 0.381mm	13.39	0.723
200	(10.5 mil) 0.267mm	18.98	0.725
300	(8 mil) 0.203mm	23.51	0.742
400	(4 mil) 0.102mm	27.09	0.846
600	(4 mil) 0.102mm	31.01	0.787
900	(2 mil) 0.051mm	43.11	0.834

The monolithic shapes and cell densities give rise to low backpressure in automotive exhaust systems. High cell density (normally 200 to 900 cells/$inch^2$), thin walls (0.051 to 0.27 mm, or 0.002 to 0.0105 inch) and high open frontal area (**OFA**) (up to 83%) are preferable conditions to achieve low backpressure (Williams, 2001).

A growing trend is to make use of ultra-thin-walled substrates to improve "light-off" performance. Here "light-off" is "typically defined as the temperature at which under the chosen reaction conditions the reactant conversion reaches the values of 50%" (Lox & Engler, 1997). Thinner walls allow the exhaust gases to flow more easily because the open frontal area is higher. Furthermore, this design means that the material has less mass overall, so it reaches the optimum reaction temperature more quickly.

Metal or alloy supports already have very thin walls; however, they have a number of disadvantages. These include high cost and poor compatibility with washcoat, because the washcoat is mainly made from porous inorganic materials.

Compared with metal or alloy supports, ceramic supports, which are made from one or more refractory materials, have better compatibility with the washcoat. Many different kinds of ceramic supports, *e.g.*, cordierite ($2MgO{\cdot}2Al_2O_3{\cdot}5SiO_2$), alumina ($Al_2O_3$), mullite ($3Al_2O_3{\cdot}2SiO_2$), lithium aluminium silicate ($Li_2O{\cdot}Al_2O_3{\cdot}4SiO_2$) and aluminium titanate ($Al_2O_3{\cdot}TiO_2$), all contain the Al_2O_3 component, which is also the main constituent in the washcoat (Alexander and Umehara, 1995).

Cordierite is made from kaolin ($Al_2O_3{\cdot}2SiO_2{\cdot}2H_2O$), talc ($3MgO{\cdot}4SiO_2{\cdot}H_2O$) and alumina ($Al_2O_3$) (Hayes and Kolaczkowski, 1997). It is generally used as support material due to its following critical characteristics (Lachman and Williams, 1992):

- Thermal shock resistance due to a low thermal expansion coefficient;
- Porosity and pore size distribution suitable for washcoat application;
- Good adherence with washcoat;
- Sufficient refractoriness because the melting point exceeds 1450 °C;
- Sufficient strength for survival in an automotive exhaust environment, and
- Compatibility with washcoat and catalysts.

Blank (uncoated) cordierite shows hardly any activity for the reactions occurring in a catalytic converter. It is of course possible to incorporate catalysts into a blank cordierite, *e.g.*, mixing noble metal catalysts into inorganic materials during the preparation of the cordierite, or by "impregnating" catalysts directly into the macropores of a blank cordierite. However, such catalysts will not exhibit a significant activity because the pore surface area of cordierite is very low, normally no more than 5 m^2/g. In blank cordierite, the pore diameter is up to several micrometers; as a result, its total pore volume may be only 0.2 cm^3/g (Alexander and Umehara, 1995).

To obtain larger surface area, and to disperse noble metal catalysts as finely as possible, it is necessary to coat at least one layer of high surface area material (commonly known as the washcoat) onto the surface of the monolith support.

2.3.2 Washcoat

Gamma alumina (γ-Al_2O_3) is one of the most common washcoat materials due to its low cost, high melting point and large surface area, which is up to 200 m^2/g (Harris *et al.*, 1982). Its disadvantage is that when the temperature reaches over 900 °C, γ-Al_2O_3 will change into δ-Al_2O_3 or θ-Al_2O_3, ultimately into α-Al_2O_3. As a result, its surface area will decrease sharply (Trimm, 1983). In a commercial catalytic converter, alumina present in the washcoat is usually a mixture of gamma and delta phases, and may also contain substantial amounts of eta, kappa and theta phases (Hindin & Dettling, 1979).

Some rare earth oxides, *e.g.* CeO_2, are also main components in washcoat materials because of their oxygen storage ability (Holmgren, 1999). During changes in driving speed and fuel mixtures, these rare earth oxides can either store or release oxygen into the exhaust gas and keep the catalyst performing consistently at a high level.

ZrO_2 may also be used as washcoat material or additive due to it thermal stability (Bekyarova *et al.*, 1998). Titania, silica and zeolite are also reported potential as washcoat materials (Bera *et al.*, 2000). Table 2.2 lists common washcoat materials and their functions.

In a catalytic converter, the washcoat may comprise of different layers. Every layer may consist of a different washcoat materials and catalysts. For example, for the layered system described by Murakami *et al.* (1999) and Morbidelli *et al.* (2001) that is illustrated in Figure 2.5a. Layer 1 is at the external surface, and consists of dispersed Pt. In Layer 2 is located the Rh layer, so that diffusion resistances for NOx reduction would be minimized and Rh would also be protected from poisoning. At the deepest location, in Layer 3, Pd catalyst provides good light-off performance, especially for aged catalysts, because of its good thermal stability. According to the authors, this

configuration also prevented undesirable alloy formation among the noble metals, which is one of the reasons causing the deactivation of catalysts.

Table 2.2 Common washcoat materials for vehicle emission control.

Materials	Functions	References
Al_2O_3, SiO_2	Disperse noble metal catalysts	Hindin *et al.* (1979) Hu *et al.* (2001)
BaO, CeO_2, ReO_2, La_2O_3, Nd_2O_3, Pr_2O_3, SiO_2, ZrO_2 M_2O_3 (M = Mg/Ca/Sr/Ba)	Stabilizer against thermal degradation	Brandenburg *et al.* (1984) Bekyarova *et al.* (1998) Hu *et al.* (2001) Koltsakis and Stamatelos (1997)
BaO	Stabilizer against poisoning with S and H_2O	Kurokawa *et al.* (1997)
	NO_x storage	Liotta *et al.* (2002)
CeO_2, N_2O_3 (N = Fe/Co/Ni)	Oxygen storage	Summers (1990) Holmgren (1999) Hu *et al.* (2001)
K_2O	Additive	Lee & Chen (1997)
Zeolite	Adsorbent of HC	Noda *et al.* (2001)

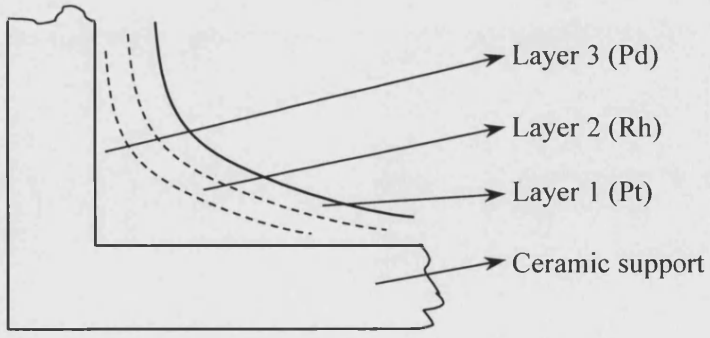

Figure 2.5a A corner of a ceramic auto-catalyst with multi-layer washcoat. (Adapted from Murakami *et al.*, 1999; Morbidelli *et al.*, 2001).

For different purposes, the distribution of catalysts in multi-layer washcoat may be different. For example, Yamamoto's invention (Yamamoto, 2003) focused on "the purification of HC, CO, and NOx with good balance". In the patent, a multi-layer washcoat is described as follows: "the zeolite layer (Layer 3) whose thickness is adjusted to a proper thickness can control the diffusion (speed) of the exhaust gases that are passed through the cell and diffused into the metal-based catalyst layer (Layer 1) and the HC adsorbent layer (Layer 2), and thus improve the cold HC purification performance" (see Figure 2.5b).

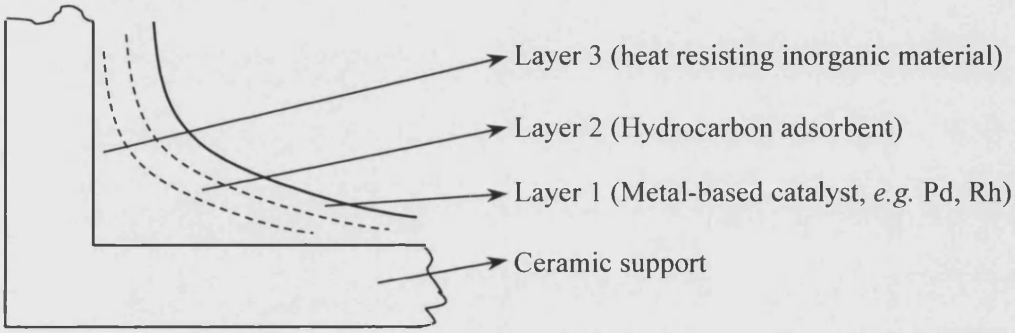

Figure 2.5b One kind of distribution of catalysts in multi-layer washcoat. (Adapted from Yamamoto, 2003).

To coat the surface of the support, washcoat materials first need to be made into a slurry (for single layer washcoat) or several slurries (for multi-layer washcoat). Then the monolith supports are partially dipped in the washcoat and the excess washcoat is blown out of the channels. The process is repeated until the desired washcoat thickness for the first layer is achieved. After drying the washcoated support, the process is repeated to coat the second layer. And then the third layer... There are many detailed descriptions in literatures of how to prepare a washcoat (*e.g.* Qin & Jiang, 2000; Labhsetwar *et al.*, 2001; Kumar *et al.*, 2004).

In practice, it is difficult to achieve a uniform thickness of washcoat around the perimeter of the cell. According to Hayes and Kolaczkowski (1997), the thickness of washcoat may vary from 10 to 150 μm around the perimeter. The ratio of the washcoat

thickness to the hydraulic diameter of the cell is very small, therefore, the washcoat layers may be assumed to have flat-plate geometry (*e.g.* Zygourakis & Aris, 1983; Zhang *et al.*, 2004). This will be convenient for simulating the performance of catalytic converters, or calculating the values of effective diffusivities in washcoat layers.

2.3.3 Catalysts

Common auto-catalysts

Platinum group metals (**PGM**), *e.g.* Pt, Pd, Rh and Ir, are the main catalysts in catalytic converters for vehicle systems due to their higher level of activity and resistance to sulphur poisoning. Among these metals, Pt and Pd are well known as oxidation catalysts, playing a key role in oxidizing carbon monoxide and hydrocarbons; whereas Rh and Ir are known as "DeNO$_x$ catalysts", being used to reduce the emission of nitrogen oxides (Merget and Rosner, 2001). Although Pt and Pd are expensive ingredients; Rh is even more expensive (Ertl *et al.*, 1997; Wijngaarden *et al.*, 1998).

Some lower-cost transition metals, *e.g.* Co, Cr, Mn, Fe, Cu and Ni (Zwinkels *et al.*, 1993; Martinez-Arias *et al.*, 1998), and some rare earth oxides, *e.g.* the oxides of La-Ce (Ciambelli *et al.*, 1999), alone or possibly with the addition of small amounts of precious metals, could create robust emission control catalysts. In particular, copper oxide exhibits activities per unit surface area similar to those of noble-metal catalysts such as Pt (Kummer, 1980).

Distribution of auto-catalysts in washcoat

Normally the components and ratios of catalysts in different washcoat layers are different. For example, Qin & Jiang (2000) described such an exhaust gas catalyst with multi-layer catalytic washcoat. The inner layer "is formed with composition active catalytic elements with approximate weight ratios of La:Ce:Mn:Co:Pd = (10-15): (10-15) : (6-10) : (6-10) : (0.1-0.3)"; whereas in the outer catalytic layer, "the weight ratio of

the active catalytic elements is Y:La:Zr:Cu:Cr:V:Pd = (1-3) : (2-6) : (2-6) : (6-10) : (10-15) : (2-6) : (0.1-0.3)".

Mussmann *et al.* (2001) described one manufacture method of multi-layer auto-catalysts in their patent:

"For providing the inner layer, the passage ways of the catalysts can be coated with an aqueous coating composition comprising the particulate support materials of the inner layer (including the first oxygen storage material). The coating composition will also be called a 'coating dispersion' in this application. .... The coating is then dried and calcined in air. Drying is preferably done at elevated temperatures of up to 150 °C. For calcining the coating, temperatures of from 200 to 500 °C for a period from 0.1 to 5 hours should be applied.

"After calcination, platinum may be dispersed onto the coated carrier body by dipping the monolith into a solution containing a precursor compound of platinum. The solution may be an aqueous or non-aqueous (organic solvent) solution. Any platinum precursor compound may be used, provided the compound is soluble in the chosen solvent and decomposes upon heating in air at elevated temperatures. Illustrative examples of these platinum compounds are chloroplatinic acid, ammonium chloroplatinate, platinum tetrachloride hydrate, platinum dichlorocarbonyl dichloride, dinitrodiamino platinum, platinum nitrate, platinum tetraammine nitrate and platinum tetraammine hydroxide. After impregnation, the coating is again calcined at temperatures between 200 and 500 °C in air."

The non-uniform catalyst distribution may also appear along the monolith length, *e.g.*, more Pt catalysts are dispersed upstream than downstream in the monolith converter. This can result in shorter warm-up period and thus lower cold-start emissions.

According to Lox *et al.* (1997), non-uniformities of catalyst distribution are "intentional and are desirable for kinetic reasons or because of specific beneficial interactions between the precious metals and the washcoat oxides". Within a single secondary

washcoat particle, the distribution of the precious metals can be assumed to be relatively homogeneous. The metal particles are present as single atoms or as small clusters of about ten atoms, with a diameter of about one nanometer.

Sub-pollution caused by auto-catalysts

Using the noble metals, especially Pt, may cause sub-pollution due to the loss of noble metal catalysts. Artelt *et al.* (1999) tested four catalytic converters and found that mean Pt emissions ranged from 7 to 123 $ng.m^{-3}$ (Pt mass concentration in unit volume of emissions) depending on the operating conditions and the age of the converters.

Recovery

About 34% of total platinum, 55% of total palladium, and 95% of total rhodium demand was used for the production of automotive catalysts in 1998, which cost more than 2.2 billion US dollars. Regrettably, less than 10% of those platinum group metals (**PGM**) from catalytic converters were recycled (Cowley, 1999). It is necessary to use an efficient way to recycle the noble metals both for saving the limited resource and for decreasing possible sub-pollution caused by PGM. In a recently published paper, one suitable method was introduced. This method can extract up to 95.9% of platinum and 92.9% of rhodium in the catalysts at 550 °C by a chlorine and carbon monoxide gas mixture (Kim *et al.*, 2000).

2.3.4 Mat and housing

The mat is a material that surrounds the monolithic support and is made either out of ceramic, or out of a metallic wire mesh. It will play at least three different roles in a catalytic converter.

- Provides an adequate gas seal around the monolith,
- Provides mechanical protection, and
- Acts as a thermal insulator, protecting also against cold thermal shock.

The converter housing, including the long section of exhaust pipe that connects with the engine, is usually made from high quality corrosion-resistant steel. The housing holds the ceramic monolith and ensures the exhaust gas flows through the ceramic monolith.

Table 2.3 shows typical values of the chemical composition and weight distribution of each section of a catalytic converter taken from a Swedish passenger car (Jobson, 1998 & 1999).

Table 2.3 The material compositions of a typical ceramic three-way catalytic converter. (Adapted from Jobson, 1998 & 1999).

Parts	Components	Weight, g
Catalyst support (crystal phase cordierite)	MgO 14%	1400
	Al_2O_3 36%	
	SiO_2 50%	
Washcoats (metal oxides slurry)	Al_2O_3 10%	170
	CeO_2 20%	
	ZrO_2 70%	
Catalysts	Pt: Pd: Rh = 1: 14: 1	2
Mat	Ceramic wire mesh	500
Converter housing	Steel	5000

2.4 Mass transfer and diffusions in catalytic converters

For typical monoliths, the Reynolds numbers vary between 25 and 400, therefore, the flow in the straight parallel passages is in the laminar flow regime (Zygourakis & Aris, 1983). The over-all process of chemical transformation in catalytic converters, as described by Gorring & deRosset (1964), involves a definite number of steps linked in series (see Figure 2.6). These are:

1. Diffusion of the reactants through the boundary layer adjacent to the external surface of the washcoat/catalysts (interphase diffusion);
2. Diffusion of the reactants through the porous matrix to the reactive surface (intraphase diffusion or pore diffusion);
3. Adsorption of the reactants on the active centres of the catalyst;
4. Chemical reaction at specific active sites;
5. Desorption of the products from the inner surface;
6. Diffusion of the products through the porous matrix to the exterior surface (intraphase diffusion or pore diffusion);
7. Diffusion of reactants away from the exterior surface and into the fluid surrounding the washcoat/catalysts (interphase diffusion).

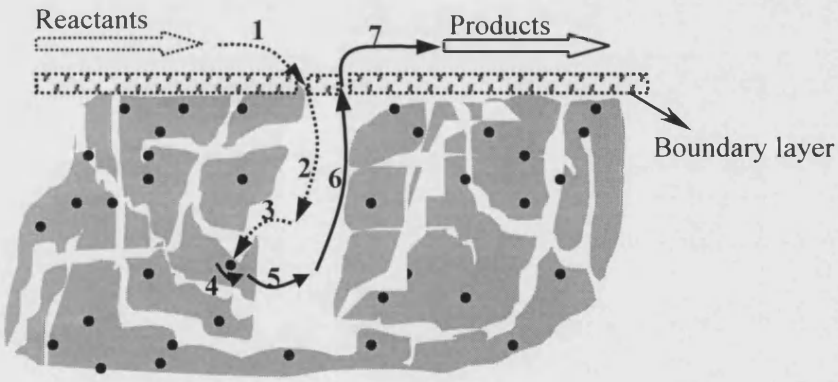

Figure 2.6 The over-all process of chemical transformation on porous materials. (Adapted from Gorring & deRosset, 1964).

When chemical reactions occur in a catalytic converter, reactants (CO, HC, NOx, *etc*) must be transported to the surface of the porous catalytic monolith and diffuse through pores to reach active catalysts. Similarly, products of the reaction (CO_2, H_2O, N_2, *etc*) must diffuse to the catalyst external surface before being transported to the surrounding bulk gas phase. The over-all reaction rate will be determined by the slowest step, which means it may be affected either by the effect of pore diffusion in the washcoat, or by

mass transfer in the gas phase, or by the number of active catalyst sites on the internal surface (Wanker *et al.*, 2000).

This process of mass transfer and diffusion is complex, which may comprise several different types of diffusions. The following paragraphs will introduce the classification of diffusions.

2.4.1 The classification of diffusions

In heterogeneous catalytic reactions, diffusion of reactants and products occurs through the pores of porous media, whose diameters may vary from 0.001 to 10 microns. These pores can be divided into three different types (based on their widths) according to the classification standard of International Union of Pure and Applied Chemistry (IUPAC) (Gregg and Sing, 1982):

Micropores (width < 2 nm)

Mesopores (2 nm < width < 50 nm)

Macropores (width > 50 nm)

There are two main types of diffusions through these pores. This includes molecular diffusion (also called bulk diffusion or free gas diffusion) and Knudsen diffusion, depending on the relation between molecule mean free path and pore width.

If the pore radius is more than 10 times the mean free path of diffusion molecules, there is much more chance of collision occurring among the molecules than that between the molecules and the wall. In this case, molecular diffusion will dominate the transport process. On the contrary, when the mean free path of the diffusion molecules are more than 10 times the pore radius, diffusion will proceed mainly by molecules and wall collisions. This is called Knudsen diffusion.

Molecular diffusion

In molecular diffusion regime, the diffusion flux of component A in component B may be described by the Stefan-Maxwell equation of diffusion (Park & Do, 1996):

$$N_A = -D_{AB}\frac{dC_A}{dz} + y_A(N_A + N_B) \tag{2.1}$$

where:

N_A	Diffusion flux of the component A, $mol.m^{-2}.s^{-1}$
D_{AB}	Molecular diffusivity, $m^{-2}.s^{-1}$
C_A	Molar concentration of A, $mol.m^{-3}$
y_A	Mole fraction of A, dimensionless

Applying the boundary conditions at the two ends of the pore, Equation 2.1 becomes:

$$N_A = \frac{C_T D_{AB}}{\sigma_{AB} L}\ln\left[\frac{1-\alpha_{AB} y_{A,2}}{1-\alpha_{AB} y_{A,1}}\right] \tag{2.2}$$

where:

C_T	Total molar concentration of gas mixture, $mol.m^{-3}$
L	Length of the catalyst, m
$y_{A,1}$	Mole fraction of A at z = 0, dimensionless
$y_{A,2}$	Mole fraction of A at z = L, dimensionless
α_{AB}	Geometric correction factor, dimensionless

σ_{AB} can be obtained from Equation 2.3:

$$\sigma_{AB} = 1 + \frac{N_B}{N_A} = 1 - \sqrt{\frac{M_A}{M_B}} \tag{2.3}$$

where $\frac{N_B}{N_A} = -\sqrt{\frac{M_A}{M_B}}$ is from Graham's law of diffusion.

The diffusion coefficient, D_{AB}, can be calculated from Chapman (1970):

$$D_{AB} = \frac{1.86\times10^{-3}\, T^{1.5} \left(\frac{1}{M_A} + \frac{1}{M_B}\right)^{0.5}}{P\sigma^2\,\Omega} \qquad (2.4)$$

where

D_{AB}	Gaseous diffusion coefficient, $m^{-2}.s^{-1}$
T	Absolute temperature, K
P	Pressure, Pa
σ	Characteristic length, Å
Ω	Diffusion collision integral, dimensionless
M_A	Molar mass of component A, $g.mol^{-1}$
M_B	Molar mass of component B, $g.mol^{-1}$

Although this estimation method is accurate, it is difficult to determine a suitable value of σ and Ω for many gases. So an empirical correlation summarised by Fuller *et al.* (1966), which included less factors, is widely used.

$$D_{AB} = \frac{1.00\times10^{-3}\, T^{1.75} \left(\frac{1}{M_A} + \frac{1}{M_B}\right)^{\frac{1}{2}}}{P\times\left[(\Sigma v)_A^{\frac{1}{3}} + (\Sigma v)_B^{\frac{1}{3}}\right]^2} \qquad (2.5)$$

where:

P	Pressure, atm
M_A	Molecular weight of A, $g.mol^{-1}$
M_B	Molecular weight of B, $g.mol^{-1}$
Σv	Diffusion volumes of molecules. The values are listed in Fuller *et al.* (1966).

Molecular diffusion may occur as a result of concentration, temperature, or pressure gradients, or because a directed external electrical or other potential is applied to a mixture (Wijngaarden *et al.*, 1998).

Knudsen diffusion

From kinetic theory, for a straight cylindrical pore in Knudsen diffusion regime, the diffusion flux of the component A is proportional to the difference of concentration between the ends of the capillary tube, but inversely proportional to the tube length. It is unaffected by the presence of the other species. The flux is represented by (Wakao & Kaguei, 1982; Park & Do, 1996):

$$N_A = -D_{K,A}\frac{\partial C}{\partial z} = -\frac{D_{K,A}}{RT}\frac{\partial P}{\partial z} = \frac{2r_p V}{3RT}\frac{\partial P}{\partial z} = \frac{2r_p}{3RT}\left(\frac{8RT}{\pi M_A}\right)^{1/2}\frac{\partial P}{\partial z} \qquad (2.6)$$

where:

$D_{K,A}$ Knudsen diffusivity of species A in the pore, $m^{-2}.s^{-1}$

r_p The pore radius, m

M_A Molecular weight of A, $g.mol^{-1}$

Integration of Equation 2.6 subjected to fixed boundary conditions gives:

$$N_A = \frac{C_T D_{K,A}}{L}(y_{A,1} - y_{A,2}) \qquad (2.7)$$

In general, Knudsen diffusivity (D_K) is related to the mean molecular velocity (v_m) and the capillary tube radius (r_p) by the following equation:

$$D_{K,A} = \frac{2v_m r_p}{3} \qquad (2.8)$$

For an ideal gas of molar mass, M_A, the velocity is:

$$v_m = \sqrt{\frac{8R_g T}{\pi \times M_A}} \tag{2.9}$$

Thus

$$D_{K,A} = \frac{2}{3} r_p \sqrt{\frac{8R_g T}{\pi \times M_A}} \tag{2.10}$$

Substituting for the value of R and π using 8.314 J/(mol.K) and 3.1416, then Equation 2.10 becomes:

$$D_{K,A} = 3.0675 \times r_p \sqrt{\frac{T}{M_A}} \tag{2.11}$$

As the pores are not cylindrical, Equation 2.11 is corrected empirically by defining a mean pore radius:

$$r_p = \frac{2V}{S} = \frac{2\theta}{S\rho} \tag{2.12}$$

where:

V	The pore volume, $m^3 \cdot g^{-1}$
S	The BET surface area, m^2
θ	The porosity
ρ	The pellet density, $kg \cdot m^{-3}$

So the effective Knudsen diffusivity can be calculated as follows (Park & Do, 1996):

$$D_{K,eff} = \frac{D_K \theta}{\tau} = 3.0675 \times \frac{2 \times \theta \times \theta}{S \times \rho \times \tau} \sqrt{\frac{T}{M_A}} = 6.135 \frac{\theta^2}{\tau \times S \times \rho} \sqrt{\frac{T}{M_A}} \tag{2.13}$$

Surface diffusion

Surface diffusion is the transport of adsorbed molecules or atoms on solid surfaces (Kast and Hohenthanner, 2000). Its contribution to the total flux depends on the particular adsorbate-adsorbent pair, system temperature, the thickness of the adsorbed layer, *etc*. Although the mobility of molecules in adsorbed layer is generally much slower than that in gas phase, the concentration is very high, and so a significant contribution of surface diffusion is possible. However, in most catalytic reactions occurring in a catalytic converter, the reaction temperatures are elevated, molecules are chemisorbed (thin mono-layer), and therefore surface diffusion is generally considered to be of little importance (Wheeler, 1955).

2.4.2 Diffusion limitation in catalytic converters

Richter *et al.* (1978) summarized the relation between the diameter of the pores and diffusion mechanisms (Figure 2.7). For auto-catalysts, because most of the pores are within the range of 0.005 to 5 microns, and the temperature at which reactions occur is much higher than the boiling points of the species, Knudsen diffusion should dominate the transport process in the pores.

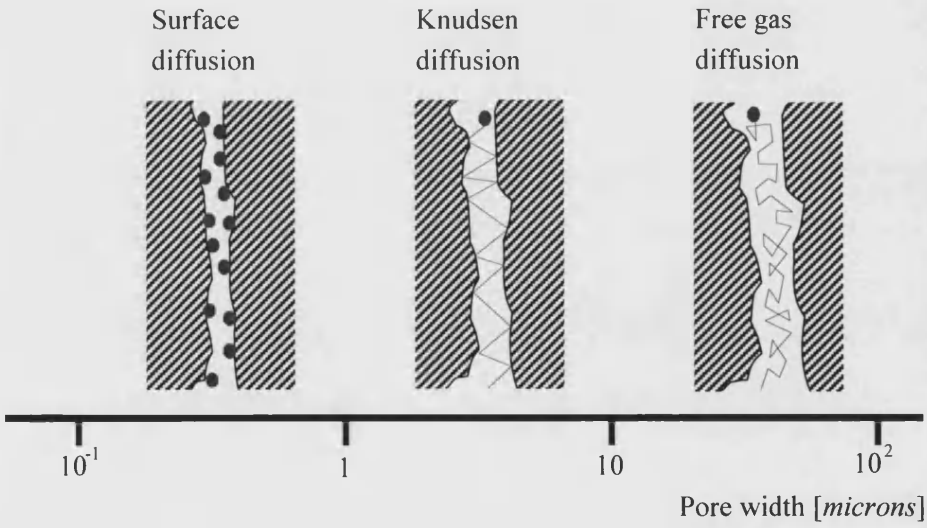

Figure 2.7 Dominating transport mechanisms as a function of the pore width. (Adapted from Richter *et al.*, 1978).

In catalytic reactions, the reactants in the bulk gas phase must diffuse through the macro-pores and micro-pores in the washcoat in order to reach the catalyst surface. At the active sites on the catalyst, the reactants react and form products. Similarly, the products must diffuse to the external surface before being transported to the surrounding bulk gas phase. During the procedure, if the rate of diffusion is slow compared to the intrinsic rate of reaction, the reaction becomes diffusion limited with effectiveness factors different from unity (Hayes & Kolaczkowski, 2000).

The washcoat on a ceramic support is so thin that the mass transfer limitations sometimes are ignored. However, Hayes and Kolaczkowski (2001) observed significant diffusion limitation in thin washcoat when examining the combustion of methane on a palladium catalyst in a monolith reactor. Groppi *et al.* (2001) investigated the effect of thin washcoat (no more than 60 μm) on mass transfer in an annular reactor. They found the effective factor decreased with the increase of washcoat thickness (see Figure 2.8). They tried to minimize the impact of diffusional processes via reactor design combined with appropriate coating techniques.

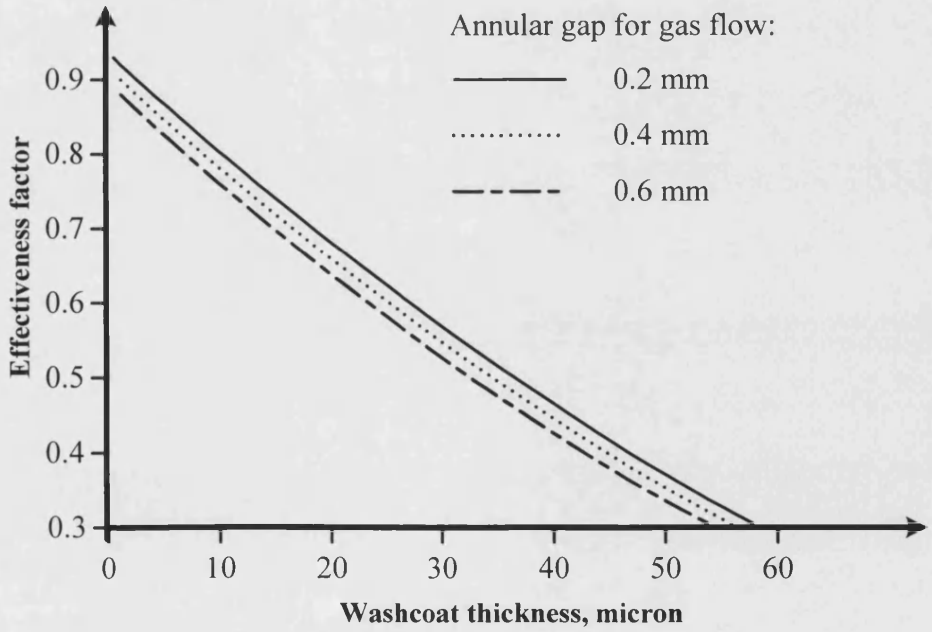

Figure 2.8 Effect of catalyst layer thickness and annular gap on the calculated global reactor effectiveness factor of the annular reactor.
(Adapted from Groppi *et al.*, 2001).

Massing *et al.* (2000) investigated the influence of propene and oxygen diffusion inside the catalytic layer of a three-way catalytic converter at steady state. They found that the concentrations of reactants significantly decrease along the thickness of washcoat. They simulated the species diffusion inside the catalytic layer. Their model demonstrated that diffusion limitations within the washcoat limited the conversion of propene. Mukadi and Hayes (2002) also developed a model for an automotive three-way catalytic converter making use of experimentally desired mechanistic kinetics. In their model, diffusion limitation in the washcoat was shown to be very significant even at relatively low operating temperatures.

Koberstein *et al.* (1991) investigated the effect of reaction temperature on the activation energy and mass transfer (see Figure 2.9) via the oxidation reaction of CO over a fresh three-way catalyst. The experimental conditions were as follows: monolith catalyst with 400 cpsi; partial pressure CO = 0.01 bar (g), partial pressure O_2 = 0.01 bar (g), balanced with N_2; Pt: 1.1 g/l, Rh: 0.2 g/l. They summarized the details as follows:

Below a gas temperature of about 470 K (Phase 0), the reaction rate is so small that almost no conversion is reached over the catalyst. From 470 K to 570 K (Phase 1), the extent of the conversion is governed by the rate of the chemical reaction, with apparent activation energy of about 100 kJ/mol. The catalyst light-off occurs in this temperature range. From 570 K to 770 K (Phase 2), the rate of the conversion is controlled by the rate of the intraparticle diffusion within the pores of the washcoat. The corresponding apparent activation energy is about 25 kJ/mol. Between 770 K and 1200 K (Phase 3), the catalyst is operated under interphase diffusion control, which is the rate of mass transfer between the gas phase and the washcoat boundary surface. Now the apparent activation energy is decreased to about 6 kJ/mol. Finally, above 1200 K (Phase 4), for some reactions a non-catalytic, homogeneous gas phase reaction occurs.

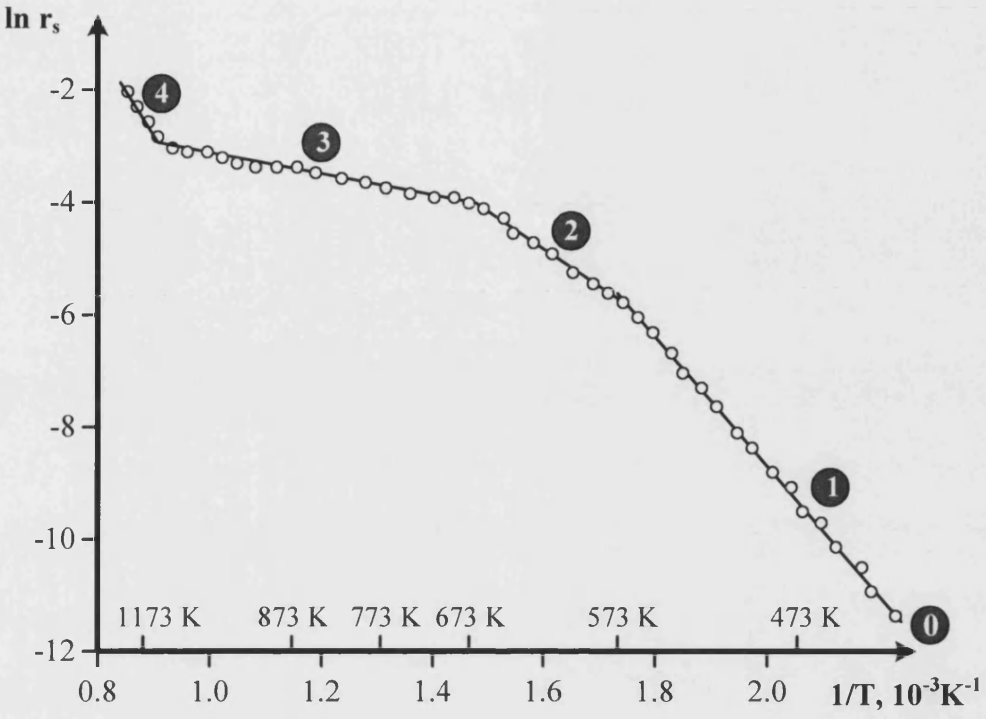

Figure 2.9 Arrhenius diagram for CO + O_2 → CO_2 recorded in a Berty reactor experiment with a fresh three-way catalyst.
(Adapted from Koberstein *et al.*, 1987).

Wijngaarden *et al.* (1998) summarized the possible profound effects that diffusion limitation may cause. Some of these are listed below:

1. The apparent activity of the catalyst is generally lowered.
2. The apparent order of the reaction may be changed.
3. The selectivity may be altered markedly.
4. The temperature gradient within catalyst may become large.

Kolaczkowski (1999) pointed out that failure to recognise the significance of diffusion limitations would in turn lead to:

- Much confusion about the magnitude of Sh and Nu numbers to be assigned in fully developed laminar flow;

- False conclusion being drawn about the activity of the catalyst;
- A reactor model without the incorporation of the diffusion limitations.

Transport limitation could be one of the main reasons to limit the conversion of pollutants in exhaust emissions.

2.5 Chemical reactions in catalytic converters

In a catalytic converter, the oxidation of carbon monoxide and hydrocarbons, and the concomitant reduction of oxides of nitrogen occur simultaneously. Since the composition of fuel is very complex (Hirao & Petfrey, 1988; Lox *et al.*, 1991), the chemical reactions occurring in catalytic converters may be represented by a series of reactions (Subramanlam & Varma, 1985; Taylor, 1993; Koltsakis and Stamatelos, 1997; Lox *et al.*, 1997; Holmgren, 1999), *e.g.*:

Oxidation reactions

$$CO + 0.5\ O_2 \rightarrow CO_2$$

$$H_2 + 0.5\ O_2 \rightarrow H_2O$$

$$C_xH_y + (x + 0.25y)\ O_2 \rightarrow x\ CO_2 + 0.5y\ H_2O$$

$$NO + 0.5\ O_2 \rightarrow NO_2 \text{ (undesired)}$$

$$SO_2 + 0.5\ O_2 \rightarrow SO_3 \text{ (undesired)}$$

Reduction reactions

$$NO + CO \rightarrow CO_2 + 0.5\ N_2$$

$$NO + H_2 \rightarrow H_2O + 0.5\ N_2$$

$$(2x + 0.5y)\ NO + C_xH_y \rightarrow x\ CO_2 + 0.5y\ H_2O + (x + 0.25y)\ N_2$$

$NO + 2.5\ CO + 1.5\ H_2O \rightarrow NH_3 + 2.5\ CO_2$ (undesired)

$NO + 2.5\ H_2 \rightarrow NH_3 + H_2O$ (undesired)

$2NO + CO \rightarrow N_2O + CO_2$ (undesired)

$2NO + H_2 \rightarrow H_2O + N_2O$ (undesired)

$SO_2 + 3\ H_2 \rightarrow H_2S + 2\ H_2O$ (undesired)

Steam reforming

$C_xH_y + x\ H_2O \rightarrow x\ CO + (x + 0.5y)\ H_2$

Water-gas shift

$CO + H_2O \rightarrow CO_2 + H_2$

CeO_2/Ce_2O_3 transfer in washcoat

$Ce_2O_3 + 0.5\ O_2 \rightarrow 2\ CeO_2$

$Ce_2O_3 + NO \rightarrow 2\ CeO_2 + 0.5\ N_2$

$Ce_2O_3 + H_2O \rightarrow 2\ CeO_2 + H_2$

$2\ CeO_2 + CO \rightarrow Ce_2O_3 + CO_2$

$2\ CeO_2 + H_2 \rightarrow Ce_2O_3 + H_2O$

Reactions based on catalysts, *e.g.* NO + CO on Rh:

$2\ Rh\text{-}O + 2\ CO \rightarrow 2\ Rh + 2\ CO_2$

$2\ Rh + NO \rightarrow Rh\text{-}N + Rh\text{-}O$

$2\ Rh\text{-}N \rightarrow 2\ Rh + N_2$

The reaction rates per unit volume of catalyst as well as their selectivity depend on both the specific catalytic activity and the surface area of the active component per unit

catalyst volume, as well as on the pore structure. These characteristics are determined by the conditions of catalyst preparation (Wijngaarden *et al.*, 1998). In order to improve the conversion of reactants and the selectivity of the reactions, as well as control reaction rates, it is very important to choose suitable materials to act as catalysts/washcoat. The selection of a suitable pore structure for the catalyst layer, and the arrangement of different layers in the washcoat are also important. Each of the layers may comprise different catalysts, washcoat materials and may have a different thickness (Hayes and Kolaczkowski, 2000; Mussmann *et al.*, 2001).

2.6 The challenges to catalytic converters

2.6.1 Deactivation of auto-catalysts

In a catalytic converter, the catalyst material has to operate in a difficult environment (*e.g.* steam and SO_2), and withstand high temperature (even more than 1000 °C); therefore, they may be subjected to various forms of deactivation. Gandhi and Shelef (1991) found even a small amount of sulphur (*e.g.* 300 ppm) in gasoline, which was equivalent to *ca.* 20 ppm SO_2 in exhaust, had multiple effects on the operation of automotive catalysts.

Angove *et al.* (1996) propose that the extent of automotive catalysts deactivation depends upon a number of factors, including contamination by residues of additives or trace elements (*e.g.*, lead and phosphorus) in fuel and/or engine oil, which generally reduce the surface area of the catalyst. Lox *et al.* (1997) summarised the physical and chemical processes including thermal deactivation occurring at different temperatures in catalytic converters (see Figure 2.10).

According to Thevenin *et al.* (2001) and Lox *et al.* (1997), the following three types of mechanism can cause the deactivation of catalyst supports, washcoats and active materials:

1. Mechanical mechanism: substrate disintegration, fouling;

2. Thermal mechanism: catalyst loss, washcoat phase transformation, active component migration, compound formation, thermal shock, hot spots, sintering;

3. Chemical mechanism: fuel poison adsorption, product adsorption, and oxidation state changes.

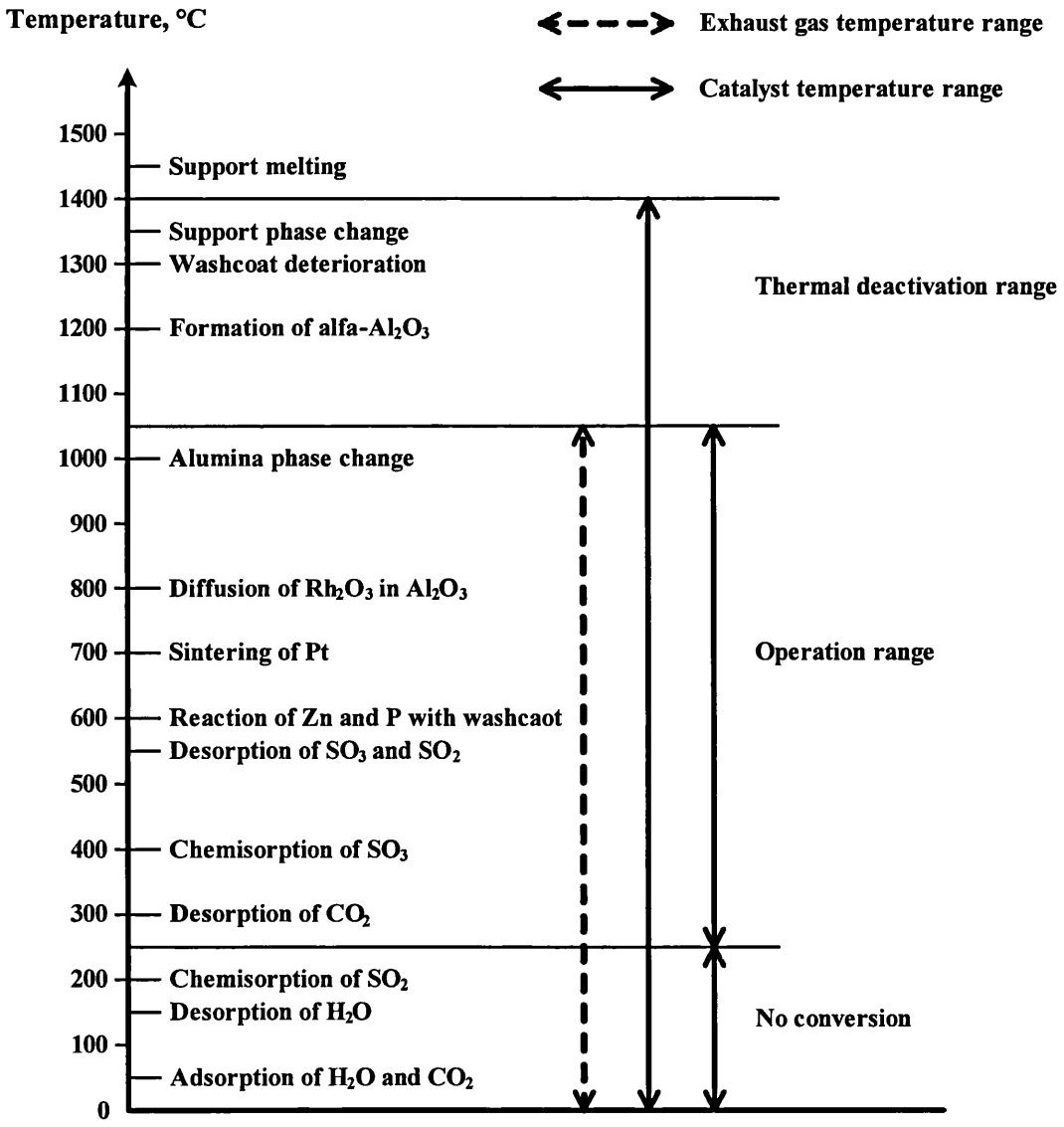

Figure 2.10 Schematic overview of some deactivation phenomena in three-way catalysts, as a function of catalyst temperature.
(Adapted from Lox *et al.*, 1997).

To minimize deactivation of automotive catalysts, further improvements are needed, especially with respect to the long-term stability and life of the catalyst. Maximizing the resistance to thermal ageing can increase the durability of the catalyst. González-Velasco *et al.* (2000) introduced a method of ageing that consisted of a treatment at 900 °C for 5 hours during which an oxidizing (2.5% O_2 plus 10% H_2O in N_2) and a reducing (5.0% CO plus 10% H_2O in N_2) feedstreams were cycled at 0.017 Hz through the catalyst.

In this thesis, the diffusion in normal commercial auto-catalysts as well as high-temperature-calcined auto-catalysts is evaluated, in order to investigate the effects of high-temperature calcination on the pores' structure and diffusion in the catalysts.

2.6.2 Cold start

Cold start period normally is within the first one to two minutes after the start of an engine at ambient temperature, where the catalyst temperature is too low for the catalytic reactions to take place (Hu *et al.*, 2001). As a result, significant amounts of unconverted pollutants pass through the catalyst.

The catalytic oxidation of CO is complex, as at low temperatures the reaction may be hindered by "self-poisoning". The CO sticks to the catalyst surface and blocks the active sites; consequently, oxygen dissociation can not take place and hardly any reaction occurs until the temperature has risen to a point where the CO starts to leave the catalyst surface. Therefore, it is very difficult to catalyze the reactions efficiently within the first 20 seconds when the catalyst temperature is lower than 200 °C (Baba *et al.*, 1996; Silveston, 1996; Holmgren, 1999; Drewsen *et al.*, 2000). This is so-called cold start problem. During the cold start period, emitted CO concentration could be up to 1% (volume ratio) or higher (Koltsakis & Stamatelos, 1997), and up to 50% to 80% of the total unburned hydrocarbons over the driving cycle are emitted (Jirat *et al.*, 2001).

Drewsen *et al.* (2000) studied the effects of the radial distribution of platinum in spherical alumina catalysts, using temperature ramp experiments with CO and air. They

showed that the homogeneous catalyst had an activity that started at a lower temperature, however, the "shell" distributed catalyst showed a fast CO "light-off" and reached total conversion earlier.

Keith *et al.* (2001) with the aid of a mathematical model proposed changes to the design of a catalytic converter. The key feature involved diverting a small portion of exhaust gas through a bypass stream, which contains an electric pre-heater and a pre-igniter, during start-up. The "light-off time" (which means the point when 50% of conversion is reached) could be decreased to 10 seconds. It is reported that the design can reduce pollution by almost 90% over current designs. Other attractive solutions to this problem include: placing the catalytic converter closer behind the engine (Holmgren, 1999); electrically heating the catalysts (Socha & Thomason, 1992); using the "lower-temperature" catalysts (Golunski *et al.*, 1995); using HC traps (Farrauto & Heck, 1999), *etc.*

In this thesis, methods to overcome the cold start problem are not considered; however, CO oxidation experiments are performed from very low temperatures, *e.g.* 50 °C, to examine the starting-reaction temperature for the selected auto-catalysts, and to estimate the temperature range in which the catalytic reactions start to be controlled by diffusion limitations.

2.6.3 Conversion efficiency

According to Duffy *et al.* (1998), the exhaust emission concentrations of benzene, toluene, total xylenes and 1,3-butadiene, even for some new catalytic converters, are up to 1.7, 28.1, 36.4, and 27.0 $mg \cdot km^{-1}$ respectively. There are at least two reasons to cause the high concentrations of aromatic compounds in vehicle exhaust emissions. One is that most automobile catalysts focus on the conversions of CO, hydrocarbons and NO_x rather than aromatic hydrocarbons; the other is that aromatic compounds are very stable. It is difficult to eliminate the aromatic compounds in the exhaust emissions using ordinary TWC or DOC catalysts.

However, even focusing on converting CO, HC and NOx, the catalyst efficiency cannot be up to 100% (see Figure 1.1). A new catalytic converter could only convert 95% of CO and HC, 90% of NOx and 70% of CH_4 (Amatayakul *et al.*, 2001). With the ageing of the converter, the efficiency will further decrease. In this case, if the sum of global vehicles always increases annually, the global vehicles exhaust emissions may also keep increasing.

To solve the problem, one method is to improve the conversions of pollutants as high as possible (100% conversions would be an ideal aim). Increasing reaction temperature is perhaps a method to improve the conversions; however, when catalytic converters work at high temperature, the diffusions of reactants and products may determine the over-all reaction rates, and so the conversions may not be improved.

To investigate how reaction rate and conversion of pollutants are affected by reaction temperatures, as well as their relation with diffusion, CO oxidation experiments over DOC catalysts are performed, and the results are discussed in this thesis.

2.7 Application of D_{eff} terms in models of catalytic converters

According to Wendland *et al.* (1991), the performance of auto-catalysts is affected by many factors, which include at least the following: support design, converter design, washcoat, precious metals, preparation, ageing, dynamic conditions, exhaust gas composition, space velocity, and reaction temperature. It is very complicated to evaluate the influence of these interdependent factors when testing the performances of catalysts.

Modelling the behaviour of catalytic converters is a good way to improve their performance, as well as to explore some of the challenges/problems without costing too much money or spending too long a time. Comparing the results with actual experimental work is an obvious advantage.

2.7.1 Main fields that catalytic converter models focus on

Over the past three decades, there has been considerable progress made with the development of models that can be applied to study the performance of catalytic converters. The models generally focus on understanding or solving a specific problem. For example:

- Sub-pollution of Pt particles (Rühle *et al.*, 1997);
- Catalyst distribution and deactivation (Psyllos & Philippopoulos, 1993; B0artholomew, 2001);
- Cold start (Kirchner & Eigenberger, 1996, 1997; Chan & Hoang, 1999);
- Air/fuel ratio control (Aimard *et al.*, 1996; Koltsakis *et al.*, 1997B; Huang, 2001);
- Mass/heat transfer and conversion (Young & Finlayson, 1976; Oh & Cavendish, 1982; Psyllos & Philippopoulos, 1992; Hayes & Kolaczkowski, 1994, 1999; Leung *et al.* 1996; Uberoi & Pereira, 1996; Jahn *et al.*, 1997; Koltsakis, 1997A; Dubien *et al.*, 1998; Holmgren & Andersson, 1998; Massing *et al.*, 2000; Gupta & Balakotaiah, 2001; Balakotaiah *et al.*, 2002; Mezedur *et al.*, 2002);
- Reaction mechanisms (Nibbelke *et al.*, 1997, 1998; Koltsakis & Stamatelos, 1999; Hoebink *et al.*, 2000; Imbihl, 2000; Keren & Sheintuch, 2000; Chatterjee *et al.*, 2001; Liu *et al.*, 2001).

From the literature, there is much work in the field of understanding mass/heat transfer and diffusion in catalytic converters, most probably because of the key role that this plays. In many of these models, "effective diffusivity" is an important factor, which represents the combined effects of bulk and Knudsen diffusion processes in a porous structure. The effective diffusivity was either calculated from suitable models, or measured experimentally.

2.7.2 Commonly quoted models for predicting effective diffusivities

As diffusion is important in catalysis, models for predicting effective diffusivities in porous catalysts feature in papers over the last 50 years. The three following models have been selected for discussion, as they represent models frequently quoted in the literature.

Parallel pore model

This type of model was developed by Wheeler's (1955), and it is assumed that the porous structure can be represented by a number of parallel capillaries that have the same size. Then, if there are "n" such capillary tubes with radius of "r" and length "L", in a unit mass of porous solid, the total surface area of the tubes is:

$$S_g = n \times 2 \times \pi \times r \times L = 2\,\pi\, n\, r\, L \tag{2.14}$$

and the total tube volume is:

$$V_g = n \times \pi \times r^2 \times L = n\,\pi\, r^2\, L \tag{2.15}$$

If "S_g" is equal to the internal surface area (usually measured in a BET apparatus), and "V_g" is equal to the pore volume of the solid, then the mean pore radius can be calculated from:

$$r_m = \frac{2V_g}{S_g} \tag{2.16}$$

The diffusion flux in a pore of mean radius (r_m), is give by (Haynes, 1982):

$$N_1 = -\left(\frac{1}{\frac{1-\beta y_1}{D_{12}} + \frac{1}{D_{K1}}} \right) \frac{dc_1}{dx} \tag{2.17}$$

where $\beta = 1 + \frac{N_2}{N_1}$ (N_2 and N_1 are diffusion flux of Components 2 and 1).

The effective diffusivity can be calculated from:

$$D_{eff} = \delta \frac{D_{12}}{\beta[(y_1)_{in} - (y_1)_{out}]} \ln \left[\frac{1 + \frac{D_{12}}{D_{K1}} - \beta(y_1)_{out}}{1 + \frac{D_{12}}{D_{K1}} - \beta(y_1)_{in}} \right] \tag{2.18}$$

where $\delta = \varepsilon_p^{\,2}$ (ε_P is the porosity of the solid).

Another typical parallel model is the cross-linked pore model, which can also be applied to a single pore of radius "r" in the solid (Johnson and Stewart, 1965). In this model, the diffusivities were interpreted as the actual values rather than effective diffusivities corrected for porosity and tortuosity.

Random pore model

Taking into account the actual pore size distribution, Wakao and Smith (1962, 1964) developed a random pore model (also called micro-macro pore model), for the estimation of effective diffusivity in specimens with a bidisperse pore structure. The model broke up the pellet pore size distribution into macro (M) and micro (μ) values for the pore volume and average pore radius: ε_M, γ_M and ε_μ, γ_μ. Often a pore size of approximately 10 nm is used as the dividing point (Froment & Bishchaff, 1990).

Based on random placement of the microparticles within the macropellet pores, a probabilistic argument for diffusion through the macro-regions, the micro-regions and series interconnection gives the indicated areas (see Figure 2.11). When adding up the various parallel contributions, the following equation can be obtained (Smith, 1981):

$$D_e = \varepsilon_M{}^2 D_M + (1-\varepsilon_M)^2 \frac{\varepsilon_\mu{}^2}{(1-\varepsilon_M)^2} D_\mu + 2[2\varepsilon_M(1-\varepsilon_M)]\frac{\varepsilon_\mu{}^2}{(1-\varepsilon_M)^2} D_\mu \qquad (2.19a)$$

$$= \varepsilon_M{}^2 D_M + \frac{\varepsilon_\mu{}^2 (1+3\varepsilon_M)}{1-\varepsilon_M} D_\mu \qquad (2.19b)$$

In the second and third terms of Equation 2.19a, the D_μ is based on the micro-void area, so the ratio of micro-void to particle area is required. In the last term of the equation, it is also assumed that in the macro-micro series part, the micro-diffusion is the dominant resistance (Froment & Bishchaff, 1990).

When $\varepsilon_M = 0$ or $\varepsilon_\mu = 0$, Equation 2.19b will become:

$$D_e = (\varepsilon_s{}^2 D)_{M \text{ or } \mu} \qquad (2.20)$$

which implies that $\tau = \frac{1}{\varepsilon_s}$, a reasonable approximation.

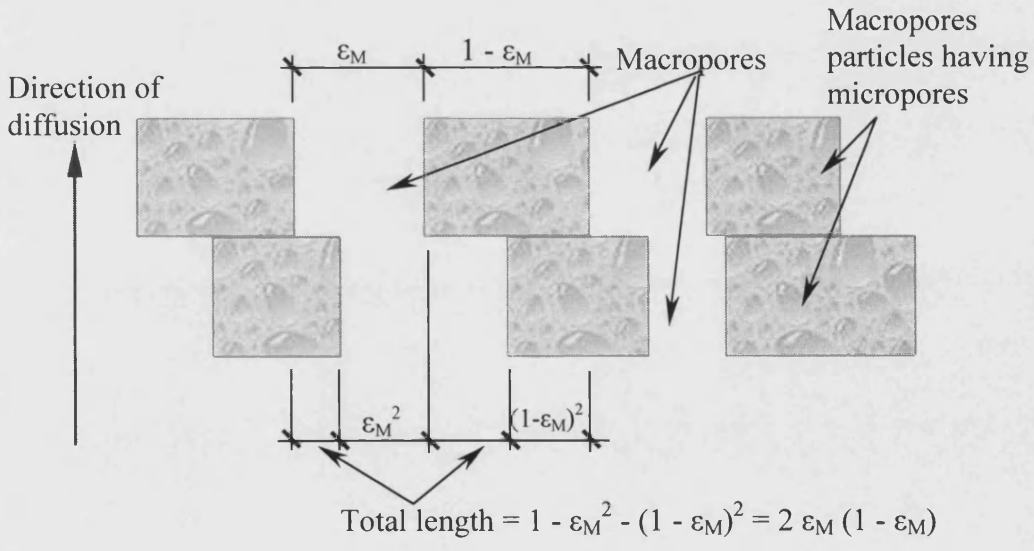

Figure 2.11 Random pore model of Wakao and Smith for a bidisperse porous solid.
(Adapted from Smith, 1981).

Dusty gas model

Evans *et al.* (1961) developed a "dusty gas" model, which is presented for the diffusion of gases in porous media in the absence of pressure gradients. In this model the porous medium is visualised as a collection of uniformly distributed "dust" particles that are constrained to be stationary. The dust particles are assumed as giant molecules; thus many of the usual results for diffusion in porous media could be simply derived from rigorous kinetic theory as special cases of multi-component mixtures.

To use the dusty gas model, it is necessary to know the volume fraction of solids or their particle size distribution. Since the physical properties of porous media are practically determined by the analysis of pore volume (through the use of capillary-surface tension, *etc*) (Kim, 2001), and there is no unique relationship between the distribution of pore sizes and the distribution of particle size (Scheidegger, 1957), the application of dusty gas model is limited and not commonly used to simulate catalytic converters.

2.7.3 Determination of the value of effective diffusivity

As pointed out by Kolaczkowski (1999), models are "only as good as the way in which the physicochemical processes are modelled and the quality of the physical and chemical parameters (*e.g.* kinetic expressions, physical properties) acquired for use in the models". Modelling of catalytic converters remains a very difficult challenge due to the following reasons (Kolaczkowski, 1999):

- The selection of appropriate kinetic expressions is difficult because of the complex competing reactions that are strongly affected by heat and mass transfer.
- The selection of heat and mass transfer correlations may be different.
- The role that intraphase diffusion may play has not been completely recognized.

- Some important factors when developing models are uncertain, *e.g.*, effective diffusivity coefficient and tortuosity factor.

Many models assume that there is no diffusion limitation in washcoat, or assume that pore diffusion effect on monolith reactors can be neglected (*e.g.* Roland & James, 1976; Ahn *et al.*, 1986; Schweich & Leclerc, 1991; Ryan *et al.*, 1991; Siemund *et al.*, 1996; Őzkan & Doğu, 1997). However, a number of authors have considered the effects of pore diffusion in the washcoat. For example:

(a) Tronconi and Groppi (2000): They evaluated the value of CO in air at temperature "T" according to

$$D_{CO} = D_{CO}{}^{0}\left(\frac{T}{T_0}\right)^{1.75} \tag{2.21}$$

Here $D_{CO}{}^{0}$ is the bulk gas diffusivity of CO in air at T_0 = 373 K, whose value is 0.32 cm^2/s quoted from Reid *et al.* (1987).

(b) Drewsen *et al.* (2000): The effective diffusion coefficient of CO in the catalyst was calculated from Knudsen diffusion coefficient in the catalyst pores and the gas bulk diffusion coefficient:

$$\frac{1}{D_{eff}} = \frac{1}{D_K} + \frac{1}{D_{bulk}} \tag{2.22}$$

The D_K was calculated from the average pore size as describe by Satterfield (1980), and D_{bulk} was calculated according to Fuller *et al.* (1966). In another model, the value of D_{eff} was calculated according to a formula in Aris (1975).

(c) Wanker *et al.* (2000): They considered that reaction rates might be affected by the effect of pore diffusion in the washcoat as well as by mass transfer in the gas phase. In their model they calculated the value of D_{eff} based on the method described in Hayes and Kolaczkowski (1994).

(d) Koci *et al.* (2004): They used approximated D_{eff} values in their model. They described: "in our approximation diffusivities of all gas components are assumed to be the same because the molar weights of individual gas components are similar." They assumed Knudsen diffusion to be dominant and used the following equation to calculate the effective diffusivities:

$$D_{eff}(T) = D_{eff,ref}\sqrt{\frac{T}{T_{ref}}}\sqrt{\frac{M_{ref}}{M}} \tag{2.23}$$

Here T_{ref} is a reference temperature, M_{ref} is molar weight of the reference component, $D_{eff,\,ref}$ is known value of effective diffusion coefficient of the reference component at the reference temperature.

From the literature, there are many methods that could be chosen to calculate the value of effective diffusivity, provided the size and the distribution of pores are known. Also their respective pore volume, as well as the value of tortuosity needs to be known. However, it is important to realize that calculated values of effective diffusivity may differ depending on the selected model. Hayes & Kolaczkowski (2000) made a comparison of the random pore model developed by Wakao and Smith, and the parallel pore model by Wheeler. They found significant differences in the calculated value of effective diffusivity for a gamma alumina monolith washcoat. The values calculated using the random pore model were found to be 3 and 7 times larger than experimentally measured values for the cordierite and wachcoat respectively. They drew a conclusion that "the random model is not appropriate for predicting the effective diffusivity in this alumina washcoat". However, they found that the values calculated from the parallel pore model did match the experimental results well. This work led to the development of a simple methodology to the selection of a suitable method of representing the effective diffusivity terms. By performing a measurement of effective diffusivity in a sample of washcoat monolith, then the choice of model can be verified, and if necessary an appropriate value of tortuosity can be back-calculated (Hayes & Kolaczkowski, 2000).

Baiker *et al.* (1982) also thought that the theoretical prediction of effective diffusivity of gases in porous catalysts was still not adequately resolved and in many cases was not accurate. Part of the reason for this is that the diffusion flux may include contribution from several mechanisms, including bulk, Knudsen and surface diffusion and in addition satisfactory geometric models for the pore structure were not at that time available.

Since effective diffusivity is "the fundamental quantity that forms the basis for calculations of diffusion and reaction in porous catalysts" (Haynes, 1988), accurate values of effective diffusivity are necessary in a rigorous model that accounts for transport of reactants and products in catalyst/washcoat layer. Data for effective diffusivity of gases are still more accurately derived from experimental measurements.

2.8 Methods to measure D_{eff} experimentally

The first significant measurements of diffusion in gases were made by Thomas Graham, starting in 1829 (Marrero & Mason, 1972). Since then, hundreds of experimental measurements have been performed. A comprehensive review of measurement methods and results has been provided in Marrero & Mason (1972) and Haynes (1988).

The effective diffusivity of a component A inside a porous catalyst is generally measured by a physical method, either a steady-state method or a transient (unsteady-state) method.

2.8.1 Transient (unsteady-state) methods

Transient methods could be categorized into three main groups (Haynes, 1988).

Time-lag method

For the case of a non-adsorbing gas A, in a porous cylindrical pellet of length L and porosity ε, according to Fick's second law, the material balance in the pellet is:

$$\varepsilon \frac{\partial C}{\partial t} = D_{eff} \frac{\partial^2 C}{\partial z^2} \tag{2.24a}$$

If one side of the pellet is maintained in an evacuated state, and the other side is held at constant pressure, then the appropriate boundary conditions are as follows:

$$C(0, t) = C_0 \tag{2.24b}$$

$$C(L, t) = 0 \tag{2.24c}$$

$$C(z, 0) = 0 \tag{2.24d}$$

The total quantity, Q, which has entered the low pressure chamber after a period of time, t, can be obtained from (Haynes, 1988):

$$Q = \frac{D_{eff} C_0}{L} \left(t - \frac{L^2}{6 D_{eff}}\right) \tag{2.24e}$$

Then the diffusivity D_{eff} can be calculated from:

$$D_{eff} = \frac{L^2 \varepsilon}{6 \tau_{lag}} \tag{2.24f}$$

where τ_{lag} is the time lag which can be observed in a plot of cumulative flow *versus* time (Haynes, 1988; Park & Do, 1996). When applying this method, the sample needs to be formed into the shape of a cylindrical pellet. Since the structure of auto-catalysts is monolith rather than pellet, time-lag method is not suitable for auto-catalysts.

Sorption rate method

Sorption rate method involves an experimental determination of the rate of adsorption or desorption of a pure compound or a component of a mixture (Haynes, 1988). Generally, this technique may be categorized according to whether the measurement is made at constant volume or constant pressure. In constant-volume experiments, samples can be equilibrated with a single-component gas in a vessel of finite volume. At time zero, a step change in pressure is introduced into the system, and the pressure response is recorded as a function of time. From a knowledge of the pressure *versus* time curve, the sorption rate can be calculated. In constant-pressure experiments, a single-component gas is introduced into a large vessel containing the sample, and the amount adsorbed is determined gravimetrically. The sorption uptake can be measured volumetrically by means of gas burette arrangements (Haynes, 1988).

Sorption rate method is particularly suitable for measurements of effective diffusivity in powders and granular materials. Since the structure of auto-catalysts is monolith rather than powder or granular, sorption rate method is not suitable for auto-catalysts

Gas chromatography (GC) method

With the development of chromatographic technique, GC was used to measure the effective diffusivity coefficient in heterogeneous catalysis under inert conditions even under reaction conditions.

In this method, a carrier gas (usually helium as it is non-adsorbed gas) is passed continuously through the column packed with catalyst. A pulse of diffusing component is injected into the inlet stream. The effluent pulse in the outlet stream is measured by a detector and a recorder (Figure 2.12). The advantages, disadvantages and limitations of GC method are listed in Table 2.4.

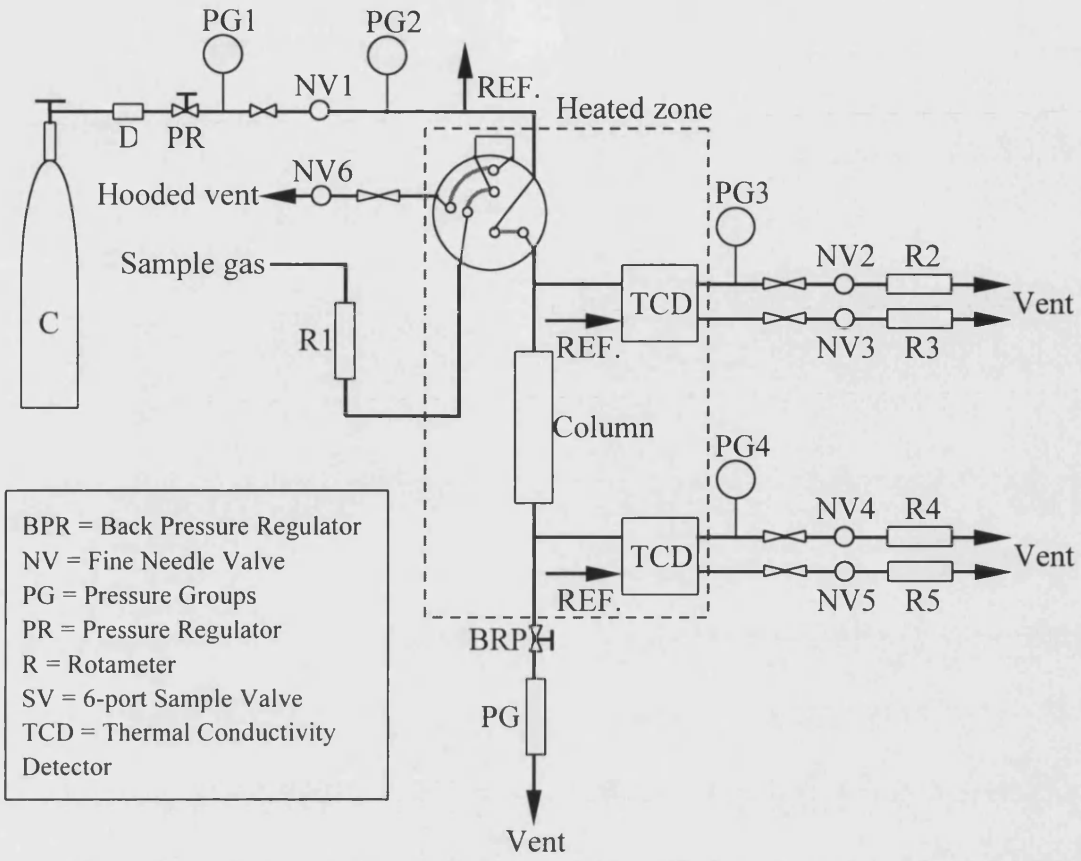

Figure 2.12 Gas chromatography diffusivity apparatus.
(Adapted from HSU & Haynes, 1981).

Table 2.4 Comparison of the advantages, disadvantages and limitations of GC method.
(Apted from Biswas *et al.*, 1987; García-Ochoa & Santos, 1994; Park & Do, 1996).

Advantages	Disadvantages	Limitations
Simple to carry out Conveniently used over wide range of temperatures and pressures Multiple pellets employed Can be used with commercial catalyst particles. Can be used even under reaction conditions.	The response used to measure D_a and D_i is a function of many factors, *e.g.*, residence time, the amount of solids in the reservoir, the external mass transfer resistance, and the non-uniformity of velocity in the case of the chromatography column. More complicated mathematical model (including axial dispersion, gas-to-solid mass transfer, possible intra-particle viscous flow) Contribution of axial dispersion to overall performance is large, which leads to inaccurate diffusivity.	Low bed porosity (~ 0.4) limits the carrier gas velocity (difficult to eliminate the flow pattern effects)

The unsteady-state methods are suitable for pellets or powders, but nor suitable for actual commercial auto-catalysts due to the following reasons (Kim, 2001; Kolaczkowski, 2002, 2003):

1. The ratio of the volume of washcoat per total monolith volume is relatively small. This leads to the problem of having a relatively small volume of porous structure to accommodate the tracer, and enable a discernable response to be detected.
2. The distribution of washcoat is not uniform, and may also vary in the axial direction. This adds a complication to the way in which the results would need to be interpreted.
3. The measured samples are so thin (no more than 300 microns) that the time delay for diffusion is insufficient to discriminate from the other time delays in the system.

2.8.2 Steady-state methods

Many of the steady-state methods described in the literature are developed or modified forms of the W-K diffusion cell (Wicke and Kallenbach, 1941), in which a sample of the catalyst is positioned between two chambers. The carrier gas flows through one of the chambers, while carrier gas and component A gas flows through the other. The pressures in the two chambers should be maintained equal, so that only the concentration difference between the two chambers (no pressure difference) provides the driving force to create a flux across the plate. As component A diffuses through the catalyst plate into the carrier gas, then simultaneously, the same number of moles of carrier gas diffuse in the other direction (see Figure 2.13). After a time, a steady state is reached in which the concentration remains constants at all points in the sample.

When interpreting the results, a number of assumptions are made (Biswas *et al.*, 1987):

1. The component and its compaction in the measured sample are uniform.
2. Pore diffusion occurs in both macropores and micropores.

3. Macropore and micropore diffusivities are independent of time and radial position.
4. Both upper and lower chambers are well mixed.
5. There is no viscous flow through the diffusion cell.
6. Adsorption isotherm is linear.
7. Adsorption in the macropore is negligible at these temperatures because of the low macropore surface area.
8. Temperatures are high enough so that surface diffusion is negligible and gas-solid adsorption rates are very fast.
9. Negligible heat release occurs during adsorption.
10. System remains at constant temperature through the process.

This method is amenable to operation over wide temperature and pressure ranges (Marrero & Mason, 1972). The main drawbacks of the steady-state method is that the diffusion in the dead end pores is not accounted for, and the measured effective diffusivity values in nonisotropic or bidispersed solids may be misleading.

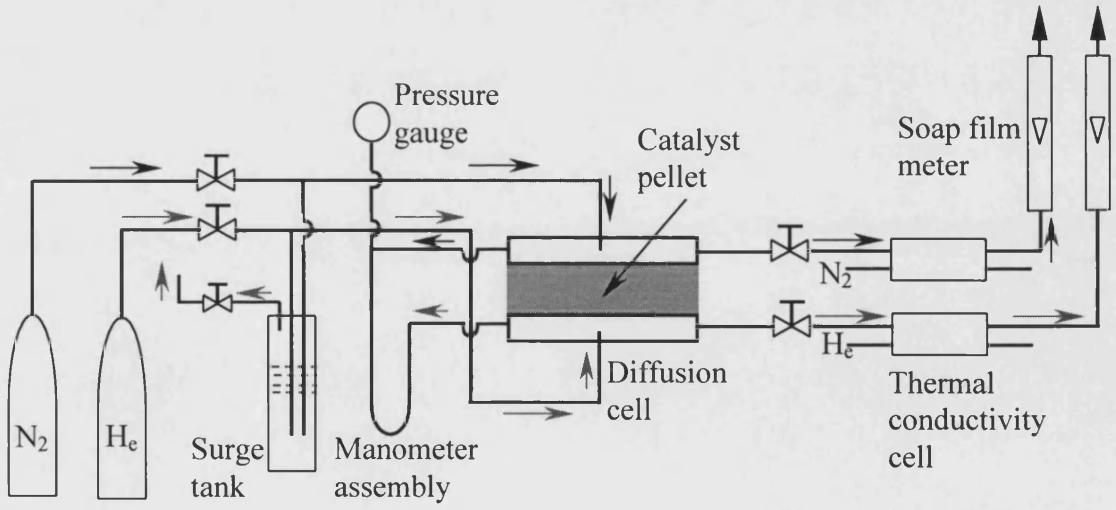

Figure 2.13 Wicke-Kallenbach diffusion apparatus.
(Adapted from Haynes, 1988).

2.8.3 Methods suitable for washcoated monolith samples

Many of the methods described were developed for pellets, so they may not be suitable for measurements on a catalyst-coated monolith. Although it is possible to cast a washcoat slurry into the shape of a pellet, or press crushed samples of material into the shape of a pellet; however, the morphological form of the pellet may not be representative of the way in which the thin layer is formed in a monolith (Kolaczkowski 2002, 2003). Pellets normally are formed under a pressure of around 1000 kg/cm^2 (Li, 1988). Compared with the actual materials (powder), the morphological form of the pressurized pellet will change as follows (Li, 1988):

- The bulk density will increase
- The porosity will decrease
- The BET surface may not vary very much.
- Both macropores and micropores (including mesopores) distribution will change.

Since high pressure will change the pore structure of the porous materials, it is difficult to ensure the measured effective diffusivity value through the pellet will be the same as that through the actual material (powder or other forms) of the pellet. So it is important to develop a technique that makes use of actual materials without modifying their pore structure. This is not an easy task as the actual washcoated monolith has a very thin layer of washcoat (no more than 300 microns), small mass of catalyst/washcoat per unit volume of monolith, and a high open free area for gas flow in the channels.

A recent review of suitable methods for monoliths was provided by Kolaczkowski (2003). The following techniques were considered in more detail and a method was then selected for this thesis.

Measurement of D_{eff} using a zirconia oxygen sensor

Mezedur *et al.* (2002) introduced a technique to measure the effective mass diffusivities of oxygen in nitrogen through a highly porous layer with different pore-size distributions at different pore length scales. They determined the oxygen concentration using a zirconia oxygen sensor mounted in the sample. The disadvantage of this technique is that the support needs to be carefully constructed and then coated with washcoat slurry, so it is not suitable for actual auto-catalysts.

Measurement of flux through the wall of a single monolith channel

Beeckman (1991) described an experimental technique to measure the effective diffusion coefficient of nitrogen monoxide through the porous walls of a monolith-type ceramic catalyst. Advantage was taken of the relatively large diameter of the channels (6 mm width and square shaped and the geometric shape of the monolith) to measure the steady-state diffusion of nitrogen monoxide through the wall of the monolith, and hence to determine the effective diffusivity (see Figure 2.14).

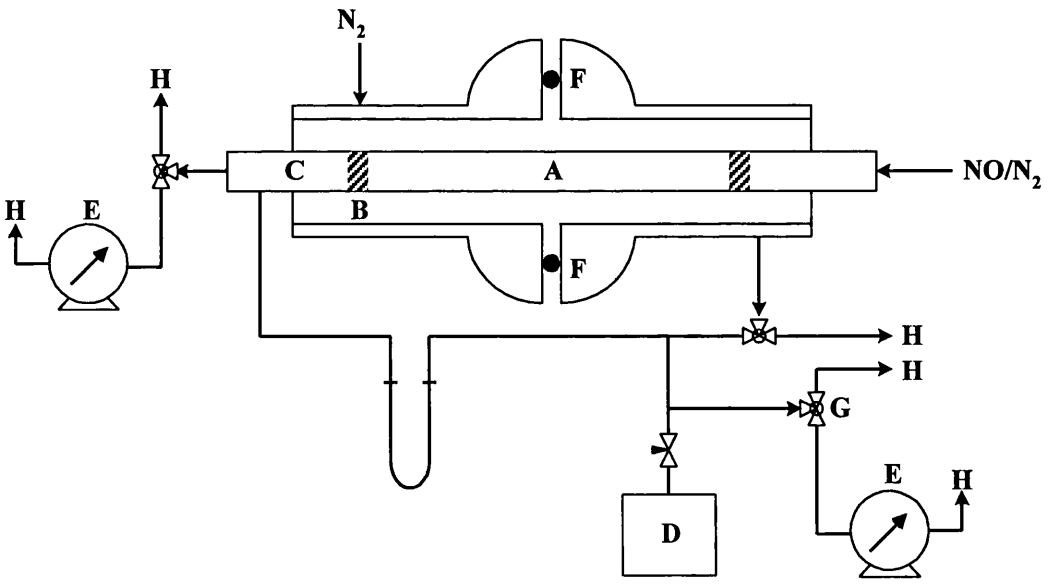

A: catalyst channel B: epoxy glue C: 1/4 inch steel tubing D: NO analyser
E: gasmeter F: O-ring closure G: 3-way valve H: vent

Figure 2.14 Experimental set-up of the single channel diffusion cell.
(Adapted from Beekman, 1991).

An obvious advantage of this method is that the measurements can be done on a real sample of monolith without making any changes to the structure. However, this method is not easy to apply to commercial auto-catalysts because the channel diameter is normally only 1 mm. This makes it very difficult to fix and seal a single channel.

Although it is possible to find a stainless steel tube whose outer diameter is less than 1 mm, the following problems would remain:

- How to cut and isolate a single channel a 1 mm × 1 mm cell, that was 10 to 50 mm long?
- How to ensure the isolated single channel had a flat outer surface (which means that extraneous cordierite wall material and washcoat on the outside surface of the channel was removed completely)?
- How to avoid damaging the fragile cordierite channel as it was sealed in the diffusion cell?
- Experimental errors could be high in such a small and delicate sample of monolith.

Measurement of flux from the centre channel to its surrounding neighbours

In order to perform measurements on a 2.36 mm channel, Li (1997) extended Beekman's technique by employing 7 channels (consisting of a central channel surrounding by six "side" channels) instead of only one. The effective diffusion coefficient of methane in nitrogen was studied in the composite structure shown in Figure 2.15. The channel had a hexagonal shape, and the wall was a composite structure consisting of 3 layers: a washcoat, then the cordierite wall, and then another washcoat. By performing experiments on an uncoated monolith, and then a coated structure, the effective diffusivity in the individual layers was calculated. When the results of the experiments were analysed, it was assumed there is no effect from the interface between the washcoat and the support structure. As discussed in Hayes & Kolaczkowski (2000)

and Kolaczkowski (2003), this assumption could be tested by performing experiments on samples prepared with differing thickness of washcoat.

Although this technique produced some interesting results on a real sample of monoliths, unfortunately for the same reasons discussed at the end of Beekman's method, this technique is still not suitable for auto-catalysts that have 1 mm cells.

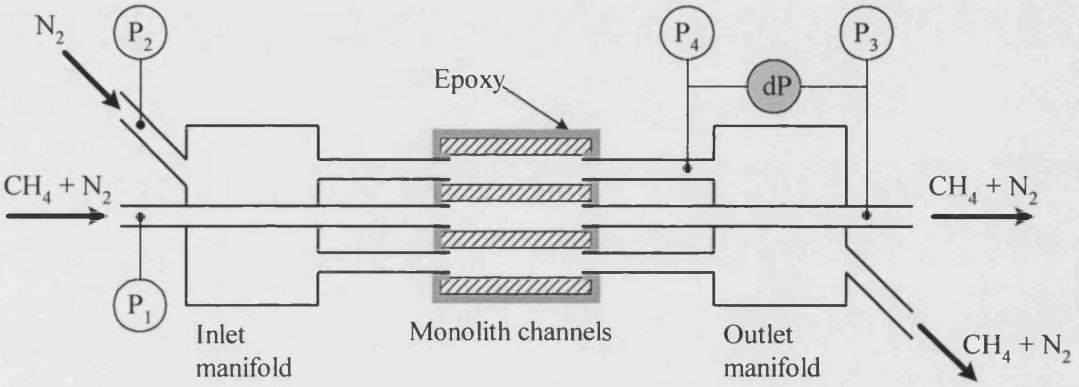

Figure 2.15 Schematic of the flow cell and manifolds connecting the monolith with the inlet tubes.
(Adapted from Li, 1997).

Using electroplated specimens for diffusion measurement

Kim (2001) applied and developed a different sample sealing technique from Beeckman (1991) or Li (1997), and measured the effective diffusivity of gasoline compounds through samples of single-plate cordierite both with/without washcoat (see Figure 2.16).

To seal the sample, a metal layer was electroplated around the sample, using an idea described by Yang and Liu (1982). One of the most important advantages of this technique is that experimental measurements can be performed at temperatures as high as 600 K (327 °C), without encountering any problems with gas leakage.

Although the measured values of effective diffusivity were repeatable, there are a number of limitations:

1. The method is only suitable for a sample that consists of a single layer on a flat plate.
2. It is only suitable for specimens, which have a smooth and compact surface. So specimens cut directly from a commercial auto-catalyst could not be easily used.
3. The method of sample preparation is difficult and may cause experimental errors. For example, before electroplating a specimen, a small piece of paper is glued onto the surface of the specimen. This paper and associated glue needs to be removed before the sample is used in the diffusion cell. Traces of glue could penetrate the pores of the sample and affect the results.
4. During the electroplating process, some of the metal ions may penetrate the pores of the sample and in turn affect the results.

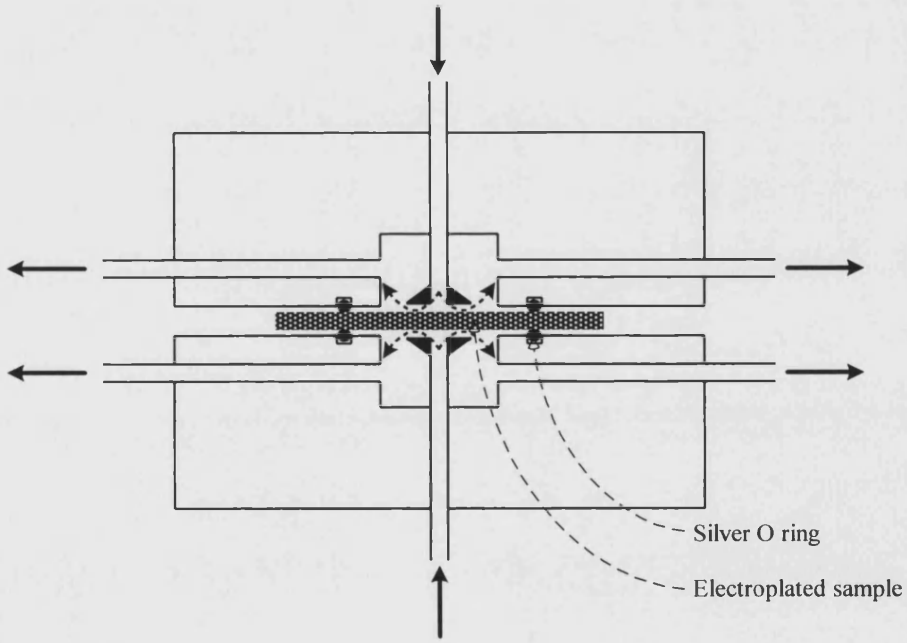

Figure 2.16 Schematic of diffusion cell which can be used at high temperature. (Adapted from Kim, 2001).

2.8.4 Decision taken on the design of diffusion cell

For the work in this thesis, a decision was taken to use a modified Wicke-Kallenbach diffusion cell to measure the effective diffusivity of CO in nitrogen through samples representative of auto-catalysts. This method combines the advantages of the techniques developed by Beekman (1991), Li (1997) and Kim (2001).

The key advantages of the method developed may be summarized as follows.

1. Actual samples of a commercial auto-catalyst may be used.
2. It is relatively easy to prepare the specimens.
3. No wax or glue needs to be coated onto the surface of the sample.
4. There are no limitations as to the width of the channels in the monolith.
5. Measurements can be made on a single layer or a multi-layer structure.

In the method used in this thesis, first a flat and thin wafer of cordierite is cut from a monolith structure. Then the wafer is grinded and coated with a thin layer of catalyst/washcoat. Next the sample is calcined and conditioned at conditions representative of a commercial unit. Finally the coated wafer is sealed with a Viton "O" ring in a modified form of Wicke-Kallenbach diffusion cell, and experiments are performed.

In designing the diffusion cell, the following factors were considered:

- How to avoid any leakage (from one chamber to another, or from chambers to the surroundings)?
- How to make sure that the diffusion cell is suited for both single-layer and multi-layer commercial auto-catalyst specimens that are very fragile?
- How to ensure that the gases fed into the cell do not create a direct impact on the surface of the sample?
- How to ensure that the gases mix well in each chamber?

In Figure 2.17, two possible methods of feeding a gas into a diffusion cell are shown. Based on a review of the literature, methods vary and these are summarised into Table 2.5.

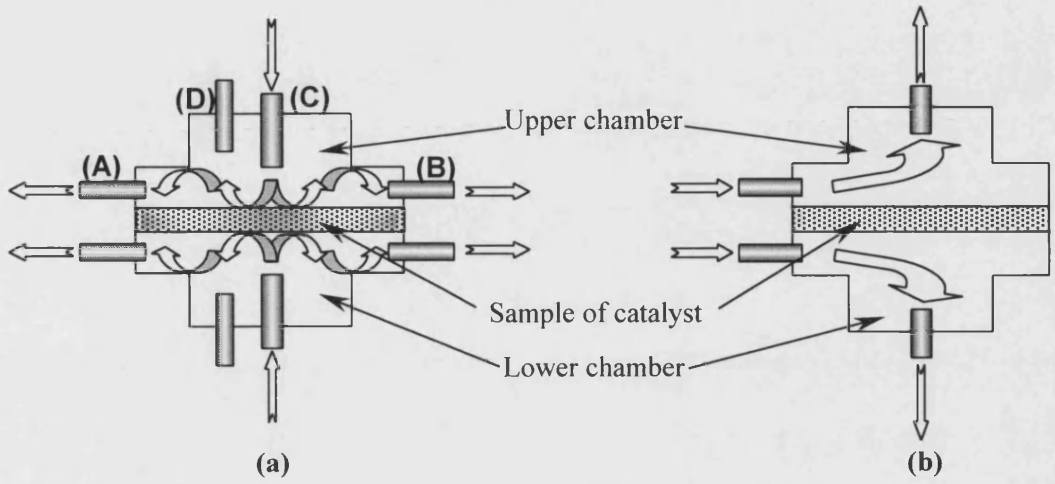

Figure 2.17 Schematic illustrating possible positioning of gas inlet and outlet ports in a diffusion cell.
(a) Gas inlet onto the face of the sample; (b) Gas inlet from the side of the chamber.

Table 2.5 Review of connection methods in the literature.
(The labels (A) to (D) refer to the labels on Figure 2.17 (a)).

Inlet connection point	Outlet connection point	Temperature test point	Pressure test point	Reference
(C)	(D)	(A)	(B)	Kim & Smith, 1974; Duduković, 1982
(C)	(A)	(D)	(B)	Robertson & Smith, 1963 Gunn & King, 1969; Doğu & Smith, 1975; Doğu, *et al.*, 1987; Kim, 2000
(A)	(B)	(C)	(D)	Wang & Smith, 1983
(A) & (B)	(C)	Other point	(D)	Al-rqobah, *et al.*, 1988

After careful consideration, it was decided to position the ports as shown in Figure 2.18. Each chamber had 5 ports in total. These consist of: 2 inlet ports, 1 outlet port, 1 temperature port and 1 pressure port. Four of the five ports had connections that could be easily and quickly changed. Gas was admitted into the upper and lower chambers from two ports located on opposite sides of the chamber, through nozzles positioned in a tangential direction (at 45° from the centre) to avoid direct jet impact on the face of the sample and to create good mixing in the chambers.

2.8.5 Decision taken on concentration of CO for the diffusion experiments

As the concentration at the inlet to the diesel oxidation catalyst can vary from 100 to 2000 ppm (volume) (see Table 1.2), the decision was taken to use a 2.4% (volume) of CO in nitrogen as the feed stream into the diffusion cell. At these conditions, the concentration of the gas in the catalyst layer would be at an appropriate of magnitude (10^2 to 10^3 ppm) and the concentration of CO in the exit stream to the gas analyser should be within the range of the instrument. The CO analyser in the laboratory had a range of 0 to 1300 ppm, and preliminary experiments would need to be undertaken to confirm that this would be adequate.

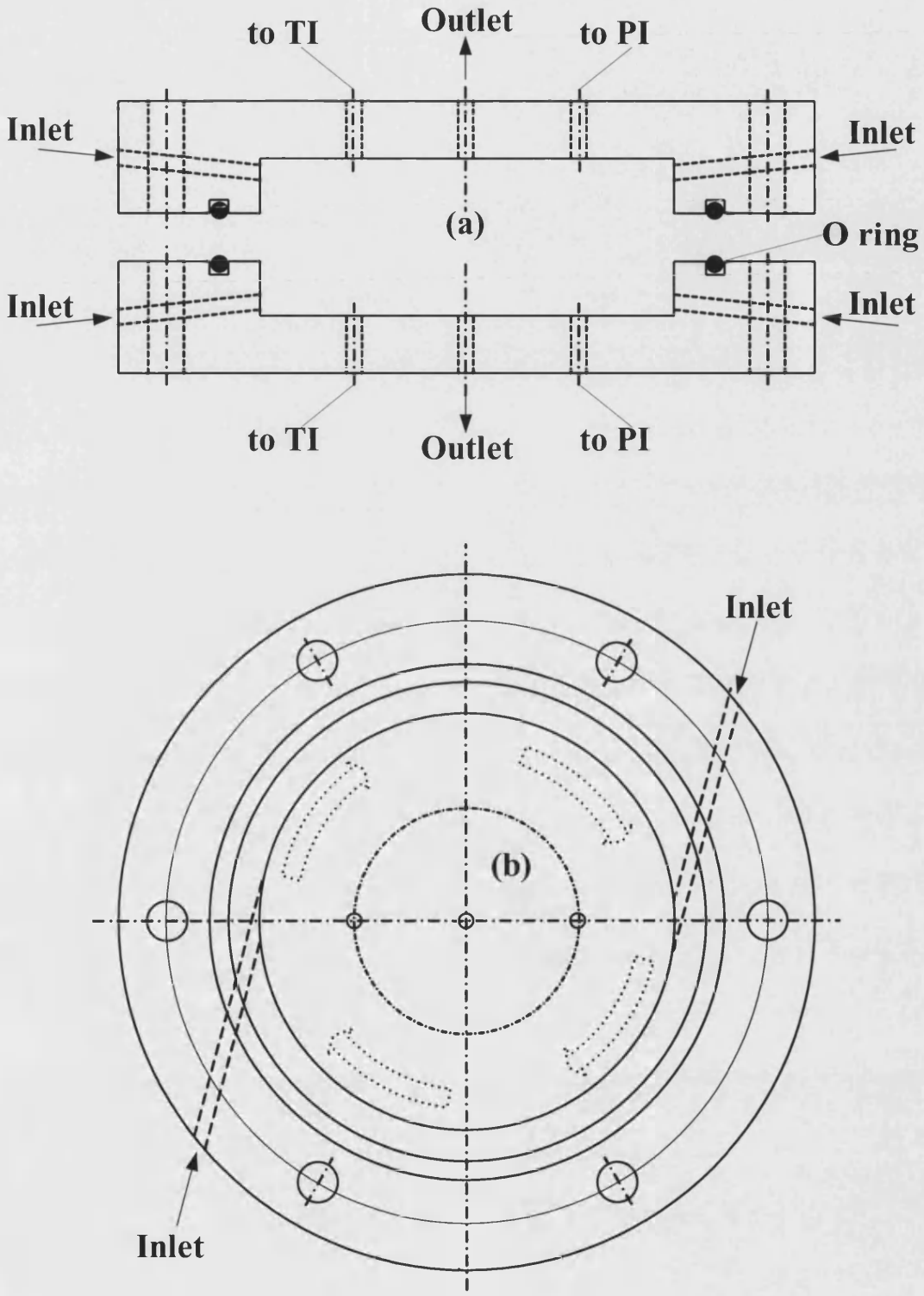

Figure 2.18 Diagram of the diffusion cell
(a) Side view of the upper chamber and the lower chamber;
(b) Plan view of the lower chamber.

2.9 Interim conclusions

1. Based on the review of the literature, it is evident that when simulating the performance of catalytic converters, intra-phase diffusion must not be ignored. If possible, the effective diffusivity should be measured in a real sample of auto-catalyst. This can then enable a tortuosity factor to be calculated, which can then be used in a model of a catalytic converter.

2. As the thickness of the layer through which diffusion is measured is very thin, a transient technique would be difficult to interpret, so a steady-state method is chosen for the measurement of effective diffusivities.

3. The decision was taken to design a modified form of Wicke-Kallenbach cell, which would enable experiments to be performed on either samples of actual cordierite coated with catalyst, or samples of auto-catalyst cut from a commercial catalyst.

4. A 2.4% (volume) CO in nitrogen mixture was selected as the concentration of the inlet gas stream into the diffusion cell.

2.10 Introduction to chapters that follow

To illustrate the connections between the various activities described in this thesis, a flowchart is provided in Figure 2.19 (a, b and c). This also shows the link between a particular experiment, a decision, and conclusions that was formed in the thesis.

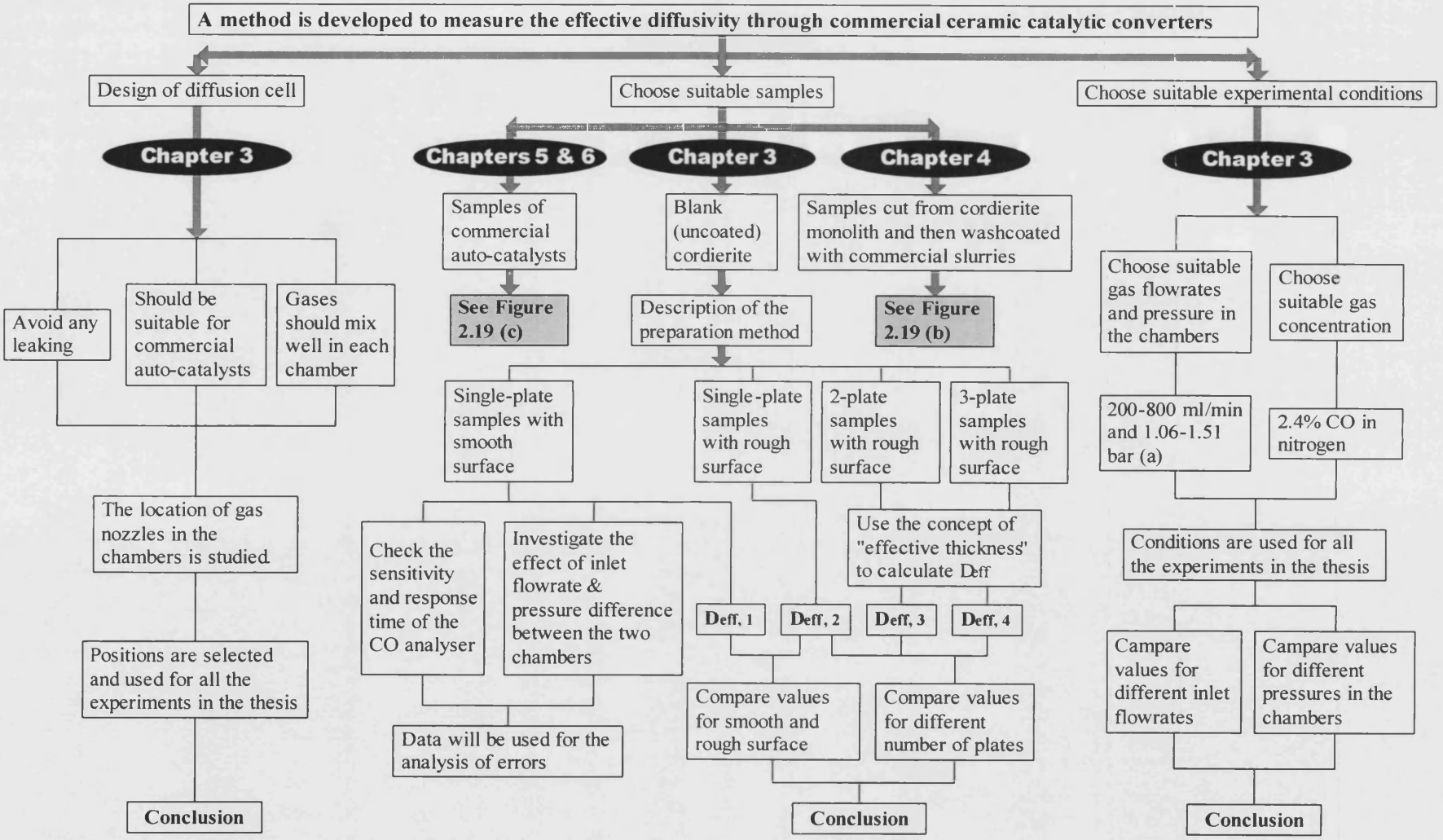

Figure 2.19 (a) Schematic illustrating the link between activities in the thesis

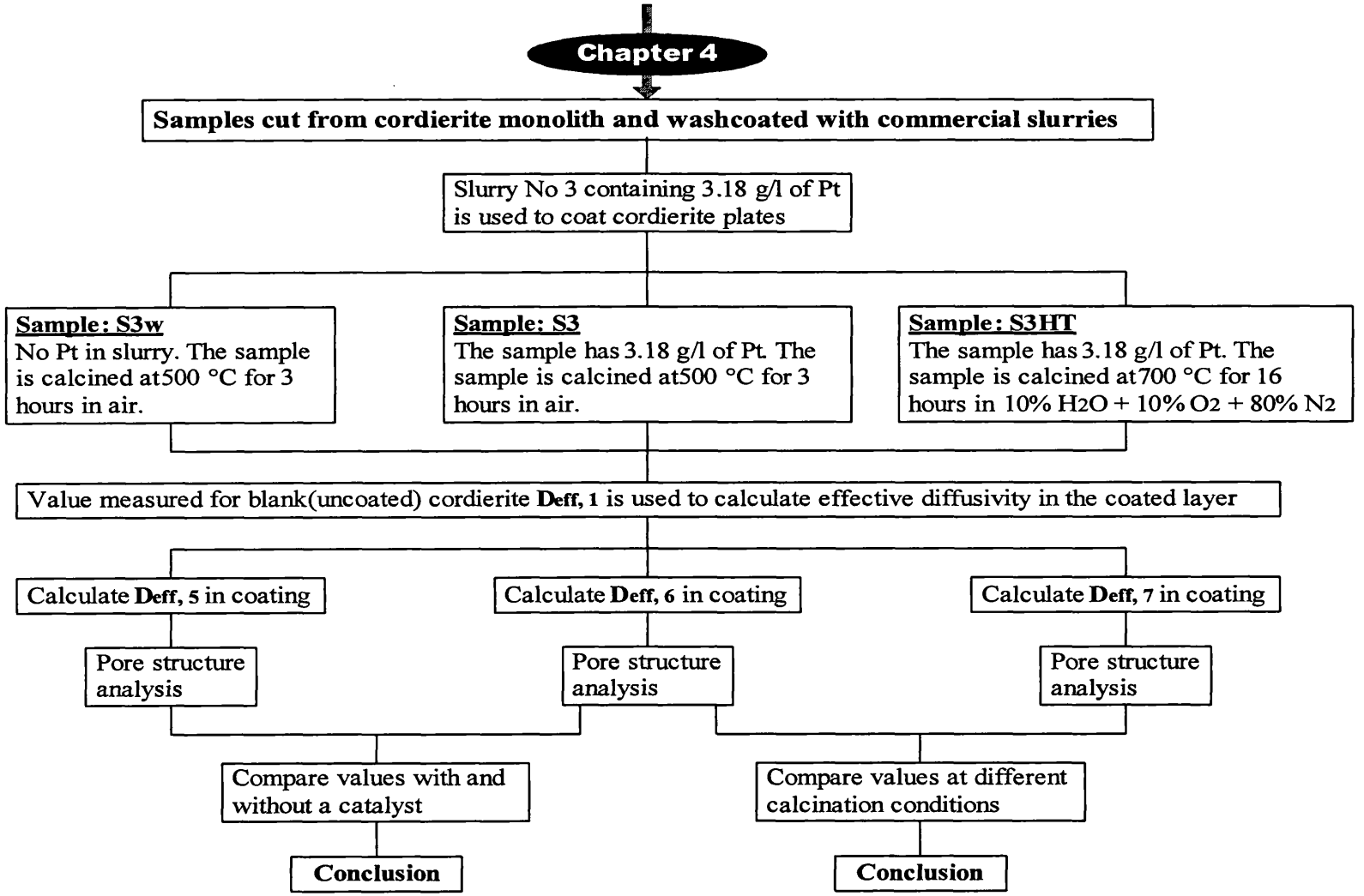

Figure 2.19(b) Schematic illustrating the link between activities in the thesis (continued from Figure 2.19(a))

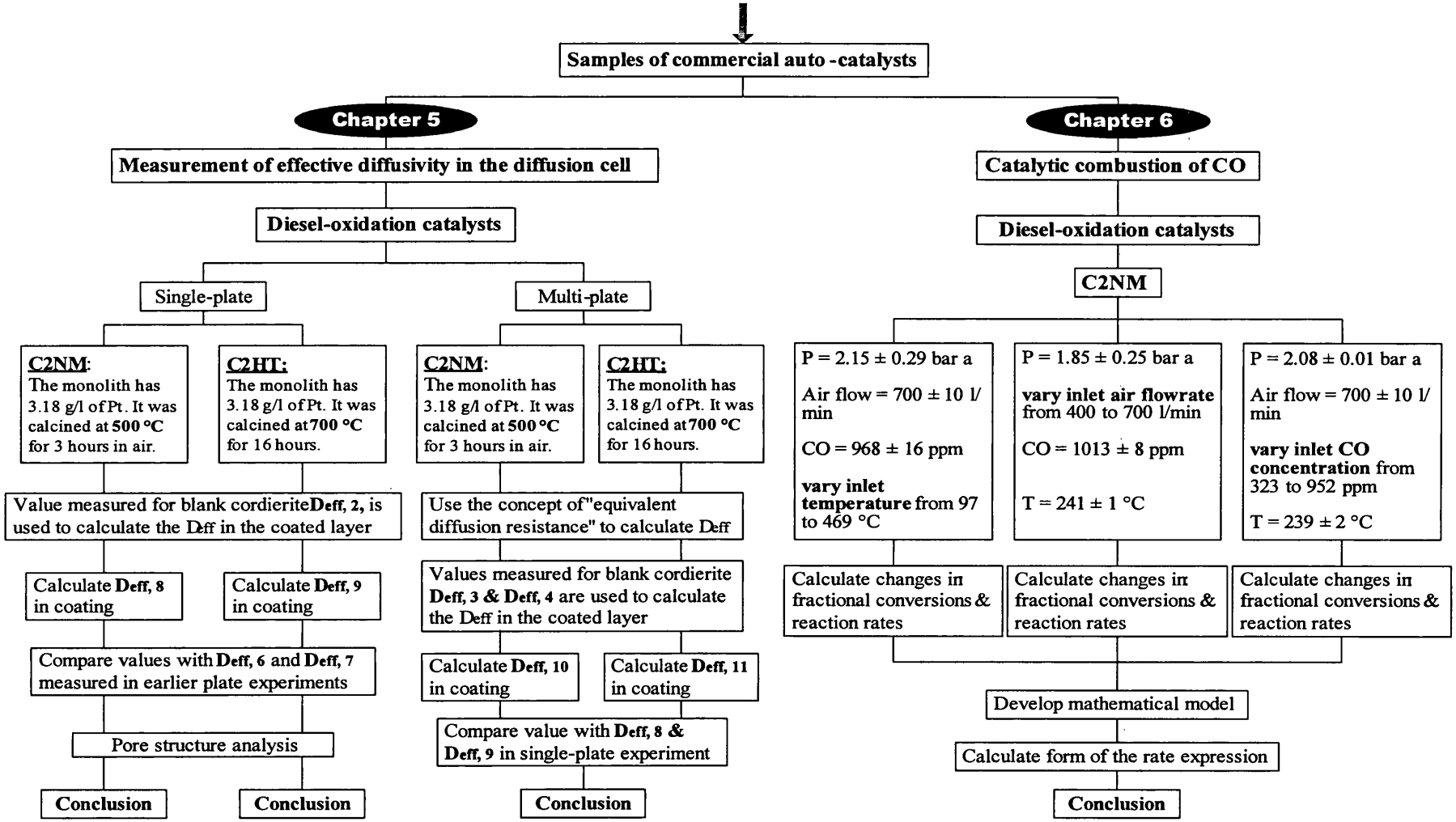

Figure 2.19(c) Schematic illustrating the link between events in the thesis (continued from Figure 2.19(a))

Chapter 3 The measurement of D_{eff} of CO in nitrogen through blank cordierite samples

In this chapter, the design of a modified form of Wicke-Kallenbach diffusion cell is described. The design had to be adapted so that the technique would be suitable for measurements on thin samples of catalyst that resembled the shape of a thin plate. Earlier work by Kim (2001) provided a useful starting point. Samples were cut from a monolith block, forming single-plate and multi-plate structures that were tested in the diffusion cell. This enabled the effective diffusivities in the cordierite support to be quantified, and the experimental method was refined in preparation for measurement on coated samples.

Figure 3.1 illustrates the procedure and logic links of the events described in this chapter.

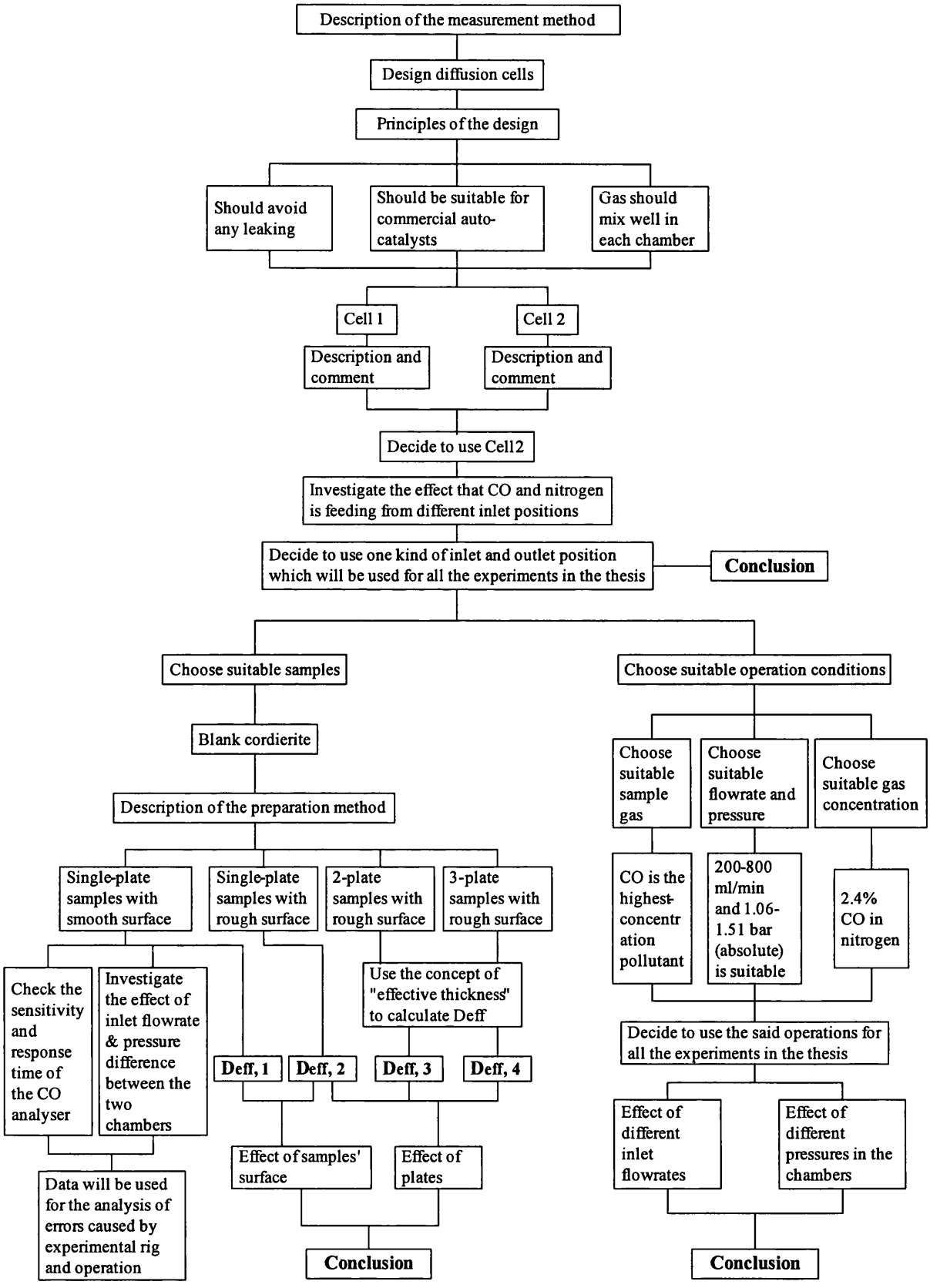

Figure 3.1 The experimental procedure and the logic links of events.

3.1 Description of experimental rig

The following is a list of the main items of equipment used in the diffusion rig:

1. CO analyser: Model: 2100 IRGA OPT; Measurement range: 0 to 1400 ppm; Made by SIGNAL Ltd, Surrey, UK.
2. Digital pressure indicator: Model: DPI 260; Made by Druck Ltd, Leicester, UK.
3. Differential pressure transducer: Model: PDCR 2111; Made by Druck Ltd.
4. Thermocouples: Made by Tempcon Instrumentation Ltd, Chichester, West Surrey, UK.
5. All the other valves and fittings: Obtained from Bristol Fluid System Technologies Ltd (Swagelok), Avonmouth, UK.

A schematic of the apparatus is illustrated in Figure 3.2 and a photograph of the rig is shown in Figure 3.3. The detailed design and dimensions of the diffusion cell are given in Figure 3.4. The outward appearance of the diffusion cell is shown in Figure 3.5.

Gas is admitted into the upper and lower chambers from two ports located on opposite sides of the chamber, through nozzles positioned in a tangential direction (at 45° from the centre) to avoid direct jet impact on the face of the sample, and to create good mixing in the chambers. Nitrogen (99.99% purity) is fed into the upper chamber and a specially ordered mixture of 2.4% (mol/mol) CO in nitrogen is fed into the lower chamber. The gas leaves the chamber from ports in the centre of the chamber (see Figures 3.4 and 3.5).

The inlet flowrate for the lower chamber varies from 200 ml/min to 800 ml/min (at experimental conditions) controlled by the needle Valve 6b and is measured with Rotameter 7b (see Figure 3.2). A similar flowrate is maintained in the upper chamber with needle Valve 6a and Rotameter 7a. The difference between the two inlet flowrates is maintained within ± 1.0% (*e.g.* 5 ml/min when the inlet flowrate is 500 ml/min), by adjusting the four needle valves (Valves 6a, 6b, 6e and 6f, see Figure 3.2).

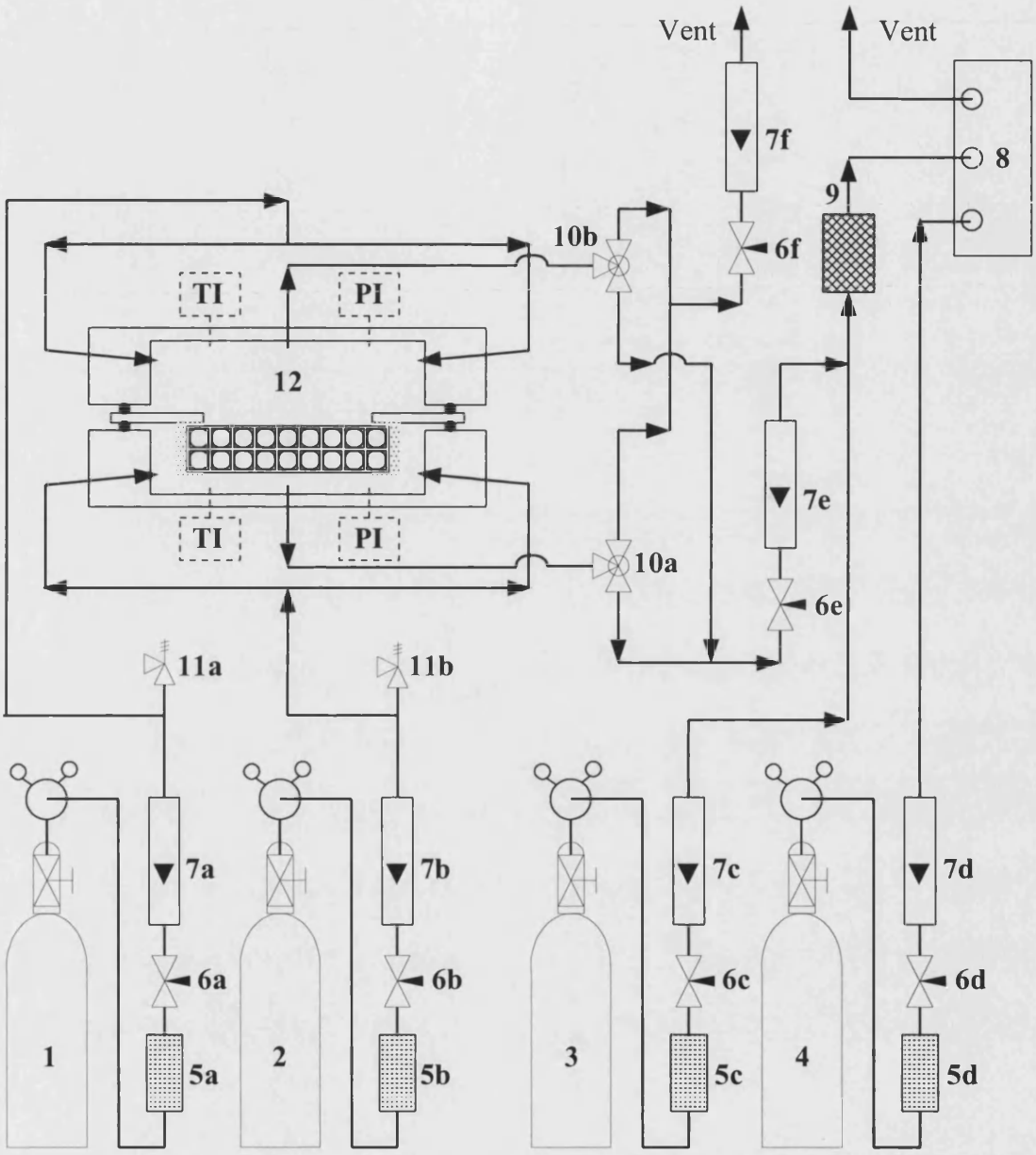

Figure 3.2 Schematic of the overall flow system for the diffusion apparatus.

1. N_2 cylinder for diffusion (99.99% purity) 2. CO cylinder for diffusion (2.4% CO in N_2) 3. CO cylinder for calibrating CO analyser (1080ppm CO in N_2) 4. N_2 cylinder providing reference gas for the CO analyser 5 (a to d). Dryers and filters 6 (a to f). Needle valves 7 (a to f). Rotameters (800 ml/min) 8. CO analyser (measurement range 0 to 1400 ppm) 9. Filter 10 (a & b). Three-way valves 11 (a & b). Relief valves 12. Diffusion cell (with TI: temperature indicator; and PI: pressure indicator).

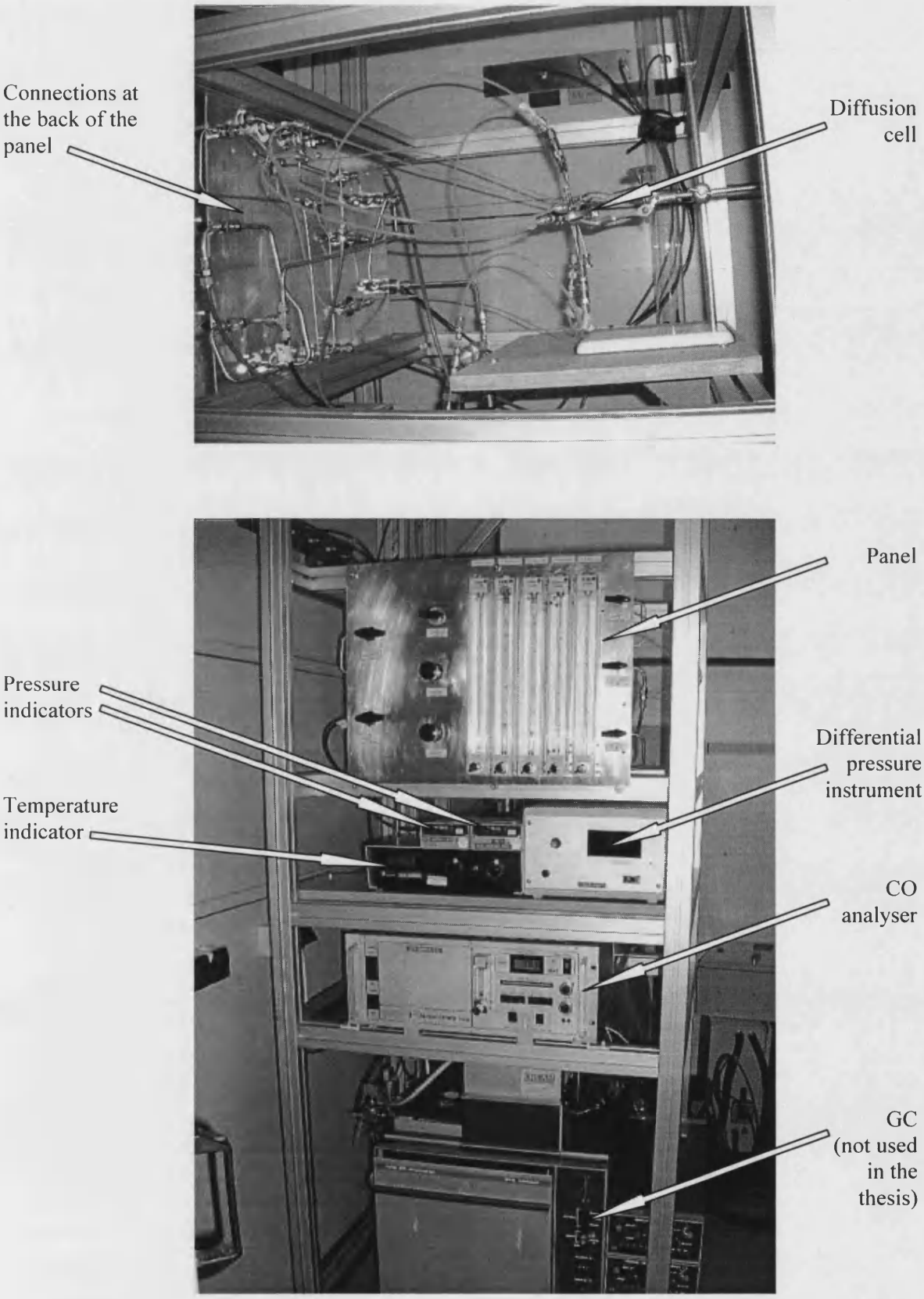

Figure 3.3 Apparatus for the measurement of effective diffusivity.

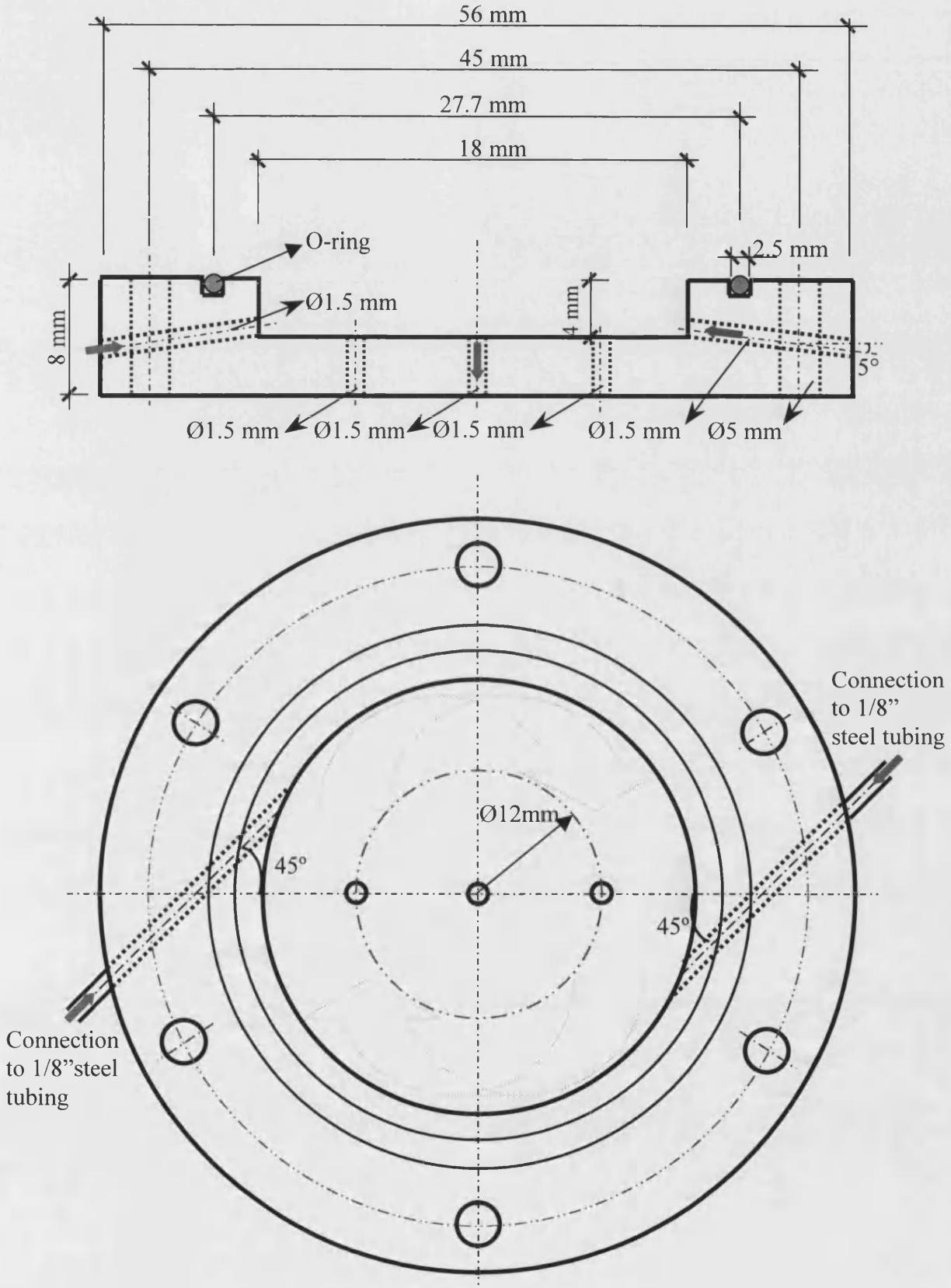

Figure 3.4 The key dimensions of the diffusion cell (based on the lower chamber).

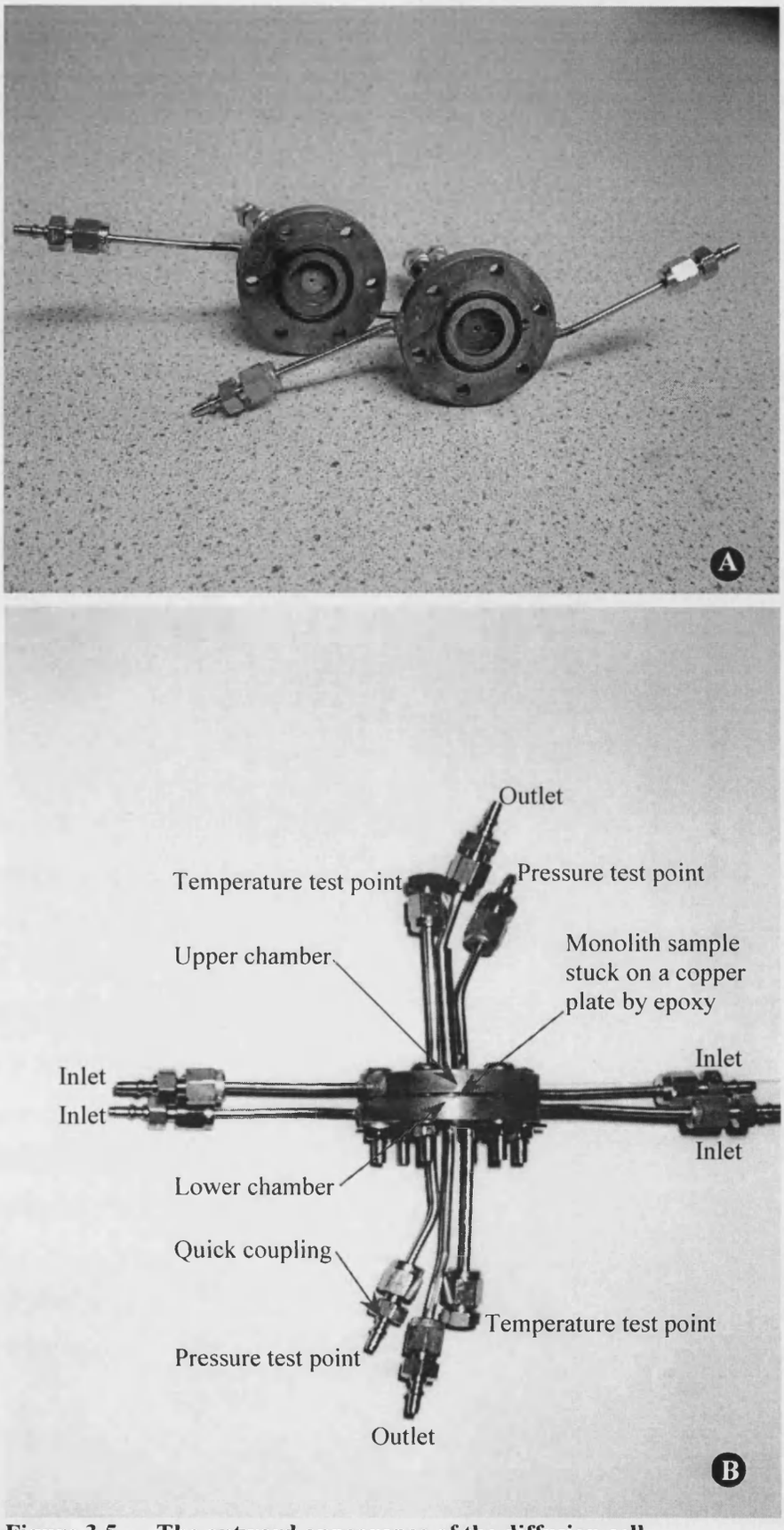

Figure 3.5 The outward appearance of the diffusion cell.

(A) View of the inside of the upper and lower chambers;
(B) View of the assembled cell.

As adjustments are made, both the gauge pressure in each chamber and the differential pressure across the two chambers is observed. Equal pressure in the two chambers is maintained by adjusting the back pressure regulating valves (Valves 6e and 6f, see Figure 3.2). Because the accuracy of the two pressure indicators is 0.0001 bar, the actual differential pressure between the two chambers is within ±10 Pa.

Gas temperature is measured with a thermocouple in each of chambers (see TI in Figure 3.2). The measured temperature was found to be close to the value measured outside of the cell.

The concentration of CO in the outlet stream of the upper chamber is measured with a CO analyser. The CO analyser works on the following principle (adapted from the operating manual for the instrument):

> The absorptivity of the infrared ray between the reference cell (filled with pure nitrogen) and the analysis cell (filled with sample gas) is different. The reference cell contains sample free air and does not absorb infrared energy. If the sample gas passing through the analysis cell also contains no absorbing gas, equal energy enters the two sides of the detector. When the sample does contain some of the absorbing gas, it reduces the amount of radiation reaching the detector at the analysis chambers. This gives rise to a minute pressure difference across the diaphragm that is deflected, thereby producing a small change in capacitance at the fixed plates. This change is measured electrically and an indication of the gas concentration is obtained on the meter (Figure 3.6).

As the CO analyser is very sensitive, great care should be taken with this instrument. The following operating procedure is critical when using the CO analyser:

1. The instrument should be warmed up for at least one hour.
2. The reference gas (pure nitrogen) should always be kept at a same flowrate, *e.g.* 500 ml/min.

3. It is essential not to move the CO analyser after calibrating it.
4. The zero and span point should be checked hourly because they may drift due to slight changes in room temperature or other factors.
5. The flowrate of sampling gas should lie in the range of 100 to 1500 ml/min, preferably 200 to 800 ml/min, same as that of the reference gas. The sampling flowrate should never be over 1500 ml/min, because this may damage the analysis cell.

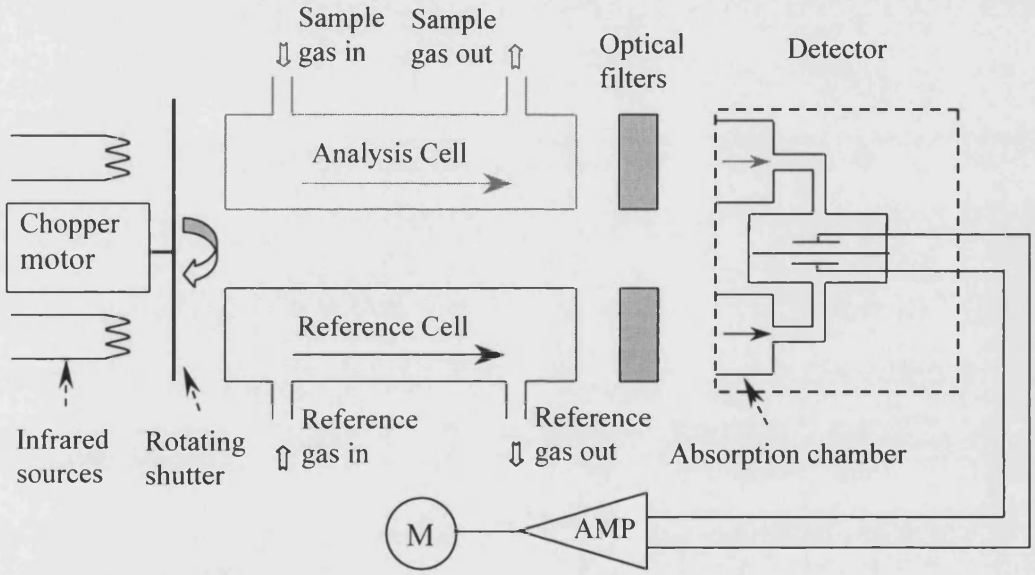

Figure 3.6 Diagram illustrating the operation principles of the CO analyser. (Adapted from "Signal Series 2000 Irga Operation Manual").

3.2 Preparation of plate samples for the diffusion cell

All the cordierite samples used in the thesis are prepared by directly cutting slices from commercial monolith cordierites, which were provided by a catalyst manufacture. The dimensions of a whole uncoated monolith cordierite as well as of a single channel are shown in Figure 3.7. Because cordierite is very fragile, care must be taken when cutting a single-plate (see Figure 3.7(A)) or a multi-plate wafer of cordierite (see Figure 3.7(B)

& (C)) with a mini saw with thin blade (about 0.5 mm). Photographs of single-plate and multi-plate cordierite samples are shown in Figure 3.8.

As shown in Figure 3.8(B), the exterior surface of cordierite samples is rough. This is due to the presence of the ridges (about 0 to 0.2 mm high somewhere) as the neighbouring walls were cut. To obtain a smooth surface, it is necessary to grind the surface as shown in Figure 3.9.

Every sample is then cut in a circular shape (14 mm diameter) by hand. This is then fixed with epoxy onto a copper plate that has a 40 mm outside diameter with a 10 mm diameter hole. The epoxy used was Araldite Resin and Araldite Hardener, made by Vantico AG Basel Switzerland. The sample needed to be positioned and sealed within 4 minutes otherwise the epoxy will start to solidify. The sample was then dried in a fume cupboard for at least 24 hours at room temperature.

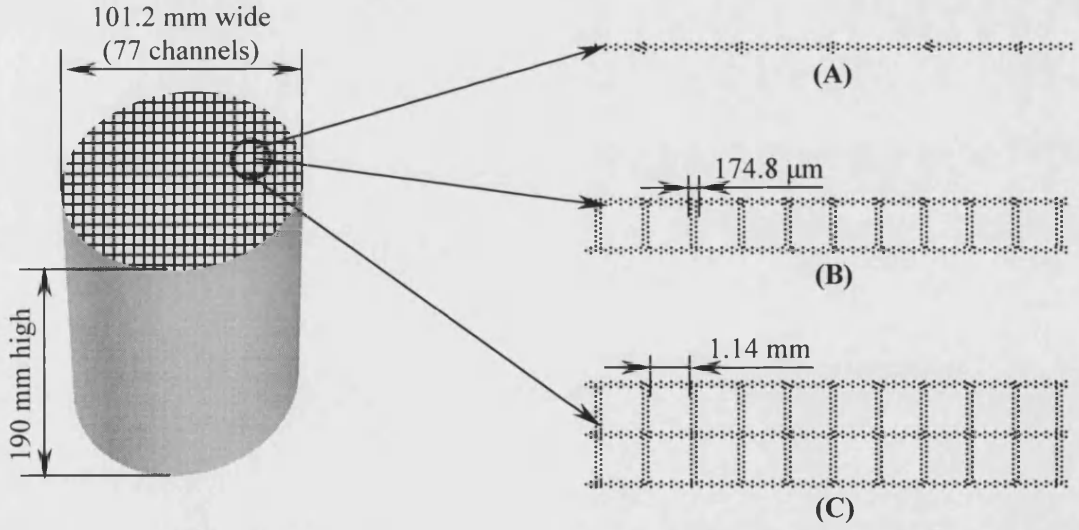

Figure 3.7 Examples of samples cut from a monolith block.

(A) Single-plate (also named half-cell) blank cordierite with rough surface;
(B) Two-plate (also named one-cell) blank cordierite with rough surface;
(C) Three-plate (also named two-cell) blank cordierite with rough surface.

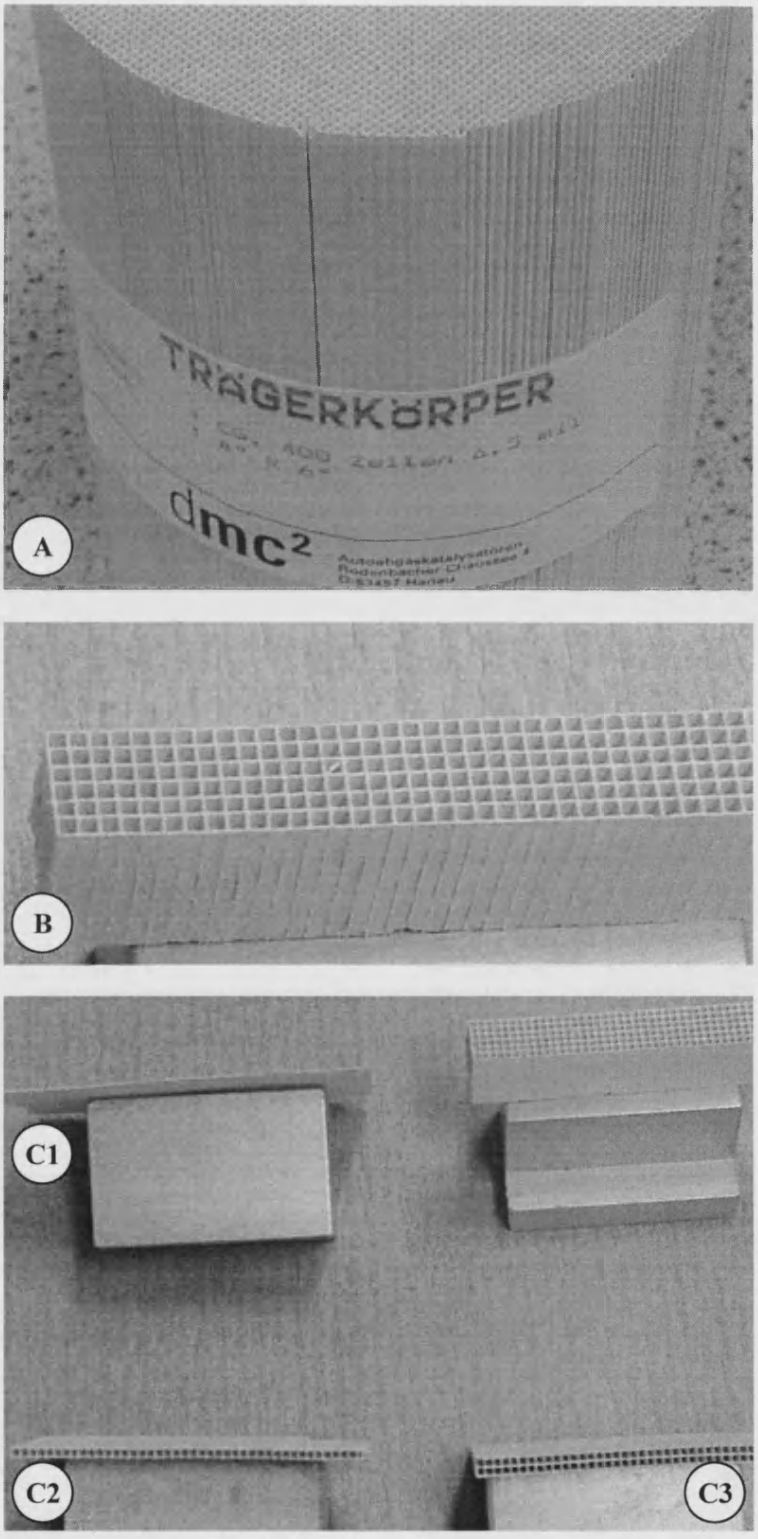

Figure 3.8 Photos of cordierite plates cut from original monolith.

(A) Original monolithic cordierite supplied by **dmc^2**, Germany;
(B) A section cut from the monolith cordierite;
(C1) Single-plate cordierite with rough surface;
(C2) Two-plate cordierite with rough surface;
(C3) Three-plate cordierite with rough surface.

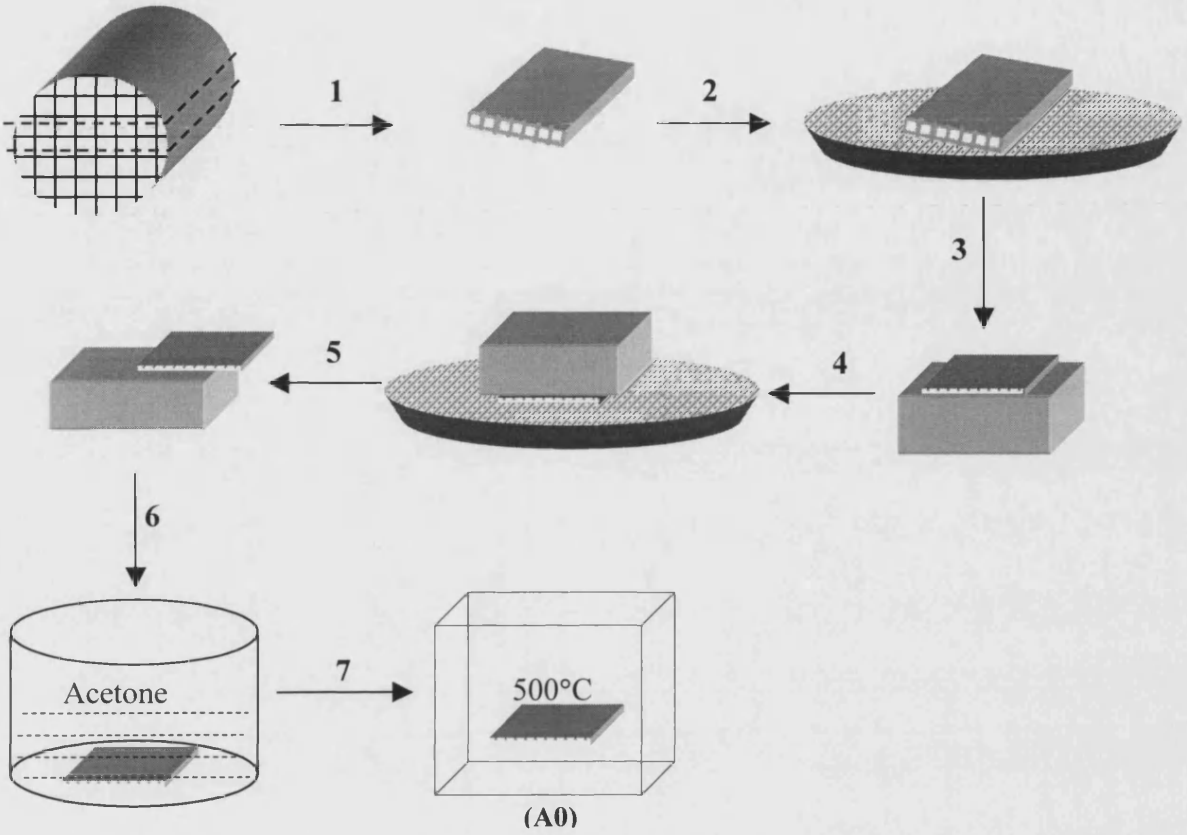

Figure 3.9 Description of the preparation procedure followed to make a single-plate cordierite sample (A0) with a smooth surface. (Adapted from Kim, 2001).

1. Cut a slice form the cordierite monolith that has at least a row of single cells.
2. Grind one of the surfaces smooth with an electric grinder.
3. Stick the smooth surface with wax onto an iron block (20 mm × 40 mm × 40mm).
4. Grind the other surface of the sample.
5. Heat the plate at 80 °C to soften the wax and release the sample.
6. Wash the sample in acetone solution to dissolve the wax.
7. Calcine the sample at 500 °C in air for 3 hours to completely eliminate the residual wax.

Using this general method, four groups of different cordierite samples (A0, A1, B & C) were prepared (see Figure 3.10, although Group A1 is not shown). Three samples were prepared of each group for comparison purpose as well as for error analysis. The details of these groups of samples are as follows:

Group A0: a single-plate with a smooth surface (this type of samples will be used as carrier for the washcoat);

Group A1: a single-plate with rough surface;

Group B: a two-plate cordierite with rough surface;

Group C: a three-plate cordierite with rough surface.

The difference between smooth surface and rough surface is that the thickness of the former is thinner than that of the latter. Besides, their pore structure of the surface may be slightly different; in other words, the pore size distributions in cordierite may not be uniform. To check this aspect, the effective diffusivity of samples taken from Group A0 & A1 is measured.

The measured value in Group A0 will also be used in the calculation of effective diffusivity in the commercial slurry coated cordierite samples. The values from Groups A1, B and C, will be used in the calculations relating to directly-cut commercial auto-catalysts with different plates. The details are as follows:

Group A1: the value will be used for single-plate commercial auto-catalysts;

Group B: the value will be used for two-plate commercial auto-catalysts;

Group C: the value will be used for three-plate commercial auto-catalysts.

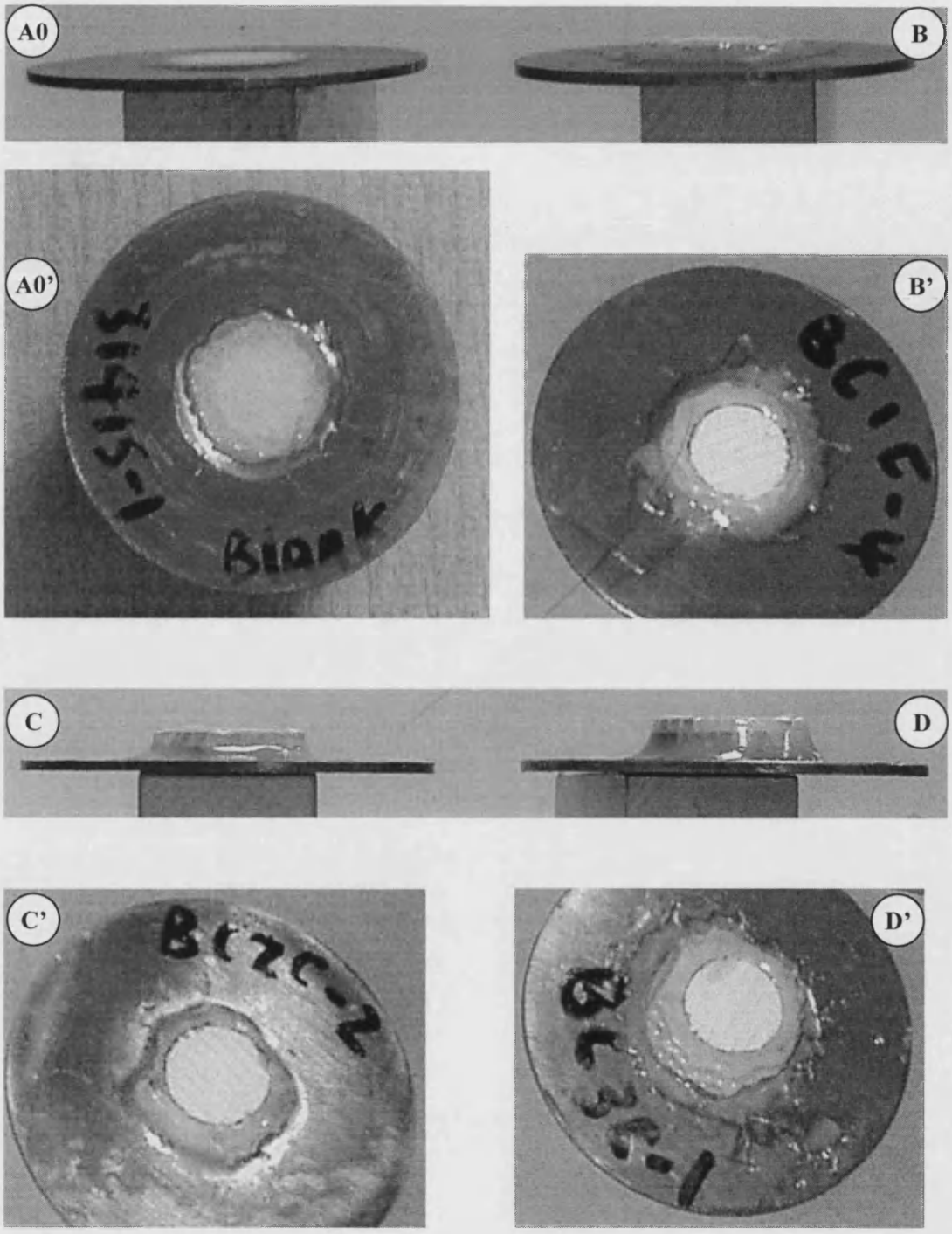

Figure 3.10 Photographs of single-plate and multi-plate blank cordierite samples (fixed on copper supports).

(A0) and (A0'): Single-plate cordierite with smooth surface;
(B) and (B'): Two-plate cordierite with rough surface;
(C) and (C'): Three-plate cordierite with rough surface;
(D) and (D'): Four-plate cordierite with rough surface (not used in the thesis).

3.3 Experimental procedures

The experimental procedures are as follows for each measurement.

3.3.1 Check to minimize leakage

As CO is a very toxic gas (even as low as 35 ppm CO in air will harm human health, according to the CO analyser manual), and minor leaks may cause significant experimental errors, any leakage (especially between the two chambers) should be avoided. To achieve this, epoxy resin is applied to stick a sample onto a copper plate, and an O-ring (made by James Walker & CO LTD, Cumbria, UK) is used to seal the copper plate in the middle of the two chambers. The type of the O ring is FR10/80. The material is dipolymer-based range with hardness of 50 to 90 IRHD. The dimension is: inner diameter 25.07 mm, O ring diameter 2.62 mm.

Leak checks were performed with nitrogen immediately after a new sample was installed. In practice, it was very difficult to ensure that there was no leakage in the whole rig. It was considered acceptable to operate if the pressure in the diffusion cell could be maintained, for example, at 0.5000 bar (g) to 0.4996 bar (g) over a 10 minute period when Valves 6a, 6b, 10a and 10b were closed (see Figure 3.2).

To check if there is any leakage between the two chambers, the pressure in one chamber was maintained about 50 mbar higher than that in the other chamber. If the differential pressure can be maintained easily (when diffusion is balanced), this means that there are no leaks. If the differential pressure trends to zero, this means there is a serious leak between the two chambers. In this case, the sample should be re-sealed or changed.

3.3.2 Calibrations

The four rotameters can measure flowrates in the range of 0 to 800 ml/min at room temperature. The optimum measurement range is 200 to 700 ml/min. The minimum

graduation is 10 ml/min. To calibrate the readings, the two nitrogen rotameters (Rotameter 7a and 7e in Figure 3.2) were calibrated using pure nitrogen at room temperature at the appropriate pressures (*e.g.* 1.06 bar (a), 1.11 bar (a), 1.21 bar (a), ..., 1.51 bar (a)), using a one-litre bubble flowmeter. The same procedure was followed for the CO rotameters (Rotameter 7b and 7f in Figure 3.2), using the 2.4% CO in nitrogen mixture. The calibration formulas for the four rotameters are listed in Table 3.1.

Table 3.1 List of calibration formulas of Rotameters 7a, 7b, 7e, and 7f (see Figure 3.2).

Q_d means displayed reading in the rotameter at the experimental conditions: 17.4 ± 2.3 °C, one atmosphere pressure.

Test pressure, bar (a)	**Rotameter 7a** (upper chamber, inlet)	**Rotameter 7e** (upper chamber, outlet)	**Rotameter 7b** (lower chamber, inlet)	**Rotameter 7f** (lower chamber, outlet)
1.06	$1.0988\times Q_d - 0.2757$	$1.0794\times Q_d - 7.5030$	$1.0790\times Q_d + 5.1219$	$1.0226\times Q_d - 3.6321$
1.11	$1.1273\times Q_d + 2.3451$	$1.0779\times Q_d - 8.3507$	$1.1138\times Q_d + 6.0710$	$1.0275\times Q_d - 8.0836$
1.21	$1.1780\times Q_d + 11.251$	$1.0869\times Q_d - 12.656$	$1.1524\times Q_d + 19.702$	$1.0300\times Q_d - 4.0289$
1.31	$1.2322\times Q_d + 16.995$	$1.0761\times Q_d - 1.4838$	$1.2145\times Q_d + 19.774$	$1.0487\times Q_d - 13.886$
1.41	$1.2919\times Q_d + 18.086$	$1.0823\times Q_d - 6.6840$	$1.2555\times Q_d + 29.478$	$1.0337\times Q_d - 6.9133$
1.51	$1.3338\times Q_d + 27.228$	$1.0695\times Q_d - 3.6936$	$1.3140\times Q_d + 29.001$	$1.0456\times Q_d - 14.062$

The CO analyser can be used to measure concentrations over the range of 0 to 1400 ppm. The optimum measurement range is 200 to 1000 ppm. The reported accuracy is ±1 ppm. The CO analyser was calibrated over 0 to 1080 ppm using pure nitrogen, mixed at various ratios (10 to 100%) with 1080 ppm CO. The calibration formula is:

$$Y_{CO,\,calibrated} = 1.0292 \times Y_{CO,\,displayed} - 28.131 \qquad (3.1)$$

The zero points on the two pressure indicators were adjusted at the start of each measurement.

3.3.3 Experiments

One sample (fixed on a copper plate) was placed into the diffusion cell. The sample faced the lower chamber. The two chambers were sealed with 6 screws. All of the connections were made (see Figure 3.11) and the valves were set in the operating positions. Check for leaks. Measurements can now be performed at different operating pressures and/or different inlet flowrates by adjusting needle Valves 6a, 6b, 6e & 6f (see Figure 3.2).

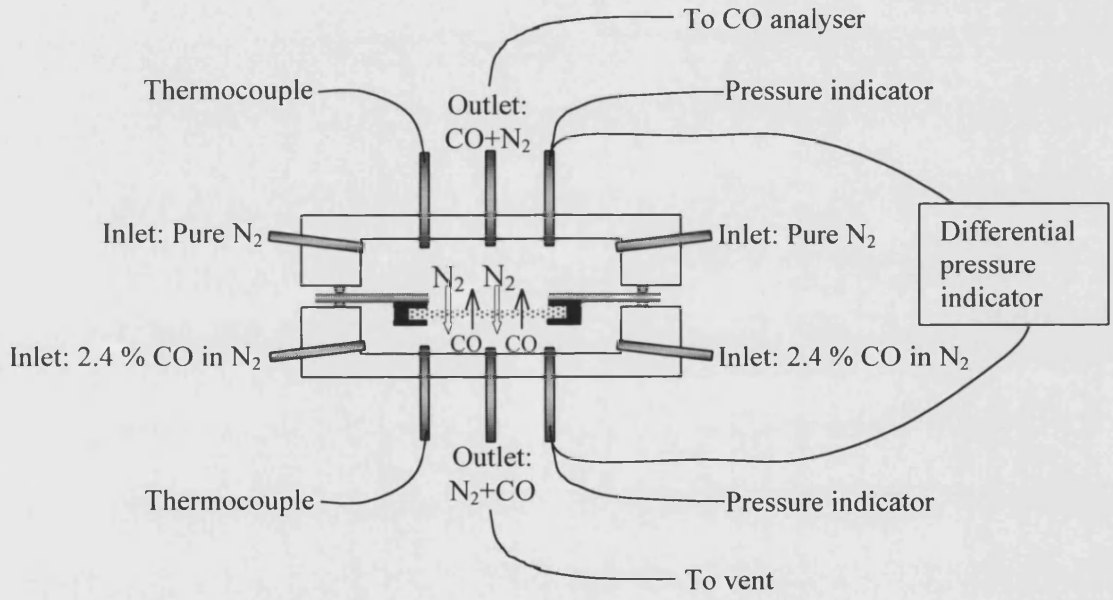

Figure 3.11 Illustration of connections on the diffusion cell.

During the measurement, care must be taken when changing pressures and/or flowrates, because the sample is likely to be damaged if the differential pressure between the two chambers is more than 80 mbar.

During the course of each experiment, when the upper inlet flowrate is same as the lower inlet flowrate, the upper outlet flowrate should also be equal to the lower outlet flowrate as equal-molar counter diffusion is assumed.

As the CO analyser requires the flowrates of sample gas to lie within the range of 100 to 1500 ml/min, the inlet flowrate to each chamber must lie in the range. When experiments are performed over this range, the molar flux of CO across the sample increases linearly with the inlet flowrate in the upper chamber (note: a similar flowrate was maintained in the lower chamber). The flux then becomes constant above a flowrate of 500 ml/min at room temperature (see Figure 3.12). This means that a steady flux can be obtained when the inlet flowrate in each chamber is more than 500 ml/min, and that external diffusion between the surface of the sample and the bulk gas is not a controlling factor. For comparison purpose, some experiments were still performed under the conditions where flowrate was less than 500 ml/min, *e.g.* 200 to 400 ml/min.

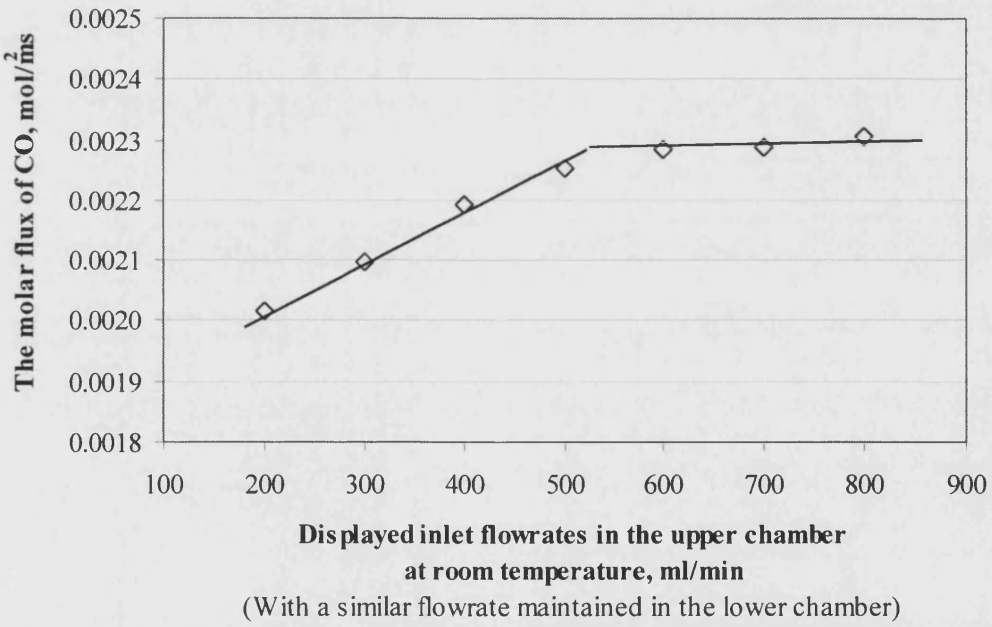

Figure 3.12 The effect of inlet flowrates on the molar flux of CO.

Exp performed on Sample BC-1C-2 (2-plate blank cordierite with rough surface).
Exp conditions: temperature: 15.8 °C; pressure: 1.0600 bar (a).

In the upper chamber, when the gas stream is fed from the two inlet points, it is assumed that the gas is well mixed in the chamber and that CO concentrations at Points B and C in Figure 3.13 are the same. The same applies to Points E and F in the lower chamber.

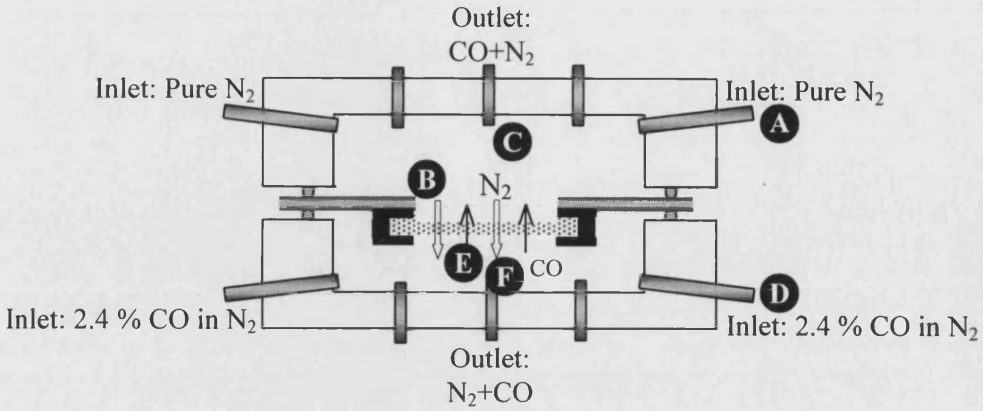

Figure 3.13 Concentrations of CO in the diffusion cell.

3.4 Characterisation of the blank (uncoated) samples

The cordierite samples were characterised by a Scanning Electron Microscope (SEM) to obtain their thickness and surface microstructure information. An X-ray technique was used to obtain information on elemental components. The instrument used was a JEOL T330 (JEOL, made in Japan) operated at 10 kV and a JEOL 6310 that was equipped with an X-ray powder diffraction (XRD) facility.

Figure 3.14 shows the SEM photos of different sections of monolith cordierite. For one unit cell, the four side walls have the roughly same thickness. The average thickness, found from the analysis of a number of cells, is 174.8 ± 5.6 microns. The variation in the thickness may be caused either by the manufacturing process, or as a result of measurements with the SEM instrument (this will be discussed in the section on error analysis). On closer examination of the cross section of a channel (see Figure 3.14(A)), it is not a perfect square. However, these variations are small (*e.g.* wall width is ± 3%).

Figure 3.14(C) shows a typical surface view of a smoothed cordierite sample. It is evident that the pores in cordierite have irregular shapes. The diameter of the pores can be as high as 10 microns, and as small as only one micron.

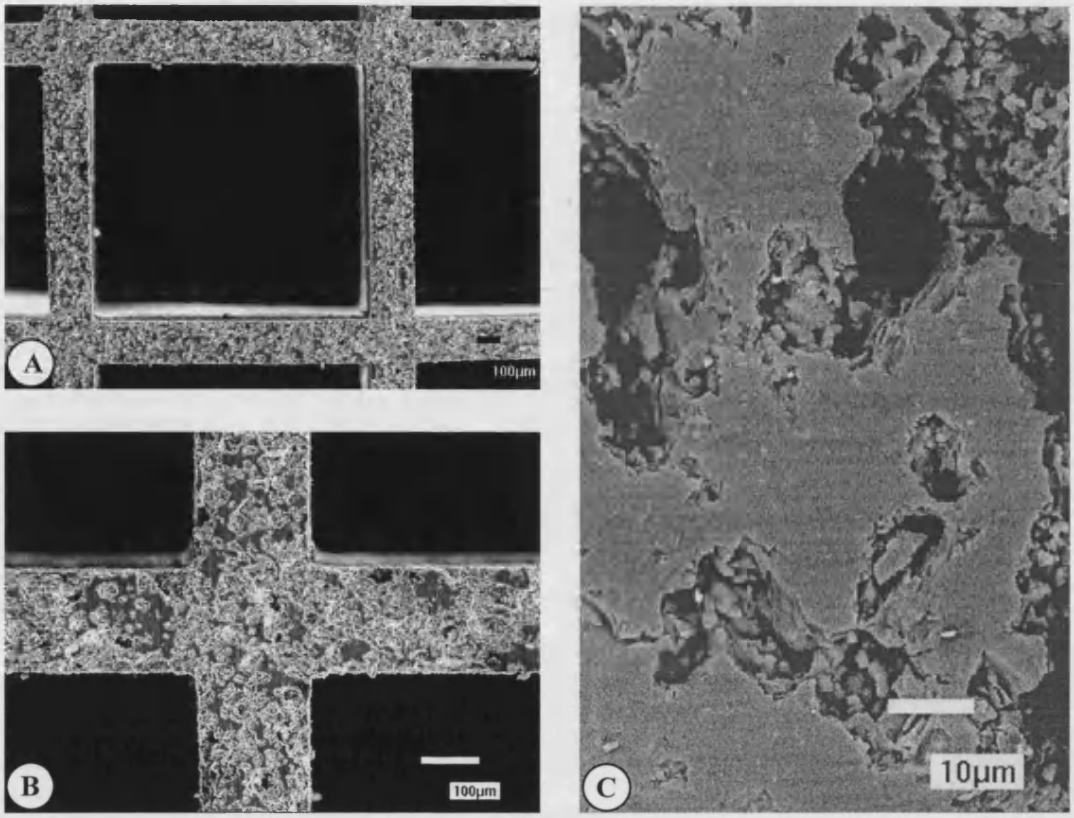

Figure 3.14 Scanning electron micrograph (SEM) of monolith cordierite samples.

(A) One square shaped cell: 1.14 mm × 1.14 mm;
(B) Walls of neighbouring cells: wall thickness = 174.8 microns;
(C) Surface view of cordierite which has been smoothed.

The result of an X-ray analysis on a sample of cordierite is shown in Figure 3.15. From the peaks, it is evident that Si is the most positive-valence element in cordierite, then Al, and Mg is the least. This is consistent with the composition of cordierite, $2MgO{\cdot}2Al_2O_3{\cdot}5SiO_2$, which has 5 Si, 4 Al and 2 Mg in one unit. Some trace elements may also exist in cordierite; however, they cannot be detected due to the accuracy of the XRD machine. Au is detected because it was coated onto the surface of the sample to improve electric conductivity.

The detailed pore size information (pore diameter, pore size distribution, *etc*) on a number of the samples was obtained using nitrogen adsorption and mercury porosimetry experiments, which were performed by Mr Julian Perfect at University College London.

For nitrogen adsorption, the Accelerated Surface Area and Porosimetry (ASAP) System 2010 machine was used. Using this equipment, pores with diameter from 0.1 nm to 1 μm can be measured. The mercury porosimeter was an AUTOPORE II 9220 (Micrometrics Instrument Co), which can measure pore diameters in the range of 3 nm to 100 μm. The result shows the median pore diameter (volume-base) is 3.405 μm (see Table 3.2 and Appendix B1). Based on the data from Appendix B1, the pore size distribution is summarized in Figure 3.16.

According to the classification standard of pores adopted by the International Union of Pure and Applied Chemistry (IUPAC), these pores are considered to be macropores. It should be noted that all the samples used for characterization are small sections of monolith cordierite and are not crushed or pressed.

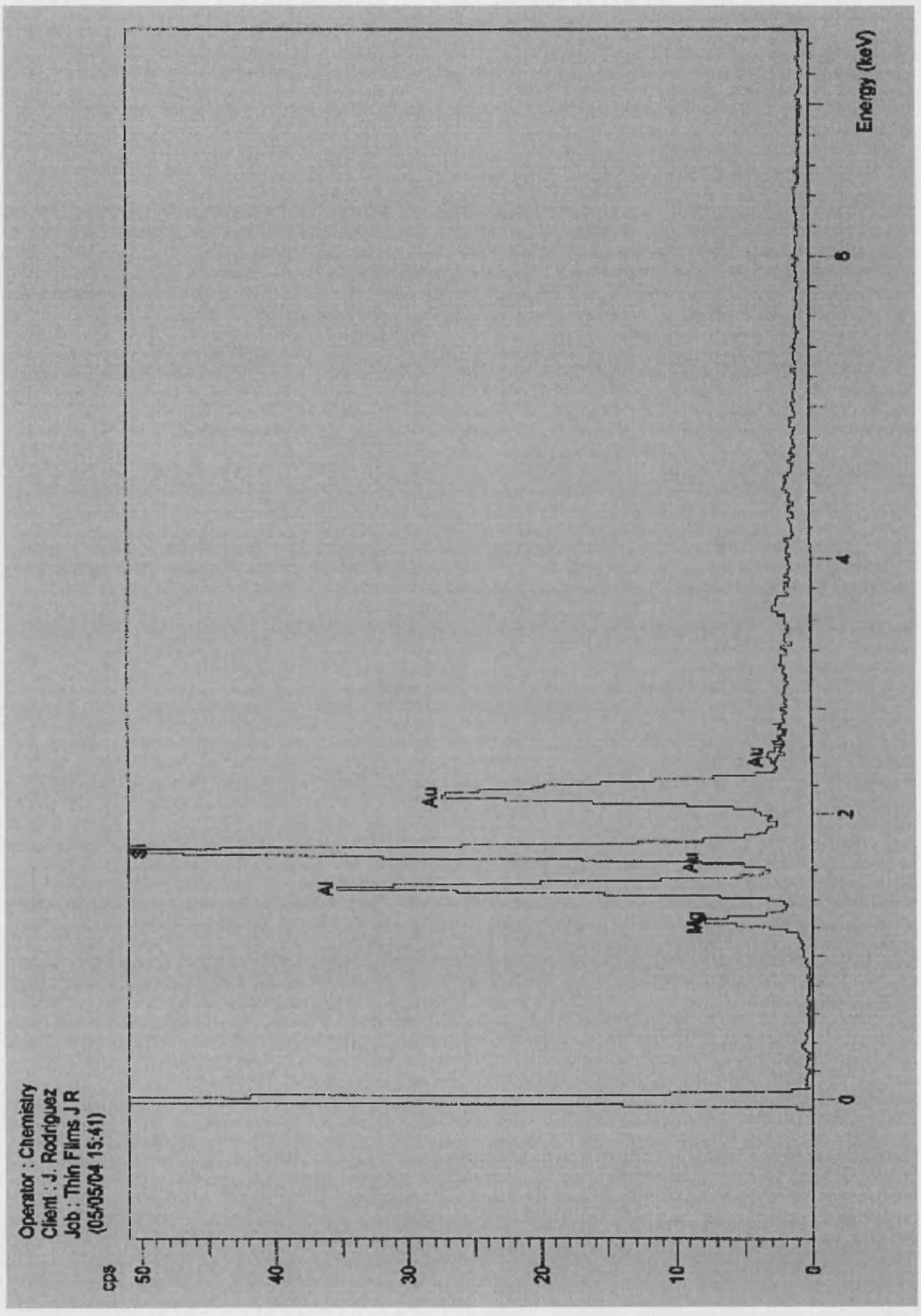

Figure 3.15 **X-ray analysis of a cordierite sample.**

Table 3.2 Summary of the properties of the uncoated cordierite.

Properties	**Data**
Cell density, cpsi	400
Thickness of the wall of channels, microns	174.8
Dimensions of a channel, micron	1140 × 1140
Fractional flow area of the monolith, %	66.4
Area from ASAP analysis	
BET surface area, m^2/g	0.2822
Micropore area, m^2/g	0.0454
Volume from ASAP analysis	
Micropore volume, cm^3/g	0.000024
Pore size from ASAP analysis	
BJH adsorption average pore diameter (4V/A), Å	100.7894
BJH desorption average pore diameter (4V/A), Å	140.6025
Intrusion data from Micromeritics	
Total intrusion volume, ml/g	0.2069
Total pore area, m^2/g	0.329
Median pore diameter (volume), μm	3.4045
Median pore diameter (area), μm	1.6283
Bulk density at 0.10 psia, g/ml	1.6613
Apparent (skeletal) density, g/ml	2.5315
Porosity, %	34.3715

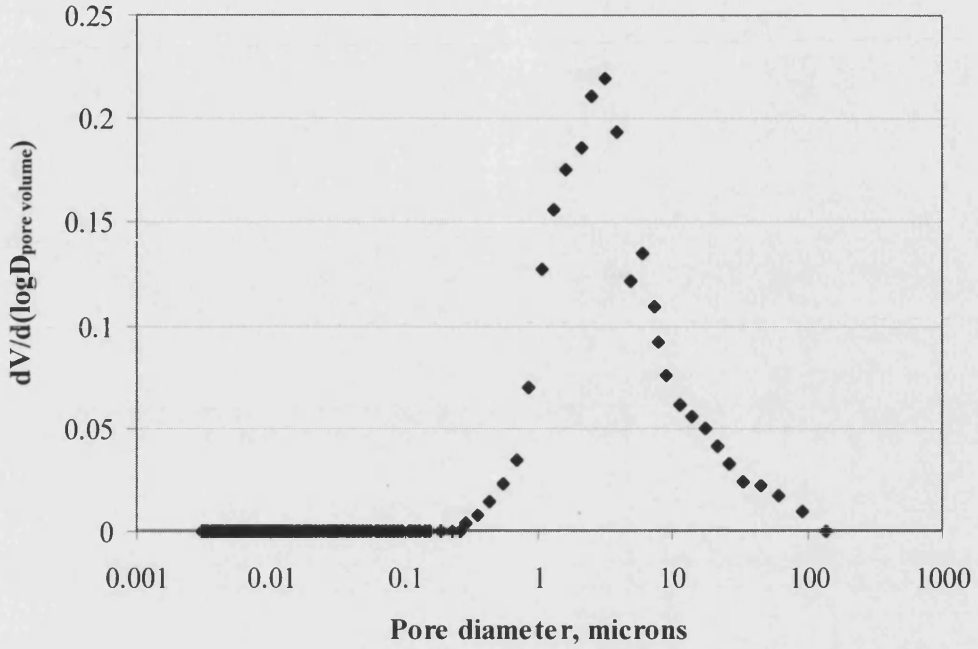

Figure 3.16 Pore size distribution measurements in a cordierite sample.

3.5 Experimental measurement of D_{eff}

3.5.1 Single-plate uncoated cordierite

In this section, experiments were performed with samples of cordierite plate that have been cut from a monolith block. These are categorized as follows:

Group A0: one plate cordierite with smooth surface, thickness = 162.0 μm;

Group A1: one plate cordierite with rough surface, thickness = 174.8 μm.

In the calculation of effective diffusivity, the concentration distribution of CO in each chamber is ignored and the following ideal conditions are assumed:

1. The concentration of CO on the lower surface of cordierite sample is uniform and same as that of outlet gases in the lower chamber.

2. The concentration of CO on the upper surface of cordierite sample is uniform and same as that of outlet gases in the upper chamber.

3. CO diffusion from the lower surface to the upper surface is driven only by concentration difference between the two sides of cordierite sample.

Based on the above assumptions, the effective diffusivity is calculated using the method described in Hayes and Kolaczkowski (2000) and Kim (2001), summarised as follows:

According to Fick's law, the flux of CO (N_{CO}) from the lower chamber to the upper chamber (through the uncoated cordierite sample) is:

$$N_{CO} = D_{eff,bc} \times \frac{\Delta C}{\Delta L} = D_{eff,bc} \times \frac{(C_{4,CO} - C_{2,CO})}{L_{bc}} \tag{3.2}$$

here

$C_{4,CO}$ The outlet concentration of CO in the lower chamber, $mol.m^{-3}$

$C_{2,CO}$ The outlet concentration of CO in the upper chamber, $mol.m^{-3}$

L_{bc} The thickness of uncoated cordierite, m;

N_{CO} can also be calculated from:

$$N_{CO} = Q_{2,s} \times \frac{C_{2,CO}}{A} \tag{3.3}$$

here

$Q_{2,S}$ The outlet flowrate in the upper chamber at standard condition, $m^3.s^{-1}$;

A Surface area available for diffusion in the diffusion cell, m^2;

From Equation 3.2 and Equation 3.3, the effective diffusivity in blank (uncoated) cordierite, $D_{eff,bc}$, can be calculated from:

$$D_{eff,bc} = \frac{Q_{2,s} \times C_{2,CO} \times L_{bc}}{A \times \Delta C} \tag{3.4}$$

A worked example (Sample BC0C-1, single-plate blank cordierite with smooth surface) of the calculation steps followed and the data for this set of experiments is available in Appendix C.

To investigate any effects of increasing flow, *versus* a decreasing flow sequence, experiments were performed on a smooth-surface cordierite sample. The results are shown in Figure 3.17, from which it is evident that the sequence does not affect the results, and the average difference between the two sets of results is less than 0.94%. This also shows good repeatability.

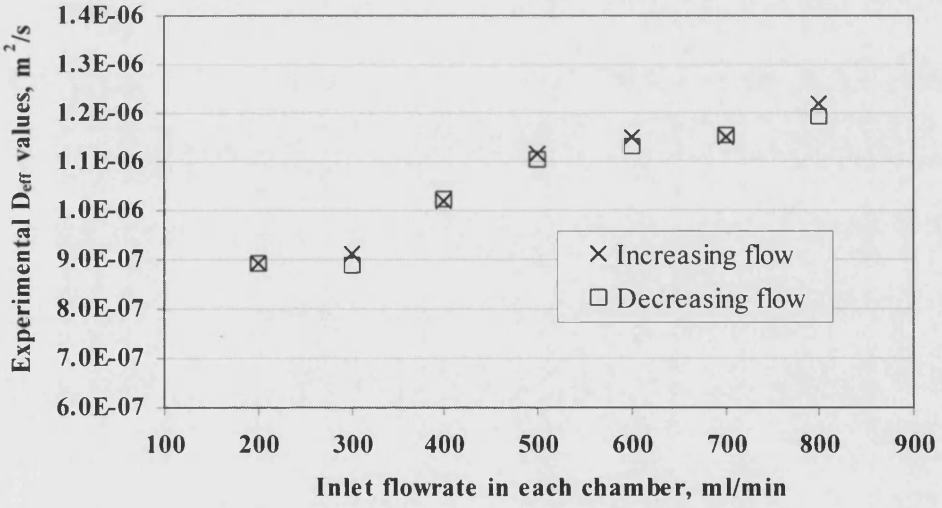

Figure 3.17 Effect of increasing/decreasing gas inlet flowrate on experimentally determined D_{eff} values for a single-plate smooth-surface cordierite sample.

The pressure in the cell was 1.1100 bar (a).

Although the order does not affect the measured results, decreasing inlet flowrates were used as it was easier to control the differential pressure across the samples to <10 mbar. This helped to protect the fragile cordierite samples.

On average, the measured D_{eff} values of the smooth-surface cordierite are about 17% higher than that of the rough surface (see Figure 3.18). The actual results are:

$(11.33 \pm 0.37) \times 10^{-7}$ m^2/s for the smooth surface (162.0 μm thick)

$(9.58 \pm 0.49) \times 10^{-7}$ m^2/s for the rough surface (174.8 μm thick)

This may indicate that the surface structure of the two samples is different, and that the distribution of the pores in the cordierite samples may not be even – the ground surface layer (about 7-micron thick) of cordierite may have more compact structure. When producing monolithic cordierite, mixed inorganic materials (14wt% MgO + 36wt% Al_2O_3 + 50wt% SiO_2 + minor amounts of substances such as Na_2O, Fe_2O_3 and CaO) are melted at over 1600 °C (Ertl *et al*, 1997) and extruded into the monolithic form. During cooling down and hardening process, the surface of cordierite will contract due to surface tension. As a result, the density of the pores (especially the open-ended pores) will be lower than that in the main body of the cordierite. When the surface layers are removed by grinding, more pores will be exposed at the surface. Clearly, this will decrease diffusion resistance.

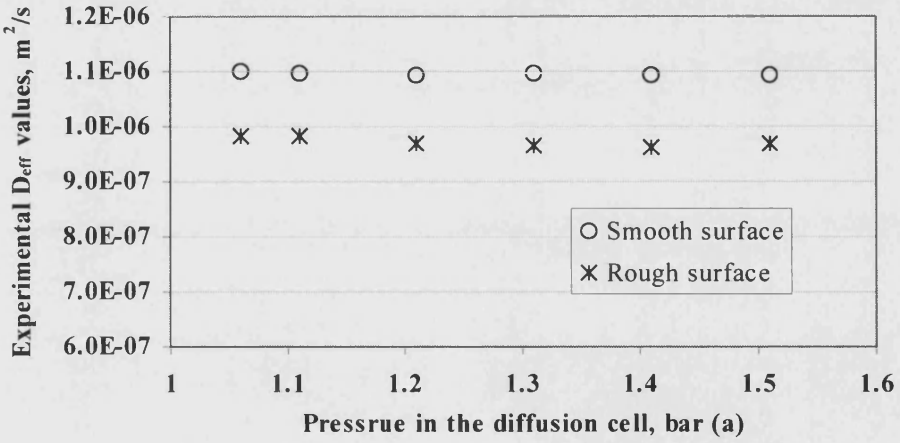

Figure 3.18 Effect of the surface structure of cordierite samples on D_{eff} values.

Based on single-plate cordierite sample, measured at different pressures with 500 ml/min inlet gas flowrate in each chamber.

3.5.2 Multi-plate uncoated cordierite

In this section, experiments were performed with samples that have been cut from a block of monolith. These are categorized as follows:

Group B: 2-plate cordierite, consisting of 1 cell in the direction of diffusion;

Group C: 3-plate cordierite, consisting of 2 cells in the direction of diffusion.

This was a new technique and there were many uncertainties about how successful it would be. If it was shown to work, then the main advantage of the method lay in the ability to perform measurements on real samples of monolith in which cell structure was preserved. Also, the samples were not as fragile as the single plate structures tested in Section 3.5.1.

From Equation 3.4, it can be found that for multi-plate uncoated cordierite samples, the challenge is how to determine their thickness, because they have more than one cordierite layers, as well as the void space between the layers.

To solve the problem, both simple methods and a complex method of analysis were used to interpret the results of measurements on these multi-plate samples. A simple method and a complex method are described in the published paper (Zhang *et al.*, 2004) on this topic (see Appendix A). The complex method was based on a two-dimensional model of the monolith and was run by Professor Hayes at the University of Alberta (Canada) utilizing one of his codes. This helped to verify the values obtained from a more simplistic approach, and hence the merits of the method.

In addition, another simplistic approach was then subsequently developed and this is described in more detail in the body of this thesis. In this simplistic approach, the thickness of the cordierite wall is assumed uniform, and each cell in the sample is assumed a perfect square.

Simplistic method applied to Group B (2-plate cordierite)

From Equation 3.2, then

$$N_{CO} = D_{eff} \times \Delta C \times \frac{A}{L} \tag{3.5}$$

here

N_{CO} The molar flow of CO, mol/s

If in the reconfigured cell structure, the ratio $\left(\frac{A}{L}\right)_{reconfigured}$ is maintained the same as $\left(\frac{A}{L}\right)_{actual\ sample}$, then for the same material (hence same D_{eff}) and same ΔC, the molar flow of CO will be the same. This premise forms the basis of the reconfiguration, which is done in a number of steps.

Step 1: Identify the zone.

In a 2-plate cordierite sample, each cell has a void channel (1140 μm × 1140 μm) with a wall (thickness = 174.8 μm). Figure 3.19 shows a magnified view of one cell. The zone that is reconfigured is indicated with dotted line, called "unit cell". The unit cell can be divided into six parts, labelled: C1, C2, C3, C4, C5 and C6 as shown in Figure 3.19.

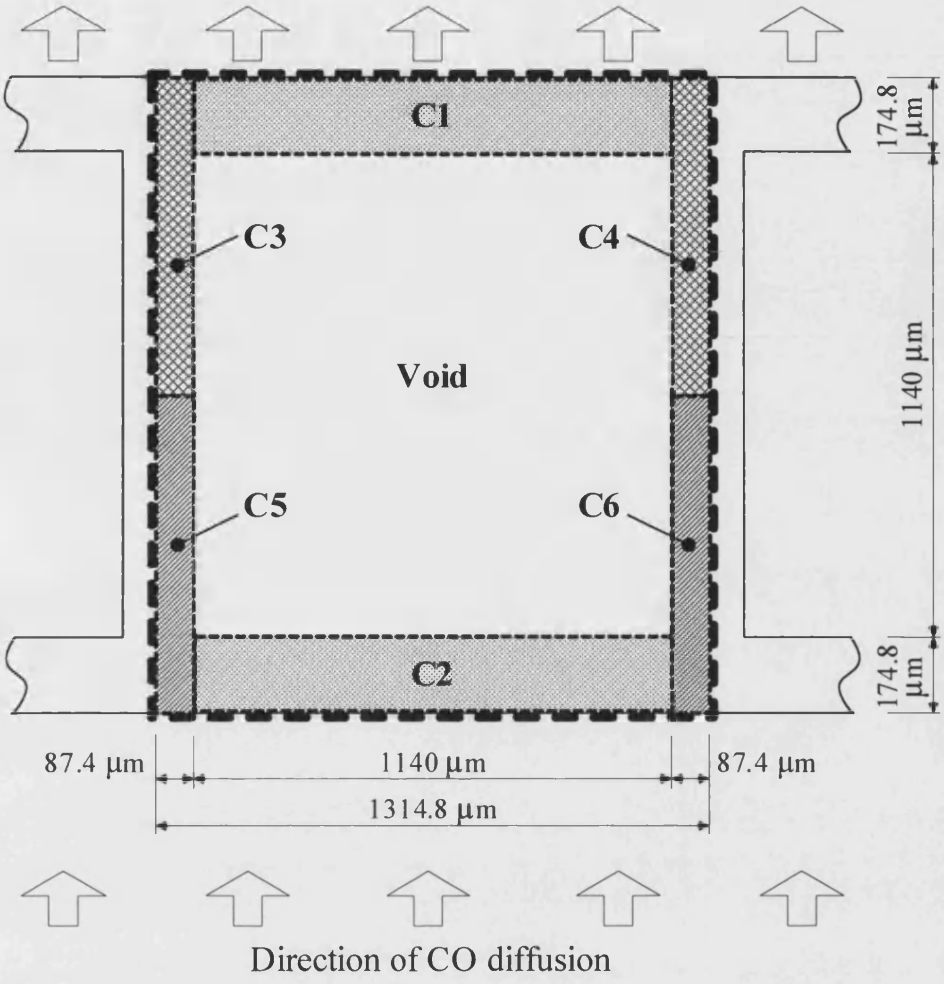

Figure 3.19 Magnified view of one cell in a Group B (2-plate cordierite)

Step 1: The dotted line indicates the zone that is reconfigured. The zone is divided into void channel part and cordierite parts (C1, C2, C3, C4, C5 and C6, which are shaded to help identify the regions).

Step 2: Reduce the height of C3, C4, C5 & C6.

The height of C3 is reduced to 174.8 µm to match the thickness of C1. The width of C3 is then reconfigured to 20.5 µm. The same procedure is applied to C4, C5 and C6, see Figure 3.20.

Step 3: Adjust the width of reconfigured cell to match the actual width.

The width of the reconfigured cell is adjusted to the original width (the width of the unit cell, 1314.8 μm) so that the reconfigured cell can match the fixed diffusion area (the hole with 10 mm diameter in the copper-supported sample). Also adjust the width of void to match the actual width of area for diffusion, see Figure 3.20.

Step 4: Combine the cordierite layers.

Combine C1, C3 and C4 into one cordierite layer – Layer 1. Combine C2, C5 and C6 into one cordierite layer – Layer 3. The reconfigured void layer is Layer 2.

Now the "apparent" dimension of the reconfigured unit cell is: 1314.8 μm (wide) × 1704.0 μm (high), having the same width as the original unit cell. The reconfigured "effective thickness" of the cordierite plates in the unit cell is: 2 × 194.6 μm = 389.2 μm. The void space has an "effective thickness" of 1314.8 μm.

An example calculation is shown in Appendix C and the results of the measurements taken are shown in Appendix D1.

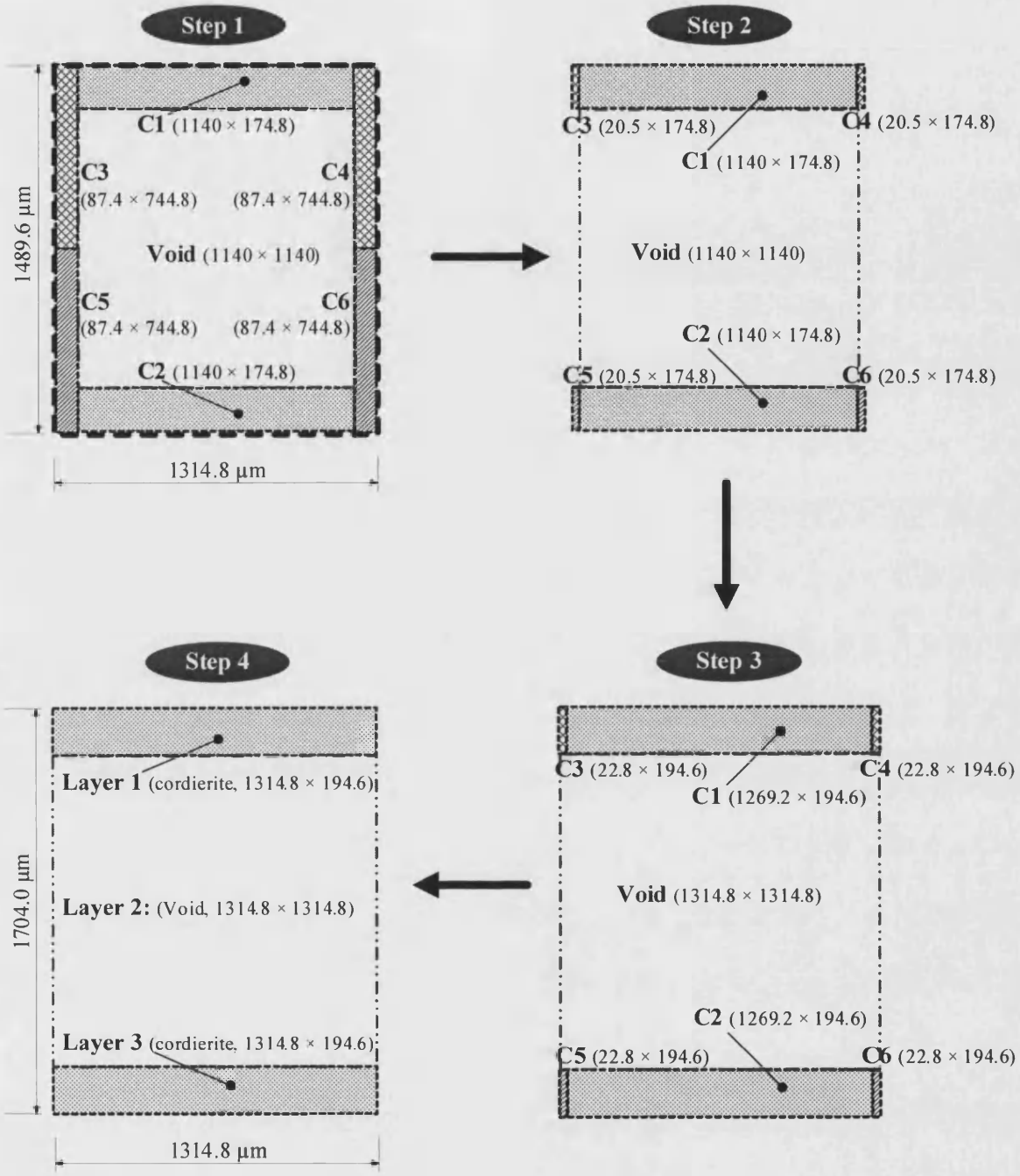

Figure 3.20 Using "equivalent diffusion resistance" method to reconfigure 2-plate cordierite sample.

Note: values of distance are in µm.

Application of simplistic method to a multi-plate sample

The above method, was also applied to a multi-plate sample. Figure 3.21 shows the "effective thickness" of different layers in a 3-plate cordierite sample.

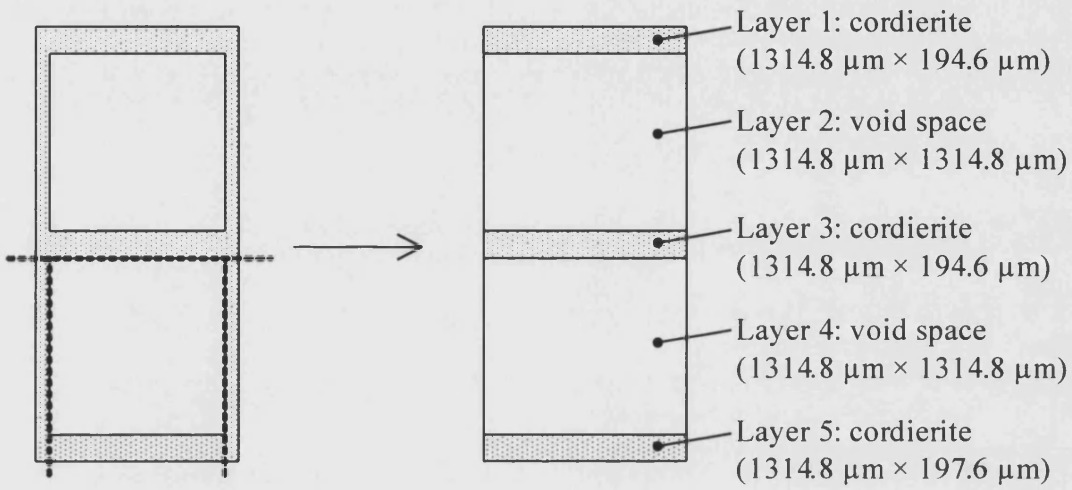

Figure 3.21 The application of the concept of "effective thickness" to a 3-plate cordierite.

A unit 3-plate cordierite (with two cells, see left figure) is reconfigured into 3 flat cordierite plates and 2 void spaces (see right figure).

Note: Layer 5 is 3 μm thicker than Layers 1 and 3 according to the reconfigured procedure.

When calculating the effective diffusivity in multi-plate cordierite, the electrical analogy can also be adopted:

$$V = I \times R_i \tag{3.6}$$

If flux of CO is N_{CO} and R_d is diffusion resistance, then:

$$(C_{CO,4} - C_{CO,2}) = N_{CO} \times R_d \tag{3.7}$$

This can be re-arranged as:

$$N_{CO} = \frac{1}{R_d}(C_{CO,4} - C_{CO,2}) \tag{3.8}$$

where for a structure of uniform composition:

$$\frac{1}{R_d} = \frac{D_{eff}}{L_{bc}} \tag{3.9}$$

Or

$$R_d = \frac{L_{bc}}{D_{eff}} \tag{3.10}$$

For a complex composite consisting of the three layers (two cordierite layers and one void layer, see Step 4 in Figure 3.20), then:

$$R_{d,total} = R_{d,Layer1} + R_{d,Layer2} + R_{d,Layer3} \tag{3.11a}$$

where:

$$R_{d,total} = \frac{L_{total}}{D_{eff,\,total}} \tag{3.11b}$$

$$R_{d,\,Layer\,1} = \frac{L_{Layer\,1}}{D_{eff,\,Layer\,1}} \tag{3.12}$$

$$R_{d,\,Layer\,2} = \frac{L_{Layer\,2}}{D_{eff,\,Layer\,2}} \tag{3.13}$$

$$R_{d,\,Layer\,3} = \frac{L_{Layer\,3}}{D_{eff,\,Layer\,3}} \tag{3.14}$$

As the composition of Layer 1 is the same as Layer 3, then $D_{eff,\,Layer\,1} = D_{eff,\,Layer\,3}$.

For the void (Layer 2), $D_{eff,\,Layer\,2}$ is the bulk gas diffusion coefficient and was calculated from Fuller *et al.* (1966):

$$D_{AB} = \frac{0.001\, T^{1.75} (1/M_A + 1/M_B)^{\frac{1}{2}}}{P\,[(\Sigma v)_A^{\frac{1}{3}} + (\Sigma v)_B^{\frac{1}{3}}]^2} \qquad (3.15)$$

where

D_{AB}	The binary diffusion coefficient, $cm^2\ s^{-1}$. Detailed calculation is summarized in Appendix E.
T	Temperature, K
M_A	The molecular weight of A, $g\ mol^{-1}$
M_B	The molecular weight of B, $g\ mol^{-1}$
P	Pressure, atm
Σ_v	Special parameters of diffusion volume. For CO the value is 18.9; for nitrogen the value is 17.9

Substituting known values into Equation 3.15, and then into Equation 3.13 and 3.11, the value of $D_{eff,\,1}$ may be calculated. The results of these experiments are summarized in Figure 3.22. D_{eff} values increase with the number of plates in the cordierite samples. Comparing the results with the D_{eff} of the single-plate sample (with rough surface), that of the 2-plate cordierite sample is 5.3% larger, and the 3-plate sample is 28.3% larger.

This may be caused by the difference in free volume in the two chambers, and the influence that swirl gas flow has. For the single-plate sample, which has a thickness of 0.1748 mm, this is much less than the height of the lower chamber (which is 4 mm), and so the effect of swirl flow in each chamber is similar. However, for the 3-plate sample, which has a thickness of up to 2.8 mm, this protrudes into the lower chamber and will dampen the effect of swirl flow in the lower chamber. As a result, the actual pressure in the centre of the lower chamber may be slightly higher than that in the upper chamber. This will cause a positive error.

These variations are relatively small, and it is not surprising that the value of D_{eff} varies slightly as the number of cells in the structure is increased. However, it is encouraging to see that the value for the single-plate structure is close to the 2-plate sample. This confirms that the method works. The value is also close to the value of $9.7 \times 10^{-7}\ m^2/s$

calculated with the two-dimensional model (Zhang *et al.*, 2004). By performing experiments on a 2-plate structure it is possible to calculate the value of D_{eff} in the cordierite support. This piece of information is important, as the calculation of the D_{eff} value for the washcoat (discussed in Chapters 4 and 5) will necessitate knowledge of D_{eff} in the cordierite support.

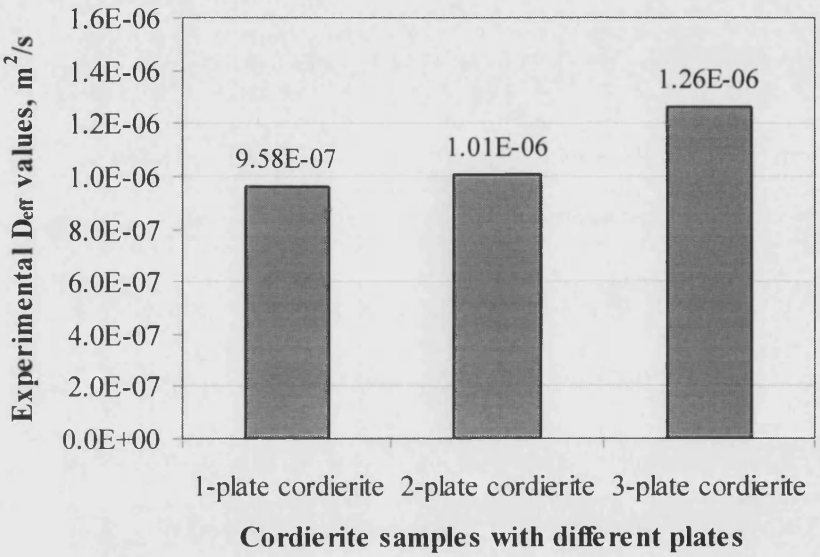

Figure 3.22 Comparison of experimental D_{eff} values in cordierite.
Exp conditions: gas flow into each chamber: 500 ml/min; pressure: 1.0600 bar (a).

3.6 Effect of operating conditions

3.6.1 Pressure in the diffusion cell

The pressure in the diffusion cell was varied from 1.06 bar (a) to 1.51 bar (a) to investigate the effect of pressure on values of effective diffusivity. Higher pressure could be measured in the rig; however, it is not necessary since the pressure in catalytic converters is only slightly higher than atmospheric.

Whilst the pressure into the diffusion cell was varied, the inlet flowrate in each chamber was still maintained at 500 ml/min (at ambient temperature and operating pressure). The results of these experiments are shown in Figure 3.23.

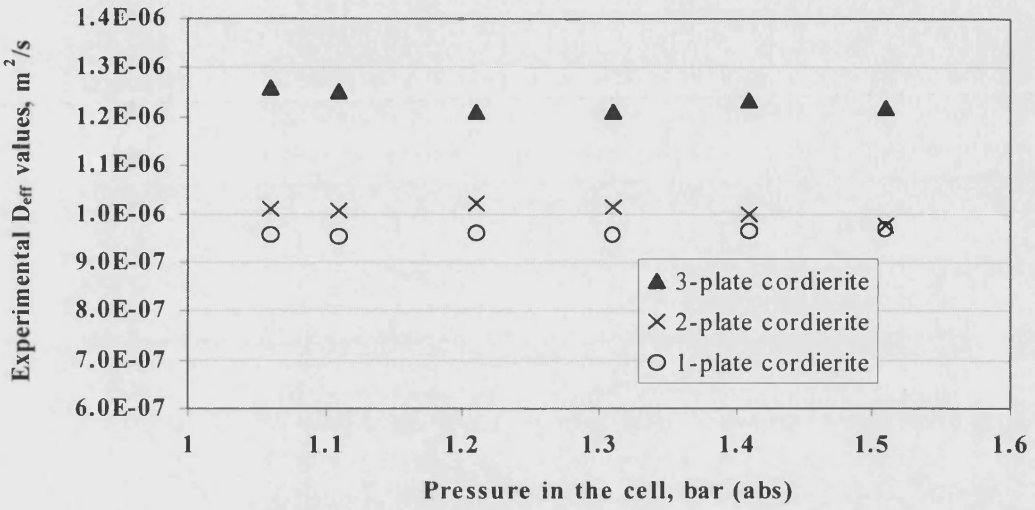

Figure 3.23 Effect of pressure in the diffusion cell on experimentally determined D_{eff} values.

Displayed inlet flowrate in each chamber was approximately 500 ml/min at conditions in the cell.

With the increase of pressure in the diffusion cell, the measured D_{eff} value decrease slightly. Since D_{eff} can be defined as a combination of D_{bulk} (diffusivity in bulk diffusion) and D_K (diffusivity in Knudsen diffusion) considering the effect of τ (tortuosity factor) and ε (porosity), the relation between P (pressure) and D_{bulk}, as well as P and D_K will reflect the relation between D_{eff} and P.

Because almost all of the pores in cordierite material have diameter more than 100 nm (see Figure 3.16), they are macropores. The diffusivity D in the macropores can be calculated from:

$$\frac{1}{D} = \frac{1}{D_{bulk}} + \frac{1}{D_K} \tag{3.16}$$

here,

$$D_{AB} = \frac{0.001\, T^{1.75} (1/M_A + 1/M_B)^{\frac{1}{2}}}{P\,[(\Sigma v)_A^{\frac{1}{3}} + (\Sigma v)_B^{\frac{1}{3}}]^2} \qquad \text{(see 3.15)}$$

and,

$$D_K = 48.5 \times d_P \sqrt{\frac{T}{M_i}} \qquad (3.17)$$

The effective diffusivity, D_{eff} is:

$$D_{eff} = \frac{\varepsilon\, D}{\tau} \qquad (3.18)$$

In Equations 3.14 to 3.18, the following factors: φ, T, M, $(\Sigma v)_A$, $(\Sigma v)_B$, d_P, ε and τ, are independent of pressure. D_K is therefore independent of pressure, and D_{bulk} will be inversely proportion to pressure. This means that D_{eff} would be expected to decrease with pressure. This was observed, however, the trend is small. Hou *et al.* (1999) performed measurement in porous catalyst pellets at pressures from 1 to 10 bars. Their results also show that the measured D_{eff} values decrease monotonically with pressure.

In the cordierite materials used in the measurement, although the mean pores diameter is up to 3.4 microns (see Table 3.2), pores whose diameter is less than 250 nm hardly exist (this mean macro pores predominate, see Figure 3.16). Because the value of D_{bulk} is normally about 20 times higher than that of D_K, then according to Equation 3.16, the value of D_{eff} will be close to the value of D_K. With the increase of pressure in the diffusion cell from 1.06 bar (abs) to 1.51 bar (abs), the value of D_{bulk} will decrease by about 28% (calculated from Equation 3.15). Because the pressure increase does not affect the value of D_K, then the value of D_{eff} will only decrease by 1.7% (calculated from Equation 3.16). This value is very close to the decrease observed in D_{eff}, which is 1.8%.

3.6.2 Inlet gas flowrate

The inlet gas was varied from 200 to 800 ml/min (at experimental conditions). The same flowrate was maintained in the lower and upper chambers. Pressure in each chamber was maintained at 1.0600 ± 0.0001 bar (a). The measurements were performed for both single-plate and multi-plate cordierite samples.

The measured D_{eff} values of single-plate and multi-plate rough-surface cordierite samples are shown in Figure 3.24. Below 500 ml/min, D_{eff} values increase with gas inlet flowrate. Above 500 ml/min, D_{eff} values are relatively independent of the inlet gas flowrate. This was also observed for the single-plate smooth-surface cordierite sample discussed earlier and shown in Figure 3.17. At gas inlet flows above 500 ml/min, mass transfer between the gas and the surface of the sample is not a significant resistance.

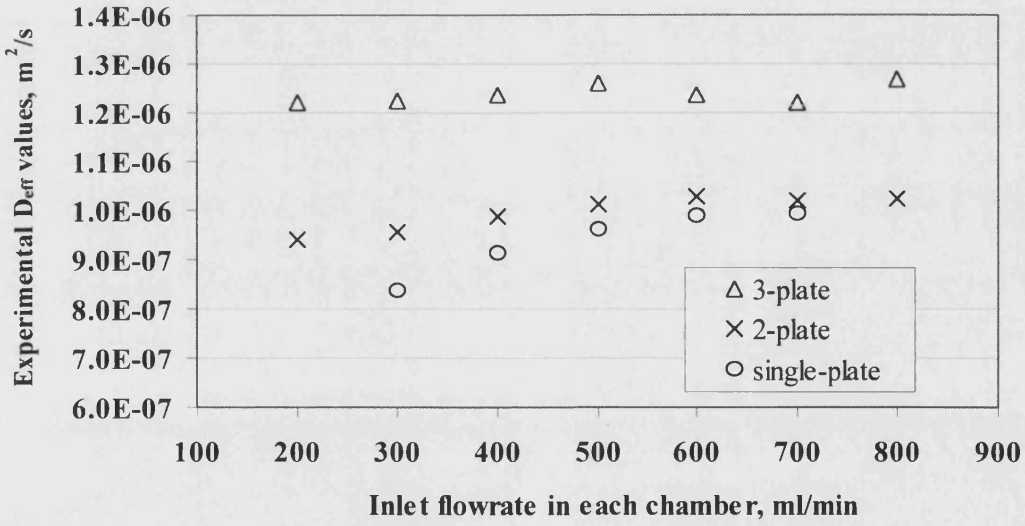

Figure 3.24 Effect of gas inlet flowrate in each chamber on experimentally determined D_{eff} values for the rough-surface cordierite plates.

The pressure in the cell was 1.0600 bar (a).

3.7 Estimation of tortuosity factor

Tortuosity factor, τ, is used to account for the tortuous nature of the pores in porous solid. It cannot be measured directly but can be back-calculated (Hayes *et al.*, 2000). From the parallel-pore model described by Wheeler (1955), for a mono-disperse material, then

$$D_{eff} = \frac{\varepsilon \times D}{\tau} \tag{3.19}$$

From Equation 3.19, the tortuosity factor (τ) can be obtained:

$$\tau = \frac{\varepsilon \times D}{D_{eff}} \tag{3.20}$$

Here ε is the overall porosity and D is the combination of the bulk diffusivity D_{bulk} and Knudsen diffusivities D_K (see Equation 3.16). In the cordierite material, only macropores are present (see Figure 3.16), therefore $D = D_M$, and this is calculated from Equation 3.21.

$$\frac{1}{D_M} = \frac{1}{D_{bulk}} + \frac{1}{(D_K)_M} \tag{3.21}$$

where D_M is the diffusion coefficients in the macropores.

The bulk diffusivity in the uncoated cordierite at 17.4 °C and 1.06 bar (a), can be calculated from Equation 3.15:

$$D_{bulk} = \frac{0.001T^{1.75}(1/M_A + 1/M_B)^{\frac{1}{2}}}{P[(\Sigma v)_A^{\frac{1}{3}} + (\Sigma v)_B^{\frac{1}{3}}]^2} \qquad \text{See (3.15)}$$

$$= \frac{0.001\times(17.4+273.15)\times(\frac{1}{28}+\frac{1}{28})^{\frac{1}{2}}}{\frac{1.06\times10^5}{101325}(18.9^{\frac{1}{3}}+17.9^{\frac{1}{3}})^2}$$

$$=0.187\ (cm^2\,s^{-1})$$

$$=1.87\times10^{-5}\ (m^2\,s^{-1})$$

Under the same condition, Knudsen diffusivity in the uncoated cordierite can be calculated from Equation 3.17. The value of d_p is chosen from "Median pore diameter (area)" in Table 3.2.

$$D_K = 48.5\times d_P\sqrt{\frac{T}{M_i}} \qquad \text{See (3.17)}$$

$$=48.5\times1.6283\times10^{-6}\times\sqrt{\frac{(17.4+273.15)}{28}}$$

$$=2.54\times10^{-4}\ m^2s^{-1}$$

From Equation 3.21 the combination of D_{bulk} and D_K can be calculated:

$$D=D_M=\frac{D_{bulk}\times D_K}{D_{bulk}+D_K} \qquad \text{See (3.21)}$$

$$=\frac{(1.87\times10^{-5}\ m^2\,s^{-1})\times(2.54\times10^{-4}\ m^2\,s^{-1})}{(1.87\times10^{-5}\ m^2\,s^{-1})+(2.54\times10^{-4}\ m^2\,s^{-1})}$$

$$=1.75\times10^{-5}\ (m^2\,s^{-1})$$

The overall porosity (ε) has been measured (the value is 0.343715, see Table 3.2. The effective diffusivity in 1-plate rough-surface cordierite is $(9.58 \pm 0.49) \times 10^{-7}$ m^2 s^{-1} (see Figure 3.22). Using Equation 3.20, the tortuosity factor (τ) is now computed:

$$\tau = \frac{\varepsilon \times D}{D_{eff}} \qquad \text{See (3.20)}$$

$$= \frac{0.343715 \times 1.75 \times 10^{-5}\ (m^2\ s^{-1})}{(9.58 \pm 0.49) \times 10^{-7}\ (m^2\ s^{-1})}$$

$$= 6.26 \mp 0.34$$

So the tortuosity factor in the 1-plate rough-surface cordierite is 6.26 ± 0.34. This value is close to some values obtained from diffusion experiments for methane-nitrogen in cordierite, *e.g.* 5.1 ± 0.5 in Kim (2001), and 8.5 in Li (1997). In general, the tortuosity factors for commercial catalysts and supports are between 3 and 7.5 (Satterfield, 1970).

3.8 Analysis of experimental errors

Experimental errors may arise from a number of sources and these are discussed in the following subsections.

3.8.1 Errors from the equipment

Rotameters

The rotameters were calibrated with a bubble flow meter, and the errors of this measurement were ± 0.2% of the flowrate. Also, fluctuations of the conical metal buoy create reading errors which could be up to 5 ml/min (about 1.0% of displayed flowrates).

CO analyser

Errors arise from the zero point drifting and the span point drifting. The drift can be as high as 2 ppm in one hour. Errors caused by instrument drift are about 1.0% of the CO reading.

3.8.2 Errors arising from the operation of the experiment

Room temperature

During the courses of an experiment the room temperature can vary between 15.1 to 19.6 °C (or 288.3 to 292.8 K). This can affect the bulk diffusion coefficient of CO, by varying it from 1.913×10^{-5} cm^2/s to 1.958×10^{-5} cm^2/s (an increase of 2.4%). Similarly the Knudsen diffusivity could increase by 0.8%. Since effective diffusivity is a combination of bulk diffusion and Knudsen diffusion, the measurement errors in D_{eff} would be no more than 2.4%.

Inlet flowrate differential between the chambers

Although it was endeavoured to maintain an equal flowrate of gas into the upper and lower chambers, a few difference of up to 10 ml/min could occur. Figure 3.25 shows the effect of the difference between the two inlet flowrates on calculated values of D_{eff}. The effect at ± 10 ml/min causes an error of ± 1.0%.

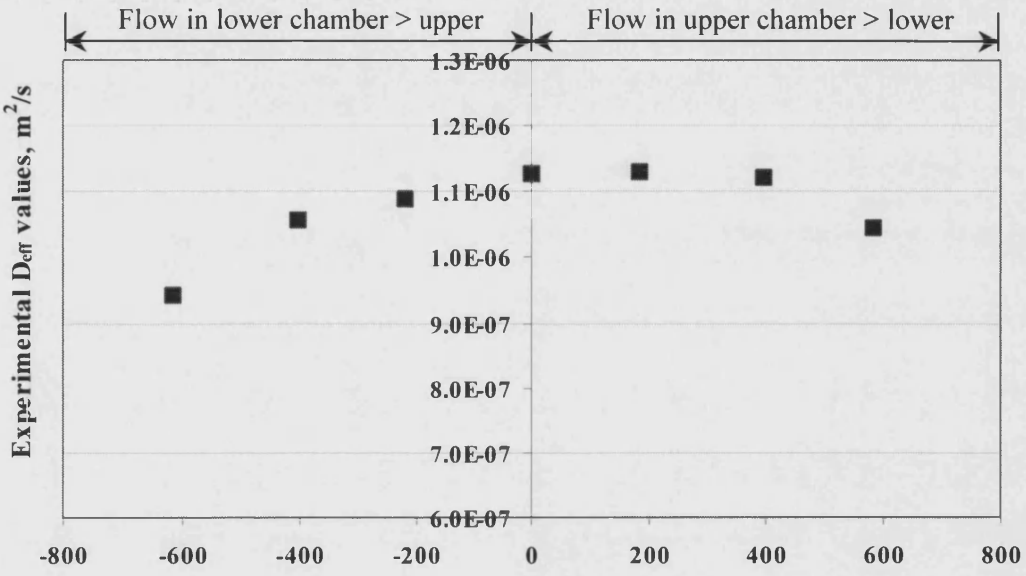

Figure 3.25 Experimental D_{eff} values when gas flow is different in the upper and lower chambers.

Experiments performed with Sample BC0C-1 (single-plate cordierite with smooth surface sample).

Pressure differential across the sample

The objective was to maintain a zero pressure difference across the sample. Two digital pressure indicators displayed the pressure in each chamber. The accuracy of the pressure indicators is ± 0.0001 bar. The pressure differential between the two chambers was measured with a differential pressure transducer. The accuracy of the transducer is ± 0.0002 bar. The effect of pressure differential on experimental measurements and hence the calculated D_{eff} values is shown in Figure 3.26, and it is clearly significant. Even if the pressure differential is as low as ± 0.2 mbar, the errors in D_{eff} will be as high

as 5%. By maintaining the pressure difference within ± 0.1 mbar, the error in D_{eff} is ± 2.0%.

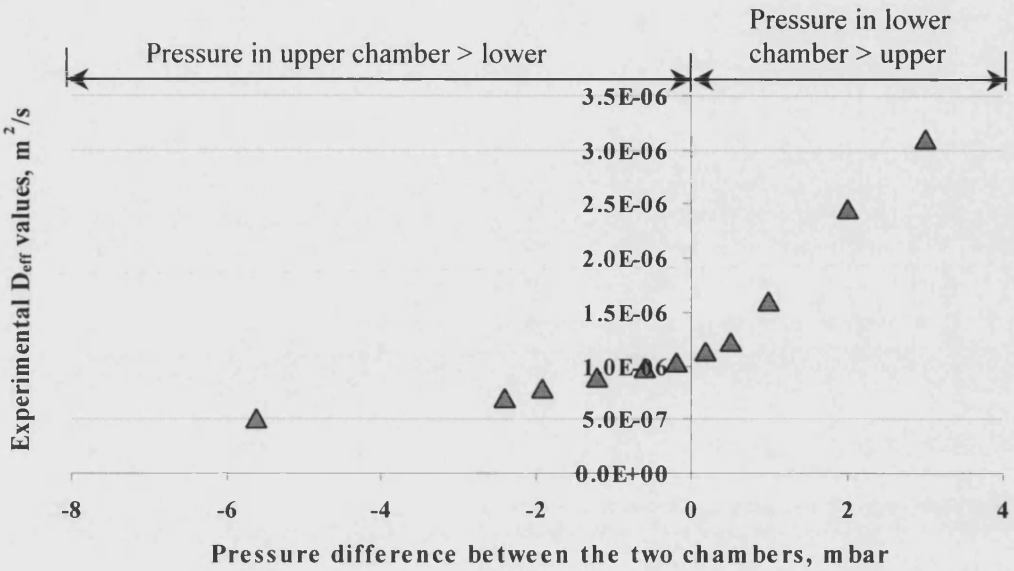

Figure 3.26 Effect of pressure difference between the two chambers.

Experiments performed with Sample BC0C-1 (single-plate cordierite with smooth surface).

It should be noted that in each chamber, the pressure near the inlet points will not be exactly the same as that in the centre of the diffusion cell. This may be due to the effect of swirl gas flow, which is fed into the chambers through the nozzles positioned in a tangential direction, see Figure 3.4. At the maximum flowrate (800 ml/min), the velocity of gas in the 1/8" stainless steel tubes (with 0.028" wall thickness) is 5.53 m/s, and this will create a small pressure difference (measured accurately by the two pressure transducers). However, as the upper chamber is exactly the same as the lower chamber, and the gas flowrate into the upper chamber is maintained the same as that into the lower one, the error caused by swirl gas flow can be minimized.

3.8.3 Errors from the preparation and characterization of the samples

Diffusion area

When calculating the D_{eff} values, it is assumed that diffusion area is same as the area of the hole in the centre of the copper support. This is 78.54 mm^2, and if the epoxy has covered an additional area of 2 mm^2, this can result in an error (in D_{eff}) of -2.5%.

To minimise the potential problems illustrated in Figure 3.27, the following methods were employed:

1. The epoxy resin is coated onto the surface of cordierite samples while the epoxy resin is becoming viscid, about 30 to 90 seconds before it starts to solidify.

2. The epoxy resin is applied quickly and evenly with a soft plastic rod whose diameter is less than 1 mm.

3. To keep the concentricity of the epoxy resin even on the two sides of the samples, another copper support is used to be as a mould. The mould's outer diameter is 40 mm, with an 11.0 mm diameter hole in the centre. Using the mould, it is easy to draw a 10.0 mm diameter circle on the cordierite sample with a pencil, and this is used to designate the section of the sample which must not be covered with resin.

Thickness of cordierite plate

The thickness of the samples was measured by SEM using the JEOL JSM-T330 Scanning Microscope, and the JEOL SEM 6310. Errors may arise from the presence of barrel-like deformation of the image at high magnification (see Figure 3.28). For smooth surface samples, additional errors may occur because the thickness of ground surface may be uneven. The thickness of the sample will be represented by its average thickness (see Figure 3.29).

The measured thickness for the rough-surface cordierite samples lie in the range of 174.8 ± 5.6 microns, which may cause a ± 3.2% error in D_{eff}. For the smooth-surface cordierite samples, the thickness is 162.0 ± 4.2 microns, which may cause an error of ± 2.6% in D_{eff}.

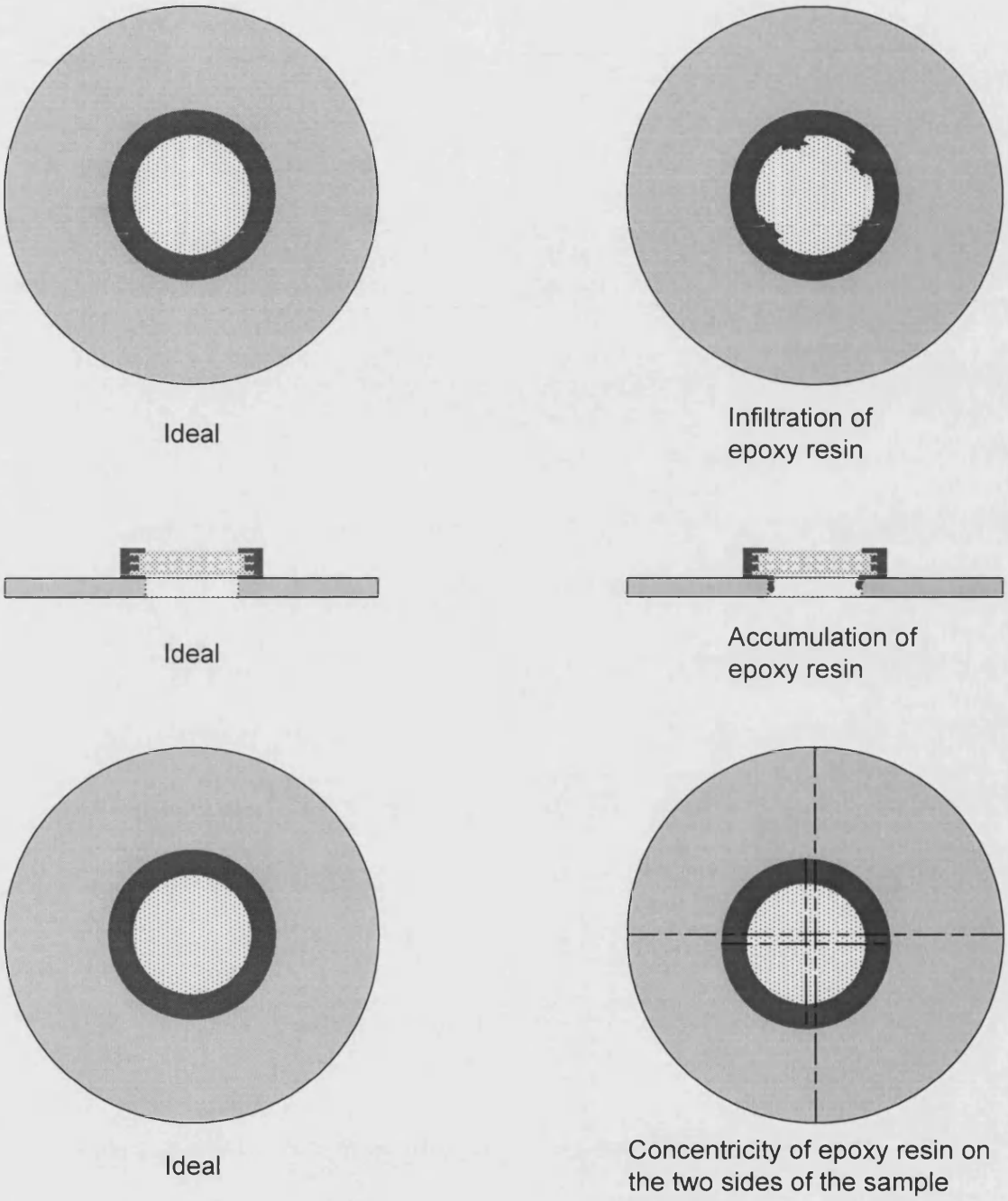

Figure 3.27 Potential problems that can cause errors as the sample is fixed to the copper plate.

Figure 3.28 Barrel-like deformation of image in SEM.

Left: ideal cross image of cordierite;
Right: barrel-like deformation (enlarged). This may occur when the magnification is more than 200 times.

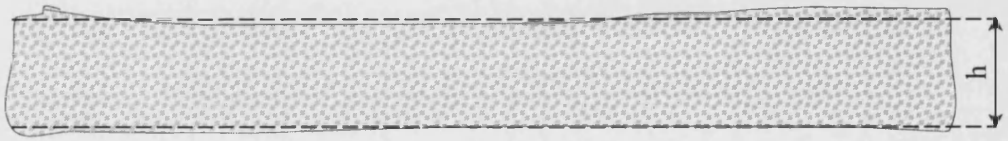

Figure 3.29 Uneven thickness of ground-smooth surface sample.

The thickness of the sample is represented by "h" when calculating D_{eff}.

Table 3.3 lists the possible effects of the above errors on the measured D_{eff} values. Because systematic errors occur on all the measured samples, and accidental errors can be minimized by repeating the measurements for a few times, the measured D_{eff} values are still suitable for comparison purpose.

Table 3.3 Impact the experimental errors may have on D_{eff} values.

Error resource	Type	Error in D_{eff} Range	Occurring on
Rotameters	Systematic error	± 1.0%	All samples
	Accidental error	± 0.5%	All samples
CO analyser	Systematic error	± 1.0%	All samples
Room temperature variation	Accidental error	± 2.4%	All samples
Flowrate differential	Accidental error	± 1.0%	Some samples
Pressure differential	Accidental error	± 2.0%	Some samples
Diffusion area	Accidental error	0% to −2.5%	Some samples
Thickness	Accidental error	± 3.2%	Some samples

3.9 Conclusions

From this experimental study, the following conclusions have been drawn:

1. A modified Wicke-Kallenbach diffusion cell is suitable for the measurement of effective diffusivity of cordierite samples, either for one-plate, two-plate or three-plate samples. For this diffusion cell and the measurement rig, the suitable operating conditions are as follows:

   Temperature: room temperature (17.4 ± 2.3 °C);

   Pressure in the cell: 1.01 to 1.51 bar (a);

   Gas inlet flowrate: 500 to 800 ml/min (measured at room temperature, and atmosphere pressure);

   Gases inlet directions: pure nitrogen from the two side-inlet points in the upper chamber; 2.4% CO (balanced by nitrogen) from the two side-inlet points in the lower chamber;

   Position of sample: always in the lower chamber and always facing down.

2. At the above operating conditions, the experimental D_{eff} values in cordierite samples are as follows:

   $(11.33 \pm 0.37) \times 10^{-7}$ m^2/s for 1-plate smooth-surface cordierite;

   $(9.58 \pm 0.49) \times 10^{-7}$ m^2/s is for 1-plate rough-surface cordierite;

   $(10.19 \pm 0.29) \times 10^{-7}$ m^2/s for 2-plate rough-surface cordierite;

   $(12.42 \pm 0.11) \times 10^{-7}$ m^2/s for 3-plate rough-surface cordierite.

These experimental values are close to the D_{eff} value of methane in cordierite, $(9.2 \pm 3.8) \times 10^{-7}$, see Hayes and Kolaczkowski (2000).

3. The back-calculated tortuosity value, τ, in the 1-plate rough-surface cordierite is 6.26 ± 0.34, which lies within the range of published data on similar materials.

4. The measured D_{eff} value of the 1-plate smooth-surface cordierite sample is about 17% greater than that of 1-plate rough-surface cordierite.

5. Experimentally determined D_{eff} values vary slightly with the operating pressure.

6. As gas inlet flowrate is increased above 500 ml/min (at experimental conditions), the D_{eff} values remain constant.

7. Although the average pore diameter of cordierite is 3.4 microns, Knudsen diffusion appears to be the dominant mode of diffusion through the cordierite.

Chapter 4 The measurement of D_{eff} of CO in cordierite plates coated with commercially-produced slurries

In this chapter, experiments are performed on cordierite plates that have been coated with a commercially-produced slurry. These coated samples were calcined at the same condition as a commercial DOC (diesel-oxidation converter). Measurements are taken both with and without the presence of Pt in the washcoat, and with a fresh and an aged sample of catalyst.

The experimental method and techniques used to evaluate the effective diffusivity are similar to those describe in Chapter 3. In addition, values of effective diffusivity for the blank (uncoated) cordierite plate determined in Chapter 3 are used in this new chapter.

4.1 Cordierite plates coated with a commercial slurry

The slurries used for these experiments were supplied by a catalyst manufacture. The cordierite plates were prepared in three different ways as described in Table 4.1.

Table 4.1 Description of coated cordierite plates with different commercial slurries

Samples reference	Description
S3	Blank cordierite plates coated with Slurry 3 which includes 3.18 g/L Pt, calcined at 500 °C for 3 hours in air.
S3w	Blank cordierite plate coated with Slurry 3 without catalyst, calcined at 500 °C for 3 hours in air.
S3HT	Sample S3 was re-calcined at 700 °C for 16 hours in 10% H_2O + 10% O_2 + 80% N_2.

(a) Effect of Pt catalyst: To investigate what effect the presence of Pt catalyst in the slurry may have on the effective diffusivity, two different slurries were used. One (Sample S3) contained the Pt catalyst; the other (named as Sample S3w) had no catalyst.

(b) Effect of washcoat thickness: To investigate the effect of washcoat thickness, more than 18 pieces of Sample S3 were prepared. The washcoat thickness of these samples varied from about 40 to 180 microns.

(c) Effect of calcination temperature/ageing: To investigate the effect of ageing, sample S3HT was calcined at a higher temperature of 700 °C in the presence of water vapour. These conditions were deemed to be appropriate by the manufacture of the auto-catalyst to represent an aged catalyst.

Figure 4.1 outlines the experimental procedure and the links between the experiments in this chapter.

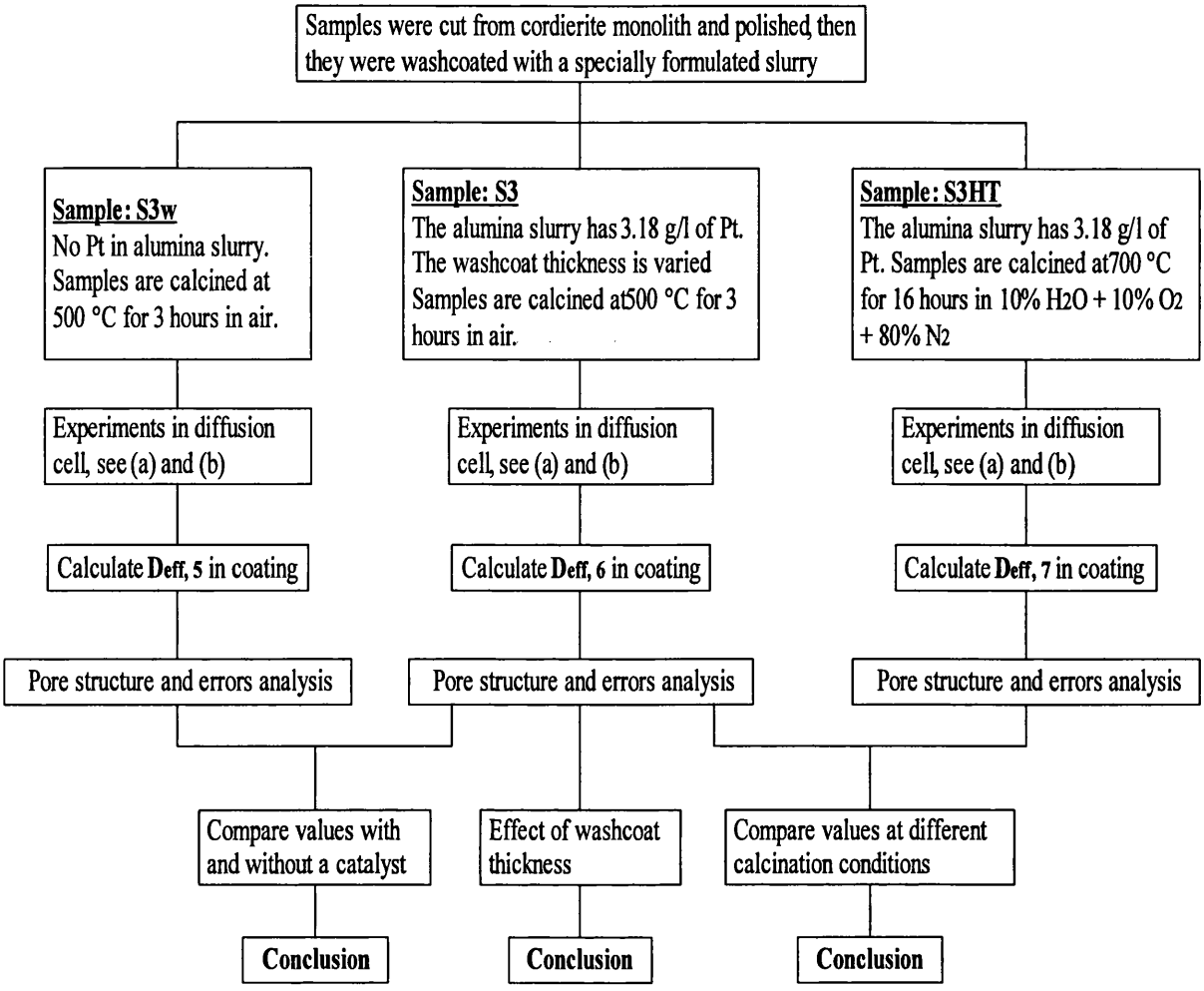

Figure 4.1 Outline of the experimental procedure and the links between the experiments in Chapter 4.

Notes:

(a) Experimental conditions for the diffusion cell were maintained the same as in Chapter 3;

(b) Values of $\mathbf{D_{eff,1}}$, determined for the blank (uncoated) cordierite plate with smooth surface (in Chapter 3) is used in the calculation of $\mathbf{D_{eff}}$ in the coated layer.

4.1.1 Preparation of the coated plates

Cordierite plates were cut following the same procedure as described earlier in Chapter 3. These were cut from a 400-cpsi blank (uncoated) monolith and ground with an electric mill to obtain a smooth surface. Each smooth-surface cordierite plate weighed about 0.4 g, and its dimensions were about 40 mm × 40 mm and 0.162 mm thick.

To coat the slurry onto the surface of the plates, many different methods were tried, including: spraying of the slurry onto the plates with a compressed-air "gun"; painting the slurry with a brush; dropping plates into the slurry and then blowing. However, some of the methods failed either because the slurry was too thick, or the cordierite plates fractured as they were very fragile. Finally, the following procedure was used, which was applied to prepare sample S3, S3w and S3HT. The method is also illustrated in Figure 4.2.

1. Weigh the smooth-surface cordierite plate and then wet the surface with water.
2. Drop about 0.5 ml of the slurry onto the cordierite plate.
3. Scrape the slurry using a metal block to make a uniform layer.
4. Dry the sample at room temperature for about 60 minutes.
5. Weigh the sample again to calculate the weight of washcoat. Assuming that the washcoat has a bulk density of 3.41 g/cm^3 (Kim, 2001), estimate the thickness of the washcoat. Repeat Step 2 to 4 until the desired thickness of washcoat has been achieved.
6. Calcine the sample by heating from room temperature to 500 °C at a rate of 2.5 °C/min; then maintaining at 500 °C for 4 hours; then allow the sample to cool until it reaches room temperature. Some plates taken from Sample S3 were then re-calcined at 700 °C for 16 hours in 10% H_2O + 10% O_2 + 80% N_2. These are labelled as S3HT.
7. Cut by hand a circular plate (approximately 14 mm in diameter) from the centre of the plate.
8. Use an epoxy resin to stick the circular plate onto the surface of an annular ring of copper (outer diameter = 50 mm, inner diameter = 10 mm, thickness = 1 mm). Fixing the smooth uncoated surface of the cordierite onto the copper support leaving the washcoat layer exposed. Wait for at least 24 hours at room temperature to allow the epoxy to solidify. Then apply more epoxy around the sides of the washcoated surface leaving a 10 mm diameter circle free. This procedure is the same as that followed in Chapter 3.

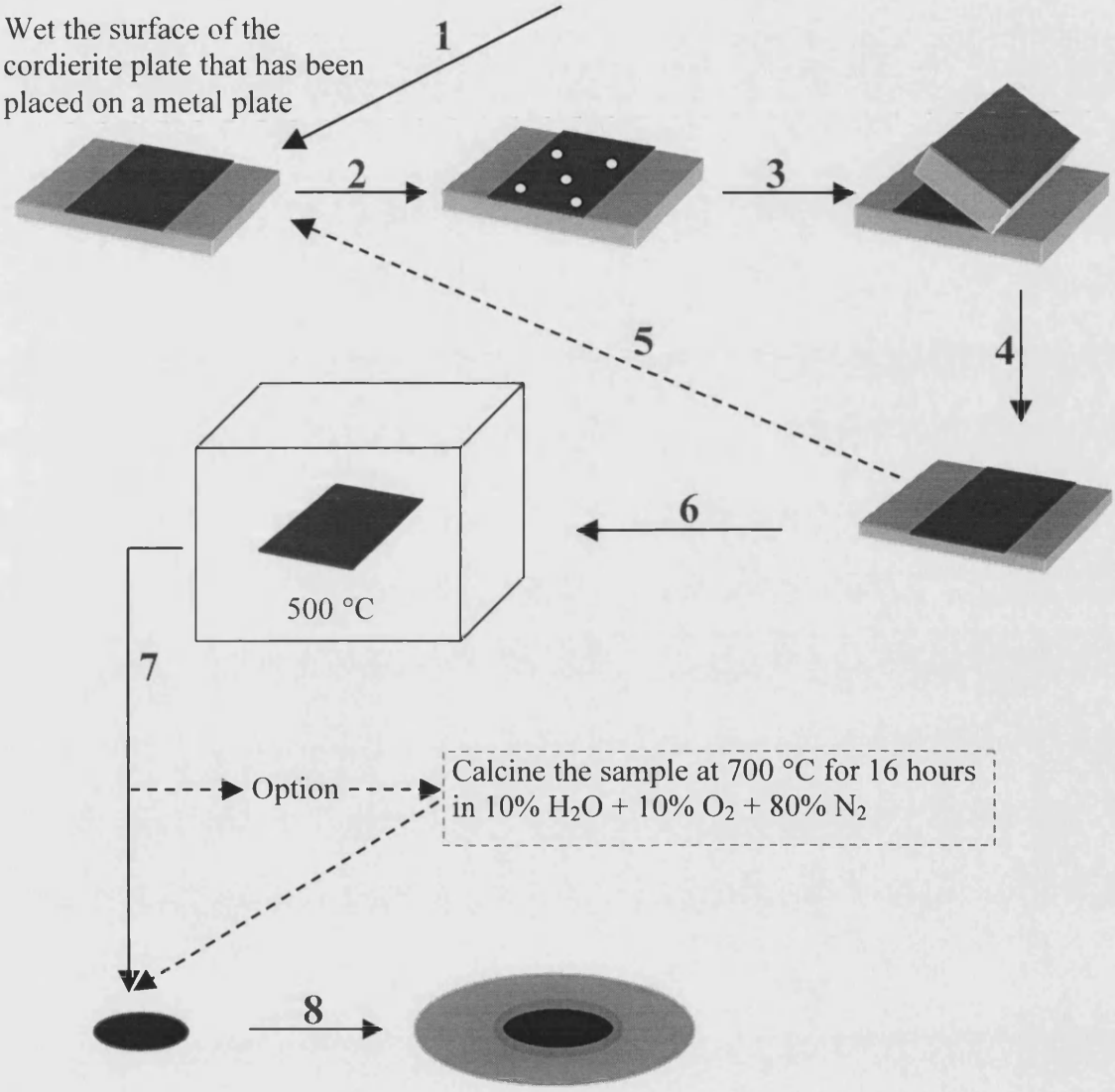

Figure 4.2 The method used to apply a specially formulated slurry onto the cordierite plate.

From Figure 4.3, it can be seen that the visual appearance of the three samples are different. Sample S3 is a dark-grey colour, whereas Sample S3w (which does not contain catalyst) is a light-yellow. Sample S3HT, which has been aged, is dark.

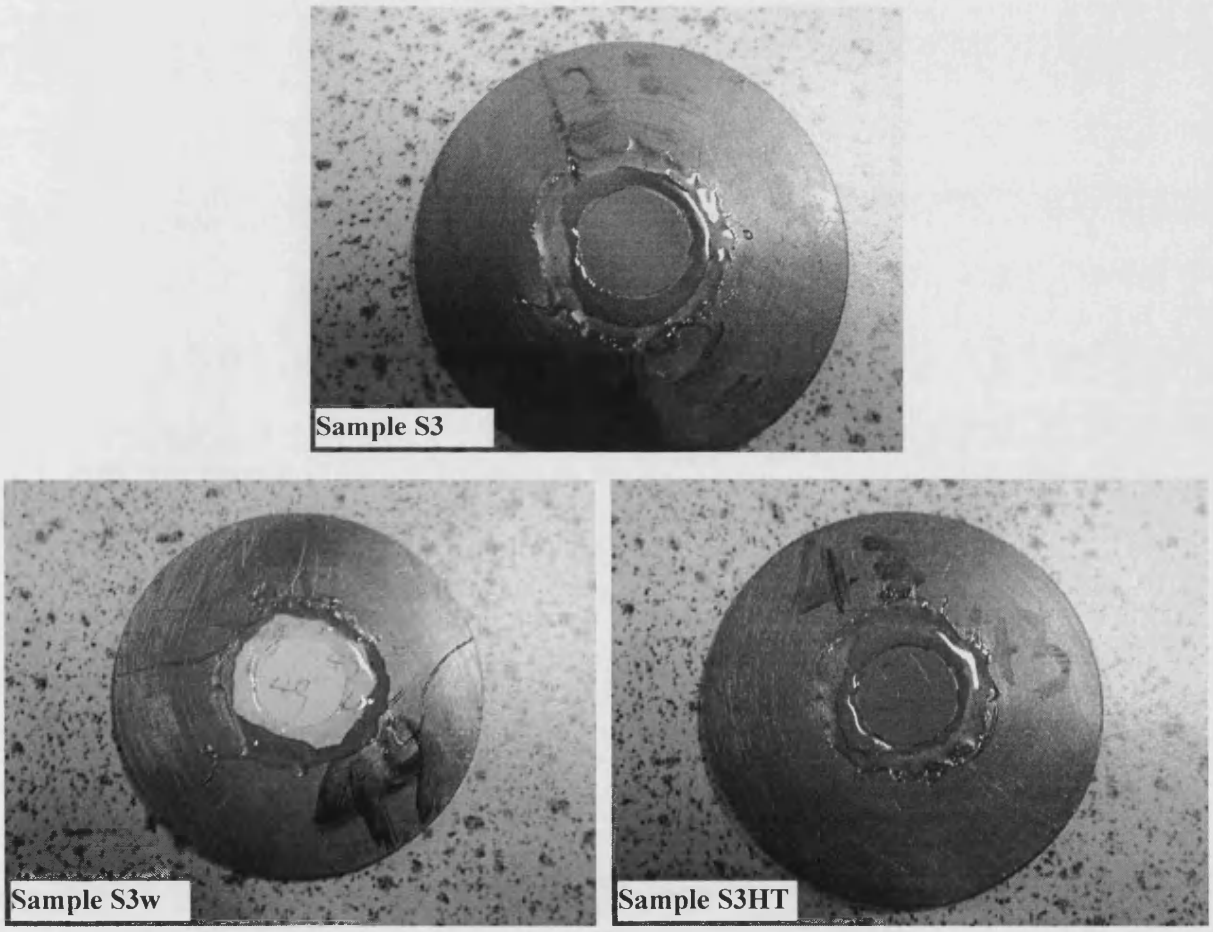

Figure 4.3 Photos of the washcoated cordierite plates that have been fixed to copper rings with epoxy resin.

4.2 Characterisation of the coated plates

All of the samples were characterized by SEM to measure the thickness of cordierite and the washcoat layer. Looking at the top layers (washcoat Layer 1) in Figure 4.4, the boundary between the washcoat and cordierite layer can be seen clearly. However, there is no apparent boundary in the washcoat, although it was coated and dried at least two times to achieve the final thickness before being calcined.

Looking at the lower side of the samples in Figure 4.4, there is a very thin washcoat layer (washcoat Layer 2). This thin layer was formed by the slurry percolating through the pores in the cordierite plate when the first washcoat layer was coated. During the percolation process, some pores in cordierite were fully or partially filled with washcoat. This can be clearly seen in Figure 4.4 (for Sample S3HT). The percolated slurry is thinner than the main slurry (this means that the cordierite has acted like a filter), because the washcoat Layer 2 is very thin (only a few microns) and very even.

Even though the "unintended" washcoat layer (washcoat Layer 2) is thin, it should not be ignored. When calculating the thickness of the washcoat, the combined thickness of the two washcoat layers is considered.

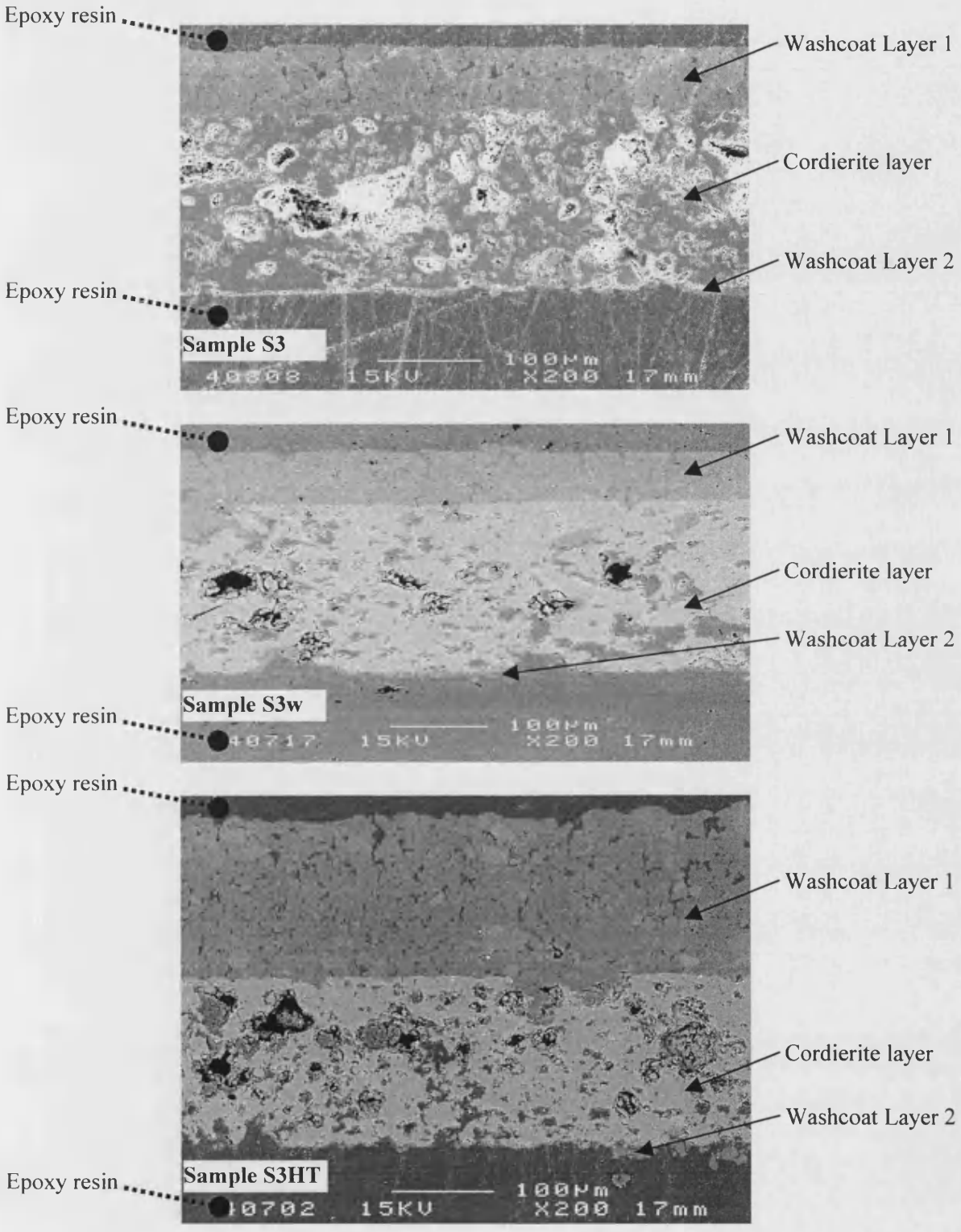

Figure 4.4 SEM photos of washcoated cordierite samples set in epoxy resin.

Pore size and volume distribution measurements were made on coated samples using ASAP and Mercury penetration methods at University College London. By subtracting the contribution of cordierite (see Figure 3.16 in Chapter 3), the pore size and pore volume distribution of washcoat can be obtained. The results are shown in Figures 4.5, 4.6, and 4.7, and additional information is listed in Table 4.2 and Appendix B2. The washcoat in Sample S3 has a bi-dispersed pore structure, which includes both macropores and mesopores. The mean diameter of the former is 104.5 nm (volume-based) whereas the latter is only 16.1 nm (BJH adsorption-based). Most of the pores have a diameter in the range of 10 to 50 nm. Compared to the pores in a cordierite support (whose mean diameter is 3404.5 nm, volume-based), the main pores in the washcoat in Sample S3 are much smaller.

Higher-temperature calcinations do not change the pore structure too much. This can be proven by comparing Figure 4.5 and Figure 4.7 and the data in Table 4.2. After 16-hour calcination at 700 °C in the presence of (10% H_2O + 10% O_2), the pore size distribution in the washcoat does not changed obviously. S3HT still has the same bi-dispersed structure. The diameter of most pores of washcoat in Sample S3HT is in the range of 10 to 50 nm. It should be pointed out that the pore diameter in Sample S3HT is about 7.5% larger (BJH adsorption-based) than that in Sample S3. This means that at higher temperatures, the presence of oxygen and water vapour enlarges the pores in the washcoat. As a result, the total pore area in Sample S3HT decreases by 3.2%, to 53.4 m^2/g.

By comparing S3 with S3w, it can be seen that the main effect of adding catalyst is to reduce the diameter of the pores by about 15.4% and also to increase the total pore area and total intrusion volume (see Figure 4.5, Figure 4.6, and Table 4.2).

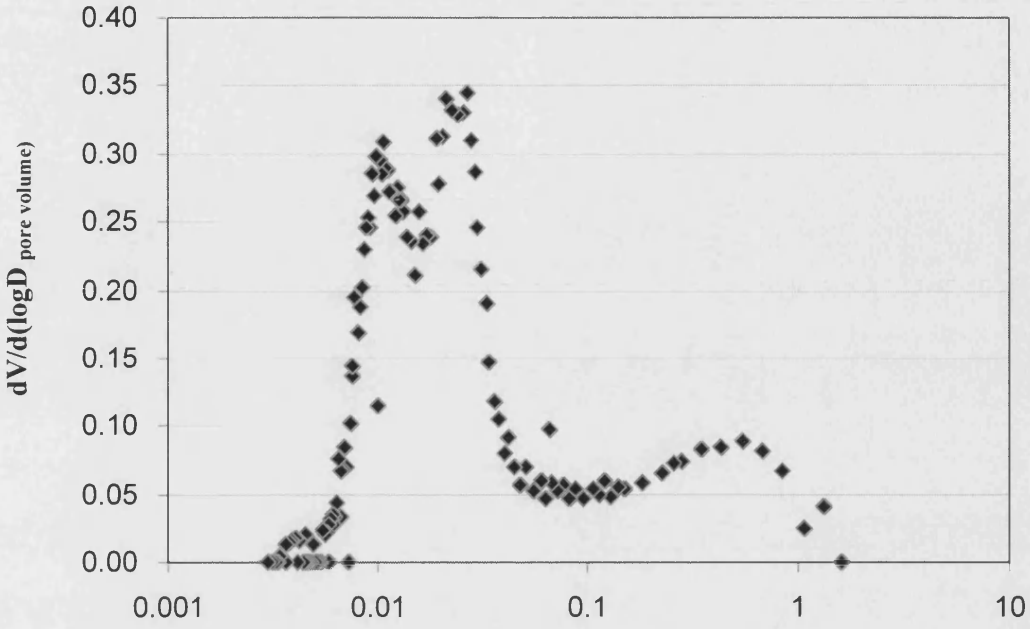

Figure 4.5 Pore size distribution of washcoat S3.

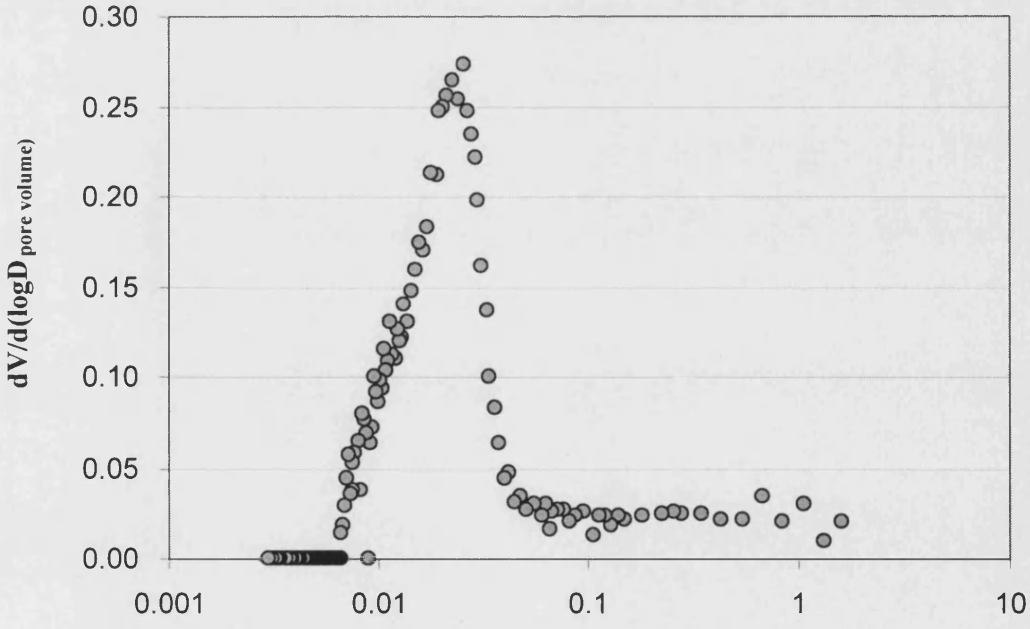

Figure 4.6 Pore size distribution of washcoat S3w.

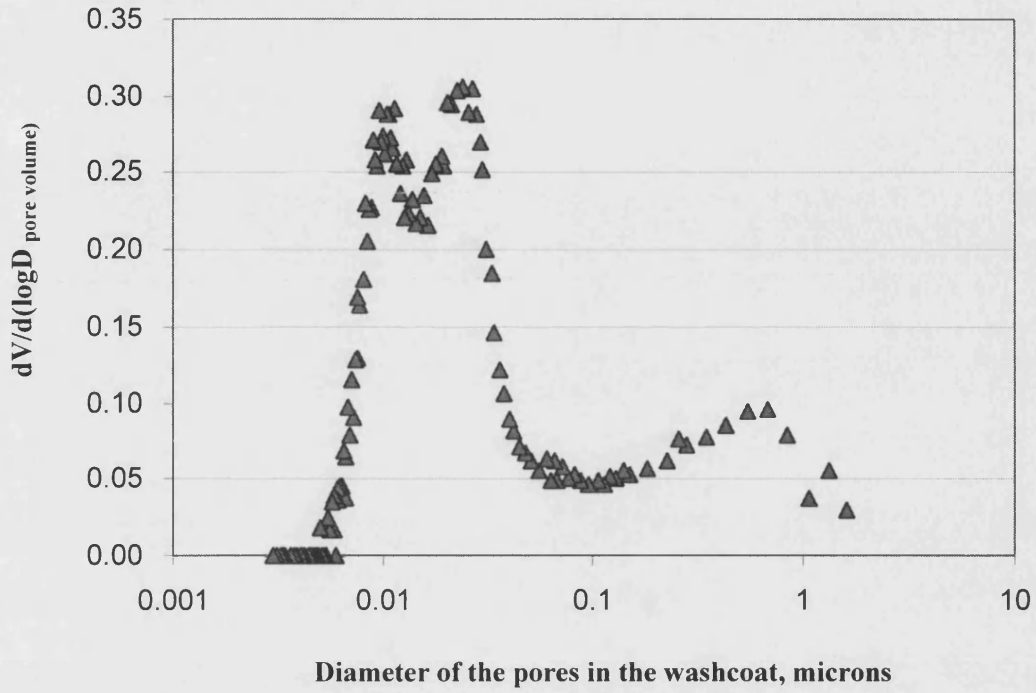

Figure 4.7 Pore size distribution of washcoat S3HT.

Table 4.2 Summary of the properties of the washcoated cordierite.

Properties	S3	S3w	S3HT
Area from ASAP analysis			
BET surface area, m^2/g	69.1458	38.0195	61.4610
Micropore area, m^2/g	21.6349	13.9079	18.7089
Volume from ASAP analysis			
Micropore volume, cm^3/g	0.011396	0.007390	0.009776
Pore size from ASAP analysis			
BJH adsorption average pore diameter (4V/A), Å	161.2548	190.6710	173.0489
BJH desorption average pore diameter (4V/A), Å	139.9434	175.7634	139.8197
Intrusion data from Micromeritics			
Total intrusion volume, ml/g	0.4314	0.3094	0.4317
Total pore area, m^2/g	55.138	27.236	53.365
Median pore diameter (volume), μm	0.1045	0.8284	0.1492
Median pore diameter (area), μm	0.0126	0.0171	0.0123
Bulk density at 0.10 psia, g/ml	1.2203	1.4271	1.2249
Apparent (skeletal) density, g/ml	2.5777	2.5555	2.6001
Porosity, %	52.6526	44.1540	52.8867

4.3 Experimental results for coated cordierite plates

The experimental data gathered during the course of this series of experiments are presented in Appendix D2. The principles behind the calculation have already been described in Section 3.5.

From Equation 3.11, then for the composite structure:

$$\frac{L_{total}}{D_{eff,total}} = \frac{L_{bc}}{D_{eff,c}} + \frac{L_w}{D_{eff,w}} \tag{4.1}$$

From this equation, as L_{total}, $D_{eff,\,total}$, L_{bc}, $D_{eff,\,c}$ and L_w are known, then the value of $D_{eff,\,w}$ can be calculated. An example calculation is presented in Appendix C.

4.4 Analysis of errors

Besides the errors discussed in Section 3.8 in Chapter 3, additional sources of errors arise in this experiment.

4.4.1 Errors caused by the method used to prepare the samples

Despite the effort to achieve a uniform washcoat layer, the thickness of the coated plate may vary by ± 3.0 microns, see Figures 4.4 and 4.8. The thinner the washcoat is, the larger the relative error will be. For example, if the washcoat thickness is 180 ± 3 microns, the error caused by the variation in thickness will be ± 1.7% in the determined value of $D_{eff,\,t}$. When calculating the D_{eff} values, an average value from at least 3 test points for each plate is used.

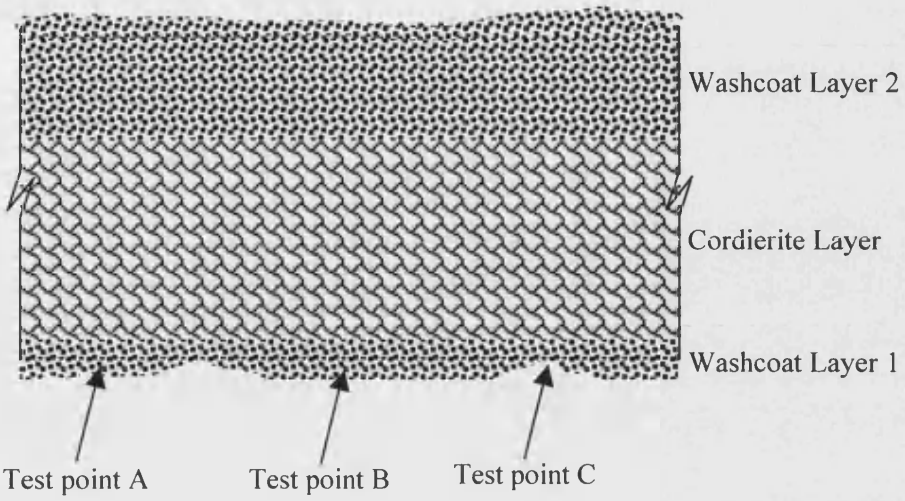

Figure 4.8 Error caused by an uneven surface of washcoat.

4.4.2 Errors caused by the calculation method

Having established a value of $D_{eff,\,t}$ for the composite structure, the contribution of the cordierite plate is considered and then the value of $D_{eff,\,w}$ is obtained. If the error described in Section 4.4.1 is considered, then its impact on the value of $D_{eff,\,w}$ is ± 3.1%.

4.5 Discussions of results

4.5.1 The effect of washcoat thickness

The experimental D_{eff} values of CO in the washcoat from Slurry S3 lie in the range of 3.71×10^{-7} to 11.97×10^{-7} m^2/s for the measured samples. It is interesting to observe that the D_{eff} values appear to increase in a linear manner with the thickness of the washcoat when the thickness is less than 200 μm. The relation between the thickness of the washcoat and the experimental D_{eff} values may be expressed by:

$$D_{eff,\,w} = 4.89 \times 10^{-3}\, L_w \ (m^2\, s^{-1}) \qquad (\text{when } L_w < 2\times10^{-4}\ m) \qquad (4.2)$$

If the thickness of washcoat is thicker than 200 μm, the curve exhibits on exponential form, that approaches an asymptote, see Figure 4.9.

One reason for the variation of measured $D_{eff,\,w}$ is that the macropores in the cordierite support become filled with impregnated washcoat (see Figure 4.4). This will increase the diffusion resistance in the cordierite, as can be seen from the extrapolated value of $D_{eff,\,w}$ when $L_w = 0$. The impregnated washcoat can be considered as "an interface layer" between the cordierite and the washcoat (although it is inside the cordierite layer). Clearly, the interface layer is increasing the total diffusion resistance in the measured sample without increasing its total thickness. This will result in a smaller experimental $D_{eff,\,total}$ value than that it should be. From Equation 4.1, a negative error on the experimental $D_{eff,\,w}$ will be caused. The thinner the washcoat thickness is, the bigger the error will be.

As the thickness of the washcoat layer is increased, then experimental errors will have less of an impact on the determined values of $D_{eff,\,w}$. This is the reason why the experimental D_{eff} values approach a constant, about $1.0 \times 10^{-6}\ m^2\ s^{-1}$. This value is very close the D_{eff} values obtained from cordierite samples in Chapter 3.

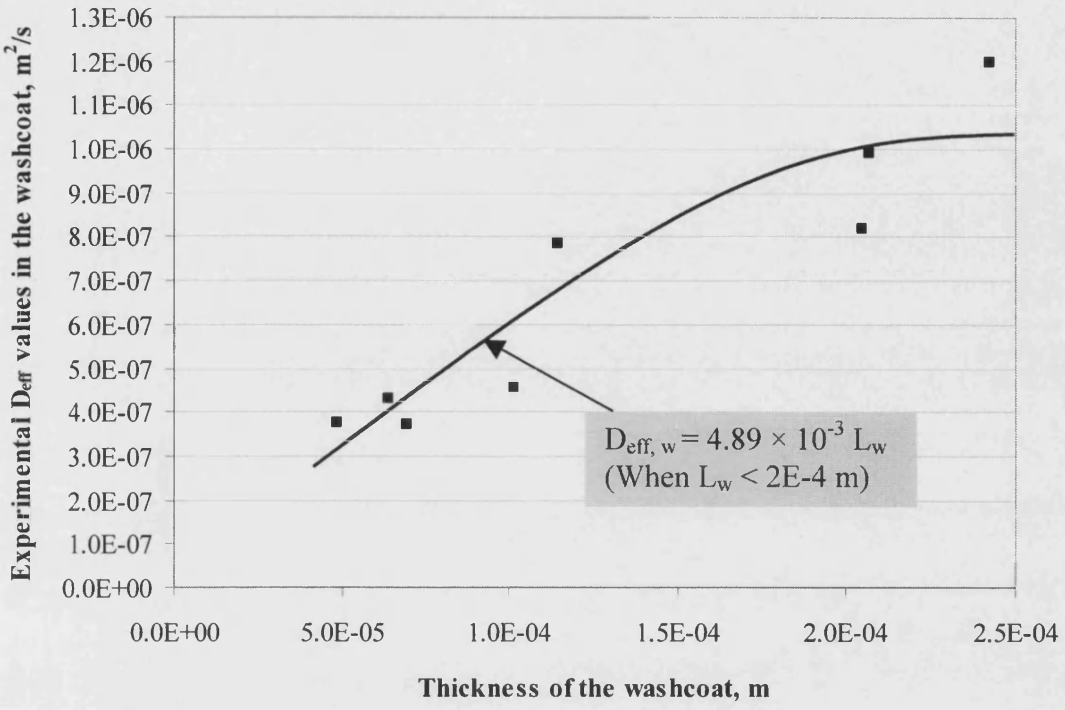

Figure 4.9 Effect of the washcoat thickness on the measured D_{eff} values (in Sample S3).

Exp conditions: displayed inlet flowrate to each chamber: 600 ml/min; pressure in each chamber: 1.1100 bar (a).

4.5.2 The effect of calcination temperature and ageing

There is much discussion amongst researchers that develop and test catalysts, about how a catalyst should be aged. An auto-catalyst manufacturer proposed that the samples from Slurry S3 that had already been calcined at 500 °C in air for 3 hours, should be re-calcined at 700 °C in 10% H_2O + 10% O_2 + 80% N_2 for 16 hours. The re-calcined and aged samples were labelled as S3HT.

The back-calculated D_{eff} values in washcoats S3 and S3HT are shown in Figure 4.10. Since it was very difficult to find two samples (one is from S3, the other is from S3HT) with same washcoat thickness, the measured D_{eff} values cannot be compared directly.

However, Equation 4.2 can be used to compare S3 with the average value for S3HT. This shows that D_{eff} values for S3HT are only 5.9% higher than that from S3. This is not a significant difference as it is within the range of experimental errors. So ageing the sample at 700 °C, did not appear to influence the effective diffusivity.

According to Trimm (1983), below 900 °C, gamma alumina is still dominant in the washcoat rather than the δ-Al_2O_3, θ-Al_2O_3 or α-Al_2O_3 forms. The other components that are present in the washcoat (possible ZrO_2 and CeO_2) are unlikely to change their microstructure when calcination temperature is raised from 500 °C to 800 °C (Ferrandon, 2001). So it is perhaps to be expected that the D_{eff} values would not have changed. However, if the calcination temperature was higher than 900 °C, then it is very likely that the D_{eff} values in washcoat would change.

4.5.3 The effect of including a Pt catalyst into the washcoat

The back-calculated D_{eff} value for the washcoat in Sample S3w is also shown in Figure 4.10. It is only about 7.6% smaller than that in S3. This is not a significant difference, and is within the range of experimental errors.

The presence of Pt catalyst, that is only several nanometers in size, does not appear to influence the effective diffusivity.

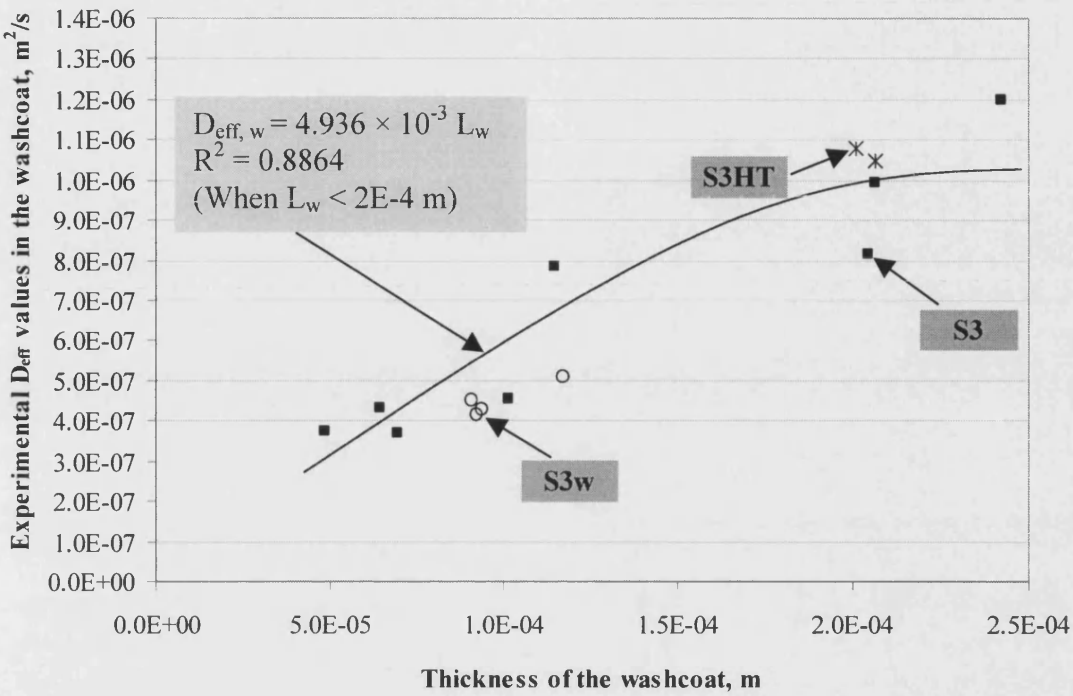

Figure 4.10 Effect of the washcoat thickness on the experimental D_{eff} values.

Exp conditions: displayed inlet flowrate to each chamber: 600 ml/min; pressure in each chamber: 1.1100 bar (a).

4.6 Estimation of tortuosity factor

The method used to estimate the tortuosity factor (τ) was described in Section 3.7. In the washcoat layer, since mesopores are prevalent (see Figures 4.5 to 4.7, and Table 4.2), the following equation will be used to evaluate D (D = D_μ see Hayes *et al.*, 2000).

$$\frac{1}{D_\mu} = \frac{1}{D_{bulk}} + \frac{1}{(D_K)_\mu} \tag{4.3}$$

where D_μ is the diffusion coefficients in the mesopores.

Applying the same procedure described in Section 3.7, the calculated values of D_μ (at 17.4 °C and 1.110 bar (a)) for S3, S3w and S3HT are obtained:

S3 $(1.77 \pm 0.01) \times 10^{-6}$ m^2/s

S3w $(2.32 \pm 0.01) \times 10^{-6}$ m^2/s

S3HT $(1.74 \pm 0.01) \times 10^{-6}$ m^2/s

Using the overall porosity (ε) in Table 4.2 and the experimental D_{eff} values (see Figure 4.10), the tortuosity factor (τ) in S3, S3w and S3HT can be obtained from Equation 3.19:

S3 1.65 ± 0.87

S3w 2.25 ± 0.23

S3HT 0.86 ± 0.02

The tortuosity factors obtained in this study for the washcoat layers are within the range of published data on similar materials (Satterfield, 1970; Garcia-Ochoa & Santos, 1994).

4.7 Conclusions

1. The modified diffusion cell is suitable for the measurement of effective diffusivity in coated cordierite samples with commercial slurries. Using the D_{eff} data of smooth-surface cordierite, the D_{eff} value in washcoat can be back-calculated.

2. The measured D_{eff} values in the washcoat (from Slurry S3 and S3w) were shown to increase with washcoat thickness. This represents the influence of an interface/penetration layer which is formed as the washcoat penetrates the macropores in the cordierite layer. As the washcoat thickness increased, D_{eff} values appeared to approach an asymptotic value of $(10.0 \pm 2.0) \times 10^{-7}$ m^2/s. This value is a factor of 2 to 15 times higher than that reported in Hayes *et al.* (2000) for an alumina based washcoat, where the values were found to lie in the range of 0.6×10^{-7} to 4.2×10^{-7} m^2/s. It should be noted that the alumina washcoat used in Hayes *et al.* (2000) had been prepared by a different supplier of catalysts. This observation is important, as it demonstrates the need to evaluate the D_{eff} in the actual washcoat used in the reactor, rather than choosing a literature value.

3. The back-calculated tortuosity factor (τ) in S3, S3w and S3HT are:

S3	1.65 ± 0.87
S3w	2.25 ± 0.23
S3HT	0.86 ± 0.02

   They are within the range of published data on similar materials.

4. Although the D_{eff} value slightly decreases (about 5.9%) for the re-calcined and aged sample (700 °C for 16 hours in 10% H_2O + 10% O_2 + 80% N_2), the difference was within experimental errors. It was a little surprising that the difference was not more significant.

5. The D_{eff} value in the presence of 3.18 g/l Pt was only 7.6% smaller than for the washcoat. This is not significant as it is within experimental errors. This observation is important, as D_{eff} values can be assigned to a washcoat without being too concerned over the effect of the dispersion of catalyst.

Chapter 5 The measurement of D_{eff} of CO in a sample cut from a commercially produced catalytic converter

In Chapter 4 it was shown that the thickness of washcoat will influence the D_{eff} value. In a commercial auto-catalyst, the washcoat thickness around the perimeter of a cell is very likely to vary, and this could be from 10 to 150 microns (Hayes and Kolaczkowski, 2000). This situation makes it difficult to assign a fixed D_{eff} value at an axial location around the perimeter of the cell.

Although the slurry used in the flat samples in Chapter 4 and the calcination conditions are the same as that in a commercial auto-catalyst; the preparation procedure of the former is not exactly the same as the latter. First of all, the washcoat in commercial converters is coated onto a rough-surface, whereas the flat samples had a smooth-surface. As described in Chapter 3, the D_{eff} values of rough-surface cordierite and the smooth-surface cordierite were different. Second, the washcoat in the commercial converter is formed by dropping the monolith into a slurry and then blowing with compressed air, whereas the flat layer was applied by a wiping action. Finally, the washcoat in the commercial converter is contained within a channel (1.1 mm width), whereas the flat sample was about 40 mm wide and had open sides. All of these factors could influence the final characteristics of the washcoat.

The technique described earlier in Section 3.5.2, was modified and applied to determine the D_{eff} values of the washcoat in samples cut from a commercial Diesel Oxidation Catalyst (DOC).

Figure 5.1 outlines the experimental procedure and the links between the experiments in this Chapter.

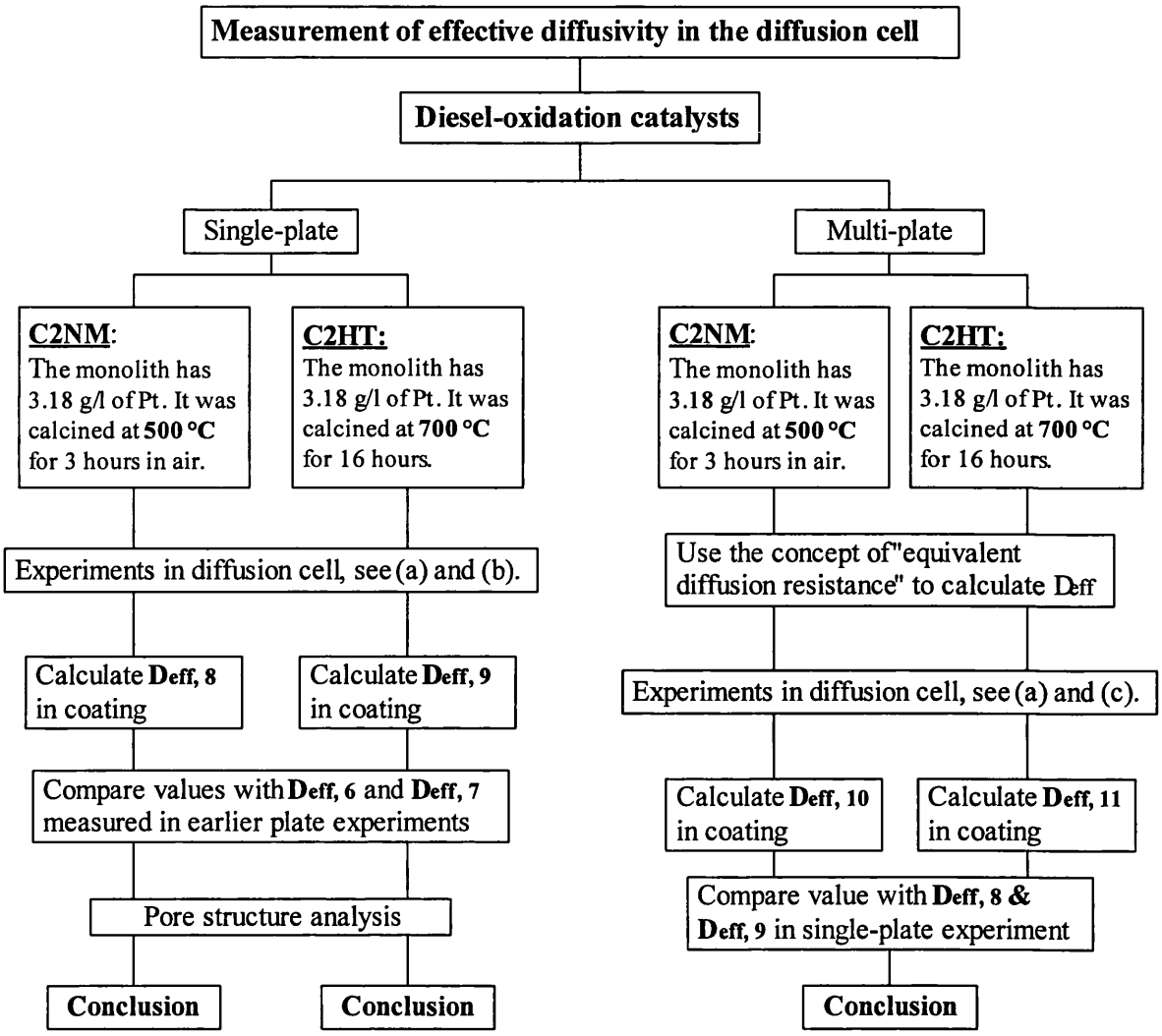

Figure 5.1 Outline of the experimental procedure and the links between the experiments in Chapter 5.

Notes:

(a) Experimental conditions for the diffusion cell were maintained the same as those in Chapter 3;

(b) Values of $\mathbf{D_{eff,2}}$, determined for the single-plate blank (uncoated) cordierite sample with rough surface (in Chapter 3) is used in the calculation of $\mathbf{D_{eff}}$ in the coated layer.

(c) Values of $\mathbf{D_{eff,3}}$ and $\mathbf{D_{eff,4}}$ determined for the multi-plate blank (uncoated) cordierite samples (in Chapter 3) are used in the calculation of $\mathbf{D_{eff}}$ in the coated layer.

To the author's knowledge, nobody else has performed this kind of experimental measurements on actual diesel oxidation catalysts before, although more and more researchers recognize the importance.

5.1 Preparation of samples cut from commercial diesel-oxidation catalysts

One of the samples (C2NM) was cut from a DOC that had been calcined at 500 °C; and the other (C2HT) was cut from a sample that had been calcined at 700 °C. Information on these samples is presented in Table 5.1.

Table 5.1 Description of the washcoat components of commercial diesel-oxidation catalysts.

Samples reference	Washcoat loading (w/w)%	Description
C2NM	23.4	**The sample represented a fresh catalyst.** The washcoat was made from 3.18 g/L Pt slurry, and calcined at 500 °C for 3 hours in air. Channel density: 400 cpsi (62 cells/cm^2)
C2HT	22.8	**The sample represented an aged catalyst.** Sample C2NM was re-calcined at 700 °C for 16 hours in the atmosphere of (10% H_2O + 10% O_2 + 80% N_2). Channel density: 400 cpsi (62 cells/cm^2)

Comparing these conditions with data in Table 4.1, it is evident that the following samples have been prepared at similar conditions:

C2NM is similar to S3

C2HT is similar to S3HT

and the results of D_{eff} measurement can therefore be compared. Photographs of C2NM and C2HT blocks cut from DOC catalysts are shown in Figure 5.2.

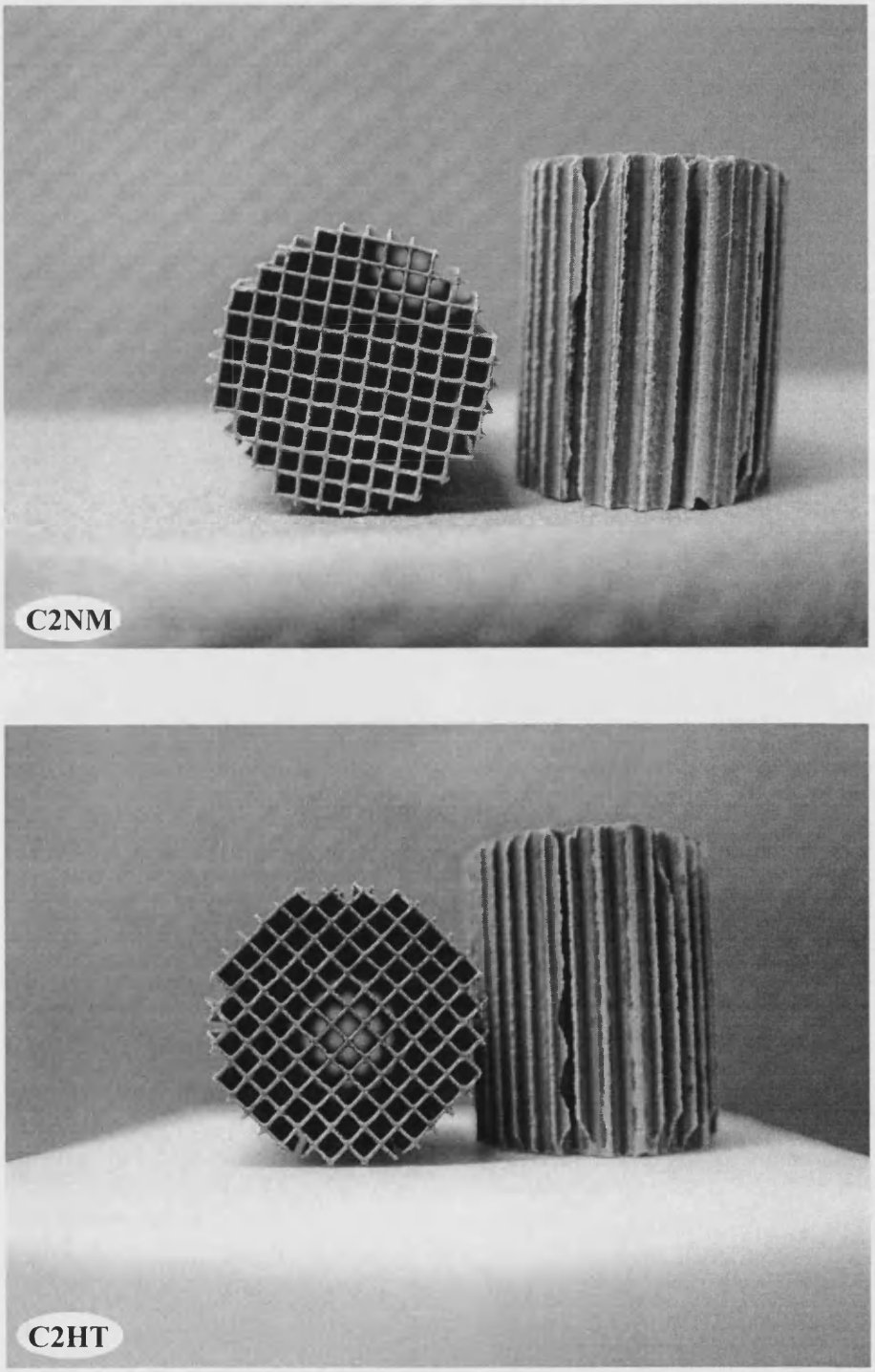

Figure 5.2 The appearance of the diesel oxidation catalyst.
These small sections were cut from a DOC monolith.

5.1.1 Preparation of "single plate" samples

By carefully cutting the connecting walls on either side of a cell, a sample was prepared of a single plate that had a coated surface on either side. Extraneous wall material on the outer surface was removed by hand. This was then cut to the correct shape and fixed with epoxy resin onto a copper support, see Figure 5.3 (A).

5.1.2 Preparation of one or two cell samples

Samples cut from a DOC monolith block to provide either a single, or a double row of cells. Extraneous wall and washcoat material on the outer surface was removed by grinding the exposed two faces to yield flat surfaces. Therefore, there was no washcoat on the exposed surface of these multi-plate samples. However, the inside surface of the cells had a coated layer. These samples were then cut to the correct shape and fixed with epoxy resin onto copper supports, see Figure 5.3 (B) and (C).

5.2 Characterization of the samples

The results of these measurements are presented in Table 5.2, Figures 5.4 and 5.5, and Appendix B3.

As shown in Figure 5.6, because of the nature of the coating process, the washcoat layers formed in the corners of the cells were thicker than those on the side walls. The geometry of the cells, including substrate thickness and washcoat distribution, was determined from SEM pictures using image analysis. Taking the average of 9 measurements, the thickness of the washcoat layer in C2NM varies from 164.6 microns in the corner to 9.7 microns on the side. For C2HT the washcoat thickness varies from 143.2 microns in the corner to 9.4 microns on the side.

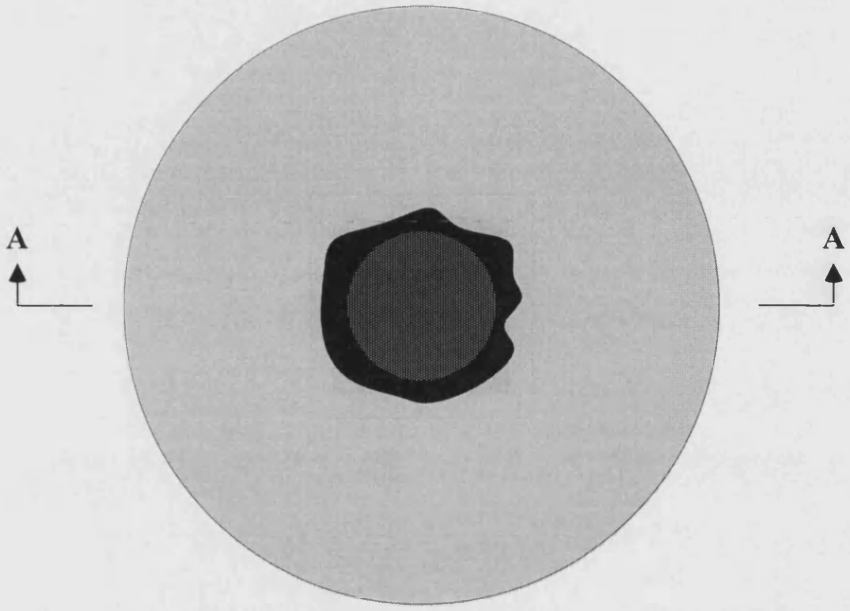

View AA:

(A) 1P: single-plate with two-side washcoat layer

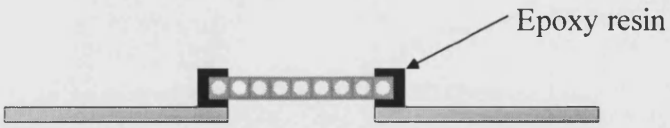

(B) 2P: two-plate with one row of cells

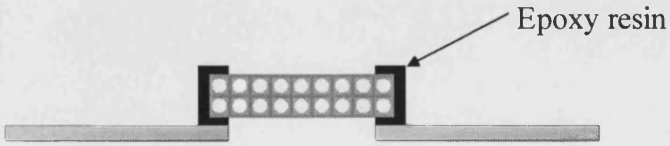

(C) 3P: three-plate with two row of cells

Figure 5.3 Schematic of samples cut from DOC for the diffusion cell.

Table 5.2 Summary of the properties of diesel-oxidation catalysts used in the measurement of D_{eff}.

Properties	C2NM	C2HT
Area from ASAP analysis		
BET surface area, m^2/g	36.2713	Not available (NA)
Micropore area, m^2/g	12.3809	NA
Volume from ASAP analysis		
Micropore volume, cm^3/g	0.006546	NA
Pore size from ASAP analysis		
BJH adsorption average pore diameter (4V/A), Å	154.0256	NA
BJH desorption average pore diameter (4V/A), Å	134.6352	NA
Intrusion data from Micromeritics		
Total intrusion volume, ml/g	0.3232	0.2710
Total pore area, m^2/g	25.154	24.120
Median pore diameter (volume), μm	1.2590	0.8622
Median pore diameter (area), μm	0.0137	0.0131
Bulk density at 0.10 psia, g/ml	1.3956	1.5061
Apparent (skeletal) density, g/ml	2.5423	2.5451
Porosity (ε), %	45.1048	40.8179

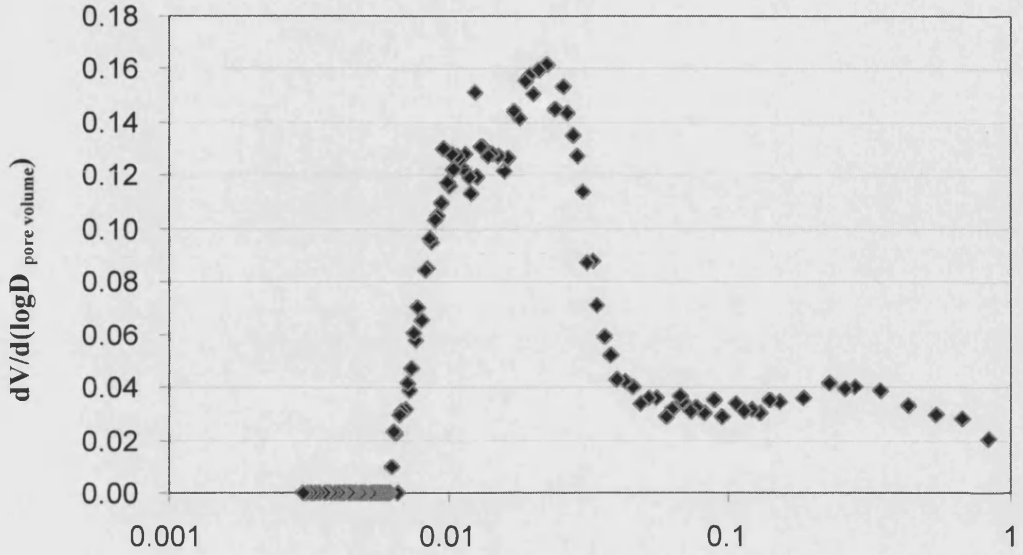

Figure 5.4 Pore size distribution of washcoat in Sample C2NM

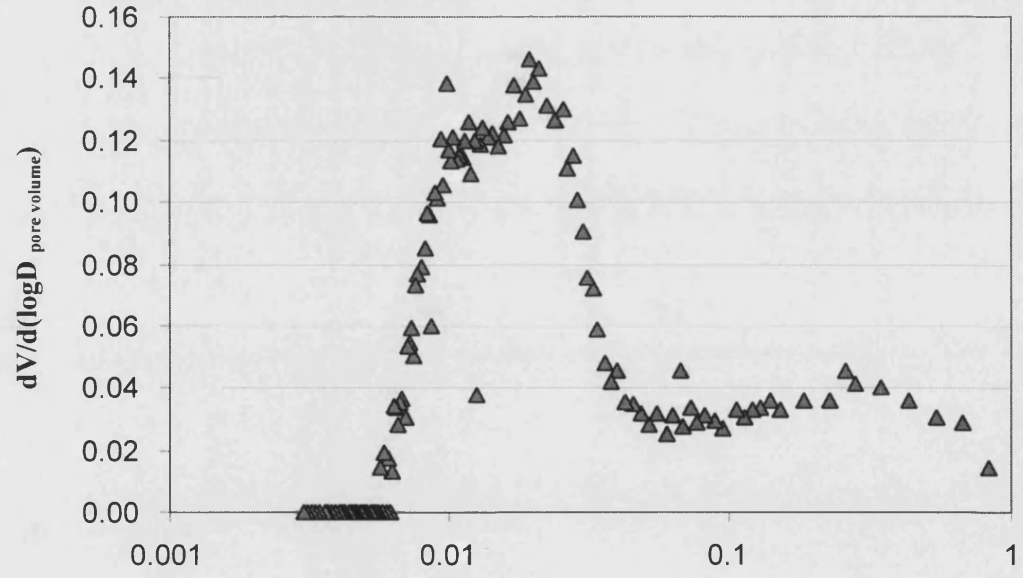

Figure 5.5 Pore size distribution of washcoat in Sample C2HT

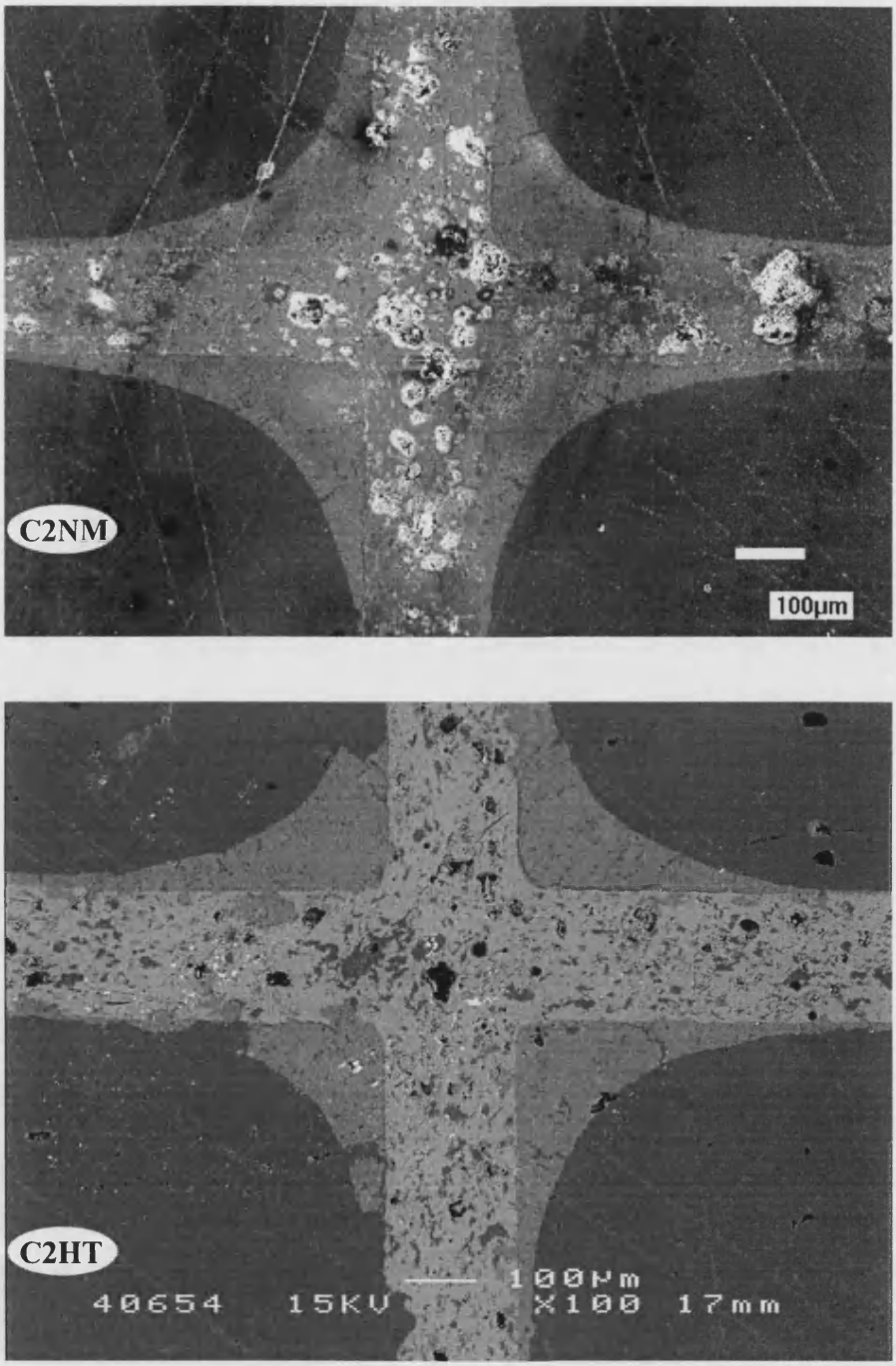

Figure 5.6 SEM photos of a section of two typical diesel-oxidation catalysts.

5.3 Experimental measurements using the diffusion cell

The experimental method and technique used to evaluate the effective diffusivity of washcoated monolith are similar to those described in Chapter 3. In addition, values of effective diffusivity for the blank (uncoated) cordierite plate with rough surface determined in Chapter 3 are used in this new chapter.

In Figure 5.3, a schematic is presented to illustrate the composite nature of the washcoat and support for the three different designs of sample. Figure 5.7 illustrates a close-up view of these samples. Because the shape of washcoat varies significantly around the perimeter of the cell, care needed to be taken with the re-configuration of this structure.

5.3.1 Re-configuration based on maintaining average thickness

One method to obtain the "effective thickness" of a washcoat is to assume that the washcoat is distributed in a uniform manner around the perimeter of the channel, as shown in Figure 5.8 (Step 1). It is then possible to use the so-called electrical analogy (Incropera and DeWitt, 2002) to define the equivalent resistance. This then leads to the reconfigured structure shown in Figure 5.8 (Step 2). This technique was applied to determine the effective diffusivity of the washcoat in a three-way catalyst, and this led to the publication of a paper (Zhang *et al.*, 2004), and this is included in Appendix A.

This technique is not described further in the body of this thesis, instead another method was developed which was tested with samples of DOC.

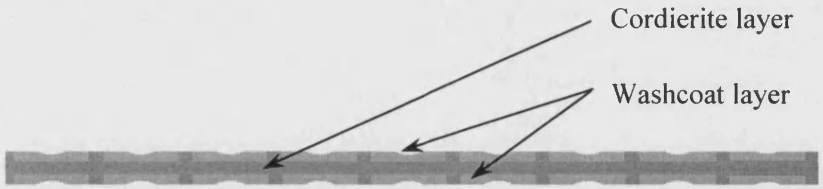

(A) 1P: single plate sample with two layers of washcoat and one layer of cordierite.

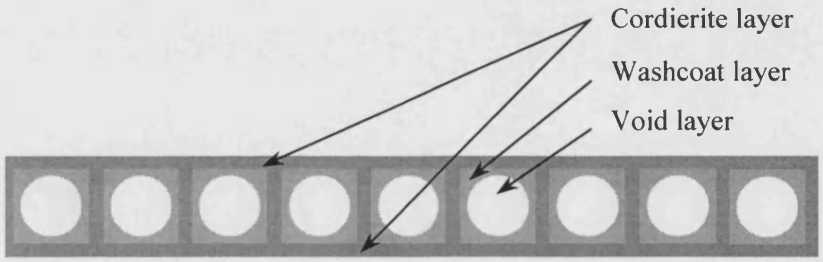

(B) 2P: 2-plate (also called "one-row") sample has two layers of washcoat and two layers of cordierite. The extraneous cordierite and washcoat has been removed from the exposed faces.

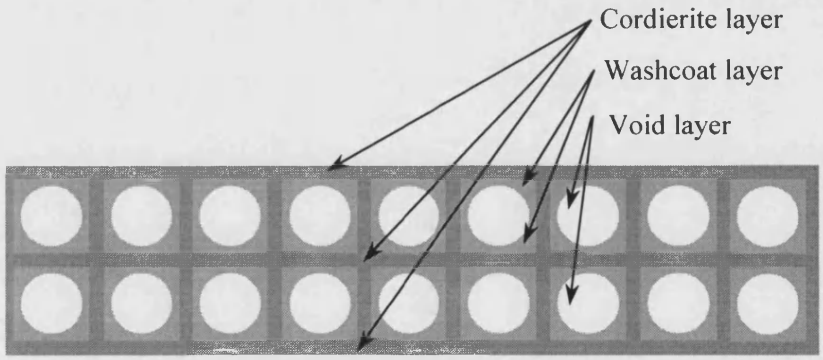

(C) 3P: 3-plate (also called "two-row") sample has four layers of washcoat and three layers of cordierite. The extraneous cordierite and washcoat has been removed from the exposed faces.

Figure 5.7 Schematic of the structure of the layers in the three different types of samples.

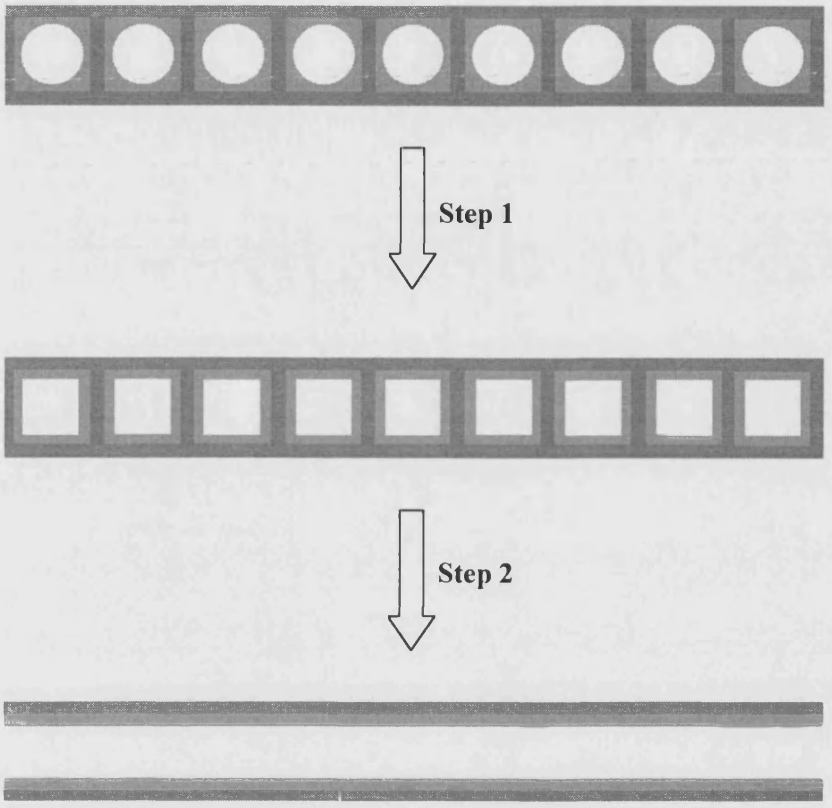

Figure 5.8 Re-configuration based on maintaining average thickness.

Step 1: Assume that the washcoat is distributed in a uniform manner around the perimeter of the channel;

Step 2: Application of technique described in the paper in Appendix A.

5.3.2 Reconfiguration allowing for the resistance of washcoat

In this method, the washcoat is split into a number of thin elements and the "equivalent diffusion resistance" is determined for each element. These values are then integrated to calculate the "effective thickness" of the total washcoat.

For a diesel-oxidation catalyst sample C2NM, the thickness of substrate wall is 174.8 μm; the width of the channel between two substrate walls is 1140 μm. The inner surface of the washcoat has a circular form, with a diameter that could vary from 1120.6 μm to 1283.6 μm (see Figure 5.9). To simplify the calculation, a circle with a minimum diameter (1120.6 μm), is selected to represent the inner surface of the washcoat (see the circle with the dotted line in Figure 5.9). So the minimum thickness of the washcoat, h, in a reconfigured circle would be:

$$h = (1140 - 1120.6) / 2 \ \mu m = 9.7 \ \mu m \qquad (5.1)$$

In this reconfigured structure, the amount of washcoat is greater than in the actual sample, see Figure 5.9.

To maintain consistent with explanations in Chapter 3, the unit cell is divided into the following parts: C1, C2, C3, C4, C5, C6, W1, W2, W3 and W4 (see Figure 5.10). Every part is now reconfigured separately. The method to reconfigure the cordierite has already been described in Chapter 3. Based on the same reconfiguration premise, information is now provided for the washcoat.

Consider a thin element in Zone W4 (the shaded part in Figure 5.11). This has a width Δx_i and a thickness y_i. Maintaining the ratio of $\frac{y_i}{\Delta x_i}$ the same, *e.g.* n (n is a constant, see Equation 5.2), then if y_i is reconfigured to h (h = 9.7 μm for Sample C2NM), Δx_i will be reconfigured to $\frac{\Delta x_i}{y_i} h$ (see Equations 5.3, 5.4 and Figure 5.11):

$$\frac{y_i}{\Delta x_i} = \frac{y_{i,\,reconfigured}}{\Delta x_{i,\,reconfigured}} = n \tag{5.2}$$

$$y_{i,\,reconfigured} = h \tag{5.3}$$

$$\Delta x_{i,\,reconfigured} = \frac{\Delta x_i}{y_i} h \tag{5.4}$$

Now divide Zone W4 into 2 parts: ABEF and BCDE (see Figure 5.12). Set up a right angle coordinate (A is the axle centre point, see Figure 5.12). For the arc EF, the coordinate of its corresponding circle centre is O(0, 570), and its radius is 560.3 μm. By using the knowledge of analytic geometry (see Protter and Morrey (1991), Page 125), the function for the quarter circle EF can be obtained:

$$x^2 + (570 - y)^2 = 560.3^2 \quad (0 \le x \le 560.3;\ 9.7 \le y \le 570) \tag{5.5}$$

For any point between A(0,0) and B(560.3, 0) on Axis X, *e.g.* Point X(x, 0), its corresponding coordinate at arc EF is Point Y(x, y), and

$$y = 570 - \sqrt{560.3^2 - x^2} \tag{5.6}$$

For each uniform segment Δx_i, when its corresponding y_i is reconfigured to $y_{i,\,reconfigured}$ which is equal to h (h = 9.7 μm), $\Delta x_{i,\,reconfigured}$ will not be uniform. So the reconfigured width (from Point A to Point B) is:

$$\sum_{i=1}^{n} \Delta x_{i,\,reconfigured} = \sum_{i=1}^{n} \frac{9.7 \times \Delta x_i}{570 - \sqrt{560.3^2 - x^2}} \ \mu m \quad (0 \le x \le 560.3) \tag{5.7}$$

The other part in W4, BCED, is also configured into a rectangle. Its height is 9.7 μm whereas its width is:

$$\frac{9.7}{570} \times 9.7\ \mu m$$

Combine the two reconfigured rectangles, and then W4 is reconfigured into such a rectangle, whose height is 9.7 μm and width can be calculated from (here n = 560):

$$\sum_{i=1}^{n} \frac{9.7 \times \Delta x_i}{570 - \sqrt{560.3^2 - x^2}}\ \mu m + \frac{9.7}{570} \times 9.7\ \mu m = 141.7\ \mu m \qquad (5.8)$$

Using the same procedure described in Section 3.5.2 (which is used to reconfigure cordierite), W4 can be further changed into a rectangle (590.5 μm wide and 40.6 μm high). The reconfigured structure should have the same width as the original unit cell, whose width is 1314.8 μm, so W4 is finally reconfigured into such a rectangle (657.4 μm wide and 45.2 μm high, see Figure 5.13).

After merging the various sections of cordierite and washcoat, the unit cell in Sample C2NM is reconfigured into two separate cordierite layers and two separate washcoat layers (see Figure 5.14). Using this method, multi-cell samples can also be reconfigured.

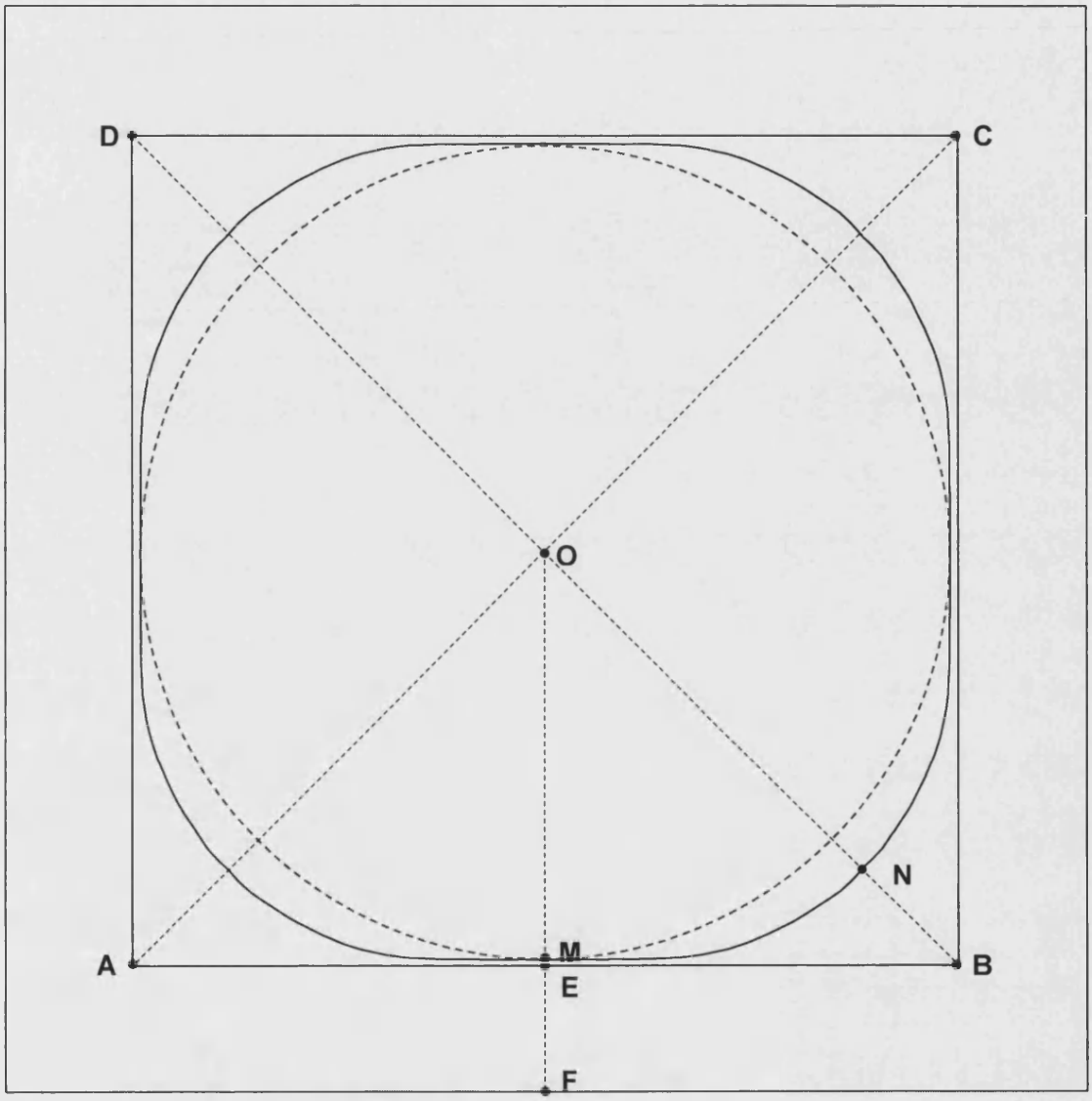

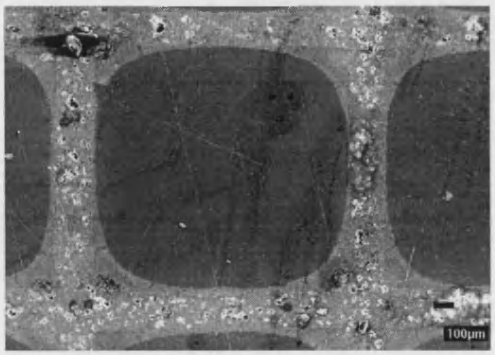

Here:

BD = AC = 1612.2 microns
AB = AD = BC = DC = 1140 microns
EF = 174.8 microns
ME = 9.7 microns
BN = 164.6 microns
OM = 560.3 microns
ON = 641.5 microns

Figure 5.9 Description of the inner perimeter of washcoat in C2NM.

All the dimensions were determined from the SEM pictures using image analysis. The attached SEM picture here is used to compare with a simplified one-cell model.

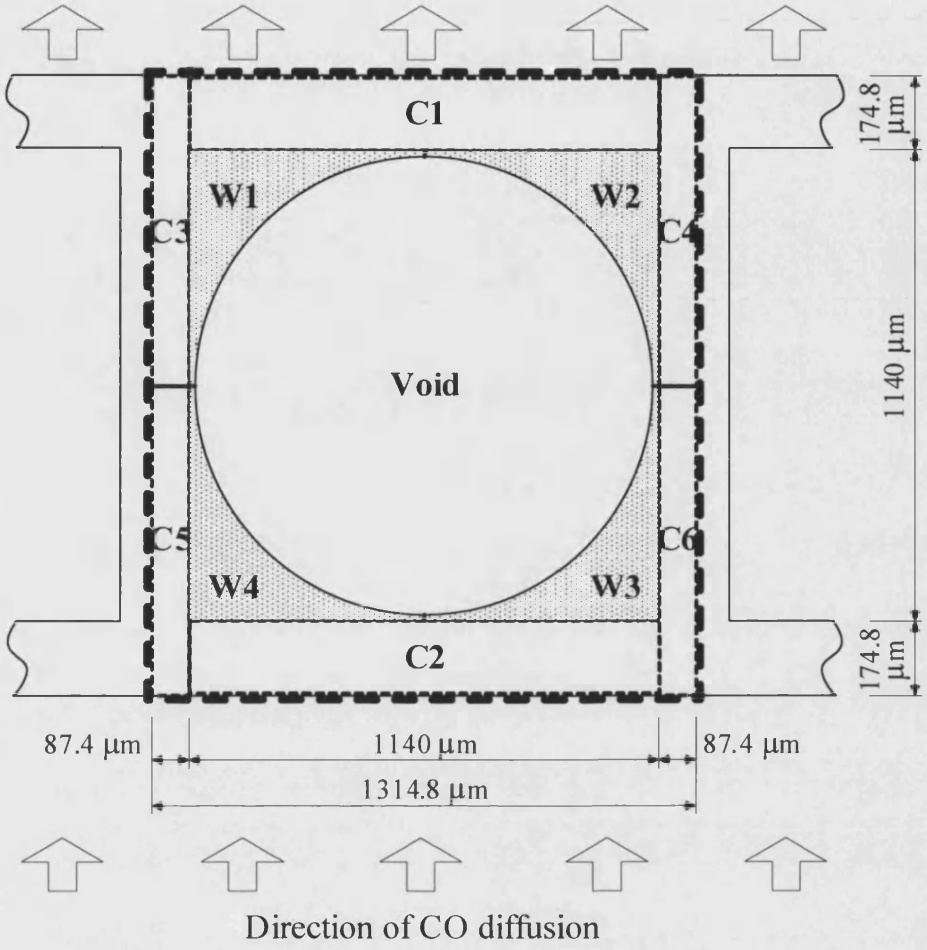

Figure 5.10 Magnified view of one cell in Sample C2NM.

The dotted line indicates the zone that is reconfigured. The zone is divided into:

(a) Void channel part;

(b) Cordierite parts (C1, C2, C3, C4, C5 and C6); and

(c) Washcoat parts (W1, W2, W3 and W4, which are shaded to help identify the regions).

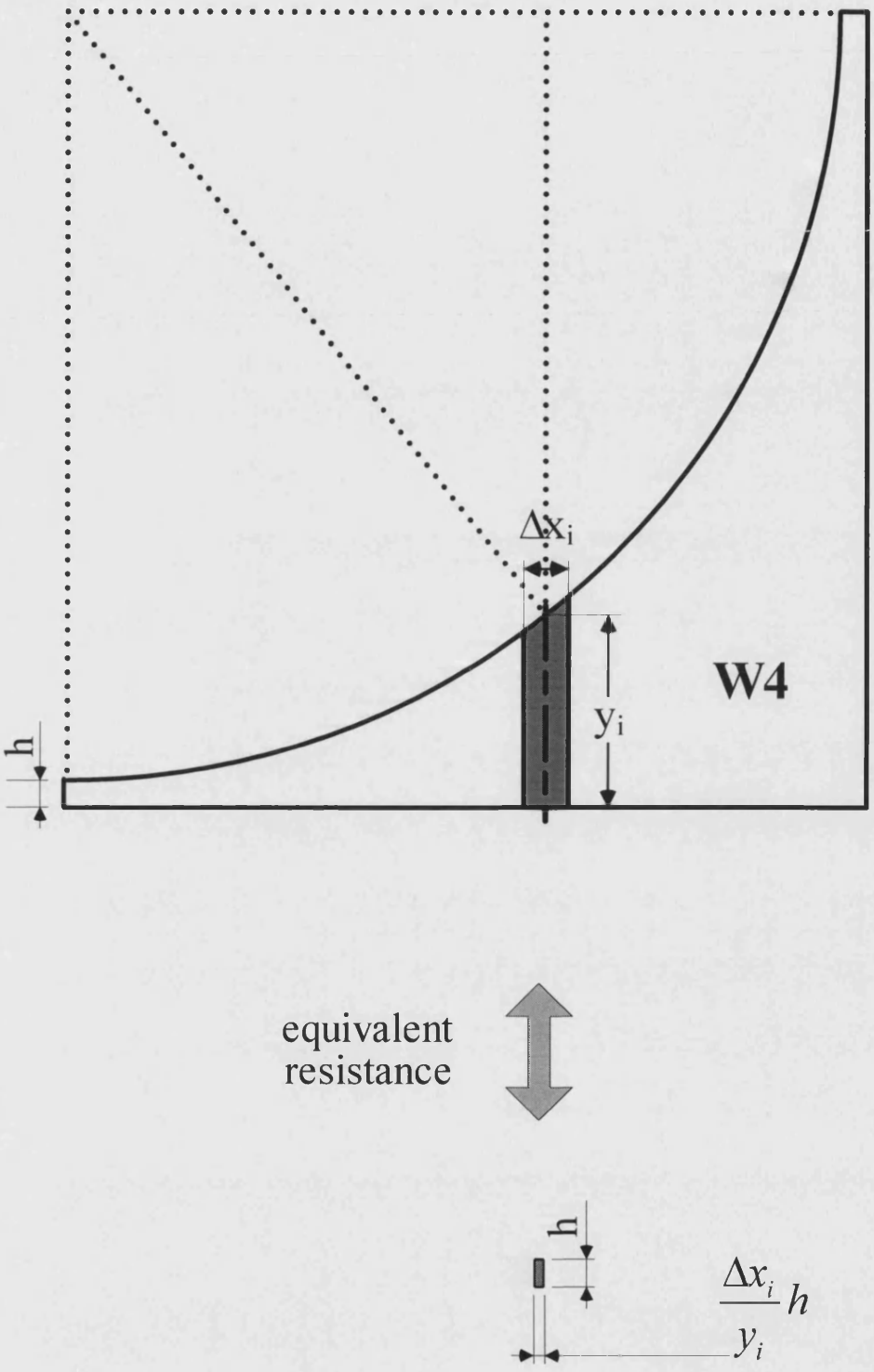

Figure 5.11 Reconfigure a thin element in W4 into the shape of a small rectangle, based on the concept of "equivalent diffusion resistance".

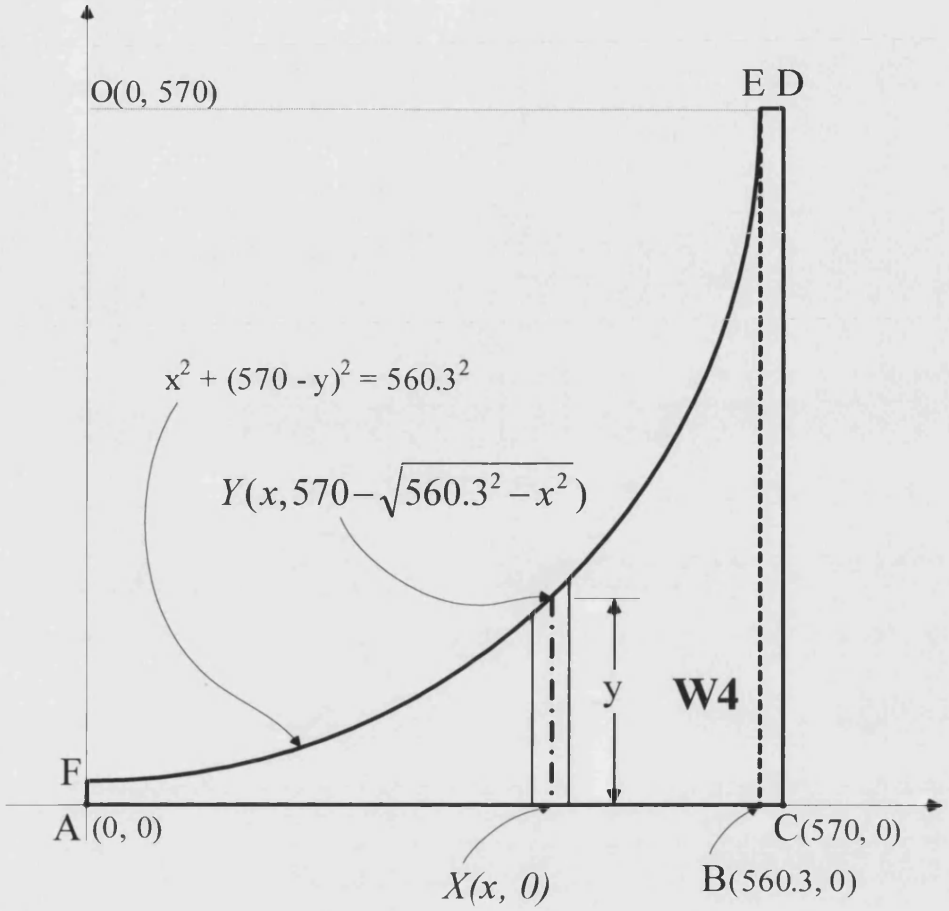

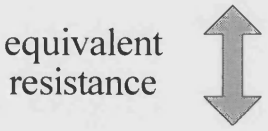

Figure 5.12 Integral of the part ABEF in the washcoat and reconfiguration of the part BCDE, based on the concept of "equivalent diffusion resistance".

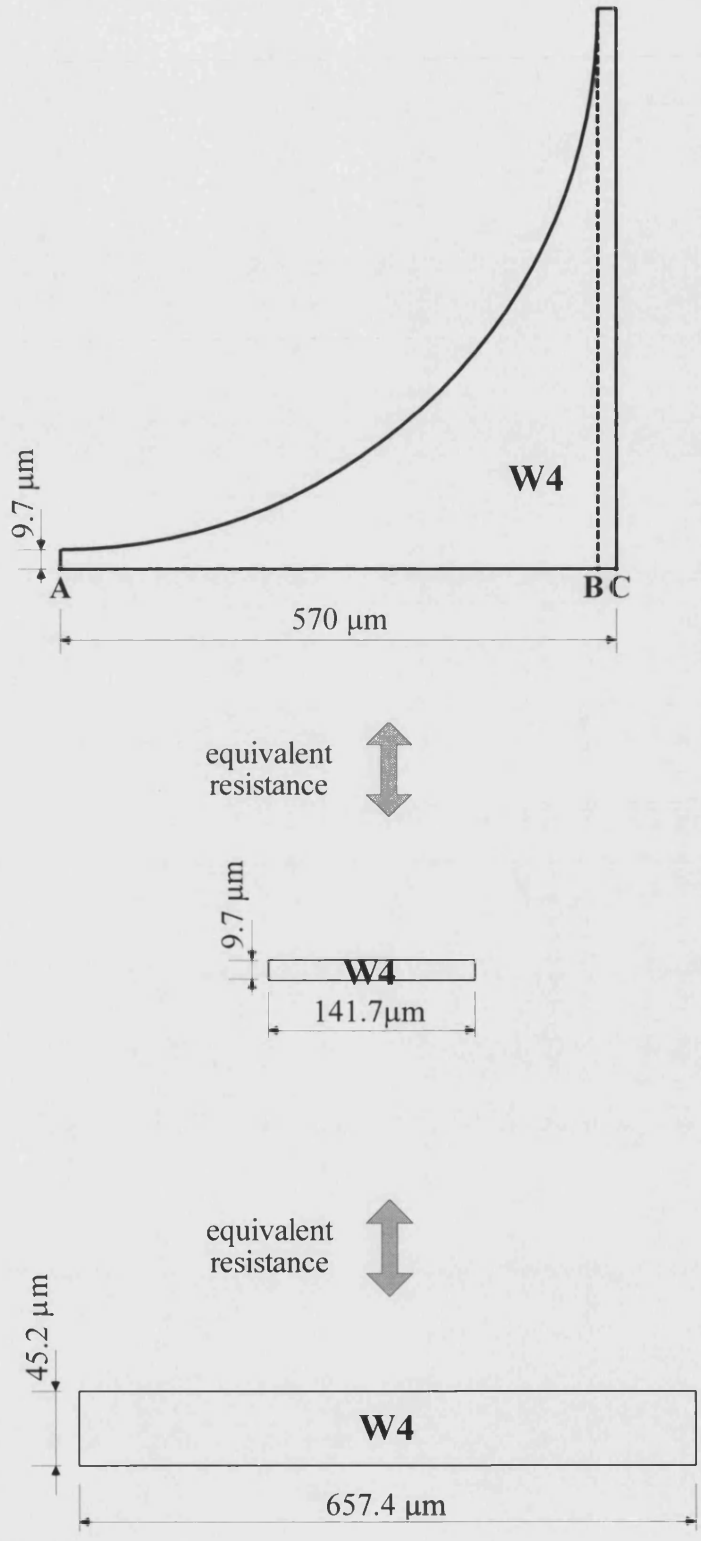

Figure 5.13 Final reconfiguration of the whole W4, based on the concept of "equivalent diffusion resistance".

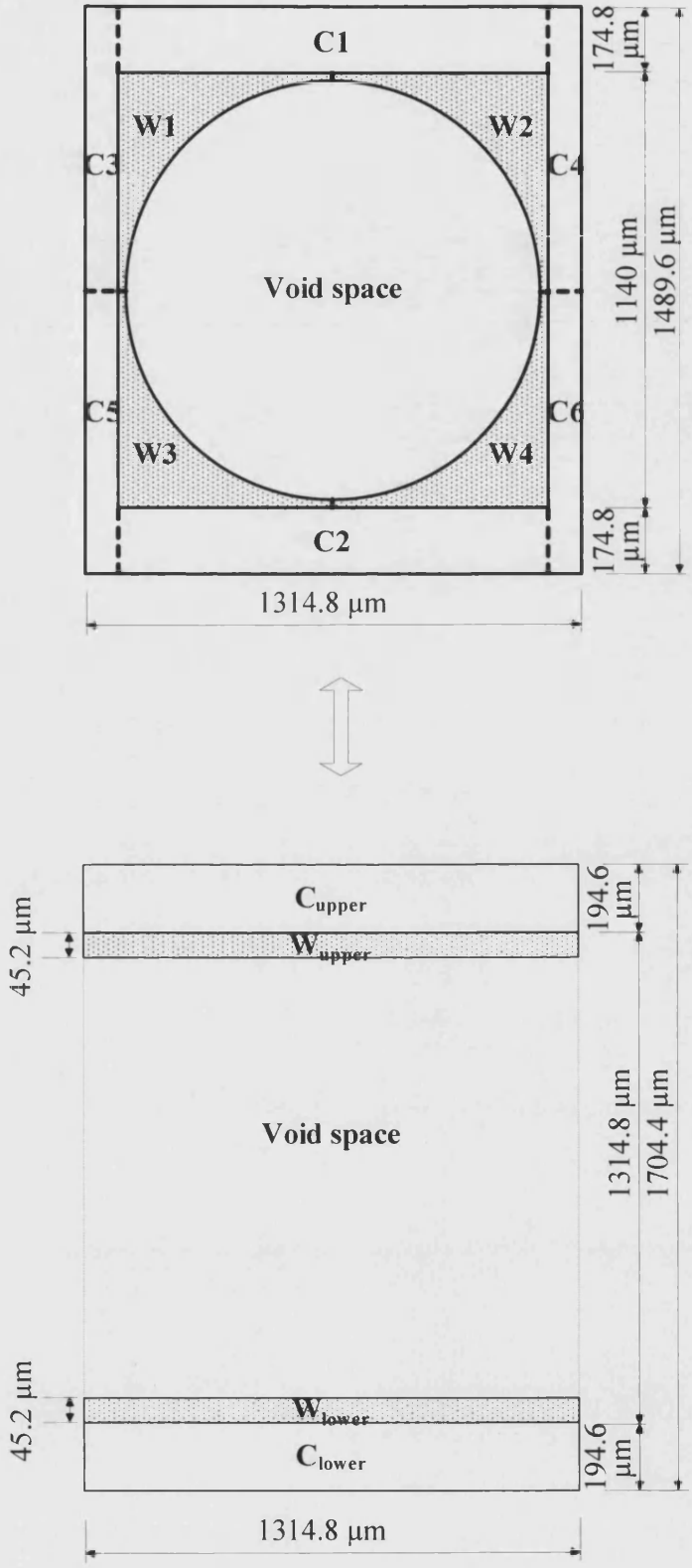

Figure 5.14 Final reconfiguration of the unit cell in Sample C2NM, based on the concept of "equivalent diffusion resistance".

5.4 Analysis of errors

Errors in the measurement of effective diffusivity through commercial diesel-oxidation catalysts may be caused by experimental apparatus, the variation of ambient temperature, the operation of the experiments, the preparation of the samples and the calculation methods *etc.* Many of these have already been discussed in earlier chapters. In this section, additional sources of errors that arise from experiments on coated monolith channels are discussed.

5.4.1 Errors arising from variations in washcoat distribution

The distribution of the washcoat in each unit cell is not exactly same, *e.g.* one cell may be coated with more washcoat than another, see Figure 5.6. Even in one cell, the distribution on the four sides is not the same. However, as the diameter of the hole in the copper support is 10 mm (about 8-channel wide), there is an averaging effect, and the assigned washcoat thickness was based on an average value calculated from 5 cells (20 test points). This can limit error within ± 5% in D_{eff}.

5.4.2 Errors from the simplification step

Errors clearly arise from the assumptions made in the reconfiguration of the cell. However, it is interesting to note that the calculated values of D_{eff} remain relatively close to one another, *e.g.*, for Sample C2NM, the experimental D_{eff} value based on a circle perimeter washcoat (see the dotted line in Figure 5.9) is only (15 ± 5)% greater than the D_{eff} value based on the actual washcoat shape.

5.4.3 Errors that may arise from the penetration of washcoat

The cordierite layer will contain a little washcoat material that has penetrated its pore structure. This will have a small effect on the assigned value of D_{eff} in the cordierite layer. This effect is discussed further in Section 5.5.1 as the results are interpreted.

5.4.4 Errors that arise from the assumption of one dimensional flow

As the structure of the cell is reconfigured and D_{eff} value are calculated, there is an inherent assumption that the flow is one directional – this is not strictly correct. However, in the analysis published by Zhang *et al.* (2004), it was shown that the difference between a one- and two- dimensional form of analysis was (8 ± 5)%.

5.5 Results and discussions

The experimental data gathered during the course of this series of experiments is presented in Appendix D3. The experimental D_{eff} values in Catalysts C2NM and C2HT as shown in Figure 5.15.

5.5.1 Effect of washcoat thickness

Comparing the D_{eff} values of washcoat in single row (2P) and double row (3P) samples (see Figure 5.15), it can be found that both for the C2NM and for the C2HT catalysts, the D_{eff} values of washcoat in 3P is about 16% to 25% higher than that in 2P. This is a similar trend that was observed for uncoated samples in Chapter 3, where D_{eff} value of 3P is about 19.4% higher than the value for a 2P sample.

The reason for these differences may arise from the assumptions made, as the real system is reconfigured into a simplified one-dimensional model. As the number of cells (or plates) increases, then the effect may also be changing.

Also, for the washcoated cells, the penetration of washcoat into the cordierite support structure may influence the results in a slightly different manner as the number of cells (or plates) is increased. There may also be a different influence of experimental errors as the thickness of the sample in the diffusion cell is changed.

Regardless of these comments, the technique does provide a very good indication of the D_{eff} for the washcoated layer, and samples can be prepared and analysed in a number of different ways.

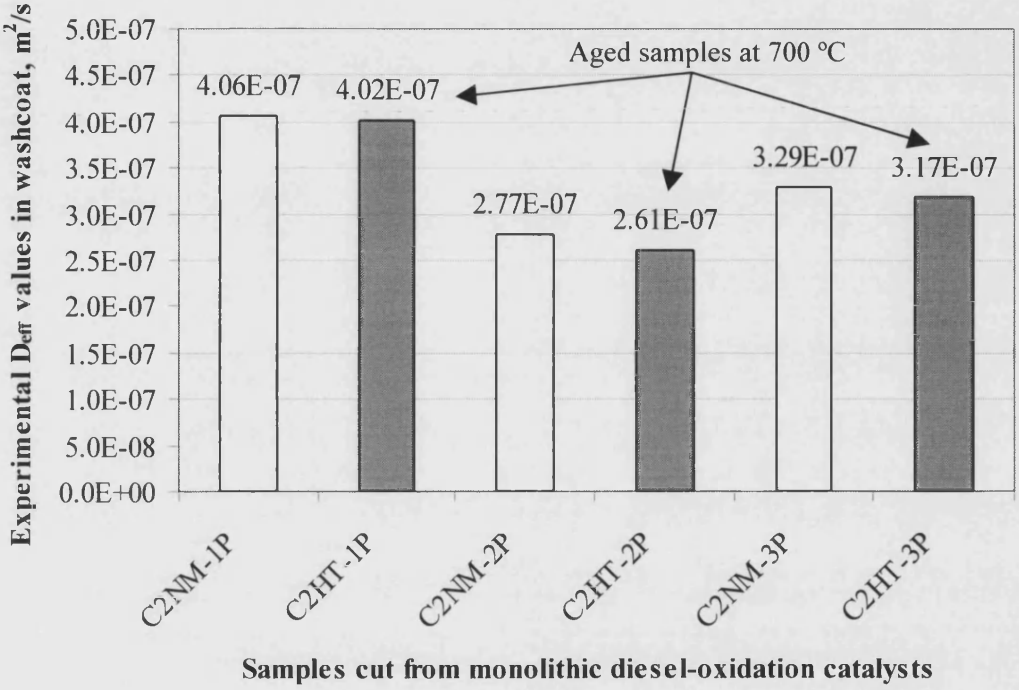

Figure 5.15 Comparison of measured D_{eff} in samples cut with a different number of plates (or cells), and aged at a higher temperature.

C2NM-1P: Sample C2NM with one plate of cordierite (surface washcoat not removed)
C2HT-1P: Sample C2HT with one plate of cordierite (surface washcoat not removed)
C2NM-2P: Sample C2NM with one row of cells (surface washcoat removed)
C2HT-2P: Sample C2HT with one row of cells (surface washcoat removed)
C2NM-3P: Sample C2NM with two rows of cells (surface washcoat removed)
C2HT-3P: Sample C2HT with two rows of cells (surface washcoat removed)

Exp conditions: displayed inlet flowrate to each chamber: 600 ml/min; pressure in each chamber: 1.1100 bar (a).

5.5.2 Effect of calcination (or aging) conditions

Comparing the measured D_{eff} values in Figure 5.16, it is clear that within measurement errors, there is no obvious difference between the fresh and the aged catalysts.

From the results of pore analysis (see Table 5.2, Figures 5.4 and 5.5) the median pore diameter (area-based) in the aged C2HT is 0.0131 micron, which is only 5% smaller than that in the fresh C2NM. The total pore area for the aged sample (C2HT) is 24.12 m^2/g, which is about 4% lower than that of the fresh C2NM. As for total intrusion volume, C2HT is 0.271 ml/g, 16% lower than C2NM. All of these results show that by re-calcining the DOC at 700 °C in the presence of water vapour, this did not change significantly the pore structure. So ageing the sample at 700 °C, did not appear to influence the effective diffusivity. This also agrees well with the measurements reported in Chapter 4.

5.5.3 Effect of coating method

The coating method for monoliths from which samples were cut in Chapter 5 is not the same as the method used to coat plate samples in Chapter 4. To compare their D_{eff} values, C2NM-1P is compared with Sample S3 (prepared in Chapter 4).

To correct for different washcoat thickness, Formula $D_{eff} = 0.004936 \times L_w$ (see Figure 4.10) is utilized to determine a D_{eff} value for S3 (using $L_w = 90.4 \times 10^{-6}$ m, the "effective" thickness of C2NM-1P). The calculated D_{eff} value is named $D_{eff, cal}$. It is then compared with experimental D_{eff} value for C2NM-1P ($D_{eff, exp}$).

This same procedure is also utilized to determine a D_{eff} value for S3HT (using $L_w = 87.6 \times 10^{-6}$ m, the "effective" thickness of C2HT-1P). The calculated D_{eff} value ($D_{eff, cal}$) is then compared with experimental D_{eff} value for C2HT-1P ($D_{eff, exp}$).

Comparing the values of $D_{eff, cal}$ (from S3) with $D_{eff, exp}$ (from C2NM-1P), it can be found that the value of $D_{eff, exp}$ is 9.0% lower than the value of $D_{eff, cal}$ (see Figure 5.16). The result is not surprising as some washcoat in the actual sample C2NM-1P has been removed; therefore the "effective thickness" of the washcoat is less than 90.4 μm. This will lead to a lower value for $D_{eff, cal}$ than 4.46×10^{-7} m^2/s. The explanation is also suitable for the comparison of D_{eff} values for S3HT *vs* C2HT-1P.

Within the range of errors, the difference between $D_{eff, exp}$ and $D_{eff, cal}$ is not significant. It can therefore be concluded that the D_{eff} values in the washcoat are similar in these two samples, and that the method of preparing coated plate samples in Chapter 4 is a viable technique. This is an important conclusion as it offers a simple method of evaluating the D_{eff} for a commercial catalyst.

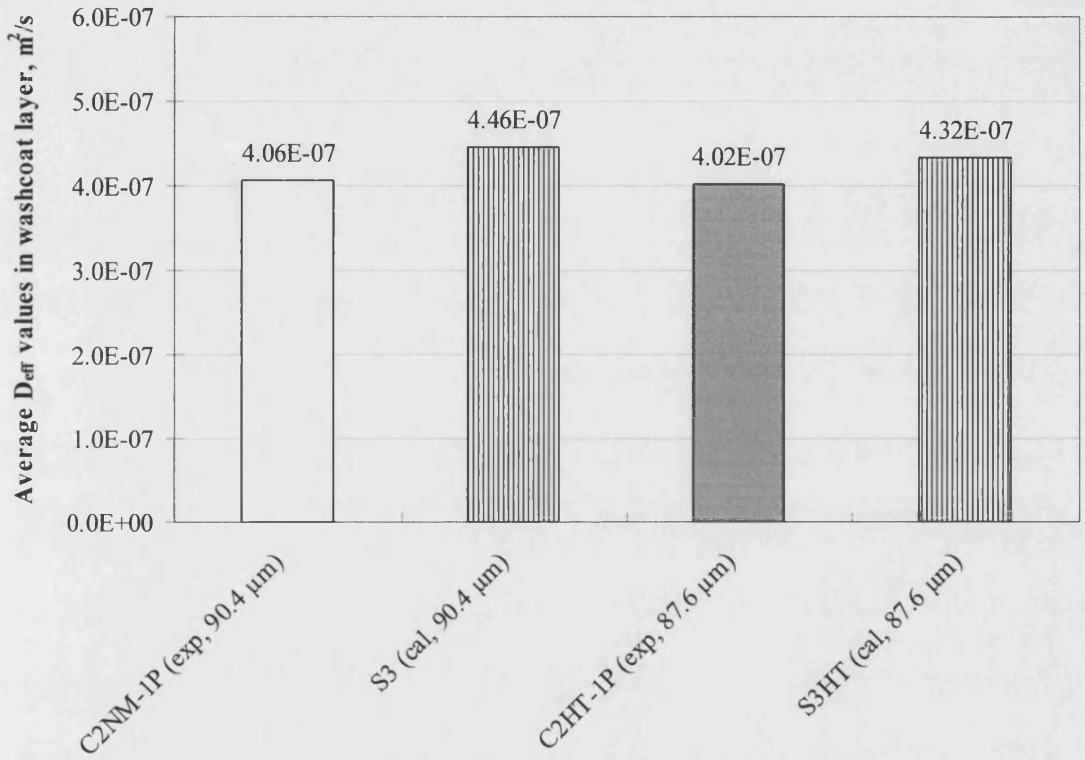

Figure 5.16 Comparison of measured effective diffusivities of Samples C2NM and C2HT – effect of coating method.

C2NM-1P (exp): Sample C2NM with one plate of cordierite (surface washcoat was not completely removed), assumed "effective thickness" of washcoat = 90.4 μm, experimental D_{eff} value;

S3 (cal): Sample S3 washcoated with the same slurry as C2NM-1P, washcoat thickness = 90.4 μm, D_{eff} value calculated from Formula $D_{eff} = 0.004936 \times L_w$ (see Figure 4.10);

C2HT-1P (exp): Sample C2HT with one plate of cordierite (surface washcoat was not completely removed), assumed "effective thickness" of washcoat = 87.6 μm, experimental D_{eff} value;

S3HT (cal): Sample S3HT washcoated with the same slurry as C2HT-1P, washcoat thickness = 87.6 μm, D_{eff} value calculated from Formula $D_{eff} = 0.004936$ (see Figure 4.10).

Exp conditions: displayed inlet flowrate to each chamber: 600 ml/min; pressure in each chamber: 1.1100 bar (a).

5.6 Estimation of tortuosity factor

The method used to estimate the tortuosity factor (τ) in the washcoat layer has already been discussed in Section 4.6. Using the same method, the calculated values of D_μ for Samples C2NM and C2HT are:

C2NM $(1.91 \pm 0.01) \times 10^{-6}$ m^2/s

C2HT $(1.84 \pm 0.01) \times 10^{-6}$ m^2/s

Using the overall porosity (ε) in Table 5.2 and the experimental Deff values (see Figure 5.16), the tortuosity factor (τ) in C2NM and C2HT can be obtained from Equation 3.20:

C2NM 2.62 ± 0.50

C2HT 2.37 ± 0.51

The tortuosity factors obtained in this study for the washcoat layers are slightly different from those in Samples S3 and S3HT, but they are still within the range of published data on similar materials (Satterfield, 1970; Garcia-Ochoa & Santos, 1994).

5.7 Conclusions

1. The modified diffusion cell is suitable for the measurement of effective diffusivity in samples cut from an actual DOC. This method can be applied to either single-plate or multi-plate samples.

2. The experimental D_{eff} values in the DOC catalysts were found to have the following values:

   $(3.42 \pm 0.65) \times 10^{-7}$ m^2/s for the fresh C2NM DOC (calcined at 500 °C);

   $(3.32 \pm 0.71) \times 10^{-7}$ m^2/s is for the aged C2HT DOC (calcined at 700 °C).

   Comparing the D_{eff} values for the fresh and aged DOC, there is no obvious difference.

3. The back-calculated tortuosity values, τ, are as follows:

   (2.62 ± 0.50) in Sample C2NM (calcined at 500 °C);

   (2.37 ± 0.51) in Sample C2HT (calcined at 700 °C).

   They lie within the range of published data on similar alumina-based materials

4. The measured value of D_{eff} in the two-cell samples is slightly higher than that in the one-cell samples.

5. The D_{eff} values determined for the washcoat in the coated monolith DOC are similar to the washcoat prepared on the coated plate. This observation is important, as it offers a simple method of evaluating the D_{eff} for a commercial catalyst.

Chapter 6 The catalytic combustion of CO in a commercial diesel-oxidation catalyst

6.1 Introduction

In this chapter, the catalytic oxidation of CO in a diesel-oxidation catalyst (DOC) is studied. This then provides a link and also acts as an illustration of the importance of quantifying the effective diffusivity in the support in order to model the performance of a DOC system. To explore the region in which the reaction is controlled more by chemical kinetics, and the region in which mass transfer within the catalyst layer plays a more dominant role, experiments are performed at very high gas velocities, corresponding to 70 to 166 m/s. At these high velocities, external mass transfer effects should be minimized. An opportunity was also taken to explore the effect of pressure on the rate of reaction. These types of experiments on DOC were not encountered in the literature.

An overview of the experiments is provided in Figure 6.1.

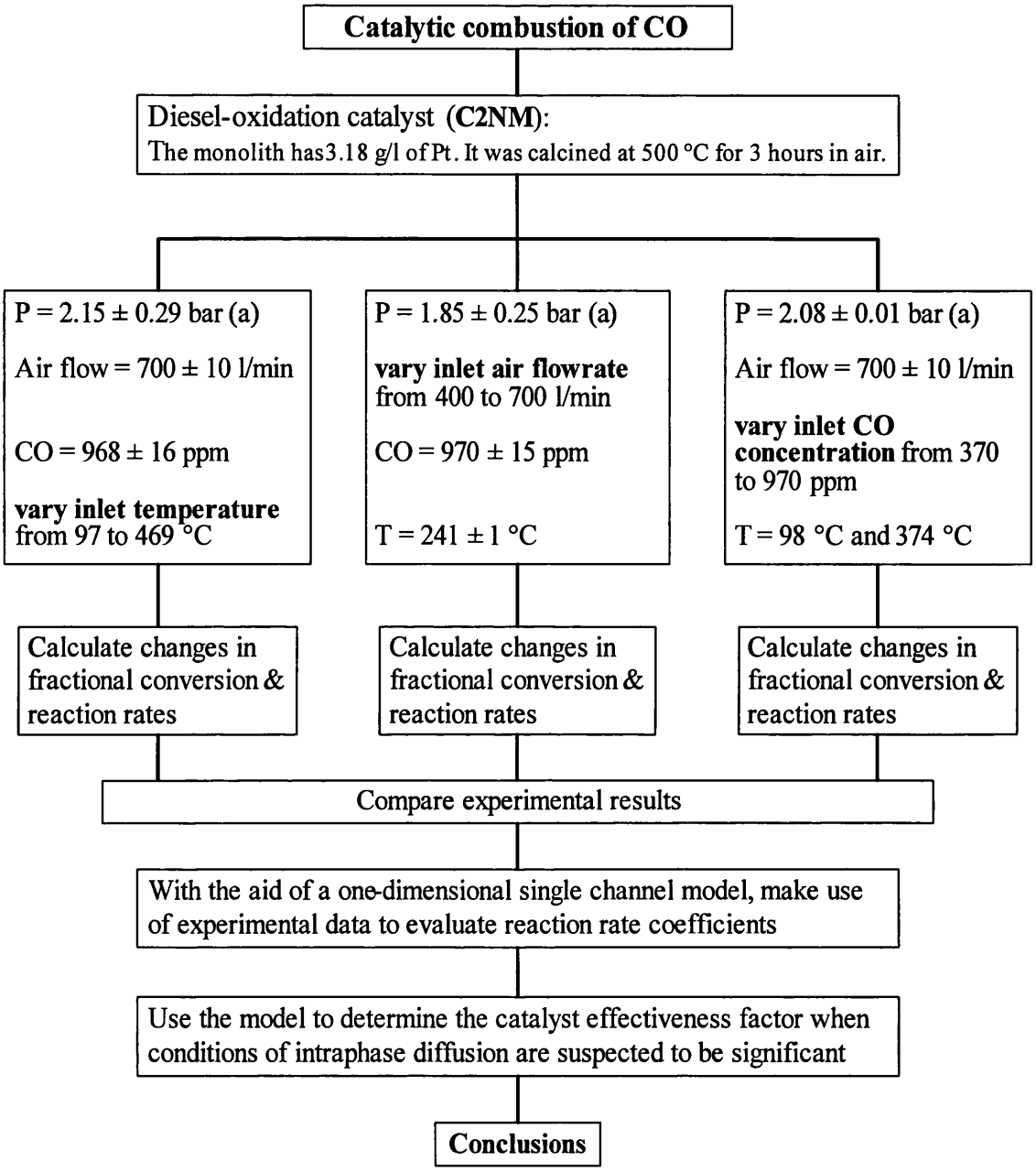

Figure 6.1 Outline of the experimental procedure and the links between the experiments in Chapter 6.

6.2 Selection of sample

6.2.1 The preparation of monolithic catalysts

For the purpose of these experiments, a sample was cut from the DOC known as C2NM. This catalytic monolith had been calcined at 500 °C for 3 hours and is cut from the same monolith that was used for experiments in Chapter 5. The properties are summarized in Table 5.1, Table 5.2, Figure 5.4, Figure 5.6 and Table 6.1. The appearance and dimensions are shown in Figure 6.2.

Table 6.1 The physical properties and chemical components of the diesel-oxidation catalyst sample C2NM.

Items	Data
Cell density, *cpsi*	400
Wall thickness, *mm*	0.18
Length, *mm*	22.0
Diameter, *mm*	15.6
Channel size, *mm*	1.0
Open area, *%*	57.6
Geometric surface area, m^2	0.0096
Catalysts	Pt
Catalyst in slurry, *g/litre slurry*	3.18
Washcoat loading, *(w/w) %*	23.4

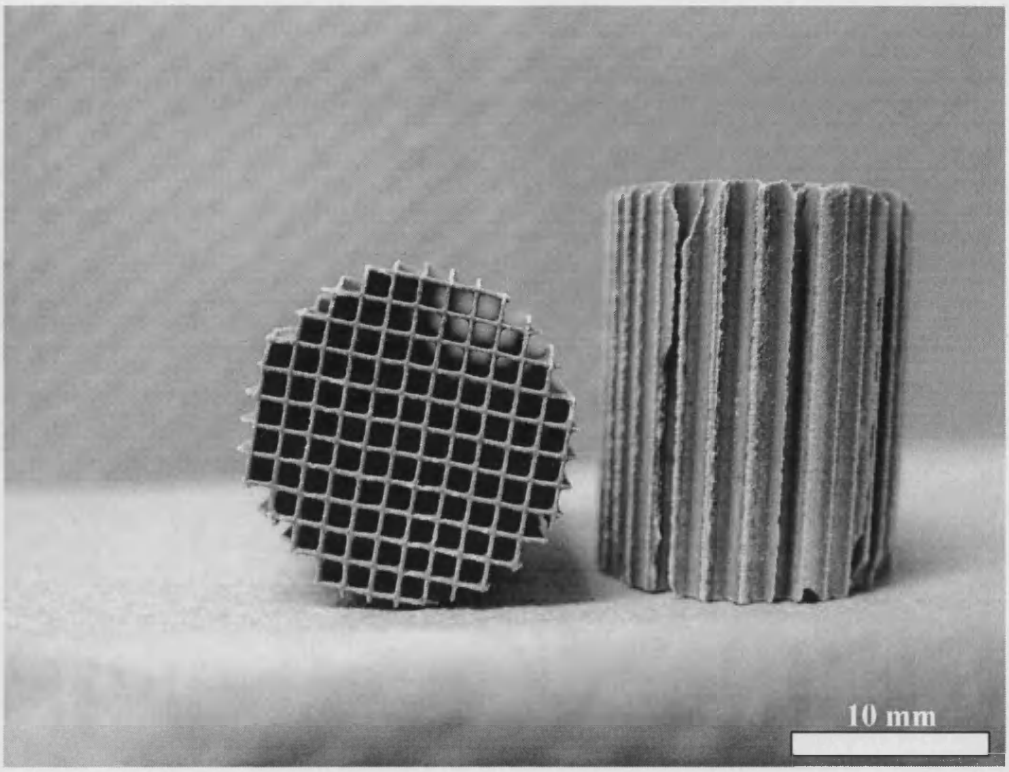

Figure 6.2 The appearance of the diesel-oxidation monolithic catalyst (Sample C2NM).

6.3 Description of the experimental apparatus and operating procedures

The experimental apparatus that was used for this project was originally developed by Li (1997) and Flatley (2001). This was then modified for the purpose of this study. A schematic of the arrangement of the experimental apparatus is shown in Figure 6.3 and a photograph is shown in Figure 6.4.

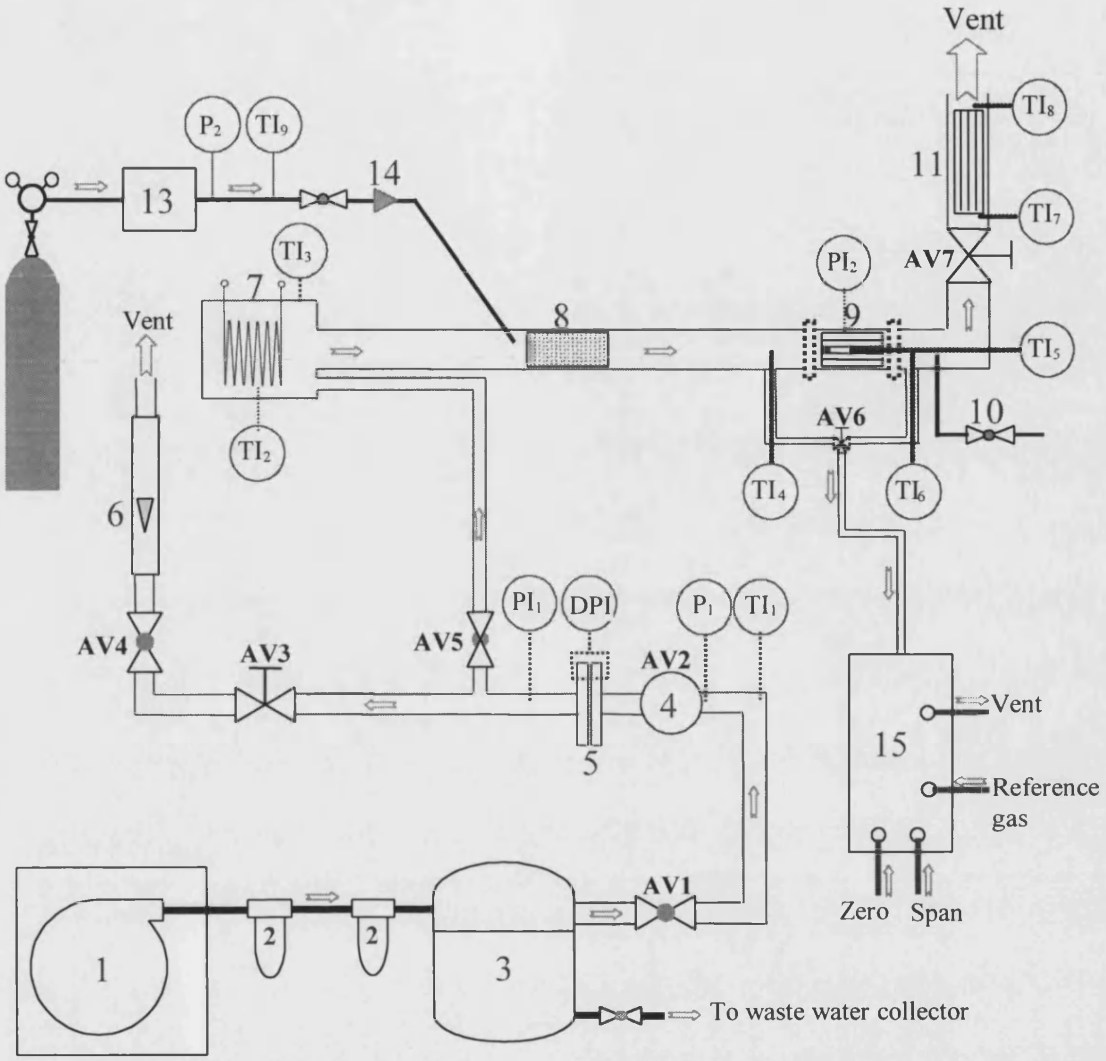

1. Air compressor (The Hydrovane Compressor Co. Ltd, England) 2. Air filter
3. Air receiver 4. Air-pressure regulator 5. Orifice plate
6. Rotameter 7. Electric heater 8. Mixer
9. Sample (monolithic catalyst) 10. Pressure relief valve
11. Monolithic catalysts for cleaning the emissions 12. Pure CO cylinder
13. Mass flow controller 14. Check valve 15. CO analyser

Figure 6.3 The schematic of experimental apparatus of CO catalytic combustion.

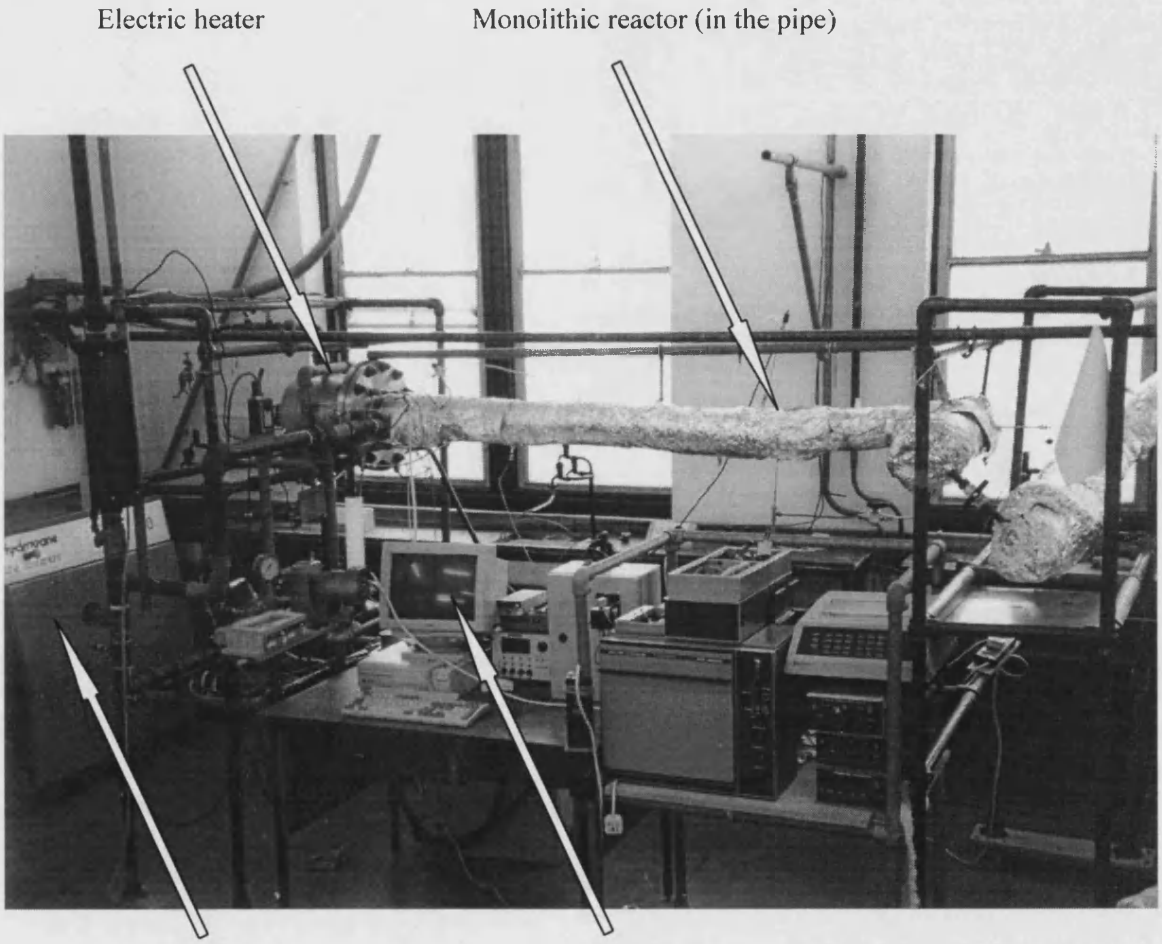

Figure 6.4 Photo of the combustion rig.

The following is a summary of important features in Figure 6.3.

(1). Before the sample was positioned inside the reactor [Item 9], the thermocouple [TI5] was mounted in the central channel, and the inlet to that channel was blocked with cement to avoid cooling by gas flow (see Figure 6.5). Two blank and uncoated monoliths [Item 5 in Figure 6.5] were used to position the sample in the reactor. The uncoated monolith behaved as an inert material and this was confirmed in preliminary trials.

(2). Temperature were measured (*e.g.* TI4, TI5, TI6) with thermocouples (type K).

(3). The CO mass flow controller was calibrated, and the CO analyser and thermocouples were checked. Further information is available in Figure 6.6 and Figure 6.7.

(4). The compressor [Item 1] maintained the air receiver [Item 3] at a pressure of 7.2 bar (g).

(5). With valve AV5 closed and AV4 open, the air flowed via the rotameter [Item 6] into the room. This enables the orifice plate [Item 5] to be calibrated. For a known differential pressure displayed on DPI and absolute pressure indicator PI1, it was possible to measure the flow on the rotameter [Item 6]. A range of conditions could be tested by varying the position of valve AV3.

(6). With valve AV4 closed and AV5 open, the air flowed into the reactor [Item 9]. The differential pressure indicator DPI across the orifice plate was measured and from a knowledge of the absolute pressure on PI1, the air flow could be determined. In practice, techniques in (5) were repeated at identical conditions to obtain a reading of air flow on the rotameter.

(7). The temperature setting on the air pre-heater [Item 7], was increased gradually at 100 °C intervals to achieve the desired gas inlet temperature to the reactor [Item 9]. Depending on the flowrate, a temperature drop of 2 to 32 °C could occur between TI3 and TI4 (a distance of 1.5 m). However, TI4 was used to record the gas inlet temperature to the reactor.

(8). To ensure that the CO mass flow controller [Item 13] operated smoothly, the gas pressure at the inlet to the mass flow controller was maintained at a pressure of 1.0 bar higher than the operating pressure of the reactor.

(9). The CO was fed into the heated air stream and mixed with an inline static mixer [Item 8].

(10). To match the range of the CO analyser (0 to 1400 ppm), experiments were performed with a CO inlet concentration that varied from 300 to 1000 ppm.

(11). The pressure in the reactor was measured with PI2, and this could be controlled by adjusting the position of valve AV7.

(12). Gas samples were taken either from the inlet or outlet of the reactor by adjusting the position of the three-way value AV6.

(13). Any un-reacted CO was oxidised in a 100 mm diameter catalytic converter [Item 11] before it was discharged outside of the laboratory. Any increase in temperature across the clean-up converter [Item 11] was detected with thermocouples TI7 and TI8.

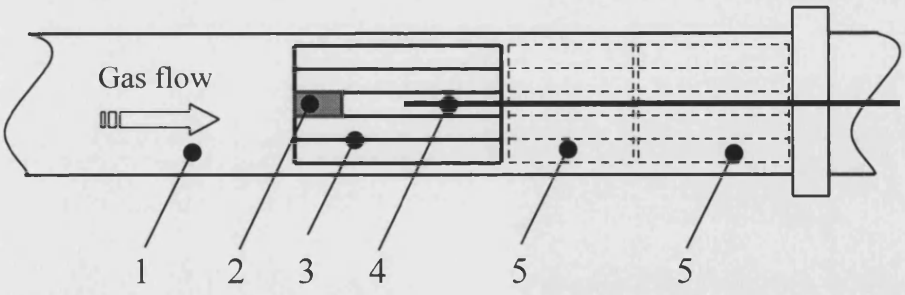

Figure 6.5 The diagram of the combustion pipe with monolithic catalysts and blank (uncoated) cordierite monolith.

1. Combustion tube 2. High-temperature cement 3. Diesel-oxidation catalysts
4. Thermocouple 5. Cordierite monolith used to fix the position of the catalysts

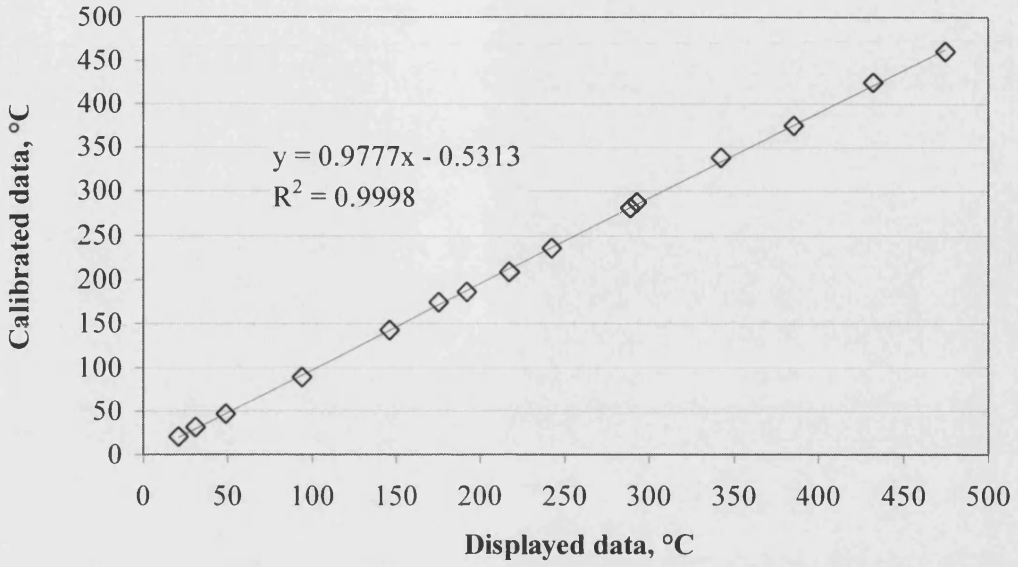

Figure 6.6 The calibration of the thermocouple used to measure the wall temperature.

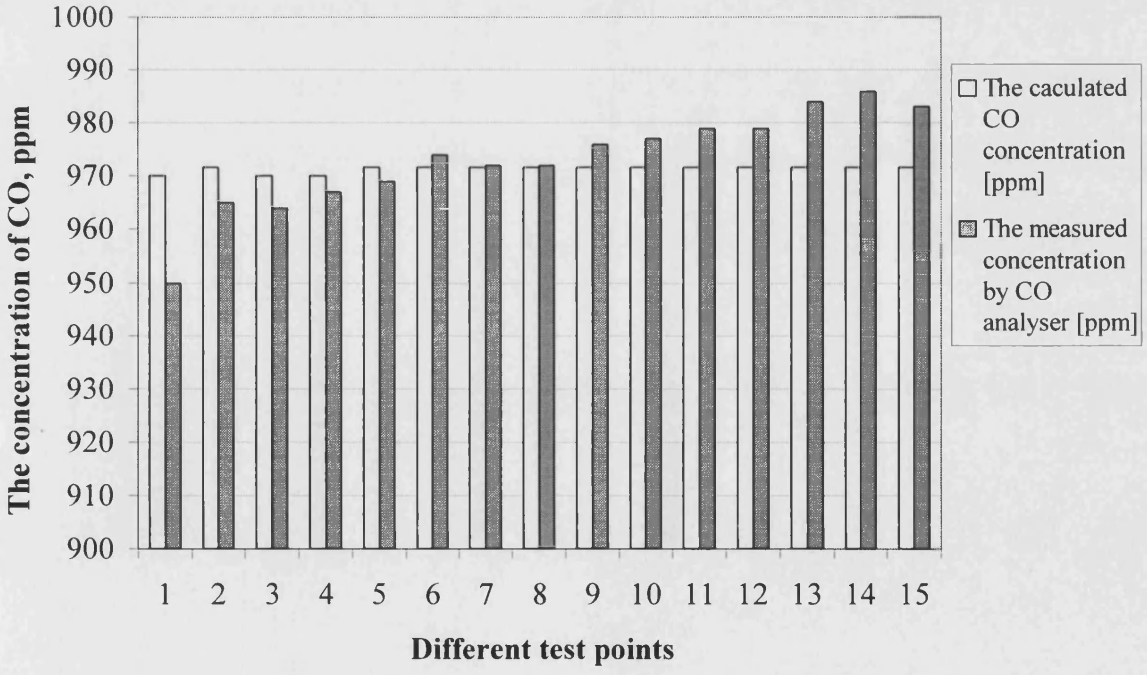

Figure 6.7 The concentration of CO between calculated data and measured data.

6.4 Choice of experimental conditions

In selecting conditions to be studied, the following questions were posed.

- Will diffusion limitations be observed when the inlet concentration of CO is low, *e.g.* 370 to 970 ppm? This is much lower than the actual concentration of CO in vehicle exhaust emissions.
- What is the "light-off" temperature for this low concentration of CO at the high gas inlet velocities used in the experiment? Will it be possible to distinguish the classic shape of the "light-off" curve?
- If the gas velocity is 50 to 100 times higher than in an auto-catalyst (*e.g.* DOC) application, then what is the temperature range at which diffusion limitations will start to become significant?
- At a high gas inlet velocity and low inlet CO concentration and temperature, is it possible to estimate the coefficients in a kinetic rate expression?

To help answer these questions, the following decisions were taken on experimental conditions:

- Gas inlet temperature: to be varied from 97 °C to 468 °C;
- CO concentration: to be varied from 370 ppm to 970 ppm;
- Oxygen concentration: to be maintained in excess and approximately 21%;
- Inlet gas flow (CO + Air): to be varied from 0.27 to 0.48 mol/s;
- Pressure in the reactor: to be maintained at approximately 2.0 bar (a).

At the above range of conditions, the gas flow represents a gas inlet channel velocity of 140.6 to 166.1 m/s in the experimental reactor (15 mm I.D.). Gas flows are therefore 50 to 100 times higher than those in an actual installation in a diesel engine. There are a number of reasons why such high gas flowrates were used. Firstly, to maintain

relatively low conversions across the monolith (in combination with short length), so that the effect of changes in operating conditions can be readily observed. Secondly, to maintain high rates of mass and heat transfer from the bulk gas to the monolith wall, and to test the sensitivity of changes in gas flow at these conditions. If mass transfer plays an important role at these flows, then it is very significant at actual inlet conditions to a converter, where the flow is relatively low, and hence mass transfer coefficients would be a lot lower.

6.5 Experimental results

In order to explore the effects of gas inlet temperature, inlet concentration and flowrate, a series of experiments were performed. For each experimental steady state condition, fractional conversion and reaction rates of CO were calculated from measurement of CO concentration across the reactor using the following expressions:

$$\left[\text{Fractional conversion of } CO\right] = 1 - \left[\frac{\text{ppm CO}_{\text{outlet}}}{\text{ppm CO}_{\text{inlet}}}\right] \tag{6.1}$$

$$\left[\text{Reaction rate of } CO\right] = \left[\text{Inlet molar flow of } CO\right] \times \left[\frac{\text{Fractional conversion}}{\text{Geometric surface area of monolith}}\right] \tag{6.2}$$

Before presenting the results of the experiments, a brief discussion is provided of processes that may limit the rate of reaction. This will help to interpret the results.

It is generally accepted that the catalytic rate expression for the oxidation of CO over a platinum catalyst is of the form (Voltz *et al.*, 1973):

$$(-R_{CO}) = \frac{A_w \exp\left(-\frac{E_w}{R_g T}\right) Y_{CO}\, Y_{O_2}}{\left[1 + A_A \exp\left(\frac{E_A}{R_g T}\right) Y_{CO}\right]^2} \qquad (6.3)$$

where:

$(-R_{CO})$	Rate of disappearance of species CO, various units
A_w	Pre-exponential factor in Arrhenius equation, various units
E_w	Activation energy in a catalytic reaction, $J.mol^{-1}$
Y_{CO}	CO fraction in the bulk fluid (mixture of gas and air), dimensionless
Y_{O2}	O_2 fraction in the bulk fluid (mixture of gas and air), dimensionless
A_A	Pre-exponential factor in adsorption constant in LHHW model, various units
E_A	Activation energy for adsorption term, $J.mol^{-1}$

When CO concentration is very low, then the value of unity dominates the denominator and with excess oxygen, the rate is first order (Hayes and Kolaczkowski, 1994). With a maximum CO inlet concentration of 970 ppm in air, these conditions apply and so the rate may be represented as:

$$R_w = A_w \exp\left(-\frac{E_w}{R_g T}\right) C_b\, Y_{CO} \qquad (6.4)$$

where:

C_b	Bulk concentration of the bulk flow, $mol.m^{-3}$

From Equation 6.4, it is clear that the rate of reaction would be expected to increase exponentially with temperature, whereas, increases in CO concentration will have a more gentle linear effect.

At the interface between the gas and the surface of the catalyst/washcoat, for a fixed position in the channel, then:

$$\left[\text{Rate of reaction in catalyst layer}\right] = \left[\text{Rate of transfer of reactants from bulk gas to surface}\right] \quad (6.5)$$

$$\eta\, A_w \exp\left(-\frac{E_w}{R_g T_w}\right) C_b\, Y_w = k_m\, C_b \left(Y_b - Y_w\right) \quad (6.6)$$

where:

Y_b	Mole fraction of CO in the bulk flow, dimensionless
C_b	Bulk concentration of the bulk flow, $mol.m^{-3}$
Y_w	Mole fraction of CO in the washcoat, dimensionless
k_m	Mass transfer coefficient, $m.s^{-1}$

A term known as the catalyst effectiveness factor (η), featuring on the left hand side of Equation 6.6, is defined as (see Hayes & Kolaczkowski (1997), Page 250):

$$\eta = \frac{\text{Average rate for a catalyst}}{\text{rate evaluated at surface conditions}} \quad (6.7)$$

The value of η can be used to recognize that the reaction is likely to be diffusion limited in the catalyst layer (where: $0 < \eta \leq 1$).

The results of the experiments, with example calculations are presented in Appendix F and Appendix G. In the sections that follow, the influence of gas inlet temperature, inlet CO concentration and gas flowrate are discussed.

6.5.1 Influences of gas inlet temperature

Maintaining a constant inlet flowrate of 0.48 mol/s, with an inlet CO concentration of 970 ppm, steady state experiments were performed over a range of gas inlet temperatures varying from about 98 °C to 468 °C. These results are shown in Figure 6.8. Data points are included that reflect experiments performed at a number of steady state conditions that were reached by gradually increasing the gas inlet temperature and then at conditions when the temperature was gradually lowered. This confirms consistency in the data and that the catalyst had not lost activity.

From these experiments, it is clear that at about 150 °C, reaction rates have rapidly increased, and the plot resembles the shape of the classic "light-off" curve, with the exception that conversion is maintained relatively low and reactants have not been depleted. From the conversion plot, it is clear that above 225 °C, although reaction rates are not increasing further with temperature, reactants still remain as only 20% of the CO has been converted. This is a clear indication that mass transfer effects between the bulk gas stream and the active catalytic sites are having a very strong influence and starting to act as a rate-determining step.

From a theoretical perspective, it has already been shown (Hayes and Kolaczkowski, 1994) that for CO oxidation in catalytic monoliths, above a temperature of 500 K to 550 K (227 °C to 277 °C), the effectiveness factor would be expected to decrease (as temperature increased), and this is consistent with the experimental results. This rapid fall in the value of η would have a very significant impact on the overall rate of reaction.

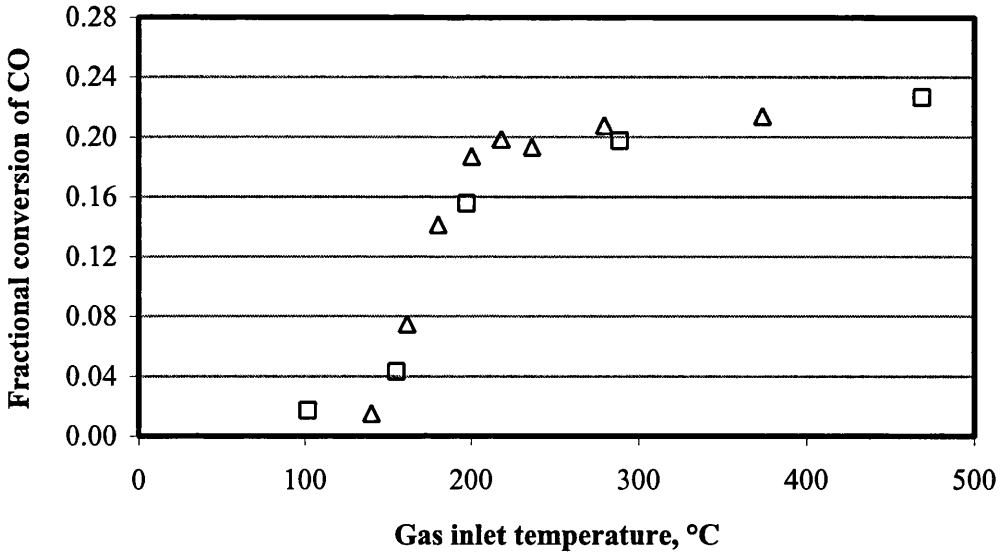

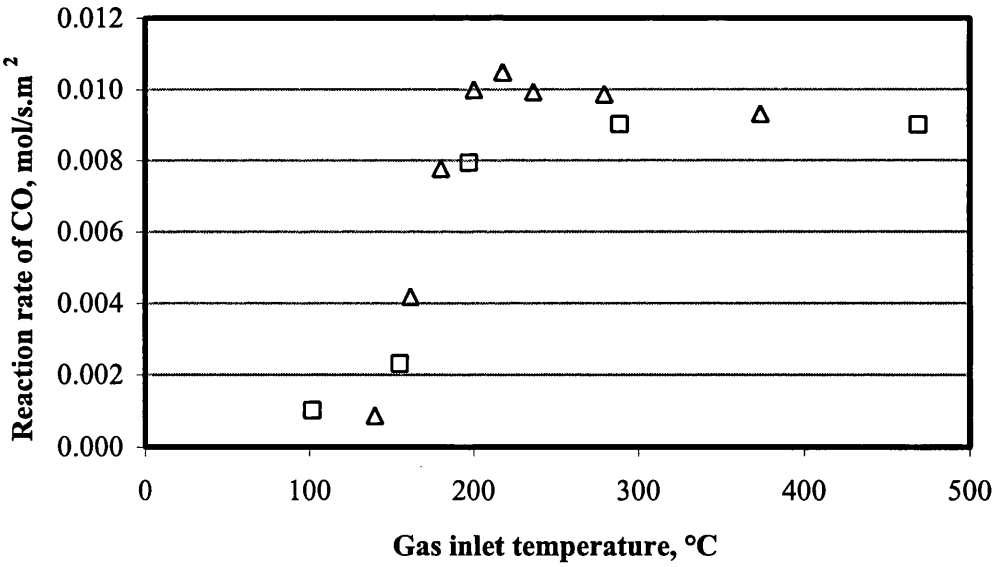

Figure 6.8 Reaction experiments with a constant inlet gas flow rate of 0.48 mol/s and 970 ppm of CO.

The Δ represents measurements as the temperature was increased and □ as the temperature was decreased.

6.5.2 Influence of inlet CO concentration

Maintaining a constant inlet flowrate of 0.48 mol/s, with a gas inlet temperature of 98 °C, steady state experiments were performed over a range of CO concentrations varying from about 370 to 970 ppm. A similar set of experiments were also performed at a higher gas inlet temperature of 374 °C. These two sets of results are shown in Figure 6.9. Both at the high and the low temperature, increasing the concentration of CO has a significant effect on reaction rates, whereas the fractional conversion of CO is hardly affected.

To confirm the combination influence of inlet CO concentrations and gas inlet temperatures, more experiments were performed over a wide range of gas inlet temperatures varying from 98 °C to 468 °C (when set temperatures in the heating chamber varying from 100 °C to 500 °C), with four different inlet CO concentrations (370 ppm, 570 ppm, 770 ppm and 970 ppm) at each temperature, maintaining a constant inlet flowrate of 0.48 mol/s. The results are shown in Figure 6.10. It can be seen that over the full inlet temperature range (from 98 °C to 468 °C) the fractional conversion of CO is hardly affected by the inlet CO concentration. However, the reaction rate of CO will increase rapidly with the increase of inlet CO concentration when the inlet temperature is higher than 150 °C. When the inlet temperature is over 275 °C, the rates of the reaction become steady, which are about 3.2, 5.0, 6.9 and 8.8×10^{-3} mol/s.m^2 at the four different inlet CO concentrations (370 ppm, 570 ppm, 770 ppm and 970 ppm), maintaining a good linear relation between the concentrations of CO and the rates of the reaction. This also confirms the order of CO mole fraction in the reaction rate expression (see Equation 6.4).

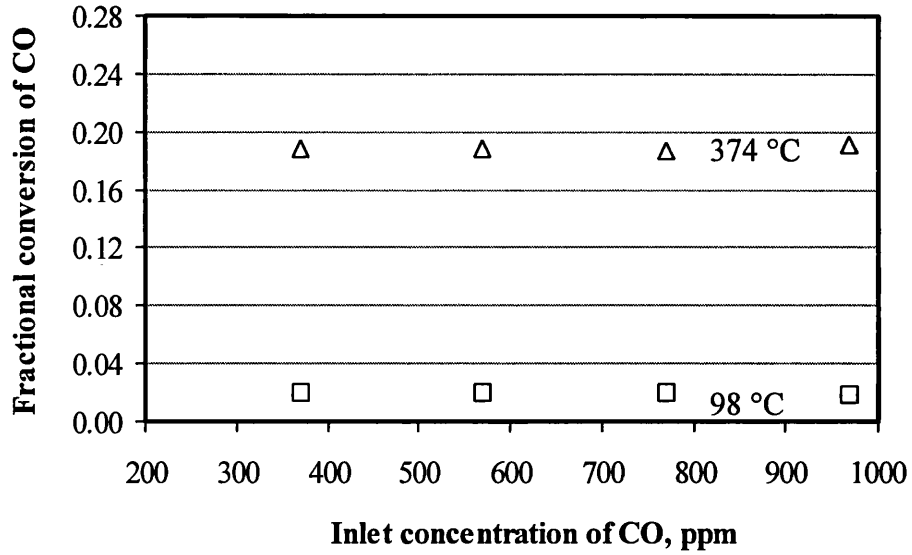

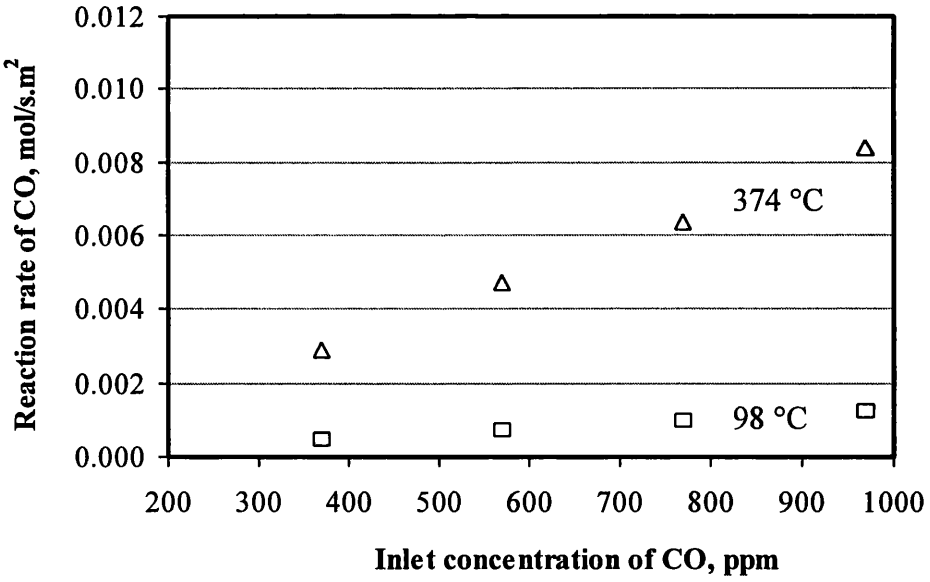

Figure 6.9 Reaction experiments with a constant inlet gas flow rate of 0.48 mol/s, and gas inlet temperature fixed at 98 °C and then 374 °C.

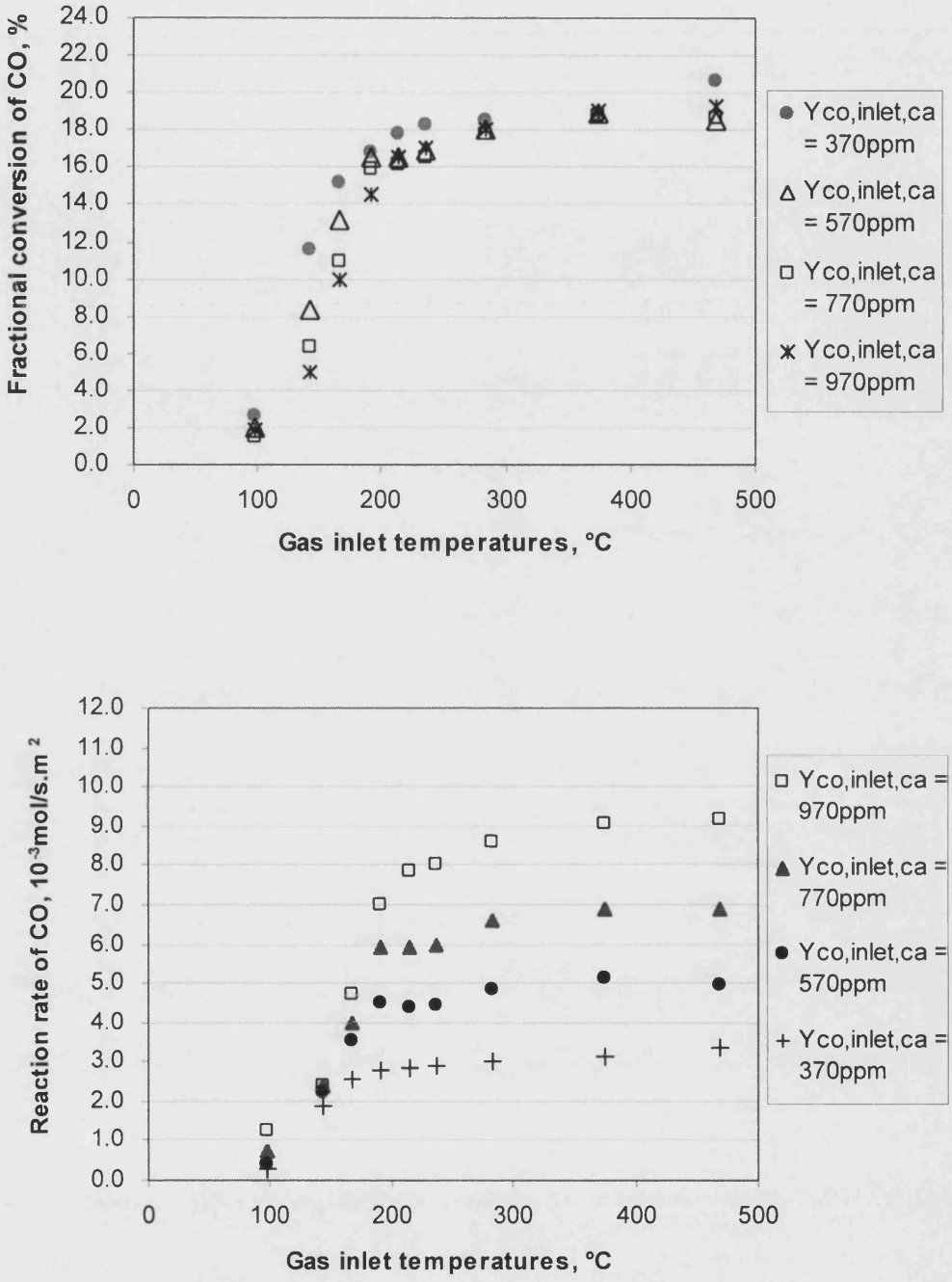

Figure 6.10 Summary of the influence of gas inlet temperatures.

Exp conditions: inlet flowrate: 700 ± 10 l/min; reaction pressure: 2.15 ± 0.29 bar (a).

6.5.3 Influence of gas flowrate

Maintaining a constant inlet CO concentration of 970 ppm, with a gas inlet temperature of 237 °C, steady state experiments were performed over a range of gas flowrates from about 0.27 to 0.48 mol/s. These results are presented in Figure 6.11. These provide a very clear indication that, by increasing the gas flow, the overall rate of reaction is increased, and hence the importance of the coupled effect described in Equation 6.6. The mechanism by which this occurs arises from the following steps:

1. Higher gas flowrates promote eddies which in turn increase the concentration of CO at the gas-solid interface.

2. High surface concentrations result in higher rates of reaction at the surface, and in parallel provide a higher concentration driving force for mass transfer within the catalyst/washcoat layer to the active sites.

This, in combination with experiments where the inlet CO concentrations were varied, confirms the importance of mass transfer.

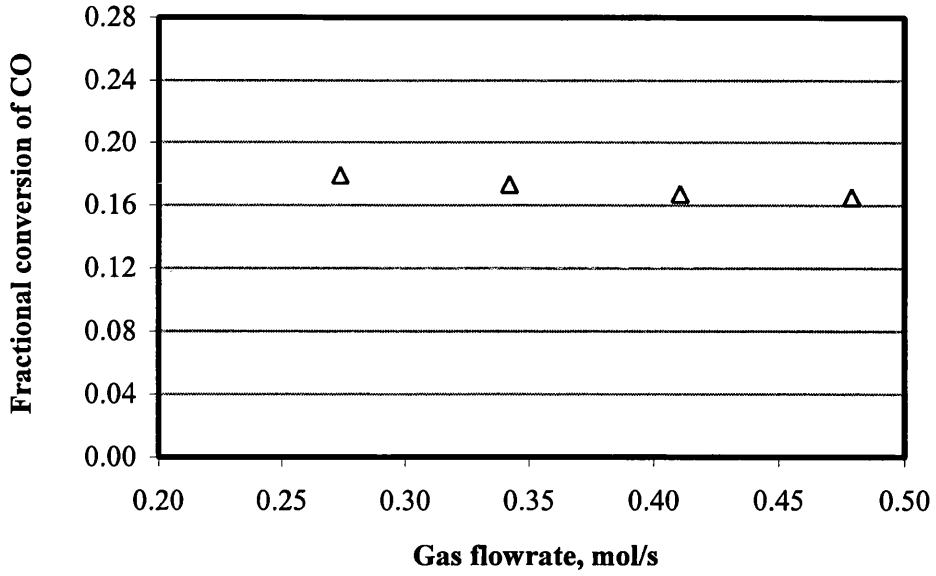

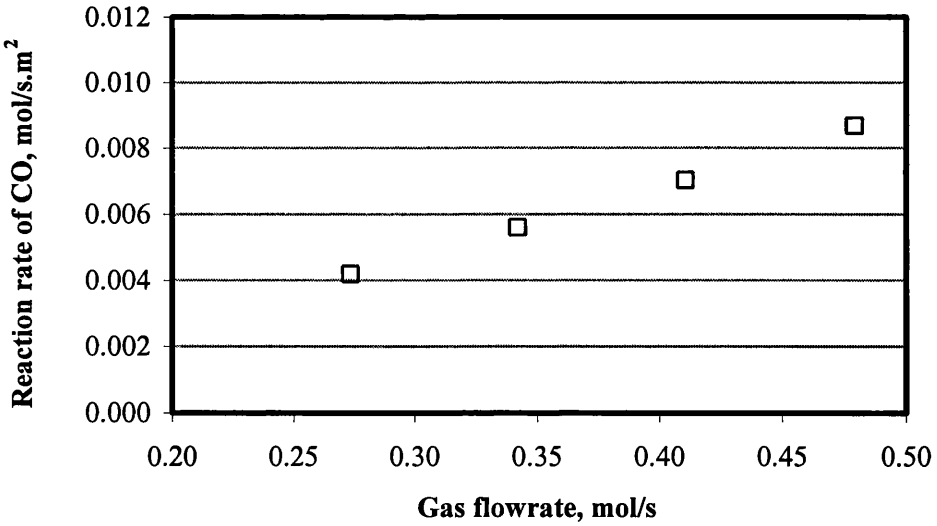

Figure 6.11 Reaction experiments with a constant inlet gas temperature of 241 °C and 970 ppm of CO.

6.6 Analysis of the data

A remaining question that was posed at the start of Section 6.4, was:

"At a high gas inlet velocity and low inlet CO concentration and temperature, is it possible to estimate the coefficients in a kinetic rate expression?

This question is answered, by looking more closely at Equation 6.8:

$$(-R_{CO}) = A_w \exp\left(-\frac{E_w}{R_g T}\right) C_b\, Y_{CO} \tag{6.8}$$

In Equation 6.8, the value of E_w is well established for the platinum catalyst and so a value of E_w = 104 kJ/mol is used, which is adapted from Voltz *et al.* (1973). However, the value of A_w is very much dependent on the dispersion and loading of the catalyst and this will need to be evaluated. According to Oh *et al.* (1980 & 1982), the value of A_w may vary from 1×10^9 to 1×10^{16} mol/(m^2.s).

As the experiments were performed at various pressures, this provided an opportunity to explore the effect of pressure. In the literature, data on the effect of pressure are scarce, and pressure does not feature in the rate expressions described by Equations 6.3 and 6.4. Pressure as a term could be included in a form of Equation 6.8, by an expression of the following form:

$$(-R_{CO}) = A_w \exp\left(-\frac{E_w}{R_g T}\right) P^{\alpha}\, C_b\, Y_w \tag{6.9}$$

where:

($-R_{CO}$) Rate of disappearance of species CO, mol.m^{-2}.s^{-1}

A_w Pre-exponential factor in Arrhenius equation, m.s^{-1}.pa$^{-\alpha}$. The unit is obtained from Equation 6.9. For more information about conversion

factors, see Appendix H.

P The reaction pressure, Pa

α Pressure coefficient, dimensionless

Substituting into Equation 6.5:

$$\eta\, A_w \exp\left(-\frac{E_w}{R_g T_w}\right) P^{\alpha}\, C_b\, Y_w = k_m\, C_b (Y_b - Y_w) \tag{6.10}$$

In Equations 6.9 and 6.10, if the coefficient $\alpha = 0$, then $P^{\alpha} = P^0 = 1$, then pressure does not have an effect. In this part of the thesis, the intention is to find suitable values of α and A_w. This will be done by making use of the data obtained in this chapter.

6.6.1 Material and energy balances

The two unknown coefficients are evaluated with the aid of a mathematical model. This is developed in the following section.

The oxidation of CO may be represented by:

$$CO + \frac{1}{2} O_2 \rightarrow CO_2$$

The equations have been formulated based on the description of the one-dimensional heterogeneous plug flow model presented in Hayes & Kolaczkowski (1997), Pages 300 to 331. The following are the key assumptions:

(1). The reactor operates at steady state conditions;

(2). Radial temperature and concentration profiles are assumed to be uniform in the bulk gas (see Figure 6.12);

(3). Radial temperature and concentration profiles are assumed to be uniform in the solid phase (see Figure 6.12);

(4). Adiabatic conditions are assumed in the monolith reactor, and the heat released by the catalytic reactions inside the washcoat is transferred to the gas phase by convection;

(5). In the washcoat species are transported in the radial direction by diffusion, and it is assumed that there is no diffusion in the axial direction along the washcoat.

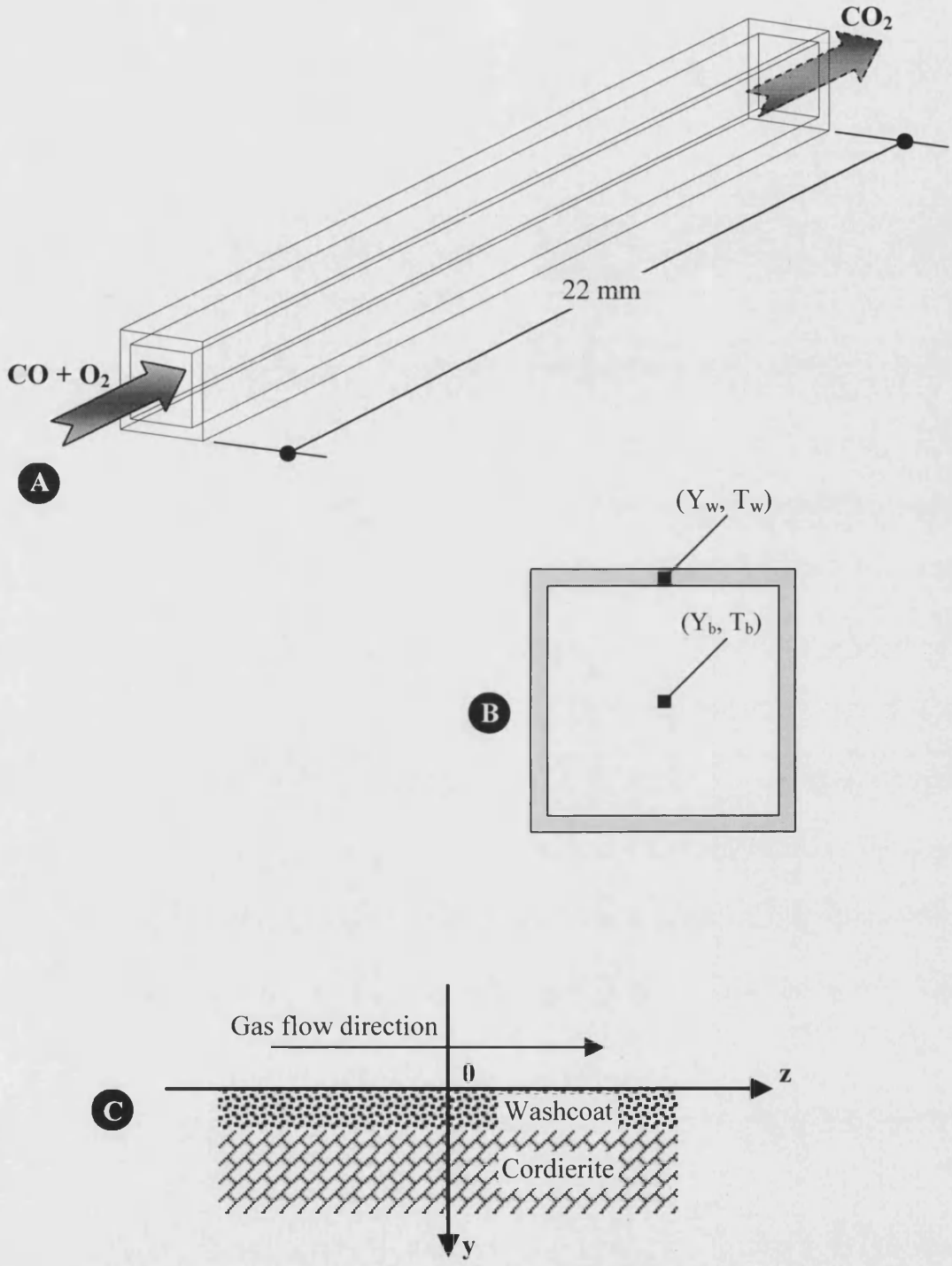

Figure 6.12 Schematic of a single channel in the monolith.

(A): The channel; (B) Cross-section; (C) Interface between the cordierite, washcoat and gas phase.

Based on a worked case study example in Hayes & Kolaczkowski (1997), Pages 318-320, the following are the equations for the catalytic monolith.

Gas phase material balance

$$\left[\text{Change in molar bulk flow of CO}\right] = \left[\text{Moles of CO transported to catalyst surface}\right] \quad (6.11)$$

$$-v\,C_b \frac{dY_b}{dz} = \frac{4}{D_H} k_m\, C_b\,(Y_b - Y_w) \quad (6.12)$$

where:

v The average velocity of the mixture gases, $m.s^{-1}$

D_H Hydraulic diameter of a single monolith channel, m. D_H is defined as:

$$\text{“}\frac{4 \times \textit{Inside cross} - \textit{Section area of channel}}{\textit{Inside perimeter of channel}}\text{”}$$

see Hayes & Kolaczkowski (1997), Page 651. The calculated value for this reactor is 1.14×10^{-3} m.

Re-arranging Equation 6.12:

$$\frac{dY_b}{dz} = \frac{4}{D_H} \frac{k_m\,(Y_w - Y_b)}{v} \quad (6.13)$$

The value of mass transfer coefficient (k_m) in Equation 6.13 can be computed from Sherwood number (Sh), see Hayes & Kolaczkowski (1997), Page 668:

$$k_m = \frac{Sh\; D_{Bulk}}{D_H} \quad (6.14)$$

The value of Sh in Equation 6.14 can be calculated from Hayes & Kolaczkowski (1997), Page 314:

$$Sh = 3.66 \times \left(1 + 0.095 \times \frac{D_H}{L} \mathrm{Re}\ Sc\right)^{0.45} \tag{6.15}$$

The value of Schmidt number (Sc) in Equation 6.15 can be obtained from Hayes & Kolaczkowski (1997), Page 668:

$$Sc = \frac{\mu}{\rho_m D_{Bulk}} \tag{6.16}$$

where:

μ Dynamic viscosity of air, Pa.s

ρ_m Inlet mass density of air, $kg.m^{-3}$

Solid phase material balance

$$[\text{Moles of CO reacted}] = [\text{Moles of CO transported to catalyst surface}] \tag{6.17}$$

$$\eta\left(-R_{CO}\right) = k_m C_b \left(Y_b - Y_w\right) \tag{6.18}$$

As

$$\left(-R_{CO}\right) = A_w \exp\left(-\frac{E_w}{R_g T_w}\right) P^{\alpha}\, C_b\, Y_w \qquad \text{(See 6.9)}$$

Then substituting Equation 6.9 into Equation 6.18:

$$\eta\, A_w \exp\left(-\frac{E_w}{R_g T_w}\right) P^{\alpha}\, C_b\, Y_w = k_m\, C_b \left(Y_b - Y_w\right) \tag{6.19}$$

The reaction rate constant (k) is defined as:

$$k = A_w \exp\left(-\frac{E_w}{R_g T_w}\right) \tag{6.20}$$

Substituting Equations 6.20 into 6.19, then Y_w can be represented as:

$$Y_w = \frac{k_m Y_b}{\eta k P^{\alpha} + k_m} \tag{6.21}$$

The value of η in Equation 6.18 can be calculated from Hayes & Kolaczkowski (1997), Page 256:

$$\eta = \frac{\tanh(\Phi)}{\Phi} \tag{6.22}$$

where Φ is the Thiele modulus, dimensionless.

As the effect of pressures is included in the rate expression, then the value of Φ for a first order reaction in a flat slab, *e.g.* Hayes & Kolaczkowski (1997), Page 254, may be also adapted to include a pressure term as follows:

$$\Phi = L\sqrt{\frac{k_v P^{\alpha}}{D_{eff}}} = L\sqrt{\frac{k P^{\alpha}}{L D_{eff}}} \tag{6.23}$$

where:

L The "effective" thickness of washcoat, m. For the used catalyst, the value is 45.2 $\times 10^{-6}$ m. The calculation method has been described in Chapter 5

k_v Reaction rate constant based on catalyst volume, $k_v = \frac{k}{L}$, $s^{-1}.Pa^{-\alpha}$

D_{eff} Effective diffusivity of CO in air under reaction conditions in the catalyst, $m^2.s^{-1}$. In this chapter, the experimental D_{eff} of CO in N_2 will

be used to represent the D_{eff} of CO in air under reaction conditions.

It is very difficult to measure D_{eff} at the temperature of reaction; however, following the method described by Hayes & Kolaczkowski (1997) (Page 246), if the porosity (ε) and the tortuosity factor (τ) of the catalyst are assumed to be independent of temperature, then this can be estimated from the following equation:

$$D_{eff,T} = \frac{\varepsilon}{\tau} D_{M,T} \tag{6.24}$$

where:

$D_{eff,T}$ Effective diffusivity of CO in N_2 at a temperature T in the catalyst, $m^2.s^{-1}$

$D_{M,T}$ Diffusion coefficient of CO in N_2 at a temperature T in the catalyst, $m^2.s^{-1}$

In the above equation, $D_{M,T}$ can be calculated from:

$$\frac{1}{D_{M,T}} = \frac{1}{D_{Bulk,T}} + \frac{1}{D_{K,T}} \tag{6.25}$$

where:

$D_{Bulk,T}$ Molecular diffusion coefficient of CO in a mixture of CO and N_2 evaluated at a mean bulk temperature (T), $m^2.s^{-1}$. The value can be obtained from Equation 3.15 or from Equation AE.3 in Appendix E. Here the former is used.

$D_{K,T}$ Knudsen diffusion coefficient in the catalyst at a temperature T, $m^2.s^{-1}$. The value can be obtained from Equation 3.17.

In Equation 6.24, the value of ε can be obtained from Table 5.2, and the method to back-calculate the value of τ in actual auto-catalysts has been described in Section 3.7

and Section 5.6. For the single-plate catalyst (C2NM-1P), the calculated value of $\frac{\varepsilon}{\tau}$ is 0.212 (see Appendix I). This value was used in Equation 6.24 to determine $D_{eff,T}$ and the results are listed in Appendix J.

Gas phase energy balance

$$[\text{Enthalpy increase of gas}] = [\text{Heat added to gas from surface}] \tag{6.26}$$

$$v \rho C_p \frac{dT_b}{dz} = \frac{4}{D_H} h (T_w - T_b) \tag{6.27}$$

where:

v	The average velocity of the gas mixture, $m.s^{-1}$
ρ	Gas mole density, $mol.m^{-3}$
C_p	Constant pressure heat capacity of air, $J.mol^{-1}.K^{-1}$. The value is adapted from Hayes & Kolaczkowski (1997), Page 104, which is: $C_{p,air} = 28.09 + 0.1965\times10^{-2}\,T + 0.4799\times10^{-5}\,T^2 - 1.965\times10^{-9}\,T^3$
T_b	Bulk gas temperature, K
h	Heat transfer coefficient, $W.m^{-2}.K^{-1}$
T_w	Washcoat temperature, K

From Equation 6.27:

$$\frac{dT_b}{dz} = \frac{4}{D_H} \frac{h(T_w - T_b)}{v \rho C_p} \tag{6.28}$$

The value of the heat transfer coefficient (h) in the above equation was calculated from Hayes & Kolaczkowski (1997), Page 664:

$$h = \frac{Nu\ k_f}{D_H} \tag{6.29}$$

where:

k_f Thermal conductivity of air, $W.m^{-1}.K^{-1}$. The value can be obtained from Hayes & Kolaczkowski (1997), Page 660, which is:

$k_f = 1.679 \times 10^{-2} + 5.073 \times 10^{-5}\ T$

The value of Nusselt number (Nu) in the above equation can be obtained from Hayes & Kolaczkowski (1997), Page 316:

$$Nu = 2.977 + 6.854 \times \left(\frac{1000}{Gz}\right)^{-0.5174} \exp\left(\frac{-42.49}{Gz}\right) \tag{6.30}$$

The value of Graetz number (Gz) in the above equation can be obtained from Hayes & Kolaczkowski (1997), Page 663:

$$Gz = \frac{D_H}{z} \text{ Re Pr} \tag{6.31}$$

where:

z Distance from the entrance in the direction of gas flow, m

The value of Reynold number (Re) in the above equation can be obtained from Hayes & Kolaczkowski (1997), Page 667:

$$\text{Re} = \frac{\rho_m D_H \nu}{\mu} \tag{6.32}$$

where:

ρ_m Inlet mass density of air, $kg.m^{-3}$

μ Dynamic viscosity of air, Pa.s. The value is obtained from Hayes &

Kolaczkowski (1997), Page 660, which is:

$\mu = 7.701\times10^{-6} + 4.166\times10^{-8}\ T - 7.531\times10^{-12}\ T^2$

The value of Prandtl number (Pr) in Equation 6.31 can be obtained from Hayes & Kolaczkowski (1997), Page 666:

$$\mathrm{Pr} = \frac{C_{p,m}\ \mu}{k_f} \tag{6.33}$$

where:

$C_{p,m}$ Mass heat capacity of air, $J.kg^{-1}.K^{-1}$

Solid phase energy balance

$$[\text{Heat released by reaction}] = [\text{Heat transferred to gas by convection}] \tag{6.34}$$

$$-\eta\,(\Delta H)_R\,(-R_{CO}) = h\,(T_w - T_b) \tag{6.35}$$

As

$$v\,\rho\,C_p\,\frac{dT_b}{dz} = \frac{4}{D_H}\,h\,(T_w - T_b) \qquad \text{(see 6.24)}$$

Then substituting Equation 6.35 into 6.24:

$$v\,\rho\,C_p\,\frac{dT_b}{dz} = -\eta\ (\Delta H)_R\ (-R_{CO})\ \frac{4}{D_H} \tag{6.36}$$

where:

$(\Delta H)_R$ Heat of reaction, J.mol^{-1}. As the value at a high temperature, *e.g.* 800 K, is approximately the same as that at 298.15 K (see Hayes & Kolaczkowski (1997), Page 120), then a fixed value of $(\Delta H)_R$ is assigned. The value of $(\Delta H)_R$ is computed from (Hayes & Kolaczkowski (1997), Page 104):

$$
\begin{aligned}
(\Delta H)_R &= \Delta H_f{}^{T}{}_{,CO_2} - \Delta H_f{}^{T}{}_{,CO} \approx \Delta H_f{}^{0}{}_{,CO_2} - \Delta H_f{}^{0}{}_{,CO} \\
&= (-393.8\,kJ.mol^{-1}) - (-110.6\,kJ.mol^{-1}) \\
&= -283.2\,kJ.mol^{-1}
\end{aligned}
$$

As ($-R_{CO}$) can be represented as:

$$(-R_{CO}) = A_w \exp\left(-\frac{E_w}{R_g T}\right) P^{\alpha}\, C_b\, Y_w \qquad \text{(see 6.9)}$$

and

$$k = A_w \exp\left(-\frac{E_w}{R_g T_w}\right) \qquad \text{(see 6.17)}$$

then Equation 6.9 will becomes:

$$(-R_{CO}) = k\, P^{\alpha}\, C_b\, Y_w \qquad (6.37)$$

From Equations 6.36 and 6.37, $\frac{dT_b}{dz}$ can be represented as:

$$\frac{dT_b}{dz} = \frac{4}{D_H} \frac{-\eta k P^{\alpha} C_b Y_w}{\rho v C_p} (\Delta H)_R \qquad (6.38)$$

Combine Equations 6.28 and 6.38, the following equation can be obtained:

$$T_w = \frac{-\eta}{h} k P^{\alpha} C_b Y_w (\Delta H_R) + T_b \tag{6.39}$$

Key equations

In summary, there are four key equations that represent the monolith reactor. These are:

$$\frac{dY_b}{dz} = \frac{4}{D_H} \frac{k_m (Y_w - Y_b)}{v} \tag{6.13}$$

$$Y_w = \frac{k_m Y_b}{\eta k P^{\alpha} + k_m} \tag{6.21}$$

$$\frac{dT_b}{dz} = \frac{4}{D_H} \frac{-\eta k P^{\alpha} C_b Y_w}{\rho v C_p} (\Delta H)_R \tag{6.38}$$

$$T_w = \frac{-\eta}{h} k P^{\alpha} C_b Y_w (\Delta H_R) + T_b \tag{6.39}$$

For the purpose of evaluating the two unknown coefficients (A_w and α), the experimental data for Figure 6.8 that is listed in Appendix G were used. This was selected for the following reasons:

(a) The temperatures range was wide (from 415.9 K to 742.1 K). This ensured that both the kinetic and intraphase diffusion regimes were covered.

(b) Gas inlet velocity was high (more than 140 $m.s^{-1}$) and this minimized the effects of mass transfer limitations between the bulk gas stream and the surface of the catalyst.

(c) Pressure varied from 1.845 to 2.302 bar (a).

The model that has been formulated is an initial value problem, where the initial conditions into the reactor are known. For example, in Run 1 (where the test points in the Matlab programme is labelled as T1 in the experiment records for Figure 6.8 in Appendix G):

Known initial conditions at z = 0 mm

Items	**Labels in Appendix G**	**Data**
T_b (inlet temperature)	T_{inlet} (after CO is fed)	415.9 K
C_b (inlet gases concentration)	Air flowrate	41.49 $mol.m^{-3}$
Y_b (inlet CO fraction)	$C_{in,c}$ (after CO is fed, calibrated)	969 ppm
Pressure	$P_{reactor}$ (after CO is fed)	1.845 bar (a)
Air velocity at reaction temperature	Air velocity at reaction temperature	140.6 $m.s^{-1}$
CO flowrate	CO flowrate	699.5 $ml.min^{-1}$
CO flowrate	CO flowrate	0.000484 $mol.s^{-1}$

Known outlet condition at z = 22 mm:

Items	**Labels in Appendix G**	**Data**
T_b (outlet temperature)	T_{oulet} (after CO is fed)	417.1 K
Y_b (outlet CO fraction)	$C_{out,a}$ (after CO is fed)	952 ppm

The equations were solved making use of a package known as MATLAB. The program was run with different values of the two unknown coefficients (A_w and α), and the calculated values of gas outlet temperatures and the mole fractions of CO in the outlet were compared with experimental data.

6.6.2 Determination of the values of A_w and α

A flowsheet of the MATLAB program is illustrated in Figure 6.13 and a listing of the code is available in Appendix K. Values of A_w and α are adjusted in a loop, searching for a good match between simulated and experimental data.

In comparing the match between the calculated values and experimental data, the following criterion was used:

$$\sigma = \sum_{n=1}^{10}\left(\frac{T_{n,measured} - T_{n,calculated}}{T_{n,measured}}\right)^2 + \sum_{n=1}^{10}\left(\frac{Y_{n,measured} - Y_{n,calculated}}{Y_{n,measured}}\right)^2 + \sum_{n=1}^{10}\frac{\left[(-R_{CO,n,measured}) - (-R_{CO,n,calculated})\right]^2}{(-R_{CO,n,measured}) \times (-R_{CO,n,calculated})} \Rightarrow Minimum \quad (6.40)$$

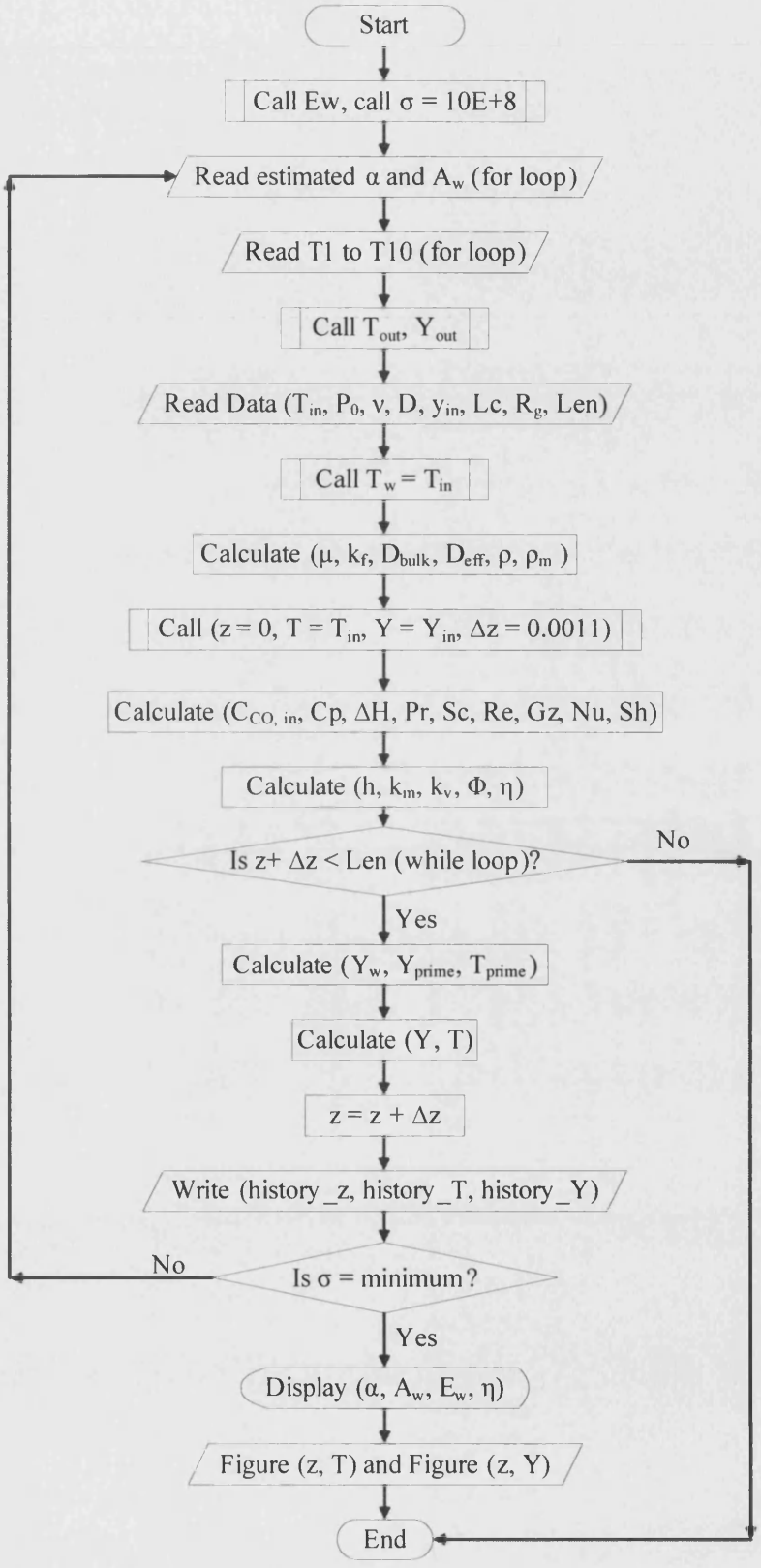

Figure 6.13 Flowsheet of the MATLAB program to estimate the values of A_w and α in the rate expression.

To find the minimum value of σ across a wide range of conditions, the following values were selected:

A_w	10^7 to 10^{16} (stepped at $10^{0.1}$) $m.s^{-1}.pa^{-\alpha}$
α	-2.6 to 0.2 (stepped at 0.1)

After running the MATLAB programme, the following results were obtained:

A_w	7.9433×10^{15} $m.s^{-1}.pa^{-\alpha}$
α	-1.10
σ	0.2037

It is therefore concluded that under the set of experimental conditions tested, for the platinum based diesel oxidation catalyst, the rate expression can be represented as:

$$(-R_{CO}) = 7.9433\times10^{15} \exp\left(-\frac{104000}{R_g T}\right) P^{-1.1}\, C_b\, Y_{CO} \quad (\text{mol.m}^{-2}.\text{s}^{-1}) \qquad (6.41)$$

As α is –1.1, this implies that pressure has an important effect on the reaction rate.

The value of effective factor (η) at different inlet temperatures were also calculated and these are shown in Figure 6.14. From this plot, it is clear that the region where the value of effective factor (η) starts to sharply decrease is 460.9 K to 512.8 K (187.7 °C to 239.6 °C). This also matches the curve shown in Figure 6.8.

The simulated outlet temperatures are compared with the experimentally measured values and these are shown in Figure 6.15. It can be seen the difference is small and the average error is less than 1%.

The simulated outlet CO fractions are also compared with the experimentally measured values and these are shown in Figure 6.16. The match is reasonable and the average error is less than 11%.

The simulated reaction rates are also compared with the experimentally measured values. The match is reasonable in the medium temperature range (*e.g.* from T3 to T6, *i.e.* 460.9 to 559.2 K). In the low and high temperature ranges, differences are observed. The reason for this may be summarised as follows:

1. At lower temperature, *e.g.* 443.7K, the reaction rate is quite slow (*e.g.* 2.84×10^{-4} $mol.s^{-1}.m^{-2}$), and the conversion of CO is also very low. The criterion in Equation 6.40 will become less sensitive to changes in the reaction rate.

2. At higher temperature, *e.g.* 654.6 to 744.3 K, the reaction is in the diffusion–controlled region. From the experimental data, it is evident that both reaction rates and the CO conversion are steady. However, in the simulation, although the effectiveness factor is approaching zero, values at high temperatures are not close enough to zero to maintain the rate of reaction constant with further increases in temperature.

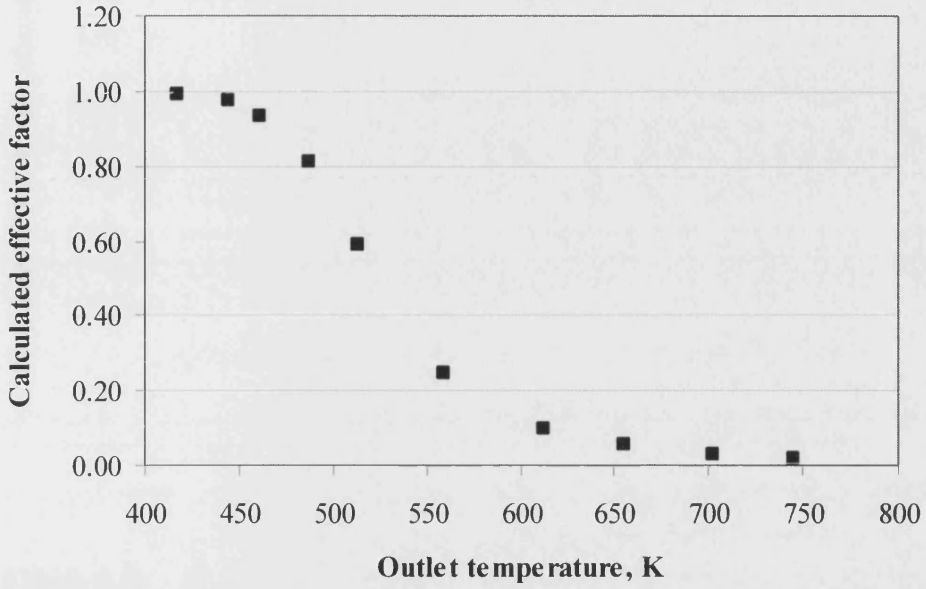

Figure 6.14 The calculated effective factors (η) at different outlet temperatures.

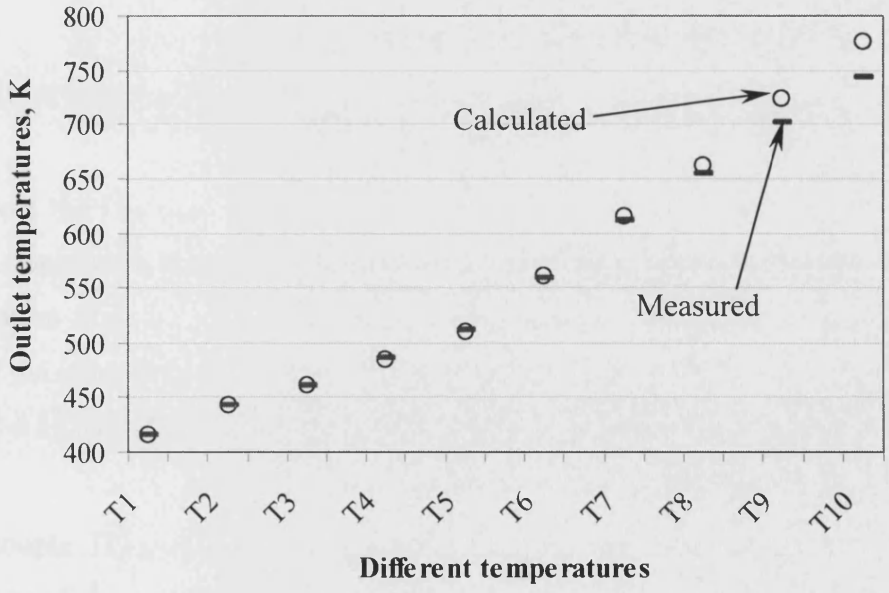

Figure 6.15 Comparison of measured and calculated outlet temperatures.

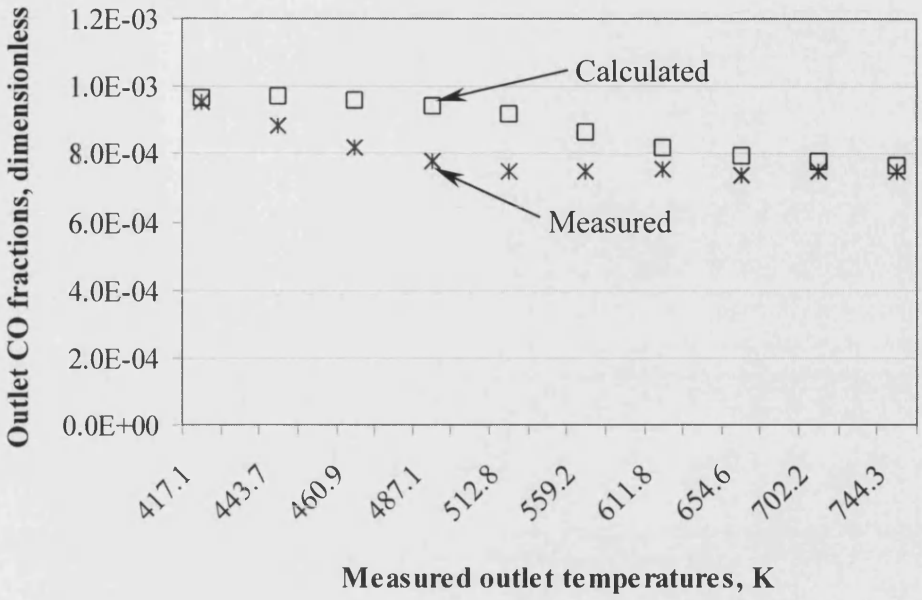

Figure 6.16 Comparison of measured and calculated outlet CO fractions at different outlet temperatures

6.7 Analysis of errors

6.7.1 Errors from the experimental apparatus

Errors from the CO analyser have already been described in Chapter 3. A comparison between measured CO concentration with the CO analyser and the calculated concentration from the ratio of CO to air in the feed is shown in Figure 6.7. It can be seen that the inlet CO concentration at 970 varies by ± 15 ppm, and air flowrate at 720 varies by ± 10 l/min. The error caused by this variation is ± 1.5%.

Thermocouple TI5 was calibrated with TI4 and TI6, see Figure 6.6 and Appendix F. This is one of the methods to minimise the relative errors of the three thermocouples. The error caused by temperatures is minor, and is less than ± 0.5%.

6.7.2 Errors from the analysis and calculation method

In order to explore the effects of gas inlet temperature, inlet concentration and flowrate, a series of experiments were performed. For each experimental steady state condition, fractional conversion and reaction rates of CO were calculated from the measurement of CO concentration across the reactor using Equation 6.1 & 6.2.

The calculation of the conversion of CO is only determined from the outlet and inlet CO concentrations, which were measured with the same CO analyser. So the error is only from the CO analyser itself, which has been analysed in Chapter 3.

The calculation of the reaction rate of CO is determined by the inlet molar flow of CO, the fraction conversion and the geometric surface area of the sample. The geometric surface area of the sample has to be estimated because some channels in the sample are not complete and the washcoat layer has been partially damaged (see Figure 6.2. Error caused by the estimation is about ± 2%.

6.8 Conclusions

From this experimental study, the following conclusions have been drawn:

1. It was shown that even at gas velocities in a channel of a catalytic converter that are 50 to 100 times higher than that in a commercial application, mass transfer effects (external and diffusion in catalyst layer) have a very strong influence, and above a gas inlet temperature of 225 °C these effects are clearly dominant.

2. In the mass transfer control region, the rate of reaction is affected by CO concentration. The reaction rate increases linearly with an increase in CO concentration.

3. In the mass transfer control region, the rate of reaction increases linearly as gas flowrate is increased.

4. Pressure has an important effect on the rate of reaction. Under the set of experimental condition studied, for the platinum based diesel oxidation catalyst, the rate expression can be represented as:

$$(-R_{CO}) = 7.9433\times10^{15} \exp\left(-\frac{104000}{R_g T}\right) P^{-1.1}\, C_b\, Y_{CO} \quad (\text{mol.m}^{-2}.\text{s}^{-1})$$

$$(-R_{CO}) = 7.9433\times10^{15} \exp$$

Chapter 7 Concluding remarks and outlook

7.1 Concluding remarks

Several important conclusions can be drawn from the discussions that have been presented in the thesis.

7.1.1 Measurement of D_{eff} in single-layer or multi-layer cordierite

From this experimental study, the following conclusions have been drawn:

1. A modified Wicke-Kallenbach diffusion cell is suitable for the measurement of effective diffusivity of cordierite samples, either for one-plate, two-plate or three-plate samples. For this diffusion cell and the measurement rig, the suitable operating conditions are as follows:

   Temperature: room temperature (17.4 ± 2.3 °C);

   Pressure in the cell: 1.01 to 1.51 bar (a);

   Gas inlet flowrate: 500 to 800 ml/min (measured at room temperature, and atmosphere pressure);

   Gases inlet directions: pure nitrogen from the two side-inlet points in the upper chamber; 2.4% CO (balanced by nitrogen) from the two side-inlet points in the lower chamber;

   Position of sample: always in the lower chamber and always facing down.

2. At the above operating conditions, the experimental D_{eff} values in cordierite samples are as follows:

   $(11.33 \pm 0.37) \times 10^{-7}$ m^2/s for 1-plate smooth-surface cordierite;

$(9.58 \pm 0.49) \times 10^{-7}$ m^2/s is for 1-plate rough-surface cordierite;

$(10.19 \pm 0.29) \times 10^{-7}$ m^2/s for 2-plate rough-surface cordierite;

$(12.42 \pm 0.11) \times 10^{-7}$ m^2/s for 3-plate rough-surface cordierite.

These experimental values are close to the D_{eff} value of methane in cordierite, $(9.2 \pm 3.8) \times 10^{-7}$, see Hayes and Kolaczkowski (2000).

3. The back-calculated tortuosity value, τ, in the 1-plate rough-surface cordierite is 6.26 ± 0.34, which lies within the range of published data on similar materials.

4. The measured D_{eff} value of the 1-plate smooth-surface cordierite sample is about 17% greater than that of 1-plate rough-surface cordierite.

5. Experimentally determined D_{eff} values vary slightly with the operating pressure.

6. As gas inlet flowrate is increased above 500 ml/min (at experimental conditions), the D_{eff} values remain constant.

7. Although the average pore diameter of cordierite is 3.4 microns, Knudsen diffusion appears to be the dominant mode of diffusion through the cordierite.

7.1.2 Measurement of D_{eff} in washcoated cordierite plates

1. The modified diffusion cell is suitable for the measurement of effective diffusivity in coated cordierite samples with commercial slurries. Using the D_{eff} data of smooth-surface cordierite, the D_{eff} value in washcoat can be back-calculated.

2. The measured D_{eff} values in the washcoat (from Slurry S3 and S3w) were shown to increase with washcoat thickness. This represents the influence of an interface/penetration layer which is formed as the washcoat penetrates the macropores in the cordierite layer. As the washcoat thickness increased, D_{eff}

values appeared to approach an asymptotic value of $(10.0 \pm 2.0) \times 10^{-7}$ m^2/s. This value is a factor of 2 to 15 times higher than that reported in Hayes *et al.* (2000) for an alumina based washcoat, where the values were found to lie in the range of 0.6×10^{-7} to 4.2×10^{-7} m^2/s. It should be noted that the alumina washcoat used in Hayes *et al.* (2000) had been prepared by a different supplier of catalysts. This observation is important, as it demonstrates the need to evaluate the D_{eff} in the actual washcoat used in the reactor, rather than choosing a literature value.

3. The back-calculated tortuosity factor (τ) in S3, S3w and S3HT are

S3	1.65 ± 0.87
S3w	2.25 ± 0.23
S3HT	0.86 ± 0.02

They are within the range of published data on similar materials.

4. Although the D_{eff} value slightly decrease (about 5.9%) for the re-calcined and aged sample (700 °C for 16 hours in 10% H_2O + 10% O_2 + 80% N_2), the difference was within experimental errors. It was a little surprising that the difference was not more significant.

5. The D_{eff} value in the presence of 3.18 g/l Pt was only 7.6% smaller than for the washcoat. This is not significant as it is within experimental errors. This observation is important, as D_{eff} values can be assigned to a washcoat without being too concerned over the effect of the dispersion of catalyst.

7.1.3 Measurement of D_{eff} in commercial catalytic converters

1. The modified diffusion cell is suitable for the measurement of effective diffusivity in samples cut from an actual DOC. This method can be applied to either single-plate or multi-plate samples.

2. The experimental D_{eff} values in the DOC catalysts were found to have the following values:

   $(3.42 \pm 0.65) \times 10^{-7}$ m^2/s for the fresh C2NM DOC (calcined at 500 °C);

   $(3.32 \pm 0.71) \times 10^{-7}$ m^2/s is for the aged C2HT DOC (calcined at 700 °C).

   Comparing the D_{eff} values for the fresh and aged DOC, there is no obvious difference.

3. The back-calculated tortuosity values, τ, are as follows:

   (2.62 ± 0.50) in Sample C2NM (calcined at 500 °C);

   (2.37 ± 0.51) in Sample C2HT (calcined at 700 °C).

   They lie within the range of published data on similar alumina-based materials

4. The measured value of D_{eff} in the two-cell samples is slightly higher than that in the one-cell samples.

5. The D_{eff} values determined for the washcoat in the coated monolith DOC are similar to the washcoat prepared on the coated plate. This observation is important, as it offers a simple method of evaluating the D_{eff} for a commercial catalyst.

7.1.4 Investigation of CO oxidation in commercial catalytic converters

1. It was shown that even at gas velocities in a channel of a catalytic converter that are 50 to 100 times higher than in a commercial application, mass transfer effects (external and diffusion in catalyst layer) have a very strong influence, and above a gas inlet temperature of 225 °C these effects are clearly dominant.

2. In the mass transfer control region, the rate of reaction is affected by CO concentration. The reaction rate increases linearly with an increase in CO concentration.

3. In the mass transfer control region, the rate of reaction increases linearly as gas flowrate is increased.

4. Pressure has an important effect on the rate of reaction. Under the set of experimental condition studied, for the platinum based diesel oxidation catalyst, the rate expression can be represented as:

$$(-R_{CO}) = 7.9433\times10^{15} \exp\left(-\frac{104000}{R_g T}\right) P^{-1.1}\, C_b\, Y_{CO} \quad (\text{mol.m}^{-2}.\text{s}^{-1})$$

7.2 Suggested direction of research

7.2.1 Preparation of pure washcoat plates without cordierite support

In this thesis, a method to measure the effective diffusivity of gases in commercial catalytic converters has been developed. This method could also be applied in many areas where catalytic monoliths are used, *e.g.* catalytic converters, catalytic combustion reactors. However, the calculation of the effective diffusivity in the washcoat is very difficult due to the irregular configuration of the coated cordierite as well as the effect

of the interface between the washcoat and the cordierite. If the measurement of D_{eff} values could be performed through a pure washcoat plate (without cordierite support), the measured results would be more reliable.

7.2.2 Variation of pores size and pores volume

It would be interesting to perform experiments on washcoats prepared by another catalytic supplier, where the particle size of the slurry could also be varied.

7.2.3 Improving D_{eff} by changing porosity and tortuosity

It would be interesting to examine in more detail how the porosity and tortuosity influence the effective diffusivity.

7.2.4 Multi-layer washcoat

It would be interesting to perform D_{eff} experiments on multi-layered washcoat structures.

7.2.5 Effect of pressure on the rate of CO oxidation reaction

In this thesis, over a limited range of operating pressures, it was shown that pressure had an important effect on the rate of reaction. It is strongly recommended that this aspect be studied in more detail over a wider range of operating pressures.

References

Ahn, T., Pinczewski, W. V., Trimm, D. L. (1986). Transient performance of catalytic combustors for gas turbine applications. *Chemical Engineering Science,* **41**(1), 55-64.

Aimard, F., Li, S., & Sorine, M. (1996). Mathematical modelling of automotive three-way catalytic converters with oxygen storage capacity. *Control Engineering Practice*, **4**(8), 1119-1124.

Akama, H., *et al.* (2002). Exhaust gas purifying system and method. *United States Patent Application Publication*, No US 2002/0053202 A1.

Alexander, J. T., & Umehara, K. (1995). Ceramic honeycomb for air pollution control. NKG Insulator Ltd., Nagoya, Japan, Reference JH-952128, July.

Al-rqobah, H. A., Kam, E. K. T., & Hughes, R. (1988). Dynamic determination of diffusion in porous particles. *Chem. Eng. Res. Des.*, **66**, 275-283.

Amatayakul, W., & Ramnäs, O. (2001). Life cycle assessment of a catalytic converter for passenger cars. *Journal of Cleaner Production*, **9**, 395-403.

Angove, D. E., Cant, N. W., Bailey, G. M., & Cohen, D. D. (1996). The application of PIXE to the mapping of contaminants deposited on a monolithic automotive catalytic converter. *Nuclear Instruments and Methods in Physics Research Section B: Beam Interactions with Materials and Atoms*, **109-110**, 563-568.

Aris, R. (1975). The mathematical theory of diffusion and reaction in permeable catalysis. *The theory of the steady state*, Volume I, Oxford: Clarendon Press.

Artelt, S., Kock, H., König, H. P., Levsen, K., & Rosner, G. (1999). Engine dynamometer experiments: platinum emissions from differently aged three-way catalytic converters. *Atmospheric Environment*, **33**(21), 3559-3567.

Baba, N., Ohsawa, K., & Sugiura, S. (1996). Analysis of transient thermal and conversion characteristics of catalytic converters during warm-up. *JSAE Review*, **17**(3), 273-279.

Baiker, A., New, M., & Richarz, W. (1982). Determination of intraparticle diffusion coefficients in catalyst pellets – a comparative study of measuring methods. *Chemical Engineering Science*, **37**(4), 643-656.

Balakotaiah, V., & West, D. H. (2002). Shape normalization and analysis of the mass

transfer controlled regime in catalytic monoliths. *Chemical Engineering Science*, **57**, 1269-1286.

Barbante, C., Veysseyre, A., Ferrari, C., van de Velde, K., Morel, C., Capodaglio, G., Cescon, P., Scarponi, G., & Boutron, C. (2001). Greenland snow evidence of large-scale atmospheric contamination for platinum, palladium and rhodium. *Environmental Science & Technology*, **35**(5), 835-839.

Barrer, R. M. (1953). A new approach to gas flow in capillary systems. *J. Phys. Chem.*, **57**, 35-40.

Bartholomew, C. H. (2001). Mechanisms of catalyst deactivation. *Applied Catalysis A: General*, **212**(1-2), 17-60.

Beekman, J. W. (1991). Measurement of the effective diffusion coefficient of nitrogen monoxide through porous monolith-type ceramic catalysts. *Ind. Eng. Chem. Res.*, **30**, 428-430.

Bekyarova, E., Fornasiero, P., Kašpar, J., & Graziani, M. (1998). CO oxidation on Pd/CeO_2–ZrO_2 catalyst. *Catalyst Today*, **45**, 179-183.

Benson, M., Bennett, C. R., Harry, J. E., Patel, M. K., & Cross, M. (2000). The recovery mechanism of platinum group metals from catalytic converters in spent automotive exhaust systems. *Resources, Conservation and Recycling,* **31**(1), 1-7.

Bera, P., Patil, K. C., & Hegde, M. S. (2000). NO reduction, CO and hydrocarbon oxidation over combustion synthesized Ag/CeO_2 catalyst. *Phys. Chem. Chem. Phys.*, **2**(16), 3715-3719.

Bettman, M., & Otto, N. C (1983). A case of negative apparent activation energy due to pore diffusion effects. *Chemical Engineering Science*, **38**(3), 491-493.

Biswas, J., Do, D. D., Greenfield, P. F., & Smith, J. M. (1987). Evaluation of bidisperse transport properties of a reforming catalyst using a diffusion cell. I. Theoretical development. *Applied Catalysis*, **32**, 217-234.

Brandenburg, J. T., & Crone, Jr., J. M. (1984). Alumina catalyst stable at high temperatures. *United States Patent*, No 4438219.

Brown, L. F. & Travis, B. J. (1983). Using diffusion measurements to determine pore-size distributions in porous materials. *Chemical Engineering Science*, **38**(6), 843-847.

Chan, S. H. & Hoang, D. L. (1999). Heat transfer and chemical reactions in exhaust system of a cold-start engine. *International Journal of Heat and Mass Transfer*, **42** (22), 4165-

4183.

Chapman, S., & Cowling, T. G. (1970). *The mathematical theory of non-uniform gases*, the 7th edition, Cambridge University Press.

Chatterjee, D., Deutschmann, O., & Warnatz, J. (2001). Detailed surface reaction mechanism in a three-way catalyst. *Faraday Discussions,* **119**, 371-384.

Ciambelli, P., Palma, V., Tikhov, S. F., Sadykov, V. A., Isupova, L. A. & Lisi, L. (1999). Catalytic activity of powder and monolith perovskites in methane combustion. *Catalysis Today*, **47**(1-4), 199-207.

Cowley, A. (1999). *Platinum.* Johnson Matthey: London.

Doğu, G., Keskin, A., & Doğu, T. (1987). Macropore and micropore effective diffusion coefficients from dynamic single-pellet experiments. *AIChE Journal*, **33**(2), 322-324.

Doğu, G., & Smith, J. M. (1975). A dynamic method for catalyst diffusivities. *AIChE Journal*, **21**(1), 58-61.

Drewsen, A., Ljungqvist, A., Skoglundh, M., & Andersson, B. (2000). Effects of the radial distribution of platinum in spherical alumina catalysts on the oxidation of CO in air. *Chemical Engineering Science,* **55**(21), 4939-4951.

Dubien, C., Schweich, D., Mabilon, G., Martin, B., & Prigent, M. (1998). Three-way catalytic converter modelling: fast- and slow-oxidizing hydrocarbons, inhibiting species, and steam-reforming reaction. *Chemical Engineering Science*, **53**(3), 471-481.

Duduković, M. P. (1982). An analytical solution for the transient response in a diffusion cell of the Wicke-Kallenbach type. *Chemical Engineering Science*, **37**(2), 153-158.

Duffy, B. L., Nelson, P. F., Ye, Y., Weeks, I. A., & Galbally, I. E. (1998). Emissions of benzene, toluene, xylenes and 1,3-butadiene from a representative portion of the Australian car fleet. *Atmospheric Environment*, **32**(14-15), 2693-2704.

Evans, R. B., III, Watson, G. M., & Mason, E. A. (1961). Gaseous diffusion in porous media at uniform pressure. *The Journal of Chemical Physics*, **35**(6), 2076-2083.

Farrauto, J. B., & Heck, M. H. (1999). Catalytic converters: state of the art and perspectives. *Catalysis Today*, **51**(3-4), 351–360.

Flatley, C. (2001). Catalytic combustion of liquid fuels. *PhD thesis,* University of Bath, UK.

Froment, G. F., & Bishchaff, R. B. (1990). *Chemical Reaction Analysis and Design*, the 2nd edition, John Wiley of Sons Inc., 125-197.

Fuller, E. N., Schettler, P. D., & Giddings, J. C. (1966). A new method for prediction of binary gas-phase diffusion coefficients. *Industrial and Engineering Chemistry*, **58**(5), 19-27.

Gandhi, H. S., & Shelef, M. (1991). Effects of sulphur on noble metal automotive catalysts. *Applied Catalysis*, **77**(2), 175-186.

García-Ochoa, F., & Santos, A. (1994). Effective diffusivity under inert and reaction conditions. *Chemical Engineering Science*, **49**(18), 3091-3102.

Golunski, S. E., Hatcher, H. A., Rajaram, R. R., & Truex, T. J. (1995). Origins of low-temperature three-way activity in Pt/CeO_2. *Applied Catalysis B: Environmental*, **5**, 367-376.

González-Velasco, J. R., Botas, J. A., Ferret, R., González-Marcos, M. P., Marc, J. -L., & Gutiérrez-Ortiz, M. A. (2000). Thermal ageing of Pd/Pt/Rh automotive catalysts under a cycled oxidising-reducing environment. *Catalysis Today*, **59**(3-4), 395-402.

Gorring, R. L., & deRosset, A. J. (1964). Gas diffusion in porous catalysts. Diffusion-controlled elution of physically adsorbed hydrocarbons. *Journal of Catalysis*, **3**, 341-352.

Gregg, S. J., & Sing, K. S. W. (1982). *Adsorption, surface area and porosity*. Academic Press, London.

Groppi, G., Tronconi, E., Forzatti, P. (1993). Modelling op catalytic combustors for gas turbine applications. *Catalysis Today*, **17**(1-2), 237-249.

Groppi, G., Ibashi, W., Tronconi, E., & Forzatti, P. (2001). Structured reactors for kinetic measurements under severe conditions in catalytic combustion over palladium supported systems. *Catalysis Today*, **69**(1-4), 399-408.

Gunn, R. D., & King, C. J. (1969). Mass transport in porous materials under combined gradients of composition and pressure. *AIChE Journal*, **15**(4), 507-514.

Gupta, N., & Balakotaiah, V. (2001). Heat and mass transfer coefficients in catalytic monoliths. *Chemical Engineering Science*, **56**, 4771-4786.

Harris, D. J., Yong, D. J., & Trimm, D. L. (1982). The sintering of alumina based catalysts. *Proceedings 10th Australian Chemical Engineering Conference*, Chemaca, Sydney, 24-26th August 1982, 175-179.

Harris, R. M. (2001). *Pollution: causes, effects, and control*. Published by The Royal Society of Chemistry, the 4th edition.

Hayes, R. E., & Kolaczkowski, S. T. (1994). Mass and heat transfer effects in catalytic monolith reactors. *Chemical Engineering Science*, **49**(21), 3587-3599.

Hayes, R. E., & Kolaczkowski, S. T. (1997). *Introduction to Catalytic Combustion*, Gordon and Breach Science Publishers, Reading.

Hayes, R. E. & Kolaczkowski, S. T. (1999). A study of Nusselt and Sherwood numbers in a monolith reactor. *Catalysis Today,* **47**(1-4), 295-303.

Hayes, R. E., Kolaczkowski, S. T., Li, P. K., & Awdry, S. (2000). Evaluating the effective diffusivity of methane in the washcoat of a honeycomb monolith. *Applied Catalyst, Part B: Environmental*, **25**(2-3), 93-104.

Hayes, R. E., Kolaczkowski, S. T., Li, P. K., & Awdry, S. (2001). The palladium catalysed oxidation of methane: reaction kinetics and the effect of diffusion barriers. *Chemical Engineering Science*, **56**(16), 4815-4835.

Haynes, H. W., Jr. (1982). Diffusion and reaction in porous media – I. *American Institute of Chemical Engineers. Modilar Instruction Series. Module E3.1.* ISSN 0270-7529/83/0516-0001.

Haynes, H. W., Jr. (1988). The experimental evaluation of catalyst effective diffusivity. *Catalysis Reviews – Science and Engineering*, **30**(4), 563-627.

Heck, R. M., & Farrauto, R. J. (2001). Automobile exhaust catalysts. *Applied Catalysis A: General,* **221**(1-2), 443-457.

Hindin, S. G., & Dettling, J. C. (1979). Catalyst manufacture. *United States Patent*, No 4134860.

Hirao, O., & Pefley, R. K. (1988). Present and future automotive fuels, A. *Wiley-Interscience Publisher*, New York.

Hoebink, J. H. B. J., van Gemert, R. A., van den Tillaart, J. A. A., & Marin, G. B. (2000). Competing reactions in three-way catalytic converters: modelling of the NOx conversion maximum in the light-off curves under net oxidising conditions. *Chemical Engineering Science*, **55**(9), 1573-1581.

Holmgren, A., & Andersson, B. (1998). Mass transfer in monolith catalysts – CO oxidation experiments and simulations. *Chemical Engineering Science*, **53**(13), 2285-2298.

Holmgren, A., (1999). Catalysts for car exhaust: oxygen storage in platinum/ceria and mass transfer in monoliths. *PhD thesis,* Chalmers University of Technology, Sweden, **1999**.

Hou, K, Fowles, M., & Hughes, R. (1999). Effective diffusivity measurement on porous catalyst pellets at elevated temperature and pressure. *Trans IChemE*, part A, **77**, 55-61.

HSU, L. -K. P., & Haynes, H. W., JR (1981). Effective diffusivity by the gas chromatography technique: analysis and application to measurement of diffusion of various hydrocarbons in zeolite nay. *AIChE Journal*, **27**(1), 81-91.

Hu, Z. -C., Heck, R. M., & Rabinowitz, H. N. (2001). Method for using a close-coupled catalyst. *US patent*, No 6254842 B1.

Huang, D. T. (2001). An integrated computer model for simulating electro-thermo-mechanical interactions of an exhaust oxygen sensor. *Finite Elements in Analysis and Design,* **37**(8), 657-672.

Imbihl, R. (2000). Model studies of catalysis with microstructured bimetallic surfaces. *Journal of Molecular Catalysis A: Chemical,* **158**(1), 101-106.

Incropera, F. P., & DeWitt, D. P. (2002). *Introduction to Heat Transfer* (Wiley, New York, USA).

Jahn, R., Šnita, D., Kubíček, M., & Marek, M. (1997). 3-D modelling of monolith reactors. *Catalysis Today*, **38**(1), 39-46.

James, C. E., Clive, R. N., Charles F. K., Mark, A. S., James, A. S., & Jinesh, C. J. (2001). Implications of platinum-group element accumulation along U.S. roads from catalytic-converter attrition. *Environment Science Technology,* **35**(19), 3816-3822.

Jelles, S. J. (1999). Diesel exhaust aftertreatment: development of catalytic systems for diesel particulate oxidation. *PhD Thesis.* Technical University of Delft, Netherlands.

Jirát, J., Kubíček, M., & Marek, M. (2001). Adsorber-reactor systems for emission treatment from mobile sources. *Chemical Engineering Science*, **56**(4), 1597-1604.

Jobson, E. (1998 & 1999). Personal communication. Gothenburg (Sweden): AB Volvo Technological Development.

Johnson, M. L. F., & Stewart, W. E. (1965). Pore structure and gaseous diffusion in solid catalysts. *Journal of Catalyst*, **4**, 248-252.

Johnson, E. (2003). LPG: a secure, cleaner transport fuel? A policy recommendation for Europe. *Energy Policy*, **31**(15), 1573-1577.

Kast, W., & Hohenthanner, C. -R. (2000). Mass transfer within the gas-phase of porous media. *International Journal of Heat and Mass Transfer*, **43**(5), 807-823.

Keith, J. M., Chang, H. -C., & Leighton, D. T., Jr. (2001). Designing a fast-igniting catalytic converter system. *AIChE Journal*, **47**(3), 650-663.

Keren, I., & Sheintuch, M. (2000). Modelling and analysis of spatiotemporal oscillatory patterns during CO oxidation in the catalytic converter. *Chemical Engineering Science*, **55**(8), 1461-1475.

Kim, C. -H., Woo, S. I., & Jeon, S. H. (2000). Recovery of Platinum-Group Metals from Recycled Automotive Catalytic Converters by Carbochlorination. *Industrial & Engineering Chemistry Research*, **39**(5), 1185-1192.

Kim, K. K., & Smith, J. M. (1974). Diffusion in nickel oxide pellets – effects of sintering and reduction. *AIChE Journal*, **20**(4), 670-678.

Kim, S. (2001). Measurement of the effective diffusivity of gasoline compounds in coated monoliths and associated factors. *PhD thesis,* University of Bath, UK.

Kirchner, T., & Eigenberger, G. (1996). Optimisation of the cold-start behaviour of automotive catalysts using an electrically heated pre-catalyst. *Chemical Engineering Science*, **51**(10), 2409-2418.

Kirchner, T., & Eigenberger, G. (1997). On the dynamic behaviour of automotive catalysts. *Catalysis Today*, **38**(1), 3-12.

Koberstein, E., & Wannemacher, G. (1987). The A/F window with three-way catalysis, In: Crucq, A., & Frennet, A. Editors, 1987, Kinetic and Surface Investigations. *Catalysis and Automotive Pollution Control*, Elsevier, Amsterdam, 155-172.

Koberstein, E., & Wannemacher, G. (1991) in *Catalysis and automotive pollution control* (Ed: Crucq, A., & Frennet, A). Elsevier, Amsterdam, 437-465.

Koci, P., Kubicek, M., & Marek, M. (2004). Multifunctional aspects of three-way catalyst – effects of complex washcoat composition. *Chemical Engineering Research and Design*, **82**(2), 284-292.

Kolaczkowski, S. T. (1999). Modelling catalytic combustion in monolith reactors – challenges faced. *Catalysis Today*, **47**, 209-218.

Kolaczkowski, S. T. (2002). Measurement of effective diffusivity in catalyst coated monoliths. *The 5th international workshop of catalytic combustion.* 15-18th May, Seoul, Korea.

Kolaczkowski, S. T. (2003). Measurement of effective diffusivity in catalyst-coated monoliths. *Catalysis Today*, **83**(1-4), 85-95.

Koltsakis, G. C. (1997A). Warm-up behaviour of monolithic reactors under non-reacting conditions. *Chemical Engineering Science,* **52**(17), 2891-2899.

Koltsakis, G. C., & Stamatelos, A. M. (1997A). Catalytic automotive exhaust aftertreatment. *Progress in Energy and Combustion Science*, **23**(1), 1-39.

Koltsakis, G. C., Konstantinidis, P. A., & Stamatelos, A. M. (1997B). Development and application range of mathematical models for 3-way catalytic converters. *Applied Catalysis B: Environmental,* **12**, 161-191.

Koltsakis, G. C., & Stamatelos, A. M. (1999). Dynamic behaviour issues in three-way catalyst modelling. *AIChE Journal*, **45**(3), 603-614.

Kruse, N., Frennet, A., & Bastin, J., -M. (1998). *Catalysis and automotive pollution control IV*. Published by Elsevier Science B.V., The Netherlands.

Kumar, S. V., Rabinowitz, H. N., & Steger, J. J. (2004). Multi-zone catalytic converter. *United States Patent*, No 20040001781.

Kummer, J. T. (1980). Catalysts for automobile emission control. *Prog. Energy Combustion Science*, **6**, 177-199.

Kurokawa, T., Takami, A., *et al.* (1997). Burned gas purifying catalyst. *US patent*, No 5677258.

Labhsetwar, N. K., Watanabe, A., Biniwale, R. B., Kumar, R., & Mitsuhashi, T. (2001). Alumina supported, perovskite oxide based catalytic materials and their auto-exhaust application. *Applied Catalysis B: Environmental*, **33**(2), 165-173.

Lachman, I. M., & Williams, J. L. (1992). Catalysts supports: chemistry, forming and characterization, extruded monolithic catalyst supports. *Catalysis Today*, **14**(2), 317-329.

Langmuir, I. (1922). The mechanism of the catalytic action of platinum in the reactions 2CO + $O_2 \leftrightarrow 2CO_2$ and $2H_2 + O_2 \leftrightarrow 2H_2O$. *Transactions of the Faraday Society*, **17**, 621-654.

Lee, C. -H., & Chen, Y. -W. (1997). Effect of support on a catalytic converter for removing CO and HC emissions from a two-stroke motorcycle. *Industrial & Engineering Chemistry Research*, **36**(12), 5160-5169.

Leung, D., Hayes, R. E., & Kolaczkowski, S. T. (1996). Diffusion limitation effects in the washcoat of a catalytic monolith reactor. *Canadian Journal of Chemical Engineering,* **74**, 94-103.

Li, D. (1988). Modelling of effective diffusivity of gases diffusion in porous catalysts. *Meng*

thesis, Dalian University of Technology, China.

Li, P. K. C. (1997). Catalytic combustion of methane in monoliths and the influence of diffusion barriers. *PhD thesis,* University of Bath, UK.

Liotta, L. F., Macaluso, A., Arena, G. E., Livi, M., Centi, G., & Deganello, G. (2002). A study of the behaviour of Pt supported on CeO_2–ZrO_2/Al_2O_3–BaO as NO_x storage–reduction catalyst for the treatment of lean burn engine emissions. *Catalysis Today*, **75**(1-4), 439-449.

Liu, B., Hayes, R. E., Checkel, M. D., Zheng M., & Mirosh E. (2001). Reversing flow catalytic converter for a natural gas/diesel dual fuel engine. *Chemical Engineering Science*, **56**(8), 2641-2658.

Lox, E. S. J., & Engler, B. H. (1997). Environmental catalysis – mobile sources. In Volume **4** of *Handbook of Heterogeneous Catalysis* edited by Ertl, G., knözinger, H., Weitkamp, J., 1559-1633. WILEY-VCH Verlag GmbH, Germany.

Lox, E. S. J., & Engler, B. H., Koberstein, E. (1991). Technical paper series 910841, *Society of automotive engineers*, Warrendale.

Marrero, T. R., & Mason, E. A. (1972). Gases diffusion coefficients. *Journal of Physical and Chemical Reference Data*, **1**(1), 1-118.

Martinez-Arias, A., Soria, J., *et al.* (1998). Influence of ceria dispersion on the catalytic performance of Cu/(CeO_2)/Al_2O_3 catalysts for the CO oxidation reaction. *Catalysis and Automotive Pollution Control IV, Studies in Surface Science and Catalysis*, **116**, 591-600.

Massing, E., Brilhac, J. F., Brillard, A., Gilot, P., & Prado, G. (2000). Modelling of the behaviour of a three-way catalytic converter at steady state influence of the propene diffusion inside the catalytic layer. *Chemical Engineering Science*, **55**(9), 1707-1716.

Merget, R., & Rosner, G. (2001). Evaluation of the health risk of platinum group metals emitted from automotive catalytic converters. *The Science of The Total Environment*, **270**(1-3), 165-173.

Mezedur, M. M., Kaviany, M., & Moore, W. (2002). Effect of Pore Structure, Randomness and Size on Effective Mass Diffusivity. *AIChE Journal*, **48**(1), 15-24.

Morbidelli, M., Gavriilidis, A., & Varma, A. (2001). Catalyst design: optimal distribution of catalyst in pellets, reactors, and membranes. Cambridge University Press.

Morlang, A., Neuhausen, U., Klementiev, K. V., Schütze, F. –W., Miehe, G., Fuess, H., and Lox, E. S. (2005). Bimetallic Pt/Pd diesel oxidation catalysts structural characterisation

and catalytic behaviour. *Applied Catalysis B: Environmental*, **60**, 195-203.

Mukadi, L. S., & Hayes, R. E. (2002). Modelling the three-way catalytic converter with mechanistic kinetics using the Newton–Krylov method on a parallel computer. *Computers & Chemical Engineering*, **26**(3), 439-455.

Murakami, H., Yamada, H., *et al.* (1999). Catalyst for purifying exhaust gas. *US patent*, No 5958828.

Mussmann, L., Lindner, D., Harris, M., Kreuzer, T., & Lox, E. (2001). Layered noble metal containing exhaust gas catalyst and its preparation. *US patent*, No 6294140 B1.

Nibbelke, R. H., Campman, M. A. J., Hoebink, J. H. B. J., & Marin, G. B. (1997). Kinetic Study of the CO Oxidation over $Pt/\gamma\text{-}Al_2O_3$and $Pt/Rh/CeO_2/\gamma\text{-}Al_2O_3$in the Presence of H_2O and CO_2. *Journal of Catalysis,* **171**(2), 358-373.

Nibbelke, R. H., Hoebink, J. H. B. J., Croon, M. H. J. M. de & Marin, G. B. (1998). Structural Stability of Kinetic Models: Anomalies Due to Irreversible Adsorption. *AIChE Journal,* **44**(4), 937-942.

Noda, N., Abe, F., & Suzuki, J. (2001). Catalyst-adsorbent for purification of exhaust gases and method for purification of exhaust gas. *US patent application publication*, No 2001/0053340 A1.

Oh, S. E., Cavendish, J. C., & Hegedus, L. L. (1980). Mathematical modeling of catalytic converter lightoff: single-pellet studies. *AIChE Journal*, **26**(6), 935-943.

Oh, S. H., & Cavendish, J. C. (1982). Transients of monolithic catalytic converters: response to step changes in feedstream temperature as related to controlling automobile emissions. *Industrial Engineering Chemical Production Research and Development*, **21**, 29-37.

Özkan, G., & Doğu, G. (1997). A Dynamic Study on Axial Dispersion and Adsorption in Catalytic Monoliths. *Industrial & Engineering Chemistry Research*, **36**(11), 4734-4739.

Park, I. –S., Do, D. D., & Rodrigues, A. E. (1996). Measurement of the effective diffusivity in porous media by the diffusion cell method. *Catal. Rev. Sci. Eng.*, **38**(2), 189-247.

Pfefferla W. C. (1977). Method of starting a combustion system utilising a catalyst. *US Patent*, No. 4019316.

Protter, M. H. & Morrey, C. B. (1991). A first course in real analysis. Second Edition. Springer-Verlag New York, Inc.

Psyllos, A. & Philippopoulos, C. (1992). Modelling of monolithic catalytic converters used

in automotive pollution control. *Applied Mathematical Modelling,* **16**(9), 484-490.

Psyllos, A. & Philippopoulos, C. (1993). Modelling of monolithic converters with axial catalyst distribution. *Applied Mathematical Modelling*, **17**(9), 459-467.

Qin, J. -W, Jiang, P. -M (2000). Heat resistant metallic oxide catalyst for reducing pollution emission. *United States Patent*, No 6107239.

Reid, R. C., Prausnitz, J. M., Poling, B. E. (1987). *The properties of Gases and Liquids*. New York: McGraw-Hill.

Richter, E., Knoblauch, K., & Jüntgen, H. (1978). Modelling Isothermer Festbettadsorber, Chem. Ing. Techn., **50**, 600-611.

Robertson, J. L., & Smith, J. M. (1963). Flow and diffusion characteristics of alumina catalyst pellets. *AICHE Journal*, **9**(3), 342-347.

Roland, H. J., & James, R. K. (1976). Mathematical modelling of monolith catalyst. *AICHE Journal*, **22**(3), 477-484.

Rühle, R. T., Schneider, H., Find, J., Herein, D., Pfänder, N., Wild, U., Nachtigall, D., Artelt, S., & Hei, U. (1997). Preparation and characterisation of Pt/Al_2O_3 aerosol precursors as model Pt-emissions from catalytic converters. *Applied Catalysis B: Environmental,* **14**(1-2), 69-84.

Ryan, M. J., Becke, E. R., & Zygourakis, K. (1991). Light-off performance of catalytic converters, the effects of heat/mass transfer characteristics. *SAE Technical paper*, 910610.

Satterfield, C. N. (1970). Mass transfer in heterogeneous catalysis. MIT press.

Satterfield, C. N. (1980). Heterogeneous catalysis in practice. McGraw-Hill, Inc., New York.

Scheidder, A. E. (1957). *The Physics of Flow through Porous Media*. University of Toronto Press, Toronto.

Schweich, D., & Leclerc, J. P. (1991). Heat flow and mass transfer in a monolithic catalytic converter. In: Crucq, A. Editor, 1991, *Catalysis and Automotive Pollution Control*, Elsevier, Amsterdam, **II**, 437-463.

Scott, D. S., & Dullien, F. A. L. (1962). Diffusion of ideal gases in capillaries and porous solids. *AICHE J.*, **8**, 113-117.

Searles, R. A. (2000). "Catalyst technologies – challenges and opportunities", paper presented to "Health Effects of Vehicles Emissions", held London 23rd and 24th February 2000. *Energy Logistics International*, 2000.

Shishu, R. C. (1972). *Ph.D. Dissertation*, University of Detroit.

Siemund, S., Leclerc, J. P., Schweich, D., Prigent, M., & Castagna, F. (1996). Three-way monolithic converter: simulations versus experiments. *Chemical Engineering Science*, **51**(15), 3709-3720.

Silveston, P. L. (1996). Automotive exhaust catalysis: is periodic operation beneficial? *Chemical Engineering Science*, **51**(10), 2419-2426.

Silversand, A. F. A., & Odenbrand, C. U. I. (1999). Modelling catalytic combustion of carbon monoxide and hydrocarbons over catalytically active wire meshes. *Chemical Engineering Journal*, **73**(3), 205-216.

Smith J. M. (1981). Chemical Engineering Kinetics (third edition). McGraw-Hill chemical engineering series.

Socha, L., & Thomason, D. (1992). Heated metal converters for low emission vehicles. *Automotive Engineering*, **100**(7), 21-25.

Spence, A., Worth, D. J., Kolaczkowski, S. T., & Crumpton, P. I. (1993). Modelling catalytic combustion in a monolith reactor: A numerical algorithm for varying solid phase peclet numbers. *Computers & Chemical Engineering*, **17**(11), 1057-1066.

Subramanlam, B. & Varma, A. (1985). Reaction kinetics on a commercial three-way catalyst: the CO-NO-O_2-H_2O system. *Industry & Engineering Chemistry Product Research and Development*, **24**(4), 512-516.

Summers, J. C. (1990). Lanthanum containing catalyst for treating automotive exhaust. *United States Patent*, No 4923842.

Taylor, K. C. (1993). Nitric oxide catalysis in automotive exhaust systems. *Catal. Rev. -Sci. Eng.*, **35**(4), 457-481.

Thevenin, P. O., Ersson, A. G., Kušar, H. M. J., Menon, P. G., & Järås, S. G. (2001). Deactivation of high temperature combustion catalysts. *Applied Catalysis, Part A: General*, **212**(1-2), 189-197.

Trimm, D. L. (1983). Catalytic combustion (Review). *Applied Catalysis*, **7**, 249-282.

Tronconi, E., & Groppi, G. (2000). A study on the thermal behaviour of structured plate-type catalysts with metallic supports for gas/solid exothermic reactions. *Chemical Engineering Science*, **55**(24), 6021-6036.

Tsolakis, A., Megaritis A., & Wyszynski, M. L. (2004). Low temperature exhaust gas fuel

reforming of diesel fuel. *Fuel*, **83**(13), 1837-1845.

Uberoi, M., & Pereira, C. J. (1996). External Mass Transfer Coefficients for Monolith Catalysts. *Industrial & Engineering Chemistry Research*, **35**(1), 113-116.

Voltz, S. E., Morgan, C. R., Liederman, D., & Jacob, S. M. (1973). Kinetic study of carbon monoxide and propylene oxidation on platinum catalysts. *Industrial Engineering Chemical Production Research Development*, **12**(4), 294-301.

Wakao, N., & Kaguei S. (1982). *Heat and Mass Transfer in Packed Beds*, Gordon and Breach, Science Publishers Inc., 94-137.

Wakao, N., & Smith, J. M. (1962). Diffusion in catalyst pellets. *Chemical Engineering Science*, **17**, 825-834.

Wakao, N., & Smith, J. M. (1964). Diffusion and reaction in porous catalysts. *Ind. Eng. Chem. Fundam.*, **3**, 123-131.

Wald, M. L. (1998). E.P.A. says catalytic converter is growing cause of global warming. *The New York Times*, May 29, 1998.

Wang, C. -T., & Smith, J. M. (1983). Tortuosity factors for diffusion in catalyst pellets. *AIChE Journal*, **29**(1), 132-136.

Wanker, R., Raupenstrauch, H., & Staudinger, G. (2000). A fully distributed model for the simulation of a catalytic combustor. *Chemical Engineering Science*, **55**(20), 4709-4718.

Wendland, D. W., Sovrell, P. L., & Kreucher, J. E. (1991). *Technical Paper Series 912372*, Society of Automotive Engineering, Warrendale.

Wheeler, A. (1955). *Catalysis,* edited by Emmett P.H., Volume **2**, Reinhold, New York.

Wicke, von E., & Kallenbach, R. (1941). The surface diffusion of carbon dioxide in activated charcoals (Die oberflächendiffusion von kohlendioxyd in aktiven kohlen), *Kolloid Zeitschrift*, **97**, 135-151.

Wijngaarden, R. J., Kronerg, A., & Westerterp, K. R. (1998). Industrial Catalysis, Optimizing Catalysts and Processes, WILEY-VCH, 1998.

Williams, J. L. (2001). Monolith structures, materials, properties and uses. *Catalysis Today*, **69**(1-4).

Yamamoto, S. (2003). Exhaust gas purifying catalyst. *United States Patent*, No 6503862.

Yang, R. T., & Liu, R. T. (1982). Gaseous diffusion in porous solids at elevated temperature.

Ind Eng Chem Fund, 21, 262-271.

Young, L. C. & Finlayson, B. A. (1976). Mathematical models of the monolith catalytic converter: part 1. Development of model and application of orthogonal collection. *American Institute of Chemical Engineers Journal,* **22**, 331-343.

Zhang, F., Hayes, R. E., & Kolaczkowski, S. T. (2004). A new technique to measure the effective diffusivity in a catalytic monolith washcoat. *Chemical Engineering Research and Design*, **82**(4), 481-489.

Zwinkels, M. M., Jaras, S. G., Menon, P. G., & Griffin, T. A. (1993). Catalytic materials for high-temperature combustion. *Catal. Rev-Sci. Eng.*, **35**(3), 319-358.

Zygourakis, K., & Aris, R. (1983). Multiple oxidation reactions and diffusion in the catalytic layer of monolith reactors. *Chemical Engineering Science*, **38**(5), 733-744.

Appendices

Appendix A A paper published at Trans IChemE, Part A, 2004

Appendix B1 Pore size distribution data for Samples BC (uncoated cordierite)

Appendix B2 Pore size distribution data for Samples S3, S3w and S3HT

Appendix B3 Pore size distribution data for Samples C2NM and C2HT

Appendix C Method adapted to calculate the value of effective diffusivity

Appendix D1 Experimental data on the measurement of D_{eff} in Chapter 3

Appendix D2 Experimental data on the measurement of D_{eff} in Chapter 4

Appendix D3 Experimental data on the measurement of D_{eff} in Chapter 5

Appendix E Estimation of CO diffusion coefficient in nitrogen

Appendix F Method adapted to calculate CO conversions and reaction rates

Appendix G Experimental data on the catalytic combustion of CO in Chapter 6

Appendix H Conversion factors used in the thesis

Appendix I Back-calculation of the tortuosity factor

Appendix J The calculation of D_{eff} at different temperatures

Appendix K Matlab programme for the calculation of A_w and α

Appendix A

A paper published at Trans IChemE, Part A, April 2004

IChemE

www.ingentaselect.com/titles/02638762.htm

0263–8762/04/$30.00+0.00

Trans IChemE, Part A, April 2004
Chemical Engineering Research and Design, 82(A4): 481–489

A NEW TECHNIQUE TO MEASURE THE EFFECTIVE DIFFUSIVITY IN A CATALYTIC MONOLITH WASHCOAT

F. ZHANG [1], R. E. HAYES [2,*] and S. T. KOLACZKOWSKI [1]

[1]*Department of Chemical Engineering, University of Bath, Bath, UK*

[2]*Department of Chemical and Materials Engineering, University of Alberta, Edmonton, Canada*

Abstract

A method is described for measuring the flux of a diffusing species through a multiple cell structure cut from a catalytic monolith honeycomb. One- and two-dimensional mathematical models are used to calculate the effective diffusivity in the catalyst/washcoat layer. This method is suitable for porous monolith supports, *e.g.* cordierite, but it is unsuitable for metal monoliths. To illustrate the technique the diffusion of CO in nitrogen is studied using a modified form of a Wicke–Kallenbach type of diffusion cell. The inlet concentration of the diffusing component is 2.4% CO in nitrogen, and experiments are performed at ambient temperature and pressures between 106 and 150 kPa on a catalytic monolith with 62 cells cm^{-2}. The technique can be applied in many areas where catalytic monoliths are used, *e.g.* catalytic converters, catalytic combustion reactors, SCR catalysts and many other applications. The method shows good agreement with the results obtained using other methods.

Keywords: catalytic converters; monoliths; diffusion; effective diffusivity; catalytic combustion; washcoat.

IChemE

www.ingentaselect.com/titles/02638762.htm

0263–8762/04/$30.00+0.00

Trans IChemE, Part A, April 2004
Chemical Engineering Research and Design, 82(A4): 481–489

A NEW TECHNIQUE TO MEASURE THE EFFECTIVE DIFFUSIVITY IN A CATALYTIC MONOLITH WASHCOAT

F. ZHANG[1], R. E. HAYES[2,*] and S. T. KOLACZKOWSKI[1]

[1]*Department of Chemical Engineering, University of Bath, Bath, UK*
[2]*Department of Chemical and Materials Engineering, University of Alberta, Edmonton, Canada*

A method is described for measuring the flux of a diffusing species through a multiple cell structure cut from a catalytic monolith honeycomb. One- and two-dimensional mathematical models are used to calculate the effective diffusivity in the catalyst/washcoat layer. This method is suitable for porous monolith supports, e.g. cordierite, but it is unsuitable for metal monoliths. To illustrate the technique the diffusion of CO in nitrogen is studied using a modified form of a Wicke–Kallenbach type of diffusion cell. The inlet concentration of the diffusing component is 2.4% CO in nitrogen, and experiments are performed at ambient temperature and pressures between 106 and 150 kPa on a catalytic monolith with 62 cells cm^{-2}. The technique can be applied in many areas where catalytic monoliths are used, e.g. catalytic converters, catalytic combustion reactors, SCR catalysts and many other applications. The method shows good agreement with the results obtained using other methods.

Keywords: catalytic converters; monoliths; diffusion; effective diffusivity; catalytic combustion; washcoat.

INTRODUCTION

The use of structured catalyst supports such as 'honeycomb' monoliths in automotive catalytic converters is common. To provide a large surface area and to minimize external mass transfer resistance, such monoliths use small sized channels, with a nominal size of 62 cells cm^{-2} (400 cells per square inch, CPSI), which corresponds to channels of approximately 1 mm, internal dimension. For ceramic monoliths, the most common channel shape is square, although hexagonal shaped cells have also been reported. The ceramic support is usually cordierite, and a high surface area material is applied to the surface as a thin coating. This coating is called a washcoat and acts as a support for the catalyst. A commonly used washcoat material is gamma alumina, which has a surface area in the region of 100–200 $m^2 g^{-1}$ (Harris *et al.*, 1982). Typically the washcoat is applied as slurry that fills the channels, and the excess is removed using an air knife (Kolb *et al.*, 1993). This process gives a washcoat that is fairly thin, but also one that has a variation in thickness around the perimeter of the channel. For example, in square channels around 1 mm in size, the washcoat is typically 10–40 μm thick at the mid-side of the channels and up to 200 μm thick (measured diagonally) in the corners. Because this layer is thin, many researchers have assumed that reaction rates in it are not limited by intraphase diffusion. However, catalytic oxidation rates are extremely fast at typical converter operating temperatures, and many researchers in this field, including commercial catalyst producers, are becoming more aware of the importance of these effects. For example, from among the many literature models of three-way catalytic converters, Siemund *et al.* (1996) compared the results of models with experimental measurements and concluded that theoretical and experimental effort must be put into internal diffusion. Other works that illustrate the role of intraphase diffusion are Leung *et al.* (1996) and Mukadi and Hayes (2002).

The ability to model the performance of a catalytic converter is becoming increasingly important to manufacturers as they compete for business in a billion dollar industry. Computer models can be used for the rapid exploration of alternative catalyst system designs, reduce the cost of catalyst system development work and increase the speed of producing a product for the marketplace. Models can also be used as a diagnostic tool to identify problems, or to improve the design. Kolaczkowski (2003) highlights how over the last decade manufacturers of catalytic converters have started to make use of thin layers to engineer a composite catalyst layer, with different reactions promoted in different layers. Examples of such structures are found in the patent literature (Frestad and Andersson, 1990; Hayashi and Kikuchi, 1998; Ishii and Nishizawa, 2001; Kachi and Nishizawa, 2001). With the aid of a model, such structures may be optimized and alternative design concepts explored.

Because intraphase diffusion strongly affects reactor performance, it must be included in any realistic reactor model. For this purpose it is essential to have reliable values

*Correspondence to: Professor R. E. Hayes, Department of Chemical and Materials Engineering, University of Alberta, Edmonton, Alberta, Canada, T6G 2G6.
E-mail: bob.hayes@ualberta.ca

for the diffusion coefficients in the washcoat, which must be measured experimentally. This paper reports on a method developed to measure diffusion coefficients in monolith washcoat and substrate materials.

DIFFUSION IN POROUS CATALYST

Correct representation of the rate of diffusion in the washcoat requires that the characteristics of the washcoat be determined experimentally. The washcoat is a consolidated porous medium consisting of a solid matrix containing a complex network of pores. Depending on the size of the pores relative to the mean free path of the diffusing species, the diffusion may be dominated by Knudsen diffusion, bulk diffusion, or a combination of the two. It is usual when modelling transport in porous media to treat the medium as a continuum and to use volume-averaged properties. For diffusion in a porous catalyst, a capillary model for the medium is often used, and hence an effective diffusivity based on the total area of the material computed. Fickian type diffusion along the normal of the concentration gradient is thus assumed. The effective diffusivity is usually related to the diffusion coefficient in the pores via the porosity of the solid, ε, and the tortuosity of the pores, τ. The latter term is included to account for the deviation of the pores from straight capillaries. The parallel pore model is a general relationship between the effective diffusivity and the pore diffusivity (Wheeler, 1955):

$$D_{\text{eff}} = \frac{\varepsilon}{\tau} D_{\text{P}} \tag{1}$$

The diffusion coefficient in the pores, D_{P}, can be determined as a combination of the Knudsen diffusion coefficient and the bulk diffusion coefficient. The Knudsen diffusion coefficient, D_{K}, depends on the temperature, the molar mass of the diffusing species and the pore diameter, d_{P}:

$$D_{\text{K}} = 48.5 d_{\text{P}} \sqrt{\frac{T}{M}} \tag{2}$$

The bulk diffusion coefficient for a binary mixture can be computed from, for example, the relationship proposed by Fuller *et al.* (1966):

$$D_{\text{B}} = \frac{1.013 \times 10^{-2} T^{1.75} \{1/M_{\text{A}} + 1/M_{\text{B}}\}^{1/2}}{P[(\sum v_i)_{\text{A}}^{1/3} + (\sum v_i)_{\text{B}}^{1/3}]^2} \tag{3}$$

For equimolar counter diffusion, the two diffusivities can be combined using the Bosanquet formula (Froment and Bischoff, 1990) to give the diffusion coefficient in the pores:

$$\frac{1}{D_{\text{P}}} = \frac{1}{D_{\text{K}}} + \frac{1}{D_{\text{B}}} \tag{4}$$

Typically, when using the parallel pore model for diffusion in porous media, a single average value is used for both the pore diameter and the tortuosity factor. As a result, this model tends to give the best results when the pores have a narrow size distribution. In practice, the average pore size, porosity and effective diffusion coefficient need to be determined experimentally, and then a tortuosity factor can be back-calculated. The effective diffusivity at other temperatures and pressures can then be calculated using this tortuosity factor, because it should only depend on the properties of the material.

There are many examples of studies of diffusion in catalysts pellets where the use of, for example, the Wicke–Kallenbach cell (Wicke and Kallenbach, 1941) is very classical. Kolaczkowski (2003) discussed the advantages and disadvantages of various methods and it is clear that there is relatively little published information on measurements of diffusion in thin catalyst layers in a monolith. This in part arises from the difficulty of performing such measurements in these thin layers, and on structures that cannot easily be mounted into a classical diffusion cell.

To overcome these problems, the washcoat/catalyst coating could be prepared on a custom-made surface, or formed into the shape of a pellet that is inserted into a classical design of diffusion cell. However, as a result of the preparation method, the morphology of the structure through which the effective diffusivity is measured may be quite different from the coated monolith. It is therefore preferable to measure the diffusivity in the actual structure as it is used.

To measure *in situ*, two techniques have been suggested. For example, the chromatographic technique, which is based on measuring the time delay and spreading of a pulse of non-adsorbing tracer, has been suggested (Kolaczkowski, 2003). The application of this method in a converter monolith, however, would require long residence times and sampling rates that are difficult to achieve with simple experiments. For monoliths of larger diameter (2 mm and above), flow cells have been used successfully (Hayes *et al.*, 2000; Beeckman, 1991). For smaller cells of the order of 1 mm, such an approach is impractical, hence the need for alternative methods. An approach inspired by the Wicke–Kallenbach method using sections of washcoated monolith is described in this paper. In this approach, a section was cut from a commercially produced catalytic monolith that used cordierite as a support. This section was mounted in a small diffusion cell that allowed the diffusion of species through the cell structure in a direction normal to the channel axis. Measurement of diffusive flux and concentration, combined with appropriate analysis, allowed the calculation of effective diffusion coefficients. This method is only suitable for porous monolith supports because it relies on the gas being able to diffuse through the porous structure. It is therefore unsuitable for metal monoliths. The results are compared to results from other investigations. The diffusion of carbon monoxide in nitrogen was studied, because it is a reactant of interest in a catalytic converter.

EXPERIMENTAL

Description of the Samples

The samples used in this work were cut from a commercial catalytic converter monolith which had 400 CPSI (62 cells cm^{-2}) and a washcoat containing a three-way catalyst. Blank monolith samples without washcoat were also used. Each circular sample was prepared by cutting through the vertical channel walls to give monolith sections that contained either one or two rows of cells. Extraneous wall material and washcoat (if present) was removed from the exposed faces to yield flat surfaces. Therefore, there was no washcoat on the exposed surfaces, but the inside surfaces had a coated layer that reflects the state of the material when the monolith reactor was produced. Figure 1 illustrates the samples used and a scanning electron microscope (SEM)

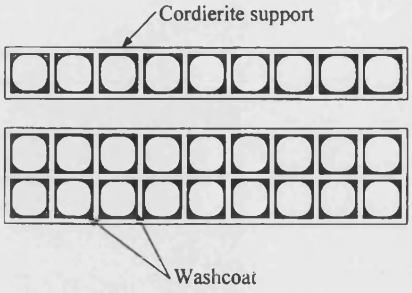

Figure 1. Representation of the samples cut from the monolith, with one or more layers of cells: (a) one layer of cell; (b) two layers of cells; and (c) three layers of cells. The washcoat from the outside surfaces was removed.

picture of a section of a typical sample is shown in Figure 2. Note the square shape of the cells and the variation of the washcoat thickness around the perimeter. Because of the nature of the coating process, thicker layers are formed in the corners of the cells. The geometry of the cells, including substrate thickness and washcoat distribution, was determined from the SEM pictures using image analysis. The dimensions used were the average values found from the analysis of a number of cells. The thickness of the washcoat layer varies from 173 μm in the corner to 31 μm on the side. If the washcoat was reconfigured so that it formed a layer of uniform thickness, then this layer was calculated to be 84.5 μm thick. The inside channel dimension was 1.14 mm, and the total thickness of the substrate was 174.8 μm.

The multi-layered monolith structure was sealed with epoxy in a metal annular ring, as shown in Figure 3. The positioning of the annular ring on either face of the sample ensured that there was a well-defined area (10 mm in diameter) through which the gases diffused between the lower and the upper chambers of the cell. The sample was then mounted in the diffusion cell.

Description of the Diffusion Cell

A schematic of the apparatus is given in Figure 4 and of the cell in Figure 5. Gas was admitted into the upper and lower chambers from two ports located on opposite sides of the

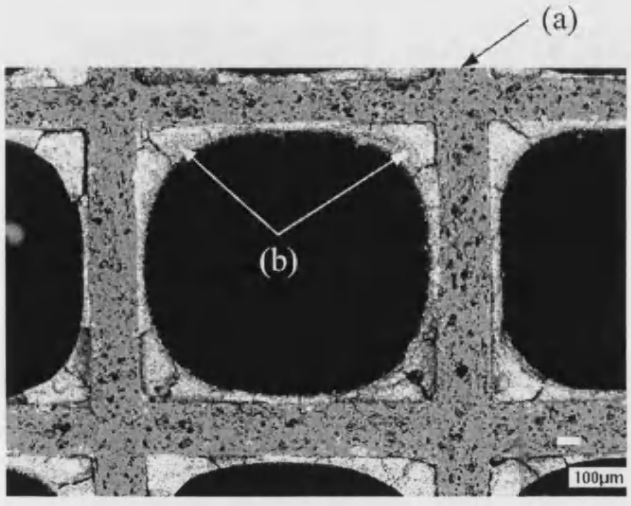

Figure 2. Scanning electron micrograph (SEM) of three-way monolithic catalyst samples: (a) cordierite support; (b) washcoat.

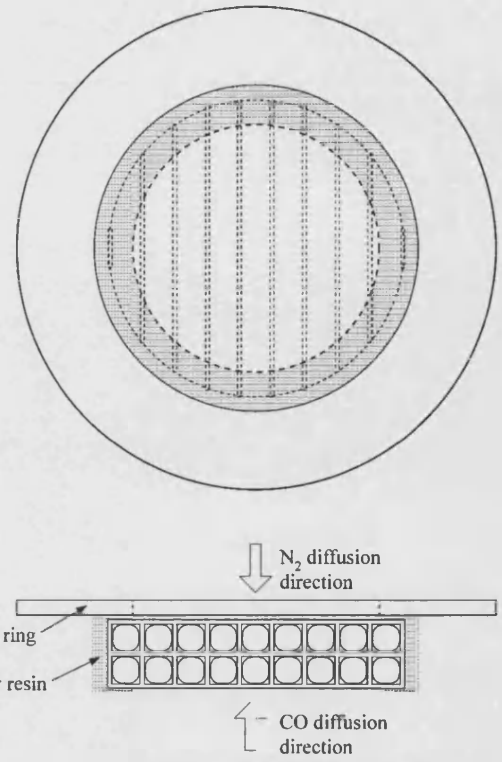

Figure 3. Two cell layered structure sealed in a metal annular ring.

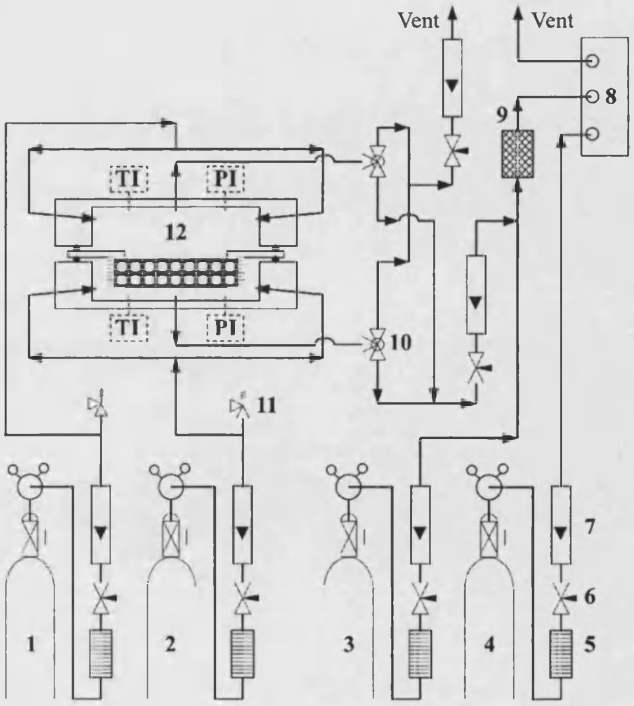

Figure 4. Schematic of the overall flow system. 1, N_2 cylinder for diffusion (99.99% purity); 2, CO cylinder for diffusion (2.4% CO in N_2); 3, CO cylinder for calibrating CO analyser (1070 ppm CO in N_2); 4, N_2 cylinder for reference of CO analyser; 5, dryer and filter; 6, needle valve; 7, rotameter (1000 ml min^{-1}); 8, CO analyser (measurement range 0–1400 ppm); 9, filter; 10, three-way valve; 11, relief valve; 12, diffusion cell (with TI, temperature indicator, and PI, pressure indicator).

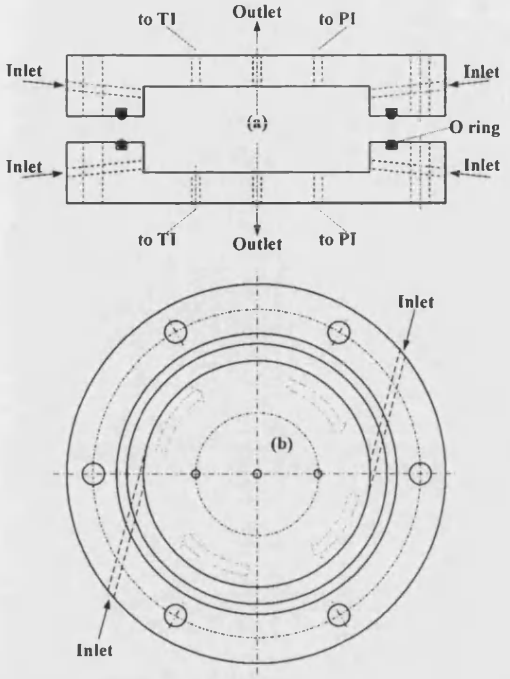

Figure 5. Diagram of the diffusion cell: (a) the upper chamber and the lower chamber; (b) the vertical view of the lower chamber.

chamber, through nozzles positioned in a tangential direction (at 45° from the centre) to avoid direct jet impact on the face of the sample and to create good mixing in the chambers. Nitrogen of 99.99% purity was fed into the upper chamber and a mixture of 2.4% by volume CO in nitrogen was fed into the lower chamber. The gas left the chamber from ports near the centre of the chamber. Gas flowrates were measured with rotameters. The concentration of CO in the gas streams was measured using a CO analyser (SIGNAL series 2000 IRGA; range 0–1400 ppm). During the course of the experiments both the total pressure and the differential pressure in the cells were measured. Equal pressure in each of the chambers (within ±20 Pa) was maintained by adjusting the back pressure regulating valves, which ensured that flow did not occur as a result of a total pressure gradient across the sample.

The diffusion cell was operated in a manner similar to the classical method developed by Wicke and Kallenbach (1941), with the exception of the method of interpreting the results.

CALCULATION OF DIFFUSION COEFFICIENTS

The washcoat shape, as shown in the SEM pictures, is clearly two-dimensional, and thus a two-dimensional analysis of the diffusion is required for the highest level of accuracy. A two-dimensional analysis is, however, more complicated than simple one-dimensional methods, and therefore a one-dimensional approximate method was tested for its predictive ability, and then compared with a two-dimensional solution.

Formulation of a Simple One-Dimensional Model

Consider a monolith cell made by cutting a section from a block of monolith. For the blank monolith, in the direction of diffusion, the total length is equal to twice the total wall thickness plus the inside channel dimension. The width of the cell for modelling purposes is equal to the inside channel dimension plus the thickness of the wall. These dimensions are the same for the monolith with washcoat monolith because there is no washcoat on the outside surfaces. The resistance to diffusion expressed in terms of Fick's law can be written as:

$$R_{eq} = \frac{\Delta x}{DA} \tag{5}$$

In equation (5), Δx is the distance normal to diffusion, A is the cross sectional area available for diffusion, D is the diffusion coefficient in the medium and R_{eq} is the equivalent or total resistance to diffusion in the medium. For heat conduction in a composite medium, use is often made of the so-called electrical analogy (Incropera and DeWitt, 2002) to define the equivalent resistance. In this method, the object is considered to be comprised of a number of individual resistances, which can be connected to form an overall circuit. The resistances are combined as a set of series and parallel resistances, which are combined using standard circuit rules. By analogy, we here extend this method to mass diffusion. Although the method is strictly exact only for a composite structure composed of a set of different media placed in series, it is nonetheless used to give a one-dimensional approximation for two-dimensional structures.

Consider a single row of monolith cells cut from a block, as previously discussed, and shown in Figure 6. Depending on how the electrical analogy is applied, two different circuits can be drawn, as shown in Figure 7. The diffusion resistance of each segment of the circuit is shown in the diagram, where the dimensions are those shown in Figure 6 and a unit depth is assumed. The equivalent resistances that correspond to each of these circuits are obtained by standard circuit analysis and are given below. For method (a) the equivalent resistance is:

$$R_{eq} = \frac{2t_S}{WD_{eff,S}} + \left[\frac{t_S D_{eff,S}}{b_S} + \frac{b_S D_B}{b_S}\right]^{-1} = \frac{2t_S}{WD_{eff,S}} + \frac{b_S}{t_S D_{eff,S} + b_S D_B} \tag{6}$$

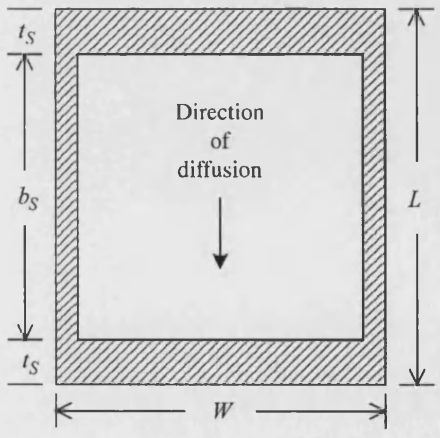

Figure 6. End view of a single cell extracted from a row of single cell thickness for a sample without washcoat. The dimensions used for constructing the equivalent electrical circuits are shown.

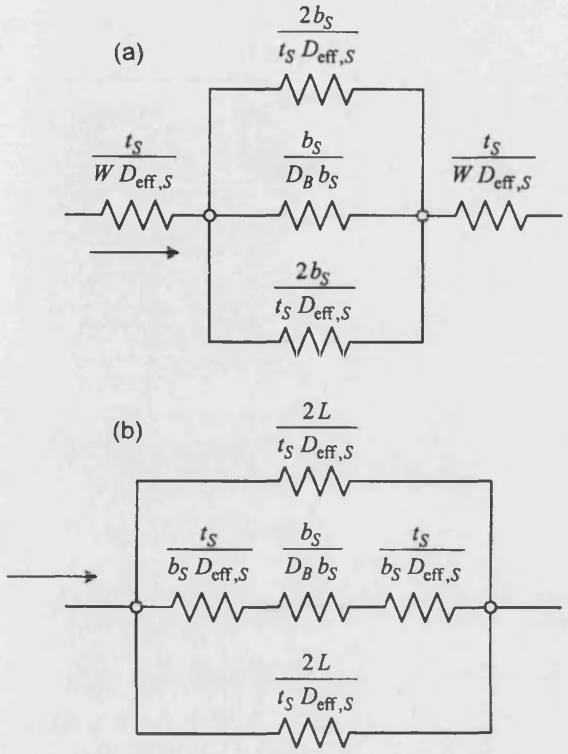

Figure 7. Analogous electrical circuits for diffusion through a blank monolith. The 'resistance' to diffusion for each component of the circuit is shown. Circuit (a) and circuit (b) result from different combinations of series and parallel resistances.

For method (b) it is:

$$R_{eq} = \left[\frac{t_S D_{eff,S}}{W + t_S} + \left(\frac{b_S}{b_S D_B} + \frac{2t_S}{b_S D_{eff,S}}\right)^{-1}\right]^{-1} = \left[\frac{t_S D_{eff,S}}{W + t_S} + b_S\left(\frac{b_S}{D_B} + \frac{2t_S}{D_{eff,S}}\right)^{-1}\right]^{-1} \quad (7)$$

The above equations can be easily extended for multiple layers of cells. For n layers of cells, the equations are, for method (a):

$$R_{eq} = \frac{(n+1)t_S}{W D_{eff,S}} + \frac{n b_S}{t_S D_{eff,S} + b_S D_B} \quad (8)$$

For method (b):

$$R_{eq} = \left[\frac{t_S D_{eff,S}}{nW + t_S} + b_S\left(\frac{nb_S}{D_B} + \frac{(n+1)t_S}{D_{eff,S}}\right)^{-1}\right]^{-1} \quad (9)$$

From the dimensions given earlier, $t_S = 174.8\,\mu m$, $b_S = 1.14$ mm and $W = b_S + t_S = 1.315$ mm.

A similar procedure can be followed for the monolith with washcoat, albeit with one important exception. Because the washcoat is distributed non-uniformly around the perimeter of the cell, it is necessary to 're-configure' the cell. This reconfiguration involves making the assumption that the washcoat is distributed in a uniform manner around the perimeter of the channel, as shown in Figure 8. For the cells used in these experiments, this uniform thickness was calculated to be $t_W = 84.5\,\mu m$. Assuming that there is no

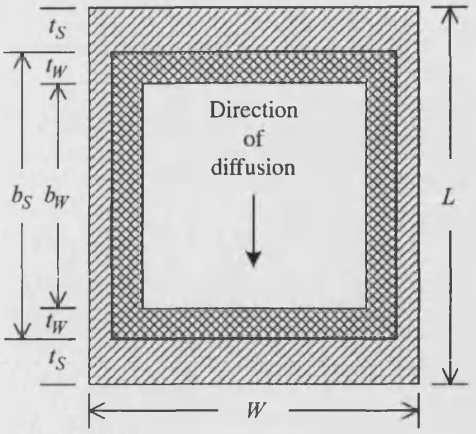

Figure 8. End view of a single cell extracted from a row of single cell thickness for a sample with washcoat. The washcoat has been reconfigured to form a uniformly thick layer around the perimeter. The total amount of washcoat is preserved. The dimensions used for constructing the equivalent electrical circuits are shown.

washcoat on the exposed surfaces, the equivalent resistances for the two circuits, for n rows of cells, are then computed for the two methods using the same technique as applied before. For method (a) the equivalent resistance is:

$$R_{eq} = \frac{(n+1)t_S}{W D_{eff,S}} + \frac{n b_W}{t_S D_{eff,S} + b_W D_B + 2t_W D_{eff,W}} + \frac{2nt_W}{t_S D_{eff,S} + b_W D_{eff,W}} \quad (10)$$

For method (b) it is:

$$R_{eq} = \left[\frac{t_S D_{eff,S}}{nW + t_S} + b_W\left(\frac{nb_W}{D_B} + \frac{(n+1)t_S}{D_{eff,S}} + \frac{2nt_W}{D_{eff,W}}\right)^{-1} + 2t_W\left(\frac{(n+1)t_S}{D_{eff,S}} + \frac{nb_W}{D_{eff,W}}\right)^{-1}\right]^{-1} \quad (11)$$

The equivalent resistance is computed from the experimental flux measurements and the value of $D_{eff,W}$ is then back-calculated. The value of $D_{eff,S}$ from the blank experiments must be used in this calculation.

The equivalent resistance may be calculated from the experimental data as follows:

$$R_{eq} = \frac{C}{W}\frac{(Y_{CO,in} - Y_{CO,out})}{N_{CO}} = \frac{P}{R_g T W}\frac{(Y_{CO,in} - Y_{CO,out})}{N_{CO}} \quad (12)$$

Formulation of a Two-Dimensional Model

The monolith cell structure represents a two dimensional domain. For the most accurate representation of the diffusion through this domain it is therefore necessary to use the two-dimensional mole balance equation and the appropriate numerical solution. The mole balance for the steady-state diffusion through the domain is represented by the

single equation, assuming that the diffusion coefficient is independent of concentration:

$$D\left(\frac{\partial^2 C}{\partial x^2}+\frac{\partial^2 C}{\partial y^2}\right)=0 \qquad (13)$$

In equation (13) the diffusion coefficient D assumes the value that corresponds to the spatial co-ordinate given by x and y. The solution can be obtained numerically using any appropriate technique. In this work, we used the Galerkin finite element method with quadratic triangular elements (P2 elements). An unstructured non-uniform mesh was used, which was built using the mesh generator Aranea (Marchand *et al.*, 2001). Element edges were superimposed along the physical interfaces of the different materials in the cell. The boundary conditions were imposed based on the experimental results. Thus, at the boundary corresponding to the inlet side of the cell, a Dirichlet condition was imposed equal to the known concentration in the inlet side of the diffusion cell. The measured diffusive flux across the cell was imposed as a Neumann boundary condition along the surface on the outlet side of the cell. The equations were then solved iteratively with different values of effective diffusivity in the solid until a value was found that gave an average concentration along the outlet side cell surface that was equal to the concentration measured experimentally in the outlet side of the diffusion cell. The linear system of equations resulting from the discretization was solved using LU factorization, and the equations were integrated using six point Gaussian quadrature. Further detail on the use of the finite element method to model diffusion in washcoats can be found in Leung *et al.* (1996) and Hayes and Kolaczkowski (1997).

In addition to performing two-dimensional simulations for the actual washcoat distribution in the channel, simulations were performed on cells with a uniform layer of washcoat imposed around the perimeter. This model was evaluated to test the effect of the uniform washcoat assumption.

Experimental Results

In the first instance experiments were performed on a blank (uncoated) monolith. The first set of results was obtained using a sample containing a single row of cells, with temperature 289–290 K and pressure 106 kPa. Figure 9 shows the results of three experiments performed on two different samples to show the reproducibility of the technique. The diffusion coefficients shown in the graph were analysed using the one-dimensional model with analysis method (a). It is seen that the results are fairly reproducible. The trend illustrated shows a decrease in the apparent diffusion coefficient below a flowrate of 500–600, which suggests that some mass transfer limitation between the fluid and solid surface was present. Figure 10 illustrates the results obtained from the two different one-dimensional methods and the full two-dimensional numerical solution. In each case, the results are the average values from three experiments. It is evident from the figure that neither one-dimensional approximation matches exactly with the two-dimensional results; however, the one-dimensional method (a) is within 2% of the two-dimensional result. The two-dimensional results indicate that the diffusion coefficient of CO in the cordierite is of the order of $0.97 \times 10^{-6}\,m^2\,s^{-1}$.

Further experiments were performed on a sample with a double layer of cells. The results are illustrated in Figure 11, which shows the average of three experiments with the results analysed from the two-dimensional model. As with the single layer, the results for the one-dimensional method (a) were closer to the two-dimensional results than method (b). It is observed that the results obtained on two cells are slightly higher than those obtained for a single layer of cells, and furthermore do not appear to be influenced by external mass transfer limitations. This latter effect may be attributed to better mixing in the apparatus, because with a two cell sample there was less space between the injected gas and the surface, which would give a shorter diffusion path. Alternatively, the doubling of the resistance of the sample would also lead to a smaller percentage effect of external mass transfer, because this resistance should have at most the same value as before.

The next set of results shown was obtained from a washcoated sample with a single row of cells. The washcoat from the external surfaces was removed. It should be noted that the calculation for the effective diffusivity in the washcoat requires that a value of effective diffusivity in the cordierite be known. These values are taken from the washcoat-free experiments, with the average value at the

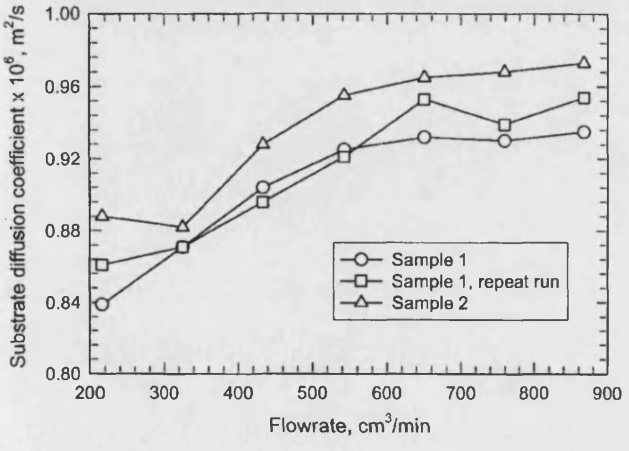

Figure 9. Experimental results from three tests performed on a sample with a single layer of cells. The effective diffusivities were analysed using the one-dimensional model with analysis method (a).

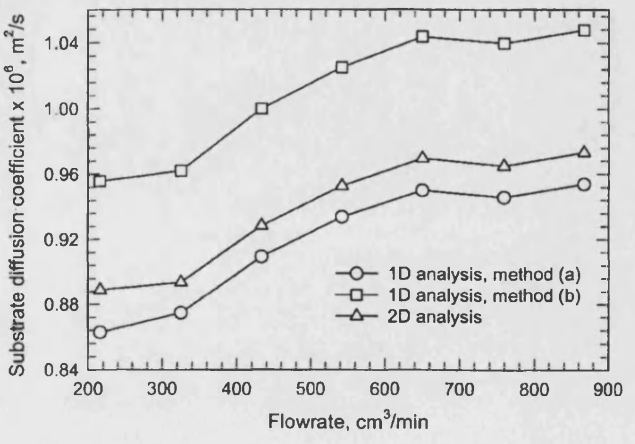

Figure 10. Comparison of three analysis methods for a sample of substrate alone with a single row of cells.

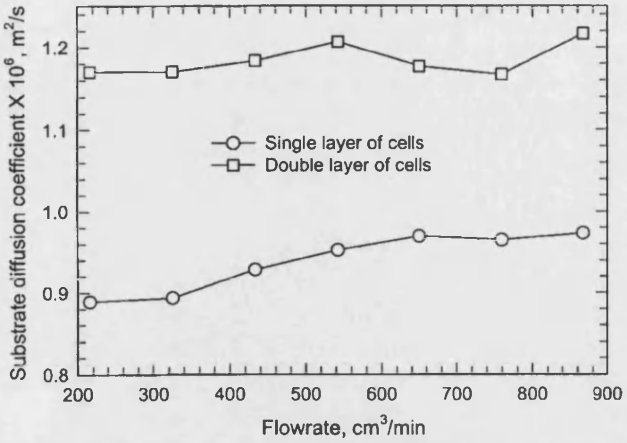

Figure 11. Comparison of results obtained from single and double layers of cells. The two-dimensional method of analysis was used to compute the effective diffusion coefficients.

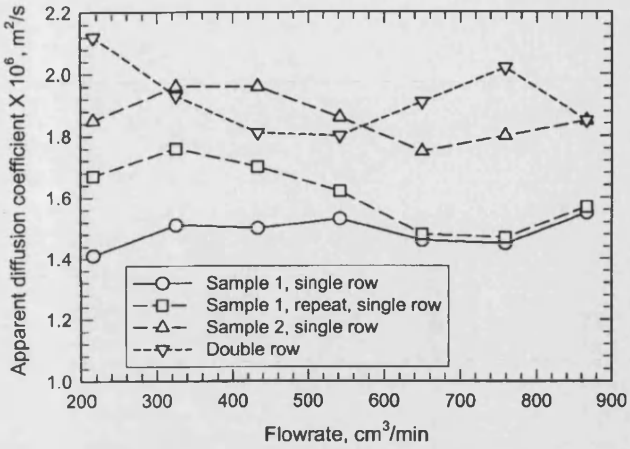

Figure 13. Experimental results from four tests performed on a washcoated sample. The effective diffusivities were analysed using the two-dimensional model.

corresponding flowrate being used. Figure 12 shows a comparison of the diffusion coefficients obtained using the three analysis methods. It can be seen that the two-dimensional solution is not well approximated by either of the two analytical methods. Recall that analysis method (a) gave a reasonable good approximation of the substrate diffusivity. The lack of agreement for the washcoat is attributed to the fact that when the analytical methods were applied for the washcoated channel, the washcoat was approximated by a uniform distribution. When the two-dimensional simulation was run for a case with a uniformly distributed washcoat, it was found that the results were essentially the same as for the analytical solution, method (a). This observation indicates that the method (a) approach would be valid for a case where the washcoat was indeed of uniform thickness, but not for the catalyst used in this investigation.

It is also interesting to note that the diffusion coefficient in the washcoat shows little or no effect of the influence of flowrate. The diffusion coefficient in the cordierite measured at the corresponding flowrate in effect includes a resistance owing to mass transfer resistance, and it would appear that this is sufficient to negate the effect on the observed value of the washcoat diffusion coefficient, because this latter value is obtained by difference. This observation is significant, because it indicates that it may not be critical to eliminate all of the external resistance, provided that the washcoat value is the primary concern.

Figure 13 shows the effect of experimental reproducibility and the variation among samples. Also shown is the result obtained from a double row of cells with washcoat. It is seen that the reproducibility is good, but there is some variation among samples. This is only to be expected, and probably results from the method of manufacture. In reality the washcoat thickness is not the same from cell to cell, however the analysis is based on a constant set of properties. Overall, the double row seems to give more reliable results, which is expected because of a reduction in the relative size of the end effects.

Figure 14 shows the effect of pressure on the calculated value of the diffusion coefficient. Results from the single layer analysed using the two-dimensional model for both the substrate and the washcoat are shown. It is observed that the effective diffusion coefficient decreases with pressure in both cases. Increasing the pressure decreases the value of the bulk diffusion coefficient, hence reducing the overall

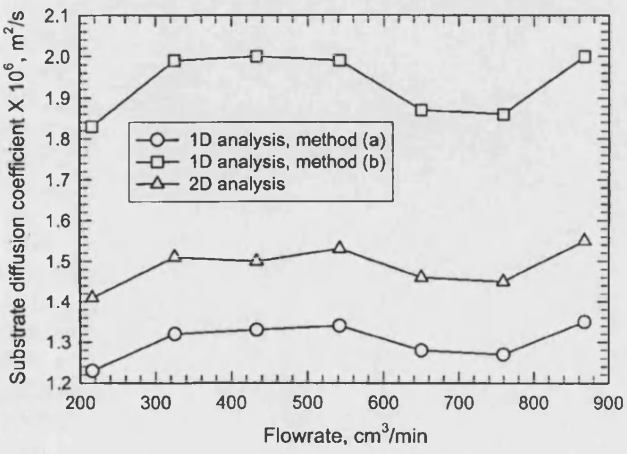

Figure 12. Comparison of three analysis methods for a washcoat with a single row of cells.

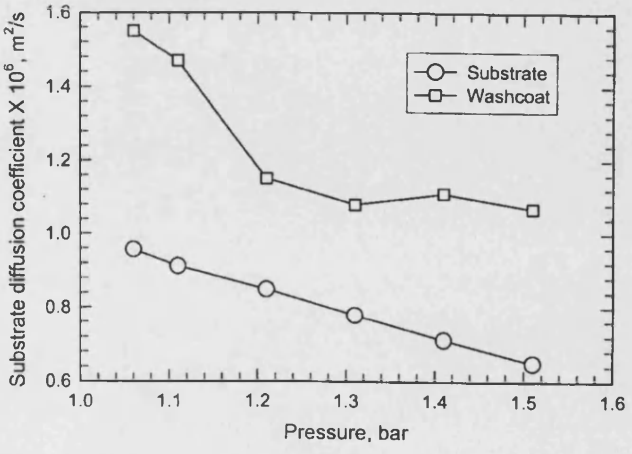

Figure 14. Effect of pressure on the effective diffusion coefficient for washcoat and substrate for a single layer of cells. The two-dimensional method of analysis was used to compute the effective diffusion coefficients.

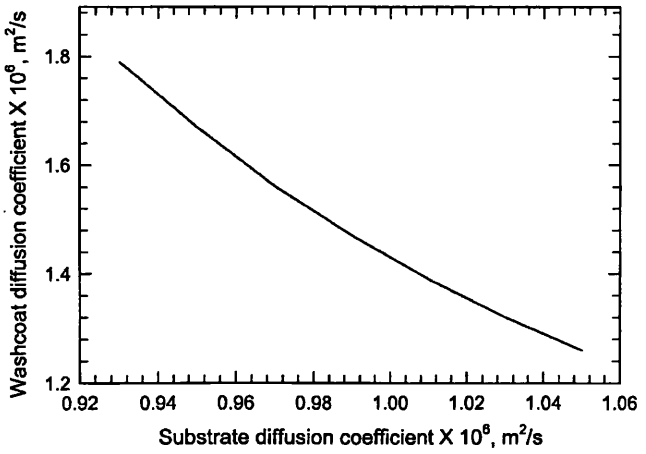

Figure 15. Effect of varying the substrate diffusion coefficient on the predicted value of the washcoat diffusion coefficient. The two-dimensional method of analysis was used on a sample with a single row of cells.

diffusion coefficient in the pores. In the substrate, macro pores predominate and the diffusion is dominated by bulk diffusion. The trend of a reduced diffusion coefficient at elevated pressure is thus expected. The washcoat contains both micro- and macropores. While Knudsen diffusion will predominate in the micropores, bulk diffusion will influence the diffusion coefficient in the macropores. The fact that the diffusion coefficient in the washcoat declines with increasing pressure indicates the presence of a macropore structure in the washcoat.

The value of the diffusion coefficient in the washcoat back calculated from the two-dimensional analysis depends on the value of the diffusion coefficient in the substrate. The latter value is measured on a separate sample. To illustrate the effect on the diffusion coefficient in the washcoat obtained from the analysis, a series of simulations was performed on a single channel experiment. The value of the diffusion coefficient in the substrate was varied to determine the magnitude of the change in the washcoat coefficient, and the variation is illustrated in Figure 15. It is obvious that the accuracy of the value of the diffusion coefficient in the washcoat depends strongly on the effective diffusivity in the substrate, which shows the importance of determining this value with accuracy and precision.

Finally, a few points should be made about the value of the diffusion coefficients determined in this study. The diffusion coefficient of CO in the cordierite is $0.97 \times 10^{-6}\,m^2\,s^{-1}$. Hayes *et al.* (2000) used a flow cell to measure the effective diffusion coefficient of methane in a cordierite substrate, and reported a value of $0.92 \times 10^{-6}\,m^2\,s^{-1}$. It is expected that the Cordierite used in both cases is essentially the same, and the agreement between these two investigations is excellent. The agreement indicates that the method proposed here is valid. The diffusion coefficient in the washcoat is higher than that reported by Hayes *et al.* (2000) by about an order of magnitude. Clearly, this difference requires an explanation, and is likely the result of different washcoat structures. The washcoat examined by Hayes *et al.* (2000) was a palladium oxidation catalyst and was shown to have a microporous structure with no macropores. The catalyst used in this work has been shown to have some macropore structure, and thus a higher diffusion coefficient would be expected. Clearly, the three way catalyst washcoat is different in properties from the palladium oxidation catalyst using in the earlier investigation. The three-way catalyst washcoat comprises a matrix consisting of pieces of alumina and ceria. Thus a macrostructure corresponding to the pores around the particles combined with a microstructure representing the porous particles is expected. These differences clearly demonstrate the need for experimental measurements for each different washcoat formulation.

CONCLUSIONS

It is shown that the method proposed in this paper is a viable way of evaluating the effective diffusivity in the washcoat of a coated monolith. A simple one-dimensional model based on a combination of series and parallel resistances does not represent adequately the results, although it will determine the correct order of magnitude. A major advantage of this technique is the ability to make measurements on actual samples of catalytic monolith produced in a commercial process. It is suggested that two or more rows of cells be used to minimize end effects.

Although in this paper the catalytic converter has been selected to illustrate the importance of being able to effectively model and measure the effective diffusivity, it should not be overlooked that the methods are also applicable to many other areas of interest were a catalytic monolith is used (e.g. catalytic combustors on gas turbines, catalytic combustion of volatile organic emissions, partial oxidation reactors to produce hydrogen for fuel cell). In addition, it would be an effective way of performing measurements on selective catalytic reduction catalysts (SCR) if they are in a monolith form that is porous throughout. In these types of catalyst systems, the catalyst is an integral part of the structure and is not coated onto a support.

NOMENCLATURE

b_S	inside dimension of the channel of the substrate, before application of the washcoat
b_W	inside dimension of the channel of the cell, after application of the washcoat
C	total molar concentration
D	generic diffusion coefficient of CO in nitrogen
D_B	bulk diffusion coefficient of CO in nitrogen
$D_{eff,S}$	effective diffusion coefficient in the substrate
$D_{eff,W}$	effective diffusion coefficient in the washcoat
L	length of the cell in the direction normal to diffusion, $L = b_S + 2t_S$
N_{CO}	molar flux of CO
n	number of rows of cells in the monolith sample
P	pressure
R_{eq}	equivalent resistance through a cell structure
R_g	universal gas constant
T	absolute temperature, K
t_S	total thickness of the wall of the substrate
t_W	total thickness of the washcoat when it is distributed uniformly around the channel
W	width of the cell in the direction orthogonal to flow, $W = b_S + t_S$
x	coordinate in cell
$Y_{CO,in}$	mole fraction of CO on the diffusion cell inlet
$Y_{CO,out}$	mole fraction of CO on the diffusion cell outlet
y	co-ordinate in cell

Greek symbols

ε	porosity of catalyst or substrate
τ	tortuosity factor

REFERENCES

Beeckman, J.W., 1991, *Ind Eng Chem Res*, 30: 428.

Frestad, A. and Andersson, S., 1990, Catalyst for purifying exhaust gases and preparation thereof, US Patent no. 4,975,406.

Froment, G.F. and Bischoff, K.B., 1990, *Chemical Reactor Analysis and Design*, 2nd edition (Wiley, New York, USA).

Fuller, E.N., Schettler, P.D., Giddings, J.C., 1966, A new method for the prediction of binary gas phase diffusion coefficients, *Ind Eng Chem*, 58(5): 19–27.

Harris, D.J., Young, D.J. and Trimm, D.L., 1982, The sintering of alumina based catalysts, in *Proceedings 10th Australian Chemical Engineering Conference, Chemeca 1982*, Sydney, August 24–26, pp 175–179.

Hayashi, T. and Kikuchi, S., 1998, Exhaust emission control catalyst comprising cerium, US Patent no. 5,753,580.

Hayes, R.E. and Kolaczkowski, S.T., 1997, *Introduction to Catalytic Combustion* (Gordon and Breach, Reading).

Hayes, R.E., Kolaczkowski, S.T., Li, P.K. and Awdry, S., 2000, Evaluating the effective diffusivity of methane in the washcoat of a honeycomb monolith, *Appl Catal B Environ*, 25: 93–104.

Incropera, F.P. and DeWitt, D.P., 2002, *Introduction to Heat Transfer* (Wiley, New York, USA).

Ishii, H. and Nishizawa, K., 2001, Exhaust emission control catalyst apparatus in internal combustion engine, US Patent no. US 6,296,813 B1.

Kachi, N. and Nishizawa, K., 2001, Catalytic converter with multi-layered catalyst system, US patent application publication, publication no. US 2001/0006934 A1.

Kolb, W.B., Papadimitriou, A.A., Cerro, R.L., Leavitt, D.D. and Summers, J.C., 1993, The ins and outs of coating monolithic structures, *Chem Eng Prog*, February: 61–67.

Kolaczkowski, S.T., 2003, Measurement of effective diffusivity in catalyst coated monoliths, *Catal Today*, 83: 85–95.

Leung, D., Hayes, R.E. and Kolaczkowski, S.T., 1996, Diffusion limitation in the washcoat of a catalytic monolith reactor, *Can J Chem Eng*, 74: 94–103.

Marchand, R., Charbonneau-Lefort, M., Dumberry, M. and Pronovost, B., 2001, Aranea, a program for generating unstructured triangular meshes with a Java Graphics User Interface, *Comput Phys Commun*, 139: 172–185.

Mukadi, L.S. and Hayes, R.E., 2002, Modelling the three-way catalytic converter with mechanistic kinetics using the Newton–Krylov method on a parallel computer, *Comput Chem Eng*, 26(3): 439–455.

Siemund, S., Leclerc, J.P., Schweigh, D., Prignet, M. and Castagna, F., 1996, Three-way monolithic converter: simulations versus experiments, *Chem Eng Sci*, 51(15): 3709–3720.

Wheeler, A., 1955, in *Catalysis*, Emmett, P.H. (ed) (Reinhold, New York, USA), Vol II, Chap. 2, p 105.

Wicke, E. and Kallenbach, R., 1941, *Kolloid Z*, 97: 135; Smith, J.M., 1981, *Chemical Engineering Kinetics*, 3rd edition (McGraw-Hill, New York, USA) (as referenced).

ACKNOWLEDGEMENTS

Financial support for this work was provided by Umicore AG. The authors also thank Professor Marchand, Physics Department, University of Alberta, for assistance with implementing Aranea.

The manuscript was received 27 November 2002 and accepted for publication after revision 1 October 2003.

Appendix B1

Pore size distribution data for Samples BC (uncoated cordierite)

This appendix includes:

- Mercury porosimetry results of blank (uncoated) cordierite
- Nitrogen adsorption results of blank cordierite (partially)

micromeritics

Dept of Chemical Engineering, UCL

AutoPore IV 9500 V1.03 Serial: 201 Port: 1/1

Calibration ID: Sample 1, BC (Pen No:16-0287) 000-066
Operator: Julian Perfect
Submitter: Fan Zhang
File: C:\9500\DATA\BLANKS\000-066.SMP

LP Analysis Time:	13/07/2004 18:27:58PM	Sample Weight:	0.9649 g
HP Analysis Time:	13/07/2004 19:43:08PM	Correction Type:	Blank
Report Time:	14/07/2004 9:15:17PM	Show Neg. Int:	No

Summary Report

Penetrometer parameters

Penetrometer:	#s/n - (16) 3 Bulb, 1.190 Stem, Powder		
Pen. Constant:	20.994 µL/pF	Pen. Weight:	54.6894 g
Stem Volume:	1.1900 mL	Max. Head Pressure:	4.6800 psia
Pen. Volume:	4.0032 mL	Assembly Weight:	101.9716 g

Hg Parameters

Adv. Contact Angle:	130.000 degrees	Rec. Contact Angle:	130.000 degrees
Hg Surface Tension:	485.000 dynes/cm	Hg Density:	13.5335 g/mL

User Parameters

Param 1:	0.000	Param 2:	0.000	Param 3:	0.000

Low Pressure:

Evacuation Pressure:	50 µmHg
Evacuation Time:	5 mins
Mercury Filling Pressure:	1.33 psia
Equilibration Time:	10 secs

High Pressure:

Equilibration Time:	10 secs

Blank Correction Sample: C:\9500\DATA\BLANKS\000-052.SMP
Blank Correction ID: Pen No:16-0287 Blank Correction 000-052

(From Pressure 0.10 to 60000.00 psia)

Intrusion Data Summary

Total Intrusion Volume =	0.2069	mL/g
Total Pore Area =	0.329	m²/g
Median Pore Diameter (Volume) =	3.4045	µm
Median Pore Diameter (Area) =	1.6283	µm
Average Pore Diameter (4V/A) =	2.5183	µm
Bulk Density at 0.10 psia =	1.6613	g/mL
Apparent (skeletal) Density =	2.5315	g/mL
Porosity =	34.3715	%
Stem Volume Used =	17	% ****

Pore Structure Summary

Threshold Pressure:	2.55	psia (Calculated)
Characteristic length =	71.0499	µm
Conductivity formation factor =	0.009	
Permeability constant =	0.00442	
Permeability =	204.9607	mdarcy
BET Surface Area =	200.0000	m²/g
Pore shape exponent =	1.00	
Tortuosity factor =	1.842	
Tortuosity =	3.0488	
Percolation Fractal dimension =	3.000	
Backbone Fractal dimension =	2.274	

Calibration ID: Sample 1, BC (Pen No:16-0287) 000-066
Operator: Julian Perfect
Submitter: Fan Zhang
File: C:\9500\DATA\BLANKS\000-066.SMP

LP Analysis Time:	13/07/2004 18:27:58PM	Sample Weight:	0.9649 g
HP Analysis Time:	13/07/2004 19:43:08PM	Correction Type:	Blank
Report Time:	14/07/2004 9:15:17PM	Show Neg. Int:	No

Mayer Stowe Summary

Interstitial porosity =	34.3715	%
Breakthrough pressure ratio =	5.9580	

Material Compressibility

Linear Coefficient =	N/A	1/psia
Quadratic Coefficient =	N/A	1/psia^2

Calibration ID: Sample 1, BC (Pen No:16-0287) 000-066
Operator: Julian Perfect
Submitter: Fan Zhang
File: C:\9500\DATA\BLANKS\000-066.SMP

LP Analysis Time:	13/07/2004 18:27:58PM	Sample Weight:	0.9649 g
HP Analysis Time:	13/07/2004 19:43:08PM	Correction Type:	Blank
Report Time:	14/07/2004 9:15:17PM	Show Neg. Int:	No

Tabular Report

Pressure (psia)	Pore Diameter (µm)	dV/dlogD Pore Volume (mL/g)	dV/dD Pore Volume (mL/g/µm)
1.33	135.7712	0.000×10^{0}	0.000×10^{0}
1.98	91.3180	9.749×10^{-3}	3.778×10^{-5}
2.98	60.7514	1.699×10^{-2}	9.836×10^{-5}
3.98	45.4941	2.192×10^{-2}	1.804×10^{-4}
5.47	33.0753	2.437×10^{-2}	2.717×10^{-4}
6.97	25.9582	3.267×10^{-2}	4.830×10^{-4}
8.46	21.3742	4.134×10^{-2}	7.610×10^{-4}
10.45	17.3034	4.935×10^{-2}	1.112×10^{-3}
12.97	13.9425	5.599×10^{-2}	1.563×10^{-3}
15.95	11.3366	6.169×10^{-2}	2.127×10^{-3}
19.95	9.0638	7.519×10^{-2}	3.215×10^{-3}
22.95	7.8802	9.205×10^{-2}	4.727×10^{-3}
24.95	7.2488	1.088×10^{-1}	6.248×10^{-3}
29.95	6.0387	1.347×10^{-1}	8.827×10^{-3}
36.83	4.9102	1.213×10^{-1}	9.657×10^{-3}
46.68	3.8744	1.933×10^{-1}	1.920×10^{-2}
56.72	3.1890	2.192×10^{-1}	2.704×10^{-2}
71.67	2.5235	2.105×10^{-1}	3.215×10^{-2}
86.89	2.0816	1.863×10^{-1}	3.524×10^{-2}
111.49	1.6222	1.754×10^{-1}	4.134×10^{-2}
136.43	1.3256	1.565×10^{-1}	4.626×10^{-2}
171.10	1.0571	1.270×10^{-1}	4.648×10^{-2}
216.54	0.8352	6.981×10^{-2}	3.219×10^{-2}
266.41	0.6789	3.409×10^{-2}	1.963×10^{-2}
327.47	0.5523	2.284×10^{-2}	1.617×10^{-2}
416.01	0.4348	1.424×10^{-2}	1.259×10^{-2}
516.84	0.3499	7.381×10^{-3}	8.202×10^{-3}
637.60	0.2837	3.456×10^{-3}	4.755×10^{-3}
697.31	0.2594	0.000×10^{0}	0.000×10^{0}
796.98	0.2269	0.000×10^{0}	0.000×10^{0}
987.10	0.1832	0.000×10^{0}	0.000×10^{0}
1197.51	0.1510	0.000×10^{0}	0.000×10^{0}

Calibration ID: Sample 1, BC (Pen No:16-0287) 000-066
Operator: Julian Perfect
Submitter: Fan Zhang
File: C:\9500\DATA\BLANKS\000-066.SMP

LP Analysis Time:	13/07/2004 18:27:58PM	Sample Weight:	0.9649 g
HP Analysis Time:	13/07/2004 19:43:08PM	Correction Type:	Blank
Report Time:	14/07/2004 9:15:17PM	Show Neg. Int:	No

Tabular Report

Pressure (psia)	Pore Diameter (µm)	dV/dlogD Pore Volume (mL/g)	dV/dD Pore Volume (mL/g/µm)
1295.64	0.1396	0.000×10^0	0.000×10^0
1397.77	0.1294	0.000×10^0	0.000×10^0
1497.07	0.1208	0.000×10^0	0.000×10^0
1596.00	0.1133	0.000×10^0	0.000×10^0
1696.51	0.1066	0.000×10^0	0.000×10^0
1895.85	0.0954	0.000×10^0	0.000×10^0
2045.16	0.0884	0.000×10^0	0.000×10^0
2194.72	0.0824	0.000×10^0	0.000×10^0
2345.30	0.0771	0.000×10^0	0.000×10^0
2495.08	0.0725	0.000×10^0	0.000×10^0
2644.49	0.0684	0.000×10^0	0.000×10^0
2693.38	0.0672	0.000×10^0	0.000×10^0
2844.18	0.0636	0.000×10^0	0.000×10^0
2993.51	0.0604	0.000×10^0	0.000×10^0
3243.49	0.0558	0.000×10^0	0.000×10^0
3490.60	0.0518	0.000×10^0	0.000×10^0
3742.06	0.0483	0.000×10^0	0.000×10^0
3990.90	0.0453	0.000×10^0	0.000×10^0
4239.40	0.0427	0.000×10^0	0.000×10^0
4485.86	0.0403	0.000×10^0	0.000×10^0
4722.17	0.0383	0.000×10^0	0.000×10^0
4982.92	0.0363	0.000×10^0	0.000×10^0
5281.50	0.0342	0.000×10^0	0.000×10^0
5478.08	0.0330	0.000×10^0	0.000×10^0
5731.02	0.0316	0.000×10^0	0.000×10^0
5977.13	0.0303	0.000×10^0	0.000×10^0
6229.84	0.0290	0.000×10^0	0.000×10^0
6477.96	0.0279	0.000×10^0	0.000×10^0
6730.03	0.0269	0.000×10^0	0.000×10^0
6979.53	0.0259	0.000×10^0	0.000×10^0
7476.64	0.0242	0.000×10^0	0.000×10^0
7978.21	0.0227	0.000×10^0	0.000×10^0

Calibration ID: Sample 1, BC (Pen No:16-0287) 000-066
Operator: Julian Perfect
Submitter: Fan Zhang
File: C:\9500\DATA\BLANKS\000-066.SMP

LP Analysis Time:	13/07/2004 18:27:58PM	Sample Weight:	0.9649 g
HP Analysis Time:	13/07/2004 19:43:08PM	Correction Type:	Blank
Report Time:	14/07/2004 9:15:17PM	Show Neg. Int:	No

Tabular Report

Pressure (psia)	Pore Diameter (µm)	dV/dlogD Pore Volume (mL/g)	dV/dD Pore Volume (mL/g/µm)
8471.10	0.0214	0.000×10^0	0.000×10^0
8969.05	0.0202	0.000×10^0	0.000×10^0
9270.15	0.0195	0.000×10^0	0.000×10^0
9570.44	0.0189	0.000×10^0	0.000×10^0
10016.48	0.0181	0.000×10^0	0.000×10^0
10463.98	0.0173	0.000×10^0	0.000×10^0
10961.52	0.0165	0.000×10^0	0.000×10^0
11455.46	0.0158	0.000×10^0	0.000×10^0
11957.18	0.0151	0.000×10^0	0.000×10^0
12558.20	0.0144	0.000×10^0	0.000×10^0
13052.17	0.0139	0.000×10^0	0.000×10^0
13602.86	0.0133	0.000×10^0	0.000×10^0
13951.31	0.0130	0.000×10^0	0.000×10^0
14289.59	0.0127	0.000×10^0	0.000×10^0
14540.96	0.0124	0.000×10^0	0.000×10^0
14946.93	0.0121	0.000×10^0	0.000×10^0
15395.89	0.0117	0.000×10^0	0.000×10^0
15748.43	0.0115	0.000×10^0	0.000×10^0
16147.49	0.0112	0.000×10^0	0.000×10^0
16596.90	0.0109	0.000×10^0	0.000×10^0
16939.92	0.0107	0.000×10^0	0.000×10^0
17294.49	0.0105	0.000×10^0	0.000×10^0
17642.61	0.0103	0.000×10^0	0.000×10^0
18048.07	0.0100	0.000×10^0	0.000×10^0
18392.90	0.0098	0.000×10^0	0.000×10^0
18744.28	0.0096	0.000×10^0	0.000×10^0
19137.75	0.0095	0.000×10^0	0.000×10^0
19741.30	0.0092	0.000×10^0	0.000×10^0
20249.76	0.0089	0.000×10^0	0.000×10^0
20756.84	0.0087	0.000×10^0	0.000×10^0
21161.30	0.0085	0.000×10^0	0.000×10^0
21617.74	0.0084	0.000×10^0	0.000×10^0

Calibration ID: Sample 1, BC (Pen No:16-0287) 000-066
Operator: Julian Perfect
Submitter: Fan Zhang
File: C:\9500\DATA\BLANKS\000-066.SMP

LP Analysis Time: 13/07/2004 18:27:58PM
HP Analysis Time: 13/07/2004 19:43:08PM
Report Time: 14/07/2004 9:15:17PM

Sample Weight: 0.9649 g
Correction Type: Blank
Show Neg. Int: No

Tabular Report

Pressure (psia)	Pore Diameter (µm)	dV/dlogD Pore Volume (mL/g)	dV/dD Pore Volume (mL/g/µm)
22022.42	0.0082	0.000×10^0	0.000×10^0
22625.85	0.0080	0.000×10^0	0.000×10^0
23179.32	0.0078	0.000×10^0	0.000×10^0
23725.61	0.0076	0.000×10^0	0.000×10^0
24079.33	0.0075	0.000×10^0	0.000×10^0
24632.47	0.0073	0.000×10^0	0.000×10^0
25029.24	0.0072	0.000×10^0	0.000×10^0
25433.29	0.0071	0.000×10^0	0.000×10^0
25883.14	0.0070	0.000×10^0	0.000×10^0
26433.41	0.0068	0.000×10^0	0.000×10^0
26935.95	0.0067	0.000×10^0	0.000×10^0
27385.40	0.0066	0.000×10^0	0.000×10^0
27786.38	0.0065	0.000×10^0	0.000×10^0
28235.61	0.0064	0.000×10^0	0.000×10^0
28984.95	0.0062	0.000×10^0	0.000×10^0
29489.15	0.0061	0.000×10^0	0.000×10^0
29987.96	0.0060	0.000×10^0	0.000×10^0
30437.55	0.0059	0.000×10^0	0.000×10^0
30887.76	0.0059	0.000×10^0	0.000×10^0
31285.51	0.0058	0.000×10^0	0.000×10^0
31789.36	0.0057	0.000×10^0	0.000×10^0
32339.08	0.0056	0.000×10^0	0.000×10^0
32886.57	0.0055	0.000×10^0	0.000×10^0
33485.34	0.0054	0.000×10^0	0.000×10^0
33987.67	0.0053	0.000×10^0	0.000×10^0
34638.07	0.0052	0.000×10^0	0.000×10^0
35486.49	0.0051	0.000×10^0	0.000×10^0
36180.21	0.0050	0.000×10^0	0.000×10^0
36980.17	0.0049	0.000×10^0	0.000×10^0
37631.83	0.0048	0.000×10^0	0.000×10^0
38426.24	0.0047	0.000×10^0	0.000×10^0
39181.33	0.0046	0.000×10^0	0.000×10^0

micromeritics

Dept of Chemical Engineering, UCL

Calibration ID: Sample 1, BC (Pen No:16-0287) 000-066
Operator: Julian Perfect
Submitter: Fan Zhang
File: C:\9500\DATA\BLANKS\000-066.SMP

LP Analysis Time:	13/07/2004 18:27:58PM	Sample Weight:	0.9649 g
HP Analysis Time:	13/07/2004 19:43:08PM	Correction Type:	Blank
Report Time:	14/07/2004 9:15:17PM	Show Neg. Int:	No

Tabular Report

Pressure (psia)	Pore Diameter (μm)	dV/dlogD Pore Volume (mL/g)	dV/dD Pore Volume (mL/g/μm)
39977.29	0.0045	0.000×10^0	0.000×10^0
40475.32	0.0045	0.000×10^0	0.000×10^0
40966.32	0.0044	0.000×10^0	0.000×10^0
42462.15	0.0043	0.000×10^0	0.000×10^0
43315.10	0.0042	0.000×10^0	0.000×10^0
43970.57	0.0041	0.000×10^0	0.000×10^0
44961.93	0.0040	0.000×10^0	0.000×10^0
46461.10	0.0039	0.000×10^0	0.000×10^0
47960.76	0.0038	0.000×10^0	0.000×10^0
49463.11	0.0037	0.000×10^0	0.000×10^0
50163.80	0.0036	0.000×10^0	0.000×10^0
52957.24	0.0034	0.000×10^0	0.000×10^0
54453.59	0.0033	0.000×10^0	0.000×10^0
55952.15	0.0032	0.000×10^0	0.000×10^0
57943.07	0.0031	0.000×10^0	0.000×10^0
59938.24	0.0030	0.000×10^0	0.000×10^0

micromeritics

Dept of Chemical Engineering, UCL

AutoPore IV 9500 V1.03 Serial: 201 Port: 1/1 Page 8

Calibration ID: Sample 1, BC (Pen No:16-0287) 000-066
Operator: Julian Perfect
Submitter: Fan Zhang
File: C:\9500\DATA\BLANKS\000-066.SMP

LP Analysis Time:	13/07/2004 18:27:58PM	Sample Weight:	0.9649 g
HP Analysis Time:	13/07/2004 19:43:08PM	Correction Type:	Blank
Report Time:	14/07/2004 9:15:17PM	Show Neg. Int:	No

Cumulative Intrusion vs Pore size

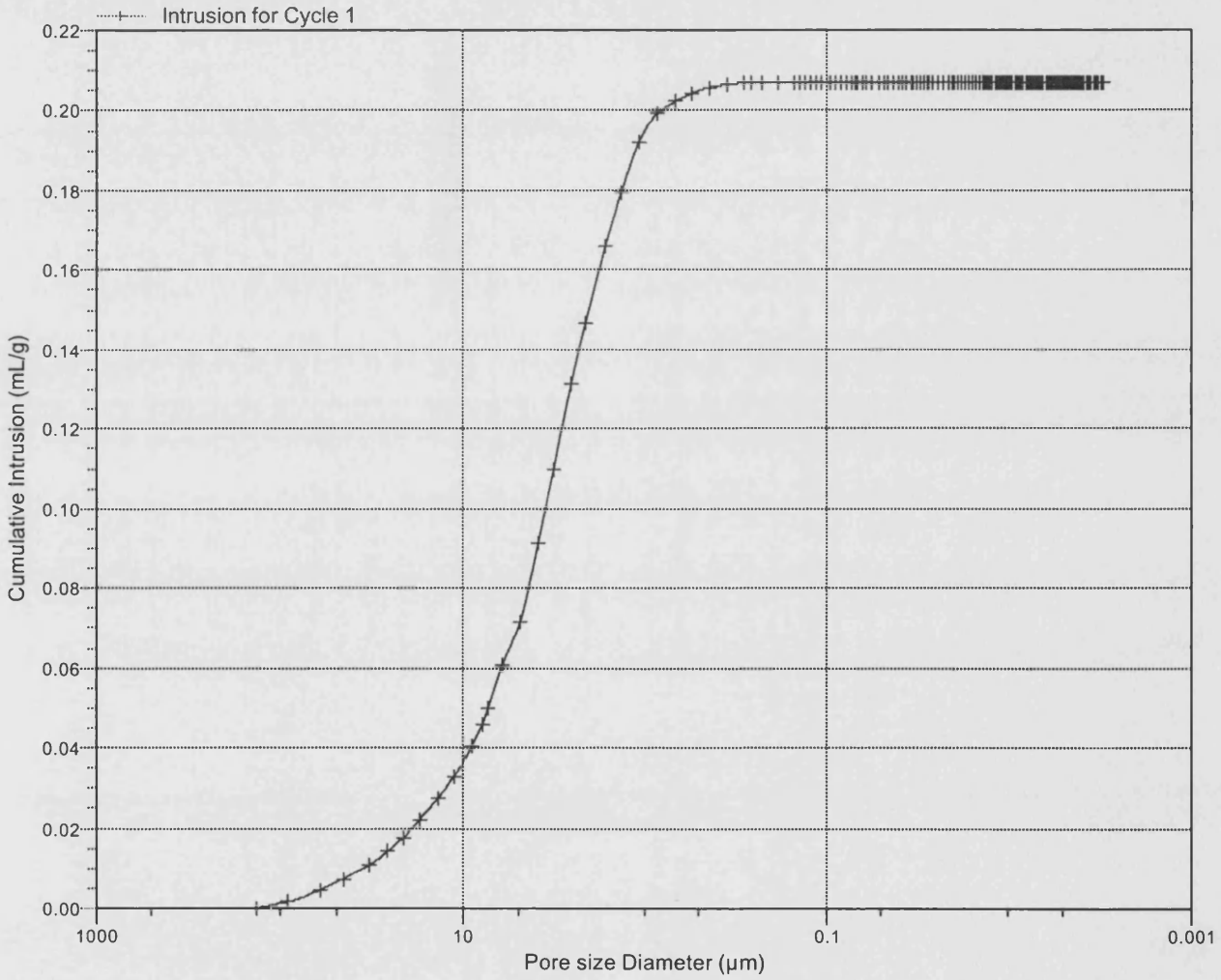

micromeritics

Dept of Chemical Engineering, UCL

AutoPore IV 9500 V1.03 Serial: 201 Port: 1/1 Page 9

Calibration ID: Sample 1, BC (Pen No:16-0287) 000-066
Operator: Julian Perfect
Submitter: Fan Zhang
File: C:\9500\DATA\BLANKS\000-066.SMP

LP Analysis Time:	13/07/2004 18:27:58PM	Sample Weight:	0.9649 g
HP Analysis Time:	13/07/2004 19:43:08PM	Correction Type:	Blank
Report Time:	14/07/2004 9:15:17PM	Show Neg. Int:	No

Incremental Intrusion vs Pressure

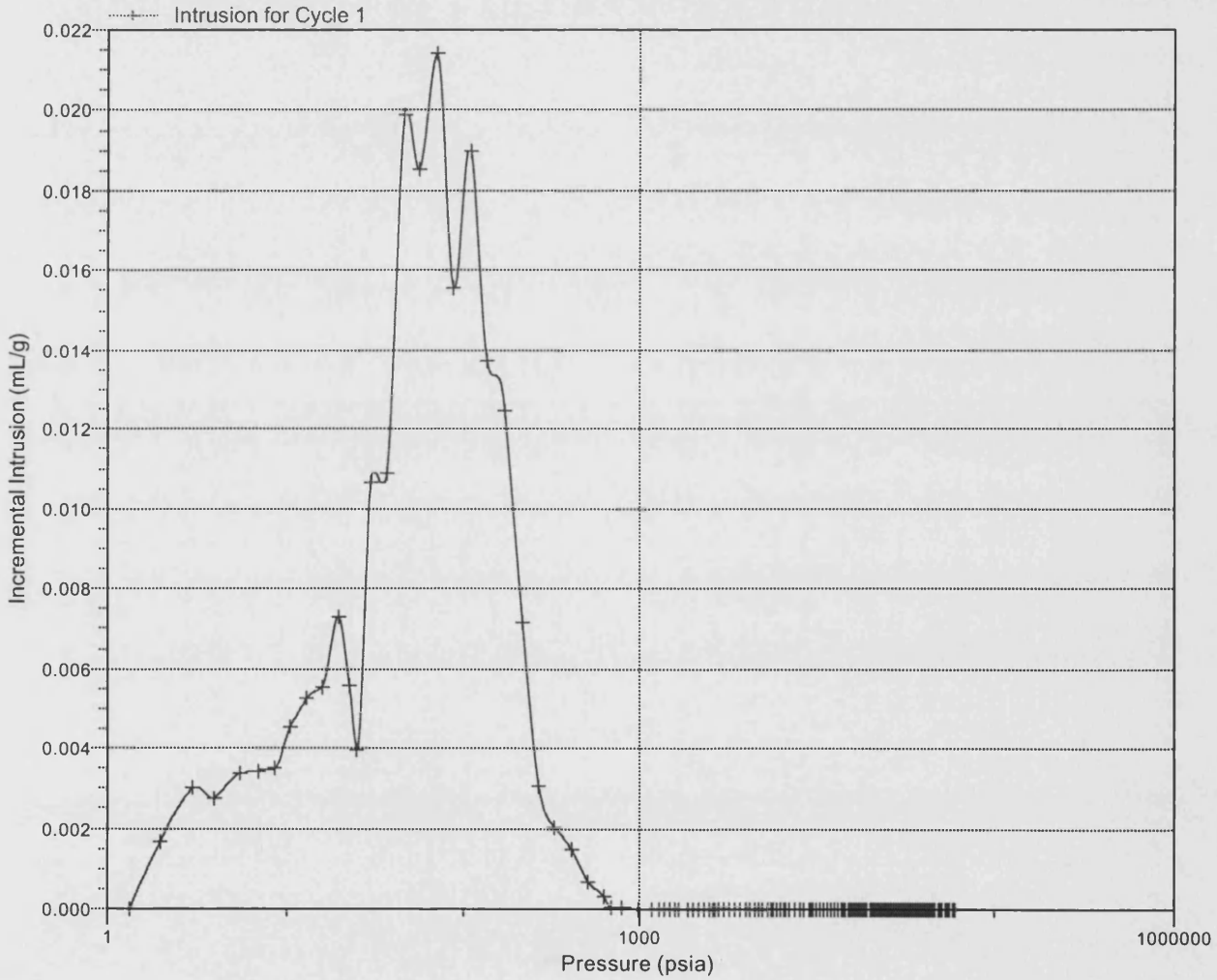

micromeritics

Dept of Chemical Engineering, UCL

AutoPore IV 9500 V1.03 Serial: 201 Port: 1/1 Page 10

Calibration ID: Sample 1, BC (Pen No:16-0287) 000-066
Operator: Julian Perfect
Submitter: Fan Zhang
File: C:\9500\DATA\BLANKS\000-066.SMP

LP Analysis Time:	13/07/2004 18:27:58PM	Sample Weight:	0.9649 g
HP Analysis Time:	13/07/2004 19:43:08PM	Correction Type:	Blank
Report Time:	14/07/2004 9:15:17PM	Show Neg. Int:	No

Differential Intrusion vs Pore size

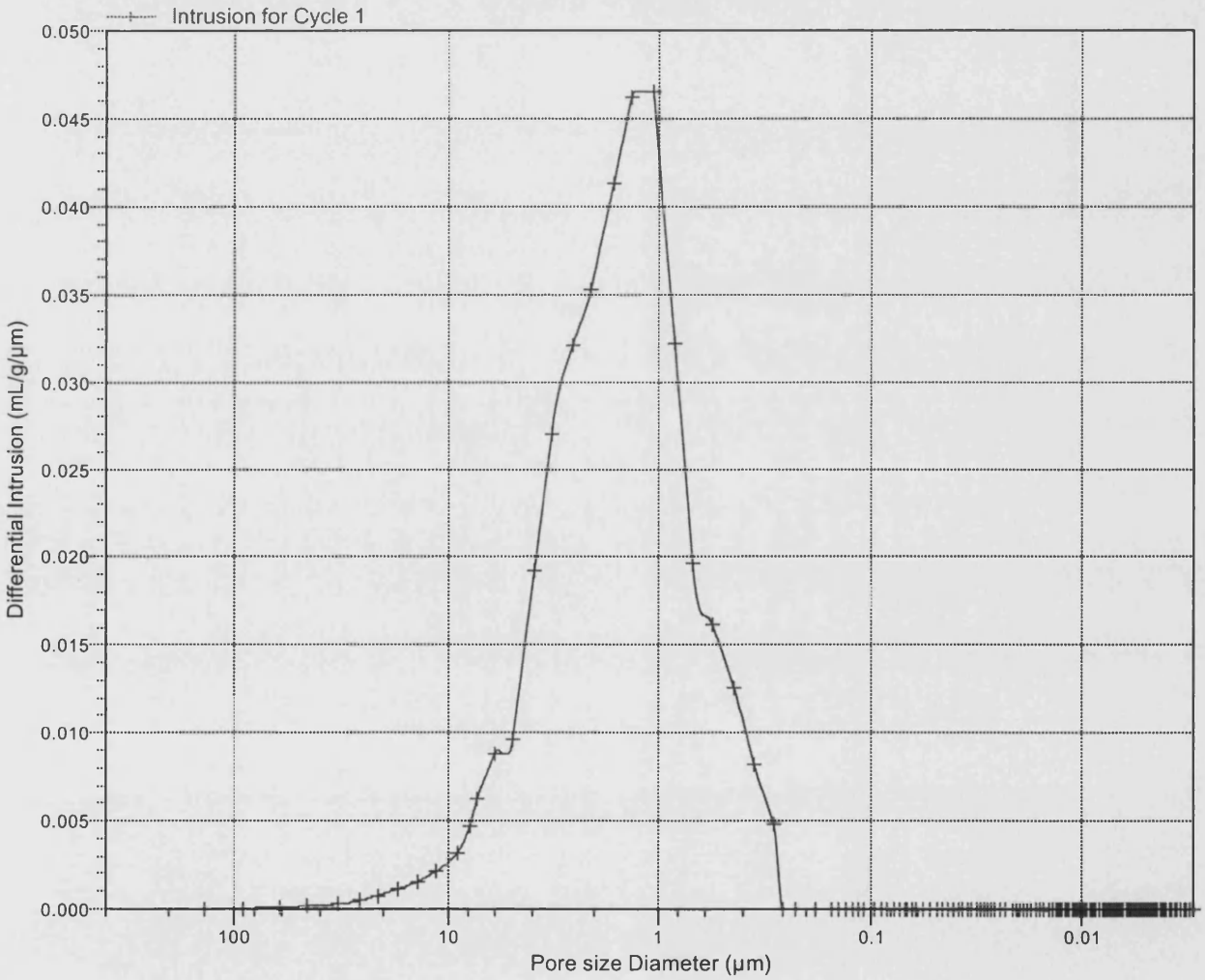

micromeritics

Dept of Chemical Engineering, UCL

AutoPore IV 9500 V1.03 Serial: 201 Port: 1/1 Page 11

Calibration ID: Sample 1, BC (Pen No:16-0287) 000-066
Operator: Julian Perfect
Submitter: Fan Zhang
File: C:\9500\DATA\BLANKS\000-066.SMP

LP Analysis Time:	13/07/2004 18:27:58PM	Sample Weight:	0.9649 g
HP Analysis Time:	13/07/2004 19:43:08PM	Correction Type:	Blank
Report Time:	14/07/2004 9:15:17PM	Show Neg. Int:	No

Log Differential Intrusion vs Pore size

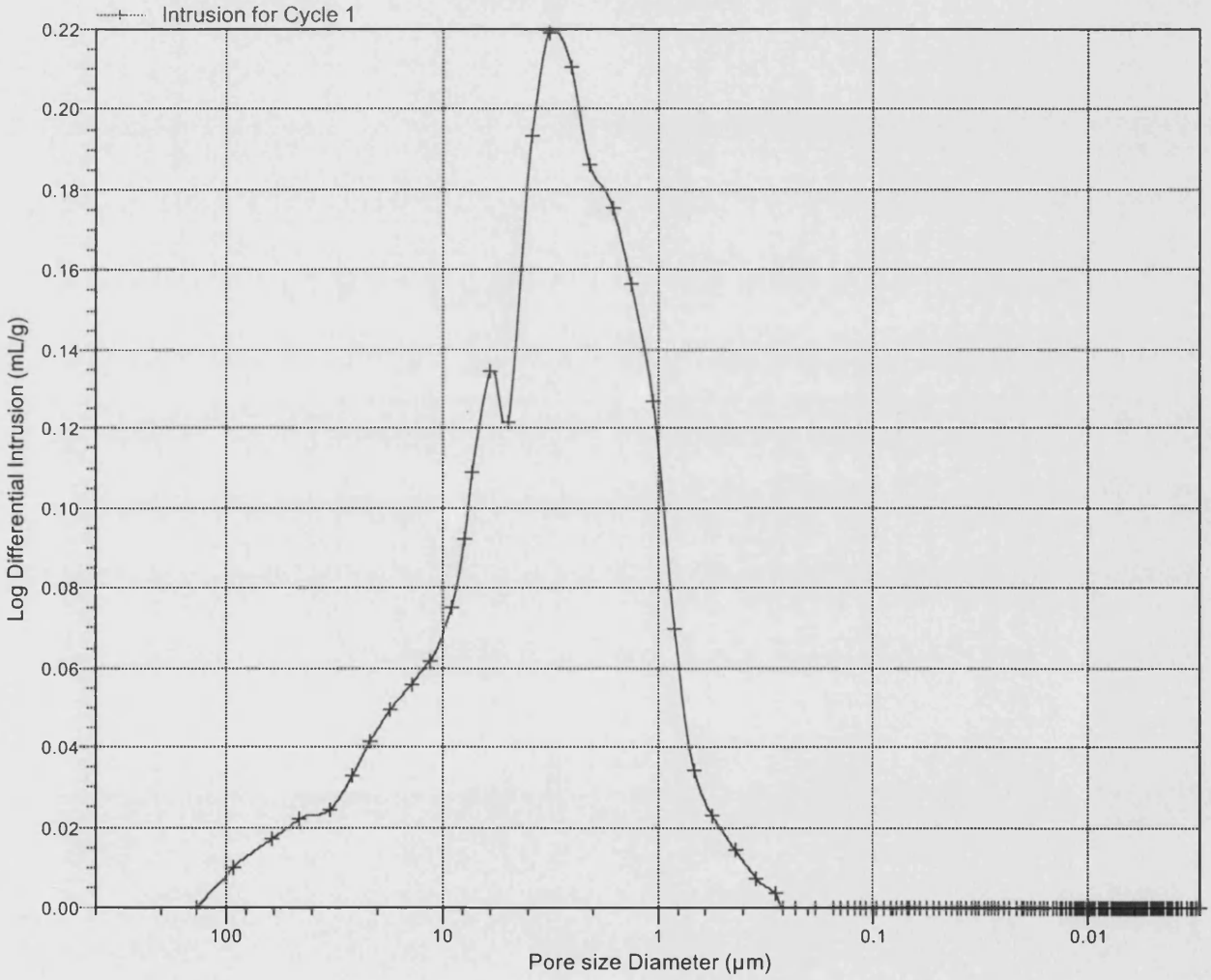

FULL ISOTHERM FOR SAMPLE 1, BC

ASAP 2010 V5.01 H Unit 1 Serial # 2727 Page 1

Sample: Sample 1, BC
Operator: Julian Perfect
Submitter: Fan Zhang
File Name: C:\ASAP2010\DATA\000-056.SMP

Started: 6/29/04 11:08:23AM Analysis Adsorptive: N2
Completed: 6/29/04 5:11:20PM Analysis Bath: 77.35 K
Report Time: 6/30/04 6:42:29PM Thermal Correction: No
Sample Weight: 2.3758 g Smoothed Pressures: No
Warm Freespace: 16.3419 cm³ Cold Freespace: 49.2292 cm³
MEASURED
Equil. Interval: 10 secs Low Pressure Dose: None
Comments:
Bulb type sample holder used with stopper and filler rod. Sample degassed, using manual mode, for ~120 hours (~28 hours @ 90C, 24 hours @ 130C and 68 hours @ 350C)

Analysis Log

Relative Pressure	Pressure (mmHg)	Vol Adsorbed (cm³/g STP)	Elapsed Time (HR:MN)	Saturation Press.(mmHg)
			02:57	768.65619
0.158557103	121.86129	0.0765	03:12	
0.161704753	124.27748	0.0790	03:15	
0.181265497	139.30858	0.0814	03:17	
0.204075662	156.83519	0.0833	03:20	
0.220024731	169.08958	0.0843	03:22	
0.251460661	193.24355	0.0867	03:25	
0.302496121	232.45792	0.0905	03:28	
0.353689717	271.79410	0.0934	03:30	
0.419298863	322.20395	0.0963	03:33	
0.469061343	360.43454	0.0993	03:36	
0.501837204	385.61081	0.1014	03:39	
0.550171436	422.74399	0.1039	03:41	
0.619250466	475.81573	0.1070	03:43	
0.669383868	514.32458	0.1112	03:46	
0.700353625	538.11176	0.1143	03:48	
0.741768304	569.91876	0.1187	03:51	
0.771998059	593.13080	0.1218	03:54	
0.800396707	614.93982	0.1250	03:56	
0.821044113	630.78796	0.1302	03:59	
0.840812880	645.96033	0.1341	04:02	
0.861360950	661.73065	0.1396	04:05	
0.876879544	673.63647	0.1461	04:08	
0.890968693	684.44910	0.1529	04:10	
0.905646412	695.70795	0.1576	04:13	
0.915586515	703.33258	0.1628	04:15	
0.925381781	710.84003	0.1703	04:18	
0.933568405	717.11145	0.1775	04:21	
0.940864062	722.70398	0.1850	04:23	
0.947941355	728.12860	0.1930	04:25	
0.955586486	733.98334	0.2025	04:28	

FULL ISOTHERM FOR SAMPLE 1, BC

ASAP 2010 V5.01 H Unit 1 Serial # 2727 Page 2

Sample: Sample 1, BC
Operator: Julian Perfect
Submitter: Fan Zhang
File Name: C:\ASAP2010\DATA\000-056.SMP

Started: 6/29/04 11:08:23AM Analysis Adsorptive: N2
Completed: 6/29/04 5:11:20PM Analysis Bath: 77.35 K
Report Time: 6/30/04 6:42:29PM Thermal Correction: No
Sample Weight: 2.3758 g Smoothed Pressures: No
Warm Freespace: 16.3419 cm³ Cold Freespace: 49.2292 cm³
MEASURED
Equil. Interval: 10 secs Low Pressure Dose: None
Comments:
Bulb type sample holder used with stopper and filler rod. Sample degassed, using manual mode, for ~120 hours (~28 hours @ 90C, 24 hours @ 130C and 68 hours @ 350C)

Analysis Log

Relative Pressure	Pressure (mmHg)	Vol Adsorbed (cm³/g STP)	Elapsed Time (HR:MN)	Saturation Press.(mmHg)
0.960277089	737.56848	0.2112	04:31	
0.964730146	740.97693	0.2195	04:33	
0.968652622	743.97180	0.2279	04:36	
0.971721400	746.31683	0.2346	04:38	
0.975405867	749.12866	0.2450	04:41	
0.977855580	750.99207	0.2535	04:44	
0.980972307	753.37366	0.2664	04:46	
0.983118811	755.00403	0.2764	04:49	
0.984915468	756.37170	0.2862	04:51	
0.987500641	758.33881	0.3023	04:54	
0.989297007	759.70007	0.3157	04:57	
			04:58	767.91296
0.990504858	760.62152	0.3257	05:02	
0.972631373	746.89624	0.2370	05:04	
0.954369063	732.87238	0.1907	05:07	
0.934736565	717.79633	0.1647	05:10	
0.916664295	703.91840	0.1481	05:13	
0.896627314	688.53174	0.1348	05:15	
0.871309796	669.09009	0.1230	05:18	
0.841551785	646.23853	0.1103	05:20	
0.822006637	631.22955	0.1020	05:23	
0.801549912	615.52057	0.0958	05:25	
0.782590467	600.96136	0.0904	05:28	
0.751738626	577.26984	0.0830	05:31	
0.723046069	555.23645	0.0768	05:33	
0.681499705	523.33246	0.0695	05:36	
0.633541976	486.50510	0.0633	05:39	
0.583066062	447.74399	0.0568	05:41	
0.531030556	407.78525	0.0509	05:44	
0.481024261	369.38477	0.0466	05:46	
0.432606689	332.20428	0.0424	05:49	

FULL ISOTHERM FOR SAMPLE 1, BC

Sample: Sample 1, BC
Operator: Julian Perfect
Submitter: Fan Zhang
File Name: C:\ASAP2010\DATA\000-056.SMP

Started: 6/29/04 11:08:23AM Analysis Adsorptive: N2
Completed: 6/29/04 5:11:20PM Analysis Bath: 77.35 K
Report Time: 6/30/04 6:42:29PM Thermal Correction: No
Sample Weight: 2.3758 g Smoothed Pressures: No
Warm Freespace: 16.3419 cm³ Cold Freespace: 49.2292 cm³
MEASURED
Equil. Interval: 10 secs Low Pressure Dose: None
Comments:
Bulb type sample holder used with stopper and filler rod. Sample degassed, using manual mode, for ~120 hours (~28 hours @ 90C, 24 hours @ 130C and 68 hours @ 350C)

Analysis Log

Relative Pressure	Pressure (mmHg)	Vol Adsorbed (cm³/g STP)	Elapsed Time (HR:MN)	Saturation Press.(mmHg)
0.381432805	292.90720	0.0378	05:51	
0.330702013	253.95036	0.0330	05:53	
0.284082540	218.15067	0.0291	05:56	
0.230809183	177.24136	0.0229	05:58	
0.181329952	139.24562	0.0172	06:01	
0.140096061	107.58158	0.0097	06:03	

FULL ISOTHERM FOR SAMPLE 1, BC

Sample: Sample 1, BC
Operator: Julian Perfect
Submitter: Fan Zhang
File Name: C:\ASAP2010\DATA\000-056.SMP

Started: 6/29/04 11:08:23AM Analysis Adsorptive: N2
Completed: 6/29/04 5:11:20PM Analysis Bath: 77.35 K
Report Time: 6/30/04 6:42:29PM Thermal Correction: No
Sample Weight: 2.3758 g Smoothed Pressures: No
Warm Freespace: 16.3419 cm³ Cold Freespace: 49.2292 cm³
MEASURED
Equil. Interval: 10 secs Low Pressure Dose: None
Comments:
Bulb type sample holder used with stopper and filler rod. Sample degassed, using manual mode, for ~120 hours (~28 hours @ 90C, 24 hours @ 130C and 68 hours @ 350C)

Summary Report

Area

Single Point Surface Area at P/Po 0.25146066 :	0.2824	m²/g
BET Surface Area:	0.2822	m²/g
Langmuir Surface Area:	0.4719	m²/g
Micropore Area:	0.0454	m²/g
External Surface Area:	0.2368	m²/g
BJH Adsorption Cumulative Surface Area of pores between 17.000000 and 3000.000000 A Diameter:	0.1834	m²/g
BJH Desorption Cumulative Surface Area of pores between 17.000000 and 3000.000000 A Diameter:	0.1362	m²/g

Volume

Single Point Desorption Total Pore Volume of pores less than 726.7631 A Diameter at P/Po 0.97263137:	0.000367	cm³/g
Micropore Volume:	0.000024	cm³/g
BJH Adsorption Cumulative Pore Volume of pores between 17.000000 and 3000.000000 A Diameter:	0.000462	cm³/g
BJH Desorption Cumulative Pore Volume of pores between 17.000000 and 3000.000000 A Diameter:	0.000479	cm³/g

Pore Size

FULL ISOTHERM FOR SAMPLE 1, BC

Sample: Sample 1, BC
Operator: Julian Perfect
Submitter: Fan Zhang
File Name: C:\ASAP2010\DATA\000-056.SMP

Started: 6/29/04 11:08:23AM
Completed: 6/29/04 5:11:20PM
Report Time: 6/30/04 6:42:29PM
Sample Weight: 2.3758 g
Warm Freespace: 16.3419 cm³
MEASURED
Equil. Interval: 10 secs
Analysis Adsorptive: N2
Analysis Bath: 77.35 K
Thermal Correction: No
Smoothed Pressures: No
Cold Freespace: 49.2292 cm³
Low Pressure Dose: None

Comments:
Bulb type sample holder used with stopper and filler rod. Sample degassed, using manual mode, for ~120 hours (~28 hours @ 90C, 24 hours @ 130C and 68 hours @ 350C)

Summary Report

Desorption Average Pore Diameter (4V/A by BET):	51.9562	A
BJH Adsorption Average Pore Diameter (4V/A):	100.7894	A
BJH Desorption Average Pore Diameter (4V/A):	140.6025	A

Appendix B2

Pore size distribution data for Samples S3, S3w & S3HT

This appendix includes:

- Mercury porosimetry results of Sample S3, S3w and S3HT
- Nitrogen adsorption results of Sample S3, S3w and S3HT (partially)

micromeritics

Dept of Chemical Engineering, UCL

AutoPore IV 9500 V1.03 Serial: 201 Port: 1/1

Calibration ID: Sample 2, S3-68 (Pen No:16-0289) 000-068
Operator: Julian Perfect
Submitter: Fan Zhang
File: C:\9500\DATA\BLANKS\000-068.SMP

LP Analysis Time:	13/07/2004 21:22:57PM	Sample Weight:	0.4512 g
HP Analysis Time:	13/07/2004 23:37:05PM	Correction Type:	Blank
Report Time:	14/07/2004 9:20:14PM	Show Neg. Int:	No

Summary Report

Penetrometer parameters

Penetrometer:	#s/n - (16) 3 Bulb, 1.190 Stem, Powder		
Pen. Constant:	20.994 µL/pF	Pen. Weight:	54.8218 g
Stem Volume:	1.1900 mL	Max. Head Pressure:	4.6800 psia
Pen. Volume:	3.9104 mL	Assembly Weight:	103.1911 g

Hg Parameters

Adv. Contact Angle:	130.000 degrees	Rec. Contact Angle:	130.000 degrees
Hg Surface Tension:	485.000 dynes/cm	Hg Density:	13.5335 g/mL

User Parameters

Param 1:	0.000	Param 2:	0.000	Param 3:	0.000

Low Pressure:

Evacuation Pressure:	50 µmHg
Evacuation Time:	5 mins
Mercury Filling Pressure:	1.34 psia
Equilibration Time:	10 secs

High Pressure:

Equilibration Time:	10 secs

Blank Correction Sample: C:\9500\DATA\BLANKS\000-053.SMP
Blank Correction ID: Pen No:16-0289 Blank Correction 000-053

(From Pressure 0.10 to 60000.00 psia)

Intrusion Data Summary

Total Intrusion Volume =	0.4314	mL/g
Total Pore Area =	55.138	m²/g
Median Pore Diameter (Volume) =	0.1045	µm
Median Pore Diameter (Area) =	0.0126	µm
Average Pore Diameter (4V/A) =	0.0313	µm
Bulk Density at 0.10 psia =	1.2203	g/mL
Apparent (skeletal) Density =	2.5777	g/mL
Porosity =	52.6526	%
Stem Volume Used =	16	% ****

Pore Structure Summary

Threshold Pressure:	91.95	psia (Calculated)
Characteristic length =	1.9671	µm
Conductivity formation factor =	0.152	
Permeability constant =	0.00442	
Permeability =	2.5980	mdarcy
BET Surface Area =	200.0000	m²/g
Pore shape exponent =	1.00	
Tortuosity factor =	1.635	
Tortuosity =	35.9793	
Percolation Fractal dimension =	2.711	
Backbone Fractal dimension =	2.490	

Calibration ID: Sample 2, S3-68 (Pen No:16-0289) 000-068
Operator: Julian Perfect
Submitter: Fan Zhang
File: C:\9500\DATA\BLANKS\000-068.SMP

LP Analysis Time:	13/07/2004 21:22:57PM	Sample Weight:	0.4512 g
HP Analysis Time:	13/07/2004 23:37:05PM	Correction Type:	Blank
Report Time:	14/07/2004 9:20:14PM	Show Neg. Int:	No

Mayer Stowe Summary

Interstitial porosity =	47.6300	%
Breakthrough pressure ratio =	3.3512	

Material Compressibility

Linear Coefficient =	N/A	1/psia
Quadratic Coefficient =	N/A	1/psia²

Calibration ID: Sample 2, S3-68 (Pen No:16-0289) 000-068
Operator: Julian Perfect
Submitter: Fan Zhang
File: C:\9500\DATA\BLANKS\000-068.SMP

LP Analysis Time: 13/07/2004 21:22:57PM
HP Analysis Time: 13/07/2004 23:37:05PM
Report Time: 14/07/2004 9:20:14PM

Sample Weight: 0.4512 g
Correction Type: Blank
Show Neg. Int: No

Tabular Report

Pressure (psia)	Pore Diameter (µm)	dV/dlogD Pore Volume (mL/g)	dV/dD Pore Volume (mL/g/µm)
1.34	135.3990	0.000×10^{0}	0.000×10^{0}
1.98	91.2177	4.866×10^{-2}	1.889×10^{-4}
2.98	60.7279	4.468×10^{-2}	2.589×10^{-4}
3.98	45.4543	4.075×10^{-2}	3.357×10^{-4}
5.47	33.0454	3.291×10^{-2}	3.673×10^{-4}
6.97	25.9641	2.331×10^{-2}	3.448×10^{-4}
8.46	21.3664	1.827×10^{-2}	3.363×10^{-4}
10.45	17.3042	1.777×10^{-2}	4.007×10^{-4}
12.97	13.9432	1.186×10^{-2}	3.309×10^{-4}
15.95	11.3374	1.208×10^{-2}	4.164×10^{-4}
19.95	9.0638	1.256×10^{-2}	5.368×10^{-4}
22.95	7.8806	1.339×10^{-2}	6.875×10^{-4}
24.95	7.2483	2.390×10^{-2}	1.373×10^{-3}
29.95	6.0387	1.676×10^{-2}	1.099×10^{-3}
36.94	4.8964	1.039×10^{-2}	8.283×10^{-4}
46.85	3.8602	1.728×10^{-2}	1.722×10^{-3}
57.03	3.1714	3.127×10^{-2}	3.875×10^{-3}
71.32	2.5361	5.821×10^{-2}	8.895×10^{-3}
86.66	2.0871	1.820×10^{-1}	3.431×10^{-2}
111.78	1.6181	3.106×10^{-1}	7.319×10^{-2}
136.33	1.3267	1.968×10^{-1}	5.825×10^{-2}
171.08	1.0572	1.512×10^{-1}	5.534×10^{-2}
216.68	0.8347	1.366×10^{-1}	6.300×10^{-2}
266.95	0.6775	1.162×10^{-1}	6.700×10^{-2}
325.82	0.5551	1.109×10^{-1}	7.840×10^{-2}
416.68	0.4341	9.886×10^{-2}	8.725×10^{-2}
516.83	0.3499	8.986×10^{-2}	9.994×10^{-2}
636.20	0.2843	7.733×10^{-2}	1.063×10^{-1}
697.28	0.2594	7.267×10^{-2}	1.162×10^{-1}
796.94	0.2269	6.475×10^{-2}	1.158×10^{-1}
987.47	0.1832	5.792×10^{-2}	1.232×10^{-1}
1196.77	0.1511	5.402×10^{-2}	1.408×10^{-1}

micromeritics

Dept of Chemical Engineering, UCL

Calibration ID: Sample 2, S3-68 (Pen No:16-0289) 000-068
Operator: Julian Perfect
Submitter: Fan Zhang
File: C:\9500\DATA\BLANKS\000-068.SMP

LP Analysis Time: 13/07/2004 21:22:57PM
HP Analysis Time: 13/07/2004 23:37:05PM
Report Time: 14/07/2004 9:20:14PM

Sample Weight: 0.4512 g
Correction Type: Blank
Show Neg. Int: No

Tabular Report

Pressure (psia)	Pore Diameter (µm)	dV/dlogD Pore Volume (mL/g)	dV/dD Pore Volume (mL/g/µm)
1296.75	0.1395	5.572×10^{-2}	1.666×10^{-1}
1396.58	0.1295	4.846×10^{-2}	1.566×10^{-1}
1496.25	0.1209	5.899×10^{-2}	2.047×10^{-1}
1596.07	0.1133	4.898×10^{-2}	1.817×10^{-1}
1696.33	0.1066	5.405×10^{-2}	2.135×10^{-1}
1895.54	0.0954	4.694×10^{-2}	2.020×10^{-1}
2046.11	0.0884	5.380×10^{-2}	2.543×10^{-1}
2195.27	0.0824	4.661×10^{-2}	2.372×10^{-1}
2343.83	0.0772	5.682×10^{-2}	3.095×10^{-1}
2495.63	0.0725	5.252×10^{-2}	3.050×10^{-1}
2644.97	0.0684	5.758×10^{-2}	3.552×10^{-1}
2693.24	0.0672	9.725×10^{-2}	6.233×10^{-1}
2843.30	0.0636	4.672×10^{-2}	3.104×10^{-1}
2993.35	0.0604	6.012×10^{-2}	4.211×10^{-1}
3243.36	0.0558	5.225×10^{-2}	3.908×10^{-1}
3492.46	0.0518	6.923×10^{-2}	5.594×10^{-1}
3741.38	0.0483	5.672×10^{-2}	4.922×10^{-1}
3991.71	0.0453	6.959×10^{-2}	6.456×10^{-1}
4239.03	0.0427	9.204×10^{-2}	9.090×10^{-1}
4485.33	0.0403	7.990×10^{-2}	8.364×10^{-1}
4723.55	0.0383	1.051×10^{-1}	1.161×10^{0}
4982.63	0.0363	1.179×10^{-1}	1.374×10^{0}
5283.25	0.0342	1.470×10^{-1}	1.811×10^{0}
5481.25	0.0330	1.907×10^{-1}	2.465×10^{0}
5731.66	0.0316	2.149×10^{-1}	2.892×10^{0}
5980.82	0.0302	2.458×10^{-1}	3.455×10^{0}
6230.14	0.0290	2.867×10^{-1}	4.202×10^{0}
6476.29	0.0279	3.095×10^{-1}	4.721×10^{0}
6728.03	0.0269	3.448×10^{-1}	5.465×10^{0}
6977.39	0.0259	3.309×10^{-1}	5.443×10^{0}
7474.60	0.0242	3.284×10^{-1}	5.694×10^{0}
7971.76	0.0227	3.316×10^{-1}	6.146×10^{0}

Calibration ID: Sample 2, S3-68 (Pen No:16-0289) 000-068
Operator: Julian Perfect
Submitter: Fan Zhang
File: C:\9500\DATA\BLANKS\000-068.SMP

LP Analysis Time:	13/07/2004 21:22:57PM	Sample Weight:	0.4512 g
HP Analysis Time:	13/07/2004 23:37:05PM	Correction Type:	Blank
Report Time:	14/07/2004 9:20:14PM	Show Neg. Int:	No

Tabular Report

Pressure (psia)	Pore Diameter (µm)	dV/dlogD Pore Volume (mL/g)	dV/dD Pore Volume (mL/g/µm)
8471.75	0.0213	3.409×10^{-1}	6.726×10^{0}
8970.69	0.0202	3.132×10^{-1}	6.555×10^{0}
9274.05	0.0195	2.784×10^{-1}	6.098×10^{0}
9567.29	0.0189	3.111×10^{-1}	7.036×10^{0}
10016.86	0.0181	2.388×10^{-1}	5.614×10^{0}
10457.77	0.0173	2.393×10^{-1}	5.880×10^{0}
10958.12	0.0165	2.338×10^{-1}	6.008×10^{0}
11462.34	0.0158	2.577×10^{-1}	6.934×10^{0}
11953.97	0.0151	2.105×10^{-1}	5.917×10^{0}
12554.95	0.0144	2.356×10^{-1}	6.931×10^{0}
13052.92	0.0139	2.387×10^{-1}	7.336×10^{0}
13605.37	0.0133	2.580×10^{-1}	8.254×10^{0}
13953.14	0.0130	2.664×10^{-1}	8.813×10^{0}
14292.62	0.0127	2.663×10^{-1}	9.028×10^{0}
14548.53	0.0124	2.746×10^{-1}	9.509×10^{0}
14951.42	0.0121	2.548×10^{-1}	9.023×10^{0}
15399.38	0.0117	2.726×10^{-1}	9.933×10^{0}
15746.88	0.0115	2.726×10^{-1}	1.019×10^{1}
16147.69	0.0112	2.886×10^{-1}	1.105×10^{1}
16592.83	0.0109	2.894×10^{-1}	1.138×10^{1}
16940.03	0.0107	3.084×10^{-1}	1.241×10^{1}
17298.36	0.0105	2.852×10^{-1}	1.172×10^{1}
17643.03	0.0103	2.949×10^{-1}	1.237×10^{1}
18043.48	0.0100	1.156×10^{-1}	4.951×10^{0}
18388.04	0.0098	2.985×10^{-1}	1.306×10^{1}
18747.72	0.0096	2.691×10^{-1}	1.200×10^{1}
19146.16	0.0094	2.854×10^{-1}	1.298×10^{1}
19743.67	0.0092	2.465×10^{-1}	1.151×10^{1}
20237.97	0.0089	2.527×10^{-1}	1.213×10^{1}
20760.76	0.0087	2.463×10^{-1}	1.212×10^{1}
21162.39	0.0085	2.293×10^{-1}	1.154×10^{1}
21614.60	0.0084	2.029×10^{-1}	1.042×10^{1}

Calibration ID: Sample 2, S3-68 (Pen No:16-0289) 000-068
Operator: Julian Perfect
Submitter: Fan Zhang
File: C:\9500\DATA\BLANKS\000-068.SMP

LP Analysis Time: 13/07/2004 21:22:57PM
HP Analysis Time: 13/07/2004 23:37:05PM
Report Time: 14/07/2004 9:20:14PM

Sample Weight: 0.4512 g
Correction Type: Blank
Show Neg. Int: No

Tabular Report

Pressure (psia)	Pore Diameter (μm)	dV/dlogD Pore Volume (mL/g)	dV/dD Pore Volume (mL/g/μm)
22022.87	0.0082	1.881×10^{-1}	9.855×10^{0}
22619.51	0.0080	1.681×10^{-1}	9.011×10^{0}
23175.28	0.0078	1.951×10^{-1}	1.073×10^{1}
23730.34	0.0076	1.364×10^{-1}	7.682×10^{0}
24077.77	0.0075	1.439×10^{-1}	8.261×10^{0}
24628.15	0.0073	1.019×10^{-1}	5.956×10^{0}
25027.04	0.0072	0.000×10^{0}	0.000×10^{0}
25431.15	0.0071	6.990×10^{-2}	4.235×10^{0}
25883.18	0.0070	8.444×10^{-2}	5.202×10^{0}
26434.59	0.0068	6.859×10^{-2}	4.308×10^{0}
26934.33	0.0067	6.720×10^{-2}	4.305×10^{0}
27384.54	0.0066	3.344×10^{-2}	2.181×10^{0}
27786.93	0.0065	7.521×10^{-2}	4.982×10^{0}
28236.32	0.0064	4.417×10^{-2}	2.971×10^{0}
28984.43	0.0062	3.357×10^{-2}	2.306×10^{0}
29486.84	0.0061	3.469×10^{-2}	2.435×10^{0}
29988.05	0.0060	2.716×10^{-2}	1.939×10^{0}
30438.71	0.0059	3.156×10^{-2}	2.290×10^{0}
30887.13	0.0059	0.000×10^{0}	0.000×10^{0}
31288.59	0.0058	2.790×10^{-2}	2.082×10^{0}
31789.64	0.0057	2.158×10^{-2}	1.634×10^{0}
32339.26	0.0056	2.073×10^{-2}	1.596×10^{0}
32883.70	0.0055	2.319×10^{-2}	1.816×10^{0}
33488.64	0.0054	0.000×10^{0}	0.000×10^{0}
33991.92	0.0053	0.000×10^{0}	0.000×10^{0}
34636.16	0.0052	0.000×10^{0}	0.000×10^{0}
35483.21	0.0051	0.000×10^{0}	0.000×10^{0}
36181.96	0.0050	0.000×10^{0}	0.000×10^{0}
36975.11	0.0049	1.363×10^{-2}	1.197×10^{0}
37628.46	0.0048	0.000×10^{0}	0.000×10^{0}
38423.36	0.0047	0.000×10^{0}	0.000×10^{0}
39181.19	0.0046	0.000×10^{0}	0.000×10^{0}

Calibration ID: Sample 2, S3-68 (Pen No:16-0289) 000-068
Operator: Julian Perfect
Submitter: Fan Zhang
File: C:\9500\DATA\BLANKS\000-068.SMP

LP Analysis Time:	13/07/2004 21:22:57PM	Sample Weight:	0.4512 g
HP Analysis Time:	13/07/2004 23:37:05PM	Correction Type:	Blank
Report Time:	14/07/2004 9:20:14PM	Show Neg. Int:	No

Tabular Report

Pressure (psia)	Pore Diameter (µm)	dV/dlogD Pore Volume (mL/g)	dV/dD Pore Volume (mL/g/µm)
39972.39	0.0045	2.038×10^{-2}	1.937×10^{0}
40470.93	0.0045	0.000×10^{0}	0.000×10^{0}
40962.97	0.0044	0.000×10^{0}	0.000×10^{0}
42459.37	0.0043	1.639×10^{-2}	1.641×10^{0}
43319.16	0.0042	0.000×10^{0}	0.000×10^{0}
43970.55	0.0041	0.000×10^{0}	0.000×10^{0}
44963.79	0.0040	1.673×10^{-2}	1.786×10^{0}
46461.50	0.0039	1.605×10^{-2}	1.761×10^{0}
47963.32	0.0038	1.388×10^{-2}	1.573×10^{0}
49462.57	0.0037	1.337×10^{-2}	1.564×10^{0}
50161.25	0.0036	0.000×10^{0}	0.000×10^{0}
52956.30	0.0034	4.793×10^{-3}	5.931×10^{-1}
54453.81	0.0033	0.000×10^{0}	0.000×10^{0}
55950.01	0.0032	0.000×10^{0}	0.000×10^{0}
57945.56	0.0031	0.000×10^{0}	0.000×10^{0}
59937.70	0.0030	0.000×10^{0}	0.000×10^{0}

micromeritics

Dept of Chemical Engineering, UCL

AutoPore IV 9500 V1.03 Serial: 201 Port: 1/1 Page 8

Calibration ID: Sample 2, S3-68 (Pen No:16-0289) 000-068
Operator: Julian Perfect
Submitter: Fan Zhang
File: C:\9500\DATA\BLANKS\000-068.SMP

LP Analysis Time:	13/07/2004 21:22:57PM	Sample Weight:	0.4512 g
HP Analysis Time:	13/07/2004 23:37:05PM	Correction Type:	Blank
Report Time:	14/07/2004 9:20:14PM	Show Neg. Int:	No

Cumulative Intrusion vs Pore size

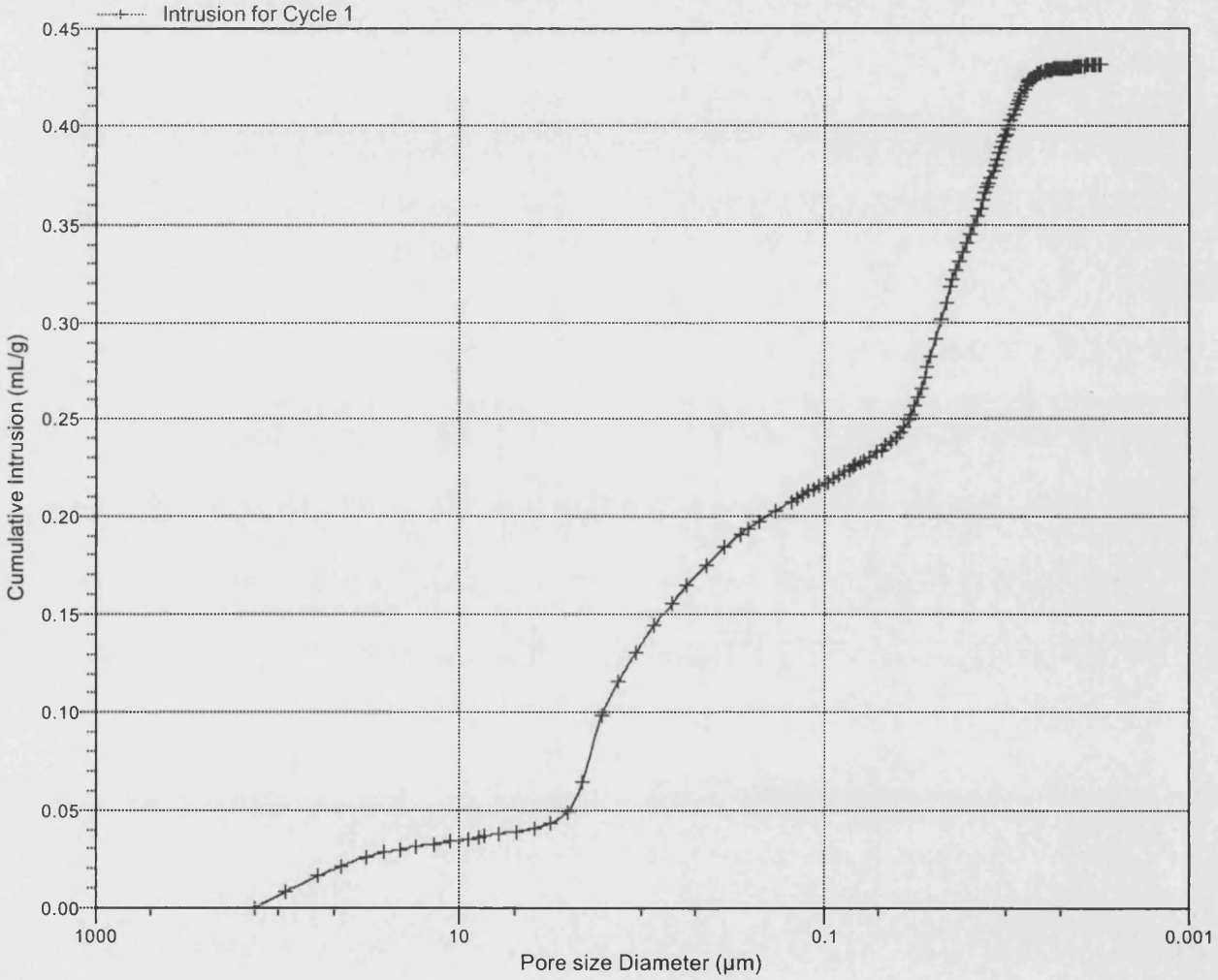

micromeritics

Dept of Chemical Engineering, UCL

AutoPore IV 9500 V1.03 Serial: 201 Port: 1/1 Page 9

Calibration ID: Sample 2, S3-68 (Pen No:16-0289) 000-068
Operator: Julian Perfect
Submitter: Fan Zhang
File: C:\9500\DATA\BLANKS\000-068.SMP

LP Analysis Time:	13/07/2004 21:22:57PM	Sample Weight:	0.4512 g
HP Analysis Time:	13/07/2004 23:37:05PM	Correction Type:	Blank
Report Time:	14/07/2004 9:20:14PM	Show Neg. Int:	No

Incremental Intrusion vs Pressure

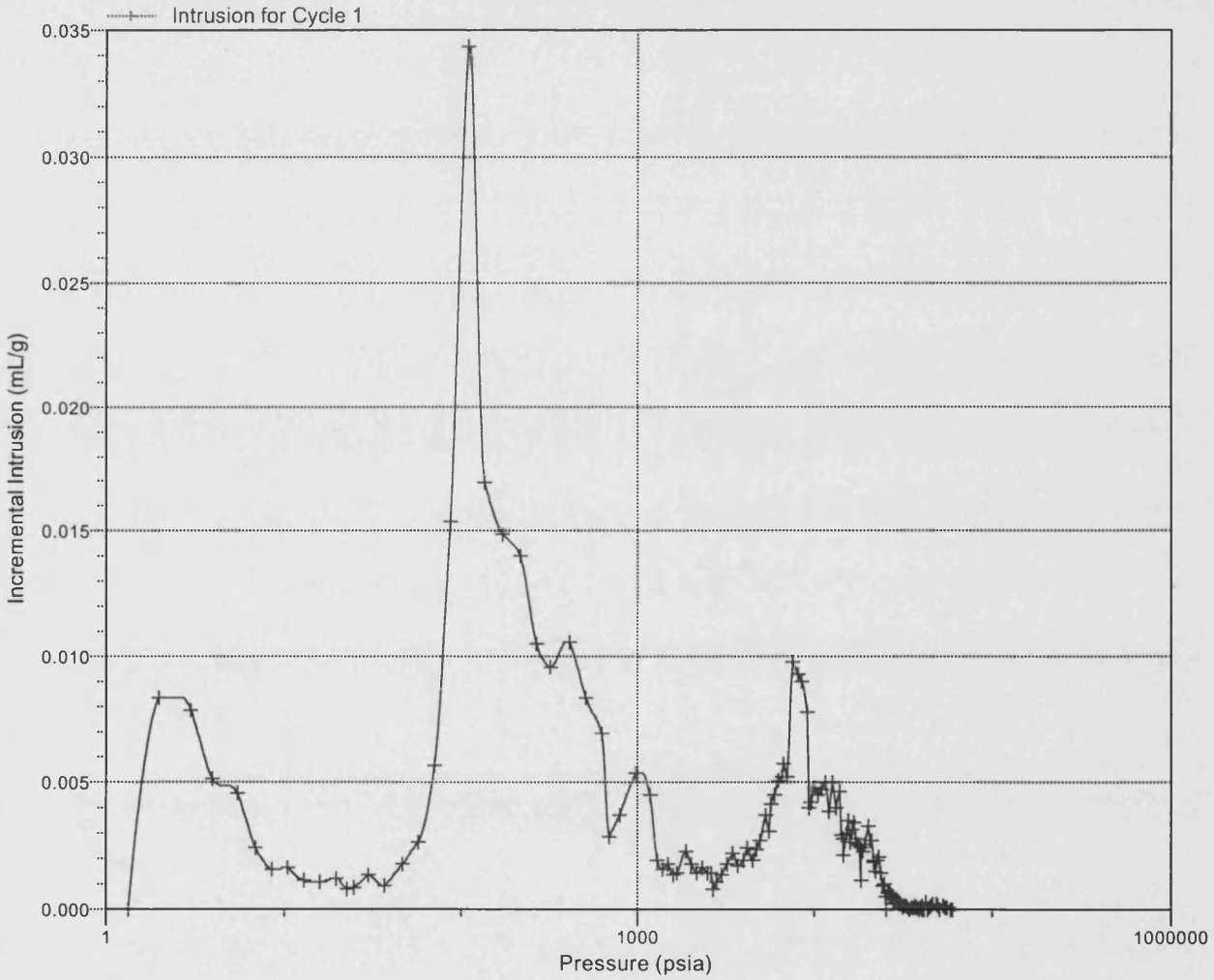

micromeritics

Dept of Chemical Engineering, UCL

AutoPore IV 9500 V1.03 Serial: 201 Port: 1/1 Page 10

Calibration ID: Sample 2, S3-68 (Pen No:16-0289) 000-068
Operator: Julian Perfect
Submitter: Fan Zhang
File: C:\9500\DATA\BLANKS\000-068.SMP

LP Analysis Time:	13/07/2004 21:22:57PM	Sample Weight:	0.4512 g
HP Analysis Time:	13/07/2004 23:37:05PM	Correction Type:	Blank
Report Time:	14/07/2004 9:20:14PM	Show Neg. Int:	No

Differential Intrusion vs Pore size

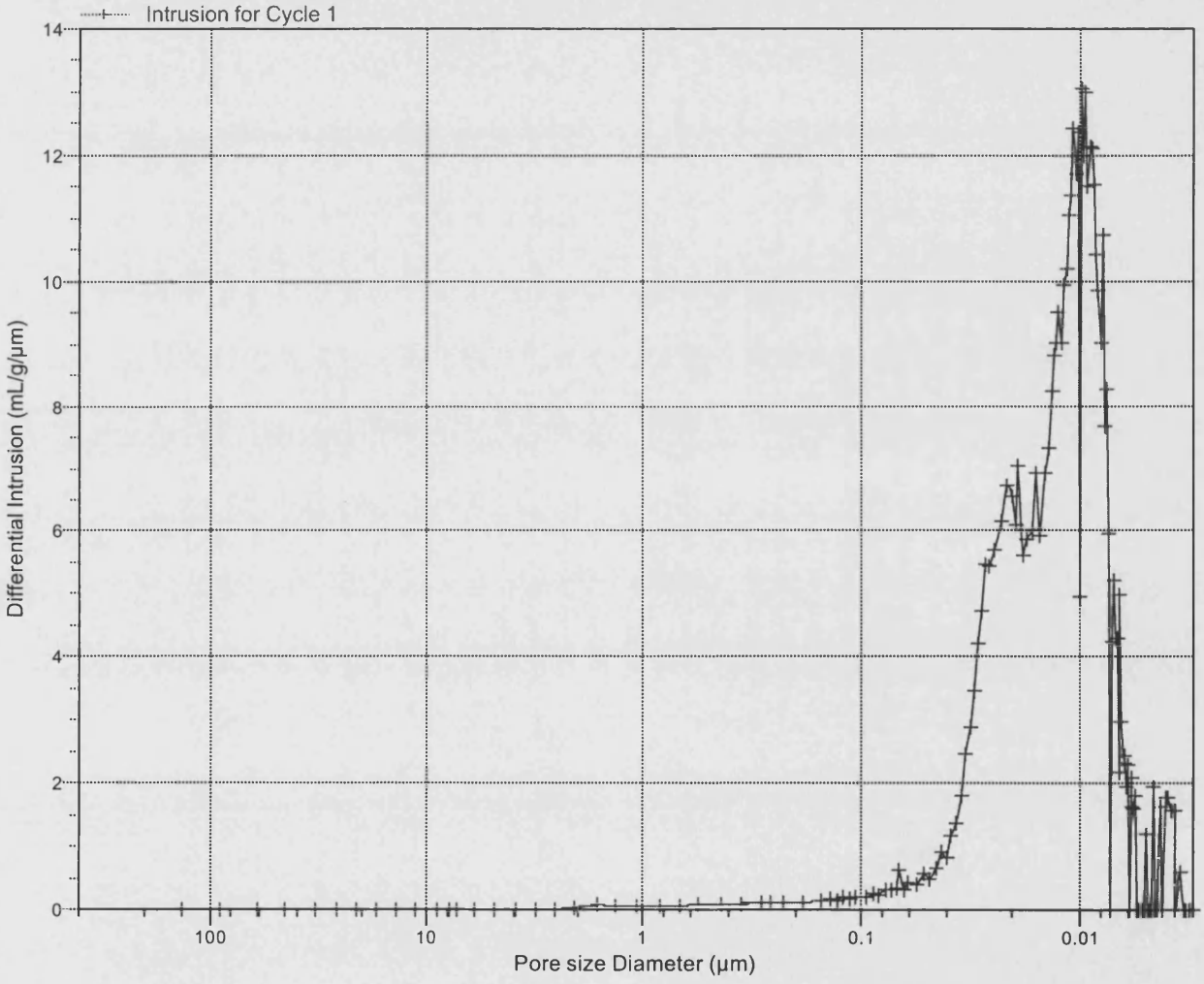

micromeritics

Dept of Chemical Engineering, UCL

AutoPore IV 9500 V1.03 Serial: 201 Port: 1/1 Page 11

Calibration ID: Sample 2, S3-68 (Pen No:16-0289) 000-068
Operator: Julian Perfect
Submitter: Fan Zhang
File: C:\9500\DATA\BLANKS\000-068.SMP

LP Analysis Time:	13/07/2004 21:22:57PM	Sample Weight:	0.4512 g
HP Analysis Time:	13/07/2004 23:37:05PM	Correction Type:	Blank
Report Time:	14/07/2004 9:20:14PM	Show Neg. Int:	No

Log Differential Intrusion vs Pore size

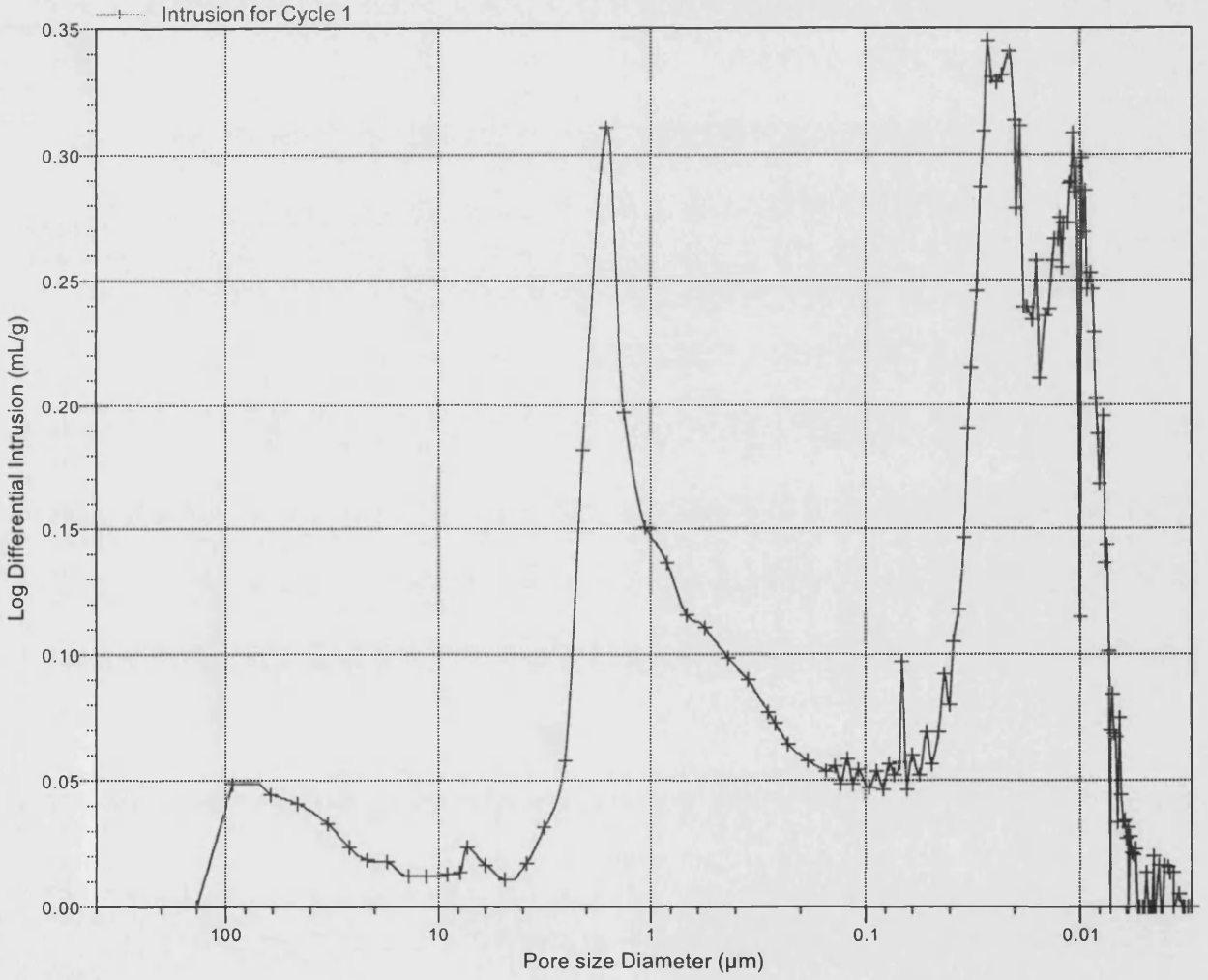

FULL ISOTHERM FOR SAMPLE 2, S3-68

ASAP 2010 V5.01 H Unit 1 Serial # 2727 Page 1

Sample: Sample 2, S3-68
Operator: Julian Perfect
Submitter: Fan Zhang
File Name: C:\ASAP2010\DATA\000-057.SMP

Started: 6/30/04 12:59:34AM Analysis Adsorptive: N2
Completed: 6/30/04 1:46:42PM Analysis Bath: 77.35 K
Report Time: 6/30/04 6:43:23PM Thermal Correction: No
Sample Weight: 0.4521 g Smoothed Pressures: No
Warm Freespace: 17.0160 cm^3 Cold Freespace: 51.4808 cm^3
MEASURED
Equil. Interval: 10 secs Low Pressure Dose: None
Comments:
Bulb type sample holder used with stopper and filler rod. Sample degassed, using manual mode, for ~130 hours (~24 hours @ 90C, 24 hours @ 130C and 82 hours @ 350C)

Analysis Log

Relative Pressure	Pressure (mmHg)	Vol Adsorbed (cm^3/g STP)	Elapsed Time (HR:MN)	Saturation Press.(mmHg)
			02:25	764.92853
0.141706802	108.35778	19.5846	02:42	
0.161508344	123.48913	20.0152	02:46	
0.183005402	139.91714	20.4547	02:49	
0.202545937	154.84737	20.8426	02:52	
0.220515589	168.57487	21.1967	02:55	
0.251938753	192.58470	21.8017	02:58	
0.302602897	231.29393	22.7699	03:02	
0.353795468	270.40622	23.7766	03:05	
0.400939715	306.41345	24.7456	03:09	
0.450883743	344.55429	25.8463	03:13	
0.500250993	382.24814	27.0537	03:17	
0.550339076	420.48654	28.4531	03:21	
0.600373153	458.67740	30.1751	03:25	
0.650818976	497.15610	32.4236	03:31	
0.699891474	534.57635	35.3467	03:37	
0.741022968	565.92279	38.5983	03:43	
0.771986107	589.47260	41.8074	03:51	
0.800961894	611.49738	45.7398	03:59	
0.822049898	627.48102	49.5631	04:08	
0.842658063	643.07928	54.3824	04:18	
0.861494876	657.30603	60.1233	04:29	
			04:31	762.95172
0.878026117	669.81677	66.3295	04:43	
0.890804155	679.49518	71.8923	04:54	
0.904531345	689.88910	78.6505	05:06	
0.915247339	697.99078	84.6100	05:17	
0.925324169	705.59027	90.7802	05:30	
0.934118982	712.22369	96.3731	05:41	
0.940920686	717.33624	100.9088	05:52	
0.947492708	722.27264	105.9141	06:03	

FULL ISOTHERM FOR SAMPLE 2, S3-68

Sample: Sample 2, S3-68
Operator: Julian Perfect
Submitter: Fan Zhang
File Name: C:\ASAP2010\DATA\000-057.SMP

Started: 6/30/04 12:59:34AM Analysis Adsorptive: N2
Completed: 6/30/04 1:46:42PM Analysis Bath: 77.35 K
Report Time: 6/30/04 6:43:23PM Thermal Correction: No
Sample Weight: 0.4521 g Smoothed Pressures: No
Warm Freespace: 17.0160 cm³ Cold Freespace: 51.4808 cm³
MEASURED
Equil. Interval: 10 secs Low Pressure Dose: None
Comments:
Bulb type sample holder used with stopper and filler rod. Sample degassed, using manual mode, for ~130 hours (~24 hours @ 90C, 24 hours @ 130C and 82 hours @ 350C)

Analysis Log

Relative Pressure	Pressure (mmHg)	Vol Adsorbed (cm³/g STP)	Elapsed Time (HR:MN)	Saturation Press.(mmHg)
0.953474639	726.75824	111.0501	06:14	
0.959282732	731.11041	116.4345	06:25	
0.964005650	734.63470	121.7224	06:36	
			06:38	762.05054
0.968742926	738.19299	127.0205	06:49	
0.971120577	739.97009	129.7796	06:59	
0.974345959	742.39642	133.4812	07:08	
0.977021032	744.40326	136.6766	07:17	
0.980450338	746.98456	140.6147	07:26	
0.982147653	748.24963	142.6207	07:34	
0.984529509	750.03259	145.3106	07:43	
0.986420865	751.44879	147.2041	07:50	
0.988191920	752.77325	148.9315	07:57	
0.989322094	753.61298	150.1492	08:03	
0.990986461	754.85956	151.6414	08:09	
0.979732482	746.26611	149.9593	08:15	
0.972410737	740.66132	147.5097	08:23	
0.966129005	735.84906	144.8485	08:31	
0.964026416	734.23041	143.7454	08:36	
0.959548594	730.79254	141.1042	08:44	
			08:46	761.59320
0.954428924	726.79279	137.2551	08:56	
0.948764947	722.37714	131.9557	09:07	
0.942587991	717.56293	125.5518	09:19	
0.935493904	712.04291	118.8013	09:32	
0.928376182	706.50671	112.4073	09:45	
0.918884085	699.16571	105.2042	09:58	
0.907604909	690.45868	98.2071	10:12	
0.892732980	679.03961	90.7178	10:24	
0.878262644	667.92084	84.3107	10:37	
0.862214492	655.61450	77.7777	10:49	

FULL ISOTHERM FOR SAMPLE 2, S3-68

Sample: Sample 2, S3-68
Operator: Julian Perfect
Submitter: Fan Zhang
File Name: C:\ASAP2010\DATA\000-057.SMP

Started: 6/30/04 12:59:34AM Analysis Adsorptive: N2
Completed: 6/30/04 1:46:42PM Analysis Bath: 77.35 K
Report Time: 6/30/04 6:43:23PM Thermal Correction: No
Sample Weight: 0.4521 g Smoothed Pressures: No
Warm Freespace: 17.0160 cm³ Cold Freespace: 51.4808 cm³
MEASURED
Equil. Interval: 10 secs Low Pressure Dose: None
Comments:
Bulb type sample holder used with stopper and filler rod. Sample degassed, using manual mode, for ~130 hours (~24 hours @ 90C, 24 hours @ 130C and 82 hours @ 350C)

Analysis Log

Relative Pressure	Pressure (mmHg)	Vol Adsorbed (cm³/g STP)	Elapsed Time (HR:MN)	Saturation Press.(mmHg)
			10:51	760.36481
0.842645786	640.71820	70.1554	11:04	
0.820443582	623.83643	62.0172	11:17	
0.799452825	607.87579	55.1023	11:29	
0.768131287	584.06000	46.8690	11:42	
0.739884524	562.58215	41.8850	11:51	
0.703497651	534.91486	37.7532	11:59	
0.653812903	497.13632	34.2773	12:06	
0.605052795	460.06085	31.9681	12:11	
0.555029144	422.02463	30.2006	12:16	
0.503402241	382.76935	28.7116	12:21	
0.450539930	342.57471	25.1135	12:26	
0.400288389	304.36520	23.9072	12:30	
0.338498832	257.38260	22.6074	12:34	
0.302032210	229.65466	21.8719	12:38	
0.252713537	192.15448	20.9087	12:41	
0.203444753	154.69223	19.9410	12:45	
0.142339946	108.23029	18.6603	12:48	

FULL

ASAP 2010 V5.01 H

Sample: Sample 2,
Operator: Julian Pe
Submitter: Fan Zhang
File Name: C:\ASAP20

Started: 6/30/04 1
Completed: 6/30/04 1
Report Time: 6/30/04 6
Sample Weight: 0.4521 g
Warm Freespace: 17.0160 c
MEASURED
Equil. Interval: 10 secs
Comments:
Bulb type sample holder used wi
manual mode, for ~130 hours (~2

FULL ISOTHERM FOR SAMPLE 2, S3-68

ASAP 2010 V5.01 H Unit 1 Serial # 2727

Sample: Sample 2, S3-68
Operator: Julian Perfect
Submitter: Fan Zhang
File Name: C:\ASAP2010\DATA\000-057.SMP

Started: 6/30/04 12:59:34AM Analysis Adsorptive: N
Completed: 6/30/04 1:46:42PM Analysis Bath: 7
Report Time: 6/30/04 6:43:23PM Thermal Correction: N
Sample Weight: 0.4521 g Smoothed Pressures: N
Warm Freespace: 17.0160 cm³ Cold Freespace: 5
MEASURED
Equil. Interval: 10 secs Low Pressure Dose: N
Comments:
Bulb type sample holder used with stopper and filler rod. Sample
manual mode, for ~130 hours (~24 hours @ 90C, 24 hours @ 130C and

Summary Report

Area

Single Point Surface Area at P

BET Surface Area:

Langmuir Surface Area:

Micropore Area:

External Surface Area:

BJH Adsorption Cumulative Surf
between 17.000000 and 3000

BJH Desorption Cumulative Surf
between 17.000000 and 3000

Single Point Surface Area at P/Po 0.25193875 :

BET Surface Area:

Langmuir Surface Area:

Micropore Area:

External Surface Area:

BJH Adsorption Cumulative Surface Area of pores
between 17.000000 and 3000.000000 A Diameter:

BJH Desorption Cumulative Surface Area of pores
between 17.000000 and 3000.000000 A Diameter:

Volume

Single Point Desorption Total
975.0306 A Diameter at

Micropore Volume:

BJH Adsorption Cumulative Pore
between 17.000000 and 3000

BJH Desorption Cumulative Pore
between 17.000000 and 3000

Single Point Desorption Total Pore Volume of pores less than
975.0306 A Diameter at P/Po 0.97973248:

Micropore Volume:

BJH Adsorption Cumulative Pore Volume of pores
between 17.000000 and 3000.000000 A Diameter:

BJH Desorption Cumulative Pore Volume of pores
between 17.000000 and 3000.000000 A Diameter:

Pore Size

FULL ISOTHERM FOR SAMPLE 2, S3-68

Sample:	Sample 2, S3-68		
Operator:	Julian Perfect		
Submitter:	Fan Zhang		
File Name:	C:\ASAP2010\DATA\000-057.SMP		
Started:	6/30/04 12:59:34AM	Analysis Adsorptive:	N2
Completed:	6/30/04 1:46:42PM	Analysis Bath:	77.35 K
Report Time:	6/30/04 6:43:23PM	Thermal Correction:	No
Sample Weight:	0.4521 g	Smoothed Pressures:	No
Warm Freespace:	17.0160 cm³ MEASURED	Cold Freespace:	51.4808 cm³
Equil. Interval:	10 secs	Low Pressure Dose:	None

Comments:
Bulb type sample holder used with stopper and filler rod. Sample degassed, using manual mode, for ~130 hours (~24 hours @ 90C, 24 hours @ 130C and 82 hours @ 350C)

Summary Report

Desorption Average Pore Diameter (4V/A by BET):	134.1843	A
BJH Adsorption Average Pore Diameter (4V/A):	161.2548	A
BJH Desorption Average Pore Diameter (4V/A):	139.9434	A

micromeritics

Dept of Chemical Engineering, UCL

AutoPore IV 9500 V1.03 Serial: 201 Port: 1/1 Page 1

Calibration ID: Sample 3, S3W-5154 (Pen No:16-0287) 000-069
Operator: Julian Perfect
Submitter: Fan Zhang
File: C:\9500\DATA\BLANKS\000-069.SMP

LP Analysis Time:	13/07/2004 23:46:06PM	Sample Weight:	0.7235 g
HP Analysis Time:	14/07/2004 0:51:06PM	Correction Type:	Blank
Report Time:	14/07/2004 9:22:27PM	Show Neg. Int:	No

Summary Report

Penetrometer parameters

Penetrometer:	#s/n - (16) 3 Bulb, 1.190 Stem, Powder		
Pen. Constant:	20.994 µL/pF	Pen. Weight:	54.7120 g
Stem Volume:	1.1900 mL	Max. Head Pressure:	4.6800 psia
Pen. Volume:	4.0032 mL	Assembly Weight:	102.7519 g

Hg Parameters

Adv. Contact Angle:	130.000 degrees	Rec. Contact Angle:	130.000 degrees
Hg Surface Tension:	485.000 dynes/cm	Hg Density:	13.5335 g/mL

User Parameters

Param 1:	0.000	Param 2:	0.000	Param 3:	0.000

Low Pressure:

Evacuation Pressure:	50 µmHg
Evacuation Time:	5 mins
Mercury Filling Pressure:	1.33 psia
Equilibration Time:	10 secs

High Pressure:

Equilibration Time:	10 secs

Blank Correction Sample: C:\9500\DATA\BLANKS\000-052.SMP
Blank Correction ID: Pen No:16-0287 Blank Correction 000-052

(From Pressure 0.10 to 60000.00 psia)

Intrusion Data Summary

Total Intrusion Volume =	0.3094	mL/g
Total Pore Area =	27.236	m²/g
Median Pore Diameter (Volume) =	0.8284	µm
Median Pore Diameter (Area) =	0.0171	µm
Average Pore Diameter (4V/A) =	0.0454	µm
Bulk Density at 0.10 psia =	1.4271	g/mL
Apparent (skeletal) Density =	2.5555	g/mL
Porosity =	44.1540	%
Stem Volume Used =	19	% ****

Pore Structure Summary

Threshold Pressure:	100.73	psia (Calculated)
Characteristic length =	1.7955	µm
Conductivity formation factor =	0.204	
Permeability constant =	0.00442	
Permeability =	2.9133	mdarcy
BET Surface Area =	200.0000	m²/g
Pore shape exponent =	1.00	
Tortuosity factor =	1.731	
Tortuosity =	41.4674	
Percolation Fractal dimension =	2.746	
Backbone Fractal dimension =	2.526	

Calibration ID: Sample 3, S3W-5154 (Pen No:16-0287) 000-069
Operator: Julian Perfect
Submitter: Fan Zhang
File: C:\9500\DATA\BLANKS\000-069.SMP

LP Analysis Time:	13/07/2004 23:46:06PM	Sample Weight:	0.7235 g
HP Analysis Time:	14/07/2004 0:51:06PM	Correction Type:	Blank
Report Time:	14/07/2004 9:22:27PM	Show Neg. Int:	No

Mayer Stowe Summary

Interstitial porosity =	44.1540	%
Breakthrough pressure ratio =	3.8123	

Material Compressibility

Linear Coefficient =	N/A	1/psia
Quadratic Coefficient =	N/A	1/psia²

Calibration ID: Sample 3, S3W-5154 (Pen No:16-0287) 000-069
Operator: Julian Perfect
Submitter: Fan Zhang
File: C:\9500\DATA\BLANKS\000-069.SMP

LP Analysis Time:	13/07/2004 23:46:06PM	Sample Weight:	0.7235 g
HP Analysis Time:	14/07/2004 0:51:06PM	Correction Type:	Blank
Report Time:	14/07/2004 9:22:27PM	Show Neg. Int:	No

Tabular Report

Pressure (psia)	Pore Diameter (µm)	dV/dlogD Pore Volume (mL/g)	dV/dD Pore Volume (mL/g/µm)
1.33	135.8874	0.000×10^{0}	0.000×10^{0}
1.98	91.2077	5.337×10^{-2}	2.068×10^{-4}
2.98	60.7180	7.123×10^{-2}	4.128×10^{-4}
3.98	45.4739	4.783×10^{-2}	3.940×10^{-4}
5.47	33.0365	4.889×10^{-2}	5.455×10^{-4}
6.97	25.9628	3.023×10^{-2}	4.472×10^{-4}
8.46	21.3772	2.265×10^{-2}	4.169×10^{-4}
10.45	17.3050	1.548×10^{-2}	3.489×10^{-4}
12.97	13.9484	1.572×10^{-2}	4.385×10^{-4}
15.96	11.3330	1.388×10^{-2}	4.786×10^{-4}
19.95	9.0637	1.307×10^{-2}	5.591×10^{-4}
22.96	7.8789	1.418×10^{-2}	7.281×10^{-4}
24.95	7.2487	1.776×10^{-2}	1.020×10^{-3}
29.95	6.0383	2.025×10^{-2}	1.328×10^{-3}
36.78	4.9181	2.074×10^{-2}	1.650×10^{-3}
46.99	3.8487	2.665×10^{-2}	2.654×10^{-3}
56.48	3.2023	3.415×10^{-2}	4.218×10^{-3}
71.45	2.5314	6.042×10^{-2}	9.194×10^{-3}
86.52	2.0905	1.363×10^{-1}	2.570×10^{-2}
112.04	1.6142	2.867×10^{-1}	6.759×10^{-2}
136.60	1.3240	2.436×10^{-1}	7.225×10^{-2}
171.43	1.0550	1.656×10^{-1}	6.071×10^{-2}
216.62	0.8349	1.156×10^{-1}	5.337×10^{-2}
266.55	0.6785	6.847×10^{-2}	3.944×10^{-2}
327.08	0.5530	4.487×10^{-2}	3.176×10^{-2}
416.75	0.4340	3.622×10^{-2}	3.203×10^{-2}
516.63	0.3501	3.238×10^{-2}	3.601×10^{-2}
636.72	0.2841	2.842×10^{-2}	3.908×10^{-2}
696.06	0.2598	2.565×10^{-2}	4.100×10^{-2}
796.68	0.2270	2.420×10^{-2}	4.324×10^{-2}
987.23	0.1832	2.335×10^{-2}	4.963×10^{-2}
1197.41	0.1510	2.187×10^{-2}	5.700×10^{-2}

Calibration ID: Sample 3, S3W-5154 (Pen No:16-0287) 000-069
Operator: Julian Perfect
Submitter: Fan Zhang
File: C:\9500\DATA\BLANKS\000-069.SMP

LP Analysis Time:	13/07/2004 23:46:06PM	Sample Weight:	0.7235 g
HP Analysis Time:	14/07/2004 0:51:06PM	Correction Type:	Blank
Report Time:	14/07/2004 9:22:27PM	Show Neg. Int:	No

Tabular Report

Pressure (psia)	Pore Diameter (µm)	dV/dlogD Pore Volume (mL/g)	dV/dD Pore Volume (mL/g/µm)
1297.54	0.1394	2.332×10^{-2}	6.979×10^{-2}
1396.22	0.1295	1.820×10^{-2}	5.880×10^{-2}
1496.30	0.1209	2.417×10^{-2}	8.388×10^{-2}
1596.04	0.1133	2.383×10^{-2}	8.841×10^{-2}
1696.35	0.1066	1.310×10^{-2}	5.174×10^{-2}
1895.60	0.0954	2.605×10^{-2}	1.121×10^{-1}
2045.90	0.0884	2.346×10^{-2}	1.109×10^{-1}
2195.06	0.0824	2.011×10^{-2}	1.023×10^{-1}
2344.60	0.0771	2.645×10^{-2}	1.441×10^{-1}
2494.12	0.0725	2.666×10^{-2}	1.548×10^{-1}
2645.55	0.0684	2.584×10^{-2}	1.594×10^{-1}
2694.64	0.0671	1.665×10^{-2}	1.068×10^{-1}
2843.73	0.0636	3.026×10^{-2}	2.011×10^{-1}
2993.43	0.0604	2.316×10^{-2}	1.622×10^{-1}
3241.68	0.0558	3.038×10^{-2}	2.271×10^{-1}
3492.03	0.0518	2.650×10^{-2}	2.141×10^{-1}
3742.25	0.0483	3.413×10^{-2}	2.962×10^{-1}
3989.61	0.0453	3.095×10^{-2}	2.871×10^{-1}
4239.08	0.0427	4.765×10^{-2}	4.705×10^{-1}
4483.51	0.0403	4.389×10^{-2}	4.594×10^{-1}
4723.69	0.0383	6.293×10^{-2}	6.953×10^{-1}
4981.55	0.0363	8.294×10^{-2}	9.660×10^{-1}
5282.52	0.0342	1.001×10^{-1}	1.232×10^{0}
5481.99	0.0330	1.366×10^{-1}	1.765×10^{0}
5731.04	0.0316	1.611×10^{-1}	2.168×10^{0}
5980.06	0.0302	1.977×10^{-1}	2.779×10^{0}
6228.53	0.0290	2.211×10^{-1}	3.240×10^{0}
6481.56	0.0279	2.340×10^{-1}	3.570×10^{0}
6727.88	0.0269	2.475×10^{-1}	3.924×10^{0}
6979.57	0.0259	2.730×10^{-1}	4.492×10^{0}
7478.51	0.0242	2.536×10^{-1}	4.398×10^{0}
7974.89	0.0227	2.646×10^{-1}	4.907×10^{0}

Calibration ID: Sample 3, S3W-5154 (Pen No:16-0287) 000-069
Operator: Julian Perfect
Submitter: Fan Zhang
File: C:\9500\DATA\BLANKS\000-069.SMP

LP Analysis Time: 13/07/2004 23:46:06PM
HP Analysis Time: 14/07/2004 0:51:06PM
Report Time: 14/07/2004 9:22:27PM

Sample Weight: 0.7235 g
Correction Type: Blank
Show Neg. Int: No

Tabular Report

Pressure (psia)	Pore Diameter (μm)	dV/dlogD Pore Volume (mL/g)	dV/dD Pore Volume (mL/g/μm)
8474.15	0.0213	2.558×10^{-1}	5.049×10^{0}
8969.58	0.0202	2.492×10^{-1}	5.216×10^{0}
9269.38	0.0195	2.475×10^{-1}	5.419×10^{0}
9567.49	0.0189	2.121×10^{-1}	4.795×10^{0}
10013.49	0.0181	2.126×10^{-1}	4.997×10^{0}
10467.78	0.0173	1.826×10^{-1}	4.489×10^{0}
10952.09	0.0165	1.700×10^{-1}	4.371×10^{0}
11458.09	0.0158	1.744×10^{-1}	4.690×10^{0}
11954.48	0.0151	1.590×10^{-1}	4.467×10^{0}
12555.60	0.0144	1.473×10^{-1}	4.332×10^{0}
13054.80	0.0139	1.303×10^{-1}	4.006×10^{0}
13600.53	0.0133	1.393×10^{-1}	4.457×10^{0}
13947.72	0.0130	1.217×10^{-1}	4.024×10^{0}
14290.27	0.0127	1.191×10^{-1}	4.037×10^{0}
14550.05	0.0124	1.253×10^{-1}	4.339×10^{0}
14950.30	0.0121	1.094×10^{-1}	3.874×10^{0}
15396.77	0.0117	1.120×10^{-1}	4.079×10^{0}
15753.45	0.0115	1.305×10^{-1}	4.879×10^{0}
16139.66	0.0112	1.087×10^{-1}	4.162×10^{0}
16597.51	0.0109	1.036×10^{-1}	4.070×10^{0}
16946.79	0.0107	1.146×10^{-1}	4.615×10^{0}
17298.17	0.0105	9.314×10^{-2}	3.829×10^{0}
17648.69	0.0102	9.745×10^{-2}	4.089×10^{0}
18042.54	0.0100	8.561×10^{-2}	3.668×10^{0}
18392.32	0.0098	9.180×10^{-2}	4.015×10^{0}
18746.51	0.0096	1.003×10^{-1}	4.472×10^{0}
19143.56	0.0094	7.204×10^{-2}	3.277×10^{0}
19741.25	0.0092	6.346×10^{-2}	2.962×10^{0}
20237.54	0.0089	0.000×10^{0}	0.000×10^{0}
20750.41	0.0087	6.868×10^{-2}	3.379×10^{0}
21159.68	0.0085	7.599×10^{-2}	3.823×10^{0}
21617.33	0.0084	7.906×10^{-2}	4.060×10^{0}

Calibration ID: Sample 3, S3W-5154 (Pen No:16-0287) 000-069
Operator: Julian Perfect
Submitter: Fan Zhang
File: C:\9500\DATA\BLANKS\000-069.SMP

LP Analysis Time: 13/07/2004 23:46:06PM
HP Analysis Time: 14/07/2004 0:51:06PM
Report Time: 14/07/2004 9:22:27PM

Sample Weight: 0.7235 g
Correction Type: Blank
Show Neg. Int: No

Tabular Report

Pressure (psia)	Pore Diameter (μm)	dV/dlogD Pore Volume (mL/g)	dV/dD Pore Volume (mL/g/μm)
22022.37	0.0082	3.780×10^{-2}	1.980×10^{0}
22620.15	0.0080	6.503×10^{-2}	3.485×10^{0}
23175.72	0.0078	5.850×10^{-2}	3.216×10^{0}
23726.79	0.0076	3.714×10^{-2}	2.091×10^{0}
24077.06	0.0075	5.226×10^{-2}	2.999×10^{0}
24629.68	0.0073	3.500×10^{-2}	2.046×10^{0}
25030.21	0.0072	5.707×10^{-2}	3.402×10^{0}
25430.15	0.0071	4.415×10^{-2}	2.675×10^{0}
25881.76	0.0070	2.914×10^{-2}	1.795×10^{0}
26434.79	0.0068	1.835×10^{-2}	1.152×10^{0}
26933.41	0.0067	1.405×10^{-2}	9.003×10^{-1}
27384.68	0.0066	0.000×10^{0}	0.000×10^{0}
27787.68	0.0065	0.000×10^{0}	0.000×10^{0}
28232.96	0.0064	0.000×10^{0}	0.000×10^{0}
28983.59	0.0062	0.000×10^{0}	0.000×10^{0}
29486.51	0.0061	0.000×10^{0}	0.000×10^{0}
29986.48	0.0060	0.000×10^{0}	0.000×10^{0}
30435.30	0.0059	0.000×10^{0}	0.000×10^{0}
30885.94	0.0059	0.000×10^{0}	0.000×10^{0}
31289.84	0.0058	0.000×10^{0}	0.000×10^{0}
31786.20	0.0057	0.000×10^{0}	0.000×10^{0}
32335.88	0.0056	0.000×10^{0}	0.000×10^{0}
32889.95	0.0055	0.000×10^{0}	0.000×10^{0}
33490.66	0.0054	0.000×10^{0}	0.000×10^{0}
33986.43	0.0053	0.000×10^{0}	0.000×10^{0}
34633.00	0.0052	0.000×10^{0}	0.000×10^{0}
35483.33	0.0051	0.000×10^{0}	0.000×10^{0}
36185.69	0.0050	0.000×10^{0}	0.000×10^{0}
36978.38	0.0049	0.000×10^{0}	0.000×10^{0}
37630.91	0.0048	0.000×10^{0}	0.000×10^{0}
38435.26	0.0047	0.000×10^{0}	0.000×10^{0}
39177.59	0.0046	0.000×10^{0}	0.000×10^{0}

Calibration ID: Sample 3, S3W-5154 (Pen No:16-0287) 000-069
Operator: Julian Perfect
Submitter: Fan Zhang
File: C:\9500\DATA\BLANKS\000-069.SMP

LP Analysis Time:	13/07/2004 23:46:06PM	Sample Weight:	0.7235 g
HP Analysis Time:	14/07/2004 0:51:06PM	Correction Type:	Blank
Report Time:	14/07/2004 9:22:27PM	Show Neg. Int:	No

Tabular Report

Pressure (psia)	Pore Diameter (µm)	dV/dlogD Pore Volume (mL/g)	dV/dD Pore Volume (mL/g/µm)
39966.98	0.0045	0.000×10^0	0.000×10^0
40462.34	0.0045	0.000×10^0	0.000×10^0
40959.75	0.0044	0.000×10^0	0.000×10^0
42473.57	0.0043	0.000×10^0	0.000×10^0
43313.64	0.0042	0.000×10^0	0.000×10^0
43961.28	0.0041	0.000×10^0	0.000×10^0
44960.83	0.0040	0.000×10^0	0.000×10^0
46464.72	0.0039	0.000×10^0	0.000×10^0
47959.93	0.0038	0.000×10^0	0.000×10^0
49461.04	0.0037	0.000×10^0	0.000×10^0
50157.25	0.0036	0.000×10^0	0.000×10^0
52953.46	0.0034	0.000×10^0	0.000×10^0
54449.03	0.0033	0.000×10^0	0.000×10^0
55945.96	0.0032	0.000×10^0	0.000×10^0
57936.08	0.0031	0.000×10^0	0.000×10^0
59923.83	0.0030	0.000×10^0	0.000×10^0

micromeritics

Dept of Chemical Engineering, UCL

AutoPore IV 9500 V1.03 Serial: 201 Port: 1/1 Page 8

Calibration ID: Sample 3, S3W-5154 (Pen No:16-0287) 000-069
Operator: Julian Perfect
Submitter: Fan Zhang
File: C:\9500\DATA\BLANKS\000-069.SMP

LP Analysis Time:	13/07/2004 23:46:06PM	Sample Weight:	0.7235 g
HP Analysis Time:	14/07/2004 0:51:06PM	Correction Type:	Blank
Report Time:	14/07/2004 9:22:27PM	Show Neg. Int:	No

Cumulative Intrusion vs Pore size

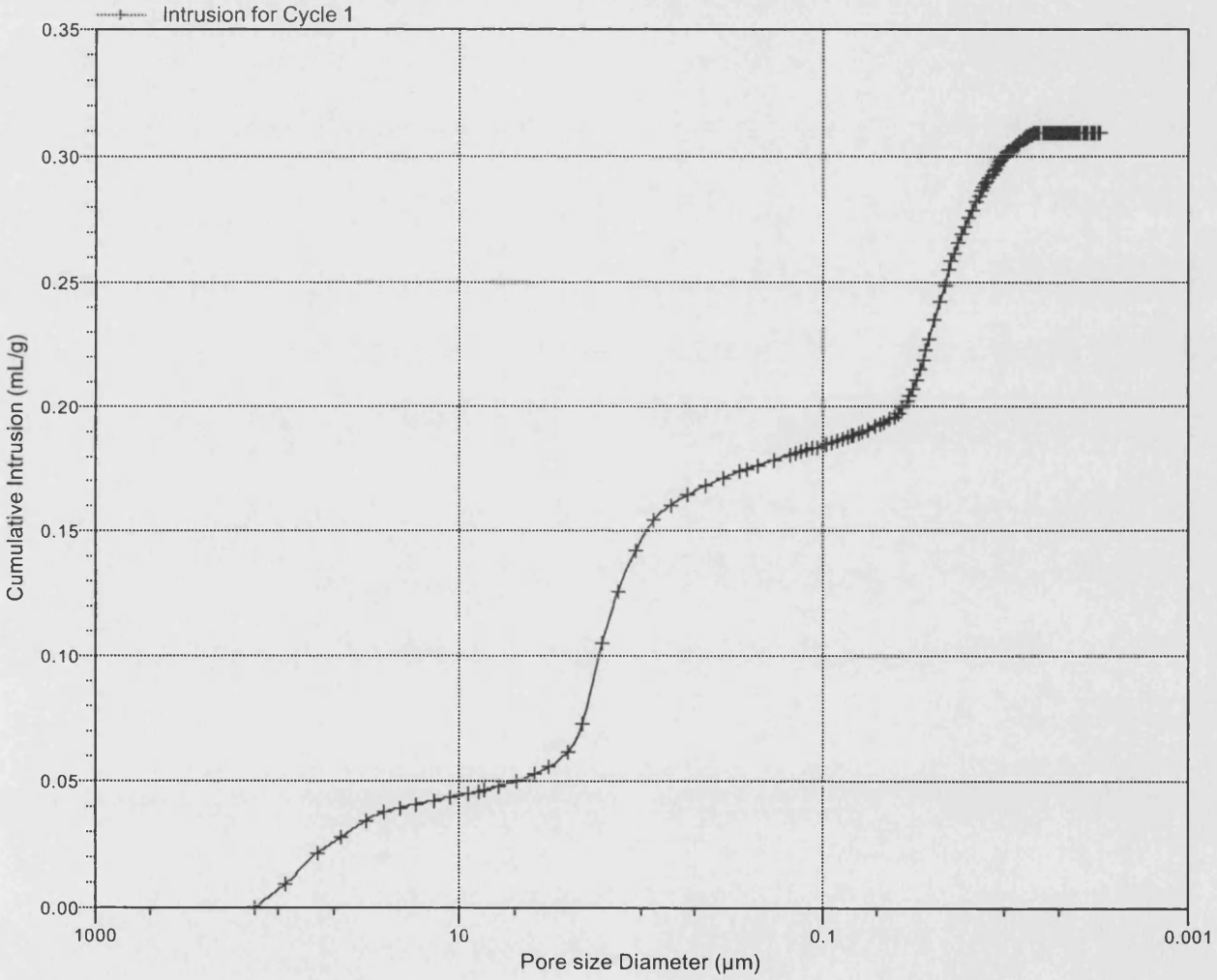

Calibration ID: Sample 3, S3W-5154 (Pen No:16-0287) 000-069
Operator: Julian Perfect
Submitter: Fan Zhang
File: C:\9500\DATA\BLANKS\000-069.SMP

LP Analysis Time:	13/07/2004 23:46:06PM	Sample Weight:	0.7235 g
HP Analysis Time:	14/07/2004 0:51:06PM	Correction Type:	Blank
Report Time:	14/07/2004 9:22:27PM	Show Neg. Int:	No

Incremental Intrusion vs Pressure

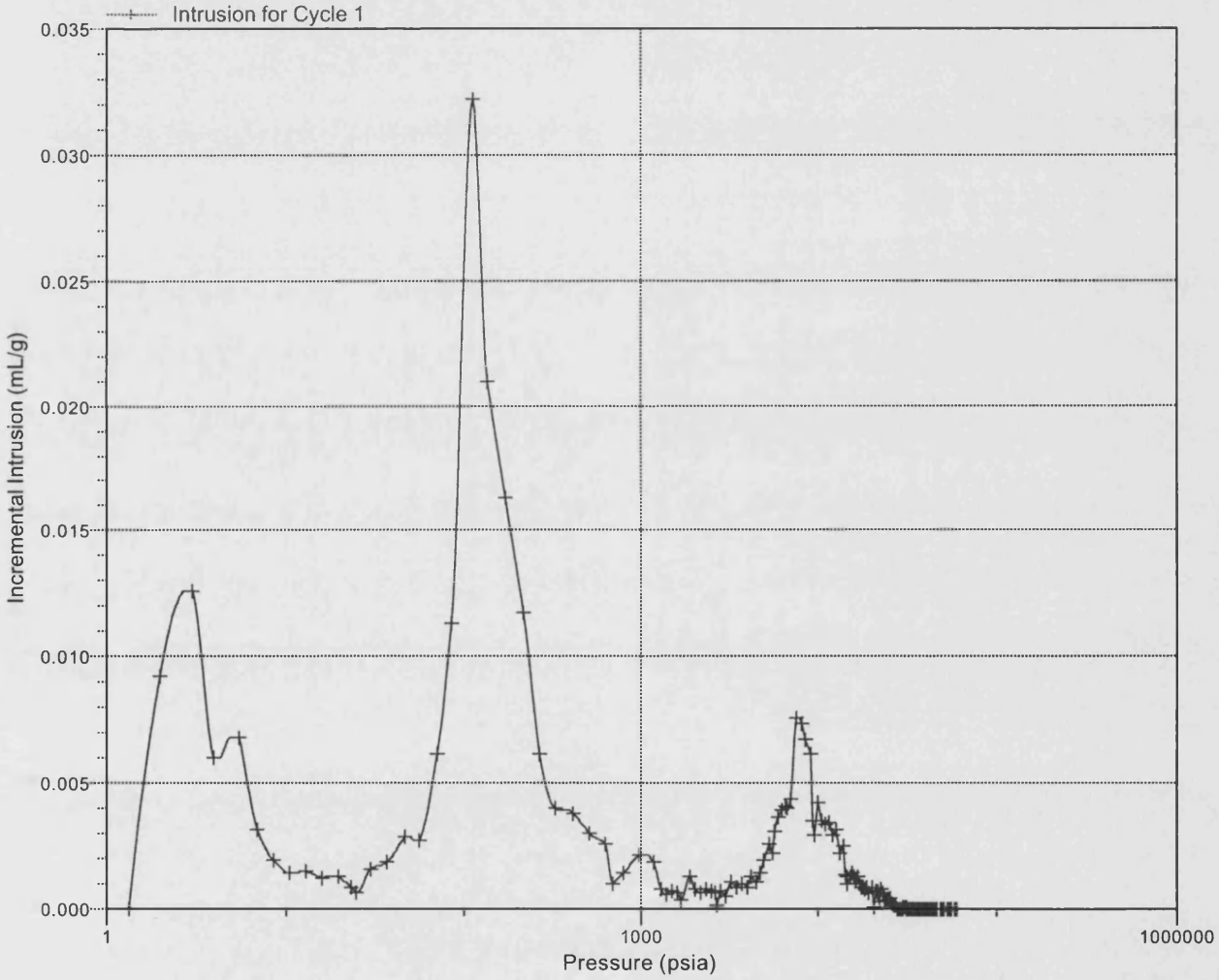

micromeritics

Dept of Chemical Engineering, UCL

AutoPore IV 9500 V1.03 Serial: 201 Port: 1/1 Page 10

Calibration ID: Sample 3, S3W-5154 (Pen No:16-0287) 000-069
Operator: Julian Perfect
Submitter: Fan Zhang
File: C:\9500\DATA\BLANKS\000-069.SMP

LP Analysis Time:	13/07/2004 23:46:06PM	Sample Weight:	0.7235 g
HP Analysis Time:	14/07/2004 0:51:06PM	Correction Type:	Blank
Report Time:	14/07/2004 9:22:27PM	Show Neg. Int:	No

Differential Intrusion vs Pore size

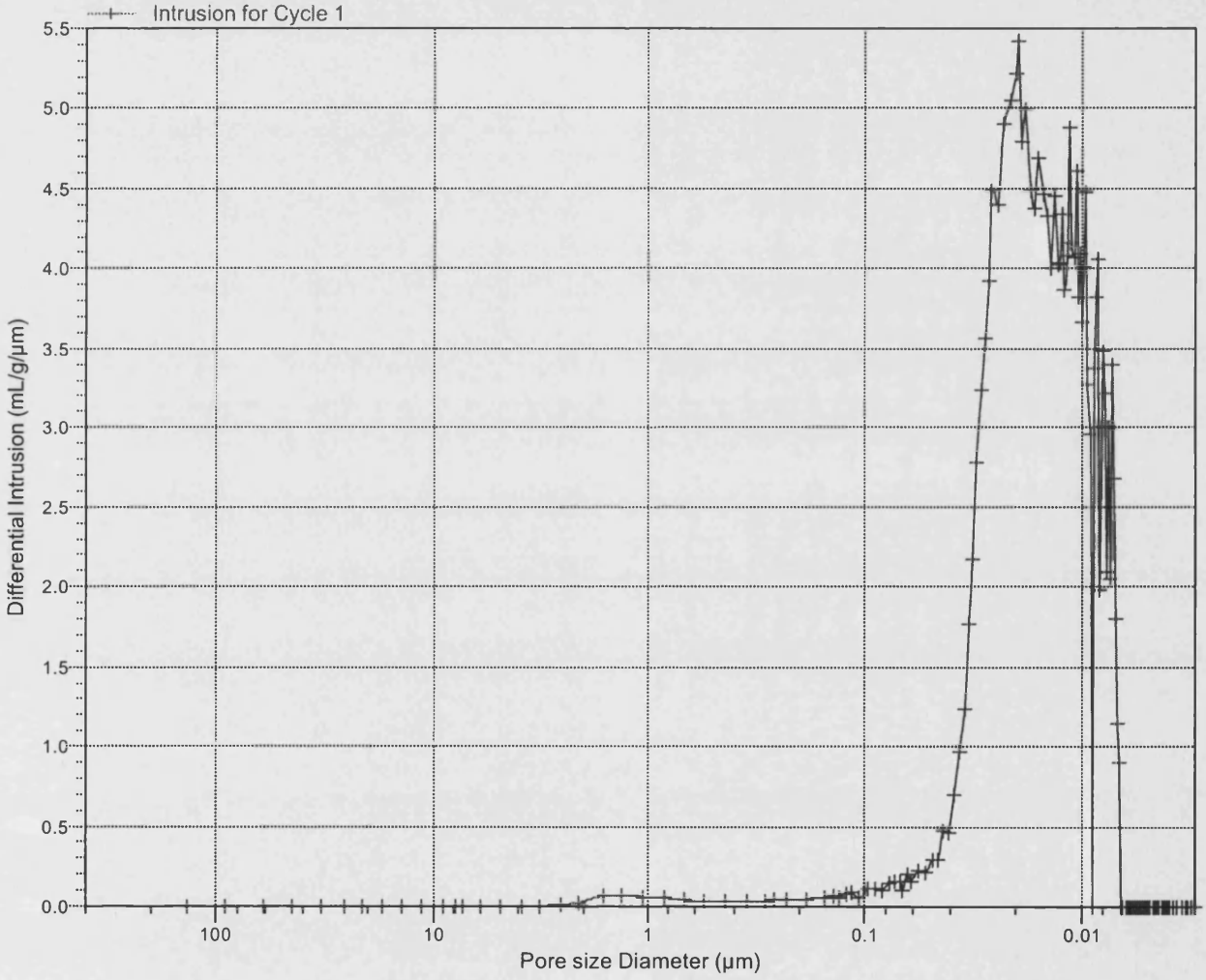

micromeritics

Dept of Chemical Engineering, UCL

AutoPore IV 9500 V1.03 Serial: 201 Port: 1/1 Page 11

Calibration ID: Sample 3, S3W-5154 (Pen No:16-0287) 000-069
Operator: Julian Perfect
Submitter: Fan Zhang
File: C:\9500\DATA\BLANKS\000-069.SMP

LP Analysis Time:	13/07/2004 23:46:06PM	Sample Weight:	0.7235 g
HP Analysis Time:	14/07/2004 0:51:06PM	Correction Type:	Blank
Report Time:	14/07/2004 9:22:27PM	Show Neg. Int:	No

Log Differential Intrusion vs Pore size

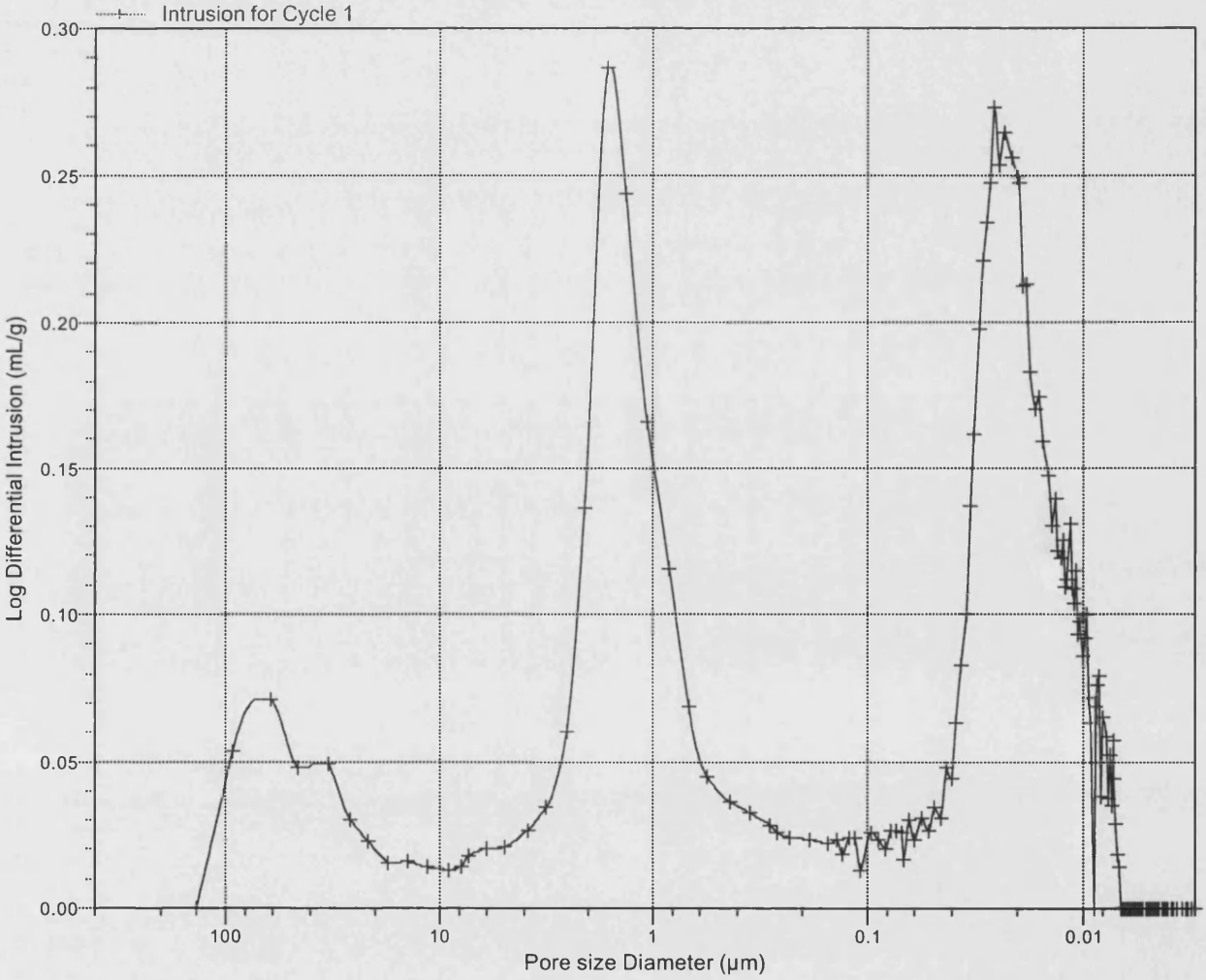

FULL ISOTHERM FOR SAMPLE 3, S3W-5154

Sample: Sample 3, S3W-5154
Operator: Julian Perfect
Submitter: Fan Zhang
File Name: C:\ASAP2010\DATA\000-061.SMP

Started: 7/12/04 11:36:26PM
Completed: 7/13/04 11:00:04AM
Report Time: 7/14/04 6:52:52PM
Sample Weight: 0.7241 g
Warm Freespace: 17.2551 cm³
MEASURED
Equil. Interval: 10 secs
Analysis Adsorptive: N2
Analysis Bath: 77.35 K
Thermal Correction: No
Smoothed Pressures: No
Cold Freespace: 51.7413 cm³
Low Pressure Dose: None

Comments:
Bulb type sample holder used with stopper and filler rod. Sample degassed, using manual mode, for ~31.75 hours (~1.25 hours @ 90C, 1.5 hours @ 120C and 29 hours @ 350C).

Analysis Log

Relative Pressure	Pressure (mmHg)	Vol Adsorbed (cm³/g STP)	Elapsed Time (HR:MN)	Saturation Press.(mmHg)
			02:26	763.51617
0.144536839	110.34328	11.0056	02:42	
0.162732736	124.23179	11.2101	02:45	
0.181181112	138.31242	11.4001	02:48	
0.201707162	153.97961	11.6093	02:50	
0.221615826	169.17381	11.8062	02:53	
0.250982836	191.58736	12.0919	02:56	
0.300065781	229.04971	12.5635	02:59	
0.353037551	269.47882	13.0775	03:02	
0.401098438	306.15768	13.5605	03:05	
0.451238494	344.41940	14.0860	03:09	
0.501281816	382.60785	14.6590	03:12	
0.551891398	421.22372	15.3053	03:16	
0.601646774	459.18539	16.0500	03:20	
0.650197226	496.22525	16.9553	03:24	
0.700783167	534.81244	18.2180	03:29	
0.740329138	564.97180	19.5919	03:34	
0.770885754	588.26910	20.9786	03:39	
0.799742463	610.26306	22.7243	03:45	
0.820852580	626.34412	24.4022	03:51	
0.840280061	641.13519	26.3689	03:58	
0.860230143	656.31866	28.9537	04:06	
0.875580162	667.99091	31.4988	04:14	
0.890729496	679.49872	34.5642	04:24	
0.905645652	690.83203	38.2451	04:33	
			04:35	762.79492
0.915987475	698.68762	41.4241	04:45	
0.925512975	705.93018	44.7599	04:55	
0.933109799	711.70355	47.8380	05:04	
0.939582480	716.61920	51.1682	05:13	

FULL ISOTHERM FOR SAMPLE 3, S3W-5154

Sample: Sample 3, S3W-5154
Operator: Julian Perfect
Submitter: Fan Zhang
File Name: C:\ASAP2010\DATA\000-061.SMP

Started: 7/12/04 11:36:26PM
Completed: 7/13/04 11:00:04AM
Report Time: 7/14/04 6:52:52PM
Sample Weight: 0.7241 g
Warm Freespace: 17.2551 cm³
MEASURED
Equil. Interval: 10 secs
Analysis Adsorptive: N2
Analysis Bath: 77.35 K
Thermal Correction: No
Smoothed Pressures: No
Cold Freespace: 51.7413 cm³
Low Pressure Dose: None

Comments:
Bulb type sample holder used with stopper and filler rod. Sample degassed, using manual mode, for ~31.75 hours (~1.25 hours @ 90C, 1.5 hours @ 120C and 29 hours @ 350C).

Analysis Log

Relative Pressure	Pressure (mmHg)	Vol Adsorbed (cm³/g STP)	Elapsed Time (HR:MN)	Saturation Press.(mmHg)
0.946329699	721.73920	54.8594	05:24	
0.951922710	725.98096	58.3291	05:34	
0.957213670	729.98969	62.2222	05:45	
0.962478201	733.97797	66.2451	05:56	
0.966647854	737.13104	69.9167	06:07	
0.970566325	740.09479	73.3387	06:17	
0.974050972	742.72754	76.3054	06:27	
0.977044186	744.98785	79.1072	06:36	
			06:38	762.48645
0.980112886	747.35608	81.9544	06:49	
0.982403197	749.12372	83.5373	06:56	
0.983030355	749.61713	84.1785	07:01	
0.986737243	752.47430	86.5827	07:11	
0.990884826	755.66473	88.6772	07:20	
0.979277651	746.83105	87.5629	07:26	
0.971481088	740.90912	85.9471	07:34	
0.965536116	736.39600	84.3237	07:41	
0.963361110	734.75500	83.5113	07:47	
0.959038545	731.48187	81.5750	07:55	
0.953888893	727.58356	78.4956	08:05	
0.949218073	724.05310	74.8247	08:16	
0.943608348	719.80902	70.3969	08:28	
0.937721985	715.35638	65.6153	08:41	
			08:42	762.86926
0.930529392	709.87347	60.2516	08:55	
0.921536259	703.01416	54.5327	09:09	
0.909895527	694.13495	48.7070	09:22	
0.894715974	682.55603	43.0475	09:35	
0.877197111	669.19238	38.0809	09:47	
0.862023201	657.61743	34.6627	09:57	

FULL ISOTHERM FOR SAMPLE 3, S3W-5154

Sample: Sample 3, S3W-5154
Operator: Julian Perfect
Submitter: Fan Zhang
File Name: C:\ASAP2010\DATA\000-061.SMP

Started: 7/12/04 11:36:26PM Analysis Adsorptive: N2
Completed: 7/13/04 11:00:04AM Analysis Bath: 77.35 K
Report Time: 7/14/04 6:52:52PM Thermal Correction: No
Sample Weight: 0.7241 g Smoothed Pressures: No
Warm Freespace: 17.2551 cm³ Cold Freespace: 51.7413 cm³
MEASURED
Equil. Interval: 10 secs Low Pressure Dose: None
Comments:
Bulb type sample holder used with stopper and filler rod. Sample degassed, using manual mode, for ~31.75 hours (~1.25 hours @ 90C, 1.5 hours @ 120C and 29 hours @ 350C).

Analysis Log

Relative Pressure	Pressure (mmHg)	Vol Adsorbed (cm³/g STP)	Elapsed Time (HR:MN)	Saturation Press.(mmHg)
0.841505137	641.96552	30.8372	10:07	
0.819992754	625.55493	27.6204	10:16	
0.801466466	611.42218	25.2758	10:23	
0.769667956	587.16437	22.1562	10:31	
0.741037453	565.32324	20.1853	10:38	
0.702046306	535.57806	18.3606	10:44	
			10:46	762.88159
0.651624779	497.11255	16.8482	10:50	
0.604378436	461.06918	15.8776	10:54	
0.553006220	421.87827	15.0765	10:58	
0.501696489	382.73502	14.4125	11:02	
0.452041283	344.85397	13.7255	11:06	
0.399712514	304.93332	13.1259	11:09	
0.350771683	267.59726	12.6222	11:12	
0.300684444	229.38663	12.1262	11:15	
0.254490481	194.14610	11.6741	11:18	
0.203652725	155.36292	11.1710	11:21	
0.141327198	107.81592	10.5069	11:25	

FULL ISOTHERM FOR SAMPLE 3, S3W-5154

Sample: Sample 3, S3W-5154
Operator: Julian Perfect
Submitter: Fan Zhang
File Name: C:\ASAP2010\DATA\000-061.SMP

Started: 7/12/04 11:36:26PM Analysis Adsorptive: N2
Completed: 7/13/04 11:00:04AM Analysis Bath: 77.35 K
Report Time: 7/14/04 6:52:52PM Thermal Correction: No
Sample Weight: 0.7241 g Smoothed Pressures: No
Warm Freespace: 17.2551 cm³ Cold Freespace: 51.7413 cm³
MEASURED
Equil. Interval: 10 secs Low Pressure Dose: None
Comments:
Bulb type sample holder used with stopper and filler rod. Sample degassed, using manual mode, for ~31.75 hours (~1.25 hours @ 90C, 1.5 hours @ 120C and 29 hours @ 350C).

Summary Report

Area

Single Point Surface Area at P/Po 0.25098284 :	39.4272	m²/g
BET Surface Area:	38.0195	m²/g
Langmuir Surface Area:	60.7593	m²/g
Micropore Area:	13.9079	m²/g
External Surface Area:	24.1116	m²/g
BJH Adsorption Cumulative Surface Area of pores between 17.000000 and 3000.000000 A Diameter:	27.8502	m²/g
BJH Desorption Cumulative Surface Area of pores between 17.000000 and 3000.000000 A Diameter:	30.7362	m²/g

Volume

Single Point Desorption Total Pore Volume of pores less than 954.0601 A Diameter at P/Po 0.97927765:	0.135442	cm³/g
Micropore Volume:	0.007390	cm³/g
BJH Adsorption Cumulative Pore Volume of pores between 17.000000 and 3000.000000 A Diameter:	0.132756	cm³/g
BJH Desorption Cumulative Pore Volume of pores between 17.000000 and 3000.000000 A Diameter:	0.135057	cm³/g

FULL ISOTHERM FOR SAMPLE 3, S3W-5154

Sample:	Sample 3, S3W-5154		
Operator:	Julian Perfect		
Submitter:	Fan Zhang		
File Name:	C:\ASAP2010\DATA\000-061.SMP		
Started:	7/12/04 11:36:26PM	Analysis Adsorptive:	N2
Completed:	7/13/04 11:00:04AM	Analysis Bath:	77.35 K
Report Time:	7/14/04 6:52:52PM	Thermal Correction:	No
Sample Weight:	0.7241 g	Smoothed Pressures:	No
Warm Freespace:	17.2551 cm³	Cold Freespace:	51.7413 cm³
	MEASURED		
Equil. Interval:	10 secs	Low Pressure Dose:	None

Comments:
Bulb type sample holder used with stopper and filler rod. Sample degassed, using manual mode, for ~31.75 hours (~1.25 hours @ 90C, 1.5 hours @ 120C and 29 hours @ 350C).

Summary Report

Pore Size

Desorption Average Pore Diameter (4V/A by BET):	142.4978	A
BJH Adsorption Average Pore Diameter (4V/A):	190.6710	A
BJH Desorption Average Pore Diameter (4V/A):	175.7634	A

micromeritics

Dept of Chemical Engineering, UCL

AutoPore IV 9500 V1.03 Serial: 201 Port: 1/1

Calibration ID: Sample 4, S3HT-44 (Pen No:16-0289) 000-070
Operator: Julian Perfect
Submitter: Fan Zhang
File: C:\9500\DATA\BLANKS\000-070.SMP

LP Analysis Time:	14/07/2004 8:06:23PM	Sample Weight:	0.5166 g
HP Analysis Time:	14/07/2004 9:19:03PM	Correction Type:	Blank
Report Time:	14/07/2004 9:38:55PM	Show Neg. Int:	No

Summary Report

Penetrometer parameters

Penetrometer:	#s/n - (16) 3 Bulb, 1.190 Stem, Powder		
Pen. Constant:	20.994 µL/pF	Pen. Weight:	54.8355 g
Stem Volume:	1.1900 mL	Max. Head Pressure:	4.6800 psia
Pen. Volume:	3.9104 mL	Assembly Weight:	102.5662 g

Hg Parameters

Adv. Contact Angle:	130.000 degrees	Rec. Contact Angle:	130.000 degrees
Hg Surface Tension:	485.000 dynes/cm	Hg Density:	13.5335 g/mL

User Parameters

Param 1:	0.000	Param 2:	0.000	Param 3:	0.000

Low Pressure:

Evacuation Pressure:	50 µmHg
Evacuation Time:	5 mins
Mercury Filling Pressure:	1.33 psia
Equilibration Time:	10 secs

High Pressure:

Equilibration Time:	10 secs

Blank Correction Sample: C:\9500\DATA\BLANKS\000-053.SMP
Blank Correction ID: Pen No:16-0289 Blank Correction 000-053

(From Pressure 0.10 to 60000.00 psia)

Intrusion Data Summary

Total Intrusion Volume =	0.4317	mL/g
Total Pore Area =	53.365	m²/g
Median Pore Diameter (Volume) =	0.1492	µm
Median Pore Diameter (Area) =	0.0123	µm
Average Pore Diameter (4V/A) =	0.0324	µm
Bulk Density at 0.10 psia =	1.2249	g/mL
Apparent (skeletal) Density =	2.6001	g/mL
Porosity =	52.8867	%
Stem Volume Used =	18	% ****

Pore Structure Summary

Threshold Pressure:	101.01	psia (Calculated)
Characteristic length =	1.7905	µm
Conductivity formation factor =	0.172	
Permeability constant =	0.00442	
Permeability =	2.4423	mdarcy
BET Surface Area =	200.0000	m²/g
Pore shape exponent =	1.00	
Tortuosity factor =	1.632	
Tortuosity =	41.4897	
Percolation Fractal dimension =	2.732	
Backbone Fractal dimension =	2.466	

Calibration ID: Sample 4, S3HT-44 (Pen No:16-0289) 000-070
Operator: Julian Perfect
Submitter: Fan Zhang
File: C:\9500\DATA\BLANKS\000-070.SMP

LP Analysis Time:	14/07/2004 8:06:23PM	Sample Weight:	0.5166 g
HP Analysis Time:	14/07/2004 9:19:03PM	Correction Type:	Blank
Report Time:	14/07/2004 9:38:55PM	Show Neg. Int:	No

Mayer Stowe Summary

Interstitial porosity =	47.6300	%
Breakthrough pressure ratio =	3.3512	

Material Compressibility

Linear Coefficient =	N/A	1/psia
Quadratic Coefficient =	N/A	1/psia²

Calibration ID: Sample 4, S3HT-44 (Pen No:16-0289) 000-070
Operator: Julian Perfect
Submitter: Fan Zhang
File: C:\9500\DATA\BLANKS\000-070.SMP

LP Analysis Time:	14/07/2004 8:06:23PM	Sample Weight:	0.5166 g
HP Analysis Time:	14/07/2004 9:19:03PM	Correction Type:	Blank
Report Time:	14/07/2004 9:38:55PM	Show Neg. Int:	No

Tabular Report

Pressure (psia)	Pore Diameter (µm)	dV/dlogD Pore Volume (mL/g)	dV/dD Pore Volume (mL/g/µm)
1.33	135.7413	0.000×10^{0}	0.000×10^{0}
1.98	91.2868	6.286×10^{-2}	2.437×10^{-4}
2.98	60.6917	5.573×10^{-2}	3.229×10^{-4}
3.98	45.4804	4.368×10^{-2}	3.598×10^{-4}
5.47	33.0599	3.027×10^{-2}	3.376×10^{-4}
6.97	25.9672	2.982×10^{-2}	4.410×10^{-4}
8.46	21.3688	2.015×10^{-2}	3.709×10^{-4}
10.45	17.3004	2.015×10^{-2}	4.543×10^{-4}
12.97	13.9423	1.795×10^{-2}	5.009×10^{-4}
15.96	11.3338	1.844×10^{-2}	6.358×10^{-4}
19.95	9.0636	2.196×10^{-2}	9.392×10^{-4}
22.95	7.8797	2.104×10^{-2}	1.080×10^{-3}
24.95	7.2487	2.680×10^{-2}	1.539×10^{-3}
29.95	6.0385	2.897×10^{-2}	1.899×10^{-3}
36.75	4.9220	3.241×10^{-2}	2.577×10^{-3}
46.70	3.8729	3.047×10^{-2}	3.024×10^{-3}
56.45	3.2039	3.881×10^{-2}	4.778×10^{-3}
71.72	2.5216	5.455×10^{-2}	8.315×10^{-3}
86.91	2.0810	1.188×10^{-1}	2.249×10^{-2}
111.41	1.6234	2.787×10^{-1}	6.568×10^{-2}
137.16	1.3187	2.116×10^{-1}	6.270×10^{-2}
172.03	1.0513	1.639×10^{-1}	6.033×10^{-2}
215.90	0.8377	1.483×10^{-1}	6.849×10^{-2}
266.29	0.6792	1.295×10^{-1}	7.444×10^{-2}
327.17	0.5528	1.171×10^{-1}	8.288×10^{-2}
416.13	0.4346	9.885×10^{-2}	8.737×10^{-2}
516.94	0.3499	8.522×10^{-2}	9.472×10^{-2}
637.50	0.2837	7.583×10^{-2}	1.043×10^{-1}
696.52	0.2597	7.622×10^{-2}	1.219×10^{-1}
796.74	0.2270	6.203×10^{-2}	1.109×10^{-1}
988.07	0.1830	5.677×10^{-2}	1.207×10^{-1}
1197.54	0.1510	5.269×10^{-2}	1.374×10^{-1}

micromeritics

Dept of Chemical Engineering, UCL

Calibration ID: Sample 4, S3HT-44 (Pen No:16-0289) 000-070
Operator: Julian Perfect
Submitter: Fan Zhang
File: C:\9500\DATA\BLANKS\000-070.SMP

LP Analysis Time:	14/07/2004 8:06:23PM	Sample Weight:	0.5166 g
HP Analysis Time:	14/07/2004 9:19:03PM	Correction Type:	Blank
Report Time:	14/07/2004 9:38:55PM	Show Neg. Int:	No

Tabular Report

Pressure (psia)	Pore Diameter (µm)	dV/dlogD Pore Volume (mL/g)	dV/dD Pore Volume (mL/g/µm)
1296.19	0.1395	5.566×10^{-2}	1.665×10^{-1}
1396.65	0.1295	4.988×10^{-2}	1.611×10^{-1}
1496.73	0.1208	5.124×10^{-2}	1.779×10^{-1}
1595.37	0.1134	4.625×10^{-2}	1.716×10^{-1}
1696.57	0.1066	4.943×10^{-2}	1.952×10^{-1}
1895.73	0.0954	4.694×10^{-2}	2.020×10^{-1}
2044.84	0.0884	4.875×10^{-2}	2.304×10^{-1}
2194.50	0.0824	5.298×10^{-2}	2.694×10^{-1}
2345.42	0.0771	5.097×10^{-2}	2.776×10^{-1}
2495.09	0.0725	5.813×10^{-2}	3.376×10^{-1}
2644.39	0.0684	4.899×10^{-2}	3.022×10^{-1}
2692.95	0.0672	6.226×10^{-2}	3.990×10^{-1}
2844.05	0.0636	4.869×10^{-2}	3.235×10^{-1}
2992.13	0.0604	6.285×10^{-2}	4.402×10^{-1}
3241.91	0.0558	5.495×10^{-2}	4.108×10^{-1}
3490.89	0.0518	6.163×10^{-2}	4.978×10^{-1}
3742.53	0.0483	6.654×10^{-2}	5.774×10^{-1}
3991.62	0.0453	7.084×10^{-2}	6.573×10^{-1}
4241.81	0.0426	8.079×10^{-2}	7.981×10^{-1}
4484.34	0.0403	8.849×10^{-2}	9.266×10^{-1}
4723.51	0.0383	1.053×10^{-1}	1.163×10^{0}
4983.25	0.0363	1.220×10^{-1}	1.421×10^{0}
5282.01	0.0342	1.459×10^{-1}	1.797×10^{0}
5480.90	0.0330	1.850×10^{-1}	2.390×10^{0}
5729.98	0.0316	2.002×10^{-1}	2.694×10^{0}
5981.76	0.0302	2.514×10^{-1}	3.533×10^{0}
6231.57	0.0290	2.701×10^{-1}	3.960×10^{0}
6475.77	0.0279	2.877×10^{-1}	4.388×10^{0}
6732.71	0.0269	3.052×10^{-1}	4.839×10^{0}
6980.18	0.0259	2.896×10^{-1}	4.766×10^{0}
7474.20	0.0242	3.057×10^{-1}	5.301×10^{0}
7972.24	0.0227	3.035×10^{-1}	5.624×10^{0}

Calibration ID: Sample 4, S3HT-44 (Pen No:16-0289) 000-070
Operator: Julian Perfect
Submitter: Fan Zhang
File: C:\9500\DATA\BLANKS\000-070.SMP

LP Analysis Time:	14/07/2004 8:06:23PM	Sample Weight:	0.5166 g
HP Analysis Time:	14/07/2004 9:19:03PM	Correction Type:	Blank
Report Time:	14/07/2004 9:38:55PM	Show Neg. Int:	No

Tabular Report

Pressure (psia)	Pore Diameter (µm)	dV/dlogD Pore Volume (mL/g)	dV/dD Pore Volume (mL/g/µm)
8474.17	0.0213	2.944×10^{-1}	5.810×10^{0}
8972.53	0.0202	2.951×10^{-1}	6.179×10^{0}
9267.23	0.0195	2.549×10^{-1}	5.581×10^{0}
9569.78	0.0189	2.611×10^{-1}	5.903×10^{0}
10014.50	0.0181	2.560×10^{-1}	6.017×10^{0}
10469.18	0.0173	2.494×10^{-1}	6.131×10^{0}
10957.53	0.0165	2.162×10^{-1}	5.559×10^{0}
11454.97	0.0158	2.352×10^{-1}	6.326×10^{0}
11956.50	0.0151	2.204×10^{-1}	6.193×10^{0}
12556.57	0.0144	2.168×10^{-1}	6.377×10^{0}
13054.53	0.0139	2.328×10^{-1}	7.155×10^{0}
13599.21	0.0133	2.239×10^{-1}	7.163×10^{0}
13944.99	0.0130	2.585×10^{-1}	8.548×10^{0}
14286.26	0.0127	2.214×10^{-1}	7.504×10^{0}
14551.42	0.0124	2.546×10^{-1}	8.814×10^{0}
14946.30	0.0121	2.360×10^{-1}	8.358×10^{0}
15398.56	0.0117	2.558×10^{-1}	9.317×10^{0}
15741.86	0.0115	2.913×10^{-1}	1.089×10^{1}
16149.67	0.0112	2.660×10^{-1}	1.019×10^{1}
16601.30	0.0109	2.723×10^{-1}	1.071×10^{1}
16941.30	0.0107	2.876×10^{-1}	1.158×10^{1}
17292.81	0.0105	2.877×10^{-1}	1.182×10^{1}
17648.95	0.0102	2.622×10^{-1}	1.100×10^{1}
18040.30	0.0100	2.732×10^{-1}	1.170×10^{1}
18390.44	0.0098	2.705×10^{-1}	1.183×10^{1}
18730.04	0.0097	2.905×10^{-1}	1.295×10^{1}
19142.01	0.0094	2.550×10^{-1}	1.159×10^{1}
19749.37	0.0092	2.589×10^{-1}	1.209×10^{1}
20239.75	0.0089	2.707×10^{-1}	1.299×10^{1}
20761.58	0.0087	2.279×10^{-1}	1.122×10^{1}
21159.33	0.0085	2.265×10^{-1}	1.140×10^{1}
21616.15	0.0084	2.048×10^{-1}	1.052×10^{1}

Calibration ID: Sample 4, S3HT-44 (Pen No:16-0289) 000-070
Operator: Julian Perfect
Submitter: Fan Zhang
File: C:\9500\DATA\BLANKS\000-070.SMP

LP Analysis Time:	14/07/2004 8:06:23PM	Sample Weight:	0.5166 g
HP Analysis Time:	14/07/2004 9:19:03PM	Correction Type:	Blank
Report Time:	14/07/2004 9:38:55PM	Show Neg. Int:	No

Tabular Report

Pressure (psia)	Pore Diameter (µm)	dV/dlogD Pore Volume (mL/g)	dV/dD Pore Volume (mL/g/µm)
22021.69	0.0082	2.301×10^{-1}	1.206×10^{1}
22621.68	0.0080	1.805×10^{-1}	9.673×10^{0}
23173.24	0.0078	1.640×10^{-1}	9.015×10^{0}
23724.27	0.0076	1.290×10^{-1}	7.264×10^{0}
24078.59	0.0075	1.690×10^{-1}	9.698×10^{0}
24627.24	0.0073	1.278×10^{-1}	7.474×10^{0}
25029.44	0.0072	9.043×10^{-2}	5.391×10^{0}
25428.77	0.0071	1.155×10^{-1}	6.997×10^{0}
25881.99	0.0070	7.872×10^{-2}	4.849×10^{0}
26428.55	0.0068	9.740×10^{-2}	6.117×10^{0}
26930.14	0.0067	3.687×10^{-2}	2.362×10^{0}
27382.27	0.0066	6.511×10^{-2}	4.246×10^{0}
27782.39	0.0065	6.899×10^{-2}	4.569×10^{0}
28234.57	0.0064	4.489×10^{-2}	3.019×10^{0}
28986.03	0.0062	4.522×10^{-2}	3.106×10^{0}
29485.37	0.0061	4.348×10^{-2}	3.053×10^{0}
29986.48	0.0060	3.649×10^{-2}	2.605×10^{0}
30433.69	0.0059	0.000×10^{0}	0.000×10^{0}
30885.96	0.0059	1.690×10^{-2}	1.244×10^{0}
31287.92	0.0058	3.856×10^{-2}	2.878×10^{0}
31783.82	0.0057	3.435×10^{-2}	2.601×10^{0}
32334.76	0.0056	1.713×10^{-2}	1.319×10^{0}
32885.57	0.0055	2.502×10^{-2}	1.959×10^{0}
33487.74	0.0054	0.000×10^{0}	0.000×10^{0}
33978.99	0.0053	0.000×10^{0}	0.000×10^{0}
34623.76	0.0052	0.000×10^{0}	0.000×10^{0}
35483.95	0.0051	0.000×10^{0}	0.000×10^{0}
36181.69	0.0050	1.780×10^{-2}	1.532×10^{0}
36984.09	0.0049	0.000×10^{0}	0.000×10^{0}
37621.02	0.0048	0.000×10^{0}	0.000×10^{0}
38412.43	0.0047	0.000×10^{0}	0.000×10^{0}
39169.71	0.0046	0.000×10^{0}	0.000×10^{0}

Calibration ID: Sample 4, S3HT-44 (Pen No:16-0289) 000-070
Operator: Julian Perfect
Submitter: Fan Zhang
File: C:\9500\DATA\BLANKS\000-070.SMP

LP Analysis Time:	14/07/2004 8:06:23PM	Sample Weight:	0.5166 g
HP Analysis Time:	14/07/2004 9:19:03PM	Correction Type:	Blank
Report Time:	14/07/2004 9:38:55PM	Show Neg. Int:	No

Tabular Report

Pressure (psia)	Pore Diameter (µm)	dV/dlogD Pore Volume (mL/g)	dV/dD Pore Volume (mL/g/µm)
39972.93	0.0045	0.000×10^0	0.000×10^0
40466.65	0.0045	0.000×10^0	0.000×10^0
40961.89	0.0044	0.000×10^0	0.000×10^0
42464.86	0.0043	0.000×10^0	0.000×10^0
43309.42	0.0042	0.000×10^0	0.000×10^0
43959.18	0.0041	0.000×10^0	0.000×10^0
44959.79	0.0040	0.000×10^0	0.000×10^0
46461.89	0.0039	0.000×10^0	0.000×10^0
47957.53	0.0038	0.000×10^0	0.000×10^0
49452.70	0.0037	0.000×10^0	0.000×10^0
50156.62	0.0036	0.000×10^0	0.000×10^0
52948.35	0.0034	0.000×10^0	0.000×10^0
54444.31	0.0033	0.000×10^0	0.000×10^0
55942.55	0.0032	0.000×10^0	0.000×10^0
57937.10	0.0031	0.000×10^0	0.000×10^0
59927.34	0.0030	0.000×10^0	0.000×10^0

micromeritics

Dept of Chemical Engineering, UCL

AutoPore IV 9500 V1.03 Serial: 201 Port: 1/1 Page 8

Calibration ID: Sample 4, S3HT-44 (Pen No:16-0289) 000-070
Operator: Julian Perfect
Submitter: Fan Zhang
File: C:\9500\DATA\BLANKS\000-070.SMP

LP Analysis Time:	14/07/2004 8:06:23PM	Sample Weight:	0.5166 g
HP Analysis Time:	14/07/2004 9:19:03PM	Correction Type:	Blank
Report Time:	14/07/2004 9:38:55PM	Show Neg. Int:	No

Cumulative Intrusion vs Pore size

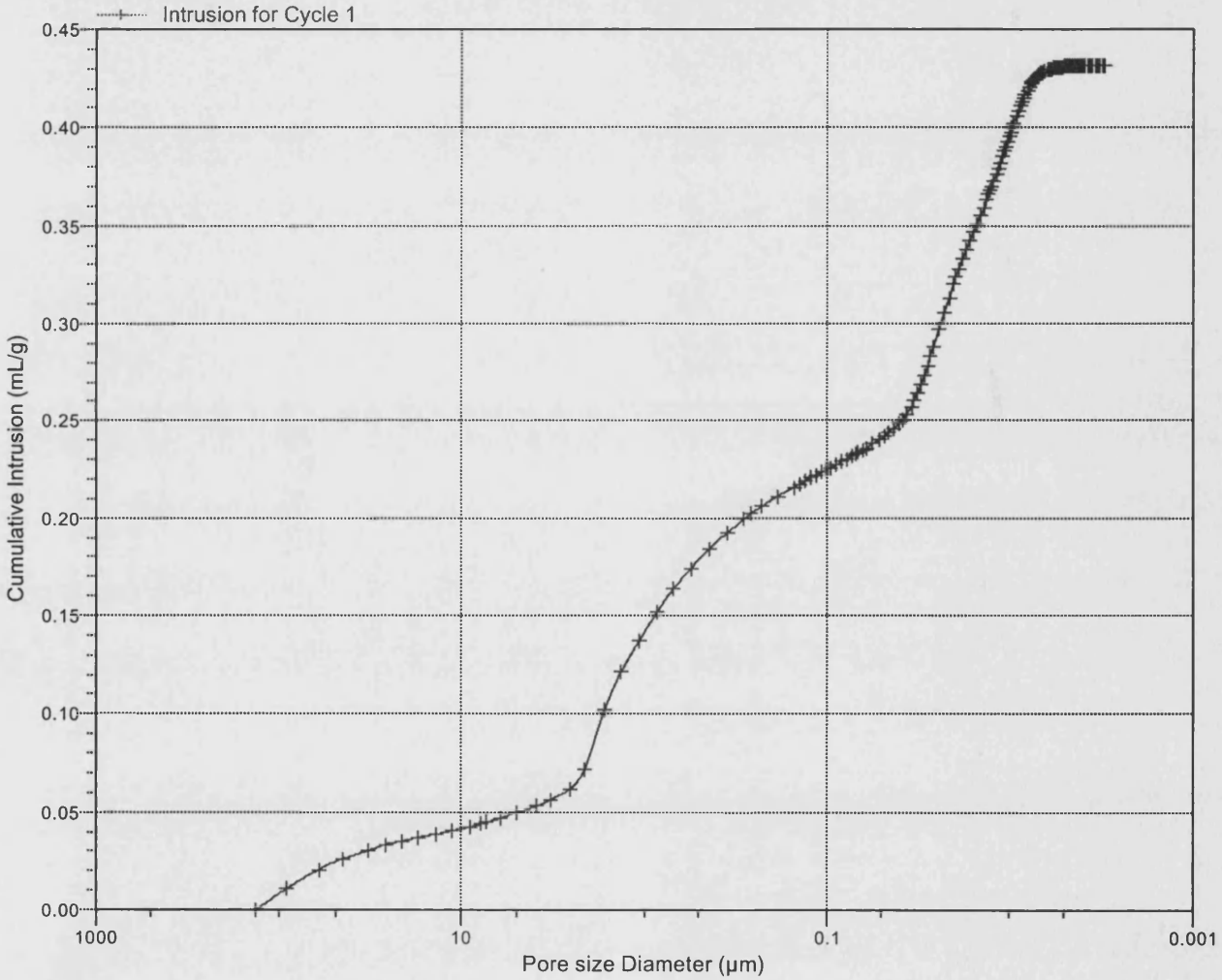

micromeritics

Dept of Chemical Engineering, UCL

AutoPore IV 9500 V1.03 Serial: 201 Port: 1/1 Page 9

Calibration ID: Sample 4, S3HT-44 (Pen No:16-0289) 000-070
Operator: Julian Perfect
Submitter: Fan Zhang
File: C:\9500\DATA\BLANKS\000-070.SMP

LP Analysis Time:	14/07/2004 8:06:23PM	Sample Weight:	0.5166 g
HP Analysis Time:	14/07/2004 9:19:03PM	Correction Type:	Blank
Report Time:	14/07/2004 9:38:55PM	Show Neg. Int:	No

Incremental Intrusion vs Pressure

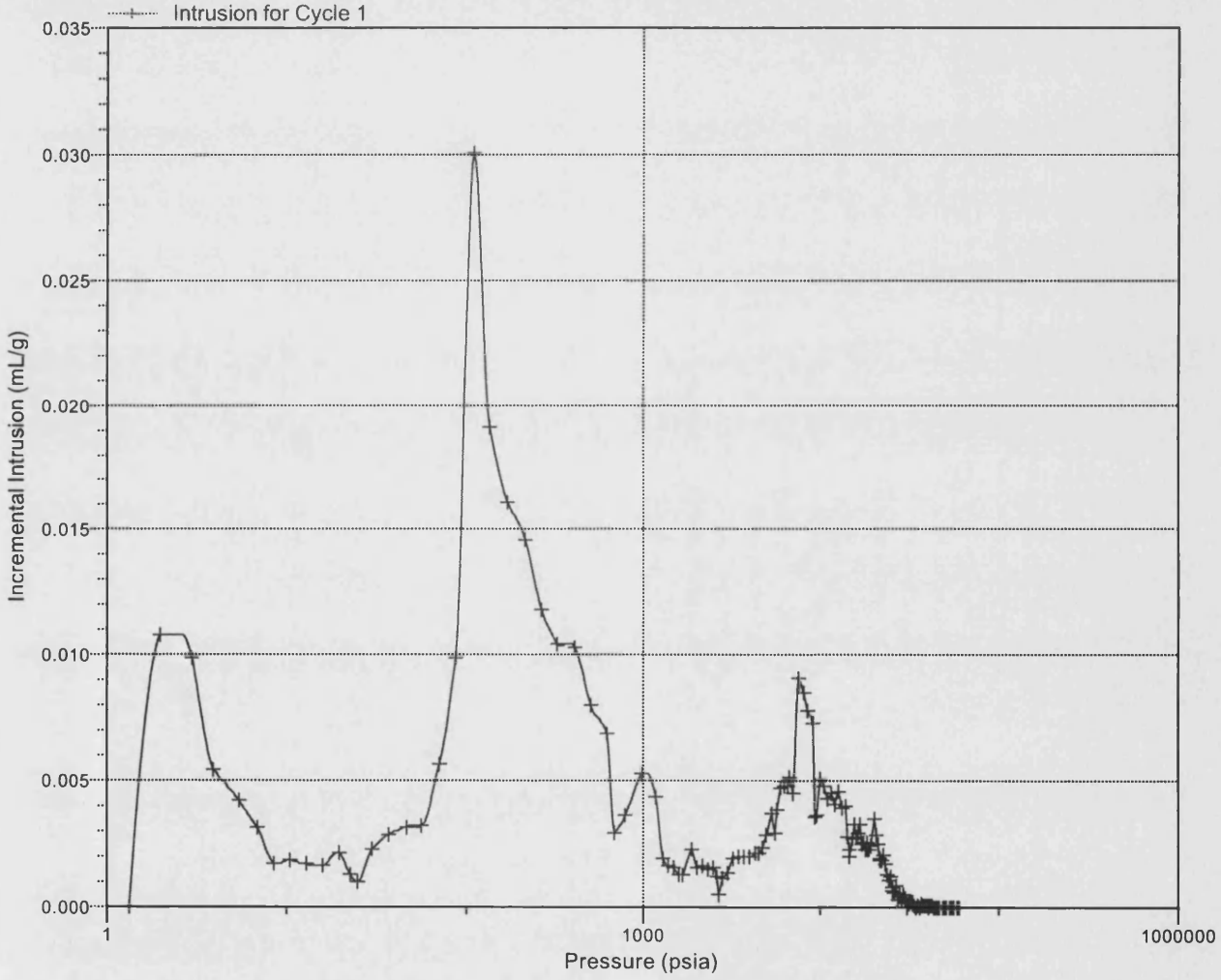

micromeritics

Dept of Chemical Engineering, UCL

AutoPore IV 9500 V1.03 Serial: 201 Port: 1/1 Page 10

Calibration ID: Sample 4, S3HT-44 (Pen No:16-0289) 000-070
Operator: Julian Perfect
Submitter: Fan Zhang
File: C:\9500\DATA\BLANKS\000-070.SMP

LP Analysis Time:	14/07/2004 8:06:23PM	Sample Weight:	0.5166 g
HP Analysis Time:	14/07/2004 9:19:03PM	Correction Type:	Blank
Report Time:	14/07/2004 9:38:55PM	Show Neg. Int:	No

Differential Intrusion vs Pore size

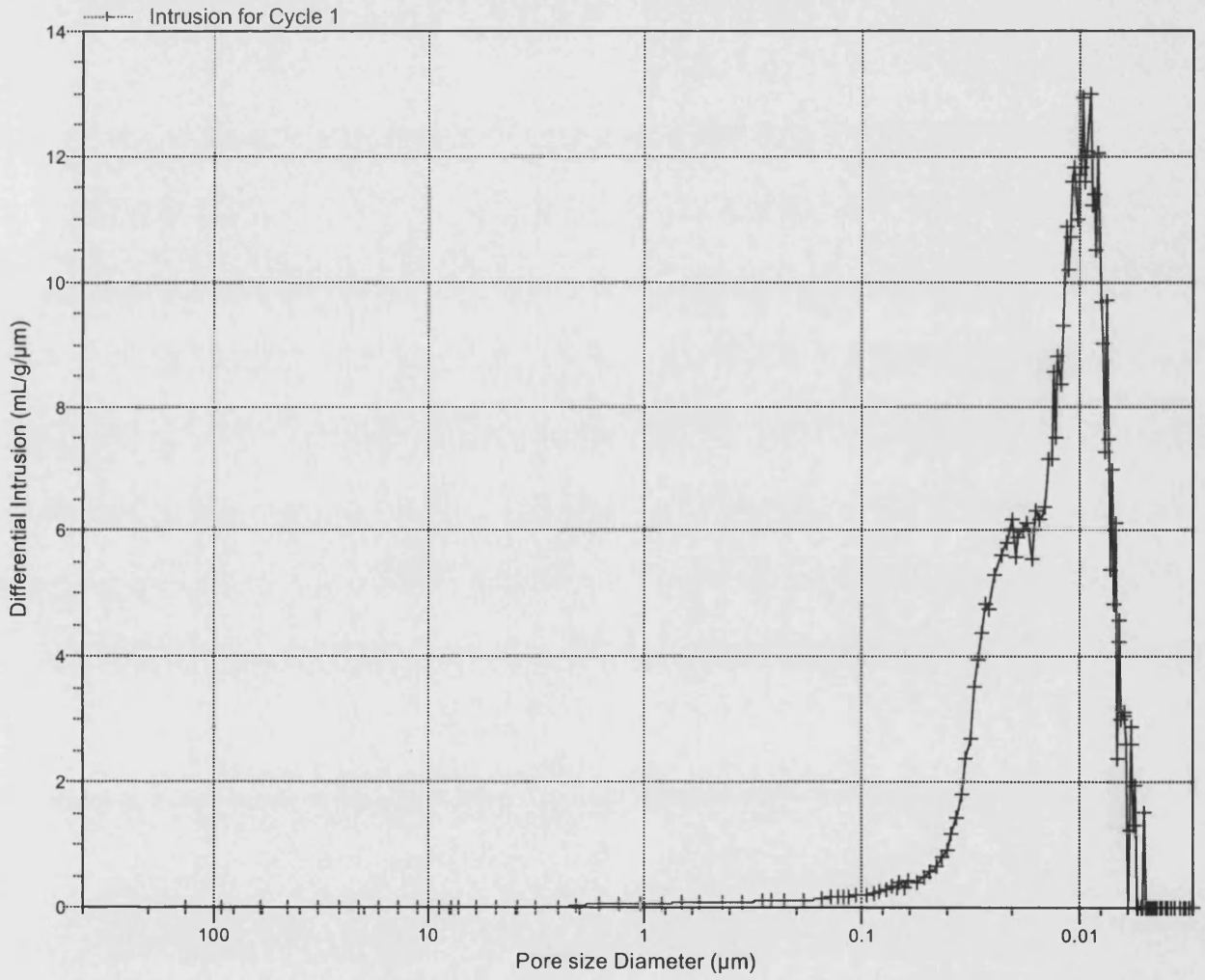

micromeritics

Dept of Chemical Engineering, UCL

AutoPore IV 9500 V1.03 Serial: 201 Port: 1/1 Page 11

Calibration ID: Sample 4, S3HT-44 (Pen No:16-0289) 000-070
Operator: Julian Perfect
Submitter: Fan Zhang
File: C:\9500\DATA\BLANKS\000-070.SMP

LP Analysis Time:	14/07/2004 8:06:23PM	Sample Weight:	0.5166 g
HP Analysis Time:	14/07/2004 9:19:03PM	Correction Type:	Blank
Report Time:	14/07/2004 9:38:55PM	Show Neg. Int:	No

Log Differential Intrusion vs Pore size

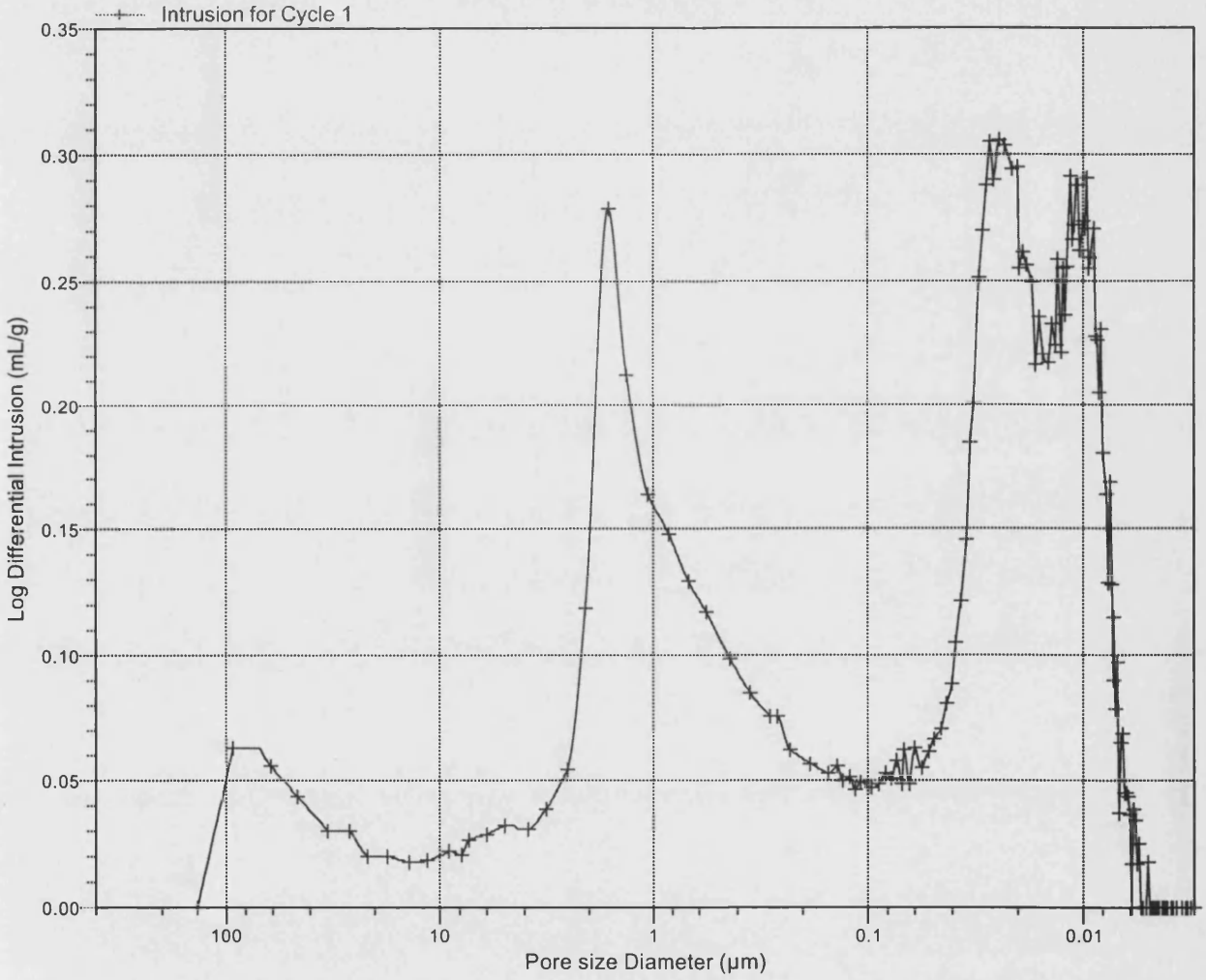

FULL ISOTHERM FOR SAMPLE 4, S3HT-44

Sample: Sample 4, S3HT-44
Operator: Julian Perfect
Submitter: Fan Zhang
File Name: C:\ASAP2010\DATA\000-062.SMP

Started: 7/13/04 2:52:08PM
Completed: 7/14/04 3:54:44AM
Report Time: 7/14/04 6:53:18PM
Sample Weight: 0.5268 g
Warm Freespace: 16.5645 cm³
MEASURED
Equil. Interval: 10 secs
Analysis Adsorptive: N2
Analysis Bath: 77.35 K
Thermal Correction: No
Smoothed Pressures: No
Cold Freespace: 50.4421 cm³
Low Pressure Dose: None

Comments:
Bulb type sample holder used with stopper and filler rod. Sample degassed, using manual mode, for ~48 hours (~1.25 hours @ 90C, 1.5 hours @ 120C and ~45 hours @ 350C).

Analysis Log

Relative Pressure	Pressure (mmHg)	Vol Adsorbed (cm³/g STP)	Elapsed Time (HR:MN)	Saturation Press.(mmHg)
			02:26	763.88562
0.135592784	103.56020	17.1925	02:43	
0.161990619	123.71815	17.7104	02:46	
0.182461201	139.34821	18.0902	02:49	
0.201939081	154.21922	18.4386	02:52	
0.220585139	168.45413	18.7653	02:55	
0.251934548	192.38908	19.3042	02:58	
0.301709212	230.39037	20.1562	03:02	
0.355825060	271.70355	21.1087	03:06	
0.401595196	306.64407	21.9530	03:09	
0.451349595	344.62134	22.9312	03:13	
0.501343504	382.77850	24.0047	03:17	
0.550166385	420.03864	25.1907	03:21	
0.599951243	458.03027	26.6241	03:25	
0.650154443	496.33347	28.4860	03:30	
0.699470844	533.95074	31.0050	03:36	
0.739826886	564.72400	33.9042	03:42	
0.770683209	588.23126	36.9217	03:50	
0.800058302	610.60437	40.8397	03:58	
0.821434357	626.86346	44.6604	04:07	
0.841288402	641.95203	49.3873	04:17	
0.860547737	656.57104	55.3767	04:29	
			04:31	762.95386
0.876207375	668.46198	61.4318	04:42	
0.889348928	678.44324	67.2808	04:53	
0.902619145	688.51312	74.1216	05:06	
0.913410829	696.69928	80.0902	05:17	
0.923096034	704.03625	85.9840	05:29	
0.931638730	710.50085	91.6077	05:41	
0.939208032	716.22650	96.7842	05:52	

FULL ISOTHERM FOR SAMPLE 4, S3HT-44

Sample: Sample 4, S3HT-44
Operator: Julian Perfect
Submitter: Fan Zhang
File Name: C:\ASAP2010\DATA\000-062.SMP

Started: 7/13/04 2:52:08PM
Completed: 7/14/04 3:54:44AM
Report Time: 7/14/04 6:53:18PM
Sample Weight: 0.5268 g
Warm Freespace: 16.5645 cm³
MEASURED
Equil. Interval: 10 secs
Analysis Adsorptive: N2
Analysis Bath: 77.35 K
Thermal Correction: No
Smoothed Pressures: No
Cold Freespace: 50.4421 cm³
Low Pressure Dose: None

Comments:
Bulb type sample holder used with stopper and filler rod. Sample degassed, using manual mode, for ~48 hours (~1.25 hours @ 90C, 1.5 hours @ 120C and ~45 hours @ 350C).

Analysis Log

Relative Pressure	Pressure (mmHg)	Vol Adsorbed (cm³/g STP)	Elapsed Time (HR:MN)	Saturation Press.(mmHg)
0.945885295	721.27118	101.8557	06:03	
0.951850282	725.76776	106.9916	06:15	
0.957614681	730.11511	112.3603	06:26	
0.962946718	734.13226	117.5980	06:37	
			06:39	762.37189
0.967307072	737.47473	122.5645	06:50	
0.970647745	740.04877	126.5521	07:01	
0.973968683	742.60547	130.4087	07:11	
0.976725458	744.73218	133.7037	07:21	
0.979686087	747.01447	137.4200	07:31	
0.982143288	748.91302	140.1817	07:41	
0.983761563	750.16449	141.9385	07:48	
0.986030800	751.91742	144.2395	07:57	
0.987755827	753.25043	145.9330	08:04	
0.988898450	754.13684	146.8721	08:10	
0.989558609	754.65033	147.5821	08:14	
0.979376481	746.90271	145.9759	08:21	
0.972349869	741.56128	143.5094	08:28	
0.966747678	737.30841	141.0628	08:36	
0.963598756	734.92395	139.4369	08:43	
			08:45	762.69177
0.959062845	731.45703	136.5965	08:54	
0.954142600	727.69086	132.4950	09:04	
0.948738655	723.55322	127.4685	09:16	
0.943115899	719.24890	121.8871	09:28	
0.936880469	714.47754	115.7242	09:40	
0.929417064	708.76862	109.0389	09:53	
0.919921809	701.50922	101.7631	10:07	
0.908958097	693.13171	95.0933	10:20	
0.894382591	682.00049	87.7035	10:33	

FULL ISOTHERM FOR SAMPLE 4, S3HT-44

Sample: Sample 4, S3HT-44
Operator: Julian Perfect
Submitter: Fan Zhang
File Name: C:\ASAP2010\DATA\000-062.SMP

Started: 7/13/04 2:52:08PM
Completed: 7/14/04 3:54:44AM
Report Time: 7/14/04 6:53:18PM
Sample Weight: 0.5268 g
Warm Freespace: 16.5645 cm³
MEASURED
Equil. Interval: 10 secs
Analysis Adsorptive: N2
Analysis Bath: 77.35 K
Thermal Correction: No
Smoothed Pressures: No
Cold Freespace: 50.4421 cm³
Low Pressure Dose: None

Comments:
Bulb type sample holder used with stopper and filler rod. Sample degassed, using manual mode, for ~48 hours (~1.25 hours @ 90C, 1.5 hours @ 120C and ~45 hours @ 350C).

Analysis Log

Relative Pressure	Pressure (mmHg)	Vol Adsorbed (cm³/g STP)	Elapsed Time (HR:MN)	Saturation Press.(mmHg)
0.878204294	669.64764	80.5396	10:46	
			10:48	762.51636
0.862565149	657.67242	74.1313	11:01	
0.842926090	642.65546	66.4166	11:13	
0.822602964	627.11200	58.9144	11:27	
0.801030534	610.62543	51.7394	11:39	
0.769804164	586.78235	43.6969	11:51	
0.740962574	564.76642	38.8504	12:01	
0.704667794	537.07837	34.9714	12:09	
0.656777354	500.55807	31.8027	12:16	
0.606427848	462.17169	29.6165	12:21	
0.553169623	421.57306	27.9183	12:25	
0.504753007	384.65311	26.0718	12:35	
0.449711043	342.69626	22.3001	12:41	
0.401832250	306.20575	21.3277	12:44	
0.338140940	257.66571	20.1405	12:48	
			12:50	761.99835
0.301138721	229.46721	19.4823	12:53	
0.251562668	191.69034	18.6242	12:57	
0.202864778	154.58263	17.7705	13:00	
0.144539382	110.13877	16.6842	13:04	

FULL ISOTHERM FOR SAMPLE 4, S3HT-44

Sample: Sample 4, S3HT-44
Operator: Julian Perfect
Submitter: Fan Zhang
File Name: C:\ASAP2010\DATA\000-062.SMP

Started: 7/13/04 2:52:08PM
Completed: 7/14/04 3:54:44AM
Report Time: 7/14/04 6:53:18PM
Sample Weight: 0.5268 g
Warm Freespace: 16.5645 cm³
MEASURED
Equil. Interval: 10 secs
Analysis Adsorptive: N2
Analysis Bath: 77.35 K
Thermal Correction: No
Smoothed Pressures: No
Cold Freespace: 50.4421 cm³
Low Pressure Dose: None

Comments:
Bulb type sample holder used with stopper and filler rod. Sample degassed, using manual mode, for ~48 hours (~1.25 hours @ 90C, 1.5 hours @ 120C and ~45 hours @ 350C).

Summary Report

Area

Single Point Surface Area at P/Po 0.25193455 :	62.8636	m²/g
BET Surface Area:	61.4610	m²/g
Langmuir Surface Area:	98.0807	m²/g
Micropore Area:	18.7089	m²/g
External Surface Area:	42.7521	m²/g
BJH Adsorption Cumulative Surface Area of pores between 17.000000 and 3000.000000 A Diameter:	52.0422	m²/g
BJH Desorption Cumulative Surface Area of pores between 17.000000 and 3000.000000 A Diameter:	65.7346	m²/g

Volume

Single Point Desorption Total Pore Volume of pores less than 958.5385 A Diameter at P/Po 0.97937648:	0.225795	cm³/g
Micropore Volume:	0.009776	cm³/g
BJH Adsorption Cumulative Pore Volume of pores between 17.000000 and 3000.000000 A Diameter:	0.225146	cm³/g
BJH Desorption Cumulative Pore Volume of pores between 17.000000 and 3000.000000 A Diameter:	0.229775	cm³/g

FULL ISOTHERM FOR SAMPLE 4, S3HT-44

Sample:	Sample 4, S3HT-44		
Operator:	Julian Perfect		
Submitter:	Fan Zhang		
File Name:	C:\ASAP2010\DATA\000-062.SMP		
Started:	7/13/04 2:52:08PM	Analysis Adsorptive:	N2
Completed:	7/14/04 3:54:44AM	Analysis Bath:	77.35 K
Report Time:	7/14/04 6:53:18PM	Thermal Correction:	No
Sample Weight:	0.5268 g	Smoothed Pressures:	No
Warm Freespace:	16.5645 cm³	Cold Freespace:	50.4421 cm³
	MEASURED		
Equil. Interval:	10 secs	Low Pressure Dose:	None

Comments:
Bulb type sample holder used with stopper and filler rod. Sample degassed, using manual mode, for ~48 hours (~1.25 hours @ 90C, 1.5 hours @ 120C and ~45 hours @ 350C).

Summary Report

Pore Size

Desorption Average Pore Diameter (4V/A by BET):	146.9521	A
BJH Adsorption Average Pore Diameter (4V/A):	173.0489	A
BJH Desorption Average Pore Diameter (4V/A):	139.8197	A

Appendix B3

Pore size distribution data for Samples C2NM & C2HT

This appendix includes:

- Mercury porosimetry results of C2NM (diesel-oxidation catalysts, from 3.18 g/l Pt slurry, calcined at 500 °C)
- Nitrogen adsorption results of C2NM (partially)
- Mercury porosimetry results of C2HT (diesel-oxidation catalysts from 3.18 g/l Pt slurry, calcined at 700 °C for 16 hours in the atmosphere of 10% H_2O + 10% O_2 + 80% N_2)

micromeritics

Dept of Chemical Engineering, UCL

AutoPore IV 9500 V1.03 Serial: 201 Port: 1/1

Calibration ID: Sample 5, C2NM (Pen No:16-0287) 000-071
Operator: Julian Perfect
Submitter: Fan Zhang
File: C:\9500\DATA\BLANKS\000-071.SMP

LP Analysis Time:	14/07/2004 6:22:25PM	Sample Weight:	1.0880 g
HP Analysis Time:	14/07/2004 7:30:12PM	Correction Type:	Blank
Report Time:	14/07/2004 9:25:27PM	Show Neg. Int:	No

Summary Report

Penetrometer parameters

Penetrometer:	#s/n - (16) 3 Bulb, 1.190 Stem, Powder		
Pen. Constant:	20.994 µL/pF	Pen. Weight:	54.7153 g
Stem Volume:	1.1900 mL	Max. Head Pressure:	4.6800 psia
Pen. Volume:	4.0032 mL	Assembly Weight:	99.4301 g

Hg Parameters

Adv. Contact Angle:	130.000 degrees	Rec. Contact Angle:	130.000 degrees
Hg Surface Tension:	485.000 dynes/cm	Hg Density:	13.5335 g/mL

User Parameters

Param 1:	0.000	Param 2:	0.000	Param 3:	0.000

Low Pressure:

Evacuation Pressure:	50 µmHg
Evacuation Time:	5 mins
Mercury Filling Pressure:	1.33 psia
Equilibration Time:	10 secs

High Pressure:

Equilibration Time:	10 secs

Blank Correction Sample: C:\9500\DATA\BLANKS\000-052.SMP
Blank Correction ID: Pen No:16-0287 Blank Correction 000-052

(From Pressure 0.10 to 60000.00 psia)

Intrusion Data Summary

Total Intrusion Volume =	0.3232	mL/g
Total Pore Area =	25.154	m²/g
Median Pore Diameter (Volume) =	1.2590	µm
Median Pore Diameter (Area) =	0.0137	µm
Average Pore Diameter (4V/A) =	0.0514	µm
Bulk Density at 0.10 psia =	1.3956	g/mL
Apparent (skeletal) Density =	2.5423	g/mL
Porosity =	45.1048	%
Stem Volume Used =	29	%

Pore Structure Summary

Threshold Pressure:	82.16	psia (Calculated)
Characteristic length =	2.2015	µm
Conductivity formation factor =	0.204	
Permeability constant =	0.00442	
Permeability =	4.3780	mdarcy
BET Surface Area =	200.0000	m²/g
Pore shape exponent =	1.00	
Tortuosity factor =	1.720	
Tortuosity =	44.8663	
Percolation Fractal dimension =	2.852	
Backbone Fractal dimension =	2.619	

Calibration ID: Sample 5, C2NM (Pen No:16-0287) 000-071
Operator: Julian Perfect
Submitter: Fan Zhang
File: C:\9500\DATA\BLANKS\000-071.SMP

LP Analysis Time:	14/07/2004 6:22:25PM	Sample Weight:	1.0880 g
HP Analysis Time:	14/07/2004 7:30:12PM	Correction Type:	Blank
Report Time:	14/07/2004 9:25:27PM	Show Neg. Int:	No

Mayer Stowe Summary

Interstitial porosity =	45.1048	%
Breakthrough pressure ratio =	3.6710	

Material Compressibility

Linear Coefficient =	N/A	1/psia
Quadratic Coefficient =	N/A	1/psia²

Calibration ID: Sample 5, C2NM (Pen No:16-0287) 000-071
Operator: Julian Perfect
Submitter: Fan Zhang
File: C:\9500\DATA\BLANKS\000-071.SMP

LP Analysis Time:	14/07/2004 6:22:25PM	Sample Weight:	1.0880 g
HP Analysis Time:	14/07/2004 7:30:12PM	Correction Type:	Blank
Report Time:	14/07/2004 9:25:27PM	Show Neg. Int:	No

Tabular Report

Pressure (psia)	Pore Diameter (µm)	dV/dlogD Pore Volume (mL/g)	dV/dD Pore Volume (mL/g/µm)
1.33	135.9530	0.000×10^{0}	0.000×10^{0}
1.98	91.3567	1.077×10^{-1}	4.171×10^{-4}
2.98	60.7372	1.209×10^{-1}	6.999×10^{-4}
3.98	45.4914	7.430×10^{-2}	6.117×10^{-4}
5.47	33.0445	5.535×10^{-2}	6.173×10^{-4}
6.97	25.9642	4.297×10^{-2}	6.356×10^{-4}
8.46	21.3763	3.624×10^{-2}	6.670×10^{-4}
10.45	17.3040	3.126×10^{-2}	7.045×10^{-4}
12.97	13.9419	3.058×10^{-2}	8.533×10^{-4}
15.96	11.3352	2.916×10^{-2}	1.006×10^{-3}
19.95	9.0639	3.024×10^{-2}	1.293×10^{-3}
22.95	7.8806	3.166×10^{-2}	1.626×10^{-3}
24.95	7.2487	3.502×10^{-2}	2.012×10^{-3}
29.95	6.0385	4.113×10^{-2}	2.696×10^{-3}
36.96	4.8941	1.965×10^{-2}	1.567×10^{-3}
46.30	3.9065	4.155×10^{-2}	4.119×10^{-3}
56.76	3.1863	7.886×10^{-2}	9.690×10^{-3}
71.86	2.5170	1.164×10^{-1}	1.780×10^{-2}
86.76	2.0846	1.639×10^{-1}	3.103×10^{-2}
111.54	1.6215	2.011×10^{-1}	4.738×10^{-2}
136.87	1.3214	1.781×10^{-1}	5.275×10^{-2}
171.48	1.0547	1.354×10^{-1}	4.972×10^{-2}
217.19	0.8327	8.996×10^{-2}	4.159×10^{-2}
266.26	0.6793	6.223×10^{-2}	3.587×10^{-2}
326.06	0.5547	5.266×10^{-2}	3.719×10^{-2}
416.25	0.4345	4.710×10^{-2}	4.157×10^{-2}
517.16	0.3497	4.613×10^{-2}	5.129×10^{-2}
636.26	0.2843	4.372×10^{-2}	6.011×10^{-2}
697.48	0.2593	3.946×10^{-2}	6.310×10^{-2}
796.94	0.2269	4.142×10^{-2}	7.409×10^{-2}
986.98	0.1832	3.620×10^{-2}	7.694×10^{-2}
1197.05	0.1511	3.421×10^{-2}	8.915×10^{-2}

Calibration ID: Sample 5, C2NM (Pen No:16-0287) 000-071
Operator: Julian Perfect
Submitter: Fan Zhang
File: C:\9500\DATA\BLANKS\000-071.SMP

LP Analysis Time:	14/07/2004 6:22:25PM	Sample Weight:	1.0880 g
HP Analysis Time:	14/07/2004 7:30:12PM	Correction Type:	Blank
Report Time:	14/07/2004 9:25:27PM	Show Neg. Int:	No

Tabular Report

Pressure (psia)	Pore Diameter (µm)	dV/dlogD Pore Volume (mL/g)	dV/dD Pore Volume (mL/g/µm)
1296.03	0.1396	3.484×10^{-2}	1.042×10^{-1}
1396.11	0.1295	3.016×10^{-2}	9.740×10^{-2}
1496.34	0.1209	3.199×10^{-2}	1.110×10^{-1}
1595.33	0.1134	3.127×10^{-2}	1.160×10^{-1}
1695.81	0.1067	3.371×10^{-2}	1.331×10^{-1}
1896.83	0.0954	2.857×10^{-2}	1.230×10^{-1}
2045.85	0.0884	3.524×10^{-2}	1.667×10^{-1}
2195.62	0.0824	2.989×10^{-2}	1.521×10^{-1}
2345.46	0.0771	3.206×10^{-2}	1.746×10^{-1}
2494.98	0.0725	3.122×10^{-2}	1.813×10^{-1}
2643.86	0.0684	3.427×10^{-2}	2.113×10^{-1}
2693.89	0.0671	3.648×10^{-2}	2.338×10^{-1}
2843.62	0.0636	3.142×10^{-2}	2.088×10^{-1}
2993.76	0.0604	2.887×10^{-2}	2.023×10^{-1}
3241.95	0.0558	3.566×10^{-2}	2.667×10^{-1}
3491.93	0.0518	3.589×10^{-2}	2.899×10^{-1}
3742.60	0.0483	3.395×10^{-2}	2.946×10^{-1}
3991.21	0.0453	3.978×10^{-2}	3.691×10^{-1}
4239.86	0.0427	4.238×10^{-2}	4.185×10^{-1}
4483.38	0.0403	4.288×10^{-2}	4.489×10^{-1}
4723.87	0.0383	5.189×10^{-2}	5.733×10^{-1}
4982.68	0.0363	5.932×10^{-2}	6.910×10^{-1}
5280.64	0.0343	7.086×10^{-2}	8.726×10^{-1}
5481.39	0.0330	8.759×10^{-2}	1.132×10^{0}
5729.19	0.0316	8.710×10^{-2}	1.172×10^{0}
5977.52	0.0303	1.140×10^{-1}	1.602×10^{0}
6229.13	0.0290	1.274×10^{-1}	1.866×10^{0}
6477.99	0.0279	1.349×10^{-1}	2.057×10^{0}
6727.78	0.0269	1.432×10^{-1}	2.270×10^{0}
6977.11	0.0259	1.532×10^{-1}	2.520×10^{0}
7475.66	0.0242	1.448×10^{-1}	2.510×10^{0}
7973.67	0.0227	1.620×10^{-1}	3.003×10^{0}

Calibration ID: Sample 5, C2NM (Pen No:16-0287) 000-071
Operator: Julian Perfect
Submitter: Fan Zhang
File: C:\9500\DATA\BLANKS\000-071.SMP

LP Analysis Time:	14/07/2004 6:22:25PM	Sample Weight:	1.0880 g
HP Analysis Time:	14/07/2004 7:30:12PM	Correction Type:	Blank
Report Time:	14/07/2004 9:25:27PM	Show Neg. Int:	No

Tabular Report

Pressure (psia)	Pore Diameter (µm)	dV/dlogD Pore Volume (mL/g)	dV/dD Pore Volume (mL/g/µm)
8472.44	0.0213	1.595×10^{-1}	3.147×10^{0}
8971.02	0.0202	1.507×10^{-1}	3.154×10^{0}
9269.00	0.0195	1.574×10^{-1}	3.445×10^{0}
9567.26	0.0189	1.553×10^{-1}	3.511×10^{0}
10018.26	0.0181	1.411×10^{-1}	3.317×10^{0}
10467.29	0.0173	1.442×10^{-1}	3.545×10^{0}
10962.21	0.0165	1.269×10^{-1}	3.264×10^{0}
11456.71	0.0158	1.218×10^{-1}	3.277×10^{0}
11958.30	0.0151	1.274×10^{-1}	3.581×10^{0}
12548.45	0.0144	1.281×10^{-1}	3.769×10^{0}
13046.29	0.0139	1.276×10^{-1}	3.919×10^{0}
13604.37	0.0133	1.308×10^{-1}	4.185×10^{0}
13948.17	0.0130	1.306×10^{-1}	4.321×10^{0}
14290.85	0.0127	1.196×10^{-1}	4.056×10^{0}
14548.51	0.0124	1.515×10^{-1}	5.244×10^{0}
14933.85	0.0121	1.131×10^{-1}	4.002×10^{0}
15397.27	0.0117	1.194×10^{-1}	4.346×10^{0}
15746.97	0.0115	1.281×10^{-1}	4.790×10^{0}
16143.92	0.0112	1.227×10^{-1}	4.696×10^{0}
16580.03	0.0109	1.260×10^{-1}	4.949×10^{0}
16939.43	0.0107	1.273×10^{-1}	5.123×10^{0}
17296.68	0.0105	1.220×10^{-1}	5.016×10^{0}
17636.84	0.0103	1.281×10^{-1}	5.371×10^{0}
18037.85	0.0100	1.161×10^{-1}	4.972×10^{0}
18388.38	0.0098	1.177×10^{-1}	5.148×10^{0}
18732.38	0.0097	1.300×10^{-1}	5.793×10^{0}
19129.25	0.0095	1.099×10^{-1}	4.995×10^{0}
19732.19	0.0092	1.049×10^{-1}	4.895×10^{0}
20245.68	0.0089	1.035×10^{-1}	4.969×10^{0}
20762.14	0.0087	9.480×10^{-2}	4.667×10^{0}
21155.23	0.0085	9.664×10^{-2}	4.863×10^{0}
21619.22	0.0084	8.532×10^{-2}	4.381×10^{0}

Calibration ID: Sample 5, C2NM (Pen No:16-0287) 000-071
Operator: Julian Perfect
Submitter: Fan Zhang
File: C:\9500\DATA\BLANKS\000-071.SMP

LP Analysis Time:	14/07/2004 6:22:25PM	Sample Weight:	1.0880 g
HP Analysis Time:	14/07/2004 7:30:12PM	Correction Type:	Blank
Report Time:	14/07/2004 9:25:27PM	Show Neg. Int:	No

Tabular Report

Pressure (psia)	Pore Diameter (μm)	dV/dlogD Pore Volume (mL/g)	dV/dD Pore Volume (mL/g/μm)
22017.53	0.0082	8.415×10^{-2}	4.408×10^{0}
22625.25	0.0080	6.569×10^{-2}	3.521×10^{0}
23174.04	0.0078	7.016×10^{-2}	3.858×10^{0}
23725.07	0.0076	5.756×10^{-2}	3.241×10^{0}
24079.80	0.0075	6.032×10^{-2}	3.462×10^{0}
24627.31	0.0073	4.713×10^{-2}	2.756×10^{0}
25030.03	0.0072	3.850×10^{-2}	2.296×10^{0}
25427.89	0.0071	4.164×10^{-2}	2.523×10^{0}
25880.16	0.0070	3.159×10^{-2}	1.946×10^{0}
26429.28	0.0068	3.122×10^{-2}	1.961×10^{0}
26931.06	0.0067	2.974×10^{-2}	1.905×10^{0}
27383.71	0.0066	0.000×10^{0}	0.000×10^{0}
27785.16	0.0065	2.249×10^{-2}	1.490×10^{0}
28231.83	0.0064	2.323×10^{-2}	1.562×10^{0}
28983.87	0.0062	1.005×10^{-2}	6.903×10^{-1}
29485.95	0.0061	0.000×10^{0}	0.000×10^{0}
29986.10	0.0060	0.000×10^{0}	0.000×10^{0}
30435.57	0.0059	0.000×10^{0}	0.000×10^{0}
30887.45	0.0059	0.000×10^{0}	0.000×10^{0}
31288.50	0.0058	0.000×10^{0}	0.000×10^{0}
31786.93	0.0057	0.000×10^{0}	0.000×10^{0}
32338.14	0.0056	0.000×10^{0}	0.000×10^{0}
32884.79	0.0055	0.000×10^{0}	0.000×10^{0}
33484.77	0.0054	0.000×10^{0}	0.000×10^{0}
33987.09	0.0053	0.000×10^{0}	0.000×10^{0}
34636.86	0.0052	0.000×10^{0}	0.000×10^{0}
35475.14	0.0051	0.000×10^{0}	0.000×10^{0}
36180.19	0.0050	0.000×10^{0}	0.000×10^{0}
36982.53	0.0049	0.000×10^{0}	0.000×10^{0}
37630.34	0.0048	0.000×10^{0}	0.000×10^{0}
38423.10	0.0047	0.000×10^{0}	0.000×10^{0}
39160.62	0.0046	0.000×10^{0}	0.000×10^{0}

Calibration ID: Sample 5, C2NM (Pen No:16-0287) 000-071
Operator: Julian Perfect
Submitter: Fan Zhang
File: C:\9500\DATA\BLANKS\000-071.SMP

LP Analysis Time:	14/07/2004 6:22:25PM	Sample Weight:	1.0880 g
HP Analysis Time:	14/07/2004 7:30:12PM	Correction Type:	Blank
Report Time:	14/07/2004 9:25:27PM	Show Neg. Int:	No

Tabular Report

Pressure (psia)	Pore Diameter (µm)	dV/dlogD Pore Volume (mL/g)	dV/dD Pore Volume (mL/g/µm)
39974.62	0.0045	0.000×10^0	0.000×10^0
40469.77	0.0045	0.000×10^0	0.000×10^0
40968.57	0.0044	0.000×10^0	0.000×10^0
42397.54	0.0043	0.000×10^0	0.000×10^0
43224.79	0.0042	0.000×10^0	0.000×10^0
43965.14	0.0041	0.000×10^0	0.000×10^0
44969.03	0.0040	0.000×10^0	0.000×10^0
46467.85	0.0039	0.000×10^0	0.000×10^0
47966.36	0.0038	0.000×10^0	0.000×10^0
49464.77	0.0037	0.000×10^0	0.000×10^0
50161.54	0.0036	0.000×10^0	0.000×10^0
52956.31	0.0034	0.000×10^0	0.000×10^0
54454.44	0.0033	0.000×10^0	0.000×10^0
55951.17	0.0032	0.000×10^0	0.000×10^0
57945.84	0.0031	0.000×10^0	0.000×10^0
59939.00	0.0030	0.000×10^0	0.000×10^0

micromeritics

Dept of Chemical Engineering, UCL

AutoPore IV 9500 V1.03 Serial: 201 Port: 1/1 Page 8

Calibration ID: Sample 5, C2NM (Pen No:16-0287) 000-071
Operator: Julian Perfect
Submitter: Fan Zhang
File: C:\9500\DATA\BLANKS\000-071.SMP

LP Analysis Time:	14/07/2004 6:22:25PM	Sample Weight:	1.0880 g
HP Analysis Time:	14/07/2004 7:30:12PM	Correction Type:	Blank
Report Time:	14/07/2004 9:25:27PM	Show Neg. Int:	No

Cumulative Intrusion vs Pore size

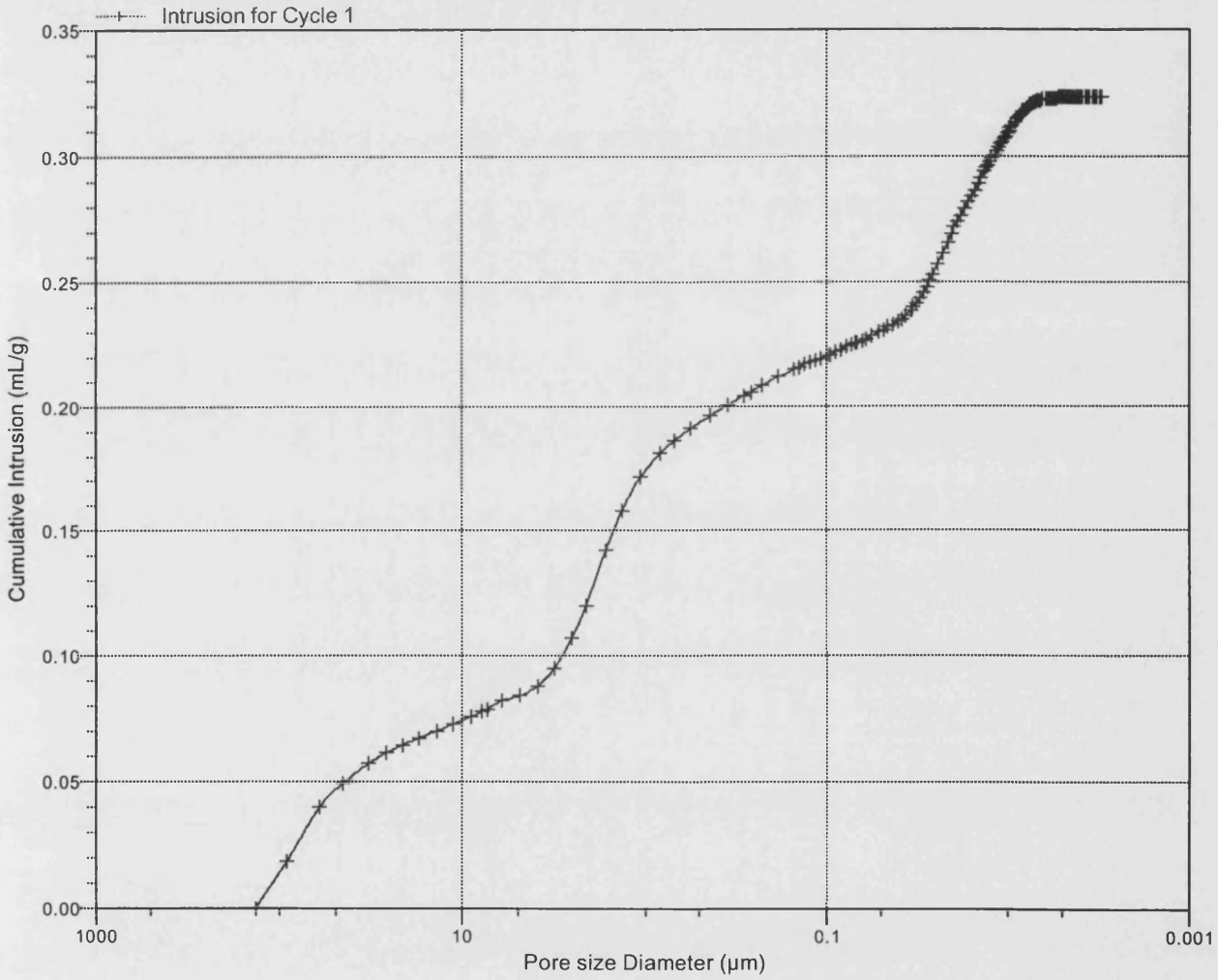

micromeritics

Dept of Chemical Engineering, UCL

AutoPore IV 9500 V1.03 Serial: 201 Port: 1/1 Page 9

Calibration ID: Sample 5, C2NM (Pen No:16-0287) 000-071
Operator: Julian Perfect
Submitter: Fan Zhang
File: C:\9500\DATA\BLANKS\000-071.SMP

LP Analysis Time:	14/07/2004 6:22:25PM	Sample Weight:	1.0880 g
HP Analysis Time:	14/07/2004 7:30:12PM	Correction Type:	Blank
Report Time:	14/07/2004 9:25:27PM	Show Neg. Int:	No

Incremental Intrusion vs Pressure

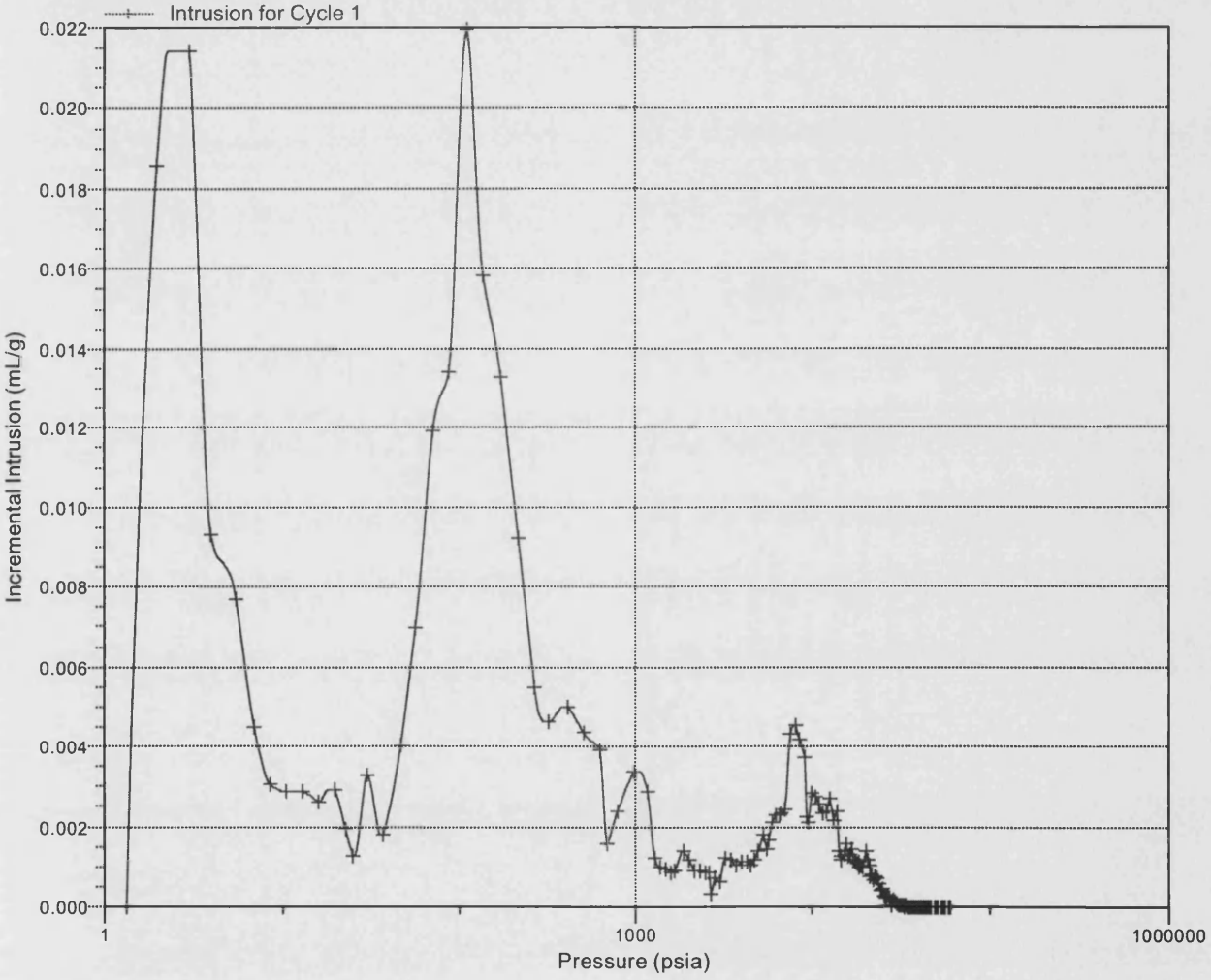

micromeritics

Dept of Chemical Engineering, UCL

AutoPore IV 9500 V1.03 Serial: 201 Port: 1/1 Page 10

Calibration ID: Sample 5, C2NM (Pen No:16-0287) 000-071
Operator: Julian Perfect
Submitter: Fan Zhang
File: C:\9500\DATA\BLANKS\000-071.SMP

LP Analysis Time:	14/07/2004 6:22:25PM	Sample Weight:	1.0880 g
HP Analysis Time:	14/07/2004 7:30:12PM	Correction Type:	Blank
Report Time:	14/07/2004 9:25:27PM	Show Neg. Int:	No

Differential Intrusion vs Pore size

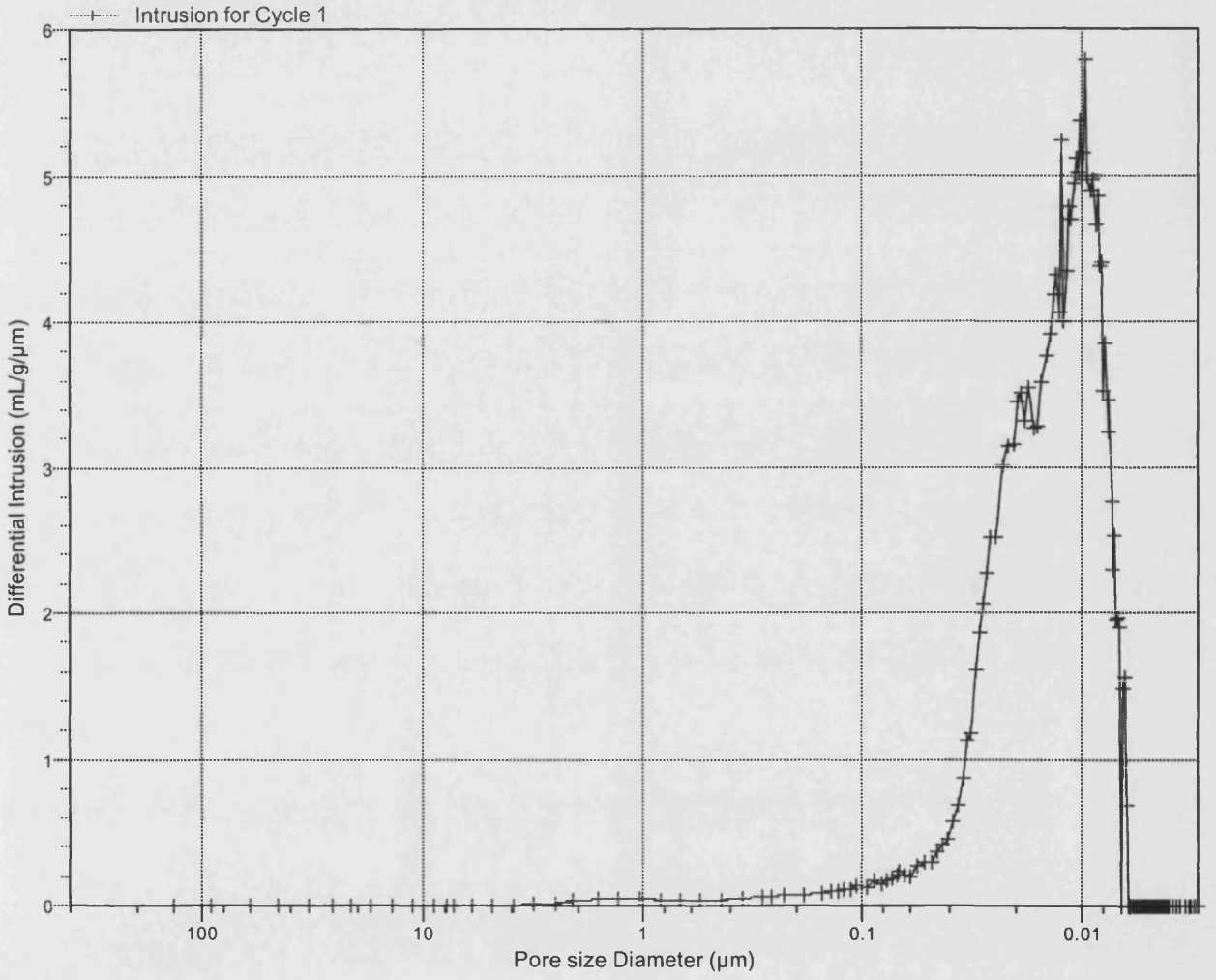

micromeritics

Dept of Chemical Engineering, UCL

AutoPore IV 9500 V1.03 Serial: 201 Port: 1/1 Page 11

Calibration ID: Sample 5, C2NM (Pen No:16-0287) 000-071
Operator: Julian Perfect
Submitter: Fan Zhang
File: C:\9500\DATA\BLANKS\000-071.SMP

LP Analysis Time:	14/07/2004 6:22:25PM	Sample Weight:	1.0880 g
HP Analysis Time:	14/07/2004 7:30:12PM	Correction Type:	Blank
Report Time:	14/07/2004 9:25:27PM	Show Neg. Int:	No

Log Differential Intrusion vs Pore size

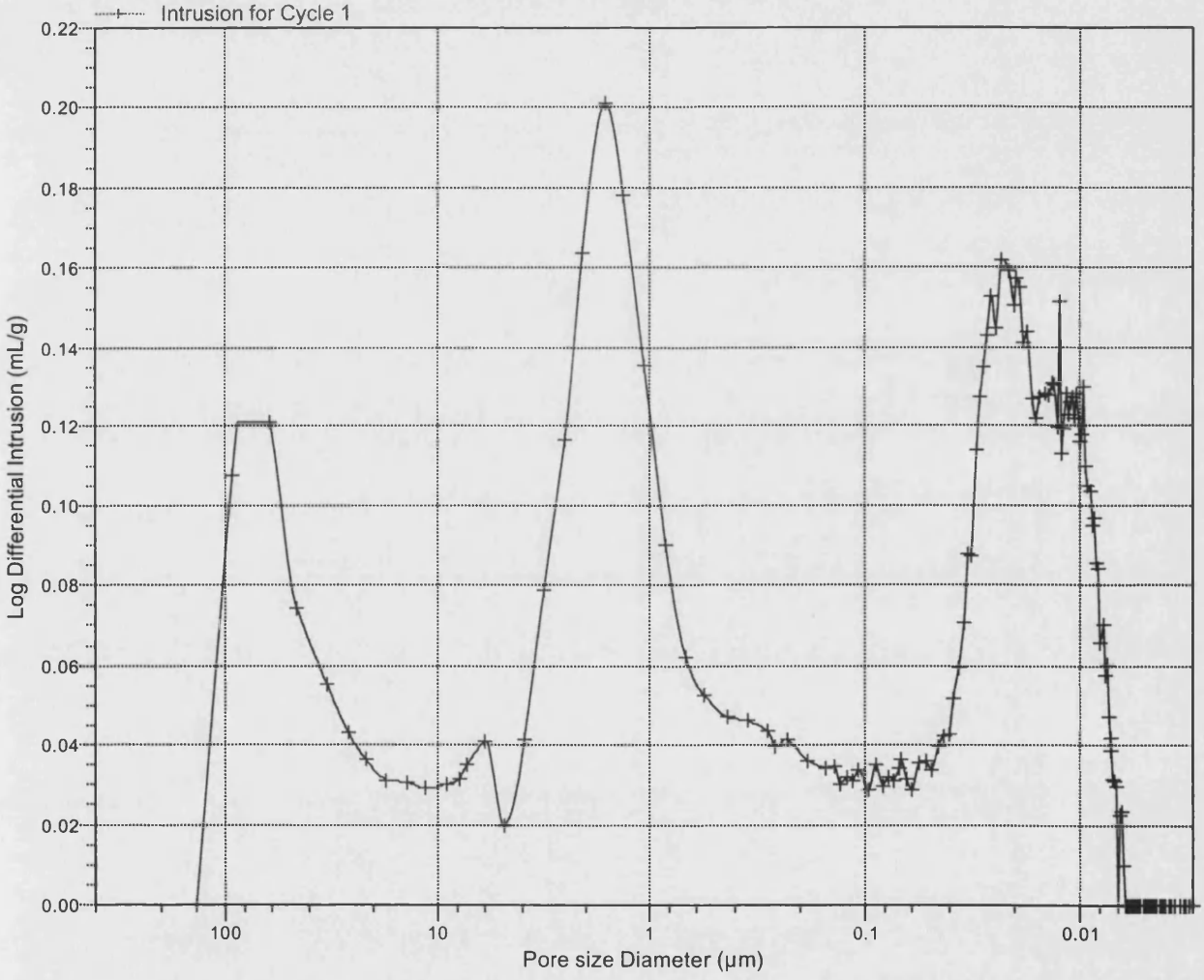

FULL ISOTHERM FOR SAMPLE 5, C2NM

ASAP 2010 V5.01 H Unit 1 Serial # 2727 Page 1

Sample: Sample 5, C2NM
Operator: Julian Perfect
Submitter: Fan Zhang
File Name: C:\ASAP2010\DATA\000-063.SMP

Started: 7/14/04 5:17:58AM Analysis Adsorptive: N2
Completed: 7/14/04 6:03:34PM Analysis Bath: 77.35 K
Report Time: 7/14/04 6:52:11PM Thermal Correction: No
Sample Weight: 1.4002 g Smoothed Pressures: No
Warm Freespace: 16.8841 cm^3 Cold Freespace: 50.5310 cm^3
MEASURED
Equil. Interval: 10 secs Low Pressure Dose: None
Comments:
Bulb type sample holder used with stopper and filler rod. Sample degassed, using manual mode, for ~29 hours (~12 hours @ 90C, 4 hours @ 120C and 14 hours @ 350C)

Analysis Log

Relative Pressure	Pressure (mmHg)	Vol Adsorbed (cm^3/g STP)	Elapsed Time (HR:MN)	Saturation Press.(mmHg)
			02:24	763.23969
0.144395710	110.19265	10.4026	02:41	
0.161784312	123.45927	10.5938	02:44	
0.182922536	139.58533	10.8127	02:48	
0.201653450	153.87468	11.0001	02:51	
0.221024708	168.65192	11.1892	02:54	
0.249873016	190.65964	11.4690	02:57	
0.300439437	229.23730	11.9559	03:00	
0.354963715	270.83051	12.4919	03:04	
0.400177721	305.31757	12.9598	03:08	
0.451550720	344.50116	13.5289	03:12	
0.500250078	381.64236	14.1279	03:16	
0.550700395	420.11325	14.8344	03:21	
0.600673248	458.21664	15.7032	03:26	
0.649200608	495.21417	16.7967	03:31	
0.699364011	533.45197	18.2870	03:37	
0.740281683	564.62909	19.8763	03:44	
0.771382593	588.31549	21.4280	03:51	
0.799670603	609.84869	23.2725	03:59	
0.820628132	625.78894	25.0603	04:07	
0.840868939	641.16962	27.2789	04:17	
0.859218750	655.10590	29.8703	04:27	
			04:29	762.43073
0.874145461	666.43213	32.3761	04:39	
0.887017413	676.20160	34.9590	04:49	
0.899972219	686.02850	37.9311	05:00	
0.910991615	694.37878	40.7585	05:11	
0.921119522	702.04840	43.6172	05:22	
0.929256159	708.19934	46.2010	05:33	
0.936766514	713.87213	48.7510	05:44	
0.943951862	719.29645	51.2783	05:55	

FULL ISOTHERM FOR SAMPLE 5, C2NM

Sample: Sample 5, C2NM
Operator: Julian Perfect
Submitter: Fan Zhang
File Name: C:\ASAP2010\DATA\000-063.SMP

Started: 7/14/04 5:17:58AM
Completed: 7/14/04 6:03:34PM
Report Time: 7/14/04 6:52:11PM
Sample Weight: 1.4002 g
Warm Freespace: 16.8841 cm³
MEASURED
Equil. Interval: 10 secs
Analysis Adsorptive: N2
Analysis Bath: 77.35 K
Thermal Correction: No
Smoothed Pressures: No
Cold Freespace: 50.5310 cm³
Low Pressure Dose: None

Comments:
Bulb type sample holder used with stopper and filler rod. Sample degassed, using manual mode, for ~29 hours (~12 hours @ 90C, 4 hours @ 120C and 14 hours @ 350C)

Analysis Log

Relative Pressure	Pressure (mmHg)	Vol Adsorbed (cm³/g STP)	Elapsed Time (HR:MN)	Saturation Press.(mmHg)
0.950020871	723.87408	53.6697	06:05	
0.955672777	728.12860	56.1094	06:16	
0.960761321	731.95331	58.5074	06:27	
0.965887187	735.81067	60.7781	06:37	
			06:39	761.78784
0.969357217	738.40234	62.6863	06:48	
0.973445645	741.47430	64.5725	06:57	
0.975871825	743.27985	66.0332	07:06	
0.979063453	745.66815	67.6926	07:15	
0.982263300	748.06244	69.1090	07:24	
0.983811579	749.20825	69.9032	07:31	
0.986821341	751.45734	71.2524	07:40	
0.988226958	752.49902	71.7783	07:46	
0.989249975	753.25409	72.2299	07:51	
0.990801835	754.40698	72.8443	07:57	
0.982511796	748.06635	72.1048	08:03	
0.977145047	743.95184	71.0965	08:09	
0.972101941	740.07465	70.1513	08:17	
0.972323626	740.22931	70.0680	08:20	
0.966950026	736.10565	68.9868	08:27	
0.962063138	732.34821	67.7546	08:35	
0.959657366	730.48438	67.0105	08:42	
			08:44	761.18323
0,954939121	726.84131	65.3292	08:53	
0.949897832	722.95740	63.2913	09:03	
0.944860380	719.07690	60.9671	09:13	
0.938816070	714.42145	58.4257	09:25	
0.925981955	704.55914	53.4662	09:46	
0.919527033	699.59338	51.1523	09:58	
0.910300274	692.52417	48.2867	10:09	
0.890305034	677.22479	43.2174	10:29	

FULL ISOTHERM FOR SAMPLE 5, C2NM

Sample: Sample 5, C2NM
Operator: Julian Perfect
Submitter: Fan Zhang
File Name: C:\ASAP2010\DATA\000-063.SMP

Started: 7/14/04 5:17:58AM
Completed: 7/14/04 6:03:34PM
Report Time: 7/14/04 6:52:11PM
Sample Weight: 1.4002 g
Warm Freespace: 16.8841 cm³
MEASURED
Equil. Interval: 10 secs
Analysis Adsorptive: N2
Analysis Bath: 77.35 K
Thermal Correction: No
Smoothed Pressures: No
Cold Freespace: 50.5310 cm³
Low Pressure Dose: None

Comments:
Bulb type sample holder used with stopper and filler rod. Sample degassed, using manual mode, for ~29 hours (~12 hours @ 90C, 4 hours @ 120C and 14 hours @ 350C)

Analysis Log

Relative Pressure	Pressure (mmHg)	Vol Adsorbed (cm³/g STP)	Elapsed Time (HR:MN)	Saturation Press.(mmHg)
0.879627848	669.05536	40.8739	10:40	
0.865503998	658.26996	37.9875	10:50	
			10:52	760.55273
0.846673225	643.93964	34.5451	11:03	
0.825460866	627.80652	31.0824	11:14	
0.803760580	611.30231	27.9059	11:25	
0.772981895	587.89349	24.2354	11:35	
0.736828877	560.39722	21.4201	11:44	
0.704520686	535.82513	19.8153	11:51	
0.638886401	485.90680	17.8246	12:00	
0.594970458	452.50641	16.9470	12:05	
0.555545805	422.52188	16.3207	12:09	
0.503871351	383.22073	15.4480	12:18	
0.449305170	341.72028	13.3023	12:24	
0.397016996	301.95236	12.6778	12:28	
0.341698623	259.87982	12.1025	12:32	
0.301187651	229.06909	11.6988	12:35	
0.253285779	192.63719	11.2342	12:39	
0.202505823	154.01636	10.7378	12:43	
0.141046749	107.27349	10.0931	12:47	

FULL ISOTHERM FOR SAMPLE 5, C2NM

Sample: Sample 5, C2NM
Operator: Julian Perfect
Submitter: Fan Zhang
File Name: C:\ASAP2010\DATA\000-063.SMP

Started: 7/14/04 5:17:58AM
Completed: 7/14/04 6:03:34PM
Report Time: 7/14/04 6:52:11PM
Sample Weight: 1.4002 g
Warm Freespace: 16.8841 cm³
MEASURED
Equil. Interval: 10 secs
Analysis Adsorptive: N2
Analysis Bath: 77.35 K
Thermal Correction: No
Smoothed Pressures: No
Cold Freespace: 50.5310 cm³
Low Pressure Dose: None

Comments:
Bulb type sample holder used with stopper and filler rod. Sample degassed, using manual mode, for ~29 hours (~12 hours @ 90C, 4 hours @ 120C and 14 hours @ 350C)

Summary Report

Area

Single Point Surface Area at P/Po 0.24987302 :	37.4515	m²/g
BET Surface Area:	36.2713	m²/g
Langmuir Surface Area:	58.0319	m²/g
Micropore Area:	12.3809	m²/g
External Surface Area:	23.8904	m²/g
BJH Adsorption Cumulative Surface Area of pores between 17.000000 and 3000.000000 A Diameter:	28.4081	m²/g
BJH Desorption Cumulative Surface Area of pores between 17.000000 and 3000.000000 A Diameter:	33.3395	m²/g

Volume

Single Point Desorption Total Pore Volume of pores less than 1126.7370 A Diameter at P/Po 0.98251180:	0.111532	cm³/g
Micropore Volume:	0.006546	cm³/g
BJH Adsorption Cumulative Pore Volume of pores between 17.000000 and 3000.000000 A Diameter:	0.109389	cm³/g
BJH Desorption Cumulative Pore Volume of pores between 17.000000 and 3000.000000 A Diameter:	0.112217	cm³/g

Pore Size

FULL ISOTHERM FOR SAMPLE 5, C2NM

Sample: Sample 5, C2NM
Operator: Julian Perfect
Submitter: Fan Zhang
File Name: C:\ASAP2010\DATA\000-063.SMP

Started: 7/14/04 5:17:58AM
Completed: 7/14/04 6:03:34PM
Report Time: 7/14/04 6:52:11PM
Sample Weight: 1.4002 g
Warm Freespace: 16.8841 cm³
MEASURED
Equil. Interval: 10 secs
Analysis Adsorptive: N2
Analysis Bath: 77.35 K
Thermal Correction: No
Smoothed Pressures: No
Cold Freespace: 50.5310 cm³
Low Pressure Dose: None

Comments:
Bulb type sample holder used with stopper and filler rod. Sample degassed, using manual mode, for ~29 hours (~12 hours @ 90C, 4 hours @ 120C and 14 hours @ 350C)

Summary Report

Desorption Average Pore Diameter (4V/A by BET):	122.9973	A
BJH Adsorption Average Pore Diameter (4V/A):	154.0256	A
BJH Desorption Average Pore Diameter (4V/A):	134.6352	A

micromeritics

Dept of Chemical Engineering, UCL

AutoPore IV 9500 V1.03 Serial: 201 Port: 1/1

Calibration ID: Sample 6, C2HT (UCL?) (Pen No:16-0289) 000-072
Operator: Julian Perfect
Submitter: Fan Zhang
File: C:\9500\DATA\BLANKS\000-072.SMP

LP Analysis Time:	14/07/2004 4:59:20PM	Sample Weight:	0.8386 g
HP Analysis Time:	14/07/2004 6:12:21PM	Correction Type:	Blank
Report Time:	14/07/2004 9:26:44PM	Show Neg. Int:	No

Summary Report

Penetrometer parameters

Penetrometer:	#s/n - (16) 3 Bulb, 1.190 Stem, Powder		
Pen. Constant:	20.994 µL/pF	Pen. Weight:	54.8372 g
Stem Volume:	1.1900 mL	Max. Head Pressure:	4.6800 psia
Pen. Volume:	3.9104 mL	Assembly Weight:	101.0623 g

Hg Parameters

Adv. Contact Angle:	130.000 degrees	Rec. Contact Angle:	130.000 degrees
Hg Surface Tension:	485.000 dynes/cm	Hg Density:	13.5335 g/mL

User Parameters

Param 1:	0.000	Param 2:	0.000	Param 3:	0.000

Low Pressure:

Evacuation Pressure:	50 µmHg
Evacuation Time:	5 mins
Mercury Filling Pressure:	1.33 psia
Equilibration Time:	10 secs

High Pressure:

Equilibration Time:	10 secs

Blank Correction Sample: C:\9500\DATA\BLANKS\000-053.SMP
Blank Correction ID: Pen No:16-0289 Blank Correction 000-053

(From Pressure 0.10 to 60000.00 psia)

Intrusion Data Summary

Total Intrusion Volume =	0.2710	mL/g
Total Pore Area =	24.120	m²/g
Median Pore Diameter (Volume) =	0.8622	µm
Median Pore Diameter (Area) =	0.0131	µm
Average Pore Diameter (4V/A) =	0.0449	µm
Bulk Density at 0.10 psia =	1.5061	g/mL
Apparent (skeletal) Density =	2.5451	g/mL
Porosity =	40.8179	%
Stem Volume Used =	19	% ****

Pore Structure Summary

Threshold Pressure:	88.74	psia (Calculated)
Characteristic length =	2.0382	µm
Conductivity formation factor =	0.164	
Permeability constant =	0.00442	
Permeability =	3.0171	mdarcy
BET Surface Area =	200.0000	m²/g
Pore shape exponent =	1.00	
Tortuosity factor =	1.769	
Tortuosity =	35.3296	
Percolation Fractal dimension =	2.845	
Backbone Fractal dimension =	2.626	

Calibration ID: Sample 6, C2HT (UCL?) (Pen No:16-0289) 000-072
Operator: Julian Perfect
Submitter: Fan Zhang
File: C:\9500\DATA\BLANKS\000-072.SMP

LP Analysis Time:	14/07/2004 4:59:20PM	Sample Weight:	0.8386 g
HP Analysis Time:	14/07/2004 6:12:21PM	Correction Type:	Blank
Report Time:	14/07/2004 9:26:44PM	Show Neg. Int:	No

Mayer Stowe Summary

Interstitial porosity =	40.8179	%
Breakthrough pressure ratio =	4.3920	

Material Compressibility

Linear Coefficient =	N/A	1/psia
Quadratic Coefficient =	N/A	1/psia^2

Calibration ID: Sample 6, C2HT (UCL?) (Pen No:16-0289) 000-072
Operator: Julian Perfect
Submitter: Fan Zhang
File: C:\9500\DATA\BLANKS\000-072.SMP

LP Analysis Time:	14/07/2004 4:59:20PM	Sample Weight:	0.8386 g
HP Analysis Time:	14/07/2004 6:12:21PM	Correction Type:	Blank
Report Time:	14/07/2004 9:26:44PM	Show Neg. Int:	No

Tabular Report

Pressure (psia)	Pore Diameter (µm)	dV/dlogD Pore Volume (mL/g)	dV/dD Pore Volume (mL/g/µm)
1.33	135.6808	0.000×10^{0}	0.000×10^{0}
1.98	91.2953	4.260×10^{-2}	1.652×10^{-4}
2.98	60.7502	4.183×10^{-2}	2.423×10^{-4}
3.97	45.5166	3.423×10^{-2}	2.817×10^{-4}
5.47	33.0436	2.739×10^{-2}	3.054×10^{-4}
6.97	25.9674	2.469×10^{-2}	3.651×10^{-4}
8.46	21.3666	2.171×10^{-2}	3.997×10^{-4}
10.45	17.3016	2.198×10^{-2}	4.955×10^{-4}
12.97	13.9448	2.135×10^{-2}	5.957×10^{-4}
15.96	11.3354	2.012×10^{-2}	6.936×10^{-4}
19.95	9.0643	2.029×10^{-2}	8.676×10^{-4}
22.95	7.8803	2.016×10^{-2}	1.035×10^{-3}
24.95	7.2486	2.252×10^{-2}	1.294×10^{-3}
29.95	6.0388	3.497×10^{-2}	2.292×10^{-3}
37.15	4.8691	2.793×10^{-2}	2.233×10^{-3}
46.78	3.8666	5.076×10^{-2}	5.070×10^{-3}
56.61	3.1948	8.213×10^{-2}	1.013×10^{-2}
71.25	2.5384	1.110×10^{-1}	1.689×10^{-2}
86.68	2.0865	1.822×10^{-1}	3.432×10^{-2}
111.52	1.6218	1.933×10^{-1}	4.552×10^{-2}
137.21	1.3181	1.569×10^{-1}	4.651×10^{-2}
171.34	1.0556	1.224×10^{-1}	4.498×10^{-2}
216.07	0.8371	8.392×10^{-2}	3.869×10^{-2}
266.57	0.6785	6.257×10^{-2}	3.599×10^{-2}
325.90	0.5550	5.319×10^{-2}	3.758×10^{-2}
417.11	0.4336	5.020×10^{-2}	4.433×10^{-2}
516.52	0.3502	4.782×10^{-2}	5.320×10^{-2}
637.08	0.2839	4.509×10^{-2}	6.199×10^{-2}
697.43	0.2593	4.580×10^{-2}	7.329×10^{-2}
796.92	0.2270	3.606×10^{-2}	6.450×10^{-2}
988.12	0.1830	3.601×10^{-2}	7.658×10^{-2}
1196.67	0.1511	3.298×10^{-2}	8.599×10^{-2}

Calibration ID: Sample 6, C2HT (UCL?) (Pen No:16-0289) 000-072
Operator: Julian Perfect
Submitter: Fan Zhang
File: C:\9500\DATA\BLANKS\000-072.SMP

LP Analysis Time:	14/07/2004 4:59:20PM	Sample Weight:	0.8386 g
HP Analysis Time:	14/07/2004 6:12:21PM	Correction Type:	Blank
Report Time:	14/07/2004 9:26:44PM	Show Neg. Int:	No

Tabular Report

Pressure (psia)	Pore Diameter (μm)	dV/dlogD Pore Volume (mL/g)	dV/dD Pore Volume (mL/g/μm)
1296.04	0.1396	3.606×10^{-2}	1.078×10^{-1}
1396.76	0.1295	3.350×10^{-2}	1.082×10^{-1}
1496.87	0.1208	3.320×10^{-2}	1.152×10^{-1}
1596.56	0.1133	3.059×10^{-2}	1.135×10^{-1}
1696.81	0.1066	3.281×10^{-2}	1.296×10^{-1}
1895.55	0.0954	2.719×10^{-2}	1.170×10^{-1}
2045.03	0.0884	2.920×10^{-2}	1.380×10^{-1}
2194.31	0.0824	3.127×10^{-2}	1.590×10^{-1}
2345.17	0.0771	2.849×10^{-2}	1.552×10^{-1}
2493.64	0.0725	3.336×10^{-2}	1.937×10^{-1}
2644.03	0.0684	2.744×10^{-2}	1.692×10^{-1}
2693.11	0.0672	4.562×10^{-2}	2.923×10^{-1}
2844.15	0.0636	3.105×10^{-2}	2.064×10^{-1}
2993.19	0.0604	2.547×10^{-2}	1.784×10^{-1}
3242.62	0.0558	3.151×10^{-2}	2.356×10^{-1}
3493.50	0.0518	2.835×10^{-2}	2.291×10^{-1}
3741.07	0.0483	3.192×10^{-2}	2.771×10^{-1}
3990.69	0.0453	3.453×10^{-2}	3.203×10^{-1}
4240.24	0.0427	3.509×10^{-2}	3.466×10^{-1}
4484.90	0.0403	4.579×10^{-2}	4.794×10^{-1}
4724.56	0.0383	4.223×10^{-2}	4.667×10^{-1}
4984.28	0.0363	4.777×10^{-2}	5.565×10^{-1}
5284.39	0.0342	5.844×10^{-2}	7.201×10^{-1}
5482.90	0.0330	7.206×10^{-2}	9.314×10^{-1}
5730.62	0.0316	7.528×10^{-2}	1.013×10^{0}
5980.52	0.0302	9.045×10^{-2}	1.271×10^{0}
6229.17	0.0290	1.008×10^{-1}	1.477×10^{0}
6477.63	0.0279	1.151×10^{-1}	1.756×10^{0}
6728.27	0.0269	1.109×10^{-1}	1.758×10^{0}
6976.83	0.0259	1.298×10^{-1}	2.135×10^{0}
7474.69	0.0242	1.265×10^{-1}	2.192×10^{0}
7976.16	0.0227	1.312×10^{-1}	2.432×10^{0}

Calibration ID: Sample 6, C2HT (UCL?) (Pen No:16-0289) 000-072
Operator: Julian Perfect
Submitter: Fan Zhang
File: C:\9500\DATA\BLANKS\000-072.SMP

LP Analysis Time:	14/07/2004 4:59:20PM	Sample Weight:	0.8386 g
HP Analysis Time:	14/07/2004 6:12:21PM	Correction Type:	Blank
Report Time:	14/07/2004 9:26:44PM	Show Neg. Int:	No

Tabular Report

Pressure (psia)	Pore Diameter (μm)	dV/dlogD Pore Volume (mL/g)	dV/dD Pore Volume (mL/g/μm)
8474.62	0.0213	1.432×10^{-1}	2.826×10^{0}
8974.11	0.0202	1.388×10^{-1}	2.905×10^{0}
9269.39	0.0195	1.460×10^{-1}	3.197×10^{0}
9568.64	0.0189	1.346×10^{-1}	3.043×10^{0}
10015.73	0.0181	1.271×10^{-1}	2.987×10^{0}
10464.10	0.0173	1.378×10^{-1}	3.386×10^{0}
10962.42	0.0165	1.256×10^{-1}	3.230×10^{0}
11452.11	0.0158	1.217×10^{-1}	3.275×10^{0}
11954.95	0.0151	1.179×10^{-1}	3.312×10^{0}
12561.33	0.0144	1.225×10^{-1}	3.605×10^{0}
13054.56	0.0139	1.211×10^{-1}	3.722×10^{0}
13607.05	0.0133	1.238×10^{-1}	3.962×10^{0}
13951.02	0.0130	1.187×10^{-1}	3.927×10^{0}
14285.83	0.0127	3.782×10^{-2}	1.282×10^{0}
14540.59	0.0124	1.198×10^{-1}	4.147×10^{0}
14952.98	0.0121	1.089×10^{-1}	3.856×10^{0}
15395.42	0.0117	1.259×10^{-1}	4.588×10^{0}
15752.61	0.0115	1.199×10^{-1}	4.483×10^{0}
16147.66	0.0112	1.144×10^{-1}	4.380×10^{0}
16598.27	0.0109	1.148×10^{-1}	4.512×10^{0}
16943.52	0.0107	1.141×10^{-1}	4.596×10^{0}
17292.78	0.0105	1.211×10^{-1}	4.975×10^{0}
17640.91	0.0103	1.130×10^{-1}	4.738×10^{0}
18038.41	0.0100	1.171×10^{-1}	5.018×10^{0}
18384.39	0.0098	1.385×10^{-1}	6.058×10^{0}
18737.85	0.0097	1.055×10^{-1}	4.703×10^{0}
19140.63	0.0094	1.206×10^{-1}	5.486×10^{0}
19744.35	0.0092	1.014×10^{-1}	4.731×10^{0}
20236.59	0.0089	1.030×10^{-1}	4.946×10^{0}
20757.46	0.0087	5.972×10^{-2}	2.939×10^{0}
21156.54	0.0085	9.606×10^{-2}	4.834×10^{0}
21614.53	0.0084	9.666×10^{-2}	4.963×10^{0}

Calibration ID: Sample 6, C2HT (UCL?) (Pen No:16-0289) 000-072
Operator: Julian Perfect
Submitter: Fan Zhang
File: C:\9500\DATA\BLANKS\000-072.SMP

LP Analysis Time:	14/07/2004 4:59:20PM	Sample Weight:	0.8386 g
HP Analysis Time:	14/07/2004 6:12:21PM	Correction Type:	Blank
Report Time:	14/07/2004 9:26:44PM	Show Neg. Int:	No

Tabular Report

Pressure (psia)	Pore Diameter (μm)	dV/dlogD Pore Volume (mL/g)	dV/dD Pore Volume (mL/g/μm)
22020.19	0.0082	8.510×10^{-2}	4.458×10^{0}
22623.33	0.0080	7.883×10^{-2}	4.225×10^{0}
23177.33	0.0078	7.666×10^{-2}	4.215×10^{0}
23727.94	0.0076	7.302×10^{-2}	4.112×10^{0}
24077.79	0.0075	5.055×10^{-2}	2.901×10^{0}
24630.61	0.0073	5.944×10^{-2}	3.476×10^{0}
25030.76	0.0072	5.465×10^{-2}	3.258×10^{0}
25434.18	0.0071	5.341×10^{-2}	3.236×10^{0}
25881.63	0.0070	3.075×10^{-2}	1.894×10^{0}
26430.50	0.0068	3.654×10^{-2}	2.295×10^{0}
26936.07	0.0067	3.553×10^{-2}	2.276×10^{0}
27387.51	0.0066	2.799×10^{-2}	1.825×10^{0}
27783.31	0.0065	3.326×10^{-2}	2.203×10^{0}
28235.34	0.0064	3.429×10^{-2}	2.306×10^{0}
28987.34	0.0062	1.336×10^{-2}	9.179×10^{-1}
29485.03	0.0061	0.000×10^{0}	0.000×10^{0}
29984.65	0.0060	1.716×10^{-2}	1.225×10^{0}
30437.08	0.0059	0.000×10^{0}	0.000×10^{0}
30888.23	0.0059	1.941×10^{-2}	1.429×10^{0}
31287.61	0.0058	0.000×10^{0}	0.000×10^{0}
31786.83	0.0057	1.461×10^{-2}	1.107×10^{0}
32334.76	0.0056	0.000×10^{0}	0.000×10^{0}
32888.05	0.0055	0.000×10^{0}	0.000×10^{0}
33488.60	0.0054	0.000×10^{0}	0.000×10^{0}
33981.59	0.0053	0.000×10^{0}	0.000×10^{0}
34630.82	0.0052	0.000×10^{0}	0.000×10^{0}
35489.41	0.0051	0.000×10^{0}	0.000×10^{0}
36180.54	0.0050	0.000×10^{0}	0.000×10^{0}
36982.38	0.0049	0.000×10^{0}	0.000×10^{0}
37635.52	0.0048	0.000×10^{0}	0.000×10^{0}
38428.62	0.0047	0.000×10^{0}	0.000×10^{0}
39174.00	0.0046	0.000×10^{0}	0.000×10^{0}

Calibration ID: Sample 6, C2HT (UCL?) (Pen No:16-0289) 000-072
Operator: Julian Perfect
Submitter: Fan Zhang
File: C:\9500\DATA\BLANKS\000-072.SMP

LP Analysis Time:	14/07/2004 4:59:20PM	Sample Weight:	0.8386 g
HP Analysis Time:	14/07/2004 6:12:21PM	Correction Type:	Blank
Report Time:	14/07/2004 9:26:44PM	Show Neg. Int:	No

Tabular Report

Pressure (psia)	Pore Diameter (μm)	dV/dlogD Pore Volume (mL/g)	dV/dD Pore Volume (mL/g/μm)
39962.64	0.0045	0.000×10^0	0.000×10^0
40456.53	0.0045	0.000×10^0	0.000×10^0
40974.81	0.0044	0.000×10^0	0.000×10^0
42462.83	0.0043	0.000×10^0	0.000×10^0
43319.02	0.0042	0.000×10^0	0.000×10^0
43969.43	0.0041	0.000×10^0	0.000×10^0
44961.14	0.0040	0.000×10^0	0.000×10^0
46463.38	0.0039	0.000×10^0	0.000×10^0
47965.10	0.0038	0.000×10^0	0.000×10^0
49456.55	0.0037	0.000×10^0	0.000×10^0
50159.25	0.0036	0.000×10^0	0.000×10^0
52956.63	0.0034	0.000×10^0	0.000×10^0
54451.22	0.0033	0.000×10^0	0.000×10^0
55951.15	0.0032	0.000×10^0	0.000×10^0
57941.65	0.0031	0.000×10^0	0.000×10^0
59923.76	0.0030	0.000×10^0	0.000×10^0

micromeritics

Dept of Chemical Engineering, UCL

AutoPore IV 9500 V1.03 Serial: 201 Port: 1/1 Page 8

Calibration ID: Sample 6, C2HT (UCL?) (Pen No:16-0289) 000-072
Operator: Julian Perfect
Submitter: Fan Zhang
File: C:\9500\DATA\BLANKS\000-072.SMP

LP Analysis Time:	14/07/2004 4:59:20PM	Sample Weight:	0.8386 g
HP Analysis Time:	14/07/2004 6:12:21PM	Correction Type:	Blank
Report Time:	14/07/2004 9:26:44PM	Show Neg. Int:	No

Cumulative Intrusion vs Pore size

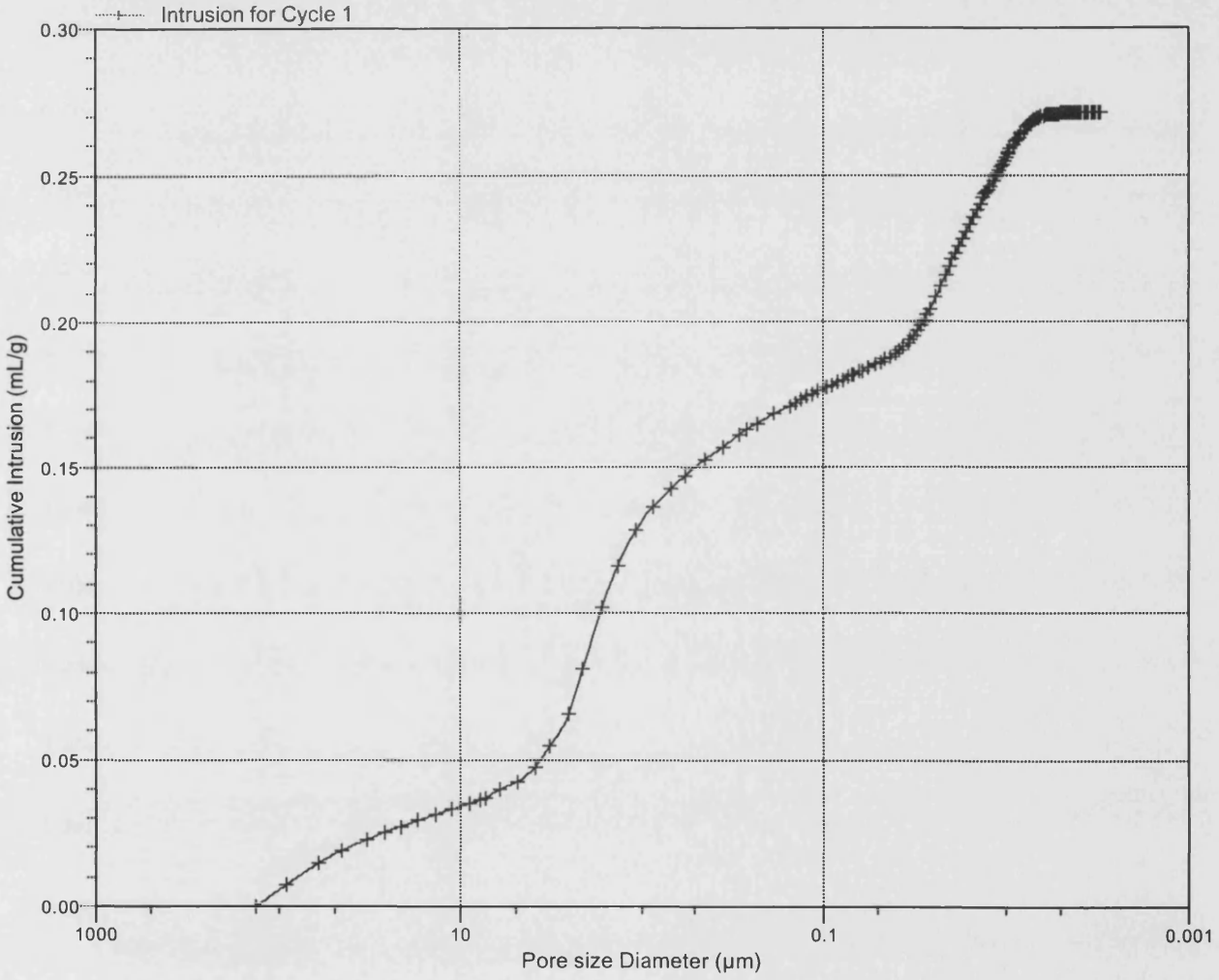

micromeritics

Dept of Chemical Engineering, UCL

AutoPore IV 9500 V1.03 Serial: 201 Port: 1/1 Page 9

Calibration ID: Sample 6, C2HT (UCL?) (Pen No:16-0289) 000-072
Operator: Julian Perfect
Submitter: Fan Zhang
File: C:\9500\DATA\BLANKS\000-072.SMP

LP Analysis Time:	14/07/2004 4:59:20PM	Sample Weight:	0.8386 g
HP Analysis Time:	14/07/2004 6:12:21PM	Correction Type:	Blank
Report Time:	14/07/2004 9:26:44PM	Show Neg. Int:	No

Incremental Intrusion vs Pressure

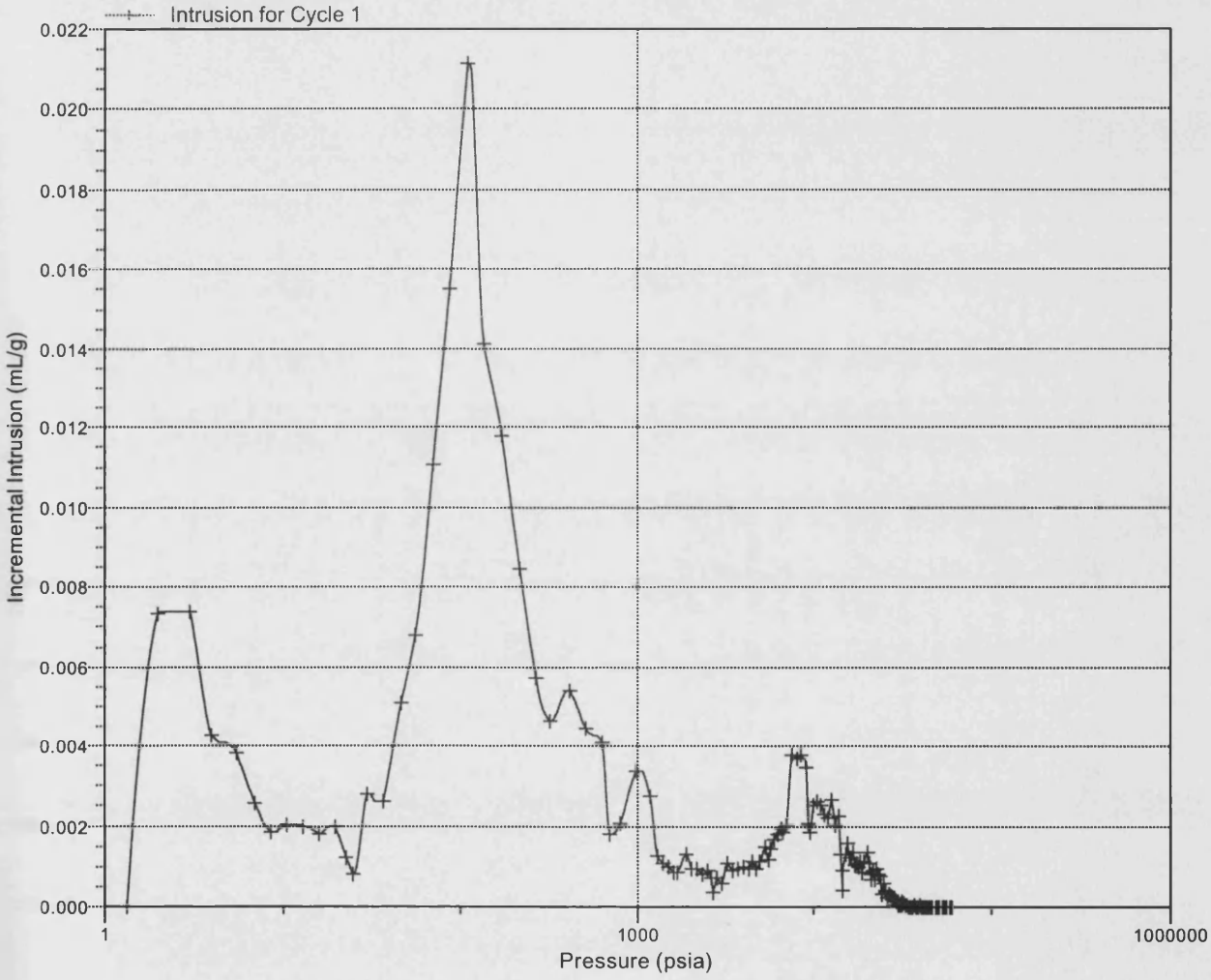

micromeritics

Dept of Chemical Engineering, UCL

AutoPore IV 9500 V1.03 Serial: 201 Port: 1/1 Page 10

Calibration ID: Sample 6, C2HT (UCL?) (Pen No:16-0289) 000-072
Operator: Julian Perfect
Submitter: Fan Zhang
File: C:\9500\DATA\BLANKS\000-072.SMP

LP Analysis Time:	14/07/2004 4:59:20PM	Sample Weight:	0.8386 g
HP Analysis Time:	14/07/2004 6:12:21PM	Correction Type:	Blank
Report Time:	14/07/2004 9:26:44PM	Show Neg. Int:	No

Differential Intrusion vs Pore size

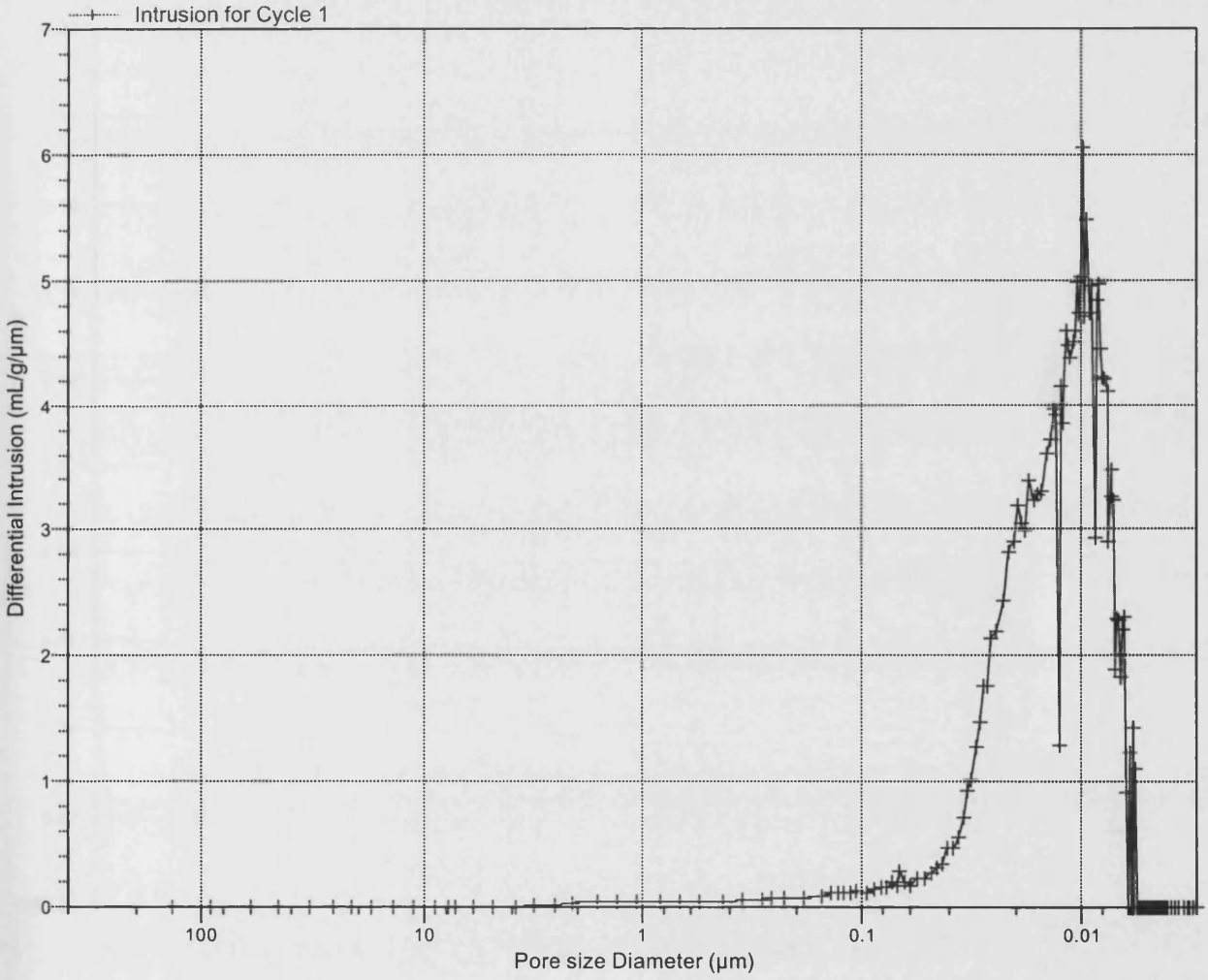

micromeritics

Dept of Chemical Engineering, UCL

AutoPore IV 9500 V1.03 Serial: 201 Port: 1/1 Page 11

Calibration ID: Sample 6, C2HT (UCL?) (Pen No:16-0289) 000-072
Operator: Julian Perfect
Submitter: Fan Zhang
File: C:\9500\DATA\BLANKS\000-072.SMP

LP Analysis Time:	14/07/2004 4:59:20PM	Sample Weight:	0.8386 g
HP Analysis Time:	14/07/2004 6:12:21PM	Correction Type:	Blank
Report Time:	14/07/2004 9:26:44PM	Show Neg. Int:	No

Log Differential Intrusion vs Pore size

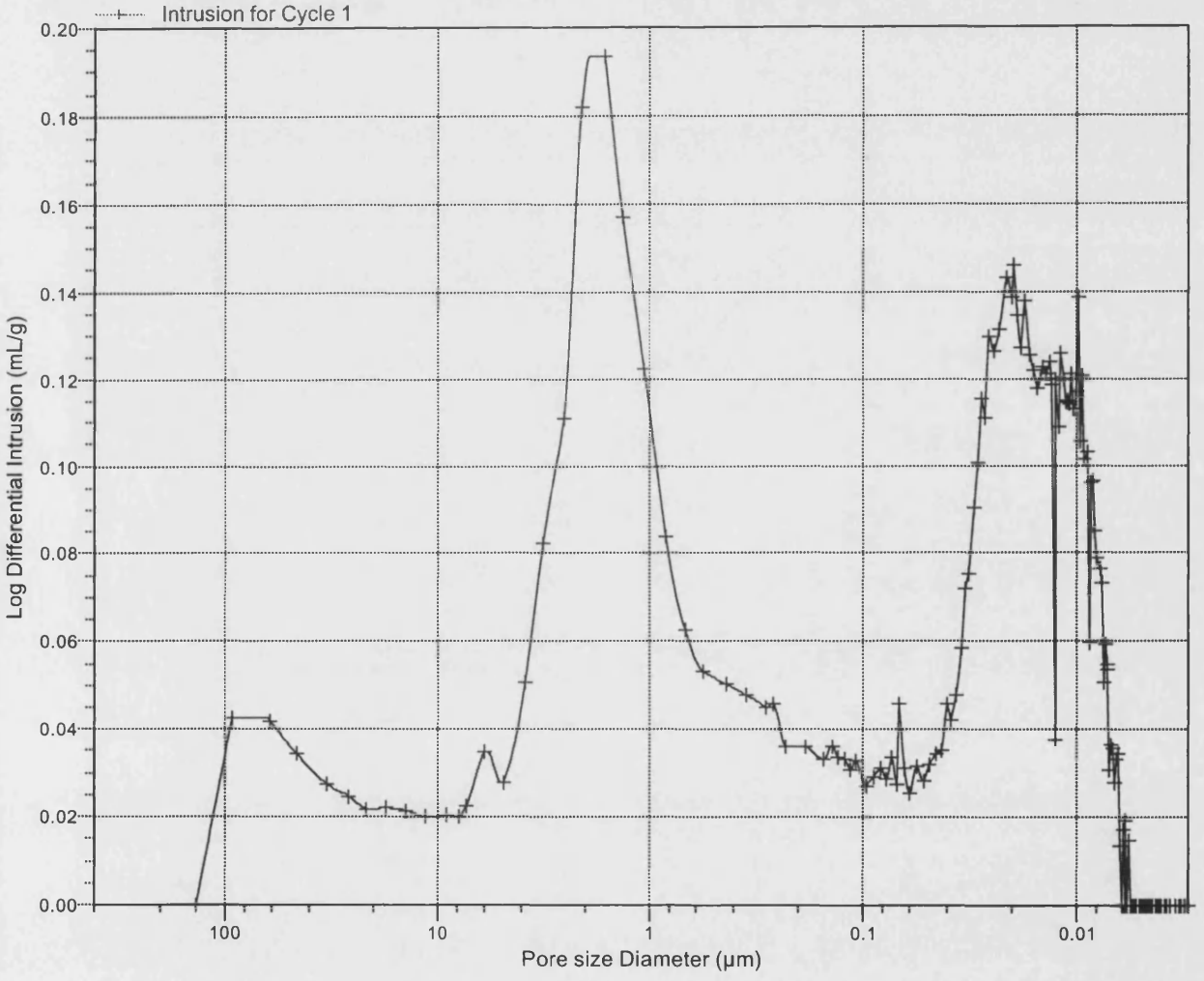

Appendix C

Method adapted to calculate the value of effective diffusivity

The following calculation is based on **Sample BC0C-1** (single-plate blank cordierite with smooth surface, see attached in the end of the appendix) and **Sample S3HT (Plate 46)** at the conditions: P_{cell} = 1.06 bar (a), inlet flowrate Q = 500 ml/min.

The diffusion cell is represented as follows. 2.4% CO stream (in nitrogen) is fed into the lower chamber and pure nitrogen is fed into the upper chamber, see Figure AC.1.

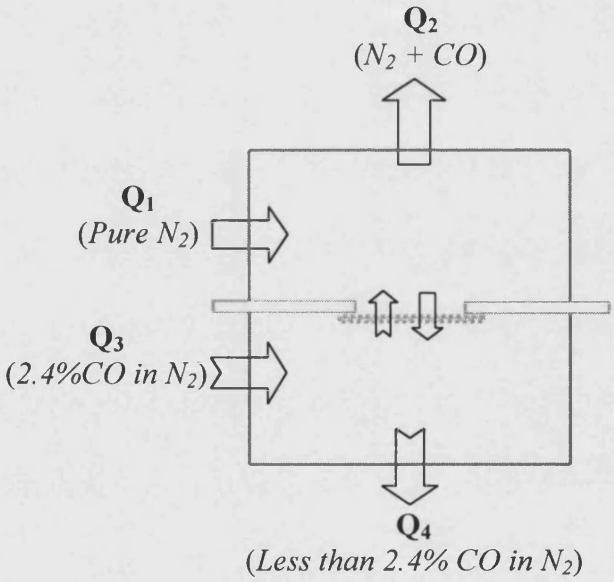

Figure AC.1 Diagram of the diffusion cell

1. Experimental condition:

T_{room} = 15.1 [℃] = 273.15 + 15.1 [*K*] = 288.25 [*K*]

P_{room} = 1 [*atm*] = 101325 [*Pa*]

$Y_{3,CO}$ = 24000 [*ppm*] ≡ 0.024

L_s = 0.000162 [*m*] (thickness of the sample with smooth surface)

D_s = 0.006 [*m*] (diameter of the diffusion area)

2. Measured data:

$Q_{1,d} = 500$ [*ml/min*]

$Q_{3,d} = 499$ [*ml/min*]

$P_{cell} = 1.06$ [*bar (a)*] = 106000 [*Pa*]

$Y_{1,CO} = 0$ [*ppm*]

$Y_{2,CO,d} = 522$ [*ppm*] $\equiv 5.22 \times 10^{-4}$

3. Calibrated data

The rotameters at a fixed operating pressure (1.06 bar (a)) were calibrated with a stopwatch and a bubble-flowmeter. The CO analyser was calibrated with the two rotameters which had been calibrated. Their calibration formulas are as follows:

For Rotameter 1, the calibration formula is $Q_{1,c} = 1.0988 \times Q_{1,d} - 0.2757$ [*ml/min*]

For Rotameter 3, the calibration formula is $Q_{3,c} = 1.0790 \times Q_{3,d} + 5.1219$ [*ml/min*]

For CO analyser, the calibration formula is $Y_{2,CO,c} = 1.0292 \times Y_{2,CO,d} - 28.131$ [*ppm*]

It should be noted that the above rotameters and the CO analyser were calibrated every few weeks to ensure they worked properly. So the calibration formulas may be different in different calculations.

The calibrated data:

$Q_{1,c} = 1.0988 \times 500$ [*ml/min*] $- 0.2757 = 549.1$ [*ml/min*]

$Q_{3,c} = 1.0790 \times 499$ [*ml/min*] $+ 5.1292 = 543.5$ [*ml/min*]

$Y_{2,CO,c} = 1.0292 \times 522$ [*ppm*] $- 28.131 = 509.1$ [*ppm*] $= 5.091 \times 10^{-4}$

4. To calculate volumetric flowrate at STP condition (1 atm, 273.15K)

All of the rotameters are calibrated at one atmosphere (outlet pressure) and room temperature, so Q_s can be obtained using ideal gas equation (assuming $P_1 = P_2$):

$$\frac{P_1 V_1}{T_1} = \frac{P_2 V_2}{T_2} \Rightarrow \frac{V_1}{T_1} = \frac{V_2}{T_2} \qquad \text{(AC.1)}$$

Equation AC.1 can also become:

$$\frac{Q_1}{T_1} = \frac{Q_2}{T_2} \Rightarrow \frac{Q_c}{T_c} = \frac{Q_s}{T_s} \qquad \text{(AC.2)}$$

So

$Q_{1,s} = Q_{1,c} \times (T_{1,s} / T_{1,c})$

$= 549.1\ [ml/min] \times 273.15\ [K]/(273.15 + 15.1)\ [K]$

$= 520.4\ [ml/min]$

$= 510.3 \times 10^{-6}\ [m^3]/60\ [s]$

$= 8.673 \times 10^{-6}\ [m^3/s]$

Following the same procedure,

$Q_{3,s} = 8.584 \times 10^{-6}\ [m^3/s]$

In the experiments, equi-molar diffusion was assumed, so

$Q_{2,s} = Q_{1,s} = 8.673 \times 10^{-6}\ [m^3/s]$

$Q_{4,s} = Q_{3,s} = 8.584 \times 10^{-6}\ [m^3/s]$

5. Completing a molar balance on CO

The inlet CO concentration marked on the cylinder was 24000 ppm.

After $F_{3,CO}$ and $F_{2,CO}$ are calculated, $F_{4,CO}$ can be calculated using CO molar balance, see Equation AC.3. Furthermore, $C_{4,CO}$ and $Y_{4,CO}$ can be obtained.

$$F_{1,CO} + F_{3,CO} = F_{2,CO} + F_{4,CO} \qquad \text{(AC.3)}$$

Obviously,

$Y_{1,CO} = 0$

So $F_{1,CO} = F_{1,t} \times Y_{1,CO} = 0$

And so Equation AC.3 will become:

$$F_{3,CO} = F_{2,CO} + F_{4,CO}$$

Or

$$F_{4,CO} = F_{3,CO} - F_{2,CO} \qquad \text{(AC.4)}$$

Because

$$F_{3,\,total} = \frac{Q_{3,s}}{0.022413\,[m^3/mol]} = \frac{8.584\times10^{-6}\,[m^3/s]}{0.022413\,[m^3/mol]}$$

$F_{3,CO} = Y_{3,CO} \times F_{3,\,total}$

$= [24000 \times 10^{-6}] \times F_{3,\,total}\ [mol/s]$

$= 9.192 \times 10^{-6}\ [mol/s]$

In a similar manner, $F_{2,CO}$ can be calculated.

$$F_{2,\,total} = \frac{Q_{2,s}}{0.022413\,[m^3/mol]} = \frac{8.673\times10^{-6}[m^3/s]}{0.022413\,[m^3/mol]}$$

$F_{2,CO} = Y_{2,CO} \times F_{2,\,total}$

$= [509.1\times 10^{-6}] \times F_{2,\,total}\ [mol/s]$

$= 1.970 \times 10^{-7}\ [mol/s]$

So $F_{4,CO} = F_{3,CO} - F_{2,CO}$

$= 9.192 \times 10^{-6}\ [mol/s] - 1.970 \times 10^{-7}\ [mol/s]$

$= 8.995 \times 10^{-6}\ [mol/s]$

Then

$Y_{4,CO} = F_{4,CO} / F_{4,\,total}$

$$= \frac{F_{4,\,CO}}{\dfrac{Q_{4,s}}{0.022413\ [\mathrm{m}^3/\mathrm{mol}]}}$$

$$= \frac{8.996\times10^{-6}\ [\mathrm{m}^3/\mathrm{mol}]}{\dfrac{8.584\times10^{-6}\ [\mathrm{m}^3/\mathrm{s}]}{0.022413\ [\mathrm{m}^3/\mathrm{mol}]}}$$

$$= 0.023486$$

$$= 23486\ [\mathrm{ppm}]$$

6. The calculation of CO D_{eff} in the combination of uncoated cordierite and washcoated monolith

Assume that diffusion between the two chambers is equi-molar diffusion. According to Fick's law,

$$N_{CO} = D_{eff,s} \times \frac{\Delta C}{\Delta L} = D_{eff,s} \times \frac{(C_{4,CO} - C_{2,CO})}{L_s} \qquad \text{(AC.5)}$$

N_{CO} can be calculated from:

$$N_{CO} = Q_{2,s} \times \frac{C_{2,CO}}{A} \qquad \text{(AC.6)}$$

$C_{4,\,CO}$ can be calculated from:

$$C_{4,CO} = Y_{4,CO} \times \frac{F_{4,\,total}}{Q_{4,\,cell}}$$

$$= Y_{4,CO} \times \frac{\dfrac{Q_{4,s}}{0.022413\ [\mathrm{m}^3/\mathrm{mol}]}}{\dfrac{P_{room} \times T_{room} \times Q_{4,s}}{P_{cell} \times T_{4,s}}}$$

$$= Y_{4,CO} \times \frac{106000\ [\mathrm{Pa}] \times 273.15\ [\mathrm{K}]}{0.022413\ [\mathrm{m}^3/\mathrm{mol}] \times 101325\ [\mathrm{Pa}] \times 288.25\ [\mathrm{K}]}$$

$$= 1.0388\ [\mathrm{mol/m}^3]$$

Following the same procedure, $C_{2,\,CO}$ and $C_{3,\,CO}$ can also be obtained.

$C_{2,CO} = 0.0225\ [mol/m^3]$

$C_{3,CO} = 1.0615\ [mol/m^3]$

So ΔC can be calculated from:

$\Delta C = C_{4,CO} - C_{2,CO}$

$= 1.0388\ [mol/m^3] - 0.0225\ [mol/m^3]$

$= 1.0163\ [mol/m^3]$

Combine Equation AC.5 and Equation AC.6, the D_{eff} of the blank cordierite can be calculated from:

$$N = Q_{2,s} \times \frac{C_{2,co}}{A} = D_{eff,s} \times \frac{\Delta C}{L_s}$$

Or

$$D_{eff,s} = \frac{Q_{2,s} \times C_{2,co} \times L_s}{A \times \Delta C} \qquad \text{(AC.7)}$$

Enter the obtained data,

$$D_{eff,s} = \frac{Q_{2,s} \times C_{2,co} \times L_s}{A \times \Delta C}$$
$$= \frac{Q_{2,s} \times C_{2,co} \times L_s}{A_s \times (C_{4,co} - C_{2,co})}$$
$$= \frac{8.673 \times 10^{-6}\ [m^3/s] \times 0.0225[mol/m^3] \times 0.000162[m]}{3.1416 \times 0.003[m] \times 0.003[m] \times 1.0163[mol/m^3]}$$
$$= 1.101 \times 10^{-6}[m^2/s]$$

Using the same method, $D_{eff,t}$, the total effective diffusivity in **Sample S3HT** (Plate 46), which is the combination of D_{eff} in washcoat and D_{eff} in cordierite, can be calculated.

T = 14.8 [℃] = 273.15 + 14.8 [*K*] = 287.95 [*K*]

P = 1 [*atm*] = 101325 [*Pa*]

$L_s = 0.000172$ [m]

$L_w = 0.000189$ [m]

$L_{total} = 0.000361$ [m]

$D = 0.010$ [m]

$D_{eff,t} = 1.033 \times 10^{-6}$ [m^2/s]

7. The calculation of the D_{eff} of CO in the washcoat

Assume both the blank cordierite surface and the washcoat surface are flat, in other word, their thickness is uniform. Then the total thickness, L_{total}, can be obtained from:

$$L_{total} = L_s + L_w \tag{AC.8}$$

The total effective diffusivity, $D_{eff,\,total}$, is represented by:

$$\frac{L_{total}}{D_{eff,t}} = \frac{L_s}{D_{eff,s}} + \frac{L_w}{D_{eff,w}} \tag{AC.9}$$

Or

$$D_{eff,w} = \frac{L_w}{\frac{L_{total}}{D_{eff,t}} - \frac{L_s}{D_{eff,s}}} \tag{AC.10}$$

According Equation AC.10, the effective diffusivity of the washcoat in **Sample S3HT** (Plate 46) can be obtained.

$$D_{eff,w} = \frac{189\times10^{-6}[\mathrm{m}]}{\frac{0.000361[\mathrm{m}]}{1.033\times10^{-6}[\mathrm{m^2/s}]} - \frac{0.000172[\mathrm{m}]}{1.101\times10^{-6}[\mathrm{m^2/s}]}}$$

$$= 9.780\times10^{-7}[\mathrm{m^2/s}]$$

Calculation in Excel:

Sample: BC0C-1 (single-plate blank cordierite with smooth surface)

Temperature [*°C*]	15.1
Thickness [*m*]	0.000162
Diameter [*m*]	0.006
Pressure in the cell [*bar abs*]	**1.06**
$Q_{1,d}$ (upper, in, displayed) [*ml/min*]	500
$Q_{1,c}$ (upper, in, calibrated) [*ml/min*]	549.1
$Q_{1,s}$ (upper, in, standard) [m^3/s]	8.67E-06
$Q_{1,s}$ (upper, in, standard) [*ml/min*]	520.4
$F_{1,CO}$ (upper, in) [*mol/s*]	0
$Q_{2,d}$ (upper, out, displayed) [*ml/min*]	500
$Q_{2,c}$ (upper, out, calibrated) [*ml/min*]	532.2
$Q_{2,c,c}$ (upper, out, assumed) [*ml/min*]	549.1
$Q_{2,s}$ (upper, out, standard) [m^3/s]	8.67E-06
$F_{2,CO}$ (upper, out) [*mol/s*]	1.97E-07
$C_{2,CO}$ (upper, out) [mol/m^3]	2.25E-02
$N_{2,CO}$ (upper, out, CO flux) [$mol/m^2.s$]	6.97E-03
$Q_{3,d}$ (lower, in, displayed) [*ml/min*]	499
$Q_{3,c}$ (lower, in, calibrated) [*ml/min*]	543.5
$Q_{3,s}$ (lower, in, standard) [m^3/s]	8.58E-06
$Q_{3,s}$ (lower, in, standard) [*ml/min*]	5.15E+02
$F_{3,CO}$ (lower, in) [*mol/s*]	9.19E-06
$C_{3,CO}$ (lower, in) [mol/m^3]	1.0615
$Q_{4,d}$ (lower, out, displayed) [*ml/min*]	530
$Q_{4,c}$ (lower, out, calibrated) [*ml/min*]	538.3
$Q_{4,c,c}$ (lower, out, assumed) [*ml/min*]	543.5
$Q_{4,s}$ (lower, out, standard) [m^3/s]	8.58E-06
$F_{4,CO}$ (lower, out) [*mol/s*]	9.00E-06
$C_{4,CO}$ (lower, out) [mol/m^3]	1.0388
dC ($C_{4,CO}$ - $C_{2,CO}$) [mol/m^3]	1.0163
A (area of the diffusion surface)[m^2]	2.83E-05
L_s (thickness of the sample) [*m*]	1.62E-04
$Y_{3,CO}$ (lower, in) [*ppm*]	24000
$Y_{2,CO,d}$ (upper, out, displayed) [*ppm*]	522
$Y_{2,CO,c}$ (upper, out, calibrated) [*ppm*]	509.1
$Y_{4,CO}$ (lower, out, caculated) [*ppm*]	23485.7
dY ($Y_{4,CO}$ - $Y_{2,CO,c}$) [*ppm*]	22976.5
$D_{eff,s}$ (blank cordierite, from dC) [m^2/s]	**1.101E-06**
$D_{eff,s}$ (blank cordierite, from dY) [m^2/s]	**1.101E-06**

Calculation in Excel:

Sample: **S3HT-plate 46**

Temperature [°C]	14.8
Total thickness [m]	3.61E-04
Washcoat thickness [m]	1.89E-04
Cordierite thickness [m]	1.72E-04
Diameter [m]	0.01
Pressure in the cell [bar a]	**1.06**
$Q_{1,d}$ (upper, in, displayed) [ml/min]	500
$Q_{1,c}$ (upper, in, calibrated) [ml/min]	538.0
$Q_{1,s}$ (upper, in, standard) [m^3/s]	8.51E-06
$F_{1,CO}$ (upper, in) [mol/s]	0
$Q_{2,d}$ (upper, out, displayed) [ml/min]	418
$Q_{2,c}$ (upper, out, calibrated) [ml/min]	443.7
$Q_{2,c,c}$ (upper, out, 2nd calibrated) [ml/min]	538.0
$Q_{2,s}$ (upper, out, standard) [m^3/s]	8.51E-06
$F_{2,CO}$ (upper, out) [mol/s]	2.29E-07
$C_{2,CO}$ (upper, out) [mol/m^3]	0.0267
$Q_{3,d}$ (lower, in, displayed) [ml/min]	499
$Q_{3,c}$ (lower, in, calibrated) [ml/min]	539.4
$Q_{3,s}$ (lower, in, standard) [m^3/s]	8.53E-06
$F_{3,CO}$ (lower, in) [mol/s]	9.13E-06
$C_{3,CO}$ (lower, in) [mol/m^3]	1.107
$Q_{4,d}$ (lower, out, displayed) [ml/min]	518
$Q_{4,c}$ (lower, out, calibrated) [ml/min]	593.6
$Q_{4,c,c}$ (lower, out, 2nd calibrated) [ml/min]	539.4
$Q_{4,s}$ (lower, out, standard) [m^3/s]	8.53E-06
$F_{4,CO}$ (lower, out) [mol/s]	8.9E-06
$C_{4,CO}$ (lower, out) [mol/m^3]	1.0360
A (area of the sample) [m^2]	7.85E-05
L_t (thickness of the sample) [m]	3.61E-04
$Y_{3,CO}$ (lower, in) [ppm]	24000
$Y_{2,CO,d}$ (upper, out, displayed) [ppm]	584
$Y_{2,CO,c}$ (upper, out, calibrated) [ppm]	603.1
$Y_{4,CO}$ (lower, out, caculated) [ppm]	23398.4
dYco ($Y_{4,CO} - Y_{2,CO}$) [ppm]	22795.2
dC ($C_{4,CO} - C_{2,CO}$) [mol/m^3]	1.0093
$D_{eff,t}$ (total, from dC) [m^2/s]	1.03E-06
$D_{eff,t}$ (total, from dY) [m^2/s]	1.03E-06
$L_t/D_{eff,t}$ (total) [s/m]	349.0
$D_{eff,s}$ (blank cordierite) [m^2/s]	1.10E-06
$L_s/D_{eff,s}$ (blank cordierite) [s/m]	1.56E+02
$(L_t/D_{eff,t}) - (L_s/D_{eff,s})$ [s/m]	192.8
$D_{eff,w}$ (washcoat) [m^2/s]	**9.780E-07**

Appendix D1

Experimental data on the measurement of D_{eff} in Chapter 3

Data used in **Figure 3.12** "The effect of inlet flowrates on the molar flux of CO".

Room temperature [*°C*]	15.8	15.8	15.8	15.8	15.8	15.8	15.8
Total thickness [*m*]	1.704E-03	1.704E-03	1.704E-03	1.704E-03	1.704E-03	1.704E-03	1.704E-03
Equivalent substrate thickness [*m*]	3.892E-04	3.892E-04	3.892E-04	3.892E-04	3.892E-04	3.892E-04	3.892E-04
Equivalent void thickness, L_v [*m*]	1.315E-03	1.315E-03	1.315E-03	1.315E-03	1.315E-03	1.315E-03	1.315E-03
Diameter [*m*]	0.01	0.01	0.01	0.01	0.01	0.01	0.01
Pressure in the cell [*bar abs*]	**1.06**	**1.06**	**1.06**	**1.06**	**1.06**	**1.06**	**1.06**
$Q_{1,d}$ (upper, in, displayed) [*ml/min*]	800	700	600	500	400	300	200
$Q_{1,c}$ (upper, in, calibrated) [*ml/min*]	867.0	758.6	650.1	541.7	433.3	324.8	216.4
$Q_{1,s}$ (upper, in, standard) [m^3/s]	1.37E-05	1.20E-05	1.02E-05	8.53E-06	6.83E-06	5.12E-06	3.41E-06
$F_{1,CO}$ (upper, in) [*mol/s*]	0	0	0	0	0	0	0
$Q_{3,d}$ (upper, out, displayed) [*ml/min*]	825	725	622	512	325	232	102
$Q_{3,c}$ (upper, out, calibrated) [*ml/min*]	868.9	768.6	665.2	554.8	367.2	273.8	143.4
$Q_{3,c,c}$ (upper, out, assumed) [*ml/min*]	867.0	758.6	650.1	541.7	433.3	324.8	216.4
$Q_{3,s}$ (upper, out, standard) [m^3/s]	1.37E-05	1.20E-05	1.02E-05	8.53E-06	6.83E-06	5.12E-06	3.41E-06
$F_{3,CO}$ (upper, out) [*mol/s*]	1.81E-07	1.80E-07	1.79E-07	1.77E-07	1.72E-07	1.65E-07	1.58E-07
$C_{3,CO}$ (upper, out) [mol/m^3]	1.31E-02	1.49E-02	1.73E-02	2.05E-02	2.49E-02	3.18E-02	4.59E-02
N_{CO} (the molar flux of CO) [$mol/m^2.s$]	**2.31E-03**	**2.29E-03**	**2.28E-03**	**2.25E-03**	**2.19E-03**	**2.10E-03**	**2.02E-03**
$Q_{2,d}$ (lower, in, displayed) [*ml/min*]	800	700	600	500	400	300	200
$Q_{2,c}$ (lower, in, calibrated) [*ml/min*]	845.2	742.1	638.9	535.8	432.6	329.5	226.3
$Q_{2,s}$ (lower, in, standard) [m^3/s]	1.33E-05	1.17E-05	1.01E-05	8.44E-06	6.82E-06	5.19E-06	3.57E-06
$F_{2,CO}$ (lower, in) [*mol/s*]	1.43E-05	1.25E-05	1.08E-05	9.04E-06	7.30E-06	5.56E-06	3.82E-06
$C_{2,CO}$ (lower, in) [mol/m^3]	1.0590	1.0590	1.0590	1.0590	1.0590	1.0590	1.0590
$Q_{4,d}$ (lower, out, displayed) [*ml/min*]	823	713	632	518	438	340	151
$Q_{4,c}$ (lower, out, calibrated) [*ml/min*]	841.8	731.5	650.2	535.9	455.6	357.3	167.7
$Q_{4,c,c}$ (lower, out, assumed) [*ml/min*]	845.2	742.1	638.9	535.8	432.6	329.5	226.3
$Q_{4,s}$ (lower, out, standard) [m^3/s]	1.33E-05	1.17E-05	1.01E-05	8.44E-06	6.82E-06	5.19E-06	3.57E-06
$F_{4,CO}$ (lower, out) [*mol/s*]	1.41E-05	1.23E-05	1.06E-05	8.86E-06	7.13E-06	5.39E-06	3.66E-06
$C_{4,CO}$ (lower, out) [mol/m^3]	1.0455	1.0438	1.0414	1.0382	1.0340	1.0276	1.0151
A (area of the sample) [m^2]	7.85E-05	7.85E-05	7.85E-05	7.85E-05	7.85E-05	7.85E-05	7.85E-05

Data used in **Figure 3.17** "Effect of increasing/decreasing gas inlet flowrates on experimentally determined D_{eff} values for a single-plate smooth-surface cordierite sample".

(Increasing gas inlet flowrates)

Temperature [°C]	16.6	16.6	16.6	16.6	16.6	16.6	16.6
Thickness [m]	1.62E-04	1.62E-04	1.62E-04	1.62E-04	1.62E-04	1.62E-04	1.62E-04
Diameter [m]	0.006	0.006	0.006	0.006	0.006	0.006	0.006
Pressure in the cell [bar abs]	**1.11**	**1.11**	**1.11**	**1.11**	**1.11**	**1.11**	**1.11**
$Q_{1,d}$ (upper, in, displayed) [ml/min]	200	300	401	502	599	700	799
$Q_{1,c}$ (upper, in, calibrated) [ml/min]	224.0	334.3	445.6	557.0	663.9	775.3	884.4
$Q_{1,s}$ (upper, in, standard) [m^3/s]	3.52E-06	5.25E-06	7.00E-06	8.75E-06	1.04E-05	1.22E-05	1.39E-05
$F_{1,CO}$ (upper, in) [mol/s]	0	0	0	0	0	0	0
$Q_{2,d}$ (upper, out, displayed) [ml/min]	214	318	416	515	613	727	818
$Q_{2,c}$ (upper, out, calibrated) [ml/min]	222.3	334.4	440.1	546.8	652.4	775.3	873.4
$Q_{2,c,c}$ (upper, out, assumed) [ml/min]	224.0	334.3	445.6	557.0	663.9	775.3	884.4
$Q_{2,s}$ (upper, out, standard) [m^3/s]	3.519E-06	5.252E-06	7.001E-06	8.751E-06	1.043E-05	1.218E-05	1.390E-05
$F_{2,CO}$ (upper, out) [mol/s]	1.536E-07	1.607E-07	1.812E-07	1.995E-07	2.071E-07	2.083E-07	2.214E-07
$C_{2,CO}$ (upper, out) [mol/m^3]	0.0451	0.0316	0.0267	0.0235	0.0205	0.0177	0.0165
$Q_{3,d}$ (lower, in, displayed) [ml/min]	202	300	400	501	601	700	800
$Q_{3,c}$ (lower, in, calibrated) [ml/min]	233.2	340.3	449.6	560.1	669.4	777.6	886.9
$Q_{3,s}$ (lower, in, standard) [m^3/s]	3.664E-06	5.347E-06	7.065E-06	8.799E-06	1.052E-05	1.222E-05	1.394E-05
$F_{3,CO}$ (lower, in) [mol/s]	3.923E-06	5.726E-06	7.565E-06	9.423E-06	1.126E-05	1.308E-05	1.492E-05
$C_{3,CO}$ (lower, in) [mol/m^3]	1.1059	1.1059	1.1059	1.1059	1.1059	1.1059	1.1059
$Q_{4,d}$ (lower, out, displayed) [ml/min]	251	350	449	553	652	768	875
$Q_{4,c}$ (lower, out, calibrated) [ml/min]	249.8	351.5	453.3	560.1	661.8	781.0	891.0
$Q_{4,c,c}$ (lower, out, assumed) [ml/min]	233.2	340.3	449.6	560.1	669.4	777.6	886.9
$Q_{4,s}$ (lower, out, standard) [m^3/s]	3.664E-06	5.347E-06	7.065E-06	8.799E-06	1.052E-05	1.222E-05	1.394E-05
$F_{4,CO}$ (lower, out) [mol/s]	3.770E-06	5.565E-06	7.384E-06	9.223E-06	1.105E-05	1.287E-05	1.470E-05
$C_{4,CO}$ (lower, out) [mol/m^3]	1.0626	1.0748	1.0794	1.0824	1.0855	1.0883	1.0895
dC ($C_{4,CO}$ - $C_{2,CO}$) [mol/m^3]	1.0175	1.0432	1.0526	1.0589	1.0650	1.0706	1.0730
A (area of the diffusion surface)[m^2]	2.827E-05	2.827E-05	2.827E-05	2.827E-05	2.827E-05	2.827E-05	2.827E-05
L_s (thickness of the cordierite) [m]	1.62E-04	1.62E-04	1.62E-04	1.62E-04	1.62E-04	1.62E-04	1.62E-04
$Y_{3,CO}$ (lower, in) [ppm]	24000	24000	24000	24000	24000	24000	24000
$Y_{2,CO,d}$ (upper, out, displayed) [ppm]	942	663	562	496	433	374	349
$Y_{2,CO,c}$ (upper, out, calibrated) [ppm]	977.9	685.8	580.1	511.0	445.0	383.3	357.1
$Y_{4,CO}$ (lower, out, caculated) [ppm]	23060.7	23326.4	23425.1	23491.8	23558.6	23617.9	23643.9
dY ($Y_{4,CO}$ - $Y_{2,CO,c}$) [ppm]	22082.8	22640.6	22845.0	22980.8	23113.5	23234.6	23286.8
$D_{eff,s}$ (blank cordierite, from dC) [m^2/s]	**8.929E-07**	**9.115E-07**	**1.019E-06**	**1.115E-06**	**1.151E-06**	**1.151E-06**	**1.221E-06**
$D_{eff,s}$ (blank cordierite, from dY) [m^2/s]	**8.929E-07**	**9.115E-07**	**1.019E-06**	**1.115E-06**	**1.151E-06**	**1.151E-06**	**1.221E-06**

Data used in **Figure 3.17** "Effect of increasing/decreasing gas inlet flowrates on experimentally determined D_{eff} values for a single-plate smooth-surface cordierite sample".

(Decreasing gas inlet flowrates)

Temperature [°C]	16.6	16.6	16.6	16.6	16.6	16.6	16.6
Thickness [m]	0.000162	0.000162	0.000162	0.000162	0.000162	0.000162	0.000162
Diameter [m]	0.006	0.006	0.006	0.006	0.006	0.006	0.006
Pressure in the cell [bar abs]	**1.11**	**1.11**	**1.11**	**1.11**	**1.11**	**1.11**	**1.11**
$Q_{1,d}$ (upper, in, displayed) [ml/min]	800	700	600	500	400	301	200
$Q_{1,c}$ (upper, in, calibrated) [ml/min]	885.5	775.3	665.0	554.8	444.5	335.4	224.0
$Q_{1,s}$ (upper, in, standard) [m^3/s]	1.39E-05	1.22E-05	1.04E-05	8.72E-06	6.98E-06	5.27E-06	3.52E-06
$F_{1,CO}$ (upper, in) [mol/s]	0	0	0	0	0	0	0
$Q_{2,d}$ (upper, out, displayed) [ml/min]	824	725	620	514	414	320	214
$Q_{2,c}$ (upper, out, calibrated) [ml/min]	879.8	773.1	659.9	545.7	437.9	336.6	222.3
$Q_{2,c,c}$ (upper, out, assumed) [ml/min]	885.5	775.3	665.0	554.8	444.5	335.4	224.0
$Q_{2,s}$ (upper, out, standard) [m^3/s]	1.39E-05	1.22E-05	1.04E-05	8.72E-06	6.98E-06	5.27E-06	3.52E-06
$F_{2,CO}$ (upper, out) [mol/s]	2.16E-07	2.09E-07	2.04E-07	1.98E-07	1.82E-07	1.57E-07	1.54E-07
$C_{2,CO}$ (upper, out) [mol/m^3]	0.0161	0.0177	0.0201	0.0234	0.0269	0.0308	0.0451
$Q_{3,d}$ (lower, in, displayed) [ml/min]	800	700	602	500	400	296	202
$Q_{3,c}$ (lower, in, calibrated) [ml/min]	886.9	777.6	670.5	559.0	449.6	335.9	233.2
$Q_{3,s}$ (lower, in, standard) [m^3/s]	1.39E-05	1.22E-05	1.05E-05	8.78E-06	7.06E-06	5.28E-06	3.66E-06
$F_{3,CO}$ (lower, in) [mol/s]	1.49E-05	1.31E-05	1.13E-05	9.4E-06	7.57E-06	5.65E-06	3.92E-06
$C_{3,CO}$ (lower, in) [mol/m^3]	1.1059	1.1059	1.1059	1.1059	1.1059	1.1059	1.1059
$Q_{4,d}$ (lower, out, displayed) [ml/min]	874	765	651	553	450	348	251
$Q_{4,c}$ (lower, out, calibrated) [ml/min]	890.0	778.0	660.8	560.1	454.3	349.5	249.8
$Q_{4,c,c}$ (lower, out, assumed) [ml/min]	886.9	777.6	670.5	559.0	449.6	335.9	233.2
$Q_{4,s}$ (lower, out, standard) [m^3/s]	1.39E-05	1.22E-05	1.05E-05	8.78E-06	7.06E-06	5.28E-06	3.66E-06
$F_{4,CO}$ (lower, out) [mol/s]	1.47E-05	1.29E-05	1.11E-05	9.21E-06	7.38E-06	5.5E-06	3.77E-06
$C_{4,CO}$ (lower, out) [mol/m^3]	1.0898	1.0882	1.0859	1.0826	1.0793	1.0751	1.0626
dC ($C_{4,CO}$ - $C_{2,CO}$) [mol/m^3]	1.0737	1.0705	1.0658	1.0592	1.0524	1.0444	1.0175
A (area of the diffusion surface)[m^2]	2.83E-05	2.83E-05	2.83E-05	2.83E-05	2.83E-05	2.83E-05	2.83E-05
L_s (thickness of the cordierite) [m]	0.000162	0.000162	0.000162	0.000162	0.000162	0.000162	0.000162
$Y_{3,CO}$ (lower, in) [ppm]	24000	24000	24000	24000	24000	24000	24000
$Y_{2,CO,d}$ (upper, out, displayed) [ppm]	341	375	425	493	565	646	942
$Y_{2,CO,c}$ (upper, out, calibrated) [ppm]	348.7	384.3	436.7	507.9	583.2	668.0	977.9
$Y_{4,CO}$ (lower, out, caculated) [ppm]	23651.8	23616.8	23566.9	23496.0	23423.4	23333.2	23060.7
dY ($Y_{4,CO}$ - $Y_{2,CO,c}$) [ppm]	23303.1	23232.5	23130.2	22988.1	22840.2	22665.2	22082.8
$D_{eff,s}$ (blank cordierite, from dC) [m^2/s]	**1.193E-06**	**1.155E-06**	**1.130E-06**	**1.103E-06**	**1.022E-06**	**8.898E-07**	**8.929E-07**
$D_{eff,s}$ (blank cordierite, from dY) [m^2/s]	**1.193E-06**	**1.155E-06**	**1.130E-06**	**1.103E-06**	**1.022E-06**	**8.898E-07**	**8.929E-07**

Data used in **Figure 3.18** "Effect of the surface structure of cordierite samples on D_{eff} values".

(Smooth surface)

Temperature [*°C*]	15.1	15.1	15.1	15.1	15.1	15.1
Thickness [*m*]	0.000162	0.000162	0.000162	0.000162	0.000162	0.000162
Diameter [*m*]	0.006	0.006	0.006	0.006	0.006	0.006
Pressure in the cell [*bar abs*]	**1.06**	**1.11**	**1.21**	**1.31**	**1.41**	**1.51**
$Q_{1,d}$ (upper, in, displayed) [*ml/min*]	500	500	500	505	498	500
$Q_{1,c}$ (upper, in, calibrated) [*ml/min*]	549.1	566.0	600.3	639.3	661.5	694.1
$Q_{1,s}$ (upper, in, standard) [m^3/s]	8.67E-06	8.94E-06	9.48E-06	1.01E-05	1.04E-05	1.10E-05
$Q_{1,s}$ (upper, in, standard) [*ml/min*]	520.4	536.3	568.8	605.8	626.8	657.8
$F_{1,CO}$ (upper, in) [*mol/s*]	0	0	0	0	0	0
$Q_{2,d}$ (upper, out, displayed) [*ml/min*]	500	515	548	589	602	639
$Q_{2,c}$ (upper, out, calibrated) [*ml/min*]	532.2	546.8	583.0	632.3	644.9	679.7
$Q_{2,c,c}$ (upper, out, assumed) [*ml/min*]	549.1	566.0	600.3	639.3	661.5	694.1
$Q_{2,s}$ (upper, out, standard) [m^3/s]	8.67E-06	8.94E-06	9.48E-06	1.01E-05	1.04E-05	1.10E-05
$F_{2,CO}$ (upper, out) [*mol/s*]	1.97E-07	1.96E-07	1.97E-07	1.97E-07	1.97E-07	1.98E-07
$C_{2,CO}$ (upper, out) [mol/m^3]	2.25E-02	2.28E-02	2.35E-02	2.39E-02	2.49E-02	2.55E-02
$N_{2,CO}$ (upper, out, CO flux) [$mol/m^2.s$]	6.97E-03	6.95E-03	6.95E-03	6.98E-03	6.97E-03	6.99E-03
$Q_{3,d}$ (lower, in, displayed) [*ml/min*]	499	498	500	502	497	500
$Q_{3,c}$ (lower, in, calibrated) [*ml/min*]	543.5	560.7	595.9	629.5	654.5	686.0
$Q_{3,s}$ (lower, in, standard) [m^3/s]	8.58E-06	8.86E-06	9.41E-06	9.94E-06	1.03E-05	1.08E-05
$Q_{3,s}$ (lower, in, standard) [*ml/min*]	5.15E+02	5.31E+02	5.65E+02	5.96E+02	6.20E+02	6.50E+02
$F_{3,CO}$ (lower, in) [*mol/s*]	9.19E-06	9.48E-06	1.01E-05	1.06E-05	1.11E-05	1.16E-05
$C_{3,CO}$ (lower, in) [mol/m^3]	1.0615	1.1116	1.2118	1.3119	1.4121	1.5122
$Q_{4,d}$ (lower, out, displayed) [*ml/min*]	530	550	591	620	649	675
$Q_{4,c}$ (lower, out, calibrated) [*ml/min*]	538.3	557.0	604.7	636.3	664.0	691.7
$Q_{4,c,c}$ (lower, out, assumed) [*ml/min*]	543.5	560.7	595.9	629.5	654.5	686.0
$Q_{4,s}$ (lower, out, standard) [m^3/s]	8.58E-06	8.86E-06	9.41E-06	9.94E-06	1.03E-05	1.08E-05
$F_{4,CO}$ (lower, out) [*mol/s*]	9.00E-06	9.29E-06	9.88E-06	1.04E-05	1.09E-05	1.14E-05
$C_{4,CO}$ (lower, out) [mol/m^3]	1.0388	1.0886	1.1881	1.2876	1.3869	1.4864
dC ($C_{4,CO}$ - $C_{2,CO}$) [mol/m^3]	1.0163	1.0658	1.1646	1.2636	1.3621	1.4610
A (area of the diffusion surface)[m^2]	2.83E-05	2.83E-05	2.83E-05	2.83E-05	2.83E-05	2.83E-05
L_s (thickness of the sample) [*m*]	1.62E-04	1.62E-04	1.62E-04	1.62E-04	1.62E-04	1.62E-04
$Y_{3,CO}$ (lower, in) [*ppm*]	24000	24000	24000	24000	24000	24000
$Y_{2,CO,d}$ (upper, out, displayed) [*ppm*]	522	506	479	453	438	420
$Y_{2,CO,c}$ (upper, out, calibrated) [*ppm*]	509.1	492.6	464.9	438.1	422.7	404.1
$Y_{4,CO}$ (lower, out, caculated) [*ppm*]	23485.7	23502.7	23531.8	23555.1	23572.8	23591.1
dY ($Y_{4,CO}$ - $Y_{2,CO,c}$) [*ppm*]	22976.5	23010.1	23066.9	23117.0	23150.2	23186.9
$D_{eff,s}$ (blank cordierite, from dC) [m^2/s]	**1.101E-06**	**1.097E-06**	**1.095E-06**	**1.096E-06**	**1.093E-06**	**1.095E-06**
$D_{eff,s}$ (blank cordierite, from dY) [m^2/s]	**1.101E-06**	**1.097E-06**	**1.095E-06**	**1.096E-06**	**1.093E-06**	**1.095E-06**

Data used in **Figure 3.18** "Effect of the surface structure of cordierite samples on D_{eff} values".

(Rough surface)

Temperature [*°C*]	16.6	16.6	16.6	16.7	16.7	16.6
Thickness [*m*]	1.748E-04	1.748E-04	1.748E-04	1.748E-04	1.748E-04	1.748E-04
Diameter [*m*]	0.006	0.006	0.006	0.006	0.006	0.006
Pressure in the cell [*bar abs*]	**1.06**	**1.11**	**1.21**	**1.31**	**1.41**	**1.51**
$Q_{1,d}$ (upper, in, displayed) [*ml/min*]	495	477	450	427	407	390
$Q_{1,c}$ (upper, in, calibrated) [*ml/min*]	543.6	540.1	541.4	543.1	543.9	547.4
$Q_{1,s}$ (upper, in, standard) [m^3/s]	8.54E-06	8.49E-06	8.51E-06	8.53E-06	8.54E-06	8.60E-06
$Q_{1,s}$ (upper, in, standard) [*ml/min*]	512.5	509.1	510.3	511.9	512.6	516.0
$F_{1,CO}$ (upper, in) [*mol/s*]	0	0	0	0	0	0
$Q_{2,d}$ (upper, out, displayed) [*ml/min*]	507	506	506	514	515	512
$Q_{2,c}$ (upper, out, calibrated) [*ml/min*]	539.8	537.1	537.3	551.6	550.7	543.9
$Q_{2,c,c}$ (upper, out, assumed) [*ml/min*]	543.6	540.1	541.4	543.1	543.9	547.4
$Q_{2,s}$ (upper, out, standard) [m^3/s]	8.54E-06	8.49E-06	8.51E-06	8.53E-06	8.54E-06	8.60E-06
$F_{2,CO}$ (upper, out) [*mol/s*]	1.60E-07	1.59E-07	1.60E-07	1.60E-07	1.61E-07	1.62E-07
$C_{2,CO}$ (upper, out) [mol/m^3]	0.0185	0.0194	0.0212	0.0228	0.0247	0.0264
$N_{2,CO}$ (upper, out, CO flux) [$mol/m^2.s$]	5.66E-03	5.64E-03	5.67E-03	5.64E-03	5.69E-03	5.72E-03
$Q_{3,d}$ (lower, in, displayed) [*ml/min*]	498	478	446	421	402	390
$Q_{3,c}$ (lower, in, calibrated) [*ml/min*]	542.5	538.5	533.7	531.1	535.0	541.5
$Q_{3,s}$ (lower, in, standard) [m^3/s]	8.52E-06	8.46E-06	8.38E-06	8.34E-06	8.40E-06	8.51E-06
$Q_{3,s}$ (lower, in, standard) [*ml/min*]	511.4	507.6	503.1	500.5	504.2	510.4
$F_{3,CO}$ (lower, in) [*mol/s*]	9.13E-06	9.06E-06	8.98E-06	8.93E-06	9.00E-06	9.11E-06
$C_{3,CO}$ (lower, in) [mol/m^3]	1.0560	1.1059	1.2055	1.3047	1.4043	1.5044
$Q_{4,d}$ (lower, out, displayed) [*ml/min*]	530	522	525	509	524	522
$Q_{4,c}$ (lower, out, calibrated) [*ml/min*]	538.3	528.3	536.7	519.9	534.7	531.7
$Q_{4,c,c}$ (lower, out, assumed) [*ml/min*]	542.5	538.5	533.7	531.1	535.0	541.5
$Q_{4,s}$ (lower, out, standard) [m^3/s]	8.52E-06	8.46E-06	8.38E-06	8.34E-06	8.40E-06	8.51E-06
$F_{4,CO}$ (lower, out) [*mol/s*]	8.97E-06	8.90E-06	8.82E-06	8.77E-06	8.84E-06	8.95E-06
$C_{4,CO}$ (lower, out) [mol/m^3]	1.0375	1.0864	1.1840	1.2814	1.3791	1.4777
dC ($C_{4,CO}$ - $C_{2,CO}$) [mol/m^3]	1.0190	1.0670	1.1628	1.2586	1.3544	1.4513
A (area of the diffusion surface)[m^2]	2.827E-05	2.827E-05	2.827E-05	2.827E-05	2.827E-05	2.827E-05
L_s (thickness of the sample) [*m*]	0.0001748	0.0001748	0.0001748	0.0001748	0.0001748	0.0001748
$Y_{3,CO}$ (lower, in) [*ppm*]	24000	24000	24000	24000	24000	24000
$Y_{2,CO,d}$ (upper, out, displayed) [*ppm*]	439	440	441	438	441	440
$Y_{2,CO,c}$ (upper, out, calibrated) [*ppm*]	420.2	421.2	422.2	419.2	422.2	421.2
$Y_{4,CO}$ (lower, out, caculated) [*ppm*]	23578.9	23577.6	23571.7	23571.3	23570.8	23574.2
dY ($Y_{4,CO}$ - $Y_{2,CO,c}$) [*ppm*]	23158.7	23156.4	23149.6	23152.1	23148.6	23153.0
$D_{eff,s}$ (blank cordierite, from dC) [m^2/s]	**9.581E-07**	**9.542E-07**	**9.590E-07**	**9.549E-07**	**9.632E-07**	**9.673E-07**
$D_{eff,s}$ (blank cordierite, from dY) [m^2/s]	**9.581E-07**	**9.542E-07**	**9.590E-07**	**9.549E-07**	**9.632E-07**	**9.673E-07**

Data used in **Figure 3.25** "Comparison of experimental D_{eff} values from samples with different plates".

Room temperature: 16.6 to 19.8 °C

Pressure, bar (a)	1.06	1.11	1.21	1.31	1.41	1.51	
Exp D_{eff}, m^2/s							**Average D_{eff}, m^2/s**
1-plate cordierite	9.581E-07	9.542E-07	9.590E-07	9.549E-07	9.632E-07	9.673E-07	**9.594E-07**
2-plate cordierite	1.008E-06	1.007E-06	1.021E-06	1.014E-06	9.997E-07	9.767E-07	**1.004E-06**
3-plate cordierite	1.260E-06	1.254E-06	1.211E-06	1.210E-06	1.231E-06	1.218E-06	**1.231E-06**

Data used in **Figure 3.26** "Effect of pressure in the diffusion cell on experimentally determined D_{eff} values".

(Single-plate)

Temperature [*°C*]	16.6	16.6	16.6	16.7	16.7	16.6
Thickness [*m*]	1.748E-04	1.748E-04	1.748E-04	1.748E-04	1.748E-04	1.748E-04
Diameter [*m*]	0.006	0.006	0.006	0.006	0.006	0.006
Pressure in the cell [*bar abs*]	**1.06**	**1.11**	**1.21**	**1.31**	**1.41**	**1.51**
$Q_{1,d}$ (upper, in, displayed) [*ml/min*]	495	477	450	427	407	390
$Q_{1,c}$ (upper, in, calibrated) [*ml/min*]	543.6	540.1	541.4	543.1	543.9	547.4
$Q_{1,s}$ (upper, in, standard) [m^3/s]	8.5414E-06	8.485E-06	8.506E-06	8.531E-06	8.543E-06	8.601E-06
$Q_{1,s}$ (upper, in, standard) [*ml/min*]	512.5	509.1	510.3	511.9	512.6	516.0
$F_{1,CO}$ (upper, in) [*mol/s*]	0	0	0	0	0	0
$Q_{2,d}$ (upper, out, displayed) [*ml/min*]	507	506	506	514	515	512
$Q_{2,c}$ (upper, out, calibrated) [*ml/min*]	539.8	537.1	537.3	551.6	550.7	543.9
$Q_{2,c,c}$ (upper, out, assumed) [*ml/min*]	543.6	540.1	541.4	543.1	543.9	547.4
$Q_{2,s}$ (upper, out, standard) [m^3/s]	8.54E-06	8.49E-06	8.51E-06	8.53E-06	8.54E-06	8.60E-06
$F_{2,CO}$ (upper, out) [*mol/s*]	1.60E-07	1.59E-07	1.60E-07	1.60E-07	1.61E-07	1.62E-07
$C_{2,CO}$ (upper, out) [mol/m^3]	0.0185	0.0194	0.0212	0.0228	0.0247	0.0264
$N_{2,CO}$ (upper, out, CO flux) [$mol/m^2.s$]	5.66E-03	5.64E-03	5.67E-03	5.64E-03	5.69E-03	5.72E-03
$Q_{3,d}$ (lower, in, displayed) [*ml/min*]	498	478	446	421	402	390
$Q_{3,c}$ (lower, in, calibrated) [*ml/min*]	542.5	538.5	533.7	531.1	535.0	541.5
$Q_{3,s}$ (lower, in, standard) [m^3/s]	8.5231E-06	8.46E-06	8.385E-06	8.341E-06	8.403E-06	8.507E-06
$Q_{3,s}$ (lower, in, standard) [*ml/min*]	511.4	507.6	503.1	500.5	504.2	510.4
$F_{3,CO}$ (lower, in) [*mol/s*]	9.1267E-06	9.059E-06	8.979E-06	8.932E-06	8.998E-06	9.11E-06
$C_{3,CO}$ (lower, in) [mol/m^3]	1.0560	1.1059	1.2055	1.3047	1.4043	1.5044
$Q_{4,d}$ (lower, out, displayed) [*ml/min*]	530	522	525	509	524	522
$Q_{4,c}$ (lower, out, calibrated) [*ml/min*]	538.3	528.3	536.7	519.9	534.7	531.7
$Q_{4,c,c}$ (lower, out, assumed) [*ml/min*]	542.5	538.5	533.7	531.1	535.0	541.5
$Q_{4,s}$ (lower, out, standard) [m^3/s]	8.52E-06	8.46E-06	8.38E-06	8.34E-06	8.40E-06	8.51E-06
$F_{4,CO}$ (lower, out) [*mol/s*]	8.97E-06	8.90E-06	8.82E-06	8.77E-06	8.84E-06	8.95E-06
$C_{4,CO}$ (lower, out) [mol/m^3]	1.0375	1.0864	1.1840	1.2814	1.3791	1.4777
dC ($C_{4,CO}$ - $C_{2,CO}$) [mol/m^3]	1.0190	1.0670	1.1628	1.2586	1.3544	1.4513
A (area of the diffusion surface)[m^2]	2.8274E-05	2.827E-05	2.827E-05	2.827E-05	2.827E-05	2.827E-05
L_s (the thickness of the sample) [*m*]	1.748E-04	1.748E-04	1.748E-04	1.748E-04	1.748E-04	1.748E-04
$Y_{3,CO}$ (lower, in) [*ppm*]	24000	24000	24000	24000	24000	24000
$Y_{2,CO,d}$ (upper, out, displayed) [*ppm*]	439	440	441	438	441	440
$Y_{2,CO,c}$ (upper, out, calibrated) [*ppm*]	420.2	421.2	422.2	419.2	422.2	421.2
$Y_{4,CO}$ (lower, out, caculated) [*ppm*]	23578.9	23577.6	23571.7	23571.3	23570.8	23574.2
dY ($Y_{4,CO}$ - $Y_{2,CO,c}$) [*ppm*]	23158.7	23156.4	23149.6	23152.1	23148.6	23153.0
$D_{eff,s}$ (blank cordierite, from dC) [m^2/s]	**9.581E-07**	**9.542E-07**	**9.590E-07**	**9.549E-07**	**9.632E-07**	**9.673E-07**
$D_{eff,s}$ (blank cordierite, from dY) [m^2/s]	**9.581E-07**	**9.542E-07**	**9.590E-07**	**9.549E-07**	**9.632E-07**	**9.673E-07**

Data used in **Figure 3.26** "Effect of pressure in the diffusion cell on experimentally determined D_{eff} values".

(2-plate)

Room temperature [*°C*]	17.6	17.6	17.6	17.6	17.6	17.6
Total thickness [*m*]	1.704E-03	1.704E-03	1.704E-03	1.704E-03	1.704E-03	1.704E-03
Equivalent substrate thickness [*m*]	3.892E-04	3.892E-04	3.892E-04	3.892E-04	3.892E-04	3.892E-04
Equivalent void channel thickness, L_v [*m*]	1.315E-03	1.315E-03	1.315E-03	1.315E-03	1.315E-03	1.315E-03
Diameter [*m*]	0.01	0.01	0.01	0.01	0.01	0.01
Pressure in the cell [*bar abs*]	**1.06**	**1.11**	**1.21**	**1.31**	**1.41**	**1.51**
$Q_{1,d}$ (upper, in, displayed) [*ml/min*]	500	500	500	500	500	500
$Q_{1,c}$ (upper, in, calibrated) [*ml/min*]	541.7	556.9	586.8	611.4	645.1	674.4
$Q_{1,s}$ (upper, in, standard) [m^3/s]	8.48E-06	8.72E-06	9.19E-06	9.57E-06	1.01E-05	1.06E-05
$F_{1,CO}$ (upper, in) [*mol/s*]	0	0	0	0	0	0
$Q_{3,d}$ (upper, out, displayed) [*ml/min*]	440	351	380	399	442	462
$Q_{3,c}$ (upper, out, calibrated) [*ml/min*]	520.2	459.7	505.3	505.1	531.0	545.5
$Q_{3,c,c}$ (upper, out, assumed) [*ml/min*]	541.7	556.9	586.8	611.4	645.1	674.4
$Q_{3,s}$ (upper, out, standard) [m^3/s]	8.48E-06	8.72E-06	9.19E-06	9.57E-06	1.01E-05	1.06E-05
$F_{3,CO}$ (upper, out) [*mol/s*]	1.78E-07	1.78E-07	1.80E-07	1.80E-07	1.78E-07	1.75E-07
$C_{3,CO}$ (upper, out) [mol/m^3]	0.0206	0.0210	0.0220	0.0228	0.0230	0.0232
N_{CO} (the molar flux of CO) [$mol/m^2.s$]	0.0023	0.0023	0.0023	0.0023	0.0023	0.0022
$Q_{2,d}$ (lower, in, displayed) [*ml/min*]	500	500	500	500	500	500
$Q_{2,c}$ (lower, in, calibrated) [*ml/min*]	535.8	548.7	582.9	615.9	644.2	680.8
$Q_{2,s}$ (lower, in, standard) [m^3/s]	8.39E-06	8.59E-06	9.13E-06	9.64E-06	1.01E-05	1.07E-05
$F_{2,CO}$ (lower, in) [*mol/s*]	8.98E-06	9.20E-06	9.77E-06	1.03E-05	1.08E-05	1.14E-05
$C_{2,CO}$ (lower, in) [mol/m^3]	1.0524	1.1021	1.2013	1.3006	1.3999	1.4992
$Q_{4,d}$ (lower, out, displayed) [*ml/min*]	525	552	581	602	612	683
$Q_{4,c}$ (lower, out, calibrated) [*ml/min*]	542.9	563.2	620.3	639.1	633.9	697.8
$Q_{4,c,c}$ (lower, out, assumed) [*ml/min*]	535.8	548.7	582.9	615.9	644.2	680.8
$Q_{4,s}$ (lower, out, standard) [m^3/s]	8.39E-06	8.59E-06	9.13E-06	9.64E-06	1.01E-05	1.07E-05
$F_{4,CO}$ (lower, out) [*mol/s*]	8.81E-06	9.02E-06	9.59E-06	1.01E-05	1.06E-05	1.12E-05
$C_{4,CO}$ (lower, out) [mol/m^3]	1.0316	1.0807	1.1792	1.2780	1.3769	1.4762
A (area of the sample) [m^2]	7.85E-05	7.85E-05	7.85E-05	7.85E-05	7.85E-05	7.85E-05
L_t (equivalent thickness) [*m*]	1.704E-03	1.704E-03	1.704E-03	1.704E-03	1.704E-03	1.704E-03
$Y_{3,CO}$ (lower, in) [*ppm*]	24000	24000	24000	24000	24000	24000
$Y_{2,CO,d}$ (upper, out, displayed) [*ppm*]	486	474	458	440	416	394
$Y_{2,CO,c}$ (upper, out, calibrated) [*ppm*]	470.3	457.4	440.1	420.7	394.7	371.0
$Y_{4,CO}$ (lower, out, caculated) [*ppm*]	23524.5	23535.8	23557.0	23582.4	23604.8	23632.5
dYco ($Y_{4,CO} - Y_{2,CO}$) [*ppm*]	23054.1	23078.4	23116.9	23161.8	23210.0	23261.6
dC ($C_{4,CO} - C_{2,CO}$) [mol/m^3]	1.0109	1.0597	1.1571	1.2552	1.3538	1.4531
$D_{eff,t}$ (total sample, calculated from dC) [m^2/s]	3.75E-06	3.75E-06	3.79E-06	3.77E-06	3.73E-06	3.65E-06
$D_{eff,t}$ (total sample, calculated from dY) [m^2/s]	3.75E-06	3.75E-06	3.79E-06	3.77E-06	3.73E-06	3.65E-06
$L_t/D_{eff,t}$ (total) [*s/m*]	453.9	454.5	449.0	451.7	457.2	466.4
D_{bulk} (bulk diffusion) [m^2/s]	1.94E-05	1.94E-05	1.94E-05	1.94E-05	1.94E-05	1.94E-05
L_v/D_{bulk} (bulk diffusion) [*s/m*]	67.91	67.91	67.91	67.91	67.91	67.91
$(L_t/D_{eff,t}) - (L_v/D_{bulk})$ [*s/m*]	385.9	386.6	381.1	383.8	389.3	398.5
$D_{eff,s}$ (substrate) [m^2/s]	**1.008E-06**	**1.007E-06**	**1.021E-06**	**1.014E-06**	**9.997E-07**	**9.767E-07**

Data used in **Figure 3.26** "Effect of pressure in the diffusion cell on experimentally determined D_{eff} values".

(3-plate)

Room temperature [*°C*]	19.6	19.6	19.6	19.6	19.6	19.6
Total thickness [*m*]	3.216E-03	3.216E-03	3.216E-03	3.216E-03	3.216E-03	3.216E-03
Equivalent substrate thickness [*m*]	5.868E-04	5.868E-04	5.868E-04	5.868E-04	5.868E-04	5.868E-04
Equivalent void thickness, Lv [*m*]	2.630E-03	2.630E-03	2.630E-03	2.630E-03	2.630E-03	2.630E-03
Diameter [*m*]	0.01	0.01	0.01	0.01	0.01	0.01
Pressure in the cell [*bar abs*]	**1.06**	**1.11**	**1.21**	**1.31**	**1.41**	**1.51**
$Q_{1,d}$ (upper, in, displayed) [*ml/min*]	500	500	500	500	500	500
$Q_{1,c}$ (upper, in, calibrated) [*ml/min*]	541.7	556.9	586.8	611.4	645.1	674.4
$Q_{1,s}$ (upper, in, standard) [m^3/s]	8.42E-06	8.66E-06	9.12E-06	9.51E-06	1.00E-05	1.05E-05
$F_{1,CO}$ (upper, in) [*mol/s*]	0	0	0	0	0	0
$Q_{3,d}$ (upper, out, displayed) [*ml/min*]	425	422	426	425	442	420
$Q_{3,c}$ (upper, out, calibrated) [*ml/min*]	507.7	515.8	539.2	525.5	531.0	510.6
$Q_{3,c,c}$ (upper, out, assumed) [*ml/min*]	541.7	556.9	586.8	611.4	645.1	674.4
$Q_{3,s}$ (upper, out, standard) [m^3/s]	8.42E-06	8.66E-06	9.12E-06	9.51E-06	1.00E-05	1.05E-05
$F_{3,CO}$ (upper, out) [*mol/s*]	1.36E-07	1.35E-07	1.32E-07	1.32E-07	1.34E-07	1.33E-07
$C_{3,CO}$ (upper, out) [mol/m^3]	0.0157	0.0160	0.0161	0.0168	0.0174	0.0177
N_{CO} (the molar flux of CO) [$mol/m^2.s$]	1.73E-03	1.73E-03	1.68E-03	1.68E-03	1.71E-03	1.70E-03
$Q_{2,d}$ (lower, in, displayed) [*ml/min*]	500	500	500	500	500	500
$Q_{2,c}$ (lower, in, calibrated) [*ml/min*]	535.8	548.7	582.9	615.9	644.2	680.8
$Q_{2,s}$ (lower, in, standard) [m^3/s]	8.33E-06	8.53E-06	9.06E-06	9.58E-06	1.00E-05	1.06E-05
$F_{2,CO}$ (lower, in) [*mol/s*]	8.92E-06	9.14E-06	9.71E-06	1.03E-05	1.07E-05	1.13E-05
$C_{2,CO}$ (lower, in) [mol/m^3]	1.0452	1.0945	1.1931	1.2917	1.3903	1.4890
$Q_{4,d}$ (lower, out, displayed) [*ml/min*]	525	550	582	642	635	668
$Q_{4,c}$ (lower, out, calibrated) [*ml/min*]	542.9	561.1	621.2	673.7	655.9	682.9
$Q_{4,c,c}$ (lower, out, assumed) [*ml/min*]	535.8	548.7	582.9	615.9	644.2	680.8
$Q_{4,s}$ (lower, out, standard) [m^3/s]	8.33E-06	8.53E-06	9.06E-06	9.58E-06	1.00E-05	1.06E-05
$F_{4,CO}$ (lower, out) [*mol/s*]	8.79E-06	9.00E-06	9.57E-06	1.01E-05	1.06E-05	1.12E-05
$C_{4,CO}$ (lower, out) [mol/m^3]	1.0293	1.0783	1.1769	1.2751	1.3730	1.4715
A (area of the sample) [m^2]	7.85E-05	7.85E-05	7.85E-05	7.85E-05	7.85E-05	7.85E-05
L_t (equivalent thickness) [*m*]	3.22E-03	3.22E-03	3.22E-03	3.22E-03	3.22E-03	3.22E-03
$Y_{3,CO}$ (lower, in) [*ppm*]	24000	24000	24000	24000	24000	24000
$Y_{2,CO,d}$ (upper, out, displayed) [*ppm*]	388	378	354	342	331	317
$Y_{2,CO,c}$ (upper, out, calibrated) [*ppm*]	361.5	350.7	324.7	311.8	299.9	284.8
$Y_{4,CO}$ (lower, out, caculated) [*ppm*]	23634.5	23644.1	23673.1	23690.5	23699.7	23717.9
dYco ($Y_{4,CO}$ - $Y_{2,CO}$) [*ppm*]	23273.0	23293.4	23348.4	23378.7	23399.8	23433.1
dC ($C_{4,CO}$ - $C_{2,CO}$) [mol/m^3]	1.0136	1.0623	1.1607	1.2583	1.3556	1.4538
$D_{eff,t}$ (total sample, calculated from dC) [m^2/s]	5.36E-06	5.34E-06	5.20E-06	5.19E-06	5.26E-06	5.22E-06
$D_{eff,t}$ (total sample, calculated from dY) [m^2/s]	5.36E-06	5.34E-06	5.20E-06	5.19E-06	5.26E-06	5.22E-06
$L_t/D_{eff,t}$ (total) [*s/m*]	600.3	602.5	618.9	619.4	610.9	616.2
D_{bulk} (bulk diffusion) [m^2/s]	1.96E-05	1.96E-05	1.96E-05	1.96E-05	1.96E-05	1.96E-05
L_v/D_{bulk} [*s/m*]	1.34E+02	1.34E+02	1.34E+02	1.34E+02	1.34E+02	1.34E+02
$(L_t/D_{eff,t}) - (L_v/D_{bulk})$ [*s/m*]	465.9	468.1	484.5	485.0	476.5	481.9
$D_{eff,s}$ (substrate) [m^2/s]	**1.260E-06**	**1.254E-06**	**1.211E-06**	**1.210E-06**	**1.231E-06**	**1.218E-06**

Data used in **Figure 3.27** "Effect of gas inlet flowrates in each chamber on experimentally determined D_{eff} values for the rough-surface cordierite plates".

(Single-plate)

Temperature [*°C*]	16.7	16.7	16.6	16.6	16.6
Thickness [*m*]	1.748E-04	1.748E-04	1.748E-04	1.748E-04	1.748E-04
Diameter [*m*]	0.006	0.006	0.006	0.006	0.006
Pressure in the cell [*bar abs*]	**1.06**	**1.06**	**1.06**	**1.06**	**1.06**
$Q_{1,d}$ (upper, in, displayed) [*ml/min*]	691	592	494	393	297
$Q_{1,c}$ (upper, in, calibrated) [*ml/min*]	759.0	650.2	542.5	431.6	326.1
$Q_{1,s}$ (upper, in, standard) [m^3/s]	1.19E-05	1.02E-05	8.52E-06	6.78E-06	5.12E-06
$Q_{1,s}$ (upper, in, standard) [*ml/min*]	715.3	612.8	511.4	406.8	307.4
$F_{1,CO}$ (upper, in) [*mol/s*]	0	0	0	0	0
$Q_{2,d}$ (upper, out, displayed) [*ml/min*]	712	603	506	409	318
$Q_{2,c}$ (upper, out, calibrated) [*ml/min*]	759.1	641.6	537.1	432.5	334.4
$Q_{2,c,c}$ (upper, out, assumed) [*ml/min*]	759.0	650.2	542.5	431.6	326.1
$Q_{2,s}$ (upper, out, standard) [m^3/s]	1.19E-05	1.02E-05	8.52E-06	6.78E-06	5.12E-06
$F_{2,CO}$ (upper, out) [*mol/s*]	1.67E-07	1.66E-07	1.61E-07	1.51E-07	1.37E-07
$C_{2,CO}$ (upper, out) [mol/m^3]	1.38E-02	1.60E-02	1.86E-02	2.20E-02	2.64E-02
$N_{2,CO}$ (upper, out, CO flux) [$mol/m^2.s$]	5.92E-03	5.87E-03	5.68E-03	5.35E-03	4.85E-03
$Q_{3,d}$ (lower, in, displayed) [*ml/min*]	692	595	495	399	292
$Q_{3,c}$ (lower, in, calibrated) [*ml/min*]	751.8	647.1	539.2	435.6	320.2
$Q_{3,s}$ (lower, in, standard) [m^3/s]	1.18E-05	1.02E-05	8.47E-06	6.84E-06	5.03E-06
$Q_{3,s}$ (lower, in, standard) [*ml/min*]	708.5	609.8	508.3	410.7	301.8
$F_{3,CO}$ (lower, in) [*mol/s*]	1.26E-05	1.09E-05	9.07E-06	7.33E-06	5.39E-06
$C_{3,CO}$ (lower, in) [mol/m^3]	1.06E+00	1.06E+00	1.06E+00	1.06E+00	1.06E+00
$Q_{4,d}$ (lower, out, displayed) [*ml/min*]	725	619	524	425	320
$Q_{4,c}$ (lower, out, calibrated) [*ml/min*]	736.9	627.9	530.3	428.6	320.7
$Q_{4,c,c}$ (lower, out, assumed) [*ml/min*]	751.8	647.1	539.2	435.6	320.2
$Q_{4,s}$ (lower, out, standard) [m^3/s]	1.18E-05	1.02E-05	8.47E-06	6.84E-06	5.03E-06
$F_{4,CO}$ (lower, out) [*mol/s*]	1.25E-05	1.07E-05	8.91E-06	7.18E-06	5.25E-06
$C_{4,CO}$ (lower, out) [mol/m^3]	1.0417	1.0396	1.0374	1.0343	1.0291
dC ($C_{4,CO}$ - $C_{2,CO}$) [mol/m^3]	1.0279	1.0235	1.0188	1.0123	1.0027
A (area of the diffusion surface)[m^2]	2.83E-05	2.83E-05	2.83E-05	2.83E-05	2.83E-05
L_s (thickness of the sample) [*m*]	1.748E-04	1.748E-04	1.748E-04	1.748E-04	1.748E-04
$Y_{3,CO}$ (lower, in) [*ppm*]	24000	24000	24000	24000	24000
$Y_{2,CO,d}$ (upper, out, displayed) [*ppm*]	333	383	441	519	620
$Y_{2,CO,c}$ (upper, out, calibrated) [*ppm*]	314.7	364.5	422.2	499.8	600.3
$Y_{4,CO}$ (lower, out, caculated) [*ppm*]	23682.3	23633.8	23575.2	23504.9	23388.6
dY ($Y_{4,CO}$ - $Y_{2,CO,c}$) [*ppm*]	23367.6	23269.4	23153.1	23005.1	22788.3
$D_{eff,s}$ (blank cordierite, from dC) [m^2/s]	**9.925E-07**	**9.889E-07**	**9.609E-07**	**9.107E-07**	**8.344E-07**
$D_{eff,s}$ (blank cordierite, from dY) [m^2/s]	**9.925E-07**	**9.889E-07**	**9.609E-07**	**9.107E-07**	**8.344E-07**

Data used in **Figure 3.27** "Effect of gas inlet flowrates in each chamber on experimentally determined D_{eff} values for the rough-surface cordierite plates".

(2-plate)

Room temperature [*°C*]	15.4	15.4	15.4	15.4	15.4	15.4	15.4
Total thickness [*m*]	1.704E-03	1.704E-03	1.704E-03	1.704E-03	1.704E-03	1.704E-03	1.704E-03
Equivalent substrate thickness [*m*]	3.892E-04	3.892E-04	3.892E-04	3.892E-04	3.892E-04	3.892E-04	3.892E-04
Equivalent void thickness, L_v [*m*]	1.315E-03	1.315E-03	1.315E-03	1.315E-03	1.315E-03	1.315E-03	1.315E-03
Diameter [*m*]	0.01	0.01	0.01	0.01	0.01	0.01	0.01
Pressure in the cell [*bar abs*]	**1.06**	**1.06**	**1.06**	**1.06**	**1.06**	**1.06**	**1.06**
$Q_{1,d}$ (upper, in, displayed) [*ml/min*]	800	700	600	500	400	300	200
$Q_{1,c}$ (upper, in, calibrated) [*ml/min*]	867.0	758.6	650.1	541.7	433.3	324.8	216.4
$Q_{1,s}$ (upper, in, standard) [m^3/s]	1.37E-05	1.2E-05	1.03E-05	8.55E-06	6.84E-06	5.13E-06	3.41E-06
$F_{1,CO}$ (upper, in) [*mol/s*]	0	0	0	0	0	0	0
$Q_{3,d}$ (upper, out, displayed) [*ml/min*]	828	722	613	508	325	210	101
$Q_{3,c}$ (upper, out, calibrated) [*ml/min*]	871.9	765.5	656.2	550.8	367.2	251.7	142.4
$Q_{3,c,c}$ (upper, out, assumed) [*ml/min*]	867.0	758.6	650.1	541.7	433.3	324.8	216.4
$Q_{3,s}$ (upper, out, standard) [m^3/s]	1.37E-05	1.2E-05	1.03E-05	8.55E-06	6.84E-06	5.13E-06	3.41E-06
$F_{3,CO}$ (upper, out) [*mol/s*]	1.87E-07	1.86E-07	1.85E-07	1.82E-07	1.76E-07	1.67E-07	1.63E-07
$C_{3,CO}$ (upper, out) [mol/m^3]	0.0136	0.0154	0.0178	0.0211	0.0255	0.0322	0.0472
N_{CO} (the molar flux of CO) [$mol/m^2.s$]	0.0024	0.0024	0.0023	0.0023	0.0022	0.0021	0.0021
$Q_{2,d}$ (lower, in, displayed) [*ml/min*]	800	700	600	500	400	300	200
$Q_{2,c}$ (lower, in, calibrated) [*ml/min*]	845.2	742.1	638.9	535.8	432.6	329.5	226.3
$Q_{2,s}$ (lower, in, standard) [m^3/s]	1.33E-05	1.17E-05	1.01E-05	8.45E-06	6.83E-06	5.2E-06	3.57E-06
$F_{2,CO}$ (lower, in) [*mol/s*]	1.43E-05	1.25E-05	1.08E-05	9.05E-06	7.31E-06	5.57E-06	3.82E-06
$C_{2,CO}$ (lower, in) [mol/m^3]	1.0604	1.0604	1.0604	1.0604	1.0604	1.0604	1.0604
$Q_{4,d}$ (lower, out, displayed) [*ml/min*]	822	710	614	535	431	250	151
$Q_{4,c}$ (lower, out, calibrated) [*ml/min*]	840.8	728.5	632.2	552.9	448.6	267.0	167.7
$Q_{4,c,c}$ (lower, out, assumed) [*ml/min*]	845.2	742.1	638.9	535.8	432.6	329.5	226.3
$Q_{4,s}$ (lower, out, standard) [m^3/s]	1.33E-05	1.17E-05	1.01E-05	8.45E-06	6.83E-06	5.2E-06	3.57E-06
$F_{4,CO}$ (lower, out) [*mol/s*]	1.41E-05	1.24E-05	1.06E-05	8.87E-06	7.13E-06	5.4E-06	3.66E-06
$C_{4,CO}$ (lower, out) [mol/m^3]	1.0465	1.0447	1.0423	1.0391	1.0349	1.0287	1.0153
A (area of the sample) [m^2]	7.85E-05	7.85E-05	7.85E-05	7.85E-05	7.85E-05	7.85E-05	7.85E-05
L_t (equivalent thickness of the sample) [*m*]	0.001704	0.001704	0.001704	0.001704	0.001704	0.001704	0.001704
$Y_{3,CO}$ (lower, in) [*ppm*]	24000	24000	24000	24000	24000	24000	24000
$Y_{2,CO,d}$ (upper, out, displayed) [*ppm*]	309	347	398	466	559	699	1013
$Y_{2,CO,c}$ (upper, out, calibrated) [*ppm*]	307.1	348.2	403.3	476.7	577.2	728.5	1067.7
$Y_{4,CO}$ (lower, out, caculated) [*ppm*]	23685.0	23644.1	23589.7	23518.0	23421.9	23281.8	22979.1
dYco ($Y_{4,CO} - Y_{2,CO}$) [*ppm*]	23377.8	23295.9	23186.4	23041.2	22844.7	22553.4	21911.5
dC ($C_{4,CO} - C_{2,CO}$) [mol/m^3]	1.0329	1.0293	1.0245	1.0181	1.0094	0.9965	0.9682
$D_{eff,t}$ (total sample, calculated from dC) [m^2/s]	3.90E-06	3.88E-06	3.87E-06	3.84E-06	3.75E-06	3.59E-06	3.61E-06
$D_{eff,t}$ (total sample, calculated from dY) [m^2/s]	3.90E-06	3.88E-06	3.87E-06	3.84E-06	3.75E-06	3.59E-06	3.61E-06
$L_t/D_{eff,t}$ (total) [*s/m*]	437.0	439.1	440.2	444.1	454.7	474.5	472.1
D_{bulk} (bulk diffusion) [m^2/s]	1.92E-05	1.92E-05	1.92E-05	1.92E-05	1.92E-05	1.92E-05	1.92E-05
L_v/D_{bulk} [*s/m*]	6.86E+01	6.86E+01	6.86E+01	6.86E+01	6.86E+01	6.86E+01	6.86E+01
$(L_t/D_{eff,t}) - (L_v/D_{bulk})$ [*s/m*]	368.4	370.4	371.6	375.5	386.1	405.8	403.4
$D_{eff,s}$ (substrate) [m^2/s]	**1.056E-06**	**1.051E-06**	**1.047E-06**	**1.036E-06**	**1.008E-06**	**9.590E-07**	**9.647E-07**

Data used in **Figure 3.27** "Effect of gas inlet flowrates in each chamber on experimentally determined D_{eff} values for the rough-surface cordierite plates".

(3-plate)

Room temperature [*°C*]	16.8	16.8	16.8	16.8	16.8	16.8	16.8
Total thickness [*m*]	3.216E-03	3.216E-03	3.216E-03	3.216E-03	3.216E-03	3.216E-03	3.216E-03
Equivalent substrate thickness [*m*]	5.868E-04	5.868E-04	5.868E-04	5.868E-04	5.868E-04	5.868E-04	5.868E-04
Equivalent void thickness, L_v [*m*]	2.630E-03	2.630E-03	2.630E-03	2.630E-03	2.630E-03	2.630E-03	2.630E-03
Diameter [*m*]	0.01	0.01	0.01	0.01	0.01	0.01	0.01
Pressure in the cell [*bar abs*]	**1.06**	**1.06**	**1.06**	**1.06**	**1.06**	**1.06**	**1.06**
$Q_{1,d}$ (upper, in, displayed) [*ml/min*]	800	700	600	500	400	300	200
$Q_{1,c}$ (upper, in, calibrated) [*ml/min*]	867.0	758.6	650.1	541.7	433.3	324.8	216.4
$Q_{1,s}$ (upper, in, standard) [m^3/s]	1.36E-05	1.19E-05	1.02E-05	8.51E-06	6.80E-06	5.10E-06	3.40E-06
$F_{1,CO}$ (upper, in) [*mol/s*]	0	0	0	0	0	0	0
$Q_{3,d}$ (upper, out, displayed) [*ml/min*]	825	724	540	380	251	175	101
$Q_{3,c}$ (upper, out, calibrated) [*ml/min*]	868.9	767.5	582.9	422.3	292.9	216.6	142.4
$Q_{3,c,c}$ (upper, out, assumed) [*ml/min*]	867.0	758.6	650.1	541.7	433.3	324.8	216.4
$Q_{3,s}$ (upper, out, standard) [m^3/s]	1.36E-05	1.19E-05	1.02E-05	8.51E-06	6.8E-06	5.1E-06	3.4E-06
$F_{3,CO}$ (upper, out) [*mol/s*]	1.38E-07	1.32E-07	1.34E-07	1.35E-07	1.33E-07	1.3E-07	1.26E-07
$C_{3,CO}$ (upper, out) [mol/m^3]	9.96E-03	1.10E-02	1.29E-02	1.57E-02	1.92E-02	2.51E-02	3.65E-02
N_{CO} (the molar flux of CO) [$mol/m^2.s$]	1.75E-03	1.69E-03	1.70E-03	1.72E-03	1.69E-03	1.65E-03	1.60E-03
$Q_{2,d}$ (lower, in, displayed) [*ml/min*]	800	700	600	500	400	300	200
$Q_{2,c}$ (lower, in, calibrated) [*ml/min*]	845.2	742.1	638.9	535.8	432.6	329.5	226.3
$Q_{2,s}$ (lower, in, standard) [m^3/s]	1.33E-05	1.17E-05	1E-05	8.41E-06	6.79E-06	5.17E-06	3.55E-06
$F_{2,CO}$ (lower, in) [*mol/s*]	1.42E-05	1.25E-05	1.07E-05	9.01E-06	7.27E-06	5.54E-06	3.81E-06
$C_{2,CO}$ (lower, in) [mol/m^3]	1.0553	1.0553	1.0553	1.0553	1.0553	1.0553	1.0553
$Q_{4,d}$ (lower, out, displayed) [*ml/min*]	822	719	646	542	351	276	170
$Q_{4,c}$ (lower, out, calibrated) [*ml/min*]	840.8	737.5	664.3	559.9	368.3	293.1	186.8
$Q_{4,c,c}$ (lower, out, assumed) [*ml/min*]	845.2	742.1	638.9	535.8	432.6	329.5	226.3
$Q_{4,s}$ (lower, out, standard) [m^3/s]	1.33E-05	1.17E-05	1E-05	8.41E-06	6.79E-06	5.17E-06	3.55E-06
$F_{4,CO}$ (lower, out) [*mol/s*]	1.41E-05	1.23E-05	1.06E-05	8.87E-06	7.14E-06	5.41E-06	3.68E-06
$C_{4,CO}$ (lower, out) [mol/m^3]	1.0451	1.0441	1.0422	1.0395	1.0361	1.0306	1.0204
A (area of the sample) [m^2]	7.85E-05	7.85E-05	7.85E-05	7.85E-05	7.85E-05	7.85E-05	7.85E-05
L_t (equivalent thickness) [*m*]	3.216E-03	3.216E-03	3.216E-03	3.216E-03	3.216E-03	3.216E-03	3.216E-03
$Y_{3,CO}$ (lower, in) [*ppm*]	24000	24000	24000	24000	24000	24000	24000
$Y_{2,CO,d}$ (upper, out, displayed) [*ppm*]	239	260	301	359	434	558	798
$Y_{2,CO,c}$ (upper, out, calibrated) [*ppm*]	226.5	249.2	293.5	356.2	437.2	571.1	830.4
$Y_{4,CO}$ (lower, out, caculated) [*ppm*]	23767.7	23745.3	23701.4	23639.9	23562.2	23436.9	23206.0
dYco ($Y_{4,CO}$ - $Y_{2,CO}$) [*ppm*]	23541.1	23496.1	23407.9	23283.8	23125.0	22865.8	22375.6
dC ($C_{4,CO}$ - $C_{2,CO}$) [mol/m^3]	1.0351	1.0332	1.0293	1.0238	1.0168	1.0054	0.9839
$D_{eff,t}$ (total sample, calculated from dY) [m^2/s]	5.36E-06	5.17E-06	5.24E-06	5.33E-06	5.27E-06	5.22E-06	5.16E-06
$L_t/D_{eff,t}$ (total) [*s/m*]	599.6	621.7	613.7	603.7	610.7	616.5	622.8
D_{bulk} (bulk diffusion) [m^2/s]	1.93E-05	1.93E-05	1.93E-05	1.93E-05	1.93E-05	1.93E-05	1.93E-05
L_v/D_{bulk} [*s/m*]	1.36E+02	1.36E+02	1.36E+02	1.36E+02	1.36E+02	1.36E+02	1.36E+02
$(L_t/D_{eff,t}) - (L_v/D_{bulk})$ [*s/m*]	463.4	485.5	477.4	467.4	474.4	480.3	486.6
$D_{eff,s}$ (substrate) [m^2/s]	**1.266E-06**	**1.209E-06**	**1.229E-06**	**1.255E-06**	**1.237E-06**	**1.222E-06**	**1.206E-06**

Data used in **Figure 3.28** "Experimental D_{eff} values when gas flow is different in the upper and lower chambers".

Temperature [°C]	15.1	15.1	15.1	15.1	15.1	15.1	15.1
Thickness [m]	1.62E-04	1.62E-04	1.62E-04	1.62E-04	1.62E-04	1.62E-04	1.62E-04
Diameter [m]	6.00E-03	6.00E-03	6.00E-03	6.00E-03	6.00E-03	6.00E-03	6.00E-03
Pressure in the cell [bar abs]	**1.11**	**1.11**	**1.11**	**1.11**	**1.11**	**1.11**	**1.11**
$Q_{1,d}$ (upper, in, displayed) [ml/min]	500	580	686	766	392	300	194
$Q_{1,c}$ (upper, in, calibrated) [ml/min]	554.8	643.0	759.8	848.0	435.7	334.3	217.4
$Q_{1,s}$ (upper, in, standard) [m^3/s]	8.76E-06	1.02E-05	1.2E-05	1.34E-05	6.88E-06	5.28E-06	3.43E-06
$F_{1,CO}$ (upper, in) [mol/s]	0	0	0	0	0	0	0
$Q_{2,d}$ (upper, out, displayed) [ml/min]	348	395	502	578	247	253	130
$Q_{2,c}$ (upper, out, calibrated) [ml/min]	366.8	417.4	532.8	614.7	257.9	264.4	131.8
$Q_{2,c,c}$ (upper, out, assumed) [ml/min]	554.8	643.0	759.8	848.0	435.7	334.3	217.4
$Q_{2,s}$ (upper, out, standard) [m^3/s]	8.76E-06	1.02E-05	1.2E-05	1.34E-05	6.88E-06	5.28E-06	3.43E-06
$F_{2,CO}$ (upper, out) [mol/s]	2.01E-07	2.02E-07	1.99E-07	1.83E-07	1.95E-07	1.88E-07	1.66E-07
$C_{2,CO}$ (upper, out) [mol/m^3]	0.0239	0.0206	0.0172	0.0142	0.0294	0.0370	0.0502
$Q_{3,d}$ (lower, in, displayed) [ml/min]	500	394	290	180	610	705	808
$Q_{3,c}$ (lower, in, calibrated) [ml/min]	559.0	443.1	329.4	209.1	679.2	783.1	895.7
$Q_{3,s}$ (lower, in, standard) [m^3/s]	8.83E-06	7E-06	5.2E-06	3.3E-06	1.07E-05	1.24E-05	1.41E-05
$F_{3,CO}$ (lower, in) [mol/s]	9.45E-06	7.49E-06	5.57E-06	3.54E-06	1.15E-05	1.32E-05	1.51E-05
$C_{3,CO}$ (lower, in) [mol/m^3]	1.1116	1.1116	1.1116	1.1116	1.1116	1.1116	1.1116
$Q_{4,d}$ (lower, out, displayed) [ml/min]	550	445	335	220	658	755	880
$Q_{4,c}$ (lower, out, calibrated) [ml/min]	557.0	449.2	336.1	218.0	668.0	767.7	896.1
$Q_{4,c,c}$ (lower, out, assumed) [ml/min]	559.0	443.1	329.4	209.1	679.2	783.1	895.7
$Q_{4,s}$ (lower, out, standard) [m^3/s]	8.83E-06	7E-06	5.2E-06	3.3E-06	1.07E-05	1.24E-05	1.41E-05
$F_{4,CO}$ (lower, out) [mol/s]	9.25E-06	7.29E-06	5.37E-06	3.35E-06	1.13E-05	1.31E-05	1.5E-05
$C_{4,CO}$ (lower, out) [mol/m^3]	1.0879	1.0817	1.0719	1.0542	1.0928	1.0958	1.0994
dC ($C_{4,CO}$ - $C_{2,CO}$) [mol/m^3]	1.0641	1.0611	1.0547	1.0400	1.0634	1.0589	1.0492
A (area of the diffusion surface)[m^2]	2.83E-05	2.83E-05	2.83E-05	2.83E-05	2.83E-05	2.83E-05	2.83E-05
L_S (thickness of the cordierite) [m]	1.62E-04	1.62E-04	1.62E-04	1.62E-04	1.62E-04	1.62E-04	1.62E-04
$Y_{3,CO}$ (lower, in) [ppm]	24000	24000	24000	24000	24000	24000	24000
$Y_{2,CO,d}$ (upper, out, displayed) [ppm]	500	433	363	300	614	770	1044
$Y_{2,CO,c}$ (upper, out, calibrated) [ppm]	515.2	445.0	371.8	305.8	634.5	797.8	1084.6
$Y_{4,CO}$ (lower, out, caculated) [ppm]	23488.7	23354.2	23142.4	22759.9	23593.0	23659.5	23736.7
dY ($Y_{4,CO}$ - $Y_{2,CO,c}$) [ppm]	22973.5	22909.1	22770.6	22454.1	22958.5	22861.6	22652.1
Flowrate difference [ml/min]	**0**	**186**	**396**	**586**	**-218**	**-405**	**-614**
$D_{eff,S}$ (blank cordierite, from dC) [m^2/s]	**1.13E-06**	**1.13E-06**	**1.12E-06**	**1.05E-06**	**1.09E-06**	**1.06E-06**	**9.42E-07**
$D_{eff,S}$ (blank cordierite, from dY) [m^2/s]	**1.13E-06**	**1.13E-06**	**1.12E-06**	**1.05E-06**	**1.09E-06**	**1.06E-06**	**9.42E-07**

Data used in **Figure 3.29** "Effect of pressure difference between the two chambers".

Temperature [°C]	15.1	15.1	15.1	15.1	15.1	15.1
Thickness [m]	1.62E-04	1.62E-04	1.62E-04	1.62E-04	1.62E-04	1.62E-04
Diameter [m]	0.006	0.006	0.006	0.006	0.006	0.006
Pressure in the cell [bar abs]	**1.11**	**1.11**	**1.11**	**1.11**	**1.11**	**1.11**
Pressure difference [mbar * 5]	2.5	-1.0	-3.0	-6.0	-9.5	-12.0
Pressure difference [mbar]	**0.5**	**-0.2**	**-0.6**	**-1.2**	**-1.9**	**-2.4**
$Q_{1,d}$ (upper, in, displayed) [ml/min]	500	500	500	500	500	500
$Q_{1,c}$ (upper, in, calibrated) [ml/min]	554.8	554.8	554.8	554.8	554.8	554.8
$Q_{1,s}$ (upper, in, standard) [m^3/s]	8.76E-06	8.76E-06	8.76E-06	8.76E-06	8.76E-06	8.76E-06
$F_{1,CO}$ (upper, in) [mol/s]	0	0	0	0	0	0
$Q_{2,d}$ (upper, out, displayed) [ml/min]	342	343	344	342	341	322
$Q_{2,c}$ (upper, out, calibrated) [ml/min]	360.3	361.4	362.4	360.3	359.2	338.7
$Q_{2,c,c}$ (upper, out, 2nd calibrated) [ml/min]	554.8	554.8	554.8	554.8	554.8	554.8
$Q_{2,s}$ (upper, out, standard) [m^3/s]	8.76E-06	8.76E-06	8.76E-06	8.76E-06	8.76E-06	8.76E-06
$F_{2,CO}$ (upper, out) [mol/s]	2.16E-07	1.85E-07	1.74E-07	1.61E-07	1.43E-07	1.27E-07
$C_{2,CO}$ (upper, out) [mol/m^3]	2.56E-02	2.20E-02	2.06E-02	1.91E-02	1.69E-02	1.50E-02
$Q_{3,d}$ (lower, in, displayed) [ml/min]	500	500	500	500	500	500
$Q_{3,c}$ (lower, in, calibrated) [ml/min]	559.0	559.0	559.0	559.0	559.0	559.0
$Q_{3,s}$ (lower, in, standard) [m^3/s]	8.83E-06	8.83E-06	8.83E-06	8.83E-06	8.83E-06	8.83E-06
$F_{3,CO}$ (lower, in) [mol/s]	9.45E-06	9.45E-06	9.45E-06	9.45E-06	9.45E-06	9.45E-06
$C_{3,CO}$ (lower, in) [mol/m^3]	1.1116	1.1116	1.1116	1.1116	1.1116	1.1116
$Q_{4,d}$ (lower, out, displayed) [ml/min]	549	533	555	561	570	578
$Q_{4,c}$ (lower, out, calibrated) [ml/min]	556.0	539.6	562.2	568.3	577.6	585.8
$Q_{4,c,c}$ (lower, out, 2nd calibrated) [ml/min]	559.0	559.0	559.0	559.0	559.0	559.0
$Q_{4,s}$ (lower, out, standard) [m^3/s]	8.83E-06	8.83E-06	8.83E-06	8.83E-06	8.83E-06	8.83E-06
$F_{4,CO}$ (lower, out) [mol/s]	9.24E-06	9.27E-06	9.28E-06	9.29E-06	9.31E-06	9.33E-06
$C_{4,CO}$ (lower, out) [mol/m^3]	1.0862	1.0898	1.0912	1.0927	1.0948	1.0967
dC ($C_{4,CO}$ - $C_{2,CO}$) [mol/m^3]	1.0606	1.0678	1.0705	1.0736	1.0779	1.0818
A (area of the diffusion surface)[m^2]	2.83E-05	2.83E-05	2.83E-05	2.83E-05	2.83E-05	2.83E-05
L_S (thickness of the cordierite) [m]	1.62E-04	1.62E-04	1.62E-04	1.62E-04	1.62E-04	1.62E-04
$Y_{3,CO}$ (lower, in) [ppm]	24000	24000	24000	24000	24000	24000
$Y_{2,CO,d}$ (upper, out, displayed) [ppm]	536	461	433	401	357	317
$Y_{2,CO,c}$ (upper, out, calibrated) [ppm]	552.9	474.4	445.0	411.6	365.5	323.6
$Y_{4,CO}$ (lower, out, caculated) [ppm]	23451.3	23529.2	23558.3	23591.5	23637.3	23678.8
dY ($Y_{4,CO}$ - $Y_{2,CO,c}$) [ppm]	22898.4	23054.9	23113.3	23180.0	23271.8	23355.2
$D_{eff,S}$ (blank cordierite, from dC) [m^2/s]	**1.212E-06**	**1.033E-06**	**9.666E-07**	**8.913E-07**	**7.884E-07**	**6.956E-07**
$D_{eff,S}$ (blank cordierite, from dY) [m^2/s]	**1.212E-06**	**1.033E-06**	**9.666E-07**	**8.913E-07**	**7.884E-07**	**6.956E-07**

Data used in **Figure 3.29** "Effect of pressure difference between the two chambers".

Temperature [°C]	15.1	15.1	15.1	15.1	15.1
Thickness [m]	1.62E-04	1.62E-04	1.62E-04	1.62E-04	1.62E-04
Diameter [m]	0.006	0.006	0.006	0.006	0.006
Pressure in the cell [bar abs]	**1.11**	**1.11**	**1.11**	**1.11**	**1.11**
Pressure difference [mbar * 5]	-28.0	5.0	10.0	15.0	1.0
Pressure difference [mbar]	**-5.6**	**1**	**2**	**3**	**0.2**
$Q_{1,d}$ (upper, in, displayed) [ml/min]	500	500	500	500	500
$Q_{1,c}$ (upper, in, calibrated) [ml/min]	554.8	554.8	554.8	554.8	554.8
$Q_{1,s}$ (upper, in, standard) [m^3/s]	8.76E-06	8.76E-06	8.76E-06	8.76E-06	8.76E-06
$F_{1,CO}$ (upper, in) [mol/s]	0	0	0	0	0
$Q_{2,d}$ (upper, out, displayed) [ml/min]	322	349	348	349	348
$Q_{2,c}$ (upper, out, calibrated) [ml/min]	338.7	367.8	366.8	367.8	366.8
$Q_{2,c,c}$ (upper, out, 2nd calibrated) [ml/min]	554.8	554.8	554.8	554.8	554.8
$Q_{2,s}$ (upper, out, standard) [m^3/s]	8.76E-06	8.76E-06	8.76E-06	8.76E-06	8.76E-06
$F_{2,CO}$ (upper, out) [mol/s]	9.21E-08	2.80E-07	4.18E-07	5.15E-07	2.01E-07
$C_{2,CO}$ (upper, out) [mol/m^3]	1.09E-02	3.32E-02	4.95E-02	6.10E-02	2.39E-02
$Q_{3,d}$ (lower, in, displayed) [ml/min]	500	500	500	500	500
$Q_{3,c}$ (lower, in, calibrated) [ml/min]	559.0	559.0	559.0	559.0	559.0
$Q_{3,s}$ (lower, in, standard) [m^3/s]	8.83E-06	8.83E-06	8.83E-06	8.83E-06	8.83E-06
$F_{3,CO}$ (lower, in) [mol/s]	9.45E-06	9.45E-06	9.45E-06	9.45E-06	9.45E-06
$C_{3,CO}$ (lower, in) [mol/m^3]	1.1116	1.1116	1.1116	1.1116	1.1116
$Q_{4,d}$ (lower, out, displayed) [ml/min]	598	546	534	521	550
$Q_{4,c}$ (lower, out, calibrated) [ml/min]	606.4	552.9	540.6	527.2	557.0
$Q_{4,c,c}$ (lower, out, 2nd calibrated) [ml/min]	559.0	559.0	559.0	559.0	559.0
$Q_{4,s}$ (lower, out, standard) [m^3/s]	8.83E-06	8.83E-06	8.83E-06	8.83E-06	8.83E-06
$F_{4,CO}$ (lower, out) [mol/s]	9.36E-06	9.17E-06	9.04E-06	8.94E-06	9.25E-06
$C_{4,CO}$ (lower, out) [mol/m^3]	1.1008	1.0786	1.0625	1.0511	1.0879
dC ($C_{4,CO}$ - $C_{2,CO}$) [mol/m^3]	1.0899	1.0454	1.0130	0.9901	1.0641
A (area of the diffusion surface)[m^2]	2.83E-05	2.83E-05	2.83E-05	2.83E-05	2.83E-05
L_s (thickness of the cordierite) [m]	1.62E-04	1.62E-04	1.62E-04	1.62E-04	1.62E-04
$Y_{3,CO}$ (lower, in) [ppm]	24000	24000	24000	24000	24000
$Y_{2,CO,d}$ (upper, out, displayed) [ppm]	233	693	1029	1266	500
$Y_{2,CO,c}$ (upper, out, calibrated) [ppm]	235.7	717.2	1068.9	1317.0	515.2
$Y_{4,CO}$ (lower, out, caculated) [ppm]	23766.1	23288.2	22939.1	22692.9	23488.7
dY ($Y_{4,CO}$ - $Y_{2,CO,c}$) [ppm]	23530.4	22571.0	21870.2	21375.9	22973.5
$D_{eff,S}$ (blank cordierite, from dC) [m^2/s]	**5.028E-07**	**1.595E-06**	**2.454E-06**	**3.093E-06**	**1.126E-06**
$D_{eff,S}$ (blank cordierite, from dY) [m^2/s]	**5.028E-07**	**1.595E-06**	**2.454E-06**	**3.093E-06**	**1.126E-06**

Appendix D2

Experimental data on the measurement of D_{eff} in Chapter 4

Data used in **Figures 9 & 10** "Effect of the washcoat thickness on the measured D_{eff} values (in **Sample S3)**".

Plate No	**31**	**33**	**36**	**37**
Slurry used	S_3	S_3	S_3	S_3
Temperature [°C]	16.0	15.7	16.2	16.1
Total thickness [m]	2.11E-04	2.26E-04	2.31E-04	2.77E-04
Washcoat thickness [m]	4.86E-05	6.41E-05	6.92E-05	1.15E-04
Cordierite thickness [m]	1.62E-04	1.62E-04	1.62E-04	1.62E-04
Diameter [m]	0.01	0.01	0.01	0.01
Pressure in the cell [bar (a)]	**1.11**	**1.11**	**1.11**	**1.11**
$Q_{1,d}$ (upper, in, displayed) [ml/min]	600	600	600	600
$Q_{1,c}$ (upper, in, calibrated) [ml/min]	645.55	645.55	645.55	645.55
$Q_{1,s}$ (upper, in, standard) [m^3/s]	1.016E-05	1.017E-05	1.016E-05	1.016E-05
$F_{1,CO}$ (CO flux, upper, in) [mol/s]	0.00	0.00	0.00	0.00
$Q_{2,d}$ (upper, out, displayed) [ml/min]	435	456	428	452
$Q_{2,c}$ (upper, out, calibrated) [ml/min]	462.04	484.70	454.48	480.39
$Q_{2,c,c}$ (upper, out, assumed) [ml/min]	645.55	645.55	645.55	645.55
$Q_{2,s}$ (upper, out, standard) [m^3/s]	1.016E-05	1.017E-05	1.016E-05	1.016E-05
$F_{2,CO}$ (upper, out) [mol/s]	2.914E-07	2.740E-07	2.436E-07	2.759E-07
$C_{2,CO}$ (concentration, upper, out) [mol/m^3]	0.0297	0.0279	0.0248	0.0281
$Q_{3,d}$ (lower, in, displayed) [ml/min]	600	600	600	600
$Q_{3,c}$ (lower, in, calibrated) [ml/min]	644.13	644.13	644.13	644.13
$Q_{3,s}$ (lower, in, standard) [m^3/s]	1.0141E-05	1.0152E-05	1.0134E-05	1.0138E-05
$F_{3,CO}$ (CO flux, lower, in) [mol/s]	1.086E-05	1.0871E-05	1.0852E-05	1.0856E-05
$C_{3,CO}$ (concentration, lower, in) [mol/m^3]	1.1543	1.1555	1.1535	1.1539
$Q_{4,d}$ (lower, out, displayed) [ml/min]	647	643	642	643
$Q_{4,c}$ (lower, out, calibrated) [ml/min]	657.99	653.90	652.88	653.90
$Q_{4,c,c}$ (lower, out, assumed) [ml/min]	644.13	644.13	644.13	644.13
$Q_{4,s}$ (lower, out, standard) [m^3/s]	1.0141E-05	1.0152E-05	1.0134E-05	1.0138E-05
$F_{4,CO}$ (lower, out) [mol/s]	1.0568E-05	1.0597E-05	1.0609E-05	1.058E-05
$C_{4,CO}$ (concentration, lower, out) [mol/m^3]	1.0784	1.0814	1.0825	1.0796
A (diffusion area in the sample) [m^2]	0.00007854	0.00007854	0.00007854	0.00007854

L_t (total thickness of the sample) [m]	2.11E-04	2.26E-04	2.31E-04	2.77E-04
$Y_{3,CO}$ (lower, in) [ppm]	24000	24000	24000	24000
$Y_{2,CO,d}$ (upper, out, displayed) [ppm]	644	605	539	610
$Y_{2,CO,c}$ (upper, out, calibrated) [ppm]	642.5	603.5	537.5	608.5
$Y_{4,CO}$ (lower, out, caculated) [ppm]	23356	23395	23461	23390
dYco ($Y_{4,CO} - Y_{2,CO}$) [ppm]	22714	22792	22924	22782
dC ($C_{4,CO} - C_{2,CO}$) [mol/m^3]	1.0488	1.0535	1.0577	1.0515
$D_{eff,t}$ (total, from dC) [m^2/s]	7.71E-07	7.76E-07	7.01E-07	9.56E-07
$D_{eff,t}$ (total, from dY) [m^2/s]	7.71E-07	7.76E-07	7.01E-07	9.56E-07
$L_t/D_{eff,t}$ (total) [s/m]	273.18	291.53	329.79	289.41
$D_{eff,s}$ (smooth surface cordierite) [m^2/s]	1.13E-06	1.13E-06	1.13E-06	1.13E-06
$Ls/D_{eff,s}$ (cordierite) [s/m]	1.43E+02	1.43E+02	1.43E+02	1.43E+02
$(L_t/D_{eff,t}) - (Ls/D_{eff,s})$ [s/m]	129.81	148.17	186.43	146.04
$D_{eff,w}$ (washcoat) [m^2/s]	3.75E-07	4.33E-07	3.71E-07	7.84E-07

Data used in **Figures 9 & 10** "Effect of the washcoat thickness on the measured D_{eff} values (in **Sample S3**)".

Plate No	**42**	**47**	**48**	**67**
Slurry used	S_3	S_3	S_3	S_3
Temperature [°C]	16.2	15.0	15.4	16.5
Total thickness [m]	2.64E-04	3.69E-04	3.66E-04	4.04E-04
Washcoat thickness [m]	1.02E-04	2.07E-04	2.04E-04	2.42E-04
Cordierite thickness [m]	1.62E-04	1.62E-04	1.62E-04	1.62E-04
Diameter [m]	0.01	0.01	0.01	0.01
Pressure in the cell [bar (a)]	**1.11**	**1.11**	**1.11**	**1.11**
$Q_{1,d}$ (upper, in, displayed) [ml/min]	600	600	600	600
$Q_{1,c}$ (upper, in, calibrated) [ml/min]	645.55	645.55	645.55	645.55
$Q_{1,s}$ (upper, in, standard) [m^3/s]	1.016E-05	1.020E-05	1.018E-05	1.015E-05
$F_{1,CO}$ (CO flux, upper, in) [mol/s]	0.00	0.00	0.00	0.00
$Q_{2,d}$ (upper, out, displayed) [ml/min]	446	439	433	453
$Q_{2,c}$ (upper, out, calibrated) [ml/min]	473.91	466.35	459.88	481.47
$Q_{2,c,c}$ (upper, out, assumed) [ml/min]	645.55	645.55	645.55	645.55
$Q_{2,s}$ (upper, out, standard) [m^3/s]	1.016E-05	1.020E-05	1.018E-05	1.015E-05
$F_{2,CO}$ (upper, out) [mol/s]	2.200E-07	2.291E-07	2.056E-07	2.329E-07
$C_{2,CO}$ (concentration, upper, out) [mol/m^3]	0.0224	0.0233	0.0209	0.0237
$Q_{3,d}$ (lower, in, displayed) [ml/min]	600	600	600	603
$Q_{3,c}$ (lower, in, calibrated) [ml/min]	644.13	644.13	644.13	647.24
$Q_{3,s}$ (lower, in, standard) [m^3/s]	1.013E-05	1.018E-05	1.016E-05	1.017E-05
$F_{3,CO}$ (CO flux, lower, in) [mol/s]	1.085E-05	1.09E-05	1.088E-05	1.089E-05
$C_{3,CO}$ (concentration, lower, in) [mol/m^3]	1.1535	1.1583	1.1567	1.1523
$Q_{4,d}$ (lower, out, displayed) [ml/min]	648	648	648	642
$Q_{4,c}$ (lower, out, calibrated) [ml/min]	659.01	659.01	659.01	652.88
$Q_{4,c,c}$ (lower, out, assumed) [ml/min]	644.13	644.13	644.13	647.24
$Q_{4,s}$ (lower, out, standard) [m^3/s]	1.013E-05	1.018E-05	1.016E-05	1.017E-05
$F_{4,CO}$ (lower, out) [mol/s]	1.063E-05	1.067E-05	1.068E-05	1.066E-05
$C_{4,CO}$ (concentration, lower, out) [mol/m^3]	1.0849	1.0886	1.0895	1.0826
A (diffusion area in the sample) [m^2]	7.854E-05	7.854E-05	7.854E-05	7.854E-05
L_t (total thickness of the sample) [m]	2.64E-04	3.69E-04	3.66E-04	4.04E-04
$Y_{3,CO}$ (lower, in) [ppm]	24000	24000	24000	24000

$Y_{2,CO,d}$ (upper, out, displayed) [ppm]	487	505	454	516
$Y_{2,CO,c}$ (upper, out, calibrated) [ppm]	485.5	503.5	452.5	514.5
$Y_{4,CO}$ (lower, out, caculated) [ppm]	23513	23495	23547	23487
dYco ($Y_{4,CO} - Y_{2,CO}$) [ppm]	23028	22992	23094	22972
dC ($C_{4,CO} - C_{2,CO}$) [mol/m^3]	1.0625	1.0653	1.0685	1.0589
$D_{eff,t}$ (total, from dC) [m^2/s]	7.19E-07	1.05E-06	9.31E-07	1.17E-06
$D_{eff,t}$ (total, from dY) [m^2/s]	7.19E-07	1.05E-06	9.31E-07	1.17E-06
$L_t/D_{eff,t}$ (total) [s/m]	366.77	351.64	393.56	345.62
$D_{eff,s}$ (smooth surface cordierite) [m^2/s]	1.13E-06	1.13E-06	1.13E-06	1.13E-06
$Ls/D_{eff,s}$ (cordierite) [s/m]	1.43E+02	1.43E+02	1.43E+02	1.43E+02
$(L_t/D_{eff,t}) - (Ls/D_{eff,s})$ [s/m]	223.41	208.28	250.20	202.26
$D_{eff,w}$ (washcoat) [m^2/s]	4.55E-07	9.93E-07	8.17E-07	1.197E-06

Data used in **Figure 4.11** "Effect of the washcoat thickness on the measured D_{eff} values (in **Sample S3w**)".

Plate No	**49**	**50**	**52**	**53**
Slurry used	S_{3w}	S_{3w}	S_{3w}	S_{3w}
Temperature [°C]	16.0	16.1	16.3	15.9
Total thickness [m]	2.79E-04	2.53E-04	2.56E-04	2.54E-04
Washcoat thickness [m]	1.17E-04	9.07E-05	9.38E-05	9.23E-05
Cordierite thickness [m]	1.62E-04	1.62E-04	1.62E-04	1.62E-04
Diameter [m]	0.01	0.01	0.01	0.01
Pressure in the cell [bar (a)]	**1.11**	**1.11**	**1.11**	**1.11**
$Q_{1,d}$ (upper, in, displayed) [ml/min]	600	600	600	600
$Q_{1,c}$ (upper, in, calibrated) [ml/min]	645.55	645.55	645.55	645.55
$Q_{1,s}$ (upper, in, standard) [m^3/s]	1.016E-05	1.016E-05	1.015E-05	1.017E-05
$F_{1,CO}$ (CO flux, upper, in) [mol/s]	0.00	0.00	0.00	0.00
$Q_{2,d}$ (upper, out, displayed) [ml/min]	451	433	451	436
$Q_{2,c}$ (upper, out, calibrated) [ml/min]	479.31	459.88	479.31	463.12
$Q_{2,c,c}$ (upper, out, assumed) [ml/min]	645.55	645.55	645.55	645.55
$Q_{2,s}$ (upper, out, standard) [m^3/s]	1.016E-05	1.016E-05	1.015E-05	1.017E-05
$F_{2,CO}$ (upper, out) [mol/s]	2.156E-07	2.332E-07	2.231E-07	2.202E-07
$C_{2,CO}$ (concentration, upper, out) [mol/m^3]	0.0220	0.0237	0.0227	0.0224
$Q_{3,d}$ (lower, in, displayed) [ml/min]	601	600	602	600
$Q_{3,c}$ (lower, in, calibrated) [ml/min]	645.17	644.13	646.21	644.13
$Q_{3,s}$ (lower, in, standard) [m^3/s]	1.016E-05	1.014E-05	1.016E-05	1.014E-05
$F_{3,CO}$ (CO flux, lower, in) [mol/s]	1.088E-05	1.086E-05	1.088E-05	1.086E-05
$C_{3,CO}$ (concentration, lower, in) [mol/m^3]	1.1543	1.1539	1.1531	1.1547
$Q_{4,d}$ (lower, out, displayed) [ml/min]	640	673	641	649
$Q_{4,c}$ (lower, out, calibrated) [ml/min]	650.83	684.58	651.85	660.04
$Q_{4,c,c}$ (lower, out, assumed) [ml/min]	645.17	644.13	646.21	644.13
$Q_{4,s}$ (lower, out, standard) [m^3/s]	1.016E-05	1.014E-05	1.016E-05	1.014E-05
$F_{4,CO}$ (lower, out) [mol/s]	1.066E-05	1.062E-05	1.066E-05	1.064E-05
$C_{4,CO}$ (concentration, lower, out) [mol/m^3]	1.0862	1.0840	1.0843	1.0861
A (diffusion area in the sample) [m^2]	7.854E-05	7.854E-05	7.854E-05	7.854E-05
L_t (total thickness of the sample) [m]	2.79E-04	2.53E-04	2.56E-04	2.54E-04
$Y_{3,CO}$ (lower, in) [ppm]	24000	24000	24000	24000
$Y_{2,CO,d}$ (upper, out, displayed) [ppm]	477	516	494	487
$Y_{2,CO,c}$ (upper, out, calibrated) [ppm]	475.5	514.5	492.5	485.5
$Y_{4,CO}$ (lower, out, caculated) [ppm]	23524	23484	23508	23513

dYco ($Y_{4,CO}$ - $Y_{2,CO}$) [ppm]	23049	22970	23015	23028
dC ($C_{4,CO}$ - $C_{2,CO}$) [mol/m^3]	1.0642	1.0602	1.0616	1.0636
$D_{eff,t}$ (total, from dC) [m^2/s]	7.45E-07	7.32E-07	7.08E-07	6.94E-07
$D_{eff,t}$ (total, from dY) [m^2/s]	7.45E-07	7.32E-07	7.08E-07	6.94E-07
$L_t/D_{eff,t}$ (total) [s/m]	374.57	345.11	361.49	366.39
$D_{eff,s}$ (smooth surface cordierite) [m^2/s]	1.13E-06	1.13E-06	1.13E-06	1.13E-06
$Ls/D_{eff,s}$ (cordierite) [s/m]	1.43E+02	1.43E+02	1.43E+02	1.43E+02
$(L_t/D_{eff,t})$ - $(Ls/D_{eff,s})$ [s/m]	231.20	201.75	218.13	223.03
$D_{eff,w}$ (washcoat) [m^2/s]	5.07E-07	4.50E-07	4.30E-07	4.14E-07

Data used in **Figure 4.11** "Effect of the washcoat thickness on the measured D_{eff} values (in **Sample S3HT)**".

Plate No	**43**	**46**
Slurry used	S_{3HT}	S_{3HT}
Temperature [°C]	16.5	16.4
Total thickness [m]	3.68E-04	3.63E-04
Washcoat thickness [m]	2.06E-04	2.01E-04
Cordierite thickness [m]	1.62E-04	1.62E-04
Diameter [m]	0.01	0.01
Pressure in the cell [bar (a)]	**1.11**	**1.11**
$Q_{1,d}$ (upper, in, displayed) [ml/min]	600	600
$Q_{1,c}$ (upper, in, calibrated) [ml/min]	645.55	645.55
$Q_{1,s}$ (upper, in, standard) [m^3/s]	1.015E-05	1.015E-05
$F_{1,CO}$ (CO flux, upper, in) [mol/s]	0.00	0.00
$Q_{2,d}$ (upper, out, displayed) [ml/min]	455	452
$Q_{2,c}$ (upper, out, calibrated) [ml/min]	483.62	480.39
$Q_{2,c,e}$ (upper, out, assumed) [ml/min]	645.55	645.55
$Q_{2,s}$ (upper, out, standard) [m^3/s]	1.015E-05	1.015E-05
$F_{2,CO}$ (upper, out) [mol/s]	2.361E-07	2.439E-07
$C_{2,CO}$ (concentration, upper, out) [mol/m^3]	0.0240	0.0248
$Q_{3,d}$ (lower, in, displayed) [ml/min]	600	600
$Q_{3,c}$ (lower, in, calibrated) [ml/min]	644.13	644.13
$Q_{3,s}$ (lower, in, standard) [m^3/s]	1.012E-05	1.013E-05
$F_{3,CO}$ (CO flux, lower, in) [mol/s]	1.084E-05	1.084E-05
$C_{3,CO}$ (concentration, lower, in) [mol/m^3]	1.1523	1.1527
$Q_{4,d}$ (lower, out, displayed) [ml/min]	643	643
$Q_{4,c}$ (lower, out, calibrated) [ml/min]	653.90	653.90
$Q_{4,c,e}$ (lower, out, assumed) [ml/min]	644.13	644.13
$Q_{4,s}$ (lower, out, standard) [m^3/s]	1.012E-05	1.013E-05
$F_{4,CO}$ (lower, out) [mol/s]	1.06E-05	1.06E-05
$C_{4,CO}$ (concentration, lower, out) [mol/m^3]	1.0822	1.0817
A (diffusion area in the sample) [m^2]	7.854E-05	7.854E-05
L_t (total thickness of the sample) [m]	3.68E-04	3.63E-04
$Y_{3,CO}$ (lower, in) [ppm]	24000	24000
$Y_{2,CO,d}$ (upper, out, displayed) [ppm]	523	540
$Y_{2,CO,c}$ (upper, out, calibrated) [ppm]	521.5	538.5
$Y_{4,CO}$ (lower, out, caculated) [ppm]	23477	23460

dYco ($Y_{4,co}$ - $Y_{2,co}$) [ppm]	22956	22922
dC ($C_{4,co}$ - $C_{2,co}$) [mol/m^3]	1.0581	1.0569
$\mathbf{D_{eff,t}}$ (total, from dC) [m^2/s]	1.08E-06	1.10E-06
$\mathbf{D_{eff,t}}$ (total, from dY) [m^2/s]	1.08E-06	1.10E-06
$\mathbf{L_t/D_{eff,t}}$ (total) [s/m]	340.74	329.38
$\mathbf{D_{eff,s}}$ (smooth surface cordierite) [m^2/s]	1.13E-06	1.13E-06
$\mathbf{Ls/D_{eff,s}}$ (cordierite) [s/m]	1.43E+02	1.43E+02
$\mathbf{(L_t/D_{eff,t}) - (Ls/D_{eff,s})}$ [s/m]	197.38	186.02
$\mathbf{D_{eff,w}}$ (washcoat) [m^2/s]	1.05E-06	1.08E-06

Appendix D3

Experimental data on the measurement of D_{eff} in Chapter 5

Data used in **Figure 5.10** "Comparison of measured effective diffusivities of Samples C2NM and C2HT – effect of calcination temperature".

Samples code	**C2NM-1P**	**C2HT-1P**	**C2NM-2P**	**C2HT-2P**	**C2NM-3P**	**C2HT-3P**
T_{room} (room temperature) [*°C*]	14.3	14.3	16.5	13.9	16.2	14.4
L_t (total thickness) [*m*]	2.652E-04	2.624E-04	1.794E-03	1.792E-03	3.397E-03	3.392E-03
L_S (equivalent substrate thickness) [*m*]	1.748E-04	1.748E-04	3.892E-04	3.892E-04	5.868E-04	5.868E-04
L_s (equivalent washcoat thickness) [*m*]	9.040E-05	8.760E-05	9.040E-05	8.760E-05	1.808E-04	1.752E-04
L_v (equivalent void channel thickness) [*m*]	0.000E+00	0.000E+00	1.315E-03	1.315E-03	2.630E-03	2.630E-03
D (diameter of the diffusion area) [*m*]	0.010	0.010	0.008	0.010	0.010	0.010
P (in the diffusion cell) [*bar (a)*]	**1.11**	**1.11**	**1.11**	**1.11**	**1.11**	**1.11**
$Q_{1,d}$ (upper, in, displayed) [*ml/min*]	600	600	600	600	600	600
$Q_{1,c}$ (upper, in, calibrated) [*ml/min*]	665.0	665.0	665.0	665.0	665.0	665.0
$Q_{1,s}$ (upper, in, at S.T.P.) [m^3/s]	1.053E-05	1.053E-05	1.045E-05	1.055E-05	1.046E-05	1.053E-05
$F_{1,CO}$ (upper, in) [*mol/s*]	0	0	0	0	0	0
$Q_{2,d}$ (upper, out, displayed) [*ml/min*]	602	634	448	629	442	634
$Q_{2,c}$ (upper, out, calibrated) [*ml/min*]	645.1	677.2	490.6	672.2	484.6	677.2
$Q_{2,c,c}$ (upper, out, assumed) [*ml/min*]	665.0	665.0	665.0	665.0	665.0	665.0
$Q_{2,s}$ (upper, out, at S.T.P.) [m^3/s]	1.053E-05	1.053E-05	1.045E-05	1.055E-05	1.046E-05	1.053E-05
$F_{2,CO}$ (upper, out) [*mol/s*]	2.098E-07	2.122E-07	7.018E-08	1.075E-07	7.259E-08	7.235E-08
$C_{2,CO}$ (upper, out, at exp conditions) [mol/m^3]	0.0189	0.0191	0.0063	0.0097	0.0065	0.0065
$C_{2,CO}$ (upper, out, at S.T.P. from $F_{2,CO}/Q_{2,S}$) [mol/m^3]	0.0199	0.0202	0.0067	0.0102	0.0069	0.0069
N_{CO} (the molar flux of CO, up, out) [$mol/m^2.s$]	2.671E-03	2.702E-03	1.396E-03	1.369E-03	9.243E-04	9.212E-04
$Q_{3,d}$ (lower, in, displayed) [*ml/min*]	600	600	600	600	600	600
$Q_{3,c}$ (lower, in, calibrated) [*ml/min*]	668.3	668.3	668.3	668.3	668.3	668.3
$Q_{3,s}$ (lower, in, at S.T.P.) [m^3/s]	1.058E-05	1.058E-05	1.050E-05	1.060E-05	1.051E-05	1.058E-05
$F_{3,CO}$ (lower, in) [*mol/s*]	1.133E-05	1.133E-05	1.125E-05	1.135E-05	1.126E-05	1.133E-05
$C_{3,CO}$ (lower, in, at exp conditions) [mol/m^3]	1.0175	1.0175	1.0098	1.0190	1.0109	1.0172
$C_{3,CO}$ (lower, in, at S.T.P., from $F_{3,CO}/Q_{3,s}$) [mol/m^3]	1.0708	1.0708	1.0708	1.0708	1.0708	1.0708
$Q_{4,d}$ (lower, out, displayed) [*ml/min*]	620	647	647	648	646	633
$Q_{4,c}$ (lower, out, calibrated) [*ml/min*]	638.2	665.3	665.3	666.3	664.3	651.2
$Q_{4,c,c}$ (lower, out, assumed) [*ml/min*]	668.3	668.3	668.3	668.3	668.3	668.3

$Q_{4,s}$ (lower, out, at S.T.P.) [m^3/s]	1.058E-05	1.058E-05	1.050E-05	1.060E-05	1.051E-05	1.058E-05
$F_{4,CO}$ (lower, out) [*mol/s*]	1.112E-05	1.112E-05	1.118E-05	1.124E-05	1.119E-05	1.126E-05
$C_{4,CO}$ (lower, out, at exp conditions) [mol/m^3]	0.9986	0.9984	1.0035	1.0093	1.0043	1.0107
$C_{4,CO}$ (lower, out, at S.T.P., from $F_{4,CO}/Q_{4,s}$) [mol/m^3]	1.0510	1.0508	1.0641	1.0607	1.0639	1.0640
A (area of the sample) [m^2]	7.854E-05	7.854E-05	5.027E-05	7.854E-05	7.854E-05	7.854E-05
L_t (thickness of the sample) [*m*]	2.652E-04	2.624E-04	1.794E-03	1.792E-03	3.397E-03	3.392E-03
$Y_{3,CO}$ (lower, in) [*ppm*]	24000	24000	24000	24000	24000	24000
$Y_{2,CO,d}$ (upper, out, displayed) [*ppm*]	445	450	149	227	154	153
$Y_{2,CO,c}$ (upper, out, calibrated) [*ppm*]	446.5	451.6	150.5	228.4	155.5	154.0
$Y_{4,CO}$ (lower, out, calculated from $F_{4,CO}/Q_{4,s}$) [*ppm*]	23555.7	23550.6	23850.2	23772.7	23845.3	23846.7
dY_{CO} ($Y_{4,CO} - Y_{2,CO}$) [*ppm*]	23109.2	23099.0	23699.7	23544.3	23689.8	23692.7
dC_{CO} ($C_{4,CO} - C_{2,CO}$) [mol/m^3]	0.9797	0.9793	0.9972	0.9996	0.9978	1.0041
$D_{eff,t}$ (total, from dC_{CO}) [m^2/s]	6.87E-07	6.88E-07	2.37E-06	2.33E-06	2.97E-06	2.96E-06
$D_{eff,t}$ (total, from dY_{CO}) [m^2/s]	6.87E-07	6.88E-07	2.37E-06	2.33E-06	2.97E-06	2.96E-06
$L_t/D_{eff,t}$ (total) [*s/m*]	3.86E+02	3.81E+02	7.57E+02	7.68E+02	1.14E+03	1.15E+03
D_{bulk} (bulk diffusion) [m^2/s]	1.92E-05	1.92E-05	1.95E-05	1.92E-05	1.95E-05	1.93E-05
L_v/D_{bulk} (bulk diffusion) [*s/m*]	0.00E+00	0.00E+00	6.74E+01	6.85E+01	1.35E+02	1.37E+02
$D_{eff,s}$ (substrate) [m^2/s]	1.07E-06	1.07E-06	1.07E-06	1.07E-06	1.28E-06	1.28E-06
$L_s/D_{eff,s}$ [*s/m*]	1.63E+02	1.63E+02	3.63E+02	3.63E+02	4.59E+02	4.59E+02
$(L_t/D_{eff,t}) - (L_v/D_{bulk}) - (L_s/D_{eff,s})$] [*s/m*]	222.7	218.2	326.5	335.6	549.7	552.1
$D_{eff,w}$ (washcoat) [m^2/s]	**4.059E-07**	**4.015E-07**	**2.769E-07**	**2.610E-07**	**3.289E-07**	**3.173E-07**
Samples code	**C2NM-1P**	**C2HT-1P**	**C2NM-2P**	**C2HT-2P**	**C2NM-3P**	**C2HT-3P**

Appendix E

Estimation of CO diffusion coefficient in nitrogen

The diffusion coefficient for a binary mixture of gases A and B can be estimated from the Fuller, Schettler, and Giddings relationship (Fuller *et al.*, 1966):

$$D_{AB} = \frac{0.001T^{1.75}(1/M_A + 1/M_B)^{\frac{1}{2}}}{P[(\Sigma v)_A^{\frac{1}{3}} + (\Sigma v)_B^{\frac{1}{3}}]^2} \qquad \text{(AE.1)}$$

where

D_{AB}	The binary diffusion coefficient, $cm^2\ s^{-1}$
T	Temperature, K
M_A	The molecular weight of A, $g\ mol^{-1}$
M_B	The molecular weight of B, $g\ mol^{-1}$
P	Pressure, atm
Σ_v	Special parameters of diffusion volume. For CO the value is 18.9; for nitrogen the value is 17.9

Under experimental conditions, *e.g.* T = 291.15K, P = 1 atm, the diffusion coefficient of CO in nitrogen can be calculated from Equation AE.1.

$$D_{AB} = \frac{0.001 \times T^{1.75} \times (\frac{1}{28} + \frac{1}{28})^{\frac{1}{2}}}{1 \times [(18.9)^{\frac{1}{3}} + (17.9)^{\frac{1}{3}}]^2}$$

$$= 0.1968 cm^2 s^{-1}$$

$$= 1.968 \times 10^{-5} m^2 s^{-1}$$

D_{AB} can also be given by the modified Gilliland equation (Gilliland, 1934) as:

$$D_{AB} = 1.8\times10^{-4} \frac{T^{\frac{1}{2}}}{[(V_A)^{\frac{1}{2}} + (V_B)^{\frac{1}{2}}]^2} \frac{M_A}{q_A} [\frac{1}{M_A} + \frac{1}{M_B}]^{\frac{1}{2}} \qquad \text{(AE.2)}$$

where

D_{AB}	The binary diffusion coefficient, $cm^2\ s^{-1}$
T	Temperature, K
M	Molecular weight, g mol^{-1}
V	Molecular volume of gas when a liquid at the normal boiling point, cm^3/g mol. For CO the value is 30.7, for N_2 the value is 36.0.

The ratio M_A/q_A in Equation AE.2 can be replaced by RT/P by use of the ideal gas law where R is the universal gas constant, 82.05 atmospheres cm^3/(mol K), and P is pressure in atmosphere (Hesketh, 1996). Substitution in Equation AE.2 the following result can be obtained:

$$D_{AB} = 1.8\times10^{-4} \frac{291.15^{\frac{1}{2}}}{(30.7^{\frac{1}{2}} + 36.0^{\frac{1}{2}})^2} \times \frac{82.05\times291.15}{1} \times (\frac{1}{28} + \frac{1}{28})^{\frac{1}{2}}$$

$$= 0.1473 cm^2\ s^{-1}$$

$$= 1.4733\times10^{-5}\ m^2\ s^{-1}$$

The third method to theoretically estimate gaseous diffusion was introduced by Chapman & Cowling (1970). They developed the following formula:

$$D_{AB} = \frac{0.001857 T^{1.5} (1/M_A + 1/M_B)^{\frac{1}{2}}}{P\sigma_{12}{}^2 \Omega} \qquad \text{(AE.3)}$$

where

D_{AB}	The binary diffusion coefficient, $cm^2\ s^{-1}$

σ_{12}	The collision diameter, Å. $\sigma_{12} = 0.5 \times (\sigma_{CO} + \sigma_{N2})$. The value of σ_{CO} is 3.690 Å; whilst σ_{N2} is 3.798 Å

At 18 °C (291 K) and 1 atm, the value of $\sigma_{12} = 0.5 \times (3.690 + 3.798) = 3.744$ Å. The values of $\frac{\varepsilon}{k_B}$ for CO and N_2 are 91.7 K and 71.4 K individually.

$$\frac{\varepsilon_{12}}{k_B T} = \frac{\sqrt{\left(\frac{\varepsilon_1}{k_B}\right)\left(\frac{\varepsilon_2}{k_B}\right)}}{T} = \frac{\sqrt{(91.7)(71.4)}}{291} = 0.2781$$

So $\frac{k_B T}{\varepsilon_{12}} = \frac{1}{0.2781} = 3.5963$

From the attached table in the literature (Chapman & Cowling, 1970), the value of Ω is 0.9058. Then D_{AB} can be calculated:

$$D_{AB} = \frac{1.86 \times 10^{-3} \times 291.15 \times \left(\frac{1}{28} + \frac{1}{28}\right)^{0.5}}{1 \times 3.744^2 \times 0.9058}$$

$$= 0.194 cm^2 s^{-1}$$

The calculated result of molecular diffusion coefficient of CO in nitrogen from Equation AE.1 is close to the result from Equation AE.3. The value is about 20 times larger than experimental effective diffusivity of CO in nitrogen through cordierite substrate.

Appendix F

Method adapted to calculate CO conversions and reaction rates

(Based on Sample **C2NM**)

1. The basic data on the monolithic catalyst

The monolithic catalyst is made from 90 g/ft^3 (or 3.18 g/l) slurry. A small section (ϕ15.4 mm × 22 mm) is cut directly from the monolith in order to well fit the catalytic combustion reactor whose inner diameter is 16.0 mm.

The physical properties of the catalyst in the reactor are as follows:

Cell type	-- square
Cells per square inch	-- 400
Diameter of a section	-- 0.0154 [m]
Length of a section	-- 0.022 [m]
Width of a channel	-- 0.001 [m]
Number of cells in a section	-- about 110 (including incomplete cells)
Number of the sections	-- one

The total geometric surface area, A, can be calculated:

$$A = 110 \times 4 \times 0.022[m] \times 0.001[m] = 0.00968[m^2]$$

2. Experimental conditions

$M_{set} = 60$

$P_{room} = 1\ [atm] = 101325\ [Pa]$

$Q_{air} = 700\ [L/min]$ (at room temperature and one atmosphere pressure)

$T_{room} = 25.4\ [℃] = 273.15 + 25.4\ [K] = 298.55\ [K]$

$T_{set} = 500\ [°C] = 500 + 273.15\ [K] = 773.15\ [K]$

3. Measured data

$P_{reactor,\,b} = 1.432\ [bar\ g] = 143200\ [Pa]$

$P_{reactor,\,a} = 1.433\ [bar\ g] = 143300\ [Pa]$

$T_{inlet,\,b} = 467.8\ [°C] = 467.8 + 273.15\ [K] = 740.95\ [K]$

$T_{wall,\,b} = 474.4\ [°C] = 474.4 + 273.15\ [K] = 747.55\ [K]$

$T_{outlet,\,b} = 464.5\ [°C] = 464.5 + 273.15\ [K] = 737.65\ [K]$

$T_{inlet,\,a} = 467.9\ [°C] = 467.9 + 273.15\ [K] = 741.05\ [K]$

$T_{wall,\,a} = 477.0\ [°C] = 477.0 + 273.15\ [K] = 750.15\ [K]$

$T_{outlet,\,a} = 465.6\ [°C] = 465.6 + 273.15\ [K] = 738.75\ [K]$

$Y_{CO,\,inlet,\,b} = 35\ [ppm]$

$Y_{CO,\,outlet,\,b} = 36\ [ppm]$

$Y_{CO,\,inlet,\,a} = 344\ [ppm]$

$Y_{CO,\,outlet,\,a} = 276\ [ppm]$

4. Calibration

4.1 The mass flow controller

The mass flow controller is calibrated by a bubble-film meter using pure CO at room temperature and one atmosphere pressure. It can be found that the linearity of Q_{CO} *vs* M_{set} is good and their slopes are also close when M_{set} is more than 60, regardless of the gas cylinder pressure ($P_{CO\ cylinder}$) is 1.0 bar (g) or 2.0 bar (g) (see Figure AF.1). So the following Equations AF.1 and AF.2 are used to calibrate the mass flow controller at different operating pressures.

$$Q_{CO} = 6.9293 \times M_{set} - 153.88 \text{ (when } P_{CO\ cylinder} = 1.0 \text{ to } 2.0 \text{ bar g)} \qquad \text{(AF.1)}$$

$$Q_{CO} = 6.9904 \times M_{set} - 160.28 \text{ (when } P_{CO\ cylinder} > 2.0 \text{ bar g)} \qquad \text{(AF.2)}$$

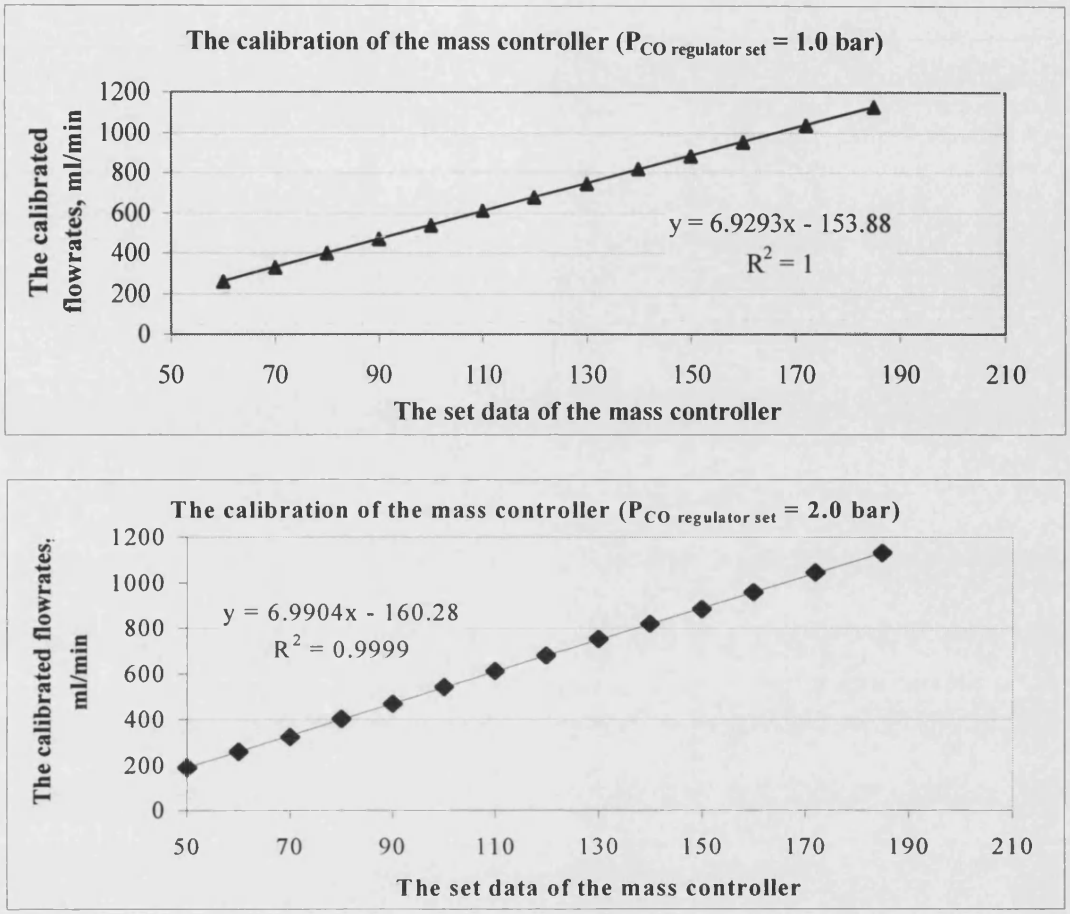

Figure AF.1 Calibration of the mass flow controller at different inlet pressures

4.2 The CO analyser

The measurement range of the CO analyser is calibrated using pure nitrogen (zero gas) and 1070 ppm CO in nitrogen (span gas) every hour in order to check zero and span drift. At most circumstance the displayed data in the CO analyser is 13 ppm to 38 ppm for zero point, and 1059 ppm to 1072 ppm for span point. For this analyser it is impossible to calibrate its zero point at 0 ppm and span point at 1070 ppm due to its accuracy limitation. So a simplified calibration method is applied, see Equation AF.3.

$$Y_{CO,\,c} = Y_{CO,\,d} - Y_{CO,\,z} \qquad \text{(AF.3)}$$

Here $Y_{CO,\,c}$ is the calibrated concentration; $Y_{CO,\,d}$ is the displayed concentration on the analyser; and $Y_{CO,\,z}$ is the displayed concentration when measuring pure nitrogen.

For example, if the displayed CO portion in the inlet gas is 344 ppm, and the displayed Y_{CO} value when measuring pure nitrogen is 15 ppm:

$$Y_{CO,\,a,\,d} = 344\ [ppm],\ Y_{CO,\,z} = 15\ [ppm]$$

Then the calibrated Y_{CO} value is:

$$Y_{CO,\,a,\,c} = 344\ [ppm] - 15\ [ppm] = 329\ [ppm]$$

4.3 The thermocouple to test wall temperature

The measured wall temperature is always higher than the inlet temperature and the outlet temperature even **before** CO is fed into the reactor. If the wall temperature is calibrated by the inlet temperature and the outlet temperature, the relative error among them will be reduced.

Assuming that the temperature dropping from the inlet to the outlet is linear before CO is fed (because no reactions occur), then $T_{wall,\,b,\,c}$, the calibrated wall temperature, can be calculated according to its distance from the inlet (or the outlet), see Figure AF.2.

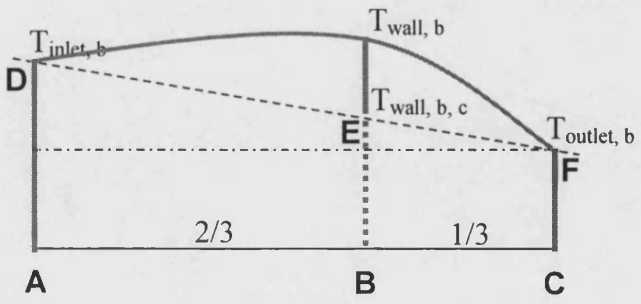

Figure AF.2 Calibration of the thermocouples

In the catalytic combustion reactor, the distance from the wall thermocouple to the inlet thermocouple is 2/3 of the total distance, which means:

$$|AB| = \frac{2}{3}|AC|$$

$$|BC| = \frac{1}{3}|AC|$$

In Figure AF.2, the relation among CF, BE and AD is:

$$\frac{|BE|-|CF|}{|AD|-|CF|} = \frac{\frac{1}{3}}{\frac{1}{3}+\frac{2}{3}} = \frac{1}{3}$$

$$\Rightarrow 3|BE|-3|CF| = |AD|-|CF|$$

$$\Rightarrow |BE| = \frac{1}{3}|AD| + \frac{2}{3}|CF|$$

This means that

$$T_{wall,b,c} = \frac{1}{3}T_{inlet,b} + \frac{2}{3}T_{outlet,b} \qquad \text{(AF.4)}$$

Using Equation AF.4, $T_{wall,\,b,\,c}$ can be calibrated:

$$T_{wall,b,c} = \frac{1}{3}T_{inlet,b} + \frac{2}{3}T_{outlet,b}$$

$$= \frac{1}{3}\times 467.8[°C] + \frac{2}{3}\times 464.5[°C]$$

$$= 465.6[°C]$$

This is the calibrated data of $T_{wall,\,b}$ at the point of 474.4 °C. Using the same method, many calibrated data can be obtained, and then a calibration formula for the wall thermocouple can be obtained, see Equation AF.5.

$$T_{wall,\,b,\,c} = 0.9777 \times T_{wall,\,b} - 0.5313 \qquad \text{(AF.5)}$$

5. The calculation of CO conversions and reaction rates

5.1 Calibrated CO portion in the inlet concentration

Q_{CO} (at room temperature and room pressure) can be calculated according to Equation AF.2 when $M_{set} = 60$.

$$Q_{CO} = 6.9904 \times M_{set} - 160.28$$
$$= 6.9904 \times 60 - 160.28$$
$$= 259.14\ [ml/min]$$

After Q_{CO} is obtained, F_{CO} can also be calculated.

$$F_{CO} = \frac{P_{room} \times Q_{CO}}{R \times T_{room}}$$
$$= \frac{101325[Pa] \times 259.14[ml/\min] \times 0.000001}{8.314[J/(mol.K)] \times (273.15 + 25.4)[K] \times 60}$$
$$= 0.000176[mol/s]$$

Similarly, F_{air} can be calculated.

$$F_{air} = \frac{P_{room} \times Q_{air}}{R \times T_{room}}$$
$$= \frac{101325[Pa] \times 700[L/\min] \times 0.001}{8.314[J/(mol.K)] \times (273.15 + 25.4)[K] \times 60}$$
$$= 0.4763\ [mol/s]$$

So $Y_{CO,\ inlet,\ cal}$, the calculated portion of CO in the inlet concentration, can be obtained using Equation AF.6.

$$Y_{CO,\ inlet,\ cal} = F_{CO} / (F_{CO} + F_{air}) \qquad \text{(AF.6)}$$

Enter the above data, the result can be obtained.

$$Y_{CO,inlet,cal} = \frac{F_{CO}}{F_{CO} + F_{air}}$$
$$= \frac{0.000176[mol/s]}{0.000176[mol/s] + 0.4763[mol/s]}$$
$$= 370.1 \times 10^{-6}$$
$$= 370.1[ppm]$$

5.2 Increased inlet temperature after CO is fed

$T_{inlet,\ b}$ (the inlet temperature before CO is fed) is different from the $T_{inlet,\ a}$ (the inlet temperature after CO is fed) for two reasons. One is that the heat of reaction (CO oxidation) causes the inlet temperature to rise; the other is that it takes a long time (*e.g.* 3 hours) to reach a steady state if the set point for the inlet temperature is changed too much, *e.g.*, more than 100 °C. So both $T_{inlet,\ b}$ and $T_{inlet,\ a}$ should be considered when calculating the temperature increase.

Figure AF.3 shows how temperatures change in the reactor before and after CO is fed. It can be found that ΔT (the increased temperature after CO is fed) should be the same as the value of $|ZM| + |NF|$, which is shown in Equation AF.7.

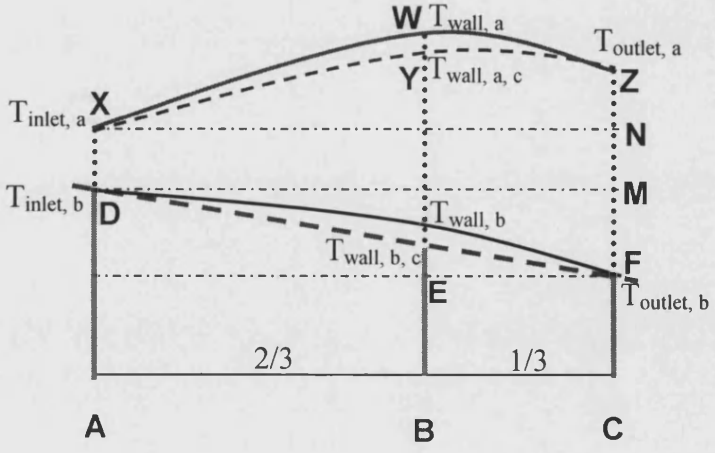

Figure AF.3 Temperatures increase in the reactor after CO is fed

$$\Delta T = (T_{outlet,\ a} - T_{inlet,\ a}) + (T_{inlet,\ b} - T_{outlet,\ b}) \quad \text{(AF.7)}$$

Using Equation AE.7, ΔT can be calculated.

$$\Delta T = (465.6\ [°C] - 467.9\ [°C]) + (467.8\ [°C] - 464.5\ [°C])$$
$$= 1.0\ [°C]$$

5.3 CO conversion

The conversion of CO can be calculated using Equation AF.9.

$$N_{CO} = \frac{Y_{CO,inlet,a} - Y_{CO,outlet,a}}{Y_{CO,inlet,a,c}} \times 100\% \qquad \text{(AF.8)}$$

In the numerator of Equation AF.9, the difference between $Y_{CO,\ inlet,\ a}$ and $Y_{CO,\ outlet,\ a}$, as displayed on the CO analyser are used. However, for the denominator the calibrated CO value is used.

An example calculation is presented as follows:

$$N_{CO} = \frac{Y_{CO,inlet,a} - Y_{CO,outlet,a}}{Y_{CO,inlet,a,c}} \times 100\%$$
$$= (344[ppm] - 276[ppm]) / 329[ppm] \times 100\%$$
$$= 20.67\%$$

5.4 The reaction rate

The total geometric surface area, A, of the sample, has been calculated, then using Equation AF.10, the reaction rate can be calculated.

$$R_{CO} = \frac{F_{CO,inlet} - F_{CO,outlet}}{A}$$
$$= \frac{F_{CO,inlet} \times N_{CO}}{A} \qquad \text{(AF.9)}$$

There is some difference between calculated value $Y_{CO,\ inlet,\ cal}$ and the calibrated value $Y_{CO,\ inlet,\ a,\ c}$ from the CO analyser (*e.g.* the former is 370 ppm, the latter is 329 ppm). The possible reason is that the mass controller is calibrated at room pressure rather than at the reaction pressure, and/or the actual air flowrate is higher than the set flowrate. So the data tested by the CO analyser is more reliable than the calculated inlet CO concentration. For the same reason, $F_{co,\ inlet}$ will be calculated from $Y_{CO,\ inlet,\ a,\ c}$.

$$\frac{F_{CO,inlet}}{F_{CO,inlet}+F_{air,inlet}} = Y_{CO,inlet,a,c}$$

$$\Rightarrow F_{CO,inlet} = \frac{Y_{CO,inlet,a,c} \times F_{air,inlet}}{(1-Y_{CO,inlet,a,c})}$$

$$\Rightarrow F_{CO,inlet} = \frac{329\times10^{-6}\times 0.4763[mol/s]}{(1-329\times10^{-6})}$$

$$\Rightarrow F_{CO,inlet} = 0.000157\,[mol/s]$$

So

$$R_{CO} = \frac{F_{CO,inlet}\times N_{CO}}{A}$$

$$= \frac{0.000157[mol/s]\times 0.2067}{0.00968[m^2]}$$

$$= 3.35\times10^{-3}[mol/s.m^2]$$

Calculation in Excel:

Sample C2NM (Pt catalyst, made from 3.18 g/l slurry)

Cell type	square
Cells per square inch	400
Length of a section [*m*]	0.022
Diameter of a section [*m*]	0.015
Number of sections	1
Width of a channel [*m*]	0.001
Number of cells in sample	110
Total geometric surface area [m^2]	0.00968
$P_{co\ cylinder}$ [*bar g*]	2.5
T_{room} [°*C*]	25.4
T_{set} [°*C*]	500
Data set (mass controller's)	*60*
Q_{CO} [*ml/min*]	259.14
$F_{CO,\ inlet,\ cal}$ [*mol/s*]	1.76E-04
Q_{air} [*l/min*]	700
$F_{air,\ inlet}$ [*mol/s*]	4.76E-01
$F_{CO,\ inlet,\ cal}$ / $F_{air,\ inlet}$ [*mol/mol*]	3.70E-04
$Y_{CO,\ inlet,\ cal}$ [*ppm*] (calculated)	370.1
$P_{air\ tube}$ [*bar g*]	4.588
$dP_{air\ tube}$ [*bar*]	0.0393
$P_{reactor,\ b}$ [*barg*] (before CO is fed)	1.432
$T_{inlet,\ b}$ [°*C*] (before CO is fed)	467.8
$T_{wall,\ b}$ [°*C*] (before CO is fed)	474.4
$T_{wall,\ b,\ c}$ [°*C*] (Calibrated)	465.6
$T_{oulet,\ b}$ [°*C*] (before CO is fed)	464.5
$Y_{CO,\ inlet,\ b}$ [*ppm*] (before CO is fed)	35
$Y_{CO,\ outlet,\ b}$ [*ppm*] (before CO is fed)	36
$P_{reactor,\ a}$ [*bar g*] (after CO is fed)	1.433
$T_{inlet,\ a}$ [°*C*] (after CO is fed)	467.9
$T_{wall,\ a}$ [°*C*] (after CO is fed)	477.0
$T_{wall,\ a,\ c}$ [°*C*] (Calibrated)	464.6
$T_{oulet,\ a}$ [°*C*] (after CO is fed)	465.6
$T_{oulet,\ a}$ [°*C*] (after CO is fed, calibrated)	468.9
dT [°*C*] (outlet - inlet)	1.0
dT_{wall} [°*C*]	-1.1
$Y_{CO,\ inlet,\ a}$ [*ppm*] (after CO is fed)	344
$Y_{CO,\ inlet,\ a,\ c}$ [*ppm*] (after CO is fed, calibrated)	329
$Y_{CO,\ outlet,\ a}$ [*ppm*] (after CO is fed)	276
$(Y_{CO,\ inlet,\ a} - Y_{CO,\ outlet,\ a})/Y_{CO,\ inlet,\ a,\ c}*100$ [%]	**20.67**
Reaction rate, [10^{-3}*mol/s.*m^2]	**3.35**

Appendix G

Experimental results of CO catalytic combustion

This appendix includes the experimental results of Sample C2NM (No 3, Pt catalyst, from 3.18 g/l slurry) at the following conditions:

- Reaction pressure P = 2.15 ± 0.29 bar (a), CO concentration C = 970 ± 15 ppm, air flowrate Q_{air} = 700 ± 20 l/min, with reaction temperature T varying from 98 to 468 °C;
- Reaction pressure P = 1.85 ± 0.25 bar (a), CO concentration C = 970 ± 15 ppm, reaction temperature T = 241 ± 1 °C, with air flowrate Q_{air} varying from 400 to 700 l/min;
- Reaction pressure P = 2.08 ± 0.20 bar (a), air flowrate Q_{air} = 700 ± 20 l/min, reaction temperature T = 98 °C and 374 °C, with CO concentration varying from C = 370 to 970 ppm.

Data used in Figure 6.8 & Matlab programme:

Sample C2NM (Pt catalyst, made from 3.18 g/l slurry)

Cell type	Square	Square	Square
Cells per square inch	400	400	400
Length of a section [m]	0.022	0.022	0.022
Diameter of a section [m]	0.015	0.015	0.015
No of sections	1	1	1
Width of a channel [m]	0.00114	0.00114	0.00114
Number of channels in the sample	110	110	110
Total geometric surface area [m^2]	0.0110352	0.0110352	0.0110352
Pressure in the CO cylinder [bar (g)]	2	2	2
Temperature of the room [°C]	20.6	20.6	20.6
Data (mass controller's)	123	123	123
CO flowrate [ml/min]	699.5	699.5	699.5
CO flowrate [mol/s]	4.84E-04	4.84E-04	4.84E-04
Air flowrate [l/min]	720	720	720
Air flowrate [mol/s]	0.498	0.498	0.498
Air flowrate [mol/m^3]	41.49	41.49	41.49
Air velocity at room temperature [m/s]	110.6	110.6	110.6
Air velocity at reaction temperature [m/s]	130.6	133.2	138.7
CO/Air [mol/mol]	9.72E-04	9.72E-04	9.72E-04
CO concentration (calculated) [ppm]	971.6	971.6	971.6
Pressure in the air tube [bar (g)]	4.66	4.662	4.663
Difference of pressure in air tube [bar]	0.0436	0.0435	0.0435
$C_{in,\,b}$ (before CO is fed) [ppm]	10	16	17
$C_{out,\,b}$ (before CO is fed) [ppm]	10	16	17
T_{set} [°C]	20.6	50	100
T_{inlet} [°C] (before CO is fed)	20.6	46.5	89.3
T_{wall} [°C] (before CO is fed)	20.6	48.9	94.1
T_{wall} [°C] (Calibrated)	20.6	46.5	88.6
T_{oulet} [°C] (before CO is fed)	20.6	46.5	88.2
$P_{reactor}$ [bar (g)] (after CO is fed)	0.635	0.682	0.735
$P_{reactor}$ [bar (a)] (after CO is fed)	1.635	1.682	1.735
T_{inlet} [°C] (after CO is fed)	20.6	48.9	92.9
T_{inlet} [K] (after CO is fed)	293.8	322.1	366.1
T_{wall} [°C] (after CO is fed)	20.6	51.3	96.6
T_{wall} [°C] (Calibrated)	19.6	49.6	93.9
T_{oulet} [°C] (after CO is fed)	20.6	48.9	91.7
T_{oulet} [K] (after CO is fed)	293.8	322.1	366.0
dT (T_{outlet}-T_{inlet}) [°C]	0.0	0.0	-0.1
$C_{in,\,a}$ [ppm] (after CO is fed)	961	975	978
$C_{in,\,c}$ [ppm] (after CO is fed, calibrated)	950	964	967
$C_{out,\,a}$ [ppm] (after CO is fed)	958	958	960
$C_{out,\,c}$ [ppm] (after CO is fed, calibrated)	947	947	949
CO conversion ((C_{in}-C_{out})/$C_{in,\,c}$) [%]	0.32	1.76	1.86
Reaction rate, [$mol/s.m^2$]	2.21E-04	1.17E-03	1.12E-03

Data used in Figure 6.8 & Matlab programme:

Sample C2NM (Pt catalyst, made from 3.18 g/l slurry)

Cell type	Square	Square	Square	Square	Square
Cells per square inch	400	400	400	400	400
Length of a section [m]	0.022	0.022	0.022	0.022	0.022
Diameter of a section [m]	0.015	0.015	0.015	0.015	0.015
No of sections	1	1	1	1	1
Width of a channel [m]	0.00114	0.00114	0.00114	0.00114	0.00114
Number of channels in the sample	110	110	110	110	110
Total geometric surface area [m^2]	0.011035	0.011035	0.011035	0.011035	0.011035
Pressure in the CO cylinder [bar (g)]	2	2	2	2	2
Temperature of the room [°C]	20.6	20.6	20.6	20.6	20.6
Data (mass controller's)	123	123	123	123	123
CO flowrate [ml/min]	699.5	699.5	699.5	699.5	699.5
CO flowrate [mol/s]	4.84E-04	4.84E-04	4.84E-04	4.84E-04	4.84E-04
Air flowrate [l/min]	720	720	720	720	720
Air flowrate [mol/s]	0.498	0.498	0.498	0.498	0.498
Air flowrate [mol/m^3]	41.49	41.49	41.49	41.49	41.49
Air velocity at room temperature [m/s]	110.6	110.6	110.6	110.6	110.6
Air velocity at reaction temperature [m/s]	**140.6**	**141.8**	**144.4**	**146.6**	**148.1**
CO/Air [mol/mol]	9.72E-04	9.72E-04	9.72E-04	9.72E-04	9.72E-04
CO concentration (calculated) [ppm]	971.6	971.6	971.6	971.6	971.6
Pressure in the air tube [bar (g)]	4.664	4.665	4.662	4.664	4.665
Difference of pressure in air tube [bar]	0.0432	0.0431	0.043	0.043	0.0432
$C_{in,\,b}$ (before CO is fed) [ppm]	16	24	18	24	18
$C_{out,\,b}$ (before CO is fed) [ppm]	16	25	18	25	19
T_{set} [°C]	150.0	175.0	200.0	225.0	250.0
T_{inlet} [°C] (before CO is fed)	142.6	173.1	186.5	210.3	237.2
T_{wall} [°C] (before CO is fed)	146.1	175.6	192.6	217.6	242.1
T_{wall} [°C] (Calibrated)	141.7	173.1	185.7	208.7	235.5
T_{oulet} [°C] (before CO is fed)	141.3	173.1	185.3	207.9	234.7
Named test points in the Matlab programme	**T1**	**T2**	**T3**	**T4**	**T5**
$P_{reactor}$ [bar (g)] (after CO is fed)	0.845	0.904	0.918	0.947	0.992
$P_{reactor}$ [bar (a)] (after CO is fed)	**1.845**	**1.904**	**1.918**	**1.947**	**1.992**
T_{inlet} [°C] (after CO is fed)	142.7	170.5	189.0	211.5	237.2
T_{inlet} [K] (after CO is fed)	**415.9**	**443.7**	**462.2**	**484.7**	**510.4**
T_{wall} [°C] (after CO is fed)	147.4	175.3	196.3	223.6	249.2
T_{wall} [°C] (Calibrated)	143.6	170.9	191.4	218.1	243.1
T_{oulet} [°C] (after CO is fed)	142.6	170.5	186.5	211.5	237.1
T_{oulet} [K] (after CO is fed)	**417.1**	**443.7**	**460.9**	**487.1**	**512.8**
dT (T_{outlet}-T_{inlet}) [°C]	1.2	0.0	-1.3	2.4	2.4
$C_{in,\,a}$ [ppm] (after CO is fed)	980	985	983	983	987
$C_{in,\,c}$ [ppm] (after CO is fed, calibrated)	**969**	**974**	**972**	**972**	**976**
$C_{out,\,a}$ [ppm] (after CO is fed)	963	893	831	790	761
$C_{out,\,c}$ [ppm] (after CO is fed, calibrated)	**952**	**882**	**820**	**779**	**750**
CO conversion ((C_{in}-C_{out})/$C_{in,\,c}$) [%]	1.75	9.45	15.64	19.86	23.16
Reaction rate, [$mol/s.m^2$]	9.92E-04	5.20E-03	8.27E-03	1.01E-02	1.15E-02

Data used in Figure 6.8 & Matlab programme:

Sample C2NM (Pt catalyst, made from 3.18 g/l slurry)

Cell type	Square	Square	Square	Square	Square
Cells per square inch	400	400	400	400	400
Length of a section [m]	0.022	0.022	0.022	0.022	0.022
Diameter of a section [m]	0.015	0.015	0.015	0.015	0.015
No of sections	1	1	1	1	1
Width of a channel [m]	0.00114	0.00114	0.00114	0.00114	0.00114
Number of channels in the sample	110	110	110	110	110
Total geometric surface area [m^2]	0.011035	0.011035	0.011035	0.011035	0.011035
Pressure in the CO cylinder [bar (g)]	2	2	2	2	2
Temperature of the room [°C]	20.6	20.6	20.6	20.6	20.6
Data (mass controller's)	123	123	123	123	123
CO flowrate [ml/min]	699.5	699.5	699.5	699.5	699.5
CO flowrate [mol/s]	4.84E-04	4.84E-04	4.84E-04	4.84E-04	4.84E-04
Air flowrate [l/min]	720	720	720	720	720
Air flowrate [mol/s]	0.498	0.498	0.498	0.498	0.498
Air flowrate [mol/m^3]	41.49	41.49	41.49	41.49	41.49
Air velocity at room temperature [m/s]	110.6	110.6	110.6	110.6	110.6
Air velocity at reaction temperature [m/s]	**152.1**	**155.7**	**159.2**	**163.0**	**166.1**
Air/CO [mol/mol]	9.72E-04	9.72E-04	9.72E-04	9.72E-04	9.72E-04
CO concentration (calculated) [ppm]	971.6	971.6	971.6	971.6	971.6
Pressure in the air tube [bar (g)]	4.667	4.656	4.662	4.658	4.663
Difference of pressure in air tube [bar]	0.043	0.0427	0.0425	0.0423	0.0423
$C_{in,\,b}$ (before CO is fed) [ppm]	20	24	22	24	23
$C_{out,\,b}$ (before CO is fed) [ppm]	21	25	22	24	24
T_{set} [°C]	300.0	350.0	400.0	450.0	500.0
T_{inlet} [°C] (before CO is fed)	283.7	341.1	379.0	429.0	467.7
T_{wall} [°C] (before CO is fed)	288.5	342.4	385.6	432.4	474.6
T_{wall} [°C] (Calibrated)	281.4	338.0	375.1	425.2	460.9
T_{oulet} [°C] (before CO is fed)	280.2	336.5	373.1	423.3	457.5
Named test points in the Matlab programme	**T6**	**T7**	**T8**	**T9**	**T10**
$P_{reactor}$ [bar (g)] (after CO is fed)	1.058	1.135	1.188	1.253	1.302
$P_{reactor}$ [bar (a)] (after CO is fed)	**2.058**	**2.135**	**2.188**	**2.253**	**2.302**
T_{inlet} [°C] (after CO is fed)	284.8	336.4	379.0	429.0	468.9
T_{inlet} [K] (after CO is fed)	**558.0**	**609.6**	**652.2**	**702.2**	**742.1**
T_{wall} [°C] (after CO is fed)	295.6	345.8	389.4	438.2	481.4
T_{wall} [°C] (Calibrated)	288.5	337.6	380.2	427.9	470.1
T_{oulet} [°C] (after CO is fed)	282.5	334.0	375.5	423.3	460.9
T_{oulet} [K] (after CO is fed)	**559.2**	**611.8**	**654.6**	**702.2**	**744.3**
dT (T_{outlet}-T_{inlet}) [°C]	1.2	2.2	2.4	0.0	2.2
$C_{in,\,a}$ [ppm] (after CO is fed)	988	990	995	997	994
$C_{in,\,c}$ [ppm] (after CO is fed, calibrated)	**977**	**979**	**984**	**986**	**983**
$C_{out,\,a}$ [ppm] (after CO is fed)	763	768	748	762	758
$C_{out,\,c}$ [ppm] (after CO is fed, calibrated)	**752**	**757**	**737**	**751**	**747**
CO conversion ((C_{in}-C_{out})/$C_{in,\,c}$) [%]	23.03	22.68	25.10	23.83	24.01
Reaction rate, [$mol/s.m^2$]	1.09E-02	1.02E-02	1.09E-02	9.95E-03	9.62E-03

Data used in Figure 6.9:

Sample C2NM (Pt catalyst, made from 3.18 g/l slurry)

Cell type	Square	Square	Square	Square
Cells per square inch	400	400	400	400
Length of a section [m]	0.022	0.022	0.022	0.022
Diameter of a section [m]	0.015	0.015	0.015	0.015
Number of sections	1	1	1	1
Width of a channel [m]	1.14E-03	1.14E-03	1.14E-03	1.14E-03
Number of cells in a sample	110	110	110	110
Total geometric surface area [m^2]	1.10E-02	1.10E-02	1.10E-02	1.10E-02
$P_{co\ cylinder}$ [bar g]	2.5	2.5	2.5	2.5
T_{room} [°C]	25.4	25.4	25.4	25.4
T_{set} [°C]	**400**	**400**	**400**	**400**
Data set (mass controller's)	60	80	100	120
Q_{CO} [ml/min]	259.14	398.95	538.76	678.57
F_{CO} [mol/s]	1.76E-04	2.71E-04	3.67E-04	4.62E-04
Q_{air} [l/min]	700	700	700	700
F_{air} [mol/s]	0.476	0.476	0.476	0.476
V_{air} [m/s]	126.1	126.1	126.3	126.2
F_{air}/F_{CO} [mol/mol]	3.70E-04	5.70E-04	7.70E-04	9.69E-04
$Y_{CO,\ ca}$ [ppm] (calculated)	370.2	569.9	769.7	969.4
$P_{air\ tube}$ [bar g]	4.600	4.598	4.598	4.598
$dP_{air\ tube}$ [bar]	0.0400	0.0400	0.0400	0.0400
$P_{reactor,\ a}$ [bar g] (after CO is fed)	1.31	1.31	1.31	1.31
$T_{inlet,\ a}$ [°C] (after CO is fed)	374.40	375.30	376.80	376.80
$T_{wall,\ a}$ [°C] (after CO is fed)	383.60	385.60	386.00	387.10
$T_{wall,\ a,\ c}$ [°C] (Calibrated)	373.80	375.74	376.13	377.20
$T_{oulet,\ a}$ [°C] (after CO is fed)	374.40	375.20	376.80	376.70
dT [°C] ($T_{outlet,\ a}$ - $T_{inlet,\ a}$)	2.40	-0.10	0.00	-0.10
$T_{wall\ increasement}$ [°C] ($T_{wall,\ a,\ c}$ - $T_{wall,\ b,\ c}$)	1.00	0.44	-0.67	0.40
$Y_{CO,\ inlet,\ a}$ [ppm] (after CO is fed)	351	567	763	981
$Y_{CO,\ inlet,\ a,\ c}$ [ppm] (after CO is fed, calibrated)	336	552	748	966
$Y_{CO,\ outlet,\ a}$ [ppm] (after CO is fed)	288	463	623	797
$(Y_{CO,\ inlet,\ a} - Y_{CO,\ outlet,\ a})/Y_{CO,\ inlet,\ a,\ c}*100$ [%]	18.75	18.84	18.72	19.05
Reaction rate [10^{-3} mol/s.m^2]	2.87	4.74	6.38	8.38

Data used in Figure 6.9:

Sample C2NM (Pt catalyst, made from 3.18 g/l slurry)

Cell type	square	square	square	square
Cells per square inch	400	400	400	400
Length of a section [m]	0.022	0.022	0.022	0.022
Diameter of a section [m]	0.015	0.015	0.015	0.015
Number of sections	1	1	1	1
Width of a channel [m]	1.14E-03	1.14E-03	1.14E-03	1.14E-03
Number of cells in a sample	110	110	110	110
Total geometric surface area [m^2]	1.10E-02	1.10E-02	1.10E-02	1.10E-02
$P_{co\ cylinder}$ [bar g]	2.0	2.0	2.0	2.0
T_{room} [°C]	24.2	24.2	24.2	24.2
T_{set} [°C]	**100**	**100**	**100**	**100**
Data set (mass controller's)	60	80	100	120
Q_{CO} [ml/min]	259.14	398.95	538.76	678.57
F_{CO} [mol/s]	1.77E-04	2.73E-04	3.68E-04	4.64E-04
Q_{air} [l/min]	700	700	700	700
F_{air} [mol/s]	0.478	0.478	0.478	0.478
V_{air} [m/s]	90.5	90.0	90.3	90.0
F_{air}/F_{CO} [mol/mol]	3.70E-04	5.70E-04	7.70E-04	9.69E-04
$Y_{CO,\ ca}$ [ppm] (calculated)	370.2	569.9	769.7	969.4
$P_{air\ tube}$ [bar g]	4.607	4.621	4.612	4.616
$dP_{air\ tube}$ [bar]	0.0397	0.0397	0.0396	0.0396
$P_{reactor,\ a}$ [bar g] (after CO is fed)	0.85	0.86	0.85	0.86
$T_{inlet,\ a}$ [°C] (after CO is fed)	98.30	98.00	98.30	97.60
$T_{wall,\ a}$ [°C] (after CO is fed)	99.50	100.50	99.50	100.00
$T_{wall,\ a,\ c}$ [°C] (Calibrated)	97.51	98.48	97.51	98.00
$T_{oulet,\ a}$ [°C] (after CO is fed)	98.30	98.10	98.30	97.60
dT [°C] ($T_{outlet,\ a}$ - $T_{inlet,\ a}$)	0.00	0.10	0.00	0.00
$T_{wall\ increasement}$ [°C] ($T_{wall,\ a,\ c}$ - $T_{wall,\ b,\ c}$)	-0.79	0.48	-0.79	0.40
$Y_{CO,\ inlet,\ a}$ [ppm] (after CO is fed)	353	567	778	999
$Y_{CO,\ inlet,\ a,\ c}$ [ppm] (after CO is fed, calibrated)	338	552	763	984
$Y_{CO,\ outlet,\ a}$ [ppm] (after CO is fed)	346	556	763	980
$(Y_{CO,\ inlet,\ a} - Y_{CO,\ outlet,\ a})/Y_{CO,\ inlet,\ a,\ c}*100$ [%]	2.07	1.99	1.97	1.93
Reaction rate [10^{-3} mol/s.m^2]	0.45	0.70	0.96	1.22

Data used in Figure 6.10:

Sample C2NM (Pt catalyst, made from 3.18 g/l slurry)

Cell type	Square	Square	Square	Square
Cells per square inch	400	400	400	400
Length of a section [m]	0.022	0.022	0.022	0.022
Diameter of a section [m]	0.015	0.015	0.015	0.015
Number of sections	1	1	1	1
Width of a channel [m]	0.001	0.001	0.001	0.001
Number of cells in sample	110	110	110	110
Total geometric surface area [m^2]	9.68E-03	9.68E-03	9.68E-03	9.68E-03
$P_{co\ cylinder}$ [$barg$]	2.5	2.5	2.5	2.5
T_{room} [$°C$]	24.2	25.4	25.4	25.4
T_{set} [$°C$]	**250**	**300**	**400**	**500**
Data set (mass controller's)	*60*	*60*	*60*	*60*
Q_{CO} [ml/min]	259.14	259.14	259.14	259.14
F_{CO} [$10^{-3}mol/s$]	0.177	0.176	0.176	0.176
Q_{air} [l/min]	700	700	700	700
F_{air} [mol/s]	0.478	0.476	0.476	0.476
F_{CO}/F_{air} [$10^{-3}mol/mol$]	370.2	370.2	370.2	370.2
$Y_{CO,\ ca}$ [ppm] (calculated)	370.1	370.1	370.1	370.1
$P_{air\ tube}$ [$barg$]	4.589	4.600	4.600	4.588
$dP_{air\ tube}$ [bar]	0.039	0.040	0.040	0.039
$P_{reactor,\ b}$ [$barg$] (before CO is fed)		1.2	1.3	1.4
$T_{inlet,\ b}$ [$°C$] (before CO is fed)		282.2	372.2	467.8
$T_{wall,\ b}$ [$°C$] (before CO is fed)		288.2	380.2	474.4
$T_{wall,\ b,\ c}$ [$°C$] (Calibrated)		282.2	370.6	465.6
$T_{oulet,\ b}$ [$°C$] (before CO is fed)		282.2	369.8	464.5
$Y_{CO,\ inlet,\ b}$ [ppm] (before CO is fed)			32	35
$Y_{CO,\ outlet,\ b}$ [ppm] (before CO is fed)			34	36
$P_{reactor,\ a}$ [$barg$] (after CO is fed)	1.08	1.175	1.307	1.433
$T_{inlet,\ a}$ [$°C$] (after CO is fed)	236.7	283.3	374.4	467.9
$T_{wall,\ a}$ [$°C$] (after CO is fed)	242.8	290.5	383.6	477.0
$T_{wall,\ a,\ c}$ [$°C$] (Calibrated)	236.9	283.3	373.8	464.6
$T_{oulet,\ a}$ [$°C$] (after CO is fed)	235.4	283.3	374.4	465.6
dT [$°C$] ($T_{outlet,\ a} - T_{inlet,\ a}$)	-1.3	0.0	2.4	1.0
$T_{wall\ increasement}$ [$°C$] ($T_{wall,\ a,\ c} - T_{wall,\ b,\ c}$)	0.2	0.0	1.0	-1.1
$Y_{CO,\ inlet,\ a}$ [ppm] (after CO is fed)	341	341	351	344
$Y_{in,\ a,\ c}$ [ppm] (after CO is fed, calibrated)	323	330	336	329
$Y_{CO,\ outlet,\ a}$ [ppm] (after CO is fed)	282	280	288	276
$(Y_{CO,\ inlet,\ a} - Y_{CO,\ outlet,\ a})/Y_{CO,\ inlet,\ a,\ c}*100$ [$\%$]				
(when $Y_{CO,\ inlet,\ ca}$ = 370ppm)	18.27	18.48	18.75	20.67
(when $Y_{CO,\ inlet,\ ca}$ = 570ppm)	16.95	18.05	18.84	18.52
(when $Y_{CO,\ inlet,\ ca}$ = 770ppm)	16.49	17.80	18.72	18.59
(when $Y_{CO,\ inlet,\ ca}$ = 970ppm)	17.02	18.07	19.05	19.27
Reaction rate, [$10^{-3}mol/s.m^2$]				
(when $Y_{CO,\ inlet,\ ca}$ = 370ppm)	2.92	3.00	3.10	3.35
(when $Y_{CO,\ inlet,\ ca}$ = 570ppm)	4.45	4.82	5.12	4.92
(when $Y_{CO,\ inlet,\ ca}$ = 770ppm)	5.98	6.60	6.89	6.89
(when $Y_{CO,\ inlet,\ ca}$ = 970ppm)	8.01	8.57	9.06	9.16

Data used in Figure 6.10:

Sample C2NM (Pt catalyst, made from 3.18 g/l slurry)

Cell type	Square	Square	Square	Square
Cells per square inch	400	400	400	400
Length of a section [m]	0.022	0.022	0.022	0.022
Diameter of a section [m]	0.015	0.015	0.015	0.015
Number of sections	1	1	1	1
Width of a channel [m]	0.00114	0.00114	0.00114	0.00114
Number of cells in sample	110	110	110	110
Total geometric surface area [m^2]	0.0110	0.0110	0.0110	0.0110
$\mathbf{P}_{\text{co cylinder}}$ [$bar\ g$]	2.0	2.0	2.0	2.0
$\mathbf{T}_{\text{room}}$ [$°C$]	23.7	23.7	23.7	23.7
$\mathbf{T}_{\text{set}}$ [$°C$]	**250**	**250**	**250**	**250**
Data set (mass controller's)	120	112	102	91
$\mathbf{Q}_{\text{CO}}$ [ml/min]	678.6	622.6	552.7	475.8
$\mathbf{F}_{\text{CO}}$ [mol/s]	4.64E-04	4.26E-04	3.78E-04	3.26E-04
$\mathbf{Q}_{\text{air}}$ [l/min]	**700**	**600**	**500**	**400**
$\mathbf{F}_{\text{air}}$ [mol/s]	0.47898	0.41055	0.34213	0.27370
$\mathbf{V}_{\text{air}}$ [m/s]	109.5	95.6	82.1	68.4
$\mathbf{F}_{\text{air}}/\mathbf{F}_{\text{CO}}$ [mol/mol]	9.69E-04	1.04E-03	1.11E-03	1.19E-03
$\mathbf{Y}_{\text{CO, ca}}$ [ppm] (calculated)	969.4	1037.7	1105.5	1189.6
$\mathbf{P}_{\text{air tube}}$ [$bar\ g$]	4.431	4.408	4.425	4.419
$\mathbf{dP}_{\text{air tube}}$ [bar]	0.0407	0.0335	0.0259	0.0188
$\mathbf{Y}_{\text{CO, inlet, b}}$ [ppm] (before CO is fed)	33			
$\mathbf{Y}_{\text{CO, outlet, b}}$ [ppm] (before CO is fed)	34			
$\mathbf{P}_{\text{reactor, a}}$ [$barg$] (after CO is fed)	1.100	0.946	0.777	0.605
$\mathbf{T}_{\text{inlet, a}}$ [$°C$] (after CO is fed)	236.2	236.1	236.2	237.8
$\mathbf{T}_{\text{wall, a}}$ [$°C$] (after CO is fed)	247.1	247.0	247.0	247.5
$\mathbf{T}_{\text{wall, a, c}}$ [$°C$] (Calibrated)	241.1	241.0	241.0	241.4
$\mathbf{T}_{\text{oulet, a}}$ [$°C$] (after CO is fed)	235.0	237.3	236.1	237.8
$\mathbf{dT}$ [$°C$] ($\mathbf{T}_{\text{outlet, a}} - \mathbf{T}_{\text{inlet, a}}$)	-1.2	1.2	-0.1	0.0
$\mathbf{T}_{\text{wall increasement}}$ [$°C$] ($\mathbf{T}_{\text{wall, a, c}} - \mathbf{T}_{\text{inlet, a}}$)	4.9	4.9	4.8	3.6
$\mathbf{Y}_{\text{CO, inlet, a}}$ [ppm] (after CO is fed)	1020	1026	1037	1036
$\mathbf{Y}_{\text{CO, inlet, a, c}}$ [ppm] (after CO is fed, calibrated)	1005	1011	1022	1021
$\mathbf{Y}_{\text{CO, outlet, a}}$ [ppm] (after CO is fed)	854	857	860	853
$(\mathbf{Y}_{\text{CO, inlet, a}} - \mathbf{Y}_{\text{CO, outlet, a}})/\mathbf{Y}_{\text{CO, inlet, a}}$	0.165	0.167	0.173	0.179
Reaction rate [$mol/s.m^2$]	0.0087	0.0070	0.0056	0.0042

Data used in Figure 6.11:

Sample C2NM (Pt catalyst, made from 3.18 g/l slurry)

Cell type	Square	Square	Square	Square
Cells per square inch	400	400	400	400
Length of a section [m]	0.022	0.022	0.022	0.022
Diameter of a section [m]	0.015	0.015	0.015	0.015
Number of sections	1	1	1	1
Width of a channel [m]	0.00114	0.00114	0.00114	0.00114
Number of cells in sample	110	110	110	110
Total geometric surface area [m^2]	0.0110	0.0110	0.0110	0.0110
$P_{co\ cylinder}$ [bar g]	2.0	2.0	2.0	2.0
T_{room} [°C]	23.7	23.7	23.7	23.7
T_{set} [°C]	**250**	**250**	**250**	**250**
Data set (mass controller's)	120	112	102	91
Q_{CO} [ml/min]	678.6	622.6	552.7	475.8
F_{CO} [mol/s]	4.64E-04	4.26E-04	3.78E-04	3.26E-04
Q_{air} [l/min]	700	600	500	400
F_{air} [mol/s]	0.47898	0.41055	0.34213	0.27370
V_{air} [m/s]	109.5	95.6	82.1	68.4
F_{air}/F_{CO} [mol/mol]	9.69E-04	1.04E-03	1.11E-03	1.19E-03
$Y_{CO,\ ca}$ [ppm] (calculated)	969.4	1037.7	1105.5	1189.6
$P_{air\ tube}$ [bar g]	4.431	4.408	4.425	4.419
$dP_{air\ tube}$ [bar]	0.0407	0.0335	0.0259	0.0188
$Y_{CO,\ inlet,\ b}$ [ppm] (before CO is fed)	33			
$Y_{CO,\ outlet,\ b}$ [ppm] (before CO is fed)	34			
$P_{reactor,\ a}$ [barg] (after CO is fed)	1.100	0.946	0.777	0.605
$T_{inlet,\ a}$ [°C] (after CO is fed)	236.2	236.1	236.2	237.8
$T_{wall,\ a}$ [°C] (after CO is fed)	247.1	247.0	247.0	247.5
$T_{wall,\ a,\ c}$ [°C] (Calibrated)	241.1	241.0	241.0	241.4
$T_{oulet,\ a}$ [°C] (after CO is fed)	235.0	237.3	236.1	237.8
dT [°C] ($T_{outlet,\ a}$ - $T_{inlet,\ a}$)	-1.2	1.2	-0.1	0.0
$T_{wall\ increasement}$ [°C] ($T_{wall,\ a,\ c}$ - $T_{inlet,\ a}$)	4.9	4.9	4.8	3.6
$Y_{CO,\ inlet,\ a}$ [ppm] (after CO is fed)	1020	1026	1037	1036
$Y_{CO,\ inlet,\ a,\ c}$ [ppm] (after CO is fed, calibrated)	1005	1011	1022	1021
$Y_{CO,\ outlet,\ a}$ [ppm] (after CO is fed)	854	857	860	853
($Y_{CO,\ inlet,\ a}$ - $Y_{CO,\ outlet,\ a}$)/$Y_{CO,\ inlet,\ a}$	0.165	0.167	0.173	0.179
Reaction rate [mol/s.m^2]	0.0087	0.0070	0.0056	0.0042

Data used in Figures 6.14 to 6.16:

When Ew = 104 kJ/mol, Alpha = -1.1, Aw = 7.9433E+15

Test points	T_{out} exp, K	T_{out} cal, K	Error on T, %	Eta
T1	417.1	415.9	-0.29	0.9957
T2	443.7	443.7	0.01	0.9756
T3	460.9	462.3	0.30	0.9332
T4	487.1	485.0	-0.43	0.8163
T5	512.8	511.1	-0.32	0.5925
T6	559.2	560.2	0.19	0.2463
T7	611.8	615.3	0.57	0.1029
T8	654.6	663.2	1.31	0.0557
T9	702.2	723.7	3.06	0.0300
T10	744.3	776.3	4.30	0.0195

When Ew = 104 kJ/mol, Alpha = -1.1, Aw = 7.9433E+15

Test points	T_{out} exp, K	Y_{out} exp, ppm	Y_{out} exp	Y_{out} cal	Error on Y_{out}, %
T1	417.1	952	9.52E-04	9.68E-04	1.72
T2	443.7	882	8.82E-04	9.70E-04	10.03
T3	460.9	820	8.20E-04	9.62E-04	17.33
T4	487.1	779	7.79E-04	9.45E-04	21.35
T5	512.8	750	7.50E-04	9.20E-04	22.62
T6	559.2	752	7.52E-04	8.66E-04	15.13
T7	611.8	757	7.57E-04	8.21E-04	8.43
T8	654.6	737	7.37E-04	7.98E-04	8.33
T9	702.2	751	7.51E-04	7.79E-04	3.71
T10	744.3	747	7.47E-04	7.64E-04	2.32

Appendix H

Conversion factors used in the thesis

Density:	**1 kg/m^3** = 0.001 g/cm^3
Energy:	**1 J** = 1 N m = 1 W s = 0.239 cal
Gas constant:	**R** = 8314.3 N m/(K kmol) = 0.082 atm liter/(mol K)
Heat capacity:	**1 J/(K kg)** = kcal/(kg °C)/4186.8
Length:	**1 m** = 3.281 ft = 39.37 inch = 100 cm = 1000 mm = 10^6 μm (micron) = 10^9 nm = 10^{10} Å
Mass:	**1 kg** = 1000 g
Mass flux:	**1 kg/(m^2 s)** = 3600 kg/(m^2 h)
Mass transfer coefficient:	**1 kg/(m^2 s)** = 3600 kg/(m^2 h)
Power:	**1 W** = J/s = N m/s = 0.239 cal/s
Pressure:	**1 atm** = 101.325 kPa = 1.01325 bar = 760 mm of mercury
	1 Pa = N/m^2 = kg/(m s^2) = 10^{-5} bar
Temperature:	**K** = °C + 273.15
	°F = 1.8 × °C + 32
Thermal diffusivity:	**1 m^2/s** = 3600 m^2/h
Velocity:	**1 m/s** = 3.6 km/h
Volume:	**1 m^3** = 35.29 ft^3 = 1000 liters

Appendix I

Back-calculation of the tortuosity factor

T	T	P (a)	d_p	$D_{bulk, cal}$	$D_{K, cal}$	D_{cal}	ε	ε/τ	τ	D_{eff}	Note
°C	K	10^5 Pa	10^{-6} m	m^2/s	m^2/s	m^2/s				m^2/s	
17.4	290.6	1.060	1.6283	1.87E-05	2.54E-04	1.75E-05	0.344	0.055	**6.26**	9.58E-07	(Cordierite)
17.4	290.6	1.060	1.6283	1.87E-05	2.54E-04	1.75E-05	0.344	0.058	**5.96**	1.01E-06	(Cordierite)
17.4	290.6	1.060	1.6283	1.87E-05	2.54E-04	1.75E-05	0.344	0.052	**6.60**	9.09E-07	(Cordierite)
17.4	290.6	1.110	0.0126	1.79E-05	1.97E-06	1.77E-06	0.527	0.209	**2.52**	3.71E-07	(S3)
17.4	290.6	1.110	0.0126	1.79E-05	1.97E-06	1.77E-06	0.527	0.675	**0.78**	1.20E-06	(S3)
17.4	290.6	1.110	0.0171	1.79E-05	2.67E-06	2.32E-06	0.442	0.178	**2.48**	4.14E-07	(S3w)
17.4	290.6	1.110	0.0171	1.79E-05	2.67E-06	2.32E-06	0.442	0.218	**2.02**	5.07E-07	(S3w)
17.4	290.6	1.110	0.0123	1.79E-05	1.92E-06	1.74E-06	0.529	0.603	**0.88**	1.05E-06	(S3HT)
17.4	290.6	1.110	0.0123	1.79E-05	1.92E-06	1.74E-06	0.529	0.622	**0.85**	1.08E-06	(S3HT)
17.4	290.6	1.110	0.0137	1.79E-05	2.14E-06	1.91E-06	0.451	0.145	**3.11**	2.77E-07	(C2NM)
17.4	290.6	1.110	0.0137	1.79E-05	2.14E-06	1.91E-06	0.451	0.212	**2.12**	4.06E-07	(C2NM-1P)
17.4	290.6	1.110	0.0131	1.79E-05	2.05E-06	1.84E-06	0.408	0.142	**2.87**	2.61E-07	(C2HT)
17.4	290.6	1.110	0.0131	1.79E-05	2.05E-06	1.84E-06	0.408	0.219	**1.86**	4.02E-07	(C2HT)

Appendix J

The calculation of D_{eff} at different temperatures

The following calculation is based on the experimental D_{eff} value in a single-plate washcoat (**C2NM** catalyst) which is 4.06×10^{-7} m^2/s.

Temp	**Temp**	**P** (a)	$D_{bulk, cal}$	$D_{K, cal}$	$D_{M, cal}$	ε	ε/τ	τ	$D_{eff, cal}$	**Note**
°C	K	10^5 Pa	cm^2/s	cm^2/s	cm^2/s				m^2/s	
16.6	**289.8**	**1.110**	**0.178**	**0.021**	**0.019**	**0.451**	**0.213**	**2.12**	**4.06E-07**	**(Measured)**
142.8	415.9	2.001	0.184	0.0256	0.0225	0.451	0.213	2.12	4.79E-07	(Calculated)
170.6	443.7	2.005	0.206	0.0265	0.0234	0.451	0.213	2.12	4.99E-07	(Calculated)
189.1	462.2	2.027	0.219	0.0270	0.0240	0.451	0.213	2.12	5.12E-07	(Calculated)
211.6	484.7	2.056	0.235	0.0276	0.0247	0.451	0.213	2.12	5.27E-07	(Calculated)
237.3	510.4	2.082	0.254	0.0284	0.0255	0.451	0.213	2.12	5.43E-07	(Calculated)
284.9	558.0	2.113	0.292	0.0297	0.0269	0.451	0.213	2.12	5.74E-07	(Calculated)
336.5	609.6	2.137	0.337	0.0310	0.0284	0.451	0.213	2.12	6.05E-07	(Calculated)
379.1	652.2	2.268	0.357	0.0321	0.0294	0.451	0.213	2.12	6.27E-07	(Calculated)
429.1	702.2	2.384	0.387	0.0333	0.0306	0.451	0.213	2.12	6.53E-07	(Calculated)
469.0	742.1	2.384	0.426	0.0342	0.0317	0.451	0.213	2.12	6.74E-07	(Calculated)

Appendix K

Matlab programme for the calculation of A_w and α

```
% Program for the calculation of Aw and alpha from T1 to T10
% in the rate expression of CO oxidation reaction

% With a plot of the solution
% any text beginning with a "%" is a comment

% The result of any calculation is written to the screen
% unless the line ends with a;

clear
% This removes any previously created variables

%Tcal = 1;                    % Stores the calculated value of T
%Ycal = 1;                    % Stores the calculated value of Y

delta1 = 100000000;      % Initial value of the sum of the squares
                         % of differences between the calculated results
                         % and experimental data

% alpha is for the power of pressure term
 for ii=-5:23
    alpha = -2.100 + 0.100*ii;

% Aw, pre-exponential factor, mol/m^2/s
 for jj=70:160
    Aw = exp(0.10*jj*log(10));

% Ew, activation energy in a catalytic reaction, J/mol
% Use the value of 104 kJ/mol, adapted from Voltz (1973).

Ew = 104000;

% For loop to calculate T and Y at different To (totally nine here from T1 to T10)
 for ll=1:10

   if ll==1            % Exp conditions at T1
   Tdata = 417.1;       % Experimental data
   Ydata = 0.000952;    % Experimental data
   To = 415.9;          % Actual inlet gas temp, K
   Po = 1.845e5;        % Actual inlet pressure, Pa (a)
   Vel = 140.6;         % Inlet velocity, m/s
   D = 0.00114;         % Tube (cell) diameter, m
   Yo = 0.000969;       % Actual initial mol fraction of CO in the gas phase
```

```
Tw = To;            % Inlet solid temp, K (initially assumed same as To)
Lc = 45.2e-6;       % Thickness of coated catalyst, m
R = 8.314;          % Gas constant, J/mol/K
Len = 0.022;        % Length of the reactor, m
end;

if ll==2            % Exp conditions at T2
Tdata = 443.7;      % Experimental data
Ydata = 0.000882;   % Experimental data
To = 443.7;         % Actual inlet gas temp, K
Po = 1.904e5;       % Actual inlet pressure, Pa (a)
Vel = 141.8;        % Inlet velocity, m/s
D = 0.00114;        % Tube (cell) diameter, m
Yo = 0.000974;      % Actual initial mol fraction of CO in the gas phase
Tw = To;            % Inlet solid temp, K (initially assumed same as To)
Lc = 45.2e-6;       % Thickness of coated catalyst, m
R = 8.314;          % Gas constant, J/mol/K
Len = 0.022;        % Length of the reactor, m
end;

if ll==3            % Exp conditions at T3
Tdata = 460.9;      % Experimental data
Ydata = 0.000820;   % Experimental data
To = 462.2;         % Actual inlet gas temp, K
Po = 1.918e5;       % Actual inlet pressure, Pa (a)
Vel = 144.4;        % Inlet velocity, m/s
D = 0.00114;        % Tube (cell) diameter, m
Yo = 0.000972;      % Actual initial mol fraction of CO in the gas phase
Tw = To;            % Inlet solid temp, K (initially assumed same as To)
Lc = 45.2e-6;       % Thickness of coated catalyst, m
R = 8.314;          % Gas constant, J/mol/K
Len = 0.022;        % Length of the reactor, m
end;

if ll==4            % Exp conditions at T4
Tdata = 487.1;      % Experimental data
Ydata = 0.000779;   % Experimental data
To = 484.7;         % Actual inlet gas temp, K
Po = 1.947e5;       % Actual inlet pressure, Pa (a)
Vel = 146.6;        % Inlet velocity, m/s
D = 0.00114;        % Tube (cell) diameter, m
Yo = 0.000972;      % Actual initial mol fraction of CO in the gas phase
Tw = To;            % Inlet solid temp, K (initially assumed same as To)
Lc = 45.2e-6;       % Thickness of coated catalyst, m
R = 8.314;          % Gas constant, J/mol/K
Len = 0.022;        % Length of the reactor, m
end;
```

```
if ll==5            % Exp conditions at T5
Tdata = 512.8;       % Experimental data
Ydata = 0.000750;    % Experimental data
To = 510.4;          % Actual inlet gas temp, K
Po = 1.992e5;        % Actual inlet pressure, Pa (a)
Vel = 148.1;         % Inlet velocity, m/s
D = 0.00114;         % Tube (cell) diameter, m
Yo = 0.000976;       % Actual initial mol fraction of CO in the gas phase
Tw = To;             % Inlet solid temp, K (initially assumed same as To)
Lc = 45.2e-6;        % Thickness of coated catalyst, m
R = 8.314;           % Gas constant, J/mol/K
Len = 0.022;         % Length of the reactor, m
end;

if ll==6            % Exp conditions at T6
Tdata = 559.2;       % Experimental data
Ydata = 0.000752;    % Experimental data
To = 558.0;          % Actual inlet gas temp, K
Po = 2.058e5;        % Actual inlet pressure, Pa (a)
Vel = 152.1;         % Inlet velocity, m/s
D = 0.00114;         % Tube (cell) diameter, m
Yo = 0.000977;       % Actual initial mol fraction of CO in the gas phase
Tw = To;             % Inlet solid temp, K (initially assumed same as To)
Lc = 45.2e-6;        % Thickness of coated catalyst, m
R = 8.314;           % Gas constant, J/mol/K
Len = 0.022;         % Length of the reactor, m
end;

if ll==7            % Exp conditions at T7
Tdata = 611.8;       % Experimental data
Ydata = 0.000757;    % Experimental data
To = 609.6;          % Actual inlet gas temp, K
Po = 2.135e5;        % Actual inlet pressure, Pa (a)
Vel = 155.7;         % Inlet velocity, m/s
D = 0.00114;         % Tube (cell) diameter, m
Yo = 0.000979;       % Actual initial mol fraction of CO in the gas phase
Tw = To;             % Inlet solid temp, K (initially assumed same as To)
Lc = 45.2e-6;        % Thickness of coated catalyst, m
R = 8.314;           % Gas constant, J/mol/K
Len = 0.022;         % Length of the reactor, m
end;

if ll==8            % Exp conditions at T8
Tdata = 654.6;       % Experimental data
Ydata = 0.000737;    % Experimental data
To = 652.2;          % Actual inlet gas temp, K
Po = 2.188e5;        % Actual inlet pressure, Pa (a)
Vel = 159.2;         % Inlet velocity, m/s
```

```
D = 0.00114;          % Tube (cell) diameter, m
Yo = 0.000984;        % Actual initial mol fraction of CO in the gas phase
Tw = To;              % Inlet solid temp, K (initially assumed same as To)
Lc = 45.2e-6;         % Thickness of coated catalyst, m
R = 8.314;            % Gas constant, J/mol/K
Len = 0.022;          % Length of the reactor, m
end;

if ll==9              % Exp conditions at T9
Tdata = 702.2;        % Experimental data
Ydata = 0.000751;     % Experimental data
To = 702.2;           % Actual inlet gas temp, K
Po = 2.253e5;         % Actual inlet pressure, Pa (a)
Vel = 163.0;          % Inlet velocity, m/s
D = 0.00114;          % Tube (cell) diameter, m
Yo = 0.000986;        % Actual initial mol fraction of CO in the gas phase
Tw = To;              % Inlet solid temp, K (initially assumed same as To)
Lc = 45.2e-6;         % Thickness of coated catalyst, m
R = 8.314;            % Gas constant, J/mol/K
Len = 0.022;          % Length of the reactor, m
end;

if ll==10             % Exp conditions at T10
Tdata = 744.3;        % Experimental data
Ydata = 0.000747;     % Experimental data
To = 742.1;           % Actual inlet gas temp, K
Po = 2.302e5;         % Actual inlet pressure, Pa (a)
Vel = 166.1;          % Inlet velocity, m/s
D = 0.00114;          % Tube (cell) diameter, m
Yo = 0.000983;        % Actual initial mol fraction of CO in the gas phase
Tw = To;              % Inlet solid temp, K (initially assumed same as To)
Lc = 45.2e-6;         % Thickness of coated catalyst, m
R = 8.314;            % Gas constant, J/mol/K
Len = 0.022;          % Length of the reactor, m
end;

Visco = 7.701e-6 + 4.166e-8*To - 7.531e-12*To^2;
% The viscosity of air in Pa.s, adapted from Hayes & Kolaczkowski (1997), Page 660

Cond = 1.679e-2 + 5.073e-5*To;
% The thermal conductivity of air in W/(m.K), adapted from Hayes & Kolaczkowski
(1997), Page 660

Diff = 1.01325*0.01*To^1.75*(1/28+1/29)^0.5/Po/(18.9^(1/3)+17.9^(1/3))^2;
% Bulk diffusion of CO in air, m^2/s, adapted from Hayes & Kolaczkowski (1997), Page
228

Dk = 48.5*1.2590*10^(-6)*(To/28)^0.5;
```

```
% Knudsen diffusion coefficient, m^2/s, adapted from Hayes & Kolaczkowski (1997),
Page 245
% In the old program Dk is
% Dk = 48.5*0.0137*10^(-6)*(To/0.028)^0.5 which is wrong

De = (Dk*Diff/(Dk+Diff))*0.212;
% The calculation of effective diffusivity at different temperatures is
% based on the results measured in single-plate washcoat C2NM, m^2/s.
% Here 0.212 is the ratio of porosity to tortuosity, which is calculated
% from the measured effective diffusivity at room temperature based on the
% sample washcoat and assumed it is constant, see Hayes & Kolaczkowski
% (1997), Page 245.

Rho = Po/(R*To);          % Inlet gas density, mol/m3
Rhom = Rho*(29/1000);     % Mass density, kg/m3

Z = 0;
T = To;
Y = Yo;
delz = 0.0011;          % step size

Co = Po/(R*To);         % Input concentration, mol/m3

history_Z = Z;          % will be used to store all the Z values
history_Y = Y;          % will be used to store all the Y values
history_T = T;          % will be used to store all the time points

Cp = 28.09 + 0.1965e-2*T + 0.4799e-5*T^2 - 1.965e-9*T^3;
% Heat capacity of air in J/(mol.K), adapted from Hayes & Kolaczkowski (1997), Page
104

DelH = -283.2*10^3;
% J/mol, Calculated from Hayes & Kolaczkowski (1997), Page 104

Pr = 0.029*Cp*Visco/Cond;
% Prandtl Number, dimensionless, used to describe heat transfer, meaning
% "(moleculare diffusivity of momentum)/(molecular diffusivity of heat)",
% adapted from Hayes & Kolaczkowski (1997), Page 666

Sc = Visco/(Rhom*Diff);
% Schmidt Number, dimensionless, used to describe mass transfer, meaning
% "(momentum diffusivity)/(mass diffusivity)", adapted from Hayes &
% Kolaczkowski (1997), Page 668

Re = Rhom*D*Vel/Visco;
% Reynold Number, dimensionless, used to describe the flow of a gas through
% a varity of media, meaning "(non-viscous forces)/(viscous forces)",
% adapted from Hayes & Kolaczkowski (1997), Page 667
```

```
Gz = (D/(Z+delz))*Re*Pr;
% Graetz Number, dimensionless, used to describe entrance effects for the
% flow of gas in a monolith channel etc, meaning "(conductive resistance to
% heat transfer in the gas phase)/(convective resistance to heat transfer in
% the gas phase)", adapted from rom Hayes & Kolaczkowski (1997), Page 663

Nu = 2.977 + 6.854*((1000/Gz)^-0.5174)*exp(-42.49/Gz);
% Nusselt Number, dimensionless, used to describe heat transfer to or from
% a flowing fluid, meaning "(conductive resistance to heat transfer in the gas
% phase)/(convective resistance to heat transfer in the gas phase)",
% adapted from rom Hayes & Kolaczkowski (1997), Pages 664 and 316

Sh = 3.66*(1+0.095*(D/Len)*Re*Sc)^0.45;
% Sherwood Number, dimensionless, used to describe flow of gas in a
% monolith channel, meaning "(diffusive resistance to mass transfer in the
% gas)/(convective resistance to mass transfer in the gas)",
% adapted from rom Hayes & Kolaczkowski (1997), Pages 668 and 314

h = (Nu*Cond)/D;              % heat transfer coefficient
km = Sh*Diff/D;               % mass transfer coefficient
kv = (Aw*exp(-Ew/R/Tw))/Lc;   % Reaction rate constant based on catalyst volume,
mol/m3/s
                              % calcualted from reaction rate constant based on area

Phi = Lc*sqrt((kv*Po^alpha)/De);  % Thile modulus
Eta = tanh(Phi)/Phi           % Effectiveness factor

% Now the main loop for Euler's method
while ((Z+delz/2) < Len)                  % repeats loop provided step,z less than
Length,L

% Now key equations:
Yw = (km*Y)/(Eta*kv*Lc*Po^alpha+km);              % Mol fraction of CO in the
solid phase,  Equation 6.21
Tw = -Eta*kv*Lc*Po^alpha*Yw*(DelH)/h*Co + T;      % from Equations 6.39
(forget to use Co in the old program)
Yprime = (4/D)*(km/Vel)*(Yw-Y);                   % finds Y derivative at the
present step, see Equation 6.13
Tprime = -4/D*Eta*kv*Lc*Po^alpha*Y*(DelH)*Co/(Rho*Cp*Vel);  % finds T
derivative at the present step, see Equation 6.38
                                  %(forget to use Co in the old program)

Y = Y  + delz*Yprime      % finds solution at next time step
T = T  + delz*Tprime      % finds solution at next time step

Z = Z + delz;             % finds next time step history_Z = [history_Z,Z] updates step
```

```
history_Z = [history_Z,Z];
history_T = [history_T,T];
history_Y = [history_Y,Y];
end                    % end of while loop

  if ll==1
    Tcal1=T;
    Ycal1=Y;
    Eta1=Eta;
    R10=Aw*2.71828^(-Ew/8.314/To)*Po^alpha*53.54*Yo*Eta; % calculated
    R20=9.92E-04;
    delta2 = 500*(T-Tdata)*(T-Tdata)/(Tdata*Tdata);
    delta3 = (Y-Ydata)*(Y-Ydata)/(Ydata*Ydata);
    delta4 = delta2 + delta3 + (R10-R20)*(R10-R20)/R10/R20;
  end;
  % Squares of difference between the calculated results and the experimental data

  if ll==2
    Tcal2=T;
    Ycal2=Y;
    Eta2=Eta;
    R11=Aw*2.71828^(-Ew/8.314/To)*Po^alpha*51.79*Yo*Eta; % calculated
    R21=5.20E-03;
    delta5 = 500*(T-Tdata)*(T-Tdata)/(Tdata*Tdata);
    delta6 = (Y-Ydata)*(Y-Ydata)/(Ydata*Ydata);
    delta7 = delta5 + delta6 + (R11-R21)*(R11-R21)/R11/R21;
  end;
  % Squares of difference between the calculated results and the experimental data

  if ll==3
    Tcal3=T;
    Ycal3=Y;
    Eta3=Eta;
    R12=Aw*2.71828^(-Ew/8.314/To)*Po^alpha*50.08*Yo*Eta; % calculated
    R22=8.27E-03;
    delta8 = 500*(T-Tdata)*(T-Tdata)/(Tdata*Tdata);
    delta9 = (Y-Ydata)*(Y-Ydata)/(Ydata*Ydata);
    delta10 = delta8 + delta9 + (R12-R22)*(R12-R22)/R12/R22;
  end;
  % Squares of difference between the calculated results and the experimental data

  if ll==4
    Tcal4=T;
    Ycal4=Y;
    Eta4=Eta;
    R13=Aw*2.71828^(-Ew/8.314/To)*Po^alpha*48.48*Yo*Eta; % calculated
    R23=1.01E-02;
    delta11 = 500*(T-Tdata)*(T-Tdata)/(Tdata*Tdata);
```

```
    delta12 = (Y-Ydata)*(Y-Ydata)/(Ydata*Ydata);
    delta13 = delta11 + delta12 + (R13-R23)*(R13-R23)/R13/R23;
end;
% Squares of difference between the calculated results and the experimental data

if ll==5
    Tcal5=T;
    Ycal5=Y;
    Eta5=Eta;
    R14=Aw*2.71828^(-Ew/8.314/To)*Po^alpha*47.10*Yo*Eta; % calculated
    R24=1.15E-02;
    delta14 = 500*(T-Tdata)*(T-Tdata)/(Tdata*Tdata);
    delta15 = (Y-Ydata)*(Y-Ydata)/(Ydata*Ydata);
    delta16 = delta14 + delta15 + (R14-R24)*(R14-R24)/R14/R24;
end;
% Squares of difference between the calculated results and the experimental data

if ll==6
    Tcal6=T;
    Ycal6=Y;
    Eta6=Eta;
    R15=Aw*2.71828^(-Ew/8.314/To)*Po^alpha*44.51*Yo*Eta; % calculated
    R25=1.15E-02;
    delta17 = 500*(T-Tdata)*(T-Tdata)/(Tdata*Tdata);
    delta18 = (Y-Ydata)*(Y-Ydata)/(Ydata*Ydata);
    delta19 = delta17 + delta18 + (R15-R25)*(R15-R25)/R15/R25;
end;
% Squares of difference between the calculated results and the experimental data

if ll==7
    Tcal7=T;
    Ycal7=Y;
    Eta7=Eta;
    R16=Aw*2.71828^(-Ew/8.314/To)*Po^alpha*42.27*Yo*Eta; % calculated
    R26=1.09E-02;
    delta20 = 500*(T-Tdata)*(T-Tdata)/(Tdata*Tdata);
    delta21 = (Y-Ydata)*(Y-Ydata)/(Ydata*Ydata);
    delta22 = delta20 + delta21 + (R16-R26)*(R16-R26)/R16/R26;
end;
% Squares of difference between the calculated results and the experimental data

if ll==8
    Tcal8=T;
    Ycal8=Y;
    Eta8=Eta;
    R17=Aw*2.71828^(-Ew/8.314/To)*Po^alpha*40.49*Yo*Eta; % calculated
    R27=1.02E-02;
    delta23 = 500*(T-Tdata)*(T-Tdata)/(Tdata*Tdata);
```

```
    delta24 = (Y-Ydata)*(Y-Ydata)/(Ydata*Ydata);
    delta25 = delta23 + delta24 + (R17-R27)*(R17-R27)/R17/R27;
  end;
  % Squares of difference between the calculated results and the experimental data

  if ll==9
    Tcal9=T;
    Ycal9=Y;
    Eta9=Eta;
    R18=Aw*2.71828^(-Ew/8.314/To)*Po^alpha*38.72*Yo*Eta; % calculated
    R28=1.09E-02;
    delta26 = 500*(T-Tdata)*(T-Tdata)/(Tdata*Tdata);
    delta27 = (Y-Ydata)*(Y-Ydata)/(Ydata*Ydata);
    delta28 = delta26 + delta27 + (R18-R28)*(R18-R28)/R18/R28;
  end;
  % Squares of difference between the calculated results and the experimental data

  if ll==10
    Tcal10=T;
    Ycal10=Y;
    Eta10=Eta;
    R19=Aw*2.71828^(-Ew/8.314/To)*Po^alpha*37.44*Yo*Eta; % calculated
    R29=9.95E-03;
    delta30 = 500*(T-Tdata)*(T-Tdata)/(Tdata*Tdata);
    delta31 = (Y-Ydata)*(Y-Ydata)/(Ydata*Ydata);
    delta32 = delta30 + delta31 + (R19-R29)*(R19-R29)/R19/R29;
  end;
  % Squares of difference between the calculated results and the experimental data

end; % end of for loop for changing Tdata

delta33=delta4+delta7+delta10+delta13+delta16+delta19+delta22+delta25+delta28+del
ta32;
% Total squares of difference between the calculated results and the experimental data

if (delta33 < delta1)
  alpha1=alpha;
  Aw1=Aw;
  Ew1=Ew;
  delta1=delta33;

  Tcal11=Tcal1;
  Tcal12=Tcal2;
  Tcal13=Tcal3;
  Tcal14=Tcal4;
  Tcal15=Tcal5;
  Tcal16=Tcal6;
  Tcal17=Tcal7;
```

```
   Tcal18=Tcal8;
   Tcal19=Tcal9;
   Tcal20=Tcal10;

   Ycal11=Ycal1;
   Ycal12=Ycal2;
   Ycal13=Ycal3;
   Ycal14=Ycal4;
   Ycal15=Ycal5;
   Ycal16=Ycal6;
   Ycal17=Ycal7;
   Ycal18=Ycal8;
   Ycal19=Ycal9;
   Ycal20=Ycal10;

   Eta11=Eta1;
   Eta12=Eta2;
   Eta13=Eta3;
   Eta14=Eta4;
   Eta15=Eta5;
   Eta16=Eta6;
   Eta17=Eta7;
   Eta18=Eta8;
   Eta19=Eta9;
   Eta20=Eta10;

   R1=R10;
   R2=R11;
   R3=R12;
   R4=R13;
   R5=R14;
   R6=R15;
   R7=R16;
   R8=R17;
   R9=R18;
   R0=R19;

   history_Z1 = history_Z;
   history_T1 = history_T;
   history_Y1 = history_Y;
end                    % end of if

   history_Z = [];
   history_T = [];
   history_Y = [];

end                    % end of for loop
end                    % end of for loop
```

```
fprintf('Value of alpha: ')
disp(alpha1)
fprintf('Value of Aw1: ')
disp(Aw1)
fprintf('Value of Ew: ')
disp(Ew1)
fprintf('\nValue of mean square error: \n')
disp(delta1/500)

fprintf('\nValue of the calculated temperature: \n')

disp(Tcal11)
disp(Tcal12)
disp(Tcal13)
disp(Tcal14)
disp(Tcal15)
disp(Tcal16)
disp(Tcal17)
disp(Tcal18)
disp(Tcal19)
disp(Tcal20)

fprintf('\nValue of the calculated mole fraction of CO: \n')

disp(Ycal11)
disp(Ycal12)
disp(Ycal13)
disp(Ycal14)
disp(Ycal15)
disp(Ycal16)
disp(Ycal17)
disp(Ycal18)
disp(Ycal19)
disp(Ycal20)

fprintf('\nValue of the calculated Eta: \n')

disp(Eta11)
disp(Eta12)
disp(Eta13)
disp(Eta14)
disp(Eta15)
disp(Eta16)
disp(Eta17)
disp(Eta18)
disp(Eta19)
disp(Eta20)
```

```
fprintf('\nValue of the calculated R1: \n')

disp(R1)
disp(R2)
disp(R3)
disp(R4)
disp(R5)
disp(R6)
disp(R7)
disp(R8)
disp(R9)
disp(R0)

% now plot the graph of Temp against t

plot(history_Z1,history_Y1)              % Does the plot
xlabel('Reactor length')                 % Labels the horizontal axis
ylabel('Mol fraction of CO')             % Labels the vertical axis
Title('Figure 1: Mol fraction versus length ')  % Puts a title on it

figure
plot(history_Z1,history_T1)              % Does the plot
xlabel('Reactor length')                 % Labels the horizontal axis
ylabel('Outlet temperature')             % Labels the vertical axis
title('Figure 2: Temperature versus length ')  % Puts a title on it


disp('equation solved, graph plotted in separate window')
```

Value of alpha: -1.1000

Value of Aw1: 7.9433e+015

Value of Ew: 104000

Value of mean square error:
0.2037

Value of the calculated temperature:
415.9056

443.7347

462.2991

484.9914

511.1374

560.2467

615.2832

663.1981

723.6937

776.3285

Value of the calculated mole fraction of CO:
9.6841e-004

9.7043e-004

9.6210e-004

9.4535e-004

9.1962e-004

8.6580e-004

8.2083e-004

7.9840e-004

7.7887e-004

7.6433e-004

Value of the calculated Eta:
0.9957

0.9756

0.9332

0.8163

0.5925

0.2463

0.1029

0.0557

0.0300

0.0195

Value of the calculated R1:
5.7318e-005

3.4720e-004

9.8262e-004

0.0029

0.0073

0.0223

0.0569

0.1104

0.2157

0.3435

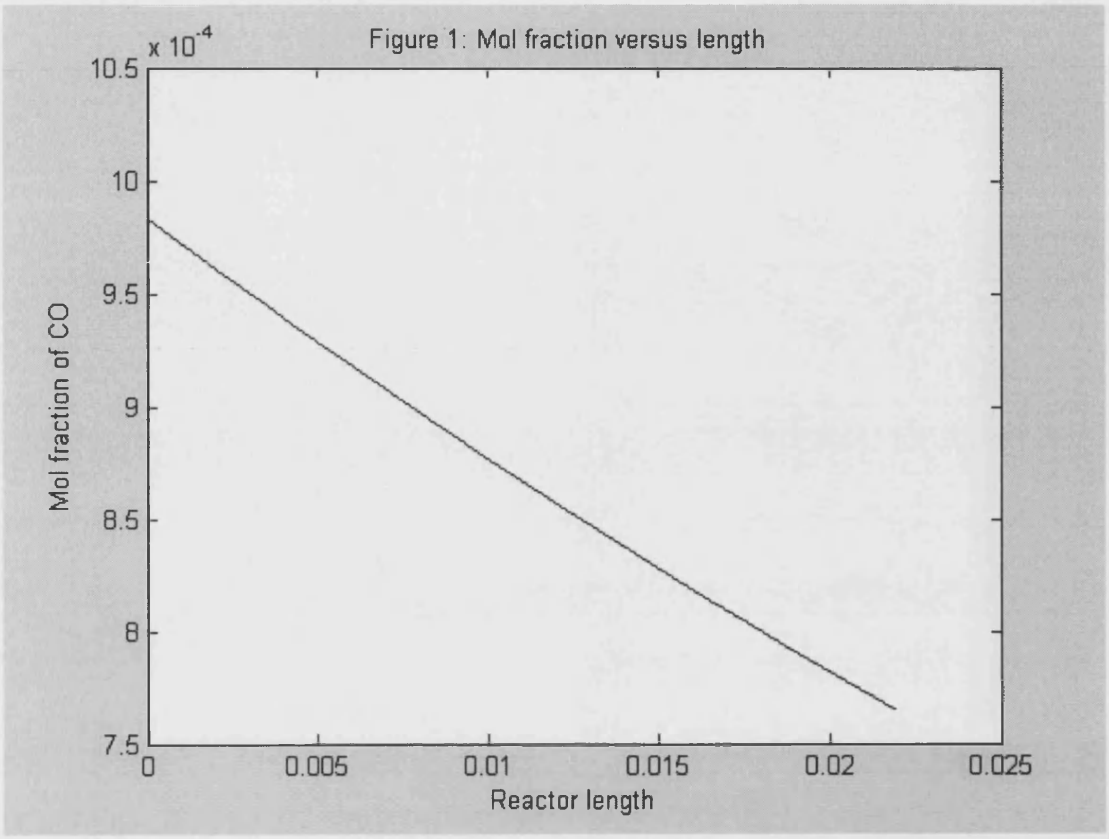
Figure 1: Mol fraction versus length
x 10^-4
10.5
10
9.5
9
8.5
8
7.5
Mol fraction of CO
0
0.005
0.01
0.015
0.02
0.025
Reactor length

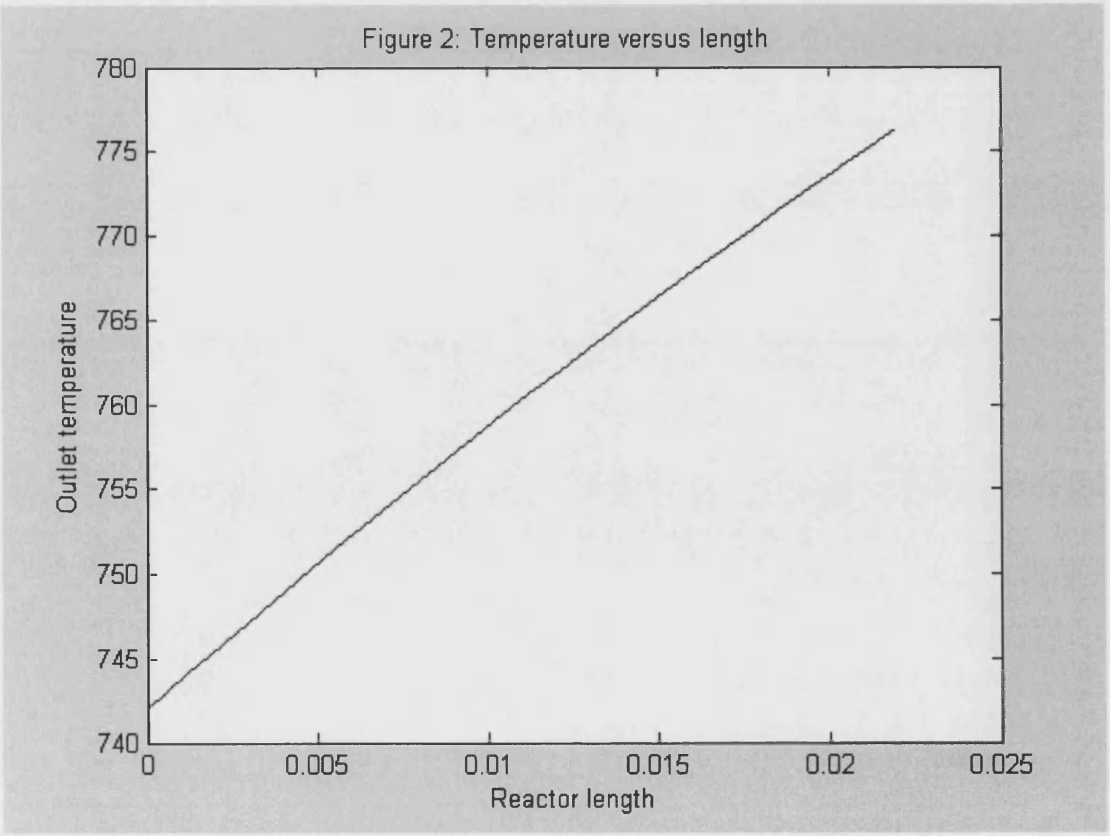
Figure 2: Temperature versus length
780
775
770
765
760
755
750
745
740
Outlet temperature
0
0.005
0.01
0.015
0.02
0.025
Reactor length